Mechanized Molecules

Euan R. Kay

Degree of Doctor of Philosophy

School of Chemistry

The University of Edinburgh

August 2006

Dedicated to My Parents

Contents

Abstract and Layout of Thesis

This Thesis describes the use of synthetic chemistry to investigate mechanisms for controlling molecular-level motion. Initially, the principles that all experimental designs for working molecular machines must follow are elucidated; tracing the development of ideas about molecular-level motion from their genesis, to the modern-day contributions of molecular biology and theoretical nonequilibrium statistical physics.

In the rest of the Thesis, these theoretical considerations are applied and extended through the construction and operation of molecular machines based on interlocked molecules. Two simple rotaxane-based examples serve to demonstrate the novel concept of 'compartmentalized' molecular machines. Correlating chemical, physical and statistical descriptions of these simple devices with their behaviour, reveals the fundamental mechanistic elements that are involved in the operation of any compartmentalized Brownian machine and suggests how these can be combined to create different types of device. This leads to the construction of a [2]catenane that is the first example of a reversible synthetic rotary molecular motor and which operates via an energy ratchet mechanism.

Next, a fundamentally different mechanism is investigated through the construction and analysis of a compartmentalized molecular machine that is the first to operate via an information ratchet mechanism.

Finally, the classic stimuli-responsive molecular shuttle design serves as an ideal test bed for investigating a new structural series of rotaxane-based molecular machines that are controlled by redox processes and which show promise for operation at surfaces.

Chapter 1 is based upon the first section of a comprehensive review article currently in press. Some minor alterations have been made in order to place it in the context of this Thesis. Chapters 2 and 3 are each presented in the form of articles that have already been published in peer-reviewed journals. No attempt has been made to rewrite this work out of context, other than to insert cross-references to other Chapters, as appropriate, and to ensure consistency of presentation throughout this Thesis. An abbreviated version of Chapter 4 has also been accepted for publication, although a fuller discussion of this material is provided here. The opening sections of

Chapter 5 have also previously been published, and here too, only minor amendments have been made so as to allow integration of the new results reported towards the end of the Chapter. Where already published, the original papers are reproduced, in their published format, in the Appendix. Additionally, each Chapter is preceded by a synopsis that puts the work reported in context, and also by a very grateful acknowledgement of the contributions of my fellow researchers. A consequence of presenting the work in this way is that many of the blind alleys, cul-de-sacs and interesting, but ultimately fruitless, avenues explored along the way have not been included. I hope the reader will forgive such omissions as well as the slight repetition that occurs in the introduction and bibliography of each Chapter.

Declaration

The scientific work described in this Thesis was carried out in the School of Chemistry at the University of Edinburgh between October 2002 and July 2006. Unless otherwise stated, it is the work of the author and has not been submitted in whole or in support of an application for another degree or qualification at this or any other University or institute of learning.

Lectures and Meetings Attended and Presentations Given

1. **Organic Research Seminars**, School of Chemistry, University of Edinburgh, UK, 2002–2006.
   Oral presentations:
   a) *Towards correlated motion in mechanically interlocked architectures*, 24 January 2003.
   b) *Doing work at the molecular level*, 23 April 2004.
   c) *Molecules that can do work: Compartmentalized molecular machines*, 4 November 2004.

2. **School of Chemistry Visiting Speaker Colloquia**, School of Chemistry, University of Edinburgh, UK, 2002–2006.

3. **Diffraction Methods**, five-lecture honours module, School of Chemistry, University of Edinburgh, UK, November–December 2002.

4. **RSC Perkin Division 31st Scottish Regional Meeting**, University of Dundee, UK, 18 December 2002.

5. **RSC Frontiers in Chemical Biology: Biomolecular Dynamics and Force Generation**, University of Manchester, UK, 4–6 September 2003.

6. **RSC Perkin Division 32nd Scottish Regional Meeting**, University of Edinburgh, UK, 17 December 2003.

7. **School of Chemistry, Organic Section Firbush Symposium**, Firbush Point Centre, University of Edinburgh, UK, 29–31 March 2004.
   Poster presentation: *Controlling molecular-level motion.*

8. **EMMMA European Training Network Meeting**, Oegstgeest, The Netherlands, 25–27 June 2004.
   Oral presentation: *Molecular-level thermal ratchets.*

9. **2nd University of Glasgow–Organon Symposium on Synthetic Chemistry**, University of Glasgow, UK, 3 September 2004.

10. **RSC Perkin Division 33rd Scottish Regional Meeting**, University of St. Andrews, UK, 20 December 2004.

11. **School of Chemistry, Organic Section Firbush Symposium**, Firbush Point Centre, University of Edinburgh, UK, 6 April 2005.
    Oral presentation: *How to do work at the molecular level.*

12. **16th SCI Postgraduate Symposium on Novel Organic Chemistry**, University of Glasgow, UK, 7 April 2005.
    Oral presentation: *How to do work at the molecular level.* Awarded 1st Prize.

13. **Graduate School of Chemistry Postgraduate Seminar Afternoon**, University of Edinburgh, UK, 27 April 2005.
Oral presentation: *How to do work at the molecular level.*

14. **EMMMA European Training Network Meeting**, Edinburgh, UK, 25–26 May 2005.
Oral presentation: *How to do work at the molecular level.*

15. **International Symposium on Reactive Intermediates and Unusual Molecules (ISRIUM 2005)**, University of Edinburgh, UK, 7–12 August 2005.
Oral presentation: *How to do work at the molecular level.*

16. **3rd University of Glasgow/WestChem–Organon Symposium on Synthetic Chemistry**, University of Glasgow, UK, 1 September 2005.

17. **EMMMA European Training Network Meeting**, Vico Equense, Italy, 3–4 February 2006.
Oral presentation: *Demons and Trapdoors – Realising a new mechanism for directional transport at the molecular level.*

18. **EMMMA European Training Network Meeting**, Villasimius, Sardinia, Italy, 1–3 June 2006.

19. **Nanonet 6th Workshop – Towards Nanodevices for the 21st Century**, Portsmouth, UK, 28 July 2006.
Oral presentation: *Switches and Beyond: Interlocked Molecular Machines.*

Acknowledgements

My first note of thanks must certainly go to my supervisor, Prof. David A. Leigh, for allowing me the opportunity to work on such fantastic science over the past five years, and for providing me with all the facilities and resources that I might need. Perhaps even more importantly, I thank him for his supportive approach and for the great number of fascinating and stretching discussions, which not only directly shaped the work reported in this Thesis, but which also taught me much about chemistry and the pursuit of science more generally. I hope they will continue for many years to come!

Theoretical conjecture is, of course, nothing without the experimental work to back it up. For that, I am indebted to those who passed on their knowledge to me, and also to those who were involved directly in the projects reported on in this Thesis – without them only a tiny fraction of this work would have been possible. In terms of the former, no member of the Leigh group should be omitted, but particular thanks must go to Dr Frédéric Coutrot, Dr Jenny Wong and Dr Stéphanie Potok for their advice, tutoring and patience while I was still an undergraduate student in the group. In the latter category, specific contributions are noted at the start of each Chapter, but special mention must go the following people: Viviana Serreli, for her persistence and determination with a particularly troublesome molecule, even with the added disadvantage of my guidance; Dr Chin-Fa Lee for adding his considerable skill and experience to the same project; Dr José Vicente-Hernández for teaching me that a little bit of madness goes a long way in the synthesis of demanding molecules; Dr Manashi Chatterjee for her friendship, curries and unshakable patience in the lab; Dr Stephen Goldup for bringing his genial presence to the office and his not inconsiderable synthetic nous to the ratchet project; and, pre-dating my time in the Leigh Group, Dr Francesco Gatti, whose work on the early rotaxane and shuttle systems forms the foundation of much of the work reported here.

Many others are of course responsible for making the Leigh group a most enjoyable place to work and I would like to thank all of the following: Jeff, for passing on just a little of his synthetic knowledge, as well as putting up with Alison's cooking on occasion; Barney and Drew, my chemistry 'brothers' of nine(!) years, for many stimulating and ridiculous conversations alike; Paul, the friendly voice of experience who always kept us right; Andrea B., Dana and Phill, my laboratory and office

neighbours, for putting up with me and teaching me the entire script of *Pulp Fiction*; James, for bringing a bit of rugby knowledge to the group, and also for letting me use his fumehood during some fraught 'finishing-up' weeks; as well as all the other group members over the past five years – Ahlem, Ai-Lan, Alé, Andrea A., Anne-Marie, Aurelian, Bill, Bryan, Claire, Diego, Elena, Emilio, Gianni, Isabel, Laure, Marius, Mark, Monica, Nick, Jong, Julia, Pepe, Popi, Raman, Roy, Smilja, Stéph C., Steve M., Tao, Trent, Vicki, Vince, Weiquan, Yun and the others I have surely forgotten.

The group would not have run so smoothly without the efforts of Louise (my only other rugby aficionado) and Stewart, and thanks also to Amanda and Annette in the office, all of the technical staff in the School of Chemistry, and the ever-friendly Derek, Kenny, Raymond and Tim in stores.

It has been a particular highlight of my studies to be involved in a European Union Research Training Network and I would like to thank all the participants in the EMMMA network, especially Coke, Giulia, Monika, Sandra and Steve, as well as Dr Fred Brouwer, Prof. Francesco Paolucci, Prof. Petra Rudolf and Prof. Francesco Zerbetto, together with their respective research groups, for some fruitful collaborations and enjoyable meetings. Beyond the network, thanks also to Alan Farrell and the group of Prof. Suzanne Jarvis at Trinity College, Dublin. I am also indebted to The Carnegie Trust for the Universities of Scotland for the award of a Scholarship for the period of my studies.

Away from the lab, I have to thank the much-neglected Graeme, Cara, Craig and Paul for trying to make sure that at least now and again I stopped being a chemistry geek. For putting up with me all of the rest of the time, my deepest thanks go to Alison, whose support and understanding have made it easy for me to concentrate on work when required and on relaxing when possible. Thank you too for looking after me so well during the 'last few months' which, in reality, have probably lasted for about a year.

Finally, thank you to my parents, Mary and Nigel, without whom this Thesis would not have happened – in many more ways than the obvious. Their counsel, love and support – financial, practical and emotional – have seen me through nine years of university education, and never once have they baulked at the prospect of yet another trip along the M8.

Abbreviations

Ac	Acetyl
Alloc	Allyloxycarbonyl
ATP	Adenosine triphosphate
b	'Backward' shuttling process
Bn	Benzyl
Boc	*tert*-Butyloxycarbonyl
br	Broad
cat.	Catalytic amount
Cbz	Benzyloxycarbonyl
CV	Cyclic voltammetry
d	Doublet
dba	Dibenzyl ammonium binding site
DCC	*N*,*N*'-Dicyclohexylcarbodiimide
decomp.	Decomposes
DMAP	4-(Dimethylamino)pyridine
DMF	*N*,*N*-Dimethylformamide
DMSO	Dimethyl sulfoxide
DNA	Deoxyribonucleic acid
EDCI·HCl	1-(3-Dimethylaminopropyl)-3-ethylcarbodiimide hydrochloride
EI	Electron impact
Et	Ethyl
ET	Energy transfer
f	'Forward' shuttling process
FAB	Fast atom bombardment
Fmoc	9-Fluorenylmethoxycarbonyl
fum	Fumaramide binding site
HOBt	1-Hydroxybenzotriazole
HRMS	High resolution mass spectrometry
IR	Infrared
m	Multiplet
mal	Maleamide binding site
mba	Monobenzyl ammonium binding site
Me	Methyl
11-MUA	11-Mercaptoundecanoic acid

n	Neutral state
NADH	Reduced nicotinamide adenine dinucleotide
NADPH	Reduced nicotinamide adenine dinucleotide phosphate
ni	Naphthalimide binding site
NMR	Nuclear magnetic resonance
3-NOBA	3-Nitrobenzyl alcohol
Ph	Phenyl
PSS	Photostationary state
q	Quartet
quant.	Quantitative
quint.	Quintet
red	Reduced state
RNA	Ribonucleic acid
rt	Room temperature
s	Singlet
SAM	Self-assembled monolayer
SPT-SIR	Spin polarization transfer by selective inversion recovery
SS	Steady state
succ	Succinamide binding site
t	Triplet
TBAF	Tetra-*n*-butylammonium fluoride
TBDMS	*tert*-Butyldimethylsilyl
TBDPS	*tert*-Butyldiphenylsilyl
TBHF	Tetra-*n*-butylammonium hexafluorophosphate
Tf	Trifluoromethanesulfonyl (Triflyl)
THF	Tetrahydrofuran
THIOG	Thioglycerol
THP	Tetrahydropyran
TLC	Thin-layer chromatography
Tr	Triphenylmethyl (Trityl)
Ts	*para*-Toluenesulfonyl (Tosyl)
UV	Ultraviolet
VT	Variable temperature

Note: conventional abbreviations for units, physical quantities and stereochemical terms are not included here.

General Comments on Experimental Data

Prior to use, isophthaloyl dichloride was purified by recrystallization from hexanes; *p*-xylylenediamine was purified by distillation under reduced pressure; triethylamine was dried by distillation from calcium hydride, then stored over 4 Å molecular sieves. Chloroform and tetrahydrofuran (THF) solvents were analytical grade, without stabilizer; dry acetonitrile, chloroform, dichloromethane, *N*,*N*-dimethylformamide (DMF), methanol, tetrahydrofuran and toluene were obtained by passing these solvents through activated alumina columns on a PureSolv^{TM} solvent purification system (Innovative Technologies, Inc., MA). Unless stated otherwise, all other reagents were purchased from commercial sources and used without further purification. Column chromatography was carried out using Kiesegel C60 (Fisher Scientific) as the stationary phase. Preparative thin-layer chromatography (TLC) was performed on glass-backed plates pre-coated with silica 60 F_{254} adsorbent (20 cm × 20 cm, with concentration zone, 0.25 mm thick, Fluka) and analytical TLC was performed on aluminium-backed sheets pre-coated with silica 60 F_{254} adsorbent (0.25 mm thick, Merck, Germany) and visualized under UV light. Photoisomerizations were carried out in quartz vessels using a multilamp photoreactor (model MLU18) manufactured by Photochemical Reactors Ltd, Reading, UK. All samples were degassed by bubbling with nitrogen prior to irradiation. Routine ^{1}H and ^{13}C NMR spectra were recorded at 400 MHz on a Bruker AV 400 instrument. Some complex ^{1}H spectra were recorded at 600 MHz on a Varian INOVA 600 instrument. Spectra were recorded at ambient temperature, unless otherwise stated. Chemical shifts (δ) are reported in parts per million from low to high field and referenced to the literature values of chemical shifts, with respect to tetramethylsilane, of residual non-deuterated solvent. Standard abbreviations indicating multiplicity are used as follows: br = broad, d = doublet, m = multiplet, q = quartet, quint. = quintet, s = singlet, t = triplet. All melting points were determined using a Sanyo Gallenkamp MPD350.BM3.5 apparatus and are uncorrected. Fast atom bombardment (FAB) and electron impact (EI) mass spectrometry was carried out by the services at the University of Edinburgh.

CHAPTER ONE

Design Principles for Molecular-Level Motors and Machines

In a slightly modified form, this Chapter forms the first section of a review article titled "*Synthetic Molecular Motors and Mechanical Machines*", accepted for publication in *Angewandte Chemie*:

E. R. Kay, D. A. Leigh, F. Zerbetto, *Angew. Chem. Int. Ed.*, DOI 10.1002/200504313

"What are the possibilities of small but movable machines? They may or may not be useful, but they surely would be fun to make...

...I can't see exactly what would happen, but I can hardly doubt that when we have some control of the arrangement of things on a small scale we will get an enormously greater range of possible properties that substances can have, and of different things that we can do."

Richard P. Feynman, 1959

Synopsis

The widespread use of controlled molecular-level motion in key natural processes suggests that great rewards could come from bridging the gap between the present generation of synthetic molecular systems – which by and large rely upon electronic and chemical effects to carry out their functions – and the machines of the macroscopic world, which utilize the synchronized movements of smaller parts to perform specific tasks. This is a scientific area of great contemporary interest and extraordinary recent growth. Yet, the notion of molecular-level machines dates back to a time when the ideas surrounding the statistical nature of matter and the Laws of Thermodynamics were first being formulated; nearly two centuries before the synthetic chemistry and instrumentation necessary to address, manipulate and characterize nanoscale structures had developed to the level required to experimentally explore them.

Despite the sophistication of modern chemical methods, clear and generally applicable precepts for the construction of molecular machines have yet to be arrived at in the literature. Furthermore, the established rules of macroscopic mechanical engineering are entirely inapplicable at the molecular level. In this Chapter, therefore, the underlying principles that all experimental molecular designs must follow are explored. Ideas about the nature of molecular-level motion, and how to control it, are drawn from such diverse fields as classical thermodynamics, molecular biology and nonequilibrium statistical physics, and are put in the context of designing synthetic molecular machines. The principles which are derived from this survey are expounded, exemplified, and extended throughout the following Chapters of this Thesis, where the construction and operation of various synthetic molecular machines is examined.

1.1 Introduction

In recent years chemists have demonstrated imagination and considerable skill in the design and construction of synthetic molecular systems in which positional displacements of submolecular components result from moving energetically downhill.[1] But what are the structural features necessary for molecules to use chemical energy to repetitively do mechanical work? How can we make a molecular machine that pumps ions to reverse a concentration gradient, say, or that moves itself energetically uphill? How can we make nanoscale structures that traverse a pre-defined path across a surface or down a track, responding to the nature of their environment to change direction? How can we make a synthetic molecular motor that rotates against an applied torque? Artificial compounds that can do such things have yet to be realized. Moreover, and perhaps more surprisingly given that nature has developed such machines and refined them to a high degree of efficiency, the literature is still largely bereft of the fundamental guidelines necessary to invent them. In this Chapter I try to address this deficiency by using theory to outline, develop and present the underlying mechanisms and principles required for future generation synthetic molecular-level machine systems.

Perhaps inevitably in a newly emerging field, there is not even a clear consensus as to what constitutes a molecular machine and what differentiates one from other molecular devices. Initially, the categorization of molecules as machines by chemists was purely iconic – the structures 'looked' like pieces of machinery – or they were so-called because they carried out a function that in the macroscopic world would require a machine to perform it. Many of the chemical systems first likened to pistons and other machines were simply host–guest complexes in which the binding could be switched 'on' or 'off' by external stimuli such as light.[1] Whilst such studies were instrumental in popularizing the notion of molecular-level machines amongst chemists, it is fair to say (with considerable hindsight[2]) that the effects of scale tell us that supramolecular decomplexation events have little in common with the motion or function of a piston (the analogy is somewhat better applied to shuttling within a rotaxane architecture because the components are always kinetically associated, but the implication of imparting momentum is still unfortunate). Similarly, a photosensitizer is not phenomenologically related to a 'light-fuelled motor'. In this

Thesis I choose to differentiate machines from other devices on the basis that the etymology and meaning of 'machine' generally implies mechanical movement – i.e. a net nuclear displacement in the molecular world – which causes something useful to happen. Thus, for our purposes, 'molecular machines' are a defined subset of 'molecular devices' (functional molecular systems) in which some stimulus triggers the controlled, large amplitude or directional mechanical motion of one component relative to another (or of a substrate relative to the machine) which results in a net task being performed. Accordingly, neither supramolecular complexes in which the components are able to exchange with others in the bulk, nor systems that function solely through changes in their electronic structure, are covered by such a definition.

1.2 Molecular-level machines and the language used to describe them

Language – especially scientific language – has to be suitably defined and correctly used in order to accurately convey concepts in a field. Nowhere is the need for accurate scientific language more apparent than in the discussion of the ideas and mechanisms by which nanoscale machines could – and do – operate.[3] Much of the terminology used to describe molecular-level machines has its origins in the observations of physicists and biologists, but their findings and descriptions have at times been misunderstood or under-appreciated by chemists. Similarly, the chemistry of molecular systems can sometimes be overlooked by other disciplines.[4]

As mechanism replaces imagery as the driving force behind advances in this field, it may be helpful for the terminology used to discuss molecular-level machine systems to become more phenomenologically based. When describing molecular behaviour scientifically, the standard dictionary definitions meant for everyday use are not always appropriate for a regime that the definitions were never intended to cover. The difference between a 'motor' and a 'switch' as basic molecular machine types, for example, is significant because 'motor' and 'switch' become descriptors of very different types of behaviour at molecular length scales, not simply iconic images (Figure 1.1). A 'switch' influences a system as a function of state whereas a 'motor' influences a system as a function of the trajectory of its components or the substrate. Returning a molecular-level switch to its original position undoes any mechanical effect it has on an external system (naturally, the molecules heat up their surroundings

as the energy from the switching stimulus is dissipated); when the components of a rotary motor return to their original position through a different pathway to the one they left by (i.e. a 360° directional rotation), a physical task performed by the machine is not inherently undone (for example, the rotating components could be used to wind up a polymer chain).

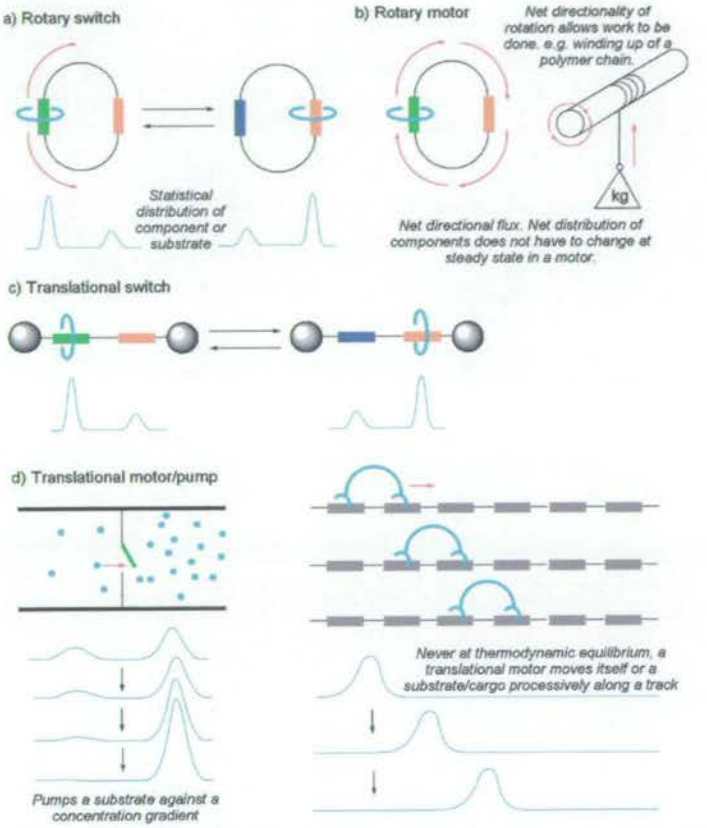

Figure 1.1 The fundamental difference between a 'switch' and a 'motor' at the molecular level. Both translational and rotary switches influence a system as a function of the switch state. They switch between two or more, often equilibrium, states. Motors, however, influence a system as a function of the trajectory of their components or a substrate. Motors function repetitively and progressively on a system; the effect of a switch is undone by resetting the machine. (a) Rotary switch. (b) Rotary motor. (c) Translational switch. (d) Translational motor or pump.

This difference is profound and the terms really should not be used interchangeably as sometimes happens in the chemistry (but not the physics[5] or biology) literature. That is not to say that molecular switches cannot use chemical energy to do mechanical work. They can, but it is undone by resetting the switch to its original state. The key reason why this point is important is that switches cannot use chemical energy to repetitively and progressively drive a system away from equilibrium whereas a motor can.[6] Other molecular machine types, also differentiated on the basis of their fundamental behaviour, can also be identified (see Chapter 2). It is an accurate reflection of the current state of the art that the vast majority of the molecular-level

machines discussed to date are switches, not motors. Similarly, thus far only 'influence-as-a-function-of-state' rather then 'influence-as-a-function-of-trajectory' molecular-level machines have been developed to the level that they can be exploited to perform tasks in the outside world.

1.3 The effects of scale

The path towards synthetic molecular machines can be traced back nearly two centuries to the observation of effects that pointed directly to the random motion experienced by all molecular-scale objects. In 1827, the Scottish botanist Robert Brown noted through his microscope the incessant, haphazard motion of tiny particles within translucent pollen grains suspended in water.[7] An explanation of the phenomenon – now known as Brownian motion or movement – was provided by Einstein in one[8] of his three celebrated papers of 1905 and was proven experimentally[9] by Perrin over the next decade.[10] Scientists have been fascinated by the implications of the stochastic nature of molecular-level motion ever since. The random thermal fluctuations experienced by molecules dominate mechanical behaviour in the molecular world. Even the most efficient nanoscale machines are swamped by its effect. A typical motor protein consumes ATP fuel at a rate of 100-1000 molecules every second, corresponding to a maximum possible power output in the region 10^{-16} to 10^{-17} W per molecule.[11] When compared with the random environmental buffeting of ~10^{-8} W experienced by molecules in solution at room temperature, it seems remarkable that *any* form of controlled motion is possible![12]

When designing molecular machines it is important to remember that the presence of Brownian motion is a consequence of scale, not of the nature of the surroundings. It cannot be avoided by putting a molecular-level structure in a near-vacuum for example. Although there would be few random collisions to set such a Brownian particle in motion, equally there would be little viscosity to slow it down. These effects always cancel each other out and as long as a temperature for an object can be defined, it will undergo Brownian motion appropriate to that temperature (which determines the kinetic energy of the particle) and only the mean free path between collisions is affected by the concentration of particles. In the absence of any other molecules, heat would still be transmitted from the hot walls of the container to the

particle by electromagnetic radiation, the random emission and absorption of the photons producing the Brownian motion. In fact, even temperature is not a particularly effective modulator of Brownian motion since the velocity of the particles depends on the square root of the temperature. So to reduce random thermal fluctuations to 10% of the amount present at room temperature, one would have to drop the temperature from 300 K to 3 K.[12, 13] It seems sensible, therefore, to try to utilize Brownian motion when designing molecular machines rather than make structures that have to fight against it. Indeed, the question of how to (and whether it is even possible to) harness the inherent random motion present at small length scales to generate motion and do work at larger length scales has vexed scientists for some considerable time.

1.3.1 The Brownian motion 'thought-machines': Maxwell's Demon, Szilard's Engine, Smoluchowski's Trapdoor and Feynman's Ratchet and Pawl

The Laws of Thermodynamics govern how systems gain, process and release energy and are central to the use of particle motion to do work on any scale. The Zeroth Law of Thermodynamics tells us about the nature of equilibrium, the First Law is concerned with the total energy of a system, while the Third Law sets the limits against which absolute measurements can be made. Whenever energy changes hands, however, (body-to-body or form-to-form) it is the Second Law of Thermodynamics that comes into play. This law provides the link between the fundamentally reversible laws of physics and the clearly irreversible nature of the universe in which we exist. And it is the Second Law, with its often counter-intuitive consequences, that governs many of the important design aspects of how to harness Brownian motion to make molecular-level machines. Indeed, the design of tiny machines capable of doing work was the subject of several celebrated historical 'thought-machines' intended to test the very nature of the Second Law.[14–18]

Maxwell's Demon

Scottish physicist James Clerk Maxwell played a major role in developing the kinetic theory of gases (along with Ludwig Boltzmann), which established the relationship between heat and particle motion and gave birth to the concept of statistical mechanics. In doing so, Maxwell realized the profundity of the statistical nature of the Second Law which had recently been formulated[19] by Rudolf Clausius and William

Thomson (later Lord Kelvin). In an attempt to illustrate this feature, Maxwell devised the thought experiment which has come to be known as Maxwell's Demon.[14, 15, 20] Maxwell envisaged a gas enclosed within a container, to and from which no heat or matter could flow. The Second Law of Thermodynamics requires that no gradient of heat or pressure can spontaneously arise in such a system, as that would constitute a reduction in entropy. Maxwell imagined the system separated into two sections by a partition (Figure 1.2). Having just proven that the molecules in a gas at a particular temperature have energies statistically distributed about a mean, Maxwell postulated a tiny 'being' able to detect the velocities of individual molecules and open and close a hole in the partition so as to allow molecules moving faster than the average to move in one direction (R → L in Figure 1.2) and molecules moving slower than the average to move in the other (L → R in Figure 1.2). All the time, the number of particles in each half and the total amount of energy in the system remains the same. The result of the demon's endeavours being successful, of course, would be that one end of the system (the 'fast' end, L) would become hot and the other (the 'slow' end, R) cold; a temperature gradient is set up without doing any work, contrary to the Second Law.

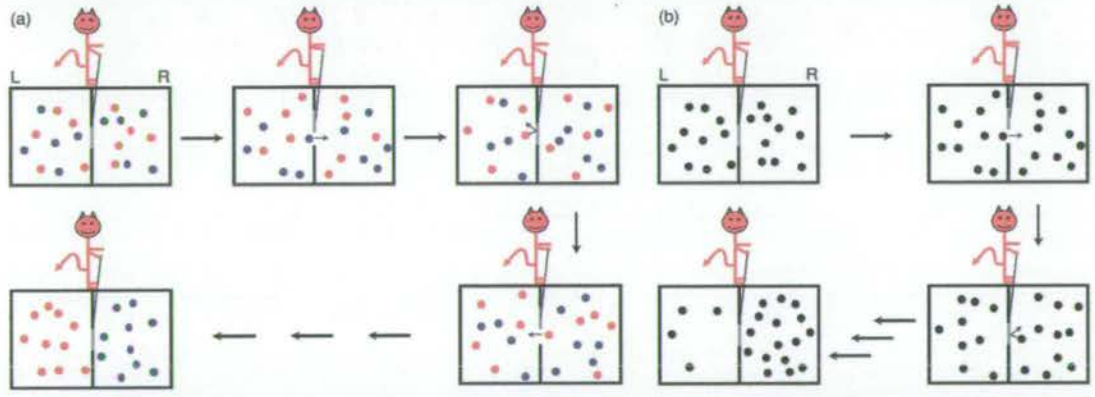

Figure 1.2 (a) Maxwell's 'temperature demon' in which a gas at uniform temperature is sorted into 'hot' and 'cold' molecules.[15] Particles with energy higher than the average are represented by red dots while blue dots represent particles with energies lower than the average. All mechanical operations carried out by the demon involve no work – i.e. the door is frictionless and it is opened and closed infinitely slowly. The depiction of the demon outside the vessel is arbitrary and was not explicitly specified by Maxwell. (b) A Maxwellian 'pressure demon' in which a pressure gradient is established by the door being opened only when a particle in the left compartment approaches it.[15c]

After its publication in '*Theory of Heat*',[15b] Thomson expanded upon Maxwell's idea in a paper[21] read before the Royal Society of Edinburgh on 16 February 1874, and published a few weeks later in *Nature*,[22] introducing the term 'demon' for Maxwell's being.[23] In using this word, Thomson apparently did not intend to suggest a malicious imp, but rather something more in keeping with the ancient Greek roots of

the word (more usually *daemon*) as a supernatural being of a nature between gods and humans. Indeed, neither Maxwell nor Thomson saw the demon as a threat to the Second Law, but rather an illustration of its limitations – an exposition of its statistical nature. This, however, has not been the view of many subsequent investigators, who have perceived the demon as an attempt to construct a perpetual motion machine driven by thermal fluctuations. The term 'Maxwell's Demon' has come to describe all manner of hypothetical constructs designed to overcome the Second Law by continually extracting energy to do work from the thermal bath.[14]

Maxwell noted that the demon principle could be demonstrated in a number of different ways; a 'pressure' demon, for example, (Figure 1.2b) could sort particles so that more end up in one end of a vessel than the other, requiring different information to operate from the original temperature demon (the direction of approach of a particle, not its speed).

Szilard's Engine

Both Maxwell and Thomson appreciated that the operation of these Brownian-particle-sorting systems appeared to rely on the demon's 'intelligence' as an animate being, but did not try to quantify this. Leo Szilard made the first attempt to mathematically relate the demon's intelligence to the thermodynamics of the process by considering the performance of a pressure-demon-based machine, Szilard's Engine (Figure 1.3).[17] Szilard realized that the operations which the demon carries out can be reduced to a simple computational process. In particular, he recognized the process requires *measurement* of the approach of the particle to gain *information* about its direction and speed, which must be *remembered* and then *acted upon*.[24]

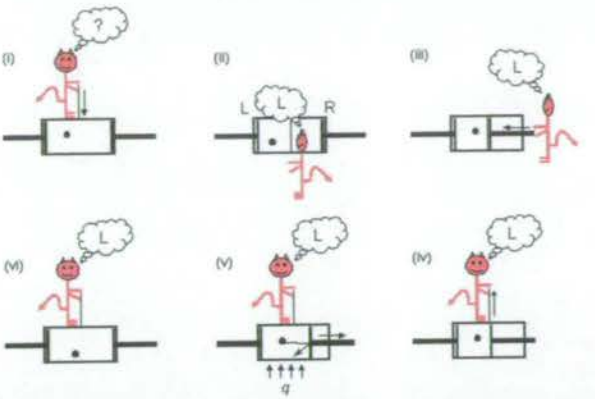

Figure 1.3 Szilard's Engine which utilizes a 'pressure demon'.[17] (i) Initially a single Brownian particle occupies a cylinder with a piston at either end. A frictionless partition is put in place to divide the container into two compartments ((i)→(ii)). (ii) The demon then detects the particle and determines in which compartment it resides. (iii) Using this information, the demon is able to move the opposite piston into position without meeting any resistance from the particle. (iv) The partition is removed, allowing (v) the 'gas' to expand against the piston, doing work against any attached load. To replenish the energy used by the piston and maintain a constant temperature, heat must flow into the system. To complete the thermodynamic cycle and reset the machine, the demon's memory of where the particle was must be erased ((vi)→(i)). In order to fully justify the application of a thermodynamic concept such as entropy to a single-particle model, a population of Szilard devices is required. The ensemble average over each of these can then be considered to represent the state of the system, comparable to the time average of a single multi-particle system at equilibrium, in a fashion similar to the statistical mechanics derivation of thermodynamic quantities.

Smoluchowski's Trapdoor

The concept of a purely mechanical Brownian motion machine which does not require any intelligent being to operate it was first explored by Marian von Smoluchowski who imagined the Maxwell system of two gas-containing compartments with a spring-loaded trapdoor in place of the demon-operated hole (Figure 1.4a).[16] If the spring is weak enough, it might appear that the door could be opened by collisions with gas molecules moving in one direction (L → R in Figure 1.4a) but not the other, and so allow transport of molecules preferentially in that direction, creating a pressure gradient between the two compartments. Smoluchowski recognized (although could not prove) that if the door had no way of dissipating the energy it gains from Brownian collisions it would be subject to the same amount of random thermal motion as the rest of the system and would not then function as the desired one-way valve.

Feynman's Ratchet and Pawl

Richard Feynman revisited these ideas in his celebrated discussion of a miniature ratchet and pawl – a construct designed to illustrate how the irreversible Second Law of Thermodynamics arises from the fundamentally reversible laws of motion.[18]

Feynman's device (Figure 1.4b) consists of a miniature axle with vanes attached to one end, surrounded by a gas at temperature T_1. At the other end of the axle is a ratchet and pawl system, held at temperature T_2. The question posed by the system is whether the random oscillations produced by gas molecules bombarding the vanes can be rectified by the ratchet and pawl so as to get net motion in one direction. Exactly analogous to Smoluchowski's trapdoor, Feynman showed that if $T_1 = T_2$ then the ratchet and pawl cannot extract energy from the thermal bath to do work. Feynman's major contribution from the perspective of molecular machines, however, was to take the analysis one stage further: if such a system cannot use thermal energy to do work, what is required in order for it to do so? Feynman showed that when the ratchet and pawl are cooler than the vanes (i.e. $T_1 > T_2$) the system does indeed rectify thermal motions and can do work (Feynman suggested lifting a hypothetical flea attached by a thread to the ratchet).[25] Of course, the machine now does not threaten the Second Law as dissipation of heat into the ratchet and pawl gas reservoir occurs, so the temperature difference must be maintained by some external means. Although insulating a molecular-sized system from the outside environment is difficult (and temperature gradients cannot be maintained over molecular-scale distances, see Section 1.4), what this hypothetical construct provides is the first example of a plausible mechanism for a molecular motor – whereby the random thermal fluctuations characteristic of this size regime are not fought against but instead are harnessed and rectified. The key ingredient is the external addition of energy to the system, not to generate motion but rather to continually or cyclically drive the system away from equilibrium, thereby maintaining a thermally-activated relaxation process that directionally biases Brownian motion towards equilibrium.[26] This profound idea is the key to the design of molecular-level systems that work through controlling Brownian motion and is expanded upon in Section 1.5.

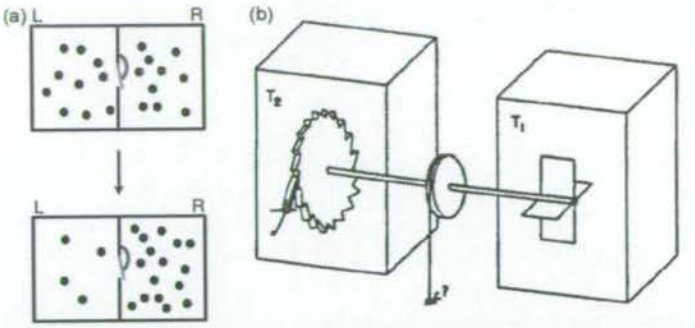

Figure 1.4 (a) Smoluchowski's Trapdoor – an 'automatic' pressure demon (the directionally-discriminating behaviour is carried out by a wholly mechanical device, a trapdoor which is intended to open when hit from one direction but not the other).[16] Like the pressure demon shown in Figure 1.2b, Smoluchowski's Trapdoor aims to transport particles selectively from the left compartment to the right. However, in the absence of a mechanism whereby the trapdoor can dissipate energy it will be at thermal equilibrium with its surroundings. This means it must spend much of its time open, unable to influence particle transport. Rarely, it will be closed when a particle approaches from the right and will open on collision with a particle coming from the left – doing its job as intended. Such events are balanced, however, by the door snapping shut on a particle from the right, pushing it into the left chamber. Overall, the probability of a particle moving from left to right is equal to that for moving right to left and so the trapdoor cannot accomplish its intended function adiabatically. (b) Feynman's Ratchet and Pawl.[18] It might appear that Brownian motion of the gas molecules on the paddle-wheel in the right-hand compartment can do work by exploiting the asymmetry of the teeth on the cog of the ratchet in the left-hand compartment. While the spring holds the pawl between the teeth of the cog, it does indeed turn selectively in the desired direction. However, when the pawl is disengaged the cog wheel need only randomly rotate a tiny amount in the other direction to move back one tooth whereas it must rotate randomly a long way to move to the next tooth forward. If the paddlewheel and ratchet are at the same temperature (i.e. $T_1 = T_2$) these rates cancel out. However, if $T_1 \neq T_2$ then the system *will* directionally rotate driven solely by the Brownian motion of the gas molecules. Part (b) reprinted with permission from ref. [18].

1.3.2 Machines that operate at low Reynolds number

Whilst rectifying Brownian motion may provide the key to powering molecular-level machines, it tells us nothing about how that power can be used to perform tasks at the nanoscale and what tiny mechanical machines can and cannot be expected to do. The constant presence of Brownian motion is not the only distinction between motion at the molecular level and in the macroscopic world. In the macroscopic world, the equations of motion are governed by inertial terms (dependent on mass). Viscous forces (dependent on particle dimensions) dampen motion by converting kinetic energy into heat, and objects do not move until provided with specific energy to do so. In a macroscopic machine this is often provided through a directional force when work is done to move mechanical components in a particular way. As objects become less massive and smaller in dimension, inertial terms decrease in importance and viscosity begins to dominate. A parameter which quantifies this effect is Reynolds number (R) – essentially the ratio of inertial to viscous forces – given by equation (1)

for a particle of length dimension a, moving at velocity v, in a medium with viscosity η and density ρ.[27]

$$R = \frac{av\rho}{\eta} \quad (1)$$

Size affects modes of motion long before we reach the nanoscale. Even at the mesoscopic level of bacteria (length dimensions ~10^{-5} m), viscous forces dominate. At the molecular level, Reynolds number is extremely low (except at low pressures in the gas phase or, possibly, in the free volume within rigid frameworks in the solid state) and the result is that molecules, or their components, cannot be given a one-off 'push' in the macroscopic sense – momentum is irrelevant. The motion of a molecular-level object is determined entirely by the forces acting on it at that particular instant – whether they be externally applied forces, viscosity or random thermal perturbations and Brownian motion. Furthermore, the tiny masses of nanoscopic objects mean that the force of gravity is insignificant for them. Since the physics which governs mechanical dynamic processes in the two size regimes is completely different, macroscopic and nanoscale motors require fundamentally different mechanisms for controlled transport or propulsion. Moreover, the high surface area:volume ratios of molecules mean they are inherently sticky and this will have a profound effect on how molecular-sized machines are organized and interact with one another. In general terms, this analysis leads to a central tenet: while the macroscopic machines we encounter in everyday life may provide the inspiration for what we might like molecular machines to achieve, drawing too close an analogy for how they might do it may not be the best design strategy. The 'rules of the game' at large and small length scales are simply too different.[1m, 12, 13, 28]

1.4 Lessons to learn from biology

Help is at hand, however, because despite all these problems, we know that motors and machines at the molecular level are conceptually feasible – they are already all around us. Nature has developed a working molecular nanotechnology that it employs to astonishing effect in virtually every significant biological process.[11] Appreciating in general terms how nature has overcome the issues of scale, environment,

equilibrium, Brownian motion and viscosity is useful for indicating general traits for the design of synthetic molecular machine systems and how they might be used.

The membranes which encase cells and their organelles allow the compartmentalization of cellular processes and constituents, thereby maintaining the nonequilibrium distributions essential for life. These lipophilic barriers contain a diverse range of functionality which facilitate the movement of various ionic and polar species through channels, via relays or the use of mobile carrier species.[29] A number of different mechanisms are employed to power motion from one compartment to another. Besides passive diffusion down a concentration gradient in the transported species, an electrochemical gradient (a transmembrane electrical potential, a concentration gradient or, most commonly, a combination of the two) originating from another species can be used. Such 'gradient pumping' mechanisms move one species against its concentration gradient at the expense of another gradient. Motion of the two species can be in the same direction (symport) or in opposite directions (antiport). If the sole power source is an electrical potential, only one species crosses the membrane (a uniport mechanism). These processes are governed by sophisticated control mechanisms which open or close highly selective channels, carriers and co-transporters in response to different stimuli, yet they all operate by relaxation down a directional transmembrane electrochemical gradient towards the thermodynamic equilibrium position.

Maintaining the primary concentration gradients which are used to power subsequent secondary transport processes are a smaller number of ion pumps. These transmembrane mechanical devices convert non-directional chemical reactions (the most abundant family, the ATPases, harness the hydrolysis of ATP) into vectorial transport of ionic species against an electrochemical gradient. The precise mechanisms by which these devices operate are still a subject of intense investigation. However, certain principles are becoming apparent. In particular, changes in the binding affinity at selective sites in the transmembrane region of the pump must be coupled to conformational changes which also modulate access to these sites from either side of the membrane so that only motion in the desired direction is achieved.[30]

A recent series of structures has revealed, in outline, how just such a mechanism operates in the sarcoplasmic reticulum Ca^{2+}-ATPase pump.[31] Calcium ions bind to

two high affinity sites which are open to the cytoplasm (**B**, Figure 1.5). Phosphorylation of the enzyme by ATP then results in a conformational change which shuts off access from either side (ratcheting[32]). Release of ADP is concomitant with a further conformational change which opens access to the lumen side and disrupts the Ca^{2+} binding residues (**A**, Figure 1.5). The calcium ions are released (escapement[32]) and swapped for protons which are subsequently occluded from the lumen by binding of a water molecule. Release of phosphate occurs with regeneration of the starting state, once again making the high-affinity Ca^{2+}-binding sites accessible to the cytoplasm. Similar mechanisms are thought to be responsible for the operation of the other members in the ATPase family. Exerting control over both binding affinities and transport kinetics in order to direct the transport of a Brownian particle in synthetic small-molecule systems is explored in Chapter 2.

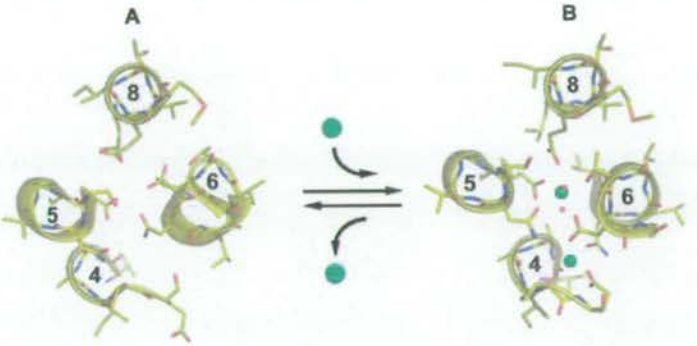

Figure 1.5 Crystal structures of the calcium-binding region in Ca^{2+}-ATPase in both low Ca^{2+}-affinity (**A**) and high Ca^{2+}-affinity (**B**) conformations.[31] Calcium ions shown in green. Numbers correspond to specific protein helices. Crystal structure pictures reprinted with permission from ref. [30b].

Pumping of protons across the energy-transducing membranes of mitochondria, chloroplasts and photosynthetic and respiratory bacteria is a particularly important process as it generates the protonmotive force necessary to operate ATP synthase (and also directly or indirectly powers the secondary transport of other species across these membranes). The ways in which nature achieves this pumping function are surprisingly diverse (by contrast, ATP synthase is highly conserved across organisms).[33] In most examples, charge-separated states and electron transfer processes are used to generate transmembrane electric potentials. Overall, therefore, a directional electrochemical driving force is set up to drive the translocation of protons, somewhat similar to the gradient pumping secondary transport processes (vide supra). Proton transport is concomitant with resetting of the redox centres in processes often termed 'redox loops' or 'Mitchell loops'.[34] Only in the case of bacteriorhodopsin –

the photosynthetic centre of certain purple bacteria – does it appear that light energy is directly converted into protonmotive force by a purely conformational pumping mechanism.[35] Again, the details of this process are not yet fully understood, but the correlation of conformational changes that control the direction in which the protons can move with changes in the affinity (i.e. pK_a) of binding sites are likely to be involved.[36]

Nature also uses molecular machines to transport objects around within cells (e.g. kinesin or dynein); to move whole organisms or their parts (e.g. myosin or the bacterial flagellar motor); to process DNA and RNA (e.g. helicases or polymerases); to convert protonmotive force into the synthesis of ATP (ATP synthase); and for many other functions besides. In these cases too, much has been learnt about the various ways in which they perform their remarkable tasks yet, equally, much remains to be discovered about each before the precise mechanisms can be elucidated.[11]

Accordingly, we can see that there are many general and fundamental differences between biological molecular machines and the man-made machines of the macroscopic world. Listed below are what appear to us to be the most significant aspects of biological machines to bear in mind when considering synthetic molecular machine design.

(i) Biological machines are soft, not rigid – their constituent molecular structures are able to constantly sample a wide range of conformations.

(ii) Biological systems operate at near-ambient temperatures, which are in turn determined by the organism's environment (heat is dissipated almost instantaneously at small length scales so temperature gradients at the cellular level cannot be exploited).

(iii) Biological motors utilize chemical energy, in the form of covalent bond breaking/formation of high-energy compounds such as ATP, NADH and NADPH, or concentration gradients.

(iv) Biomachines operate in solution, or at surfaces, under conditions of intrinsically high viscosity.

(v) Nature utilizes – rather than opposes – Brownian motion. Biomolecular machines need not use chemical energy to initiate movement – their components are constantly in motion – rather, they function by manipulating (ratcheting) that movement. Furthermore, constant thermal motion and small

'reaction vessels' (cells and their organelles) ensure that the mixing of biological machines, their substrates and their fuel is extremely rapid, in spite of the high viscosity they experience.

(vi) The viscous environment and constant thermal motion mean that biological machines have no use for smooth, low-friction surfaces. Genuinely smooth features are not possible on the molecular scale, of course, since the machine component dimensions are close to the dimensions of the intrinsic unit of matter – the atom.

(vii) Biomotors and other mobile molecular machines utilize architectures (e.g. tracks) which serve to restrict most of the degrees of freedom of the machine components and/or the substrate(s) they act upon. The molecular machine and the substrate(s) it is acting upon remain kinetically associated during the operation of the machine. For example, kinesin only functions as it 'walks' processively down a microtubule, not by simply binding to the microtubule at different places (i.e., not by completely detaching, exchanging with the bulk, and re-binding). Similarly, pumps work by internally compartmentalizing ions so that they cannot exchange with others outwith the machine.

(viii) The operation and structure of biological machines are governed by noncovalent interactions (intramolecular and intermolecular), many of which exploit the aqueous environment in which the machines assemble and operate.

(ix) Biological machines are made by combinations of multiple parallel synthesis and self-assembly processes utilizing a relatively small range of building blocks: amino acids, nucleic acids, lipids and saccharides.

(x) Living organisms intrinsically and necessarily function far from equilibrium – a state maintained by the compartmentalization of processes into cells, vesicles and organelles.

We should also remember, however, that the mechanisms and function of biomolecular machines are restricted by evolutionary constraints. Over billions of years, evolution has led to machines of a complexity not yet possible through rational design, but it intrinsically proceeds through small iterations and tends to retain the first successful solution arrived at for each problem. The human molecular machine designer has at his or her disposal a much larger chemical toolbox, a wider range of possible operating conditions and a design approach that favours innovation.

Furthermore, whilst an appreciation of the characteristics of biological machines can give us broad clues about how to make molecular-level devices that exploit mechanical motion, we understand few of the precise details of how their designs work. How does an inherently mechanically directionless chemical reaction, the conversion of ATP into ADP, drive the directional motion of calcium ions by Ca^{2+}-ATPase? What is the detailed nature of the conformational changes which can set-up or disrupt the highly selective binding sites? Why exactly do the movements of the individual peptide subunits that cause this to happen occur in that particular sequence? What are the details of the pathways connecting the binding sites with the outside? What is the role of the kinetics and thermodynamics of each amino acid in this mechanism? In fact, biological motors and machines are so complex that studying simple synthetic chemical systems may help in the understanding of exactly how they work. Likewise, finding out biology's solutions can only aid the design of sophisticated artificial systems. At present, however, much of the most detailed information for devising the basic mechanisms for synthetic molecular machines comes not from biology, but from nonequilibrium statistical mechanics.

1.5 Lessons to learn from physics, mathematics and statistical mechanics

1.5.1 Breaking detailed balance

The Principle of Detailed Balance[37] states that, at equilibrium, transitions between any two states take place in either direction at the same rate so that no net flux is generated. This rules out the maintenance of equilibria by cyclic processes such as A→B→C→A rather than A⇆B + B⇆C + C⇆A (ref. [12]) and is a formal indication that machines such as Smoluchowski's Trapdoor and Feynman's Ratchet and Pawl cannot operate adiabatically. However, in an out-of-equilibrium system (e.g. if $T_1 \neq T_2$ for the Feynman Ratchet and Pawl), 'detailed balance' is broken and as the system moves spontaneously towards equilibrium, net work can be done by the fluxional exchange process.

To understand the mechanisms by which mechanical machines can operate at length scales on which Brownian motion occurs, it is useful to appreciate precisely *why* work can be done by a random exchange process between two states only while detailed balance is broken. A simple analogy helps illustrate why detailed balance holds in a

fluxionally exchanging system at equilibrium and the requirements necessary to break it. Consider a pair of scales with many ants running randomly between the two sides, the scales will be statistically balanced (but not necessarily horizontal, that only occurs if the pivot of the scale is positioned in the middle) and remain more or less steady at a stable angle. Even if a barrier is suddenly placed between the scales, stopping the two sides being in equilibrium, they remain balanced. However, if ants are added to one side or the other the scales become unbalanced and will tip accordingly. Remove the barrier and the ants (assuming they can overcome the effect of gravity!) resume scurrying between the two sides, eventually equilibrium – and balance – will be restored. Note that even if we start without the barrier in place, if ants are suddenly added to one side balance will be broken for some time – and the scale will tip – until the roaming ants establish equilibrium and balance is restored. The breaking of balance allows a task to be performed as the exchanging system returns toward equilibrium. The net displacement that arises as the scales tip over – or as they right themselves – could be used to lift a feather the scale was attached to. Breaking detailed balance is the key to doing work with a machine that operates at length scales on which Brownian motion occurs.

During the past decade, a number of remarkable theoretical formalisms have been developed in mathematics (particularly game theory) and nonequilibrium statistical physics that explain how the directional transport of Brownian particles over periodic potential energy surfaces can occur from unbiased periodic or stochastic perturbations of the system.[38, 39] Underlying each of these Brownian ratchet or motor mechanisms are three components:[39b] (i) a randomizing element;[40] (ii) an energy input to avoid falling foul of the Second Law of Thermodynamics; and (iii) asymmetry in the energy or information potential in the dimension in which the motion occurs.[41] It is now widely accepted that ratchet mechanisms have a central role in explaining the operation of biological motor proteins.[42, 43] They have also been successfully used to develop transport and separation devices for mesoscopic particles and macromolecules, microfluidic pumping and quantum and electronic applications.[43, 44] For molecular-level motors and other machines, the necessary randomizing element can be Brownian motion of the substrate or the machine components. The other two requirements (energy and anisotropy) can be supplied in different ways according to the type of fluctuation-driven transport mechanism.

1.5.2 Fluctuation-driven transport mechanisms

Many different possible types of theoretical fluctuation-driven ('Brownian ratchet') mechanisms have been proposed, including flashing ratchets, tilting ratchets, Seebeck ratchets, drift ratchets, Hamiltonian ratchets, temperature ratchets, entropic ratchets.[39] They can be classified and grouped together in many different (not always mutually exclusive) ways, and mechanisms that might be indistinguishable in chemical terms can be differentiated because of the nature of the physics involved. Whilst it is not clear (at least to us!) how some of the theoretical mechanisms could be applied to molecular structures, many offer clear design opportunities for the synthetic chemist. The details of the various mechanisms have been discussed extensively in the physics literature, so we will limit our discussion here to some specific variations which appear particularly well-suited for chemical systems. We choose to distinguish between two overarching classes of mechanism: energy ratchets, which fall into two basic types – pulsating ratchets and tilting ratchets – and are the subject of a recent major review by Reimann;[39f] and information ratchets, which are much less common in the physics literature, but have been discussed by Astumian, Parrondo and others.[39h, 42b, 45] Both energy ratchets and information ratchets bias the movement of a Brownian substrate.[46] However, we will also see that they offer clues for how to go beyond a simple switch with a chemical machine, performing tasks through the nonequilibrium control of conformational and co-conformational changes within molecular structures.

Pulsating ratchets[39f]

Pulsating ratchets are a general category of energy ratchet in which potential energy minima and maxima are varied in a periodic or stochastic fashion, independent of the position of the particle on the potential energy surface. In its simplest form, this can be considered as an asymmetric sawtooth potential being repetitively turned on and off faster than Brownian particles can diffuse over more than a small fraction of the potential energy surface (an 'on–off' ratchet, Figure 1.6). The result is net directional transport of the particles across the surface (left to right in Figure 1.6).

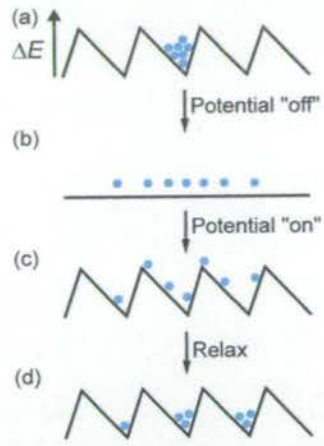

Figure 1.6 An example of a pulsating ratchet mechanism – an on–off ratchet.[39f] (a) The Brownian particles start out in energy minima on the potential energy surface with the energy barriers >> k_BT. (b) The potential is turned off so that free Brownian-motion-powered diffusion is allowed to occur for a short time period (much less than required to reach global equilibrium). (c) On turning the potential back on again, due to the asymmetry of the potential, the particles have a greater probability of being trapped in the adjacent well to the right rather than the adjacent well to the left. Note this step involves raising the energy of the particles. (d) Relaxation to the local energy minima (during which heat is emitted) leads to the average position of the particles moving to the right. Repeating steps (b)-(d) progressively moves the Brownian particles further and further to the right.

More general than the special case of an on–off ratchet, *any* asymmetric periodic potential may be regularly or stochastically varied to give a ratchet effect (such mechanisms are generally termed 'fluctuating potential' ratchets). As with the simple on–off ratchet, most commonly encountered examples involve switching between two different potentials and are therefore often termed 'flashing' ratchets. A classic example, which has particular relevance for explaining a number of biological processes[42b] as well as being the basis for a [2]catenane rotary motor (see Chapter 3), is illustrated in Figure 1.7. It consists, in physical terms, of an asymmetric potential energy surface (comprising a periodic series of two different minima and two different maxima) along which a Brownian particle is directionally transported by sequentially raising and lowering each set of minima and maxima. The particle starts in a green or orange well (Figure 1.7a or 1.7c). Raising that energy minimum while lowering those in adjacent wells provides the impetus for the particle to change position by Brownian motion (Figure 1.7b → 1.7c or 1.7d → 1.7e). By simultaneously (or beforehand) changing the relative heights of the energy barriers to the adjacent energy wells, the kinetics of the Brownian motion in each direction are different and the particle is transported from left to right. Note that the position of the particle does not influence the sequence in which (or when or if) the energy minima and maxima are changed. Nor does the switching of the potential have to be regular.

As long as the relationship (be it simultaneous or sequential) between the switching of minima and maxima is maintained, the particle will tend to be transported from left to right in Figure 1.7, even though occasionally it may move over a barrier in the wrong direction.

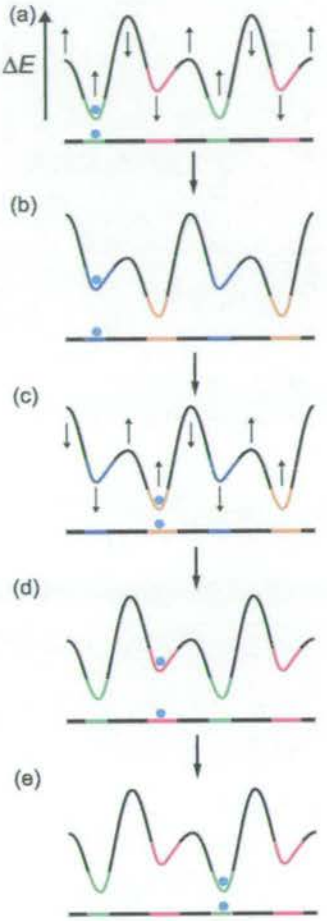

Figure 1.7 Another example of a pulsating ratchet mechanism – a flashing ratchet.[42b] For details of its operation, see main text.

The basic pulsating ratchet requirements can also be realized in another way. A potential such as that shown in Figure 1.7a can be given a directional drift velocity. Such systems are often termed 'travelling potential' ratchets. This principle is essentially the same as macroscopic devices such as Archimedes' Screw, yet in the presence of thermal fluctuations these systems exhibit Brownian ratchet characteristics (particularly when the fluctuations are of similar energy to the barrier heights) and are closely related to tilting the potential in one direction (as discussed below). Clearly, however, an asymmetric potential is not absolutely required, nor in fact are thermal fluctuations; imagine, for example, a particle 'surfing' on a travelling wave on the surface of a liquid. This category of mechanism is at the boundary

between fluctuation-driven transport and transport due to potential gradients, with the precise location on this continuum dependent on the importance of thermal fluctuations and spatial asymmetry under the conditions chosen. The travelling motion does not have to be continuous, but rather may take place in discrete steps. Furthermore, arranging a continuously travelling potential to 'jump' distances which are multiples of its period, at random or regular intervals, can be used to escape from the inherent directionality of the travelling wave scheme and it has been shown that the ratchet dynamics are essentially unaffected. In the limit, this can be reduced to dichotomous switching between two spatially shifted potentials which are otherwise identical, which is very similar to a rocking ratchet (vide infra).

Tilting ratchets[39f]

In this category, the underlying intrinsic potential remains unchanged and detailed balance is broken by application of an unbiased driving force to the Brownian particle. Perhaps the most obvious unbiased driving force is heat, and ratchet mechanisms based on periodic or stochastic temperature variations are generally termed 'temperature' or 'diffusion' ratchets. In its simplest form (Figure 1.8), this mechanism is very similar to the on–off ratchet. Initially the thermal energy is low so that the particles cannot readily cross the energy barriers. A sudden increase in temperature can be applied so that k_BT is much greater that the potential amplitude, causing the particles to diffuse as if over a virtually flat potential energy surface (Figure 1.8b, cf. Figure 1.6b). Returning to the original, lower, temperature (Figure 1.8c) is equivalent to turning the potential back on in Figure 1.6c and more particles will have moved to the next well to the right than to the left. Under this scheme, therefore, it seems that applying temperature variations to any process which involves an asymmetric potential energy surface could result in a ratchet effect.[47] In chemical terms, this means that the rotation of a chiral group around a covalent bond, at least in principle, can be made unidirectional in such a manner.

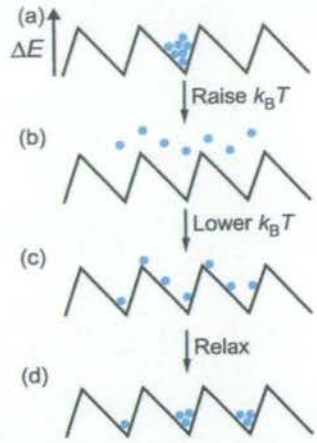

Figure 1.8 A temperature (or diffusion) ratchet.[39f] (a) The Brownian particles start out in energy minima on the potential energy surface with the energy barriers $>> k_BT_1$. (b) The temperature is increased so that the height of the barriers is $<< k_BT_2$ and effectively free diffusion is allowed to occur for a short time period (much less than required to reach global equilibrium). (c) The temperature is lowered to T_1 once more, and due to the asymmetry of the potential, each particle is statistically more likely to be captured by the adjacent well to the right rather than the well to the left. (d) Relaxation to the local energy minimum (during which heat is emitted) leads to the average position of the particles moving to the right. Repeating steps (b)-(d) progressively moves the Brownian particles further and further to the right. Note the similarities between this mechanism and that of the on–off ratchet shown in Figure 1.6.

An unbiased driving force can also be achieved by applying a directional force in a periodic manner so that, over time, the bias averages to zero – a 'rocking' ratchet. The simplest form of this is shown in Figure 1.9. Periodic application towards the left and then right of a driving force that allows the particle to surmount the barriers (say, by applying an external field if the particle is charged) results in transport. Motion over the steep barrier is again most likely as it involves the shortest distance. Such a mechanism is physically equivalent to tilting the ratchet potential in one direction then the other. Of course, if the driving force is strong enough and is constantly applied in one direction or the other, thermal fluctuations are not necessary, which would then correspond to a power stroke.[46]

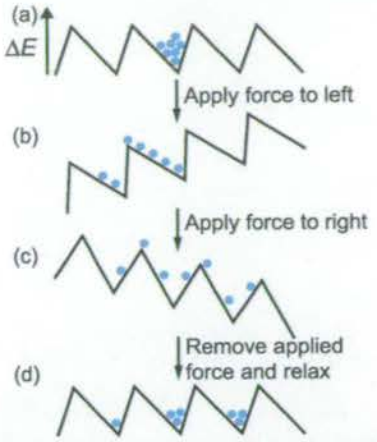

Figure 1.9 A rocking ratchet.[39f] (a) The Brownian particles start out in energy minima on the potential energy surface with the energy barriers >> k_BT. (b) A directional force is applied to the left. (c) An equal and opposite directional force is applied to the right, such that, in the absence of an asymmetric underlying potential, the effect of step (b) is precisely balanced. (d) Removal of the force and relaxation to the local energy minimum leads to the average position of the particles moving to the right. Repeating steps (b)-(d) progressively moves the Brownian particles further and further to the right.

Analogues of a rocking ratchet in which the applied driving force is a form of stochastic noise are known as 'fluctuating force' ratchets (in certain cases, also 'correlation' ratchets). Finally, a tilting ratchet can be achieved in a symmetric potential if the perturbation itself results in spatial asymmetry (becoming very similar to the travelling-potential models discussed above). This may be rather obvious for the periodic force cases (imagine applying the electric field discussed above for longer in one direction than the other) but is less so for stochastic driving forces. In general, these mechanisms are known as 'asymmetrically tilting' ratchets.

Information ratchets[39h, 42b, 45]

In the pulsating and tilting types of energy ratchet mechanisms, perturbations of the potential energy surface – or of the particle's interaction with it – are applied globally and *independent of the particle's position*, while the periodicity of the potential is invariant. Information ratchets (Figure 1.10, for example) directionally transport a Brownian particle by changing the effective kinetic barriers to Brownian motion *depending on the position of the particle* on the surface. In other words, the heights of the maxima on the potential energy surface change according to the location of the particle (this requires information to be transferred from the particle to the surface) whereas the potential energy minima do not necessarily need to change at all. This switching does not require raising the potential energy of the particle at any stage, rather the motion can be powered with energy taken entirely from the thermal bath by

using information about the position of the particle. This is directly analogous to the mechanism required of Maxwell's Pressure Demon (Figure 1.2b, Section 1.3.1), but does not break the Second Law of Thermodynamics as the required information transfer (actually, information erasure[48]) has an intrinsic energy cost that has to be met externally.

It appears to us that information ratchet mechanisms of relevance to chemical systems can arise in at least three ways: (i) a localized change to the intrinsic potential energy surface depending on the position of the particle (e.g. Figure 1.10); (ii) a position-dependent change in the state of the particle which alters its interaction with the potential energy surface at that point; or (iii) switching between two different intrinsic periodic potentials according to the position of the particle.[39h] An example of the first of these types, in which the system responds to the 'information' from the particle by lowering the energy barrier to the right-hand side (and only to the right-hand side) of the particle, is shown in Figure 1.10.

The particle starts in one of the identical-minima energy wells (Figure 1.10a). The presence of the particle lowers the kinetic barrier for passage to the adjacent right-hand well and it moves there by Brownian motion (Figure 1.10b → Figure 1.10c). At this point it can sample two energy wells by Brownian motion, and a random reinstatement of the barrier has a 50% chance of returning the particle to its starting position and a 50% chance of trapping it in the newly accessed well to the right (Figure 1.10d, of course a more efficient mechanism could be envisaged in which a second information transfer signals the occupation of the right-hand well and raises the barrier at this point only). The particle can no longer go back to the starting well but is now allowed access to the next well further to the right. Even though no enthalpic driving force ever exists for the particle to move from left to right, it is inevitably transported in that direction through such a mechanism. The potential surface in Figure 1.10 is asymmetric, but this is not necessary if some other means can be devised of directionally communicating the position of the particle (and therefore breaking spatial inversion symmetry). A synthetic molecular machine that operates by such a mechanism is discussed in Chapter 4.

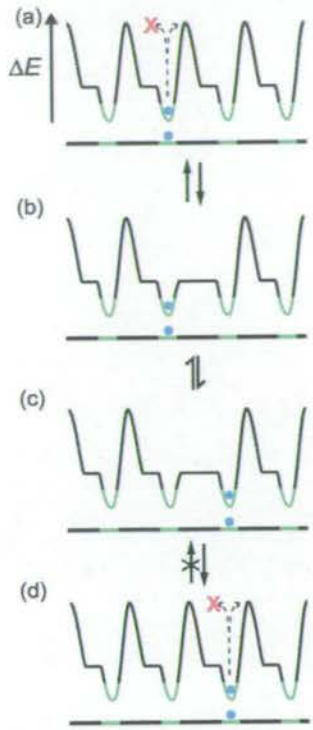

Figure 1.10 A type of information ratchet mechanism for Brownian particle transport along a potential energy surface.[39h, 42b, 45] Dotted arrows indicate the transfer of information that signals the position of the particle. If the signal is distance dependent – say, energy transfer from an excited state causing lowering of an energy barrier – then the asymmetry in the particle's position between two barriers provides the 'information' which transports the particle directionally along the potential energy surface.

Both energy ratchets and information ratchets could provide valid operating mechanisms for synthetic molecular-level machines. Furthermore, hybrid mechanisms appear to be possible. For example, using asymmetry in the Brownian particle (e.g. a cyclodextrin) rather than in the potential energy surface to induce directionality of motion.[49] Indeed, it seems that the realization of functioning synthetic chemical machine systems could have as much to offer theoretical nonequilibrium statistical physics as the other way around, just as progress in understanding biological molecular motors has both benefited from and stimulated developments in the physics field.

A similar complementary relationship has recently arisen between the physics of these nonequilibrium systems and the mathematics of probability and game theory. While Brownian ratchet theories model the behaviour of a Brownian particle over continuous space and time, it has recently been shown that the such mechanisms can be discretized in space and time as two gambling games. The games are chosen such that, when each is played individually, the odds are stacked against the gambler, but paradoxically, when they are played in an alternating fashion (either periodically, or

randomly) the gambler tends to win.[39i, 50] This observation, which has come to be known as 'Parrondo's Paradox', provides a conceptual link between Brownian ratchet models of particles moving in changing potentials to *any* process where switching between two dynamics, in each of which some variable decreases ('losing'), can result in increases of that variable ('winning'). Applying the well-established language of probability theory presents different opportunities for analysis and suggests different fields of application for these models (such as economics and social dynamics, which already have established links with game theory and probability); illustrating the importance of ratchet theories in explaining a diverse range of fluctuation-driven phenomena.

1.6 Design principles for synthetic molecular machines

Theoretical fluctuation-driven transport mechanisms have generally been considered in terms of either two-minima potential energy surfaces or an infinitely repeating potential energy surface. The former can be the basis for molecular switches, while the latter can be employed directly as designs for molecular-level motors.[51] But what other general ideas can we glean from how these systems work from the viewpoint of designing other types of synthetic molecular-level machines that exploit Brownian motion?

(i) *Asymmetry in some part of the fluctuation-driven transport cycle is necessary to ensure that time-reversal symmetry is broken, meaning that the particles undergo non-reciprocal motion during the operating cycle, generating a directional flux.* This means that the particles are not subjected to the opposite of the initial transport process as the potential is being reset to begin another cycle.

(ii) In all these mechanisms (e.g. Figures 1.6-1.10) we can see that *the particles are always under the influence of the potential energy surfaces responsible for transporting them.* Even in the on–off ratchet (Figure 1.6), the sawtooth potential can only be switched off for a short time. If it were switched off for long enough for the particles to reach an equilibrium distribution over the surface then the mechanism would not be able to directionally transport the particles progressively, it could only switch between one (average) equilibrium

distribution and another. In other words, for a machine to operate by these types of mechanisms which manipulate nonequilibrium states, Brownian substrates must remain kinetically associated with the machine throughout its operation – not necessarily in physical contact, but rather, not able to exchange with substrates in the bulk, which are not under the influence of the machine. (This is why we rule out host–guest complexes that are under thermodynamic control acting as such machines (Section 1.2).) Exchanging with the bulk while entering the machine at one end and when leaving at the other is allowed when the two bulk regions are themselves otherwise separated (e.g. a transmembrane pump).

(iii) *The particles in all fluctuation-driven transport mechanisms can be considered to be 'compartmentalized'*, in that at any moment the particles are free to move only over a localized area (which continually changes during the operating cycle of the machine). The compartment boundaries are not necessarily physical ones; when the sawtooth potential in the on–off ratchet in Figure 1.6 is switched off, it is the short time before the potential is reapplied that prevents the particles coming to global equilibrium over the surface.

(iv) *It is the manipulation of the Brownian particles in terms of which and when compartments are 'linked'* (able to exchange particles) *and the statistical balance of the populations of linked compartments with respect to the potential energy surface* (in the case of energy ratchets) *or information* (in the case of information ratchets) *that enables the transport mechanism to function.*

(v) Energy ratchets (in which the Brownian substrate is passive) have been the most widely considered fluctuation-driven transport mechanisms in the physics literature. However, the components of chemical systems are not always passive. *For molecular structures it seems likely that information ratchets* (where the position of the Brownian particle or fragment affects the potential energy surface) *will also prove of great utility and importance.*

(vi) Fluctuation-driven transport mechanisms are often considered in terms of charged particles with electric fields being applied, typically to generate an infinitely repeating potential energy surface. *In chemical systems, noncovalent interactions and binding interactions can provide the necessary changing potential energy surface, which can be of limited length and not uniform, with*

the Brownian substrate being either another ion or molecule, or it could be another fragment of the same molecule.[52]

(vii) *Although the mechanisms for fluctuation-driven transport have been developed to direct the flow of particles in a given direction, we can consider applying the same sorts of ideas to generate other sorts of nonequilibrium distributions within molecular-level structures.* It should be possible to design molecular-level machine systems that are neither simple switches nor motors, by utilizing small numbers of real or virtual 'compartments' within a molecular (or supramolecular) structure that can be 'linked' (and 'unlinked') and 'balanced' (and 'unbalanced') in particular ways, perhaps using Boolean logic operations, and addressed via orthogonal inputs to perform some function (e.g. see the 'sorting-and-separating' machine suggested in Chapter 2, Figure 2.7). Fluctuation-driven transport mechanisms are illustrative of the general principles through which nonequilibrium distributions of supramolecular, molecular and submolecular structures can be created, controlled, ordered and manipulated via inputs of energy.

If biology, mathematics and physics provide the inspiration and strategies for controlling molecular-level motion, it is through chemistry that artificial molecular-level machine mechanisms must be designed, constructed and made to work. The minimum requirements for such systems must be the restriction of the 3D-motion of the machine components, the substrate, or both, and a change in their relative positions induced by an input of energy.

In the following Chapters, these requirements are met by the remarkable characteristics of interlocked molecules[53] – particularly, catenanes and rotaxanes – which provide remarkable scope for applying the above principles to the control of motion in synthetic molecular systems. Even though the interlocked components in these molecules are not covalently connected, catenanes and rotaxanes are molecules – not supramolecular complexes – as covalent bonds must be broken in order to separate the constituent parts. In these structures,[54] the mechanical bond severely restricts the relative degrees of freedom of the components in several directions, while often permitting extraordinarily large amplitude motion in an allowed vector. This is in many ways analogous to the restriction of movement imposed on biological motors by a track[55] and is one reason interlocked structures continue to play a central role in

the development of synthetic molecular machines.[1c, 1h, 1m, 56] (For more details on specific examples, refs. [1m, 56m] can be found reprinted in the Appendix.)

The above principles (which, it is interesting to note, are equally relevant for the design of interacting chemical reaction cascades and catalytic cycles that operate far from equilibrium) are used to develop the concepts for compartmentalized molecular machines, as described in Chapter 2. These are then employed and extended in molecular realizations of an energy ratchet and an information ratchet in Chapters 3 and 4, respectively. Following these fundamental considerations, in Chapter 5 we return to the well-established concept of rotaxane-based molecular shuttles[1c, 1h, 1m, 56] in order to explore a new series of chemical structures that can be used to control the thermodynamics and kinetics for motion of a Brownian particle. Furthermore, we explore the operation of such devices on surfaces. Both these types of investigation are essential in the ongoing development of molecular machines – irrespective of mechanism – towards technological applications.

1.7 References and notes

[1] Although it is nearly 50 years since Richard Feynman's famous and prescient presentation to the American Physical Society, proposing the construction of mechanical devices at the nano- and molecular-level [(a) R. P. Feynman, *Eng. Sci.* **1960**, *23*, 22-36; a copy of the manuscript can be found under http://www.its.caltech.edu/~feynman], it is only in the past 15 years that successful molecular designs have been achieved: b) A. P. Davis, *Nature* **1999**, *401*, 120-121; c) V. Balzani, A. Credi, F. M. Raymo, J. F. Stoddart, *Angew. Chem. Int. Ed.* **2000**, *39*, 3349-3391; d) B. L. Feringa, *Nature* **2000**, *408*, 151-154; e) Special issue on "Molecular Machines": *Acc. Chem. Res.* **2001**, *34*, 409-522; f) Volume on "Molecular Machines and Motors": *Struct. Bond.* **2001**, *99*, 1-281; g) V. Balzani, A. Credi, M. Venturi, *Chem. Eur. J.* **2002**, *8*, 5524-5532; h) V. Balzani, M. Venturi, A. Credi, *Molecular Devices and Machines. A Journey into the Nanoworld*, Wiley-VCH, Weinheim, **2003**; i) C. J. Easton, S. F. Lincoln, L. Barr, H. Onagi, *Chem. Eur. J.* **2004**, *10*, 3120-3128; j) C. P. Mandl, B. König, *Angew. Chem. Int. Ed.* **2004**, *43*, 1622-1624; k) G. S. Kottas, L. I. Clarke, D. Horinek, J. Michl, *Chem. Rev.* **2005**, *105*, 1281-1376; l) K. Kinbara, T. Aida, *Chem. Rev.* **2005**, *105*, 1377-1400; m) E. R. Kay, D. A. Leigh in *Functional Artificial Receptors* (Eds.: T. Schrader, A. D. Hamilton), Wiley-VCH, Weinheim, **2005**, pp. 333-406 (reprinted, in full, in the Appendix); n) Volume on "Molecular Machines": *Top. Curr. Chem.* **2005**, *262*, 1-236. For a recent view of the molecular machines field from the perspective of the physics community, see: o) Special issue on "Molecular Motors": *J. Phys.: Condens. Matter* **2005**, *17*, S3661-S4024.

[2] This is in no sense a criticism of the terminology used at the time to report these pioneering experiments, which filled a generation of chemists with excitement at the prospect of making molecular-sized machines. Language can only ever be used in the context of the knowledge of the day.

[3] E. R. Kay, D. A. Leigh, *Nature* **2006**, *440*, 286-287 (reprinted, in full, in the Appendix).

[4] a) R. E. Smalley, *Sci. Am.* **2001**, *285* (3), 68-69; b) G. M. Whitesides, *Sci. Am.* **2001**, *285* (3), 70-75; c) Point/counterpoint debate between R. E. Smalley and K. E. Drexler, *Chem. Eng. News* **2003**, *81* (48), 37–42.

[5] In fact, physicists sometimes differentiate thermal ratchets from motors in that the former do not bear a load. However, as they are mechanistically identical, this distinction is unnecessary for the design of chemical systems.

[6] 'Motor molecules' can also act as switches; the change in distribution or position of the components can be used to affect a system as a function of state.

[7] a) R. Brown, *Philos. Mag.* **1828**, *4*, 171-173; b) R. Brown, *Edinb. New Philos. J.* **1828**, *5*, 358-371; c) R. Brown, *Philos. Mag.* **1829**, *6*, 161-166. Brown's accounts of these investigations are also reprinted in d) R. Brown in *The Miscellaneous Botanical Works of Robert Brown, Vol. 1* (Ed.: J. J. Bennett), Ray Society, London, **1866**, pp. 463-486. Although (by his own admission) not the first to observe such effects, Brown's key contribution was to make a systematic study of the phenomenon, giving the lie to the notion that it is a manifestation of some sort of 'life force' in matter of organic origin, showing instead that it is a physical phenomenon, occurring in all types of material – still anathema to some at the time. For a modern reconstruction of the original experiments, see: e) B. J. Ford, *The Microscope* **1992**, *40*, 235-241.

[8] A. Einstein, *Ann. Phys.* **1905**, *17*, 549-560; reprinted in *Einstein's Annalen Papers: The Complete Collection 1901-1922* (Ed.: J. Renn), Wiley-VCH, Weinheim, **2005**, pp. 182-193.

[9] J. Perrin, *Atoms* (English Translation: D. L. Hammick), 2nd English ed., Constable & Co., London, **1923**.

[10] For more detailed accounts of these discoveries and their impact on the scientific world, see: a) M. D. Haw, *J. Phys.: Condens. Matter* **2002**, *14*, 7769-7779; b) G. Parisi, *Nature* **2005**, *433*, 221-221; c) M. Haw, *Phys. World* **2005**, *18* (1), 19-22; d) P. Hänggi, F. Marchesoni, *Chaos* **2005**, *15*, 026101; e) J. Renn, *Ann. Phys.* **2005**, *14*, S23-S37; reprinted in *Einstein's Annalen Papers: The Complete Collection 1901-1922* (Ed.: J. Renn), Wiley-VCH, Weinheim, **2005**, pp. 23-37.

[11] *Molecular Motors* (Ed.: M. Schliwa), Wiley-VCH, Weinheim, **2003**.

[12] R. D. Astumian, P. Hänggi, *Phys. Today* **2002**, *55* (11), 33-39.

[13] R. A. L. Jones, *Soft Machines: Nanotechnology and Life*, Oxford University Press, Oxford, **2004**.

[14] For reprints of key papers and commentary on some of the main issues regarding Maxwell's Demon and the other related thought-machines, see: *Maxwell's Demon 2. Entropy, Classical and Quantum Information, Computing* (Eds.: H. S. Leff, A. F. Rex), Institute of Physics Publishing, Bristol, **2003**.

[15] The first (a) private and (b) public written discussions of the 'temperature demon' were: a) J. C. Maxwell, *Letter to P. G. Tait, 11 December 1867*. Quoted in C. G. Knott, *Life and Scientific Work of Peter Guthrie Tait*, Cambridge University Press, London, **1911**, pp. 213-214; and reproduced in *The Scientific Letters and Papers of James Clerk Maxwell Vol. II 1862-1873* (Ed.: P. M. Harman), Cambridge University Press, Cambridge, **1995**, pp. 331-332. b) J. C. Maxwell, *Theory of Heat*, Longmans, Green and Co., London, **1871**, Chapter 22. c) Maxwell introduced the idea of a 'pressure demon' in a later letter to Tait (believed to date from early 1875). Quoted in C. G. Knott, *Life and Scientific Work of Peter Guthrie Tait*, Cambridge University Press, London, **1911**, pp. 214-215; and reproduced in *The Scientific Letters and Papers of James Clerk Maxwell Vol. III 1874-1879* (Ed.: P. M. Harman), Cambridge University Press, Cambridge, **2002**, pp. 185-187. "*Concerning Demons...Is the production of an inequality of temperature their only occupation? No, for less intelligent demons can produce a difference in pressure as well as temperature by merely allowing all particles going in one direction while stopping all those going the other way. This reduces the demon to a valve.*" More formally, a pressure demon would operate in a system linked to a constant-temperature reservoir with the sole effect of using energy transferred as heat from that reservoir to do work (see Szilard's Engine, Figure 1.3 and ref. [17]). This is in conflict with the Kelvin–Planck form of the Second Law whereas the temperature demon challenges the Clausius definition.

[16] a) M. von Smoluchowski, *Physik. Z.* **1912**, *13*, 1069-1080; b) M. von Smoluchowski, *Vortgage über die Kinetische Theorie der Materie und der Elektrizitat* (Ed.: M. Planck), Teubner und Leipzig, Berlin, **1914**, pp. 89-121. Maxwell had earlier eluded to the basic premise behind Smoluchowski's Trapdoor in private correspondence [(c) J. C. Maxwell, *Letter to J. W. Strutt, 6 December 1870*. Reproduced in *The Scientific Letters and Papers of James Clerk Maxwell Vol. II 1862-1873* (Ed.: P. M. Harman), Cambridge University Press, Cambridge, **1995**, pp. 582-583], describing his "*finite being*" as a "*doorkeeper, very intelligent and exceedingly quick*" adding that "*I do not see why even intelligence might not be dispensed with and the thing be made self-acting*".

[17] L. Szilard, *Z. Phys.* **1929**, *53*, 840-856. An English translation by A. Rapoport and M. Knoller is reprinted in ref. [14], pp. 110-119.

[18] R. P. Feynman, R. B. Leighton, M. Sands, *The Feynman Lectures on Physics, Vol. 1*, Addison-Wesley, Reading, MA, **1963**, Chapter 46.

[19] *The Second Law of Thermodynamics. Memoirs by Carnot, Clausius and Thomson: Harper's Scientific Memoirs* (Ed.: W. F. Magie), Harper & Brothers, New York, **1899**.

[20] a) W. Ehrenberg, *Sci. Am.* **1967**, *217* (5), 103-110; b) C. H. Bennett, *Sci. Am.* **1987**, *257* (5), 88-96.

[21] W. Thomson, *Proc. R. Soc. Edinb.* **1874**, *8*, 325-334.

[22] W. Thomson, *Nature* **1874**, *9*, 441-444.

[23] In fact, Thomson thought that Maxwell had coined the term 'demon' but Maxwell corrects this in ref. [15c].

[24] This insight is all the more remarkable coming as it did before the advent of the electronic computer. The deconstruction of the reasoning processes of a living being to simple computational steps is the basis for the modern field of cybernetics.

[25] For a modern critique of Feynman's analysis, see: a) J. M. R. Parrondo, P. Español, *Am. J. Phys.* **1996**, *64*, 1125-1130; b) K. Sekimoto, *J. Phys. Soc. Jpn.* **1997**, *66*, 1234-1237; and for other modern treatments of this model, see: c) H. Sakaguchi, *J. Phys. Soc. Jpn.* **1998**, *67*, 709-712; d) T. Hondou, F. Takagi, *J. Phys. Soc. Jpn.* **1998**, *67*, 2974-2976; e) M. O. Magnasco, G. Stolovitzky, *J. Stat. Phys.* **1998**, *93*, 615-632; f) C. Jarzynski, O. Mazonka, *Phys. Rev. E* **1999**, *59*, 6448-6459; g) D. Abbott, B. R. Davis, J. M. R. Parrondo, in *Proceedings of the Second International Conference on Unsolved Problems of Noise and Fluctuations* (Adelaide, 1999), *AIP Conf. Proc. 511* (Eds.: D. Abbott, L. B. Kiss), American Institute of Physics, New York, **2000**, pp. 213-218; h) S. Velasco, J. M. M. Roco, A. Medina, A. C. Hernández, *J. Phys. D: Appl. Phys.* **2001**, *34*, 1000-1006; i) R. Kawai, X. Sailer, L. Schimansky-Geier, C. Van den Broeck, *Phys. Rev. E* **2004**, *69*, 051109; j) C. Van den Broeck, R. Kawai, P. Meurs, *Phys. Rev. Lett.* **2004**, *93*, 090601; k) C. Van den Broeck, P. Meurs, R. Kawai, *New J. Phys.* **2005**, *7*, 10.

[26] In more recent times, Skordos and Zurek have carried out a simulation of the Smoluchowski Trapdoor which showed Smoluchowski's intuitive conclusions (and Feynman's theoretical considerations) to be correct: a) P. A. Skordos, W. H. Zurek, *Am. J. Phys.* **1992**, *60*, 876-882; reprinted in ref. [14], pp. 94-100. Cooling the trapdoor every time it approaches the closed position results in the success of the ratcheting mechanism and creates a pressure gradient between the two compartments. Rex and Larsen have presented a similar analysis, quantifying the statistical entropy loss on sorting the particles and showing this to be less than the thermodynamic entropy gained on cooling the trapdoor: b) A. F. Rex, R. Larsen, in *Proceedings of the Workshop on Physics and Computation* (PhysComp, Dallas, 1992), IEEE Computer Society Press, Los Alamitos, **1992**, pp. 93-101; reprinted in [14], pp. 101-109.

[27] E. M. Purcell, *Am. J. Phys.* **1977**, *45*, 3-11.

[28] J. Siegel, *Science* **2005**, *310*, 63-64.

[29] R. B. Gennis, *Biomembranes – Molecular Structure and Function*, Springer-Verlag, New York, **1989**.

[30] a) P. Läuger, *Electrogenic Ion Pumps*, Sinauer Associates, Sunderland, MA, **1991**; b) E. Gouaux, R. MacKinnon, *Science* **2005**, *310*, 1461-1465.

[31] a) C. Toyoshima, G. Inesi, *Annu. Rev. Biochem.* **2004**, *73*, 269-292; b) J. V. Møller, P. Nissen, T. L.-M. Sørensen, M. le Maire, *Curr. Opin. Struct. Biol.* **2005**, *15*, 387-393.

[32] M. N. Chatterjee, E. R. Kay, D. A. Leigh, *J. Am. Chem. Soc.* **2006**, *128*, 4058-4073 (reprinted, in full, in the Appendix and the basis for Chapter 2).

[33] D. G. Nicholls, S. J. Ferguson, *Bioenergetics 3*, Academic Press, London, **2002**.

[34] The precise mechanisms in each case are, of course, complex and the details difficult to elucidate. In part this is because elements of a conformational and a gradient-driven pumping mechanism can be in operation at the same time.

[35] A close analogue, halorhodopsin, is a light-powered chloride conformational pump.

[36] a) J. K. Lanyi, H. Luecke, *Curr. Opin. Struct. Biol.* **2001**, *11*, 415-419; b) R. Neutze, E. Pebay-Peyroula, K. Edman, A. Royant, J. Navarro, E. M. Landau, *Biochim. Biophys. Acta* **2002**, *1565*, 144-167.

[37] L. Onsager, *Phys. Rev.* **1931**, *37*, 405-426.

[38] For an introduction to ratchet mechanisms, see ref. [12] and: R. D. Astumian, *Sci. Am.* **2001**, *285* (1), 56-64.

[39] For reviews on Brownian ratchet mechanisms, see: a) P. Hänggi, R. Bartussek in *Nonlinear Physics of Complex Systems – Current status and future trends: Lecture Notes in Physics, Vol. 476* (Eds.: J. Parisi, S. C. Müller, W. Zimmermann), Springer, Berlin, **1996**, pp. 294-308; b) R. D. Astumian, *Science* **1997**, *276*, 917-922; c) M. Bier, *Contemp. Phys.* **1997**, *38*, 371-379; d) F. Jülicher, A. Ajdari, J. Prost, *Rev. Mod. Phys.* **1997**, *69*, 1269-1281; e) Special issue on "The constructive role of noise in fluctuation driven transport and stochastic resonance": *Chaos* **1998**, *8*, 533-664; f) P. Reimann, *Phys. Rep.* **2002**, *361*, 57-265; g) P. Reimann, P. Hänggi, *Appl. Phys. A* **2002**, *75*, 169-178; h) J. M. R. Parrondo, B. J. De Cisneros, *Appl. Phys. A* **2002**, *75*, 179-191; i) J. M. R. Parrondo, L. Dinís, *Contemp. Phys.* **2004**, *45*, 147-157; j) B. J. Gabryś, K. Pesz, S. J. Bartkiewicz, *Physica A* **2004**, *336*, 112-122; k) H. Linke, M. T. Downton, M. J. Zuckermann, *Chaos* **2005**, *15*, 026111. The terms 'thermal ratchet' and 'Brownian ratchet' are often used interchangeably in the physics and biophysics literature ('Brownian rectifier' and 'stochastic ratchet' are also occasionally used). This reflects the fact that *thermal* energy, in the form of *Brownian* motion, is the source of randomization in such

schemes. Although the latter term is more common in the recent literature, it has to be said that some researchers (see, for example, Refs. [39f-h] above) prefer the former on the basis that 'Brownian ratchet' was first coined [(l) S. M. Simon, C. S. Peskin, G. F. Oster, *Proc. Natl. Acad. Sci. USA* **1992**, *89*, 3770-3774] for the specific phenomenon of protein translocation through pores, during which Brownian motion is ratcheted by binding events on one side of the membrane. There can also be confusion between the terms 'thermal ratchet' and 'temperature ratchet'; the latter should properly be reserved only for ratchet systems that operate on the basis of temperature gradients, a sub-class of thermal ratchets. We believe, therefore, that both force of numbers and the illustrative nature of the term 'Brownian ratchet' commend it for use here, particularly as 'Brownian motor' is commonly used to describe a machine which operates by such a mechanism (see Ref. [5]).

[40] Randomizing influences other than Brownian motion can be used in ratchet mechanisms. For example, in quantum ratchets, quantum effects such as tunnelling or electron-wave interference play this role. See, for example: H. Linke, T. E. Humphrey, P. E. Lindelof, A. Lofgren, R. Newbury, P. Omling, A. O. Sushkov, R. P. Taylor, H. Xu, *Appl. Phys. A* **2002**, *75*, 237-246.

[41] The source of spatial inversion symmetry-breaking is most commonly an inherently asymmetric (or 'ratchet') potential. In certain cases, however, a symmetric potential is sufficient if the energy input (although unbiased) brings about spatial asymmetry. Also possible is spontaneous symmetry breaking in coupled symmetric systems driven away from equilibrium (not discussed here). Of course, spatial inversion symmetry may also be broken by a combination of the above.

[42] a) R. D. Astumian, M. Bier, *Biophys. J.* **1996**, *70*, 637-653; b) R. D. Astumian, I. Derényi, *Eur. Biophys. J.* **1998**, *27*, 474-489; c) L. Mahadevan, P. Matsudaira, *Science* **2000**, *288*, 95-99; d) R. Lipowsky in *Stochastic Processes in Physics, Chemistry and Biology: Lecture Notes in Physics, Vol. 557* (Eds.: J. A. Freund, T. Pöschel), Springer, Berlin, **2000**, pp. 21-31; e) C. Bustamante, D. Keller, G. Oster, *Acc. Chem. Res.* **2001**, *34*, 412-420; f) R. D. Astumian, *Appl. Phys. A* **2002**, *75*, 193-206; g) A. Mogilner, G. Oster, *Curr. Biol.* **2003**, *13*, R721-R733; h) G. Oster, H. Y. Wang, *Trends Cell Biol.* **2003**, *13*, 114-121; i) M. Kurzyński, P. Chełminiak, *Physica A* **2004**, *336*, 123-132.

[43] For a recent snapshot of the current status of experiment and application with respect to both biological systems and future technology, see: Special issue on "Ratchets and Brownian motors: Basics, experiments and applications": *Appl. Phys. A* **2002**, *75*, 167-352.

[44] For a selection of experimental examples, see: a) J. Rousselet, L. Salome, A. Ajdari, J. Prost, *Nature* **1994**, *370*, 446-448; b) L. P. Faucheux, L. S. Bourdieu, P. D. Kaplan, A. J. Libchaber, *Phys. Rev. Lett.* **1995**, *74*, 1504-1507; c) L. P. Faucheux, G. Stolovitzky, A. Libchaber, *Phys. Rev. E* **1995**, *51*, 5239-5250; d) L. P. Faucheux, A. Libchaber, *J. Chem. Soc. Faraday Trans.* **1995**, *91*, 3163-3166; e) L. Gorre, E. Ioannidis, P. Silberzan, *Europhys. Lett.* **1996**, *33*, 267-272; f) L. Gorre-Talini, S. Jeanjean, P. Silberzan, *Phys. Rev. E* **1997**, *56*, 2025-

2034; g) L. Gorre-Talini, P. Silberzan, *J. Phys. I* **1997**, *7*, 1475-1485; h) L. Gorre-Talini, J. P. Spatz, P. Silberzan, *Chaos* **1998**, *8*, 650-656; i) A. Lorke, S. Wimmer, B. Jager, J. P. Kotthaus, W. Wegscheider, M. Bichler, *Physica B* **1998**, *251*, 312-316; j) H. Linke, W. Sheng, A. Lofgren, H. Q. Xu, P. Omling, P. E. Lindelof, *Europhys. Lett.* **1998**, *44*, 341-347; k) C. Mennerat-Robilliard, D. Lucas, S. Guibal, J. Tabosa, C. Jurczak, J. Y. Courtois, G. Grynberg, *Phys. Rev. Lett.* **1999**, *82*, 851-854; l) A. van Oudenaarden, S. G. Boxer, *Science* **1999**, *285*, 1046-1048; m) J. S. Bader, R. W. Hammond, S. A. Henck, M. W. Deem, G. A. McDermott, J. M. Bustillo, J. W. Simpson, G. T. Mulhern, J. M. Rothberg, *Proc. Natl. Acad. Sci. USA* **1999**, *96*, 13165-13169; n) C. F. Chou, O. Bakajin, S. W. P. Turner, T. A. J. Duke, S. S. Chan, E. C. Cox, H. G. Craighead, R. H. Austin, *Proc. Natl. Acad. Sci. USA* **1999**, *96*, 13762-13765; o) M. Switkes, C. M. Marcus, K. Campman, A. C. Gossard, *Science* **1999**, *283*, 1905-1908; p) H. Linke, T. E. Humphrey, A. Lofgren, A. O. Sushkov, R. Newbury, R. P. Taylor, P. Omling, *Science* **1999**, *286*, 2314-2317; q) R. W. Hammond, J. S. Bader, S. A. Henck, M. W. Deem, G. A. McDermott, J. M. Bustillo, J. M. Rothberg, *Electrophoresis* **2000**, *21*, 74-80; r) H. Linke, W. D. Sheng, A. Svensson, A. Lofgren, L. Christensson, H. Q. Xu, P. Omling, P. E. Lindelof, *Phys. Rev. B* **2000**, *61*, 15914-15926; s) E. M. Hohberger, A. Lorke, W. Wegscheider, M. Bichler, *Appl. Phys. Lett.* **2001**, *78*, 2905-2907; t) C. Marquet, A. Buguin, L. Talini, P. Silberzan, *Phys. Rev. Lett.* **2002**, *88*, 168301; u) S. Matthias, F. Müller, *Nature* **2003**, *424*, 53-57; v) L. R. Huang, E. C. Cox, R. H. Austin, J. C. Sturm, *Anal. Chem.* **2003**, *75*, 6963-6967. The implications of Brownian ratchet theory, however, are far-reaching and elements of a wide range of noise-assisted physical phenomena may be modelled as ratchet processes, see refs. [39f, 43].

[45] a) H. X. Zhou, Y.-D. Chen, *Phys. Rev. Lett.* **1996**, *77*, 194-197; b) I. Derényi, M. Bier, R. D. Astumian, *Phys. Rev. Lett.* **1999**, *83*, 903-906; c) A. Parmeggiani, F. Jülicher, A. Ajdari, J. Prost, *Phys. Rev. E* **1999**, *60*, 2127-2140.

[46] A 'power stroke' is not intrinsically different in mechanistic terms to these ratchet mechanisms. The distinction solely concerns the relative importance of random fluctuations and any *directional* external force (i.e. moving down an energy gradient) in generating particle motion.

[47] A net flux of particles may also be achieved in a symmetric periodic potential if it is subject to a spatially periodic variation in temperature of the same periodicity as, but out of phase with, the potential. Such systems have their origin in the demonstration by Rolf Landauer that, in a bistable potential well, a localized inhomogeneity in temperature can alter the relative stabilities of the two minima [(a) R. Landauer, *Phys. Rev. A* **1975**, *12*, 636-638]. Büttiker [(b) M. Büttiker, *Z. Phys. B* **1987**, *68*, 161-167] and van Kampen [(c) N. G. van Kampen, *IBM J. Res. Dev.* **1988**, *32*, 107-111] independently modelled this effect and showed that if extended to a periodic potential (i.e. repeating the bistable well in a linear fashion or allowing motion in a closed loop), directional particle transport would occur. Shortly after, Landauer further extended this model [(d) R. Landauer, *J. Stat. Phys.* **1988**, *53*, 233-248] which is now often termed 'Landauer's blowtorch' [see also: e) K. Sinha, F. Moss, *J.*

Stat. Phys. **1989**, *54*, 1411-1423; f) M. Bekele, S. Rajesh, G. Ananthakrishna, N. Kumar, *Phys. Rev. E* **1999**, *59*, 143-149]. Although realization of such a scheme on a microscopic scale would be problematic (see Section 1.4), circulating currents in a closed loop were first observed in electronics by Thomas Johann Seebeck in 1821. An electric current flows in a circuit composed of two resistors which are held at different temperatures (the modern equivalent of such thermoelectric circuits is a thermogenerator, in which a semiconductor diode is held at a different temperature to the rest of a circuit). For this reason, particle transport over symmetric periodic potentials, driven by spatial variations in temperature, is also often known as a 'Seebeck ratchet'. Clearly, such schemes also bear a close resemblance to Feynman's Ratchet and Pawl (Section 1.3.1) when $T_1 \neq T_2$ and, indeed, mathematical equivalence of the two models can be shown, see ref. [25].

[48] R. Landauer, *IBM J. Res. Dev.* **1961**, *5*, 183-191.

[49] The directional threading that occurs in cyclodextrin and other unsymmetrical macrocycle-based rotaxanes, polyrotaxanes and pseudorotaxanes could be used in this respect, but only if coupled to an appropriate energy input (e.g. olefin or azobenzene isomerization), see: a) R. Isnin, A. E. Kaifer, *J. Am. Chem. Soc.* **1991**, *113*, 8188-8190; b) H. Yonemura, M. Kasahara, H. Saito, H. Nakamura, T. Matsuo, *J. Phys. Chem.* **1992**, *96*, 5765-5770; c) A. Abou-Hamdan, P. Bugnon, C. Saudan, P. G. Lye, A. E. Merbach, *J. Am. Chem. Soc.* **2000**, *122*, 592-602; d) J. E. H. Buston, J. R. Young, H. L. Anderson, *Chem. Commun.* **2000**, 905-906; e) M. R. Craig, M. G. Hutchings, T. D. W. Claridge, H. L. Anderson, *Angew. Chem. Int. Ed.* **2001**, *40*, 1071-1074; f) C. Saudan, F. A. Dunand, A. Abou-Hamdan, P. Bugnon, P. G. Lye, S. F. Lincoln, A. E. Merbach, *J. Am. Chem. Soc.* **2001**, *123*, 10290-10298; g) J. S. Lock, B. L. May, P. Clements, S. F. Lincoln, C. J. Easton, *Org. Biomol. Chem.* **2004**, *2*, 337-344; h) J. W. Park, H. J. Song, *Org. Lett.* **2004**, *6*, 4869-4872; i) J. W. Park, S. Y. Lee, H. J. Song, K. K. Park, *J. Org. Chem.* **2005**, *70*, 9505-9513; j) T. Oshikiri, Y. Takashima, H. Yamaguchi, A. Harada, *J. Am. Chem. Soc.* **2005**, *127*, 12186-12187; k) Q.-C. Wang, X. Ma, D.-H. Qu, H. Tian, *Chem. Eur. J.* **2006**, *12*, 1088-1096; l) A. G. Cheetham, M. G. Hutchings, T. D. W. Claridge, H. L. Anderson, *Angew. Chem. Int. Ed.* **2006**, *45*, 1596-1599; m) G. Wenz, B.-H. Han, A. Müller, *Chem. Rev.* **2006**, *106*, 782-817.

[50] a) P. V. E. McClintock, *Nature*, **1999**, *401*, 23-24; b) G. P. Harmer, D. Abbott, *Nature*, **1999**, *402*, 864; c) G. P. Harmer, D. Abbott, *Stat. Sci.* **1999**, *14*, 206-213; d) G. P. Harmer, D. Abbott, P. G. Taylor, *Proc. R. Soc. Lond. A* **2000**, *456*, 247-259; e) R. D. Astumian, *Am. J. Phys.* **2005**, *73*, 178-183.

[51] J. V. Hernández, E. R. Kay, D. A. Leigh, *Science* **2004**, *306*, 1532-1537 (reprinted, in full, in the Appendix and the basis for Chapter 3).

[52] It seems to us that these ideas could prove useful in understanding protein folding and, perhaps, how some chaperones, foldases and prions function.

[53] a) G. Schill, *Catenanes, Rotaxanes and Knots*, Academic Press, New York, **1971**; b) D. M. Walba, *Tetrahedron* **1985**, *41*, 3161-3212; c) D. B. Amabilino,

J. F. Stoddart, *Chem. Rev.* **1995**, *95*, 2725-2828; d) S. A. Nepogodiev, J. F. Stoddart, *Chem. Rev.* **1998**, *98*, 1959-1976; e) D. A. Leigh, A. Murphy, *Chem. Ind.* **1999**, 178-183; f) G. A. Breault, C. A. Hunter, P. C. Mayers, *Tetrahedron* **1999**, *55*, 5265-5293; g) *Molecular Catenanes Rotaxanes and Knots* (Eds.: J.-P. Sauvage, C. Dietrich-Buchecker), Wiley-VCH, Weinheim, **1999**.

[54] There are some examples of catenanes and rotaxanes constructed under thermodynamic control using dynamic processes such as olefin metathesis or imine bond formation (see for example: R. L. E. Furlan, S. Otto, J. K. M. Sanders, *Proc. Natl. Acad. Sci. USA* **2002**, *99*, 4801-4804 and references therein). Such systems cannot act as molecular machines if they exchange components with the bulk quicker than the timescale of their stimuli-induced motion.

[55] Myosin requires an actin track to move along: a) S. M. Block, *Cell* **1996**, *87*, 151-157; while kinesin progresses along the pathway provided by microtubule filaments: b) S. M. Block, *Cell* **1998**, *93*, 5-8; even ion pumps operate through precisely defined structural channels: c) J. C. Skou, *Angew. Chem. Int. Ed.* **1998**, *37*, 2321-2328.

[56] a) A. C. Benniston, *Chem. Soc. Rev.* **1996**, *25*, 427-435; b) V. Balzani, M. Gómez-López, J. F. Stoddart, *Acc. Chem. Res.* **1998**, *31*, 405-414; c) J.-P. Sauvage, *Acc. Chem. Res.* **1998**, *31*, 611-619; d) M.-J. Blanco, M. C. Jiménez, J.-C. Chambron, V. Heitz, M. Linke, J.-P. Sauvage, *Chem. Soc. Rev.* **1999**, *28*, 293-305; e) J.-P. Collin, C. Dietrich-Buchecker, P. Gaviña, M. C. Jiménez-Molero, J.-P. Sauvage, *Acc. Chem. Res.* **2001**, *34*, 477-487; f) M. C. Jiménez-Molero, C. Dietrich-Buchecker, J.-P. Sauvage, *Chem. Commun.* **2003**, 1613-1616; g) M. J. Gunter, *Eur. J. Org. Chem.* **2004**, 1655-1673; h) A. H. Flood, R. J. A. Ramirez, W. Q. Deng, R. P. Muller, W. A. Goddard, J. F. Stoddart, *Aust. J. Chem.* **2004**, *57*, 301-322; i) P. M. Mendes, A. H. Flood, J. F. Stoddart, *Appl. Phys. A* **2005**, *80*, 1197-1209; j) V. Balzani, A. Credi, B. Ferrer, S. Silvi, M. Venturi, *Top. Curr. Chem.* **2005**, *262*, 1-27; k) J.-P. Collin, V. Heitz, J.-P. Sauvage, *Top. Curr. Chem.* **2005**, *262*, 29-62; l) N. N. P. Moonen, A. H. Flood, J. M. Fernández, J. F. Stoddart, *Top. Curr. Chem.* **2005**, *262*, 99-132; m) E. R. Kay, D. A. Leigh, *Top. Curr. Chem.* **2005**, *262*, 133-177 (reprinted, in full, in the Appendix).; n) A. B. Braunschweig, B. H. Northrop, J. F. Stoddart, *J. Mater. Chem.* **2006**, *16*, 32-44; o) H. Tian, Q.-C. Wang, *Chem. Soc. Rev.* **2006**, *35*, 361-374.

CHAPTER TWO

Beyond Switches: Ratcheting a Particle Energetically Uphill with a Compartmentalized Molecular Machine

Published in *Journal of the American Chemical Society* as "*Beyond Switches: Ratcheting a Particle Energetically Uphill with a Compartmentalized Molecular Machine*":

M. N. Chatterjee, E. R. Kay, D. A. Leigh, *J. Am. Chem. Soc.* **2006**, *128*, 4058-4073.

Acknowledgements and contributions

Synthesis and characterization of all new compounds and performance of the machine operation steps reported in this Chapter were shared equally with Dr Manashi N. Chatterjee, whose contribution is very gratefully acknowledged. The author also developed the concepts explored herein, designed the specific molecular systems used to illustrate them, analysed the results and wrote this Chapter and the paper it is based upon. Prof. David A. Leigh provided guidance and input at all stages.

Synopsis

In Chapter 1, the principles for designing molecular-level machines were explored by considering the problem from a number of different perspectives. A key feature that allows Brownian particles to be driven energetically uphill is 'compartmentalization' of the machine and control over the kinetics for exchange between compartments. Stimuli-responsive molecular shuttles – the classic synthetic molecular machines constructed form rotaxanes and catenanes – have no such control, and at all times exhibit equilibrium distributions of macrocycle between the stations.

Here we correlate chemical (covalent), physical (thermodynamic), and statistical (population distribution) descriptions of behaviour with the way that two new types of simple compartmentalized molecular machines (the threads of rotaxanes) perform the task of transporting a Brownian substrate (the rotaxane macrocycle) between two distinguishable binding sites. The first machine–substrate ensemble is a [2]rotaxane that operates through a mechanism that intrinsically causes it to change the average position of the macrocycle irreversibly – unlike stimuli-responsive molecular shuttles, which act as reversible molecular switches. The second system is a molecular machine that is able to pump its substrate energetically uphill using the energy provided by a photon by means of an olefin photoisomerization. Resetting this compartmentalized molecular machine does not undo the work it has carried out or the task performed, a significant difference to a simple molecular switch and a characteristic we recognize as 'ratcheting'.

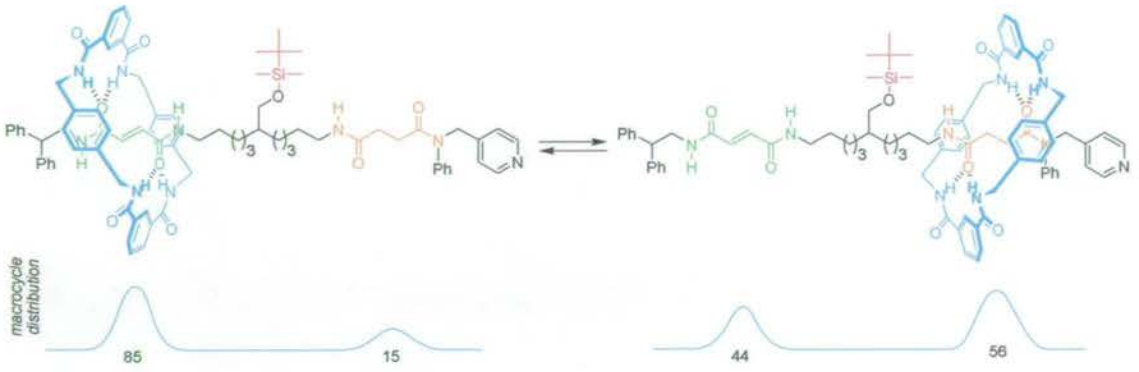

The ratcheting mechanism allows the [2]rotaxane to carry out the transport function envisaged for the historical thought-machines Smoluchowski's Trapdoor and Maxwell's Pressure Demon, albeit via an unrelated mechanism and using an input of energy. The terms 'ratcheting' and 'escapement' are defined and exemplified in

mechanical terms for the molecular level and the fundamental phenomenological differences that exist between what constitutes a two-state Brownian switch, a two-state Brownian memory or 'flip-flop' and a (two-stroke) Brownian motor are outlined. We also suggest that considering the relationship between the parts of a molecular machine and a substrate in terms of 'statistical balance' and 'linkage' could be useful in the design of more complex systems, and in helping to understand the role of individual amino acids and peptide fragments during the directional transport of substrates by biological pumps and motors.

2.1 Introduction

In recent years it has proved possible to design synthetic molecular systems in which positional displacements of submolecular components result from moving energetically downhill,[1] but what are the structural features necessary for molecules to convert chemical energy into mechanical work? How can we make a synthetic molecular machine that pumps ions against a gradient, say, or moves itself or a substrate energetically uphill along a track? We know that nature has developed such machines and refined them to a high degree of efficiency[2] and yet the chemistry literature is surprisingly poor when it comes to the fundamental guidelines necessary to invent them. Here we examine the way that some simple molecular machines carry out the task of transporting a particle along a one-dimensional, two minimum, potential energy surface and attempt to correlate the chemical (covalent structure), physical potential (thermodynamic and kinetic properties governed by attractive and repulsive noncovalent interactions), and statistical (population distribution) behaviour of the system with aspects of the task performance. The results begin to provide the phenomenological framework necessary for chemists to design more complex compartmentalized molecular-level machines (assemblies of simpler machines that each act as components by performing a set task). It may also prove useful in understanding the roles played by individual submolecular fragments during the operation of biological machines.

2.2 The two-compartment Brownian particle 'thought-machines'

The design of tiny machines capable of transporting Brownian particles selectively between two compartments – i.e. effectively along a one-dimensional, two minimum, potential energy surface – was the subject of several celebrated historical 'thought-machines' (Figure 2.1, see Chapter 1 for more details).[3–7] Both Maxwell's Demon[4] (Figures 2.1a and 2.1b) and Smoluchowski's Trapdoor[5] (Figure 2.1d) were concerned with trying to set up temperature or pressure gradients in systems containing multiple Brownian particles through their controlled exchange between two compartments; Szilard's Engine[6] (Figure 2.1c) endeavoured to utilize the pressure exerted by one Brownian particle located in one of two compartments to do work. The behaviours of all four 'Gedankenmaschinen' were considered without an

external energy source (other than a heat reservoir at the same temperature as the Gedankenmaschine system) – their purpose was to test the nature of the Second Law of Thermodynamics, not to see how a working Brownian machine could be achieved (that was probably first discussed[7, 8] by Feynman). However, modern synthetic routes allow us to make molecules in which the Brownian motion of substrates *does* occur between two well-defined locations, e.g. rotaxane-based molecular shuttles. This enables us to re-visit the question of how to transport a Brownian particle between two distinguishable sites, not from the point of view of doing so adiabatically, but rather to see how such a task can be performed by a molecular-level machine.

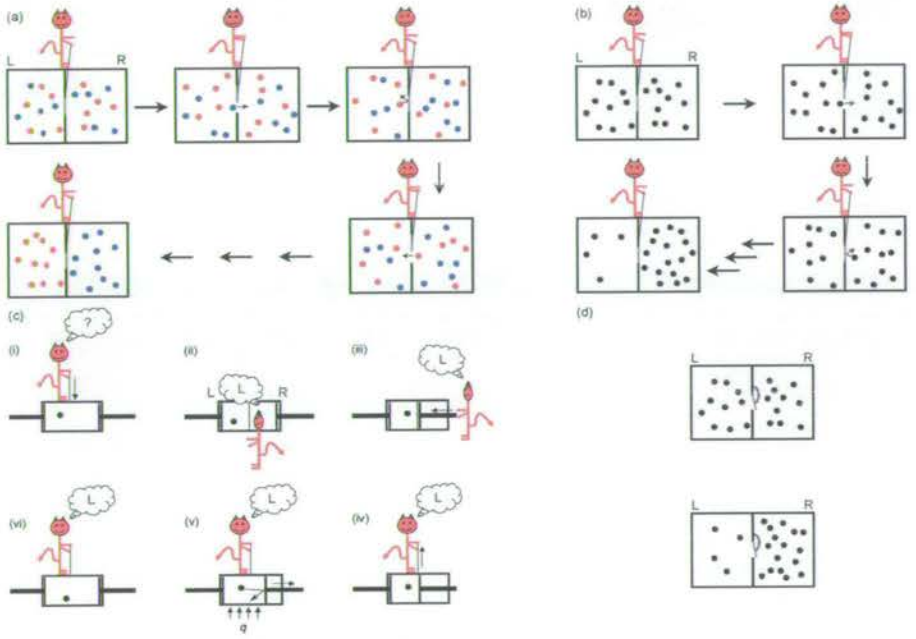

Figure 2.1 Examples of two-compartment Brownian 'thought-machines' (for more details, see Chapter 1): (a) Maxwell's 'temperature demon' in which a gas at uniform temperature is sorted into 'hot' and 'cold' molecules.[4] Particles with energy higher than the average are represented by red dots while blue dots represent particles with energies lower than the average. (b) A Maxwellian 'pressure demon' in which a pressure gradient would be created if the door was only opened when a particle in the left compartment approached it.[4c] (c) Szilard's Engine, which attempts to do work with a piston using heat drawn from an external reservoir by a pressure demon.[6] (i) Initially, a single Brownian particle occupies a cylinder with a piston at either end. A frictionless partition is put in place to divide the container into two compartments ((i)→(ii), unlinking stimulus). (ii) The demon then detects the particle and determines in which compartment it resides (the left (L) compartment in the depicted example). (iii) Using this information, the demon is able to move the opposite piston into position without meeting any resistance from the particle. (iv) The partition is removed (linking stimulus), allowing (v) the 'gas' to expand against the piston, doing work against any attached load. To replenish the energy used by the piston and maintain a constant temperature, heat must flow into the system. To complete the thermodynamic cycle and reset the machine, the demon's memory of where the particle was must be erased ((vi)→(i)). (d) Smoluchowski's Trapdoor – an 'automatic' pressure demon. The directionally discriminating behaviour is carried out by a wholly mechanical device, a trapdoor that is intended to open when hit from one direction but not the other (note, this still involves the communication of information between the particle and the machine; the demon is incorporated into the door mechanism).[5]

2.3 Rotaxanes and molecular shuttles

Rotaxanes are chemical structures in which one or more macrocycles are mechanically prevented from de-threading from linear chains by bulky 'stoppers'.[9] Even though the rings are not covalently attached to the threads, rotaxanes are molecules – not supramolecular complexes – as covalent bonds must be broken in order to separate the components from each other.[9, 10] The interactions generally used to direct the synthesis of rotaxanes often 'live-on' in the product, providing a well-defined binding site or 'station' for the ring on the thread. If two or more stations are present on a thread with a traversable path between them the rotaxane can be considered a 'molecular shuttle'[11] in which the ring is incessantly and randomly exchanged between the binding sites.[12] Stimuli-responsive molecular shuttles are rotaxanes in which the net position of the macrocycle on the thread (i.e. the statistical distribution of the ring between the stations) changes in response to external triggers (light,[13] heat,[14] electrons,[15] chemical,[16] pH,[17] binding events,[18] etc.). Generally, the external stimulus alters the structure of one of the binding sites so as to change the relative binding affinities of the stations for the macrocycle, placing the system out of co-conformational[19] equilibrium. Relaxation towards the new global minimum subsequently occurs by the macrocycle moving along the thread. A typical example[13j] of a light-switchable amide-based molecular shuttle is shown in Scheme 2.1.

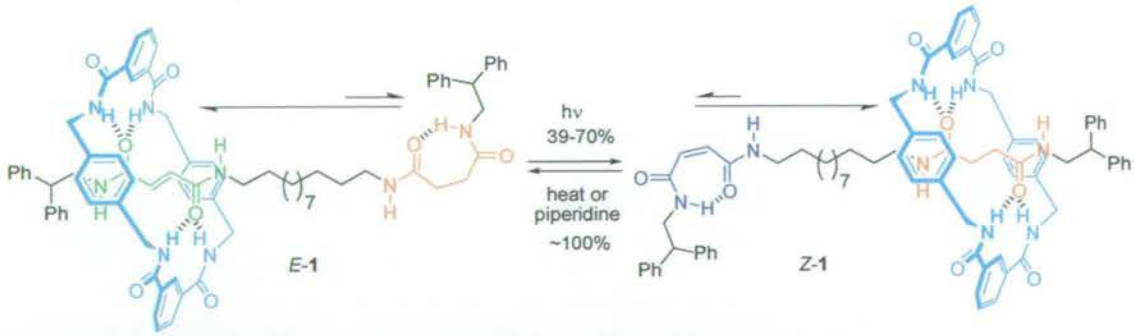

Scheme 2.1 A previously reported[13j] [2]rotaxane, **1**, that functions as a stimuli-responsive molecular shuttle. At 254 nm the photostationary state is 61:39 *E*:*Z*,[13j] at 312 nm it is ~50:50 and at 350 nm with a benzophenone sensitizer it is 40:60 *E*:*Z*[13j] and can be increased up to 30:70 *E*:*Z*[20j] for some derivatives.

However, we can also think of stimuli-responsive molecular shuttles in another way; we can consider just the thread portion of such a molecule as a machine that directionally transports a particle – the interlocked macrocycle – between two sites

(compartments) on a one-dimensional potential energy surface.[20] The significance of considering a rotaxane in this way is that over the past decade physicists have developed formal theoretical mechanisms, deeply rooted in nonequilibrium statistical mechanics, which explain how the directional transport of Brownian particles can occur from periodic changes in a potential energy surface (e.g. by applying an oscillating electric field).[21, 22] Many different possible types of these theoretical 'Brownian ratchet' mechanisms have been suggested, including energy ratchets, information ratchets, flashing ratchets, tilting ratchets, and rocking ratchets (see Chapter 1).[22] These mechanisms have been successfully applied to the development of transport and separation devices for mesoscopic particles and macromolecules, microfluidic pumping, and quantum and electronic applications,[23, 24] and have also been shown to successfully account for the general principles that govern the operation of complex biological motors.[24, 25] However, to date it is not known how such theoretical mechanisms correlate with the changes that occur in molecular structure during the operation of biological machines. What do individual peptide fragments do in order to bring about transport of an ion or molecule by a Brownian ratchet mechanism and why? We wondered whether examining how these principles can be applied to some much less sophisticated (in terms of function as well as structure) synthetic molecular machines could tell us something about how they might apply to more complex systems, both artificial and natural.

2.4 The statistical balance of a dynamically exchangeable substrate or quantity (The Principle of Detailed Balance)

If we ignore the normally small population of rings on the thread, at equilibrium the macrocycle in a molecular shuttle can be considered to continuously fluctuate between the two stations. However, even for a molecular shuttle with two different stations, at equilibrium no net task can be performed by these movements. This is a consequence of the 'Principle of Detailed Balance';[26] at equilibrium transitions between any two states take place in either direction at the same rate so that no flux is generated. This rules out the maintenance of equilibria by cyclic processes such as A→B→C→A rather than A⇆B + B⇆C + C⇆A (ref. [21b]) and is a formal indication that a machine such as Smoluchowski's Trapdoor (Figure 2.1d) cannot operate (at least not in the way originally envisaged). However, in an out-of-

equilibrium system, detailed balance is broken and as the system moves spontaneously towards equilibrium net work *can* be done by the fluxional exchange process. It is well established that breaking detailed balance is a requirement for doing work with stochastic transport systems.[22] However, we recently pointed out that detailed balance could be considered to result from two separate properties of a system:[8d] the statistical distribution of a quantity (an imbalance in which provides the thermodynamic impetus for net transport) and the ability of that quantity to be dynamically exchanged (which provides the communication necessary for transport to occur). It is no coincidence that all four of the Gedankenmaschinen shown in Figure 2.1 disconnect the compartments at various stages during their operation in order to try and achieve net particle transportation. The molecular examples in this paper (vide infra) show that the deconvolution of the statistical 'balance' and the 'linkage' of compartments is useful for establishing the phenomenological nature of ratcheting and escapement (the counterpart to ratcheting) in Brownian transport processes.

2.5 Systematic behaviour of some simple molecular machines

Let us consider how a stimuli-responsive rotaxane such as **1** (Scheme 2.1) performs the mechanical task of changing the average position of the ring along the thread. So that we can clearly see how the system evolves as this task is performed we will represent it at each stage (Scheme 2.2) in terms of the covalent structure of the machine, that is the thread (chemical status), the average potential energy surface (physical status of the machine, governed by noncovalent interactions – attractive forces between machine and substrate such as hydrogen bonding, and repulsive forces such as steric barriers), and the statistical distribution of the substrate being transported (the macrocycle). In these types of schemes, which we shall call 'machine-performance representations', we will use bold numbers to show different systems (**1**, **2**, **3**... etc.) and lettered suffixes to differentiate states of the system (**1A**, **1B**, **1C**... etc.). In Scheme 2.2 we assume the photostationary state is 50:50 *E*:*Z*, and that the preferred ratio of occupancy between fumaramide (green) and succinamide (orange) stations is 90:10 and between maleamide (dark blue) and succinamide 10:90.

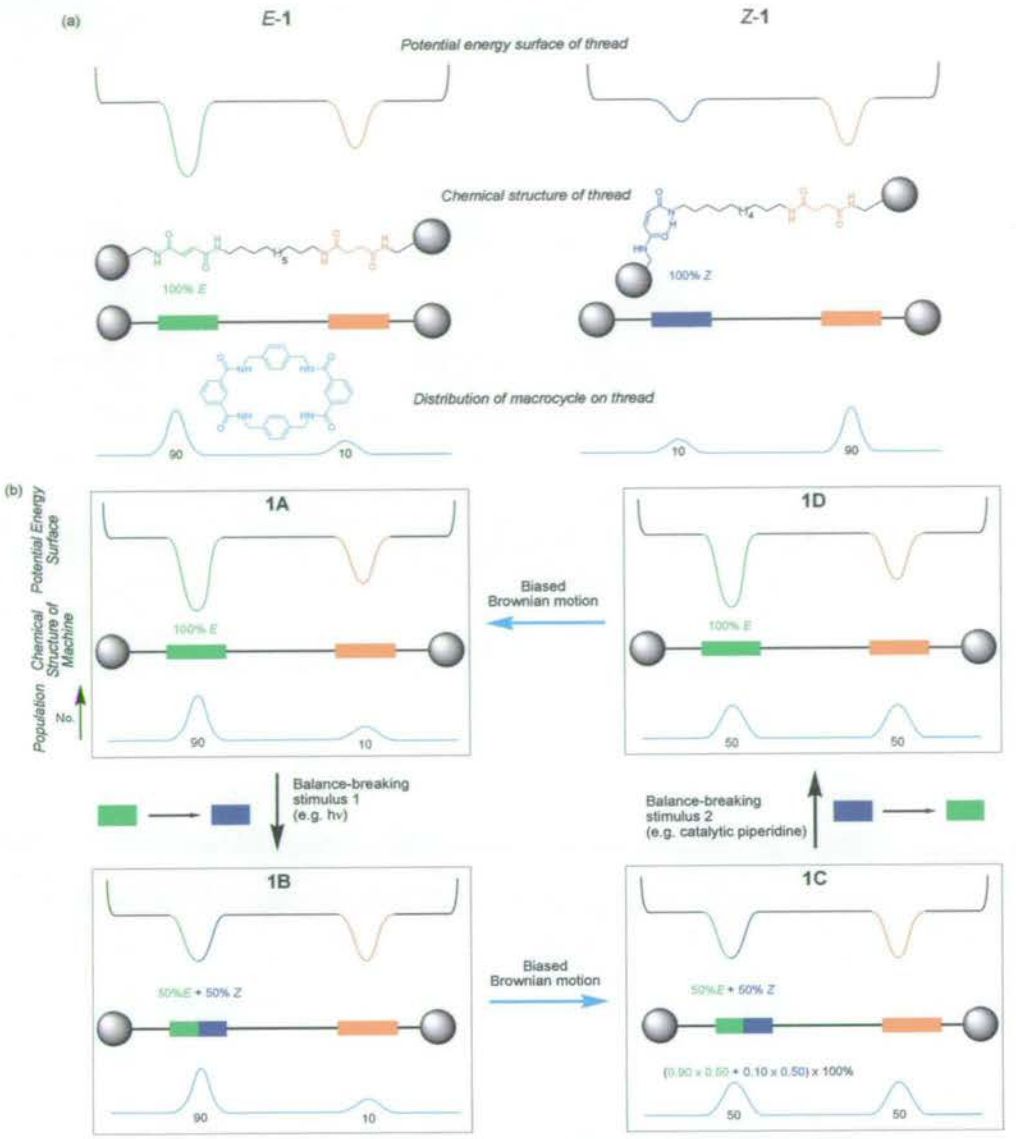

Scheme 2.2 (a) Description of *E*-**1** and *Z*-**1** in covalent, thermodynamic and statistical terms, assuming a 90:10 distribution of translational isomers in each olefin diastereomer. (b) 'Machine-performance representation' of the forward (**1A**→**1C**) and backward (**1C**→**1A**) operations of machine–substrate system **1**, assuming a 50:50 olefin mixture at the photostationary state. The chemical structure of the machine (thread) is shown at each stage in cartoon form with the fraction of olefin diastereomers indicated in terms of colour of a station. The potential energy surface shown is the average potential energy surface of the thread for the macrocycle at that stage of the machine operation, i.e. the appropriately weighted combination of the potential energy surfaces for each of the olefin diastereomers (see (a)) contributing to the mixture. The population trace shows the overall distribution of the substrate over the machine.

The initial state of the system (**1A**) is statistically balanced. The average position of the macrocycle (from the Boltzmann distribution) is very close to the green station. A photonic stimulus ('balance-breaking stimulus') causes isomerization of some of the olefins from *E* to *Z*, putting the position of the macrocycle in the molecules that are isomerized momentarily out of equilibrium (**1B**, similarly **1D**). The system acts to restore balance through biased Brownian motion of the macrocycles and we arrive at

the final state, **1C**. The change in state between **1B** and **1C** (and also between **1D** and **1A**) is not triggered externally, rather it is a thermally activated relaxation step, in which the average position of the macrocycle (given by the Boltzmann distributions within the olefin isomers multiplied by their contribution to the photostationary state) moves along the thread towards the orange station. Note, however, that the machine – the thread – cannot use the energy from the photon to perform the transportation task in such a way that the position of the substrate becomes independent of the state of the machine; applying a second stimulus to reset the machine (e.g. adding piperidine to reform the *E*-olefin of the thread) undoes the net displacement of the macrocycle (**1C→1A**).

Now let us consider a new type of rotaxane system, **2**, in which a stimuli-induced change of position of the macrocycle also occurs but through a clearly different mechanism to the previous shuttle (Scheme 2.3). In **2** the two stations are structurally identical (but distinguishable – note the differently depicted stoppers) and a bulky group acts as a barrier which prevents the ring from moving between them. If we start with 100% of the rings on the first station, *succ1*-**2**,[27] and then remove the barrier, the system moves towards equilibrium, causing an average displacement of the macrocycle of half the distance separating the two stations.

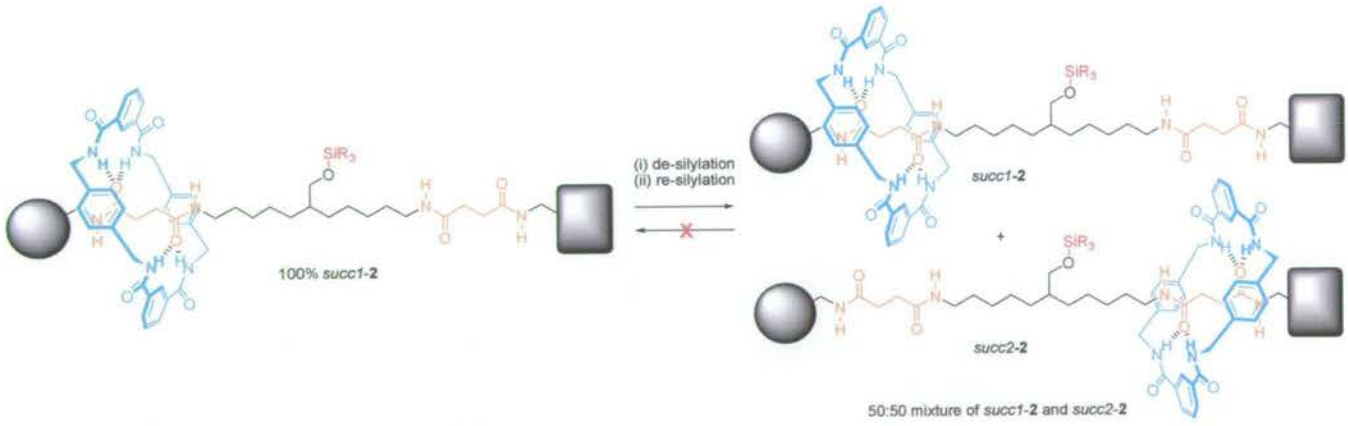

Scheme 2.3 A type of [2]rotaxane that can act as an irreversible mechanical switch. R_3SiO– is a silyl ether that is too bulky to allow macrocycle exchange between the succinamide stations.

Again, we can see how this system evolves more clearly using a 'machine-performance representation' (Scheme 2.4). Unlike system **1**, machine–substrate system **2** starts out statistically unbalanced (**2A**). The stimulus required is also different from that used in the first system: a 'linking stimulus' lowers the barrier between the two stations (**2B**), allowing the system to fulfil the impetus to restore

balance and move to equilibrium by biased Brownian motion of the macrocycle (**2C**, note that the energy well-depths of the two stations are the same; the macrocycle is not held more tightly by the station it moves to). Raising the barrier by applying an 'unlinking stimulus' resets the machine – the thread – but this time the task it has performed is *not* undone (**2D**). However, we note that if we try applying the linking stimulus again after the machine is reset, the machine does not change the average position of the macrocycle because the system is already statistically balanced (Scheme 2.4).

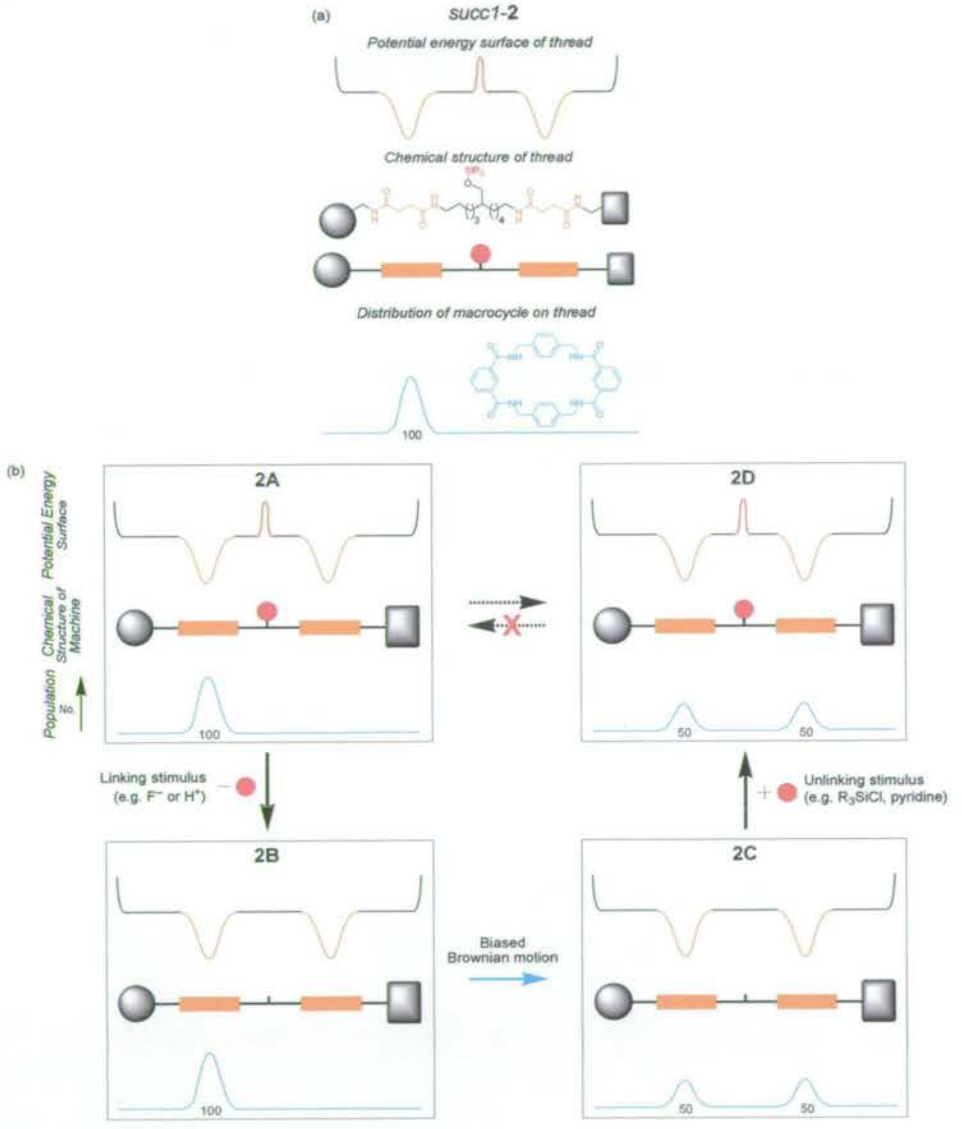

Scheme 2.4 (a) Description of *succ1*-**2** in covalent, thermodynamic and statistical terms. (b) 'Machine-performance representation' of a [2]rotaxane that acts as an irreversible mechanical switch. **2A:** The macrocycle is locked on one of the two energetically identical but distinguishable stations by a large kinetic energy barrier. **2B:** A linking stimulus lowers the barrier. **2C:** The thermal bath restores equilibrium via biased Brownian motion. **2D:** An unlinking stimulus resets the machine. Note that repeating the cycle of chemical reactions would not change the distribution of the macrocycle for a second time.

This stimuli-induced irreversible net change of position of the macrocycle represents a new type of molecular shuttle in phenomenological terms and so we prepared an experimental example, **3**, in single translational isomer form (*succ1*-**3**) according to Scheme 2.5. The unoccupied thread, **4**, was also synthesized as a comparison for ^{1}H NMR purposes. To be able to distinguish between the two succinamide stations through ^{1}H NMR spectroscopy, but still keep them similar in terms of macrocycle binding affinity, the terminal right-hand side (as depicted in Scheme 2.5) amide group was derivatized with a phenyl group. Aryl-substituted tertiary amides preferentially adopt an *anti*-arrangement of the alkyl groups so there is no complication with slowly interconverting rotamers in the ^{1}H NMR spectra.[28, 29] (Tertiary aryl-substituted fumaramide groups are excellent templates for benzylic amide macrocycle rotaxane formation.[30]) A 4-picolyl fragment provides the necessary bulk for the rest of the stopper.

The synthetic route to *succ1*-**3** is worthy of some comment. The 'gated' spacer that separates the two stations was prepared by double alkylation (orthogonal amine protecting groups) and subsequent Krapcho decarboxylation[31] of dimethyl malonate (Scheme 2.5, (i)-(v)). A fumaramide group was then attached, both to maximize the yield of rotaxane formation (step (viii), 68%) and to provide a common route for the synthesis of *fum-E*-**5** (vide infra). Unmasking of the Fmoc-protected amine, followed by coupling with a succinic acid derivative (step (ix)) was followed by hydrogenation (step (x)) of the fumaramide moiety. Perhaps surprisingly, the macrocycle appears to offer no significant protection to the thread functionality in this step,[32] which readily affords the two station rotaxane, **3**, as a single translational isomer, *succ1*-**3** (however, careful solvent selection is necessary to avoid cleavage of the silyl ether[33]).

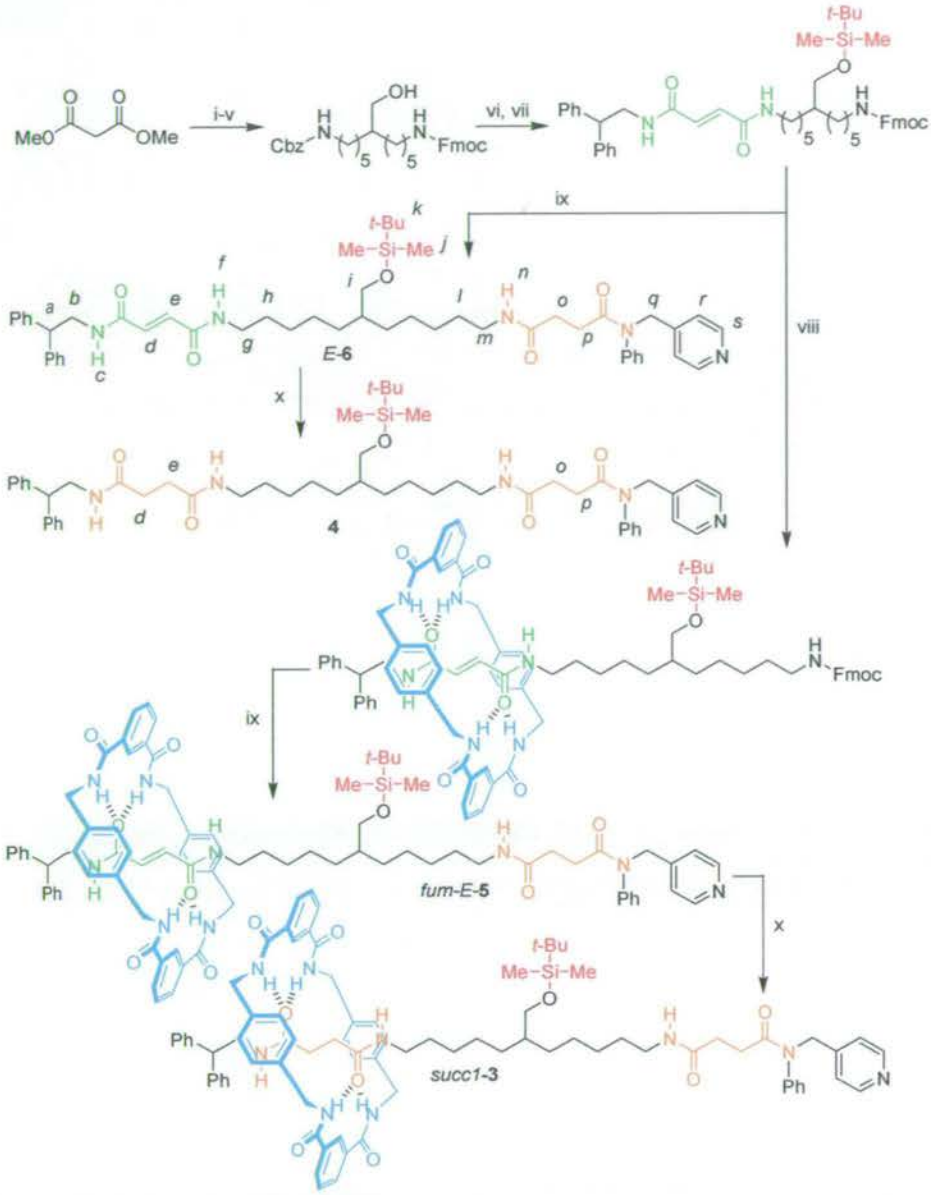

Scheme 2.5 Synthesis of single translational isomer [2]rotaxanes *succ1*-**3** and *fum*-*E*-**5** and the corresponding threads, **4** and *E*-**6**. Reaction conditions (unless otherwise stated, reactions were carried out at room temperature): (i) a. NaH, THF, 0 °C to 40 °C, 2 h; b. Bu_4NI, *N*-benzyloxycarbonyl-5-bromo-1-pentylamine, THF, reflux, 12 h, 88%; (ii) a. NaH, THF, 0 °C to r.t, 2 h; b. Bu_4NI, *N*-allyloxycarbonyl-5-bromo-1-pentylamine, THF, reflux, 12 h, 58%; (iii) LiCl, DMSO, H_2O, 160 °C, 4 h, 66%; (iv) diisobutylaluminium hydride (1M in toluene), THF, –78 °C, 4 h, 68%; (v) a. $PhSiH_3$, $Pd(PPh_3)_4$, CH_2Cl_2, 45 min; b. fluorenylmethylchloroformate (Fmoc-Cl), Et_3N, 45 min, 56%; (vi) a. H_2, 10% Pd/C, HCl (1M in Et_2O), MeOH, 1 atm, 1 h; b. (*E*)-3-(2,2-diphenylethylcarbamoyl)-acrylic acid, 1-[3-dimethylaminopropyl]-3-ethylcarbodiimide hydrochloride (EDCI·HCl), 1-hydroxybenzotriazole hydrate (HOBt·H_2O), Et_3N, CH_2Cl_2, 0 °C to rt, 4 h, 60%; (vii) *tert*-butyldimethylsilyl chloride (TBDMSCl), imidazole, 4-(dimethylamino)pyridine (DMAP), CH_2Cl_2, 2 h, 63%; (viii) *p*-xylylenediamine, isophthaloyl dichloride, Et_3N, $CHCl_3$, 3 h, 68%; (ix) a. piperidine, THF/CH_3CN (1:3), 2.5 h; b. 4-oxo-4-(phenyl(pyridin-4-ylmethyl)amino)butanoic acid, EDCI·HCl, HOBt·H_2O, Et_3N, CH_2Cl_2, 0 °C to rt, 14 h, 47% (*E*-**6**), 48% (*fum*-*E*-**5**); (x) H_2, 10% Pd/C, THF, 1 atm, 6 h, 90% (**4**), 90% (*succ1*-**3**). For full experimental details, see Section 2.9.2.

The system functions (Scheme 2.6) as predicted in Scheme 2.4. De-silylation of *succ1*-**3** (Scheme 2.6, step (i)) followed by re-silylation (step (ii)) afforded a ~1:1 mixture of the two translational isomers of **3**. Note, because *succ1*-**3** and *succ2*-**3** are not in equilibrium with each other, unlike *fum-E*-**1** and *succ-E*-**1** for example (Scheme 2.1), the translational isomers of **3** are actually diastereoisomers.[10] The ^{1}H NMR spectra of the machine in the absence of the substrate (i.e. the free thread, Figure 2.2a),[29] the machine–substrate ensemble in its initial state (Figure 2.2b), and after application of the linking and unlinking stimuli (Figure 2.2c) are shown in Figure 2.2.

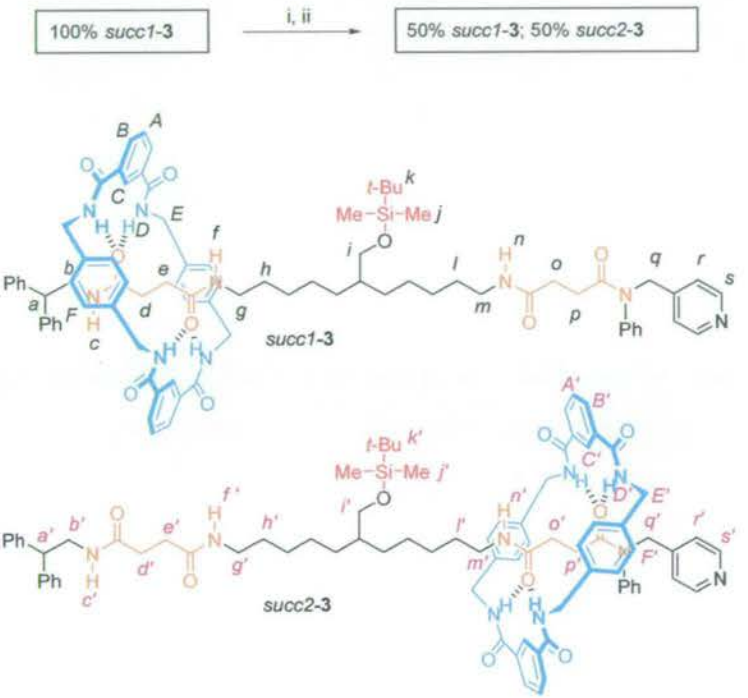

Scheme 2.6 Chemical representation of the irreversible net translocation of the macrocycle that occurs through the transformation *succ1*-**3** → [*succ2*-**3** + *succ1*-**3**] (50:50 ±2). Reaction conditions: (i) 80% aqueous acetic acid, 60 °C, 1 h; (ii) TBDMSCl, imidazole, DMAP, CH_2Cl_2, rt, 1 h. For full experimental details, see Section 2.9.1.

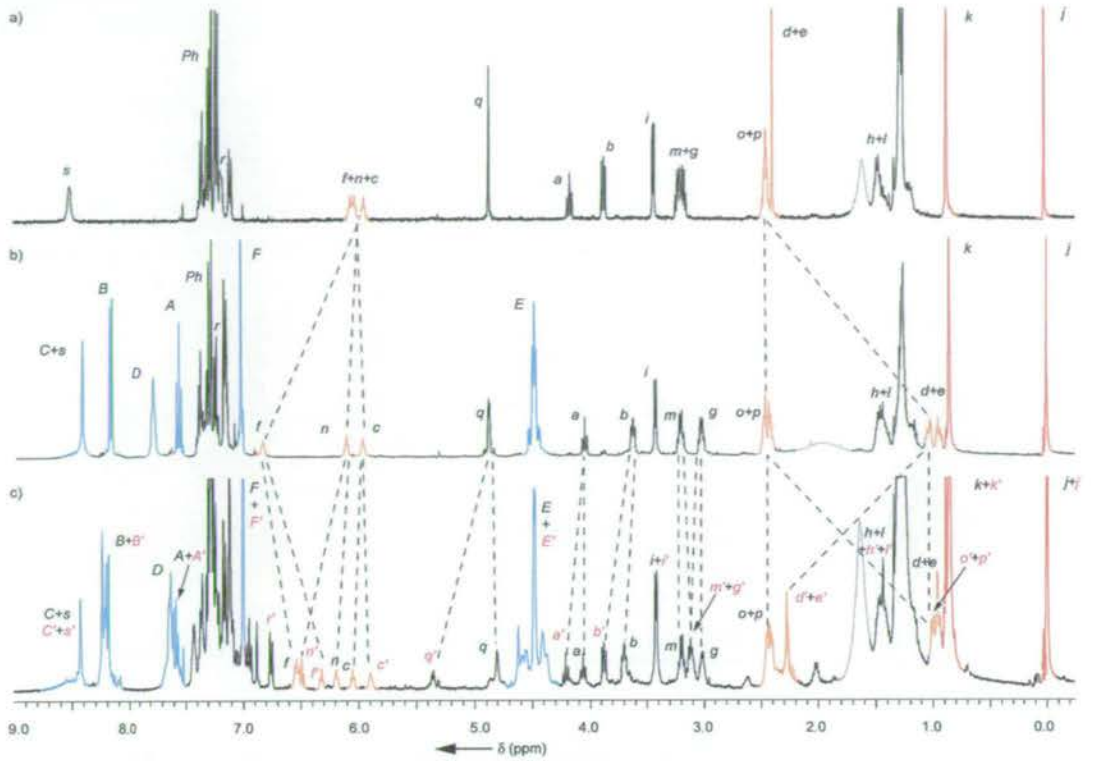

Figure 2.2 ^{1}H NMR Spectra (400 MHz, $CDCl_3$, 298 K) of: (a) free thread **4**; (b) *succ1*-**3**; (c) mixture of translational isomers *succ1*-**3** and *succ2*-**3** after the two step operation (Scheme 2.6, (i) and (ii)). Integration shows the *succ1*-**3**:*succ2*-**3** ratio in (c) is 50:50 (± 2%). The ^{1}H NMR assignments and colouring correspond to the labelling in Schemes 2.5 and 2.6. Residual water peaks are shown in grey.

Again, let us consider what the mechanism of operation of the machine is: the stimuli applied to **3** switch 'on' and 'off' whether the stations are able to exchange the macrocycle or not. Linking of two parts of the machine which interact with the substrate allows the system to move towards equilibrium, that is towards a statistically balanced state. This is a molecular-level form of 'escapement', the element of the mechanism that controls the release of potential energy to drive mechanical motion in clocks and other macroscopic mechanical devices.[34]

Let us combine the features of the first two rotaxanes, **1** and **3**, to invent a third type of molecular machine system, **5**, and see how it functions. Rotaxane **5** was synthesized as a single configurational and translational isomer, *fum-E*-**5**, along with the corresponding thread *E*-**6**, according to Scheme 2.5. The reaction profile of this rotaxane is outlined in Scheme 2.7 in standard chemical terms and its performance as a machine–substrate ensemble is shown in Scheme 2.8.

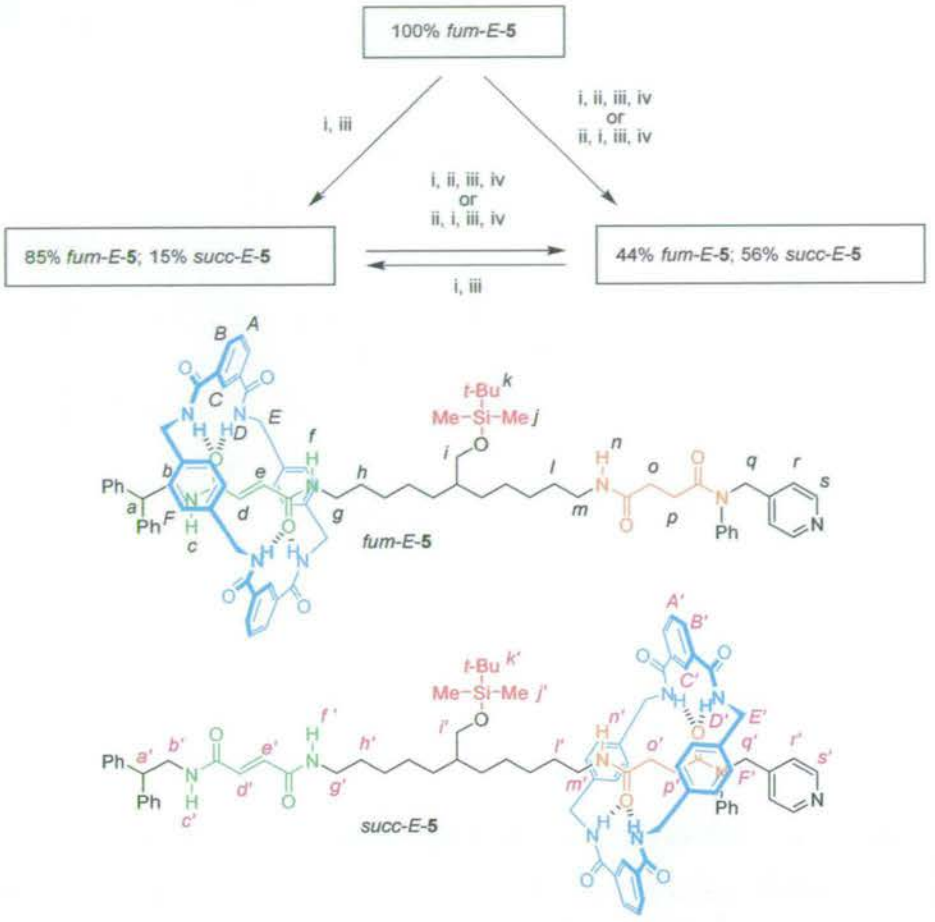

Scheme 2.7 Chemical representation of the operation of machine–substrate system **5**. Reaction conditions: (i) 80% aqueous acetic acid, 60 °C, 1 h; (ii) *hv* at 312 nm (5 × 5 min irradiation),[35] CH_2Cl_2, rt; (iii) TBDMSCl, imidazole, DMAP, CH_2Cl_2, rt, 1 h; (iv) piperidine, CH_2Cl_2, rt, 12 h, quantitative. For full experimental details, see Section 2.9.1.

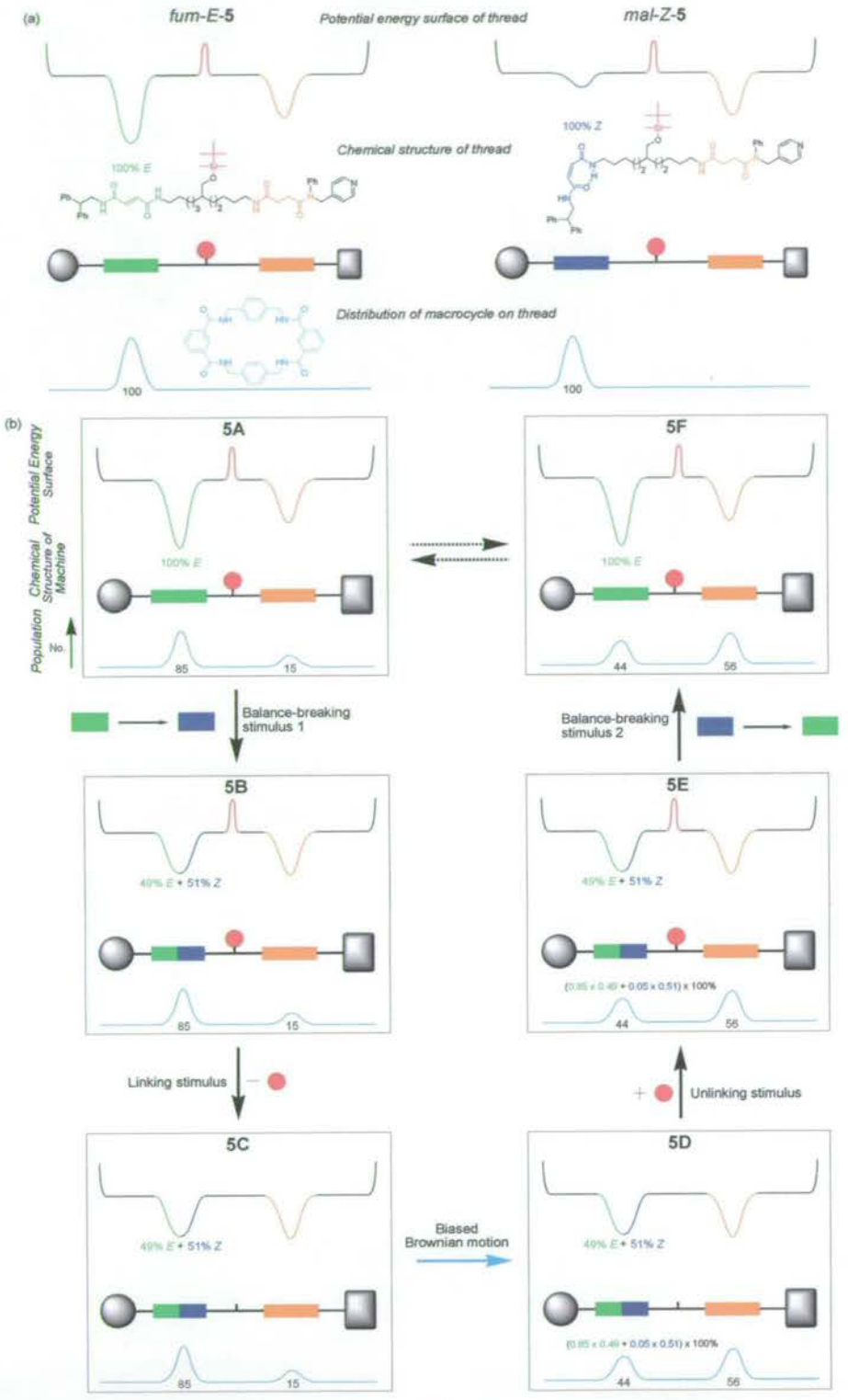

Scheme 2.8 (a) Description of *fum-E*-**5** and *mal-Z*-**5** in covalent, thermodynamic and statistical terms. (b) 'Machine-performance representation' of a compartmentalized molecular machine that can transport a substrate energetically uphill and be reset without undoing the task. **5A:** Initially balanced and unlinked. **5B:** Unbalanced and unlinked. **5C:** Unbalanced and linked (detailed balance is broken). **5D:** Balanced and linked. **5E:** Balanced and unlinked. **5F:** Unbalanced and unlinked. Note the chemical structure of the thread in **5F** is identical to that in **5A** – the machine has been reset – but the population distribution of the macrocycle has changed. The machine has successfully utilized the energy of the photon, via the olefin isomerization reactions, to do the work required to transport the substrate energetically uphill. The stimuli correspond to the reaction conditions given in Scheme 2.7.

The xylylene rings of the macrocycle shield the regions of the thread that they encapsulate and the resulting shifts in the ^{1}H NMR spectra are diagnostic of the position of the macrocycle on the thread.[13j] Thus, the operation of the machine and its effect on the substrate can be followed by ^{1}H NMR spectroscopy (Figure 2.3). In particular, it is instructive to observe the change in intensity of the unoccupied fumaramide station protons $H_{d'}$ and $H_{e'}$ (H_d and H_e in *E*-**6**) during the operation of the machine. In the free thread they appear as a pair of doublets at 6.86 ppm and 7.02 ppm (Figure 2.3a); they are absent in the spectrum of pure *fum*-*E*-**5** (Figure 2.3b); in the statistically balanced (unlinked) system (Figure 2.3c) they account for ~15% of the overall population; in the final ratcheted system (Figure 2.3d) they are ~56% of the reaction mixture.

So, in Scheme 2.8, the two parts of the machine start out (**5A**) statistically balanced (85% of the macrocycles on the fumaramide station; 15% on the succinamide station) and unlinked (and therefore not in equilibrium). A balance-breaking stimulus (*hv* at 312 nm,[35] which generates a 49:51 ± 2% *E*:*Z* photostationary state by ^{1}H NMR, not shown) is applied, giving **5B**. Removal of the barrier ('linking stimulus'; 80% aqueous acetic acid) gives **5C** and allows balance to be restored through moving to equilibrium by biased Brownian motion of the ring (**5D**). Restoring the barrier ('unlinking stimulus'; TBDMSCl, base) makes the system unlinked and not in equilibrium, although statistically balanced (**5E**). The resetting step (a different balance-breaking stimulus; catalytic piperidine, to promote the *Z*→*E* olefin isomerization), makes the system statistically unbalanced, unlinked, and not in equilibrium (**5F**).

After the operational cycle of the machine (i.e. **5F**) the unoccupied fumaramide station protons $H_{d'}$ and $H_{e'}$ account for ~56% of the reaction mixture (Figure 3d).[36] Given that the photostationary state from irradiation of *E*-**5** at 312 nm is 49:51 ± 2% *E*:*Z*, and that the statistically balanced distribution of the macrocycle is 85:15 between the *fum* and *succ* stations of *E*-**5** (Figure 2.3c), the final 44:56 *fum*-*E*-**5**:*succ*-*E*-**5** ratio indicates that the equilibrium distribution of translational isomers between the *mal* and *succ* stations in the de-silylated (linked) derivative of *Z*-**5** is ~5:95 in CH_2Cl_2 at room temperature.[37] The transportation of the macrocycle in **5** is repeatedly reversible between the statistically balanced 85:15 and statistically unbalanced 44:56 ratios of *fum*-*E*-**5** to *succ*-*E*-**5**.[38]

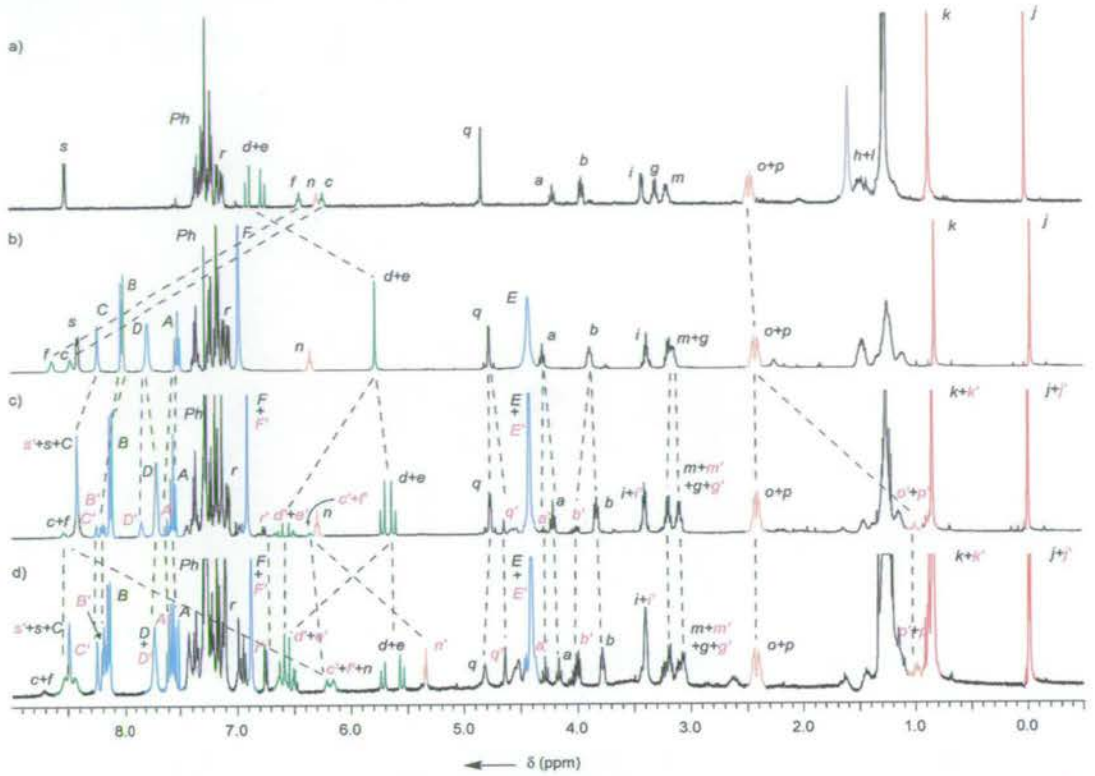

Figure 2.3 ^{1}H NMR Spectra (400 MHz, $CDCl_3$, 298 K) of: (a) free thread *E*-**6**; (b) *fum*-*E*-**5**; (c) statistically balanced *E*-**5**, the 85:15 mixture of *fum*-*E*-**5** and *succ*-*E*-**5** that results from desilylation/resilylation of *fum*-*E*-**5** (Scheme 2.7, (i) and (iii)); (d) 44:56 (± 2%) mixture of *fum*-*E*-**5** and *succ*-*E*-**5** that results from the four step operation of the machine, either starting from *fum*-*E*-**5** or the 85:15 *fum*-*E*-**5**:*succ*-*E*-**5** statistically balanced mixture (Scheme 2.7, (i), (ii), (iii), (iv) or (ii), (i), (iii), (iv); Scheme 2.8, **5A**→**5F**). The ^{1}H NMR assignments and colouring correspond to the labelling in Schemes 2.5 and 2.7. Residual water peaks are shown in grey.

The thread has therefore successfully performed the task of directionally changing the net position of the macrocycle – and since the succinamide station binds the macrocycle more weakly than the fumaramide station, the thread has moved the macrocycle energetically uphill! – while the machine, the thread, has returned to its initial state. We recognize this behaviour as 'ratcheting', a characteristic of the operating mechanism of many biological molecular machines. For the first time, we have a molecular shuttle which is more sophisticated in terms of task performance than a simple mechanical switch. The compartmentalized machine achieves this result by applying four different stimuli which govern in turn the thermodynamics and the kinetics for transport between the two stations: balance-breaking 1; linking; unlinking; balance-breaking 2 (resetting – of the machine, not the substrate).[39]

Through its operation in Schemes 2.7 and 2.8, rotaxane **5** establishes a thermodynamically unfavourable distribution of the macrocycle between the compartments. This is the function envisaged for the pressure demon thought-

machines shown in Figures 2.1b and 2.1d, albeit featuring many machines each acting on one Brownian particle in the case of the rotaxane rather than a single machine acting on many Brownian particles. However, the way in which **5** achieves this result is very different to either Gedankenmaschine design. During the operation of **5** the Brownian particle's position does not determine when or whether the linking stimulus is applied. This would require the communication of information regarding the particle's position to the machine, which *is* possible but would correspond to an 'information ratchet'[25b] mechanism (see Chapter 4 for a molecular realization of this type of mechanism). Rather, the rotaxane machine carries out its operations independent of the position of the particle by varying the potential energy surface minima as well as maxima in a partial so-called 'energy ratchet'[8d, 25b] mechanism (Figure 2.4).

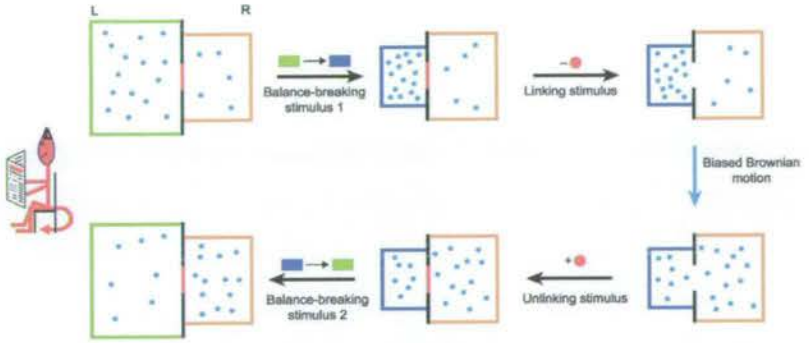

Figure 2.4 The operation of machine–substrate system **5** in Schemes 2.7 or 2.8 is the experimental realization (albeit nonadiabatic) of the transportation task required of Smoluchowski's Trapdoor[5] (Figure 2.1d) and Maxwell's Pressure Demon[4c] (Figure 2.1b). The mechanistic equivalent of the cartoons from Figure 2.1 is shown above. The colours of the compartments, particles and door are the same as the corresponding elements of **5**. The initially balanced (in proportion to the sizes of the two compartments) distribution of the Brownian particles between the left (L) and right (R) compartments becomes statistically unbalanced by a change in volume of the left-hand compartment. Opening the door allows the particles to redistribute themselves according to the new size-ratio of the compartments. Closing the door ratchets the new distribution of particles. Restoring the left-hand compartment to its original size then results in a concentration gradient of the Brownian particles across the two compartments. There is no role for an information-gathering demon in this mechanism.

As mechanical work is done by its operation, is it correct to categorize **5** as a molecular motor? No. Although the machine component of **5** acts to transport a substrate energetically uphill and can be reset without undoing the work done on the substrate, it cannot do so repetitively – a key requirement of a motor – because the succinamide compartment cannot be emptied of the ratcheted substrate. The escapement of the ratcheted quantity is the missing element required for **5** to operate for a second time without undoing the previously performed task by the action of resetting the machine.[40] This feature is present in a previously reported[8d]

[2]catenane, **7**, in which the larger macrocycle acts as a motor that repetitively transports the small macrocycle directionally around itself according to a cyclic reaction scheme (Scheme 2.9, discussed in greater detail in Chapter 3). As with **5**, the olefin isomerization reactions in Scheme 2.9 are balance-breaking steps (depending on where one starts in the scheme, either can be considered to reset the machine); the manipulation of the trityl and silyl protecting groups are pairs of linking–unlinking steps which determine the pathway through which escapement of the ratcheted substrate occurs. Thus, the molecular machine in Scheme 2.9 operates by the following sequence: [balance-breaking 1; escapement (pathway A); ratcheting; balance-breaking 2 (reset machine); escapement (pathway B); ratcheting]$_n$.

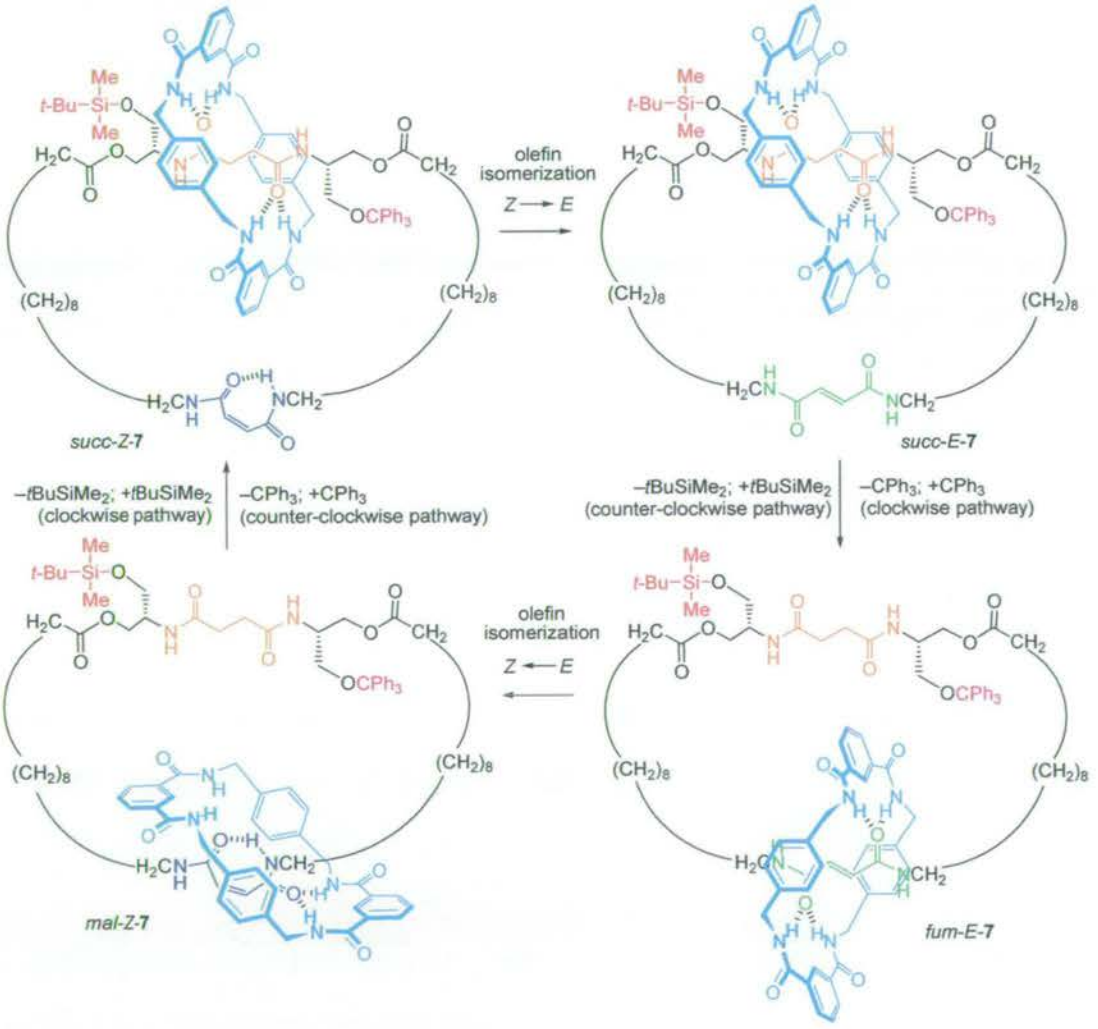

Scheme 2.9 A previously reported[8d] synthetic molecular rotary motor **7** that operates through a full Brownian ratchet mechanism. For a full discussion of this molecule, see Chapter 3.

Although rotaxane **5** does not fulfil the requirements for a motor, neither is it a simple switch since the machine part can be reset without influencing the distribution of the

substrate. Significantly, examining the state of the machine (the rotaxane thread) in **5** does not provide information regarding the state (distribution) of the substrate. It is only from the history of the machine's operations that the distribution of the substrate can be known; in other words, the net position of the macrocycle in rotaxane **5** is a consequence of a form of sequential logic. This type of logic is different to that utilized in most of the Boolean logic chemical systems investigated to date, which feature combinational logic (the outputs are solely a function of the inputs at that moment in time).[41] In fact, the behaviour of **5** is characteristic of a two-state (one bit) memory or 'flip-flop' component in electronics.[42] A flip-flop maintains its effect on a system indefinitely until an input pulse operates on it, causing its output to change to a new indefinitely stable state according to defined rules.[43] Different variants include T-, S-R-, J-K- and D-type flip-flops. We suggest that a molecule such as **5** should be termed a 'two-state' Brownian flip-flop because the substrate must exist in one of two compartments in each molecule. However, there is an important difference that arises because of the statistical nature of a two-state Brownian flip-flop compared to the digital nature of its electronic counterpart. If we wish to utilize the effect of *many* molecules of **5** on a system, the operation of the flip-flop can vary the bulk population distribution of the substrate between the two compartments over a continuum from 85:15 to 44:56 *fum*:*succ* by modifying the balance-breaking reaction parameters (e.g. by changing the time for which the photoisomerization stimulus is applied). If, on the other hand, we use a *single* molecule of **5** to influence a system its effect is strictly binary – the molecule is in one state or the other – with the *fum*:*succ* ratios corresponding to the *probability* that the substrate will be in a particular compartment given the history of the inputs. In contrast, an electronic flip-flop is generally utilized as a single entity in a circuit and its effect is therefore always binary.

2.6 The language necessary to describe the operation and mechanisms of molecular-level mechanical machines

Up to now the categorization of molecules as machines by chemists has largely been iconic – the structures 'look' like pieces of machinery – or they are so-called because they carry out a function that in the macroscopic world would require a machine to perform it.[1] However, as function and mechanism replaces imagery as the driving force behind advances in this field, the use of language needs to become more

phenomenologically based. For this reason, on the basis of the systems described in this Chapter and those developed previously by ourselves, Kelly, Feringa, Stoddart and others,[8, 10, 13–18] we suggest below definitions for four significant phenomenological terms – ratcheting, escapement, balance and linkage – which are crucial for machines that operate by controlled Brownian motion. Ratcheting is an often used, but previously ill-defined, process in chemical terms. Unfortunately, this vagueness has led to the term sometimes being applied to describe phenomena that are unrelated to Brownian ratchet mechanisms. Escapement is the counterpart to ratcheting and, as far as we are aware, has only rarely been used to describe molecular-level events. The statistical balance of a dynamic substrate, and whether the parts of the machine acting on the substrate allow exchange of the substrate or not, appear to be key factors that determine whether the machine can perform a task or not. In fact, it appears that the behaviour of a molecular machine towards a substrate can be defined by the changing relationship (linked/unlinked; balanced/unbalanced) between the parts of machine interacting with the substrate.

(a) 'Ratcheting' is the capturing of a positional displacement of a substrate through the imposition of a kinetic energy barrier which prevents the displacement being reversed when the thermodynamic driving force is removed. The key feature of ratcheting is that the ratcheted part of the system is not linked with (i.e. not allowed to exchange the substrate with) any part of the system that it is ratcheted from. Ratcheting is a crucial requirement for allowing a Brownian machine to be reset without undoing the task it has performed. An example of ratcheting is the unlinking step **5D→5E** in Scheme 2.8. Because it is used to kinetically stabilize an ultimately thermodynamically unfavourable state, ratcheting is intrinsically associated with a sequential logic sequence applied to a Brownian substrate.

(b) 'Escapement' is the (directional) release of a ratcheted substrate in a statistically unbalanced system by lowering a kinetic energy barrier (i.e. by linking). The key feature of escapement is that it requires the linking of two unbalanced parts of a system that were previously unlinked. An escapement step must be subsequently ratcheted in order for a machine to be able to do work repetitively on a substrate. An example of escapement is the de-silylation step during the

operation of the irreversible molecular shuttle *succ1*-**3** (Scheme 2.6, step (i)) or the analogous step for system **5** (**5B**→**5C**, Scheme 2.8).

(c) 'Balance' is the thermodynamically preferred distribution of an exchangeable quantity or substrate over a machine or parts of a machine. The impetus for net transportation of a substrate comes from balance being broken. (Note that 'balance' being broken is not the same as 'detailed balance' being broken; breaking statistical 'balance' provides a thermodynamic driving force for 'detailed balance' to be broken.)

(d) 'Linkage' is the communication necessary for transportation of a substrate to occur between parts of a machine. However, the ability to exchange the substrate between the linked parts is not in itself enough for a task to be performed, there must also be a driving force for it to occur (vide supra). Linking and unlinking operations are purely kinetic parameters and so can be accomplished by simply changing the rate of reactions rather than introducing or removing physical steric barriers.

2.7 Types of compartmentalized molecular machines

During development of the terminology necessary to describe molecular-level behaviour scientifically, the standard dictionary definitions meant for everyday use are not always appropriate for regimes that the definitions were never intended to cover (see Chapter 1). As we have seen through the examples given in this Chapter, the difference between a molecular motor and a molecular switch is fundamental and profound because 'motor' and 'switch' become different phenomenological descriptors at Brownian length scales, not just iconic classifications of macroscopic objects. As another example, simple switches that operate through biasing Brownian motion do not stay in the same state if the thermodynamic driving force is turned off and it is important to distinguish them from other Brownian machines that do. Indeed, we can identify three different fundamental types of simple Brownian machines that act through various combinations of balance-breaking, linking/unlinking, ratcheting and escapement steps – a Brownian switch (Figures 2.5a and 2.5b), a Brownian flip-flop (Figure 2.5c) and a Brownian motor (Figure 2.6). Each of these simple machine

types can also function as components in more complex molecular-level machines (Figure 2.7).

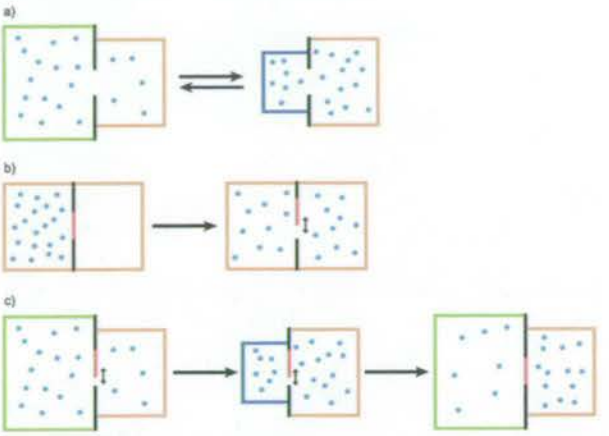

Figure 2.5 Schematic representations of some simple compartmentalized molecular-level machines. (a) A two-state Brownian switch. (b) An irreversible Brownian switch. (c) A two-state Brownian flip-flop (shown operating through a partial energy ratchet mechanism; other mechanisms can achieve the same machine function).

(a) A 'Two-state (or multi-state) Brownian switch' is a machine that can reversibly change the distribution of a Brownian substrate (a moiety which undergoes Brownian motion) between two (or more) distinguishable sites as a function of state of the machine. It does this by biasing the Brownian motion of the substrate (Figure 2.5a). Classic stimuli-responsive molecular shuttles, such as *E*/*Z*-**1** (Scheme 2.1) and those listed in refs. [13-18, 20], are examples of two-state (or three-state[14]) Brownian switches. An 'irreversible Brownian switch' is a 'once only' machine, such as *succ1*-**3** (Scheme 2.6), which irreversibly changes the distribution or position of a Brownian substrate in response to an external stimulus (Figure 2.5b).

(b) A 'Two-state (or multi-state) Brownian flip-flop' is a machine that can reversibly change the distribution of a Brownian substrate between two (or more) distinguishable sites and can be reset without restoring the original distribution of the substrate (Figure 2.5c). The statistical distribution of the substrate cannot be determined from the state of the flip-flop (unlike a switch, which influences a substrate as a function of state) but rather is determined by the history of operation of the machine, i.e. through a form of sequential logic. Rotaxane **5** is an example of a two-state Brownian flip-flop. It operates through a partial Brownian ratchet mechanism[44] consisting of the following steps applied to a pair of compartments: balance breaking, escapement, ratcheting,

and resetting of the machine (a second balance-breaking step). The original substrate distribution is restored by an escapement–unlinking sequence.

(c) A 'Brownian motor' is a machine that can repetitively and progressively change the distribution of a Brownian substrate, during which the machine is reset without restoring the original distribution of the substrate (Figure 2.6). Like a flip-flop, a Brownian motor affects a system as a function of the pathway that the machine takes, not as a function of state. Catenane **7** (Scheme 2.9) is an example of a two-stroke rotary Brownian motor (Figure 2.6a).[8d] The substrate is repetitively transported between two sites via two alternating pathways. We shall shortly report on the synthesis and operation of a linear three compartment Brownian motor (Figure 2.6b).[45]

(d) By combining the three fundamental Brownian machine types, which work through combinations of balance breaking, linking/unlinking, ratcheting and escapement, with other combinational and/or sequential operations based on Boolean logic, machines that can carry out more complex functions, such as variable, directional, travel (Figure 2.7a) and 'sorting and separating' (Figure 2.7b), can be envisaged.

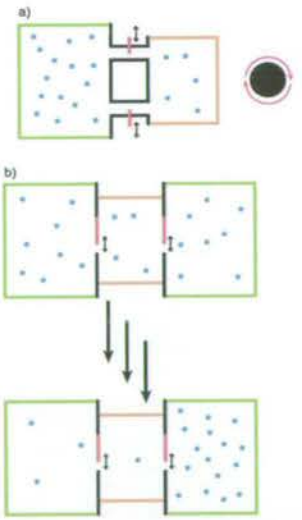

Figure 2.6 Schematic representations of two types of Brownian motors: (a) a two-stroke rotary motor; (b) a three-compartment translational motor or pump.

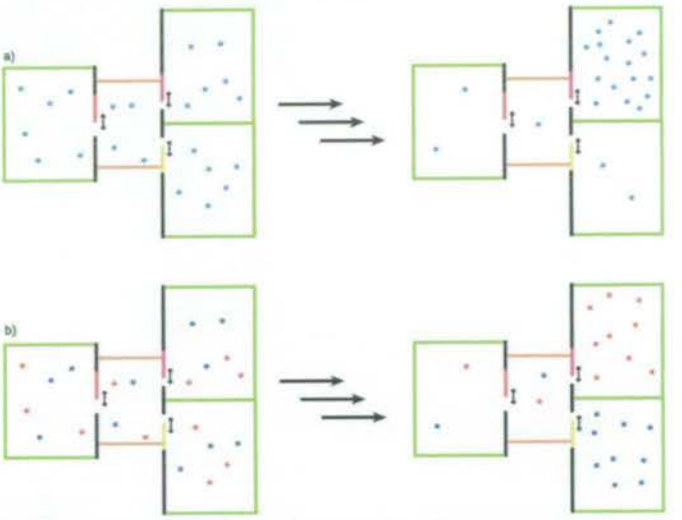

Figure 2.7 Schematic representations of some possible compartmentalized molecular-level machines that combine ratcheting and escapement with Boolean logic operations: (a) a four-compartment Brownian machine that pumps a substrate in a given (variable) direction. Deciding which one of the pink or yellow gates is used for ratcheting determines whether the substrate is transported to the top compartment or the bottom. (b) A four-compartment Brownian machine that sorts and separates different ions (e.g. red = Na^+; blue = K^+). A logic operation providing selective access through each of the pink and yellow gates ensures one type of ion is pumped into each compartment.

2.8 Conclusions

Apart from allowing a large amplitude one-dimensional motion to be considered independently of other movements, there is nothing special about rotaxanes in terms of mechanical mechanisms.[12, 46] The relationships described in this paper are applicable to any type of molecular-level construct, with controlled motion possible in a kinetically-associated structure in two or three dimensions as well as just one. They may also be useful in understanding the changes involved in biological machines as they bring about movement, function and the transport of Brownian substrates (molecules and ions) in 1-D channels, across membranes and between parts of a protein.

To appreciate the technological potential of controlled molecular-level motion one only has to consider that it lies at the heart of virtually every biological process. When we learn how to build synthetic structures that can rectify random dynamic processes and interface their effects directly with other molecular-level substructures and the outside world, it will add a new dimension to functional molecule and materials design. An improved understanding of biological pumps, motors and other cellular machines will surely also follow.

2.9 Experimental section

2.9.1 Experimental procedures for the operation of machine–substrate systems 3 and 5

Machine–substrate system 3

Step (i). A solution of [2]rotaxane *succ1*-**3** (80 mg, 0.057 mmol) in aqueous acetic acid (80%, 10 mL) was heated at 60 °C for 1 h. The reaction mixture was concentrated under reduced pressure and traces of acetic acid were removed with a toluene azeotrope (3 × 50 mL). To remove non-rotaxane impurities, the crude reaction mixture was filtered through a plug of silica gel (neat dichloromethane then methanol/dichloromethane, 5:95) and the solvent was removed under reduced pressure to furnish fully de-silylated material.

Step (ii). The de-silylated product from step (i) was dissolved in dichloromethane (20 mL) and treated with imidazole (70 mg, 1.0 mmol), *tert*-butyldimethylsilyl chloride (90 mg, 0.60 mmol) and a catalytic amount (5.0 mg) of 4-(dimethylamino)pyridine. The mixture was stirred at room temperature for 1 h. To remove non-rotaxane impurities, the crude reaction mixture was filtered through a plug of silica gel (neat dichloromethane then methanol/dichloromethane, 2:98) and the solvent removed under reduced pressure. The ^{1}H NMR spectrum in $CDCl_3$ of the isomeric mixture of *succ1*-**3** and *succ2*-**3** resulting from this two step operation is shown in Figure 2.2c.

Machine–substrate system 5

Step (i). A solution of [2]rotaxane *fum-E*-**5** (30 mg, 0.021 mmol) in aqueous acetic acid (80%, 2.0 mL) was heated at 60 °C for 1 h. The reaction mixture was concentrated under reduced pressure and traces of acetic acid were removed with a toluene azeotrope (3 × 5 mL). To remove non-rotaxane impurities the crude reaction mixture was filtered through a plug of silica gel (neat dichloromethane then methanol/dichloromethane, 5:95) and the solvent was removed under reduced pressure to furnish fully de-silylated material.

Step (ii). A solution of the de-silylated product from step (i) (20 mg) in dichloromethane (50 mL) was placed in a quartz vessel, degassed with argon (15 min), and irradiated at 312 nm using a multilamp photoreactor for five successive 5 min sessions. The progress of the reaction was monitored by ^{1}H NMR spectroscopy. The photostationary state was reached after 20 min (4 × 5 min irradiations). The

reaction mixture was concentrated under reduced pressure and used directly in the next step.

Step (iii). The de-silylated photoisomerized material (20 mg) was dissolved in dichloromethane (2.0 mL) and treated with imidazole (20 mg, 0.29 mmol), *tert*-butyldimethylsilyl chloride (26 mg, 0.17 mmol) and a catalytic amount (5.0 mg) of 4-(dimethylamino)pyridine. The reaction mixture was stirred for 2 h, during which time a colourless precipitate appeared. Water (2 mL) was added and the reaction mixture extracted with dichloromethane (5 mL). The organic layer was separated, washed with brine (sat., 5 mL), dried (Na_2SO_4) and concentrated under reduced pressure to furnish the crude re-silylated isomeric mixture of rotaxanes. To remove non-rotaxane impurities, the mixture was filtered through a plug of silica gel (ethyl acetate/petroleum ether, 1:4 then methanol/dichloromethane, 1:4). This mixture was concentrated under reduced pressure and used directly in the next step.

Step (iv). To a solution of the re-silylated isomeric mixture of four rotaxanes from step (iii) (20 mg) in dichloromethane (1.0 mL) was added piperidine (100 μL, 1.0 mmol). The reaction was stirred for 12 h. To remove non-rotaxane impurities, the crude reaction mixture was filtered through a plug of silica gel (neat dichloromethane then methanol/dichloromethane, 1:4) and the solvent removed under reduced pressure. The ^{1}H NMR spectrum in $CDCl_3$ of the isomeric mixture of *fum-E*-**5** and *succ-E*-**5** obtained after the four step operation is shown in Figure 2.3d. An essentially identical ^{1}H NMR spectrum was obtained upon reversing the sequence of steps (i) and (ii).

2.9.2 Synthesis

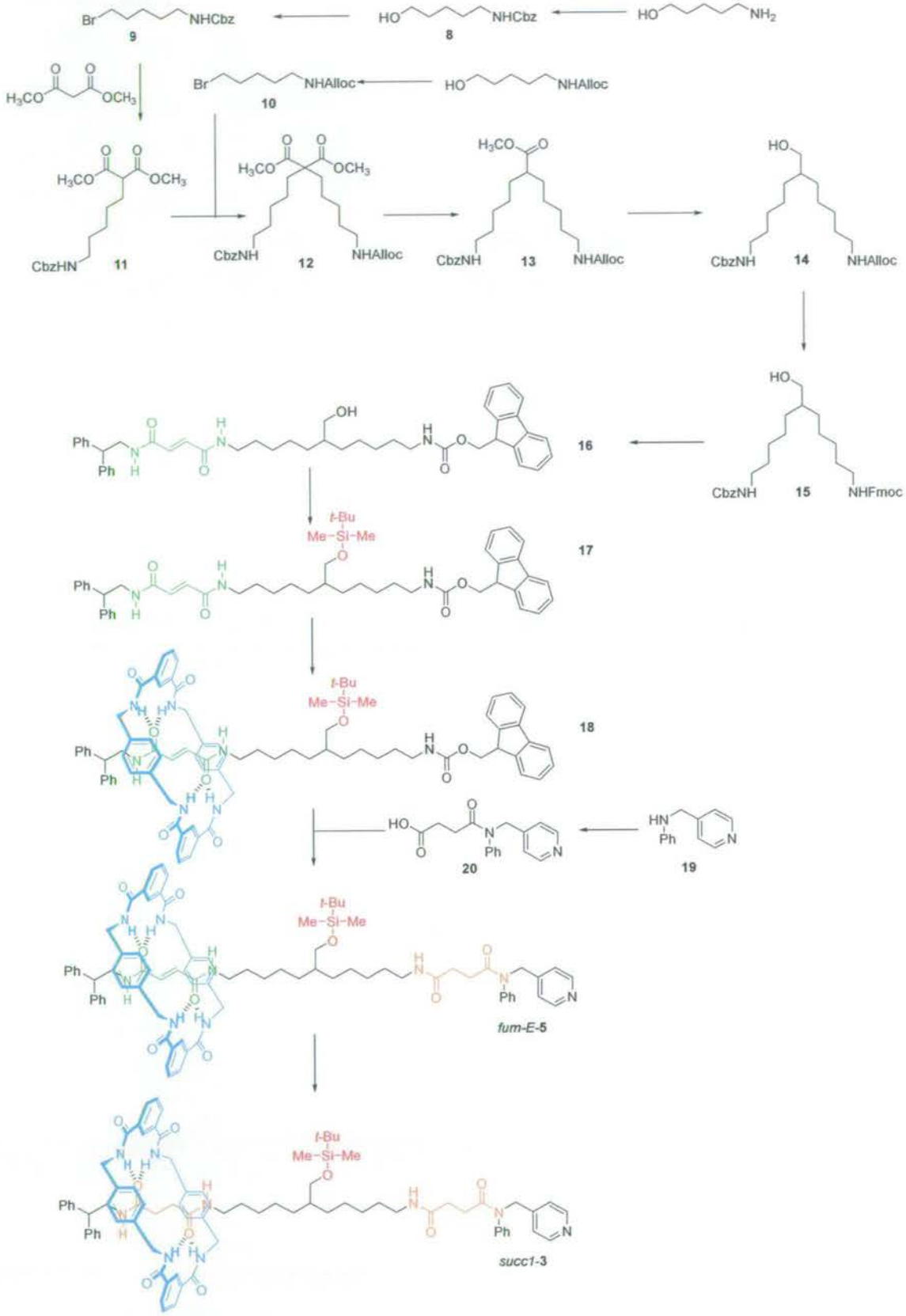

Scheme 2.10 Synthesis of single translational isomer [2]rotaxanes *succ1*-**3** and *fum-E*-**5**.

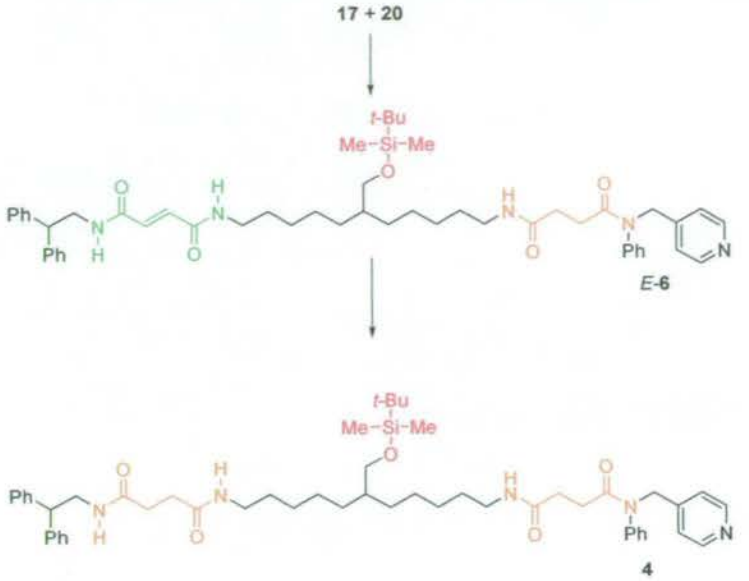

Scheme 2.11 Synthesis of thread molecules *E*-**7** and **5**.

Benzyl (5-hydroxypentyl)carbamate (8)[47]

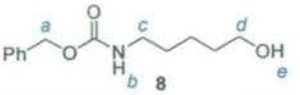

To a solution of 5-aminopentanol (12.4 g, 120 mmol) and sodium hydrogen carbonate (30.2 g, 360 mmol) in water (120 mL) was added a solution of benzylchloroformate (27.5 g, 162 mmol) in tetrahydrofuran (120 mL) at 0 °C. The reaction mixture was warmed to room temperature and stirred vigorously for 12 h. The organic layer was separated and the aqueous layer extracted with ethyl acetate (2 × 70 mL). The combined organics were washed with brine (sat., 200 mL), dried (Na_2SO_4) and concentrated under reduced pressure. The crude product was triturated with *n*-hexane. The resulting powder was collected by filtration, washed with diethyl ether and dried under reduced pressure to afford **8** as a colourless low melting solid (27.5 g, 97%); mp 43-44 °C; ^{1}H NMR (400 MHz, $CDCl_3$): δ = 7.37-7.29 (m, 5H, H_{Ph}), 5.09 (s, 2H, H_a), 4.82 (br t, 1H, H_b), 3.63 (t, J = 6.4 Hz, 2H, H_d), 3.23-3.18 (m, 2H, H_c), 1.62 (br s, 1H, H_e), 1.61-1.35 (m, 6H, alkyl CH_2); ^{13}C NMR (100 MHz, $CDCl_3$): δ = 156.5 (C=O), 136.5 (ArC_q), 128.4 (ArCH), 128.0 (2 × ArCH), 66.5 ($CH_{2(a)}$), 62.3 ($CH_{2(d)}$), 40.8 ($CH_{2(c)}$), 32.0 (CH_2), 29.6 (CH_2), 22.8 (CH_2); HRMS (EI): m/z = 237.1364 [$M^{+\bullet}$] (anal. calcd for $C_{13}H_{19}NO_3^{+\bullet}$: m/z = 237.1364).

Benzyl (5-bromopentyl)carbamate (9)[48]

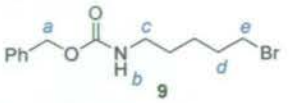

9

Alcohol **8** (28.0 g, 118 mmol) in dichloromethane (800 mL) was cooled to 0 °C. Tetrabromomethane (59.0 g, 177 mmol) and triphenylphosphine (46.5 g, 177 mmol) were added in portions and the solution was allowed to warm to room temperature. The reaction was stirred for a further 4 h after which time TLC indicated complete consumption of the starting material. The reaction was quenched by addition of water (400 mL) and the organic layer was separated, washed with water (400 mL) and brine (sat., 400 mL) then dried (Na_2SO_4). Solvent was removed under reduced pressure and the crude material purified by flash chromatography (SiO_2; ethyl acetate/petroleum ether, 1:9 to 3:7) to furnish bromide **9** as colourless low melting solid (29.0 g, 82%); mp 44-45 °C; ^{1}H NMR (400 MHz, $CDCl_3$): δ = 7.36-7.30 (m, 5H, H_{Ph}), 5.09 (s, 2H, H_a), 4.85 (br s, 1H, H_b), 3.39 (t, J = 6.7 Hz, 2H, H_e), 3.22-3.17 (m, 2H, H_c), 1.86 (quint., 2H, J = 6.9 Hz, H_d), 1.56-1.42 (m, 4H, alkyl CH_2); ^{13}C NMR (100 MHz, $CDCl_3$): δ = 156.3 (C=O), 136.5 (ArC_q), 128.5 (ArCH), 128.0 (2 × ArCH), 66.6 ($CH_{2(a)}$), 40.7 ($CH_{2(c)}$), 33.5 ($CH_{2(e)}$), 32.2 (CH_2), 29.1 (CH_2), 25.2 (CH_2); HRMS (EI): m/z = 299.0517 and 301.0405 [$M^{+\bullet}$] (anal. calcd for $C_{13}H_{18}NO_2{}^{79}Br^{+}$: m/z = 299.0521 and for $C_{13}H_{18}NO_2{}^{81}Br^{+\bullet}$: m/z = 301.0502).

Allyl (5-bromopentyl)carbamate (10)

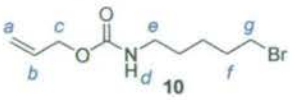

10

5-(Allyloxycarbonylamino)-1-pentanol (Fluka, UK) (22.0 g, 117 mmol) in dichloromethane (800 mL) was cooled to 0 °C. Tetrabromomethane (58.5 g, 176 mmol) and triphenylphosphine (46.5 g, 177 mmol) were added in portions and the solution was allowed to warm to room temperature. The reaction was stirred for an additional 4 h after which time TLC indicated complete consumption of the starting material. The reaction was quenched by addition of water (200 mL) and the organic layer was separated, washed with water (400 mL) and brine (sat., 400 mL), then dried (Na_2SO_4). Solvent was removed under reduced pressure and the crude material was purified by flash chromatography (SiO_2; ethyl acetate/petroleum ether, 1:9 to 3:7) to furnish bromide **10** as a colourless oil (27.0 g, 93%); ^{1}H NMR (400 MHz, $CDCl_3$): δ

= 5.85-5.75 (m, 1H, H_b), 5.20-5.07 (m, 2H, H_a & H_d), 5.08 (d, J = 10.4 Hz, 1H, $H_{a'}$), 4.43 (d, J = 5.4 Hz, 2H, H_c), 3.30 (t, J = 6.8 Hz, 2H, H_g), 3.07 (q, J = 6.4 Hz, 2H, H_e), 1.76 (quint., J = 7.0 H, 2H, H_f), 1.47-1.32 (m, 4H, alkyl CH_2); ^{13}C NMR (100 MHz, $CDCl_3$): δ = 156.1 (C=O), 132.7 (CH_b), 117.1 ($CH_{2(a)}$), 65.0 ($CH_{2(c)}$), 40.4 ($CH_{2(e)}$), 33.3 ($CH_{2(g)}$), 32.0 (CH_2), 28.7 (CH_2), 24.9 (CH_2); HRMS (EI): m/z = 249.0446 and 251.0345 [$M^{+\bullet}$] (anal. calcd for $C_9H_{16}NO_2{}^{79}Br^{+\bullet}$: m/z = 249.0364 and for $C_9H_{16}NO_2{}^{81}Br^{+\bullet}$: m/z = 251.0345).

Dimethyl (5-{[(benzyloxy)carbonyl]amino}pentyl)malonate (11)

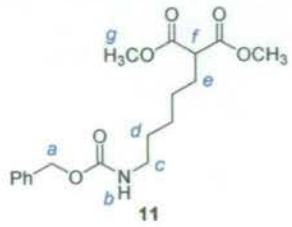

11

Dimethyl malonate (23.8 g, 181 mmol) was added to a suspension of sodium hydride (5.41 g, 60.0% w/w in oil, 135 mmol) in tetrahydrofuran (250 mL) over 1 h, keeping the reaction at 0 °C, resulting in formation of a gel. The reaction mixture was allowed to warm to ambient temperature and was then heated to 40 °C to dissolve the gel. The reaction mixture was allowed to stir for further 1 h at this temperature. Tetrabutylammonium iodide (333 mg, 0.903 mmol) was added, followed by dropwise addition of a solution of bromide **9** (27.0 g, 90.3 mmol) in tetrahydrofuran (250 mL). After addition was complete, the reaction mixture was refluxed for 12 h during which time a solid precipitated. The reaction mixture was filtered, and the solid precipitate washed with tetrahydrofuran. The resulting liquors were then quenched with NH_4Cl (sat. aq., 200 mL). The organic layer was separated and washed with brine (sat., 200 mL), then dried (Na_2SO_4) and concentrated under reduced pressure. The resulting oil was purified by flash chromatography (SiO_2; ethyl acetate/petroleum ether, 1:4 to 2:3) to furnish unreacted dimethyl malonate (6.00 g, 45.5 mmol) and the desired compound **11** as colourless oil (28.0 g, 88%); ^1H NMR (400 MHz, $CDCl_3$): δ = 7.29-7.25 (m, 5H, H_{Ph}), 5.08 (br t, 1H, H_b), 5.03 (s, 2H, H_a), 3.67 (s, 6H, H_g), 3.30 (t, J = 7.5 Hz, 1H, H_f), 3.14-3.07 (m, J = 6.3 Hz, 2H, H_c), 1.86-1.84 (m, 2H, H_e), 1.44-1.42 (m, 2H, H_d), 1.28-1.25 (m, 4H, alkyl CH_2); ^{13}C NMR (100 MHz, $CDCl_3$): δ = 169.6 (ester C=O), 156.2 (carbamate C=O), 136.5 (ArC_q), 128.3 (ArCH), 127.8 (2 × ArCH), 66.3 ($CH_{2(a)}$), 52.2 (CH_3), 51.3 (CH_f), 40.6 ($CH_{2(c)}$), 29.4 (CH_2), 28.5 (CH_2), 26.7

(CH_2), 26.1 (CH_2); HRMS (FAB, 3-NOBA matrix): m/z = 352.1764 [$(M+H)^+$] (anal. calcd for $C_{18}H_{26}NO_6^+$: m/z = 352.1760).

Dimethyl (5-{[(allyloxyoxy)carbonyl]amino}pentyl)(5-{[(benzyloxy)carbonyl]amino}pentyl)malonate (12)

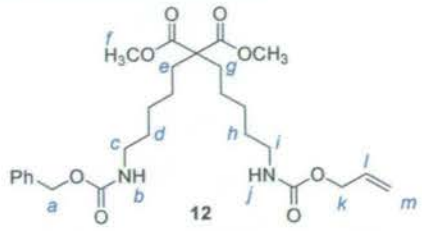

Malonate **11** (22.0 g, 62.7 mmol) was added to a suspension of sodium hydride (3.60 g, 60.0% w/w in oil, 94.0 mmol) in tetrahydrofuran (300 mL) over 1 h, keeping the reaction temperature at 0 °C. The reaction mixture was allowed to warm to room temperature and was stirred for a further 1 h. Tetrabutylammonium iodide (255 mg, 0.690 mmol) was added, followed by dropwise addition of a solution of bromide **10** (17.0 g, 69.0 mmol) in tetrahydrofuran (250 mL). After complete addition, the reaction mixture was refluxed for 12 h, during which time a solid precipitated. The reaction mixture was filtered and the solid precipitate washed with tetrahydrofuran. The resulting liquors were then quenched with NH_4Cl (sat. aq., 200 mL). The phases were separated, and the aqueous layer extracted with ethyl acetate (200 mL). The combined organics were washed with brine (sat., 200 mL), dried (Na_2SO_4) and concentrated under reduced pressure to furnish an oil which was purified by flash chromatography (SiO_2; ethyl acetate/petroleum ether, 1:4 to 2:3) to furnish compound **12** as a colourless oil (19.0 g, 58%); ^{1}H NMR (400 MHz, $CDCl_3$): δ = 7.31-7.27 (m, 5H, H_{Ph}), 5.89-5.81 (m, 1H, H_l), 5.24 (d, J = 16.3 Hz, 1H, H_m), 5.15 (d, J = 10.3 Hz, 1H, $H_{m'}$), 5.04 (s, 2H, H_a), 4.95 (br s, 2H, H_b & H_j), 4.50 (m, 2H, H_k), 3.65 (s, 6H, H_f), 3.13-3.10 (m, 4H, H_c & H_i), 1.83-1.79 (m, 4H, H_e & H_g), 1.45 (br s, 4H, H_d & H_h), 1.31-1.24 (m, 4H, alkyl CH_2), 1.15-1.08 (m, 4H, alkyl CH_2); ^{13}C NMR (100 MHz, $CDCl_3$): δ = 172.1 (ester C=O), 156.3 (benzyl carbamate C=O), 156.1 (allyl carbamate C=O), 136.5 (ArC_q), 132.9 (CH_l), 128.3 (ArCH), 127.9 (2 × ArCH), 117.3 ($CH_{2(m)}$), 66.3 ($CH_{2(a)}$), 65.2 ($CH_{2(k)}$), 57.3 ($C_q(CO_2CH_3)_2$), 52.2 (CH_3), 40.72 ($CH_{2(c\ or\ i)}$), 40.67 ($CH_{2(c\ or\ i)}$), 32.2 (2 × CH_2), 29.5 (2 × CH_2), 26.7 (2 × CH_2), 23.6 (2 × CH_2); HRMS (FAB, 3-NOBA matrix): m/z = 521.2854 [$(M+H)^+$] (anal. calcd for $C_{27}H_{41}N_2O_8^+$: m/z = 521.2863).

Methyl 7-{[(allyloxy)carbonyl]amino}-2-(7-{[(benzyloxy)carbonyl]amino}pentyl)heptanoate (13)

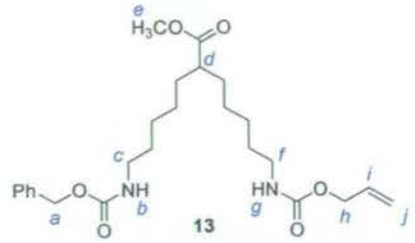

Diester **12** (8.00 g, 15.4 mmol) was dissolved in dimethyl sulfoxide (30 mL). Anhydrous lithium chloride (1.90 g, 46.1 mmol) and water (304 µL, 16.9 mmol) were added and the reaction mixture was heated at 160 °C for 4 h. The reaction mixture was allowed to cool to ambient temperature and was then diluted with water (135 mL). The mixture was extracted with diethyl ether (3 × 130 mL). The combined organic layers were washed with water (3 × 400 ml) and brine (sat., 350 mL), then dried (Na_2SO_4) and concentrated under reduced pressure. The crude oil was purified by flash chromatography (SiO_2; ethyl acetate/petroleum ether, 1:4 to 2:3) to furnish monoester **13** as a colourless oil (4.70 g, 66%); ^{1}H NMR (400 MHz, $CDCl_3$): δ = 7.34-7.25 (m, 5H, H_{Ph}), 5.98-5.86 (m, 1H, H_i), 5.30 (d, J = 17.2 Hz, 1H, H_j), 5.20 (d, J = 10.3 Hz, 1H, $H_{j'}$), 5.08 (s, 2H, H_a), 4.74 (br s, 2H, H_b & H_g), 4.54 (d, J = 5.0 Hz, 2H, H_h), 3.65 (s, 3H, H_e), 3.17-3.14 (m, 4H, H_c & H_f), 2.31-2.29 (m, 1H, H_d), 1.47-1.13 (m, 16H, alkyl CH_2); ^{13}C NMR (100 MHz, $CDCl_3$): δ = 176.8 (ester C=O), 156.3 (benzyl carbamate C=O), 156.2 (allyl carbamate C=O), 136.6 (ArC_q), 133.0 (CH_i), 128.5 (ArCH), 128.1 (2 × ArCH), 117.6 ($CH_{2(j)}$), 66.6 ($CH_{2(a)}$), 65.4 ($CH_{2(h)}$), 51.4 (CH_3), 45.4 (CH_d), 40.93 ($CH_{2(c\ or\ f)}$), 40.89 ($CH_{2(c\ or\ f)}$), 32.3 (2 × CH_2), 29.8 (2 × CH_2), 27.0 (2 × CH_2), 26.6 (2 × CH_2); HRMS (FAB, 3-NOBA matrix): m/z = 463.2808 [$(M+H)^+$] (anal. calcd for $C_{25}H_{39}N_2O_6^+$, m/z = 463.2808).

Allyl benzyl [6-(hydroxymethyl)undecane-1,11-diyl]biscarbamate (14)

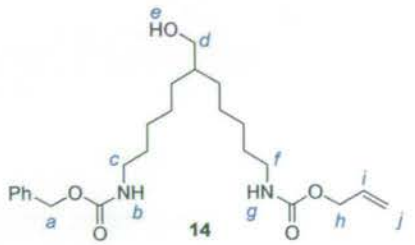

Di-isobutylaluminium hydride (43 mL, 1.0 M in toluene, 43 mmol) was added dropwise to a solution of ester **13** (5.00 g, 10.8 mmol) in freshly distilled

tetrahydrofuran (60 mL) at –78 °C under argon. The reaction mixture was stirred at this temperature for 4 h, after which time TLC indicated complete consumption of the starting material. Methanol (30 mL) was added to quench the reaction and the mixture was brought to room temperature. Citric acid (10 % aq., 120 mL) was added to bring the reaction mixture to pH 3, resulting in the formation of two layers. The organic layer was separated and the aqueous layer extracted with diethyl ether (2 × 120 mL). The combined organics were washed with brine (sat., 200 mL), dried (Na_2SO_4) and concentrated under reduced pressure to furnish the crude product as an oil which was purified by flash chromatography (SiO_2; ethyl acetate/petroleum ether, 3:7 to 2:3) to give alcohol **14** as an oil which solidified on standing to a low melting, colourless solid (3.20 g, 68%); mp 44-46 °C; ^{1}H NMR (400 MHz, $CDCl_3$): δ = 7.34-7.25 (m, 5H, H_{Ph}), 5.95-5.86 (m, 1H, H_i), 5.29 (d, J = 17.2 Hz, 1H, H_j), 5.20 (d, J = 10.4 Hz, 1H, $H_{j'}$), 5.08 (s, 2H, H_a), 4.82-4.79 (br s, 2H, H_b & H_g), 4.54 (d, J = 5.3 Hz, 2H, H_h), 3.51 (d, J = 5.3 Hz, 2H, H_d), 3.20-3.14 (m, 4H, H_c & H_f), 1.49-1.13 (m, 17H, alkyl CH_2 & alkyl CH); ^{13}C NMR (100 MHz, $CDCl_3$): δ = 156.4 (benzyl carbamate C=O), 156.3 (allyl carbamate C=O), 136.6 (ArC_q), 132.9 (CH_i), 128.5 (ArCH), 128.0 (2 × ArCH), 117.5 ($CH_{2(j)}$), 66.5 ($CH_{2(a)}$), 65.4 ($CH_{2(h)}$), 65.3 ($CH_{2(d)}$), 40.92 ($CH_{2(c\ or\ f)}$), 40.87 ($CH_{2(c\ or\ f)}$), 40.2 ($CHCH_2OH$), 30.7 (2 × CH_2), 29.8 (2 × CH_2), 26.9 (2 × CH_2), 26.3 (2 × CH_2); HRMS (FAB, 3-NOBA matrix): m/z = 435.2852 [$(M+H)^+$] (anal. calcd for $C_{24}H_{39}N_2O_5^+$: m/z = 435.2860).

Benzyl 9*H*-fluoren-9-ylmethyl [6-(hydroxymethyl)undecane-1,11-diyl]biscarbamate (15)

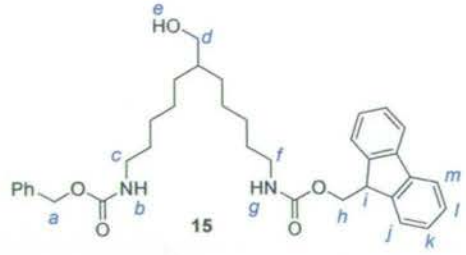

Phenylsilane (746 mg, 6.89 mmol) and a solution of tetrakis(triphenylphosphine)palladium(0) (80.0 mg, 69.2 nmol) in dry dichloromethane (60 mL) were added under nitrogen to a solution of alcohol **14** (1.50 g, 3.45 mmol) in dry dichloromethane (10 mL). The mixture was stirred for 45 min during which time the light yellow solution turned brown and the disappearance of

starting material was monitored by TLC. 9-Fluorenylmethylchloroformate (1.00 g, 3.88 mmol) and triethylamine (1.30 g, 13.0 mmol) were added to the above reaction mixture. The reaction was allowed to stir for 45 min and before being quenched with water (20 mL). Hydrochloric acid (1 N, 4 mL) was added and the organic layer was separated, washed with brine (sat., 10 mL), dried (Na_2SO_4) and concentrated under reduced pressure. The resulting crude brown foam was purified by flash chromatography (SiO_2; ethyl acetate/petroleum ether, 3:7 then 1:1 to 7:3). Appropriate fractions were concentrated to obtain a semi-solid which on trituration with diethyl ether furnished the desired alcohol, **15** as an off-white solid (1.10 g, 56%); mp 94-96 °C; ^{1}H NMR (400 MHz, $CDCl_3$): δ = 7.77 (d, 2H, J = 7.6 Hz, H_m), 7.60 (d, J = 7.6 Hz, 2H, H_j), 7.41 (t, J = 7.6 Hz, 2H, H_l), 7.36-7.30 (m, 7H, H_{Ph} & H_k), 5.10 (s, 2H, H_a), 4.85-4.82 (m, 2H, H_b & H_g), 4.40 (d, J = 6.9 Hz, 2H, H_h), 4.22 (t, J = 6.9 Hz, 1H, H_i), 3.52 (d, J = 5.3 Hz, 2H, H_d), 3.21-3.16 (m, 4H, H_c & H_f), 1.50-1.25 (m, 17H, alkyl CH_2 & alkyl CH); ^{13}C NMR (100 MHz, $CDCl_3$): δ = 156.41 (C=O), 156.37 (C=O), 144.0 (Fmoc ArC_q), 141.2 (Fmoc ArC_q), 136.6 (phenyl ArC_q), 128.5 (phenyl ArCH), 128.1 (2 × phenyl ArCH), 127.6 ($ArCH_l$), 127.0 ($ArCH_k$), 125.0 ($ArCH_j$), 119.9 ($ArCH_m$), 66.5 ($CH_{2(h)}$), 66.4 ($CH_{2(a)}$), 65.3 ($CH_{2(d)}$), 47.2 (CH_i), 40.9 ($CH_{2(c)}$ & $CH_{2(f)}$), 40.3 ($CHCH_2OH$), 30.7 (2 × CH_2), 29.8 (2 × CH_2), 27.0 (2 × CH_2), 26.3 (2 × CH_2); HRMS (FAB, 3-NOBA matrix): m/z = 573.3332 [$(M+H)^+$] (anal. calcd for $C_{35}H_{45}N_2O_5^+$: m/z = 573.3338).

9*H*-Fluoren-9-ylmethyl [11-{[(2*E*)-4-(diphenylethylamino)-4-oxobut-2-enoyl]amino}-6-(hydroxymethyl)undecyl]carbamate (16)

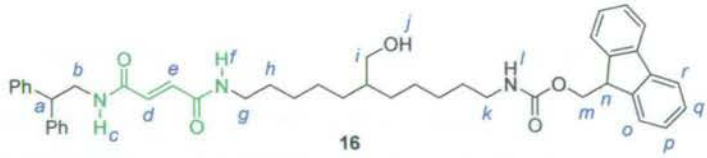

16

To a solution of **15** (740 mg, 1.28 mmol) in methanol (10 mL) was added ethereal hydrochloric acid (1.0 M, 2.7 mL) and 10% Pd/C (150 mg). The mixture was stirred under an atmosphere of hydrogen (1 atm) for 1 h. The reaction mixture was filtered through Celite, washed with methanol (15 mL) and concentrated under reduced pressure to furnish a colourless solid on cooling, which was used without any further purification. (*E*)-3-(2,2-Diphenylethylcarbamoyl)acrylic acid[13j] (535 mg, 1.80 mmol) was dissolved in dichloromethane (10 mL) and the solution was cooled to 0 °C. 1-[3-

Dimethylaminopropyl]-3-ethylcarbodiimide hydrochloride (433 mg, 2.20 mmol), 1-hydroxybenzotriazole hydrate (345 mg, 2.20 mmol) and triethylamine (333 mg, 3.20 mmol) were added at 0 °C and the reaction mixture was allowed to warm to room temperature and stir for 30 min. A solution of the above amine hydrochloride in dichloromethane (15 mL) and triethylamine (210 mg, 2.01 mmol) was added to the activated acid. The reaction mixture was stirred for 4 h, diluted with chloroform (15 mL) and washed with hydrochloric acid (1 N, 10 mL), resulting in formation of a precipitate. The solid was removed by filtration, and the organic layer was washed with sodium hydrogen carbonate (sat. aq., 15 mL). The organic layer was further washed with brine (sat., 10 mL), dried (Na_2SO_4) and concentrated under reduced pressure. The crude material was purified by flash chromatography (SiO_2; ethyl acetate/petroleum ether, 1:1 then methanol/dichloromethane, 2:98) to furnish compound **16** as a colourless solid (550 mg, 60%); mp 116-118 °C; ^{1}H NMR (400 MHz, $CDCl_3$): δ = 7.77 (d, J = 7.5 Hz, 2H, H_r), 7.59 (d, J = 7.4 Hz, 2H, H_o), 7.40 (t, J = 7.5 Hz, 2H, H_q), 7.32-7.18 (m, 12H, H_{Ph} & H_p), 6.93 (d, J = 14.9 Hz, 1H, $H_{d\text{ or }e}$), 6.75 (d, J = 14.9 Hz, 1H, $H_{d\text{ or }e}$), 6.47 (t, J = 5.7 Hz, 1H, H_f), 6.14 (br t, 1H, H_c), 4.90 (br t, 1H, H_l), 4.37 (d, J = 6.8 Hz, 2H, H_m), 4.22-4.17 (m, 2H, H_a & H_n), 3.94 (dd, J = 7.7 Hz and J = 5.8 Hz, 2H, H_b), 3.50 (d, J = 5.5 Hz, 2H, H_i), 3.29 (q, J = 6.7 Hz, 2H, H_g), 3.19-3.15 (m, 2H, H_k), 1.53-1.22 (m, 17H, alkyl CH_2 & alkyl CH & H_h); ^{13}C NMR (100 MHz, $CDCl_3$): δ = 164.3 (amide C=O), 164.2 (amide C=O), 156.5 (carbamate C=O), 144.0 (Fmoc ArC_q), 141.5 (phenyl ArC_q), 141.3 (Fmoc ArC_q), 133.4 ($CH_{(d\text{ or }e)}$), 132.6 ($CH_{(d\text{ or }e)}$), 128.8 (phenyl ArCH), 127.9 (phenyl ArCH), 127.7 ($ArCH_q$), 127.0 ($ArCH_p$), 126.9 (phenyl ArCH), 125.0 ($ArCH_o$), 119.9 ($ArCH_r$), 66.5 ($CH_{2(m)}$), 65.4 ($CH_{2(i)}$), 50.3 (CH_a), 47.2 (CH_n), 44.1 ($CH_{2(b)}$), 40.9 ($CH_{2(k)}$), 40.1 ($CHCH_2OH$), 39.7 ($CH_{2(g)}$), 30.7 (CH_2), 30.6 (CH_2), 29.8 (CH_2), 29.7 (CH_2), 27.0 (CH_2), 26.9 (CH_2), 26.3 (CH_2), 26.1 (CH_2); HRMS (FAB, 3-NOBA matrix): m/z = 716.4063 [$(M+H)^+$] (anal. calcd for $C_{45}H_{54}N_3O_5^+$: m/z = 716.4064).

9*H*-Fluoren-9-ylmethyl [11-{[(2*E*)-4-(2,2-diphenylethylamino)-4-oxobut-2-enoyl]amino}-6-(*tert*-butyldimethylsilyloxymethyl)undecyl]carbamate (17)

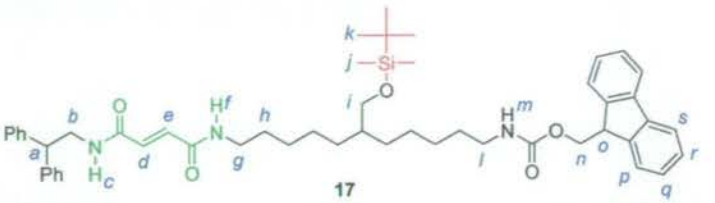

17

To a slurry of alcohol **16** (545 mg, 0.762 mmol) in dichloromethane (10 mL) was added imidazole (204 mg, 3.00 mmol) and *tert*-butyldimethylsilyl chloride (228 mg, 1.52 mmol). The reaction mixture was stirred for 2 h during which time a colourless precipitate appeared. Water (2 mL) was added, and the reaction mixture was extracted with dichloromethane (5 mL). The organic layer was separated, washed with brine (sat., 5 mL), dried (Na_2SO_4) and concentrated to furnish the crude material which was purified by flash chromatography (SiO_2; ethyl acetate/petroleum ether, 1:4 to 1:1). Appropriate fractions were concentrated to furnish compound **17** as a colourless solid (400 mg, 63%); mp 118-120 °C; ^{1}H NMR (400 MHz, $CDCl_3$): δ = 7.76 (d, J = 7.5 Hz, 2H, H_s), 7.59 (d, J = 7.5 Hz, 2H, H_p), 7.40 (t, J = 7.4 Hz, 2H, H_r), 7.41-7.18 (m, 12H, H_{Ph} & H_q), 6.93 (d, J = 14.9 Hz, 1H, $H_{d \text{ or } e}$), 6.75 (d, J = 14.6 Hz, 1H, $H_{d \text{ or } e}$), 6.32 (t, J = 5.0 Hz, 1H, H_f), 6.02 (br t, 1H, H_c), 4.86 (br t, 1H, H_m), 4.37 (d, J = 6.8 Hz, 2H, H_n), 4.23-4.17 (m, 2H, H_a & H_o), 3.94 (br dd, 2H, H_b), 3.43 (d, J = 5.3 Hz, 2H, H_i), 3.29 (q, J = 6.5 Hz, 2H, H_g), 3.20-3.15 (m, 2H, H_l), 1.51-1.19 (m, 17H, alkyl CH_2 & alkyl CH & H_h), 0.88 (s, 9H, H_k), 0.02 (s, 6H, H_j); ^{13}C NMR (100 MHz, $CDCl_3$): δ = 164.2 (amide C=O), 164.1 (amide C=O), 156.4 (carbamate C=O), 144.0 (Fmoc ArC_q), 141.5 (phenyl ArC_q), 141.3 (Fmoc ArC_q), 133.4 ($CH_{(d \text{ or } e)}$), 132.5 ($CH_{(d \text{ or } e)}$), 128.8 (phenyl ArCH), 127.9 (phenyl ArCH), 127.6 ($ArCH_r$), 127.01 ($ArCH_q$), 126.95 (phenyl ArCH), 125.0 ($ArCH_p$), 119.9 ($ArCH_s$), 66.5 ($CH_{2(n)}$), 65.6 ($CH_{2(i)}$), 50.3 (CH_a), 47.3 (CH_o), 44.1 ($CH_{2(b)}$), 41.1 ($CH_{2(l)}$), 40.2 ($CHCH_2OTBDMS$), 39.8 ($CH_{2(g)}$), 30.7 (2 × CH_2), 29.9 (CH_2), 29.3 (CH_2), 27.2 (CH_2), 27.1 (CH_2), 26.44 (CH_2), 26.37 (CH_2), 25.9 ($CH_{3(k)}$), 18.3 ($C_q(CH_3)_3$), –5.4 ($CH_{3(j)}$); HRMS (FAB, 3-NOBA matrix): m/z = 830.4923 [$(M+H)^+$] (anal. calcd for $C_{51}H_{68}N_3O_5Si^+$: m/z = 830.4928).

[2]-(1,4,7,14,17,20-Hexaaza-2,6,15,19-tetraoxo-3,5,9,12,16,18,22,25-tetrabenzocyclohexacosane)-(9*H*-Fluoren-9-ylmethyl [11-{[(2*E*)-4-(diphenylethylamino)-4-oxobut-2-enoyl]amino}-6-(*tert*-butyldimethylsilyloxymethyl)undecyl]carbamate)-rotaxane (18)

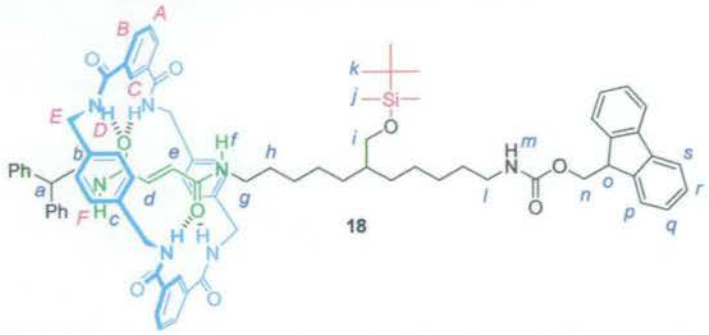

Thread **17** (180 mg, 0.217 mmol) and triethylamine (100 μL) were dissolved in chloroform (30 mL) under nitrogen and stirred vigorously whilst solutions of the mixture of *p*-xylylenediamine (237 mg, 1.74 mmol) and triethylamine (448 μL, 4.34 mmol) in chloroform (12 mL) and isophthaloyl dichloride (353 mg, 1.74 mmol) in chloroform (12 mL) were simultaneously added over a period of 3 h using motor-driven syringe pumps. The reaction mixture was stirred for a further 2 h under nitrogen. The resulting precipitate was removed by filtration and washed with chloroform. The filtrates were evaporated under reduced pressure to afford a solid which was purified by flash chromatography on silica to yield, in order of elution, the unconsumed thread **17** (ethyl acetate/petroleum ether, 1:1) and the desired rotaxane **18** (methanol/chloroform, 2:98) as a colourless solid (200 mg, 68%); mp 248-250 °C; ^{1}H NMR (400 MHz, $CDCl_3$): δ = 8.27 (br s, 2H, H_C), 8.06 (d, J = 7.8 Hz, 4H, H_B), 8.02 (br s, 1H, H_c), 7.74 (d, J = 7.6 Hz, 2H, H_s), 7.71 (br t, 4H, H_D), 7.59-7.53 (m, 5H, H_A & H_f & H_p), 7.37 (t, J = 7.5 Hz, 2H, H_r), 7.28-7.13 (m, 12H, H_{Ph} & H_q), 6.95 (s, 8H, H_F), 5.71 (s, 2H, H_d & H_e), 5.00 (t, J = 5.8 Hz, 1H, H_m), 4.42 (br s, 8H, H_E), 4.34 (d, J = 7.1 Hz, 2H, H_n), 4.26 (t, J = 7.8 Hz, 1H, H_a), 4.19 (t, J = 6.9 Hz, 1H, H_o), 3.85 (t, J = 6.4 Hz, 2H, H_b), 3.40 (d, J = 5.0 Hz, 2H, H_i), 3.14-3.10 (m, 4H, H_g & H_l), 1.46-1.22 (m, 17H, alkyl CH_2 & alkyl CH & H_h), 0.82 (s, 9H, H_k), –0.03 (s, 6H, H_j); ^{13}C NMR (100 MHz, $CDCl_3$): δ = 166.6 (macrocycle C=O), 165.7 (amide C=O), 165.3 (amide C=O), 156.5 (carbamate C=O), 143.9 (Fmoc ArC_q), 141.4 (phenyl ArC_q), 141.2 (Fmoc ArC_q), 136.8 (xylyl ArC_q), 133.5 (isophthaloyl ArC_q), 131.2 ($ArCH_B$), 129.8 ($CH_{(d \text{ or } e)}$), 129.6 ($CH_{(d \text{ or } e)}$), 129.1 ($ArCH_A$ & $ArCH_F$), 128.9 (phenyl ArCH), 127.8 (phenyl ArCH), 127.6 ($ArCH_r$), 127.2 ($ArCH_q$), 127.0 (phenyl ArCH), 125.0 ($ArCH_p$), 124.5 ($ArCH_C$), 119.9 ($ArCH_s$), 66.5 ($CH_{2(n)}$), 65.4 ($CH_{2(i)}$), 50.3 (CH_a),

47.2 (CH_o), 44.8 ($CH_{2(b)}$), 44.2 ($CH_{2(E)}$), 41.0 ($CH_{2(l)}$), 40.1 ($CH_{2(g)}$), 40.0 ($CHCH_2OTBDMS$), 30.9 (CH_2), 30.8 (CH_2), 29.9 (CH_2), 29.2 (CH_2), 27.5 (CH_2), 27.1 (CH_2), 26.51 (CH_2), 26.45 (CH_2), 25.9 ($CH_{3(k)}$), 18.2 ($C_q(CH_3)_3$), –5.4 ($CH_{3(f)}$); HRMS (FAB, 3-NOBA matrix): m/z = 1362.7038 [$(M+H)^+$] (anal. calcd for $C_{83}H_{96}N_7O_9Si^+$: m/z = 1362.7037).

_N_-(Pyridin-4-ylmethyl)aniline (19)

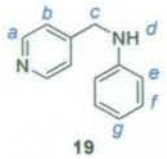

19

Aniline (3.00 mL, 33.0 mmol) in methanol (200 mL) was treated with pyridine-4-carboxaldehyde (3.18 mL, 33.3 mmol) to give a yellow solution which was heated at reflux for 3 h. The reaction mixture was then cooled to 0 °C and sodium borohydride (3.80 g, 99.9 mmol) was added portionwise. The resulting mixture was allowed to stir for 16 h, warming slowly to room temperature. After this time, the reaction was quenched with sodium hydrogen carbonate (½ sat. aq., 100 mL) and extracted with diethyl ether (3 × 200 mL). Combined organics were washed with brine (sat., 400 mL) then dried ($MgSO_4$) and evaporated under reduced pressure. The crude material was filtered through a silica plug, (neat dichloromethane then methanol/dichloromethane, 2:98) to give **19** as a colourless solid which turns pale yellow in air (3.85 g, 64%); mp 104-106 °C; ^{1}H NMR (400 MHz, $CDCl_3$): δ = 8.55 (d, J = 5.8 Hz, 2H, H_a), 7.30 (d, J = 5.3 Hz, 2H, H_b), 7.17 (t, J = 7.8 Hz, 2H, H_f), 6.74 (dt, J = 7.3 Hz and J = 0.8 Hz, 1H, H_g), 6.58 (dd, J = 8.3 Hz and J = 0.8 Hz, 2H, H_e), 4.39 (s, 2H, H_c), 4.22 (br s, 1H, H_d); ^{13}C NMR (100 MHz, $CDCl_3$): δ = 149.9 ($ArCH_a$), 149.1 (pyridyl ArC_q), 147.4 (phenyl ArC_q), 129.3 ($ArCH_f$), 122.1 ($ArCH_b$), 118.1 ($ArCH_g$), 112.8 ($ArCH_e$), 47.0 (CH_2); HRMS (FAB, 3-NOBA matrix): m/z = 185.1077 [$(M+H)^+$] (anal. calcd for $C_{12}H_{13}N_2^+$: m/z = 185.1079).

4-Oxo-4-[phenyl(pyridin-4-ylmethyl)amino]butanoic acid (20)

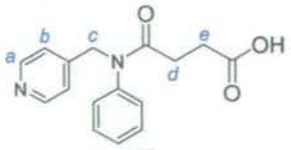

20

To a solution of succinic anhydride (701 mg, 7.01 mmol) in tetrahydrofuran (15 mL) was added 4-(dimethylamino)pyridine (10.0 mg, 82.0 nmol) followed by dropwise addition of amine **19** (1.29 g, 7.01 mmol) in tetrahydrofuran (20 mL). The resulting mixture was heated to reflux for 24 h, during which time a colourless precipitate formed. After cooling to room temperature, **20** was recovered as a colourless solid by filtration and washing with a small amount of cold dichloromethane (1.61 g, 81%); mp 190-192 °C; ^{1}H NMR (400 MHz, CD_3OD): δ = 8.44 (d, J = 5.9 Hz, 2H, H_a), 7.44-7.26 (m, 7H, H_{Ph} & H_b), 4.96 (s, 2H, H_c), 2.60 (t, J = 6.4 Hz, 2H, H_e), 2.41 (t, J = 6.4 Hz, 2H, H_d); ^{13}C NMR (100 MHz, CD_3OD): δ = 176.5 (acid C=O), 174.5 (amide C=O), 150.1 ($ArCH_a$), 149.5 (pyridyl ArC_q), 143.4 (phenyl ArC_q), 131.0 (phenyl ArCH), 129.7 (phenyl ArCH), 129.4 (phenyl ArCH), 124.8 ($ArCH_b$), 53.4 ($CH_{2(c)}$), 30.3 ($CH_{2(d\ or\ e)}$), 30.2 ($CH_{2(d\ or\ e)}$); HRMS (FAB, THIOG matrix): m/z = 285.1240 [$(M+H)^+$] (anal. calcd for $C_{16}H_{17}N_2O_3^+$: m/z = 258.1239).

[2]-(1,4,7,14,17,20-Hexaaza-2,6,15,19-tetraoxo-3,5,9,12,16,18,22,25-tetrabenzocyclohexacosane)-{(2*E*)-*N*-[6-(*tert*-Butyldimethylsilyloxymethyl)-11-({4-oxo-4-[phenyl(pyridin-4-ylmethyl)amino]butanoyl}amino)undecyl]-*N'*-(2,2-diphenylethyl)but-2-enediamide}-rotaxane (*fum-E*-5)

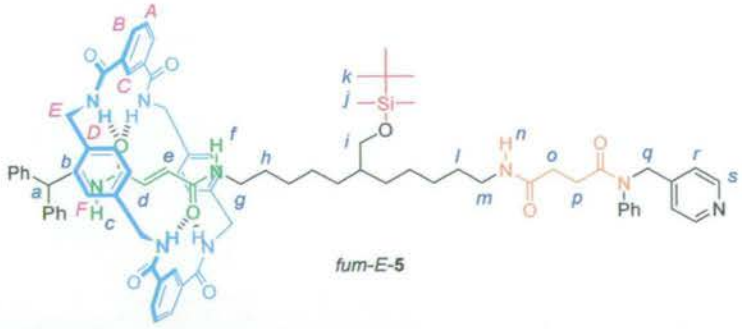

fum-E-5

Rotaxane **18** (200 mg, 0.147 mmol) was dissolved in tetrahydrofuran/acetonitrile (1:3, 8 mL). Piperidine (700 mg, 8.22 mmol) was added and the reaction was allowed to stir for 2.5 h. The reaction mixture was concentrated under reduced pressure and the crude material was purified by flash chromatography (SiO_2; methanol/dichloromethane, 2:98 then methanol/ammonia/dichloromethane, 6:0.75:93) to afford the free amine, which was used directly in the following step.

Carboxylic acid **20** (50.3 mg, 0.176 mmol) was dissolved in dichloromethane (5 mL) and the solution was cooled to 0 °C. 1-[3-Dimethylaminopropyl]-3-ethylcarbodiimide hydrochloride (41.0 mg, 0.211 mmol), 1-hydroxybenzotriazole hydrate (29.0 mg, 0.211 mmol) and triethylamine (90.0 μL, 0.849 mmol) were added at 0 °C. The reaction mixture was allowed to stir at room temperature for 30 min. A solution of the above amine in tetrahydrofuran (15 mL) was added to the activated acid. The reaction mixture was stirred for 14 h. Solvent was removed under reduced pressure and the residue taken up in dichloromethane (15 mL), washed with sodium hydrogen carbonate (sat. aq., 10 mL) and brine (sat., 10 mL), then dried (Na_2SO_4) and concentrated under reduced pressure to furnish the crude product which was purified by flash chromatography (SiO_2; methanol/dichloromethane, 1:99 to 3:97) to give *fum-E*-**5** as a colourless solid (100 mg, 48%); mp > 300 °C (decomp.); ^{1}H NMR (400 MHz, $CDCl_3$): δ = 8.64 (br t, 1H, H_f), 8.48 (br t, 1H, H_c), 8.41 (d, J = 5.0 Hz, 2H, H_s), 8.24 (s, 2H, H_C), 8.03 (d, J = 7.9 Hz, 4H, H_B), 7.77 (br s, 4H, H_D), 7.52 (t, J = 7.7 Hz, 2H, H_A), 7.39-7.06 (m, 17H, H_{Ph} & H_r), 6.98 (s, 8H, H_F), 6.35 (t, J = 5.5 Hz, 1H, H_n), 5.78 (s, 2H, H_d & H_e), 4.79 (d, J = 15.6 Hz, 1H, H_q), 4.75 (d, J = 16.0 Hz, 1H, $H_{q'}$), 4.43 (br s, 8H, H_E), 4.30 (t, J =7.8 Hz, 1H, H_a), 3.89 (br dd, 2H, H_b), 3.42-3.34 (m, 2H, H_i), 3.21-3.14 (m, 4H, H_g & H_m), 2.45-2.39 (m, 4H, H_o & H_p), 1.51-1.42 (m, 4H, H_h & H_l), 1.34-1.10 (m, 13H, alkyl CH_2 & alkyl CH), 0.83 (s, 9H, H_k), –0.03 (s, 6H, H_j); ^{13}C NMR (100 MHz, $CDCl_3$): δ = 172.7 (succinamide C=O), 172.0 (succinamde C=O), 166.6 (macrocycle C=O), 165.7 (fumaramide C=O), 165.4 (fumaramide C=O), 148.6 ($ArCH_s$), 146.5 (pyridyl ArC_q), 141.9 (phenyl ArC_q), 141.5 (phenyl ArC_q), 136.9 (xylyl ArC_q), 133.6 (isophthaloyl ArC_q), 131.2 ($ArCH_B$), 130.0 (phenyl ArCH), 129.9 ($CH_{(d \text{ or } e)}$), 129.4 ($CH_{(d \text{ or } e)}$), 129.1 ($ArCH_F$), 128.9 ($ArCH_A$), 128.8 (phenyl ArCH), 128.5 (phenyl ArCH), 127.9 (phenyl ArCH), 127.8 (phenyl ArCH), 127.1 (phenyl ArCH), 124.6 ($ArCH_C$), 123.3 ($ArCH_r$), 65.6 ($CH_{2(i)}$), 52.7 ($CH_{2(q)}$), 50.4 (CH_a), 44.8 ($CH_{2(b)}$), 44.2 ($CH_{2(E)}$), 40.2 ($CHCH_2OTBDMS$), 40.0 ($CH_{2(g)}$), 39.5 ($CH_{2(m)}$), 31.4 (CH_2), 30.71 (CH_2), 30.66 (CH_2), 29.9 (CH_2), 29.7 (CH_2), 29.5 (CH_2), 29.1 (CH_2), 27.4 (CH_2), 27.2 (CH_2), 26.4 (CH_2), 25.9 ($CH_{3(k)}$), 18.3 ($C_q(CH_3)_3$), –3.3 ($CH_{3(j)}$); HRMS (FAB, 3-NOBA matrix): m/z = 1406.7405 [$(M+H)^+$] (anal. calcd for $C_{84}H_{100}N_9O_9Si^+$: m/z = 1406.7413).

[2]-(1,4,7,14,17,20-Hexaaza-2,6,15,19-tetraoxo-3,5,9,12,16,18,22,25-tetrabenzocyclohexacosane)-{*N*-(2,2-Diphenylethyl)-*N'*-[6-(*tert*-butyldimethylsilyloxymethyl)-11-([4-oxo-4-[phenyl(pyridin-4-ylmethyl)amino]butanoyl}amino)undecyl]succinamide}-rotaxane (*succ1*-3)

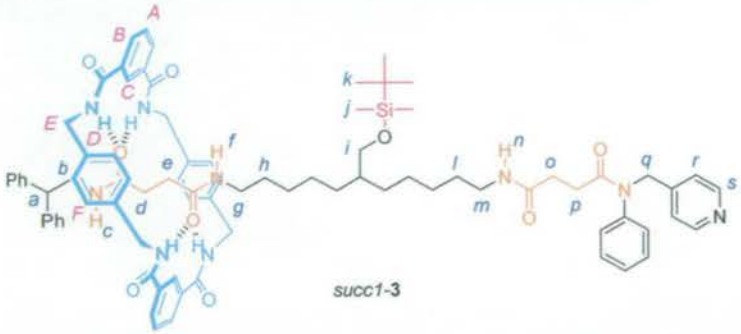

A solution of *fum-E*-**5** (10.0 mg, 711 nmol) in tetrahydrofuran (5.0 mL) was treated with Pd/C (10 %, 10 mg portions added every 2 h) and stirred under an atmosphere of H_2 at 1 atm for 6 h. The reaction mixture was filtered through Celite. The filtrate was concentrated under reduced pressure to furnish *succ1*-**3** as a colourless solid (8.85 mg, 90%); mp > 300 °C (decomp.); ^{1}H NMR (400 MHz, $CDCl_3$): δ = 8.41 (br s, 4H, H_C & H_s), 8.16 (dd, J = 7.8 Hz and J = 1.3 Hz, 4H, H_B), 7.77 (br t, 4H, H_D), 7.55 (t, J = 7.8 Hz, 2H, H_A), 7.38-7.13 (m, 17H, H_{Ph} & H_r), 7.02 (s, 8H, H_F), 6.82 (br t, 1H, H_f), 6.09 (t, J = 5.2 Hz, 1H, H_n), 5.95 (br t, 1H, H_c), 4.89 (d, J = 15.6 Hz, 1H, H_q), 4.84 (d, J = 15.8 Hz, 1H, $H_{q'}$), 4.53-4.42 (m, 8H, H_E), 4.04 (t, J = 7.9 Hz, 1H, H_a), 3.61 (dd, J = 7.4 Hz and J = 5.9 Hz, 2H, H_b), 3.41 (d, J = 5.6 Hz, 2H, H_i), 3.19 (q, J = 6.5 Hz, 2H, H_m), 3.01 (q, J = 6.5 Hz, 2H, H_g), 2.47-2.41 (m, 4H, H_o & H_p), 1.48-1.39 (m, 4H, H_h & H_l), 1.33-1.13 (m, 13H, alkyl CH_2 & alkyl CH), 1.05-0.91 (m, 4H, H_d & H_e), 0.85 (s, 9H, H_k), 0.00 (s, 6H, H_j); ^{13}C NMR (100 MHz, $CDCl_3$): δ = 172.92 (succinamide C=O), 172.88 (succinamide C=O), 172.7 (succinamide C=O), 172.0 (succinamide C=O), 166.5 (macrocycle C=O), 148.7 ($ArCH_s$), 146.6 (pyridyl ArC_q), 141.9 (phenyl ArC_q), 141.5 (phenyl ArC_q), 137.9 (xylyl ArC_q), 133.9 (isophthaloyl ArC_q), 131.5 ($ArCH_B$), 130.0 (phenyl ArCH), 129.14 ($ArCH_F$), 129.09 ($ArCH_A$), 128.9 (phenyl ArCH), 128.6 (phenyl ArCH), 127.9 (phenyl ArCH), 127.8 (phenyl ArCH), 127.1 (phenyl ArCH), 124.1 ($ArCH_C$), 123.5 ($ArCH_r$), 65.7 ($CH_{2(i)}$), 52.7 ($CH_{2(q)}$), 50.4 (CH_a), 44.0 ($CH_{2(b)}$), 43.9 ($CH_{2(E)}$), 40.2 ($CHCH_2OTBDMS$), 39.8 ($CH_{2(g)}$), 39.6 ($CH_{2(m)}$), 31.3 (CH_2), 30.7 (CH_2), 30.6 (CH_2), 29.8 (CH_2), 29.7 (CH_2), 29.5 (CH_2), 29.4 (CH_2), 29.3 (CH_2), 27.3 (CH_2), 27.2 (CH_2), 26.5 (CH_2), 26.4 (CH_2), 25.9 ($CH_{3(k)}$), 18.3 ($C_q(CH_3)_3$), –4.7 ($CH_{3(j)}$); HRMS (FAB, 3-NOBA matrix): m/z = 1408.7105 [$(M+H)^+$] (anal. calcd for $C_{84}H_{102}N_9O_9Si^+$: m/z = 1408.7113).

(2*E*)-*N*-[6-(*tert*-Butyldimethylsilyloxymethyl)-11-({4-oxo-4-[phenyl(pyridin-4-ylmethyl)amino]butanoyl}amino)undecyl]-*N'*-(2,2-diphenylethyl)but-2-enediamide (*E*-6)

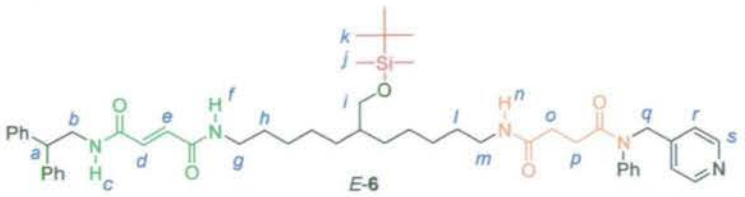

Compound **17** (40.0 mg, 0.0483 mmol) was dissolved in tetrahydrofuran/acetonitrile (1:3, 800 µL). Piperidine (170 mg, 1.99 mmol) was added and the reaction was allowed to stir for 2.5 h at room temperature. The reaction mixture was concentrated under reduced pressure and the crude material was purified by flash chromatography (SiO_2; methanol/dichloromethane, 2:98 then methanol/ammonia/dichloromethane, 6:2:92) to afford the free amine, which was used directly in the following step.

Carboxylic acid **20** (13.8 mg, 0.0487 mmol) was dissolved in dichloromethane (1.0 mL) and the solution was cooled to 0 °C. 1-[3-Dimethylaminopropyl]-3-ethylcarbodiimide hydrochloride (12.0 mg, 0.0625 mmol), 1-hydroxybenzotriazole hydrate (9.56 mg, 0.0625 mmol) and triethylamine (40.0 mg, 0.396 mmol) were added at 0 °C. The reaction mixture was allowed to stir at room temperature for 30 min. A solution of the above amine in tetrahydrofuran (15 mL) was added to the activated acid. The reaction mixture was stirred for 14 h. Solvent was removed under reduced pressure and the residue taken up in dichloromethane (15 mL), washed with sodium hydrogen carbonate (sat. aq., 10 mL) and brine (sat., 10 mL), then dried (Na_2SO_4) and concentrated to furnish the crude product which was purified by flash chromatography (SiO_2; methanol/dichloromethane, 1:99 to 5:95) to give *E*-**6** as a colourless oil (20.0 mg, 47%); ^{1}H NMR (400 MHz, $CDCl_3$): δ = 8.51 (d, J = 5.8 Hz, 2H, H_s), 7.38-7.10 (m, 17H, H_{Ph} & H_r), 6.89 (d, J = 14.8 Hz, 1H, $H_{d \text{ or } e}$), 6.76 (d, J = 14.9 Hz, 1H, $H_{d \text{ or } e}$), 6.44 (t, J = 5.5 Hz, 1H, H_f), 6.29 (t, J = 5.2 Hz, 1H, H_n), 6.23 (t, J = 5.6 Hz, 1H, H_c), 4.83 (s, 2H, H_q), 4.21 (t, J = 7.9 Hz, 1H, H_a), 3.95 (br dd, 2H, H_b), 3.41 (d, J = 5.4 Hz, 2H, H_i), 3.30 (q, J = 6.6 Hz, 2H, H_g), 3.23-3.18 (m, 2H, H_m), 2.50-2.44 (m, 4H, H_o & H_p), 1.53-1.45 (m, 4H, H_h & H_l), 1.42-1.25 (m, 13H, alkyl CH_2 & alkyl CH), 0.87 (s, 9H, H_k), 0.01 (s, 6H, H_j); ^{13}C NMR (100 MHz, $CDCl_3$): δ = 172.7 (succinamide C=O), 171.9 (succinamide C=O), 164.5 (fumaramide C=O), 164.4 (fumaramide C=O), 149.8 ($ArCH_s$), 146.4 (pyridyl ArC_q), 141.8 (phenyl ArC_q), 141.7 (phenyl ArC_q), 133.5 ($CH_{(d \text{ or } e)}$), 132.5 ($CH_{(d \text{ or } e)}$), 129.9 (phenyl ArCH), 128.7

(phenyl ArCH), 128.4 (phenyl ArCH), 128.0 (phenyl ArCH), 127.9 (phenyl ArCH), 126.9 (phenyl ArCH), 123.0 ($ArCH_r$), 65.8 (CH_i), 52.4 ($CH_{2(q)}$), 50.3 (CH_a), 44.2 ($CH_{2(b)}$), 39.8 ($CHCH_2OTBDMS$), 39.6 ($CH_{2(g\ or\ m)}$), 39.5 ($CH_{2(g\ or\ m)}$), 31.3 (CH_2), 30.3 (CH_2), 30.2 (CH_2), 29.8 (CH_2), 29.4 (CH_2), 29.1 (CH_2), 27.0 (CH_2), 26.8 (CH_2), 26.3 (CH_2), 26.0 (CH_2), 25.9 ($CH_{3(k)}$), 18.3 ($C_q(CH_3)_3$), –5.4 ($CH_{3(j)}$); HRMS (FAB, 3-NOBA matrix): m/z = 874.5303 [$(M+H)^+$] (anal. calcd for $C_{52}H_{72}N_5O_5Si^+$: m/z = 874.5303).

_N_-(2,2-Diphenylethyl)-_N'_-[6-(*tert*-butyldimethylsilyloxymethyl)-11-([4-oxo-4-[phenyl(pyridin-4-ylmethyl)amino]butanoyl}amino)undecyl]succinamide (4)

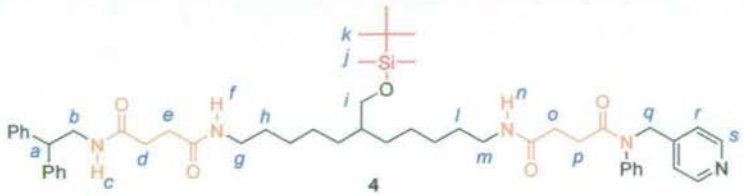

4

A solution of *E*-**6** (20.0 mg, 0.0229 mmol) in tetrahydrofuran (5.0 mL) was treated with Pd/C (10 %, 10 mg portions added every 2 h) and stirred under an atmosphere of H_2 at 1 atm for 6 h. The reaction mixture was filtered through Celite. The filtrate was concentrated under reduced pressure to furnish **4** as a colourless oil (18.1 mg, 90%); ^{1}H NMR (400 MHz, $CDCl_3$): δ = 8.52 (br s, 2H, H_s), 7.38-7.09 (m, 17H, H_{Ph} & H_r), 6.07-6.01 (m, 2H, H_c & $H_{f\ or\ n}$), 5.95 (t, J = 5.1 Hz, 1H, $H_{f\ or\ n}$), 4.87 (s, 2H, H_q), 4.17 (t, J = 8.0 Hz, 1H, H_a), 3.86 (dd, J = 7.9 Hz and J = 5.8 Hz, 2H, H_b), 3.43 (d, J = 5.5 Hz, 2H, H_i), 3.23-3.14 (m, 4H, H_g & H_m), 2.48-2.42 (m, 4H, H_o & H_p), 2.39 (m, 4H, H_d & H_e), 1.50-1.45 (m, 4H, H_h & H_l), 1.42-1.17 (m, 13H, alkyl CH_2 & alkyl CH), 0.87 (s, 9H, H_k). 0.02 (s, 6H, H_j); ^{13}C NMR (100 MHz, $CDCl_3$): δ = 172.5 (succinamide C=O), 172.2 (succinamide C=O), 172.0 (succinamide C=O), 171.9 (succinamide C=O), 149.3 ($ArCH_s$), 145.9 (pyridyl ArC_q), 141.83 (phenyl ArC_q), 141.79 (phenyl ArC_q), 130.0 (phenyl ArCH), 128.7 (phenyl ArCH), 128.5 (phenyl ArCH), 128.0 (2 × phenyl ArCH), 126.8 (phenyl ArCH), 123.3 ($ArCH_r$), 65.6 ($CH_{2(i)}$), 52.5 ($CH_{2(q)}$), 50.5 (CH_a), 43.8 ($CH_{2(b)}$), 40.1 ($CHCH_2OTBDMS$), 39.60 ($CH_{2(g\ or\ m)}$), 39.55 ($CH_{2(g\ or\ m)}$), 31.8 (CH_2), 31.7 (CH_2), 31.4 (CH_2), 30.7 (CH_2), 30.6 (CH_2), 29.9 (CH_2), 29.7 (CH_2), 29.5 (CH_2), 29.4 (CH_2), 27.0 (CH_2), 26.9 (CH_2), 26.2 (CH_2), 25.9 ($CH_{3(k)}$), 18.3 ($C_q(CH_3)_3$), –4.4 ($CH_{3(j)}$); HRMS (FAB, 3-NOBA matrix): m/z = 876.5451 [$(M+H)^+$] (anal. calcd for $C_{52}H_{74}N_5O_5Si^+$: m/z = 876.5459).

2.10 References and notes

[1] a) V. Balzani, A. Credi, F. M. Raymo, J. F. Stoddart, *Angew. Chem. Int. Ed.* **2000**, *39*, 3349-3391; b) Special issue on "Molecular Machines": *Acc. Chem. Res.* **2001**, *34*, 409-522; c) V. Balzani, M. Venturi, A. Credi, *Molecular Devices and Machines. A Journey into the Nanoworld*, Wiley-VCH, Weinheim, **2003**; d) C. J. Easton, S. F. Lincoln, L. Barr, H. Onagi, *Chem. Eur. J.* **2004**, *10*, 3120-3128; e) A. H. Flood, R. J. A. Ramirez, W.-Q. Deng, R. P. Muller, W. A. Goddard, J. F. Stoddart, *Aust. J. Chem.* **2004**, *57*, 301-322; f) G. S. Kottas, L. I. Clarke, D. Horinek, J. Michl, *Chem. Rev.* **2005**, *105*, 1281-1376; g) K. Kinbara, T. Aida, *Chem. Rev.* **2005**, *105*, 1377-1400; h) E. R. Kay, D. A. Leigh in *Functional Artificial Receptors* (Eds.: T. Schrader, A. D. Hamilton), Wiley-VCH, Weinheim, **2005**, pp. 333-406 (reprinted, in full, in the Appendix); i) Special issue on "Molecular Machines": *Top. Curr. Chem.* **2005**, *262*, 1-236.

[2] *Molecular Motors* (Ed.: M. Schliwa), Wiley-VCH, Weinheim, **2003**.

[3] *Maxwell's Demon 2. Entropy, Classical and Quantum Information, Computing* (Eds.: H. S. Leff, A. F. Rex), Institute of Physics Publishing, Bristol, **2003**.

[4] The first (a) private and (b) public written discussions of the 'temperature demon' were: a) J. C. Maxwell, *Letter to P. G. Tait, 11 December 1867.* Quoted in C. G. Knott, *Life and Scientific Work of Peter Guthrie Tait*, Cambridge University Press, London, **1911**, pp. 213-214. b) J. C. Maxwell, *Theory of Heat*, Longmans, Green and Co., London, **1871**, Chapter 22. c) Maxwell introduced the idea of a 'pressure demon' in a later (undated) letter to Tait, also quoted in C. G. Knott, *Life and Scientific Work of Peter Guthrie Tait*, Cambridge University Press, London, **1911**, pp. 214-215 and ref. [3]. A pressure demon is able to operate in a system linked to a constant-temperature reservoir with the sole effect of using energy transferred as heat from that reservoir to do work (see Szilard's engine, Figure 2.1c, ref. [6]). This is in conflict with the Kelvin–Planck form of the Second Law, whereas the temperature demon challenges the Clausius definition.

[5] Smoluchowski's trapdoor [(a) M. von Smoluchowski, *Physik. Z.* **1912**, *13*, 1069-1080; (b) M. von Smoluchowski, *Vortgage über die Kinetische Theorie der Materie und der Elektrizitat* (Ed.: M. Planck), Teubner und Leipzig, Berlin, **1914**, pp. 89-121] aims to transport particles selectively from the left compartment to the right in Figure 2.1d. However, in the absence of a mechanism whereby the trapdoor can dissipate energy, it will be at thermal equilibrium with its surroundings. This means that it must spend much of its time open, unable to influence particle transport. Rarely, it will be closed when a particle approaches from the right and will open on collision with a particle coming from the left – doing its job as intended. Such events are balanced, however, by the door snapping shut on a particle from the right, pushing it into the left chamber. Overall, the probability of a particle moving from left to right

is equal to that for moving right to left and so the trapdoor cannot accomplish its intended function adiabatically.

[6] L. Szilard, *Z. Phys.* **1929**, *53*, 840-856.

[7] R. P. Feynman, R. B. Leighton, M. Sands, *The Feynman Lectures on Physics, Vol. 1*, Addison-Wesley, Reading, MA, **1963**, Chapter 46.

[8] For the realization of Feynman's ratchet-and-pawl in molecular form, see: a) T. R. Kelly, I. Tellitu, J. P. Sestelo, *Angew. Chem. Int. Ed. Engl.* **1997**, *36*, 1866-1868. For nonadiabatic molecular versions which unidirectionally rotate, see: b) T. R. Kelly, H. De Silva, R. A. Silva, *Nature* **1999**, *401*, 150-152; c) D. A. Leigh, J. K. Y. Wong, F. Dehez, F. Zerbetto, *Nature* **2003**, *424*, 174-179; d) J. V. Hernández, E. R. Kay, D. A. Leigh, *Science* **2004**, *306*, 1532-1537 (reprinted, in full, in the Appendix and the basis for Chapter 3). For other types of rotary molecular motors, see: e) N. Koumura, R. W. J. Zijlstra, R. A. van Delden, N. Harada, B. L. Feringa, *Nature* **1999**, *401*, 152-155; f) N. Koumura, E. M. Geertsema, A. Meetsma, B. L. Feringa, *J. Am. Chem. Soc.* **2000**, *122*, 12005-12006; g) N. Koumura, E. M. Geertsema, M. B. van Gelder, A. Meetsma, B. L. Feringa, *J. Am. Chem. Soc.* **2002**, *124*, 5037-5051; h) E. M. Geertsema, N. Koumura, M. K. J. ter Wiel, A. Meetsma, B. L. Feringa, *Chem. Commun.* **2002**, 2962-2963; i) R. A. van Delden, N. Koumura, N. Harada, B. L. Feringa, *Proc. Natl. Acad. Sci. USA* **2002**, *99*, 4945-4949; j) M. K. J. ter Wiel, R. A. van Delden, A. Meetsma, B. L. Feringa, *J. Am. Chem. Soc.* **2003**, *125*, 15076-15086; k) R. A. van Delden, N. Koumura, A. Schoevaars, A. Meetsma, B. L. Feringa, *Org. Biomol. Chem.* **2003**, *1*, 33-35; l) M. K. J. ter Wiel, R. A. van Delden, A. Meetsma, B. L. Feringa, *J. Am. Chem. Soc.* **2005**, *127*, 14208-14222; m) D. Pijper, R. A. van Delden, A. Meetsma, B. L. Feringa, *J. Am. Chem. Soc.* **2005**, *127*, 17612-17613; n) M. K. J. ter Wiel, R. A. van Delden, A. Meetsma, B. L. Feringa, *Org. Biomol. Chem.* **2005**, *3*, 4071-4076; o) R. A. van Delden, M. K. J. ter Wiel, M. M. Pollard, J. Vicario, N. Koumura, B. L. Feringa, *Nature* **2005**, *437*, 1337-1340; p) T. Fujita, S. Kuwahara, N. Harada, *Eur. J. Org. Chem.* **2005**, 4533-4543; q) S. Kuwahara, T. Fujita, N. Harada, *Eur. J. Org. Chem.* **2005**, 4544-4556; r) S. P. Fletcher, F. Dumur, M. M. Pollard, B. L. Feringa, *Science* **2005**, *310*, 80-82; s) Y. Lin, B. J. Dahl, B. P. Branchaud, *Tetrahedron Lett.* **2005**, *46*, 8359-8362.

[9] a) G. Schill, *Catenanes, Rotaxanes and Knots*, Academic Press, New York, **1971**; b) D. B. Amabilino, J. F. Stoddart, *Chem. Rev.* **1995**, *95*, 2725-2828; c) *Molecular Catenanes Rotaxanes and Knots* (Eds.: J.-P. Sauvage, C. O. Dietrich-Buchecker), Wiley-VCH, Weinheim, **1999**.

[10] J. S. Hannam, S. M. Lacy, D. A. Leigh, C. G. Saiz, A. M. Z. Slawin, S. G. Stitchell, *Angew. Chem. Int. Ed.* **2004**, *43*, 3260-3264.

[11] a) P. L. Anelli, N. Spencer, J. F. Stoddart, *J. Am. Chem. Soc.* **1991**, *113*, 5131-5133. For the first example of an amide-based molecular shuttle, see: b) A. S. Lane, D. A. Leigh, A. Murphy, *J. Am. Chem. Soc.* **1997**, *119*, 11092-11093.

[12] The key feature of a rotaxane architecture from the point of view of molecular-level machines is that movement of the macrocycle in any direction other than along the thread is resisted by enormous steric forces up until the breaking point of covalent bonds in the macrocycle or the thread. This is a fundamentally different situation to a host–guest complex when, following de-complexation from the binding site, the motion of the ring is not restricted in any dimension and it is free to exchange with others in the medium. Simple host–guest/supramolecular systems cannot function as nanoscale mechanical machines unless restrictions on the exchange of the unbound species with the bulk apply (as happens with kinetically stable pseudorotaxanes) or the binding event brings about a mechanical (i.e. conformational) change in one of the molecular components. Similarly, molecules that are not kinetically stable – this includes some rotaxanes that are thermodynamically stable but kinetically labile – cannot behave as molecular machines if they exchange components with the bulk quicker than the timescale of their stimuli-induced change of position. Molecular machines designed to exploit motion have to be kinetically associated with their substrates throughout the operation of the machine.

[13] For examples of photochemically responsive molecular shuttles, see: a) A. C. Benniston, A. Harriman, *Angew. Chem. Int. Ed. Engl.* **1993**, *32*, 1459-1461; b) A. C. Benniston, A. Harriman, V. M. Lynch, *Tetrahedron Lett.* **1994**, *35*, 1473-1476; c) A. C. Benniston, A. Harriman, V. M. Lynch, *J. Am. Chem. Soc.* **1995**, *117*, 5275-5291; d) H. Murakami, A. Kawabuchi, K. Kotoo, M. Kunitake, N. Nakashima, *J. Am. Chem. Soc.* **1997**, *119*, 7605-7606; e) N. Armaroli, V. Balzani, J.-P. Collin, P. Gaviña, J.-P. Sauvage, B. Ventura, *J. Am. Chem. Soc.* **1999**, *121*, 4397-4408; f) P. R. Ashton, R. Ballardini, V. Balzani, A. Credi, K. R. Dress, E. Ishow, C. J. Kleverlaan, O. Kocian, J. A. Preece, N. Spencer, J. F. Stoddart, M. Venturi, S. Wenger, *Chem. Eur. J.* **2000**, *6*, 3558-3574; g) G. W. H. Wurpel, A. M. Brouwer, I. H. M. van Stokkum, A. Farran, D. A. Leigh, *J. Am. Chem. Soc.* **2001**, *123*, 11327-11328; h) A. M. Brouwer, C. Frochot, F. G. Gatti, D. A. Leigh, L. Mottier, F. Paolucci, S. Roffia, G. W. H. Wurpel, *Science* **2001**, *291*, 2124-2128; i) C. A. Stanier, S. J. Alderman, T. D. W. Claridge, H. L. Anderson, *Angew. Chem. Int. Ed.* **2002**, *41*, 1769-1772; j) A. Altieri, G. Bottari, F. Dehez, D. A. Leigh, J. K. Y. Wong, F. Zerbetto, *Angew. Chem. Int. Ed.* **2003**, *42*, 2296-2300; k) W. Abraham, L. Grubert, U. W. Grummt, K. Buck, *Chem. Eur. J.* **2004**, *10*, 3562-3568; l) H. Murakami, A. Kawabuchi, R. Matsumoto, T. Ido, N. Nakashima, *J. Am. Chem. Soc.* **2005**, *127*, 15891-15899; m) S. Schmidt-Schaffer, L. Grubert, U. W. Grummt, K. Buck, W. Abraham, *Eur. J. Org. Chem.* **2006**, 378-398; n) Q.-C. Wang, Q. Ma, D.-H. Qu, H. Tian, *Chem. Eur. J.* **2006**, *12*, 1088-1096; o) V. Balzani, M. Clemente-León, A. Credi, B. Ferrer, M. Venturi, A. H. Flood, J. F. Stoddart, *Proc. Natl. Acad. Sci. USA* **2006**, *103*, 1178-1183.

[14] For an example of entropy-driven shuttling, see: G. Bottari, F. Dehez, D. A. Leigh, P. J. Nash, E. M. Pérez, J. K. Y. Wong, F. Zerbetto, *Angew. Chem. Int. Ed.* **2003**, *42*, 5886-5889.

[15] For examples of electrochemically responsive molecular shuttles, see refs. [13e, 13f, 13o] and: a) R. A. Bissell, E. Córdova, A. E. Kaifer, J. F. Stoddart, *Nature* **1994**, *369*, 133-137; b) J.-P. Collin, P. Gaviña, J.-P. Sauvage, *New J.*

Chem. **1997**, *21*, 525-528; c) R. Ballardini, V. Balzani, W. Dehaen, A. E. Dell'Erba, F. M. Raymo, J. F. Stoddart, M. Venturi, *Eur. J. Org. Chem.* **2000**, 591-602; d) A. Altieri, F. G. Gatti, E. R. Kay, D. A. Leigh, D. Martel, F. Paolucci, A. M. Z. Slawin, J. K. Y. Wong, *J. Am. Chem. Soc.* **2003**, *125*, 8644-8654 (reprinted, in full, in the Appendix and the basis for Chapter 5); e) B. Long, K. Nikitin, D. Fitzmaurice, *J. Am. Chem. Soc.* **2003**, *125*, 15490-15498; f) N. Kihara, M. Hashimoto, T. Takata, *Org. Lett.* **2004**, *6*, 1693-1696; g) H.-R. Tseng, S. A. Vignon, P. C. Celestre, J. Perkins, J. O. Jeppesen, A. Di Fabio, R. Ballardini, M. T. Gandolfi, M. Venturi, V. Balzani, J. F. Stoddart, *Chem. Eur. J.* **2004**, *10*, 155-172; h) A. H. Flood, A. J. Peters, S. A. Vignon, D. W. Steuerman, H.-R. Tseng, S. Kang, J. R. Heath, J. F. Stoddart, *Chem. Eur. J.* **2004**, *10*, 6558-6564; i) H.-R. Tseng, D. M. Wu, N. X. L. Fang, X. Zhang, J. F. Stoddart, *ChemPhysChem* **2004**, *5*, 111-116; j) D. W. Steuerman, H.-R. Tseng, A. J. Peters, A. H. Flood, J. O. Jeppesen, K. A. Nielsen, J. F. Stoddart, J. R. Heath, *Angew. Chem. Int. Ed.* **2004**, *43*, 6486-6491; k) J. O. Jeppesen, S. Nygaard, S. A. Vignon, J. F. Stoddart, *Eur. J. Org. Chem.* **2005**, 196-220.

[16] For examples of chemically responsive molecular shuttles, see refs. [11b, 15g, 15k] and: a) C. G. Gong, H. W. Gibson, *Angew. Chem. Int. Ed. Engl.* **1997**, *36*, 2331-2333; b) C. G. Gong, T. E. Glass, H. W. Gibson, *Macromolecules* **1998**, *31*, 308-313; c) M. C. Jiménez, C. Dietrich-Buchecker, J.-P. Sauvage, *Angew. Chem. Int. Ed.* **2000**, *39*, 3284-3287; d) J. W. Lee, K. P. Kim, K. Kim, *Chem. Commun.* **2001**, 1042-1043; e) M. C. Jimenez-Molero, C. Dietrich-Buchecker, J.-P. Sauvage, *Chem. Eur. J.* **2002**, *8*, 1456-1466; f) T. Da Ros, D. M. Guldi, A. F. Morales, D. A. Leigh, M. Prato, R. Turco, *Org. Lett.* **2003**, *5*, 689-691; g) H.-R. Tseng, S. A. Vignon, J. F. Stoddart, *Angew. Chem. Int. Ed.* **2003**, *42*, 1491-1495; h) B. W. Laursen, S. Nygaard, J. O. Jeppesen, J. F. Stoddart, *Org. Lett.* **2004**, *6*, 4167-4170; i) T. J. Huang, H.-R. Tseng, L. Sha, W. X. Lu, B. Brough, A. H. Flood, B.-D. Yu, P. C. Celestre, J. P. Chang, J. F. Stoddart, C.-M. Ho, *Nano Lett.* **2004**, *4*, 2065-2071; j) D. A. Leigh, E. M. Pérez, *Chem. Commun.* **2004**, 2262-2263; k) K. Nørgaard, B. W. Laursen, S. Nygaard, K. Kjaer, H.-R. Tseng, A. H. Flood, J. F. Stoddart, T. Bjørnholm, *Angew. Chem. Int. Ed.* **2005**, *44*, 7035-7039.

[17] For examples of pH-responsive molecular shuttles, see ref. [15a] and: a) M.-V. Martínez-Díaz, N. Spencer, J. F. Stoddart, *Angew. Chem. Int. Ed. Engl.* **1997**, *36*, 1904-1907; b) P. R. Ashton, R. Ballardini, V. Balzani, I. Baxter, A. Credi, M. C. T. Fyfe, M. T. Gandolfi, M. Gómez-López, M.-V. Martínez-Díaz, A. Piersanti, N. Spencer, J. F. Stoddart, M. Venturi, A. J. P. White, D. J. Williams, *J. Am. Chem. Soc.* **1998**, *120*, 11932-11942; c) A. M. Elizarov, S.-H. Chiu, J. F. Stoddart, *J. Org. Chem.* **2002**, *67*, 9175-9181; d) J. D. Badjić, V. Balzani, A. Credi, S. Silvi, J. F. Stoddart, *Science* **2004**, *303*, 1845-1849; e) C. M. Keaveney, D. A. Leigh, *Angew. Chem. Int. Ed.* **2004**, *43*, 1222-1224; f) S. Garaudée, S. Silvi, M. Venturi, A. Credi, A. H. Flood, J. F. Stoddart, *ChemPhysChem* **2005**, *6*, 2145-2152; g) J. D. Badjić, C. M. Ronconi, J. F. Stoddart, V. Balzani, S. Silvi, A. Credi, *J. Am. Chem. Soc.* **2006**, *128*, 1489-1499.

[18] For examples of molecular shuttles switched by alkali metal ion complexation, competitive binding, or allosteric regulation, see: a) S. A. Vignon, T.

Jarrosson, T. Iijima, H.-R. Tseng, J. K. M. Sanders, J. F. Stoddart, *J. Am. Chem. Soc.* **2004**, *126*, 9884-9885; b) T. Iijima, S. A. Vignon, H.-R. Tseng, T. Jarrosson, J. K. M. Sanders, F. Marchioni, M. Venturi, E. Apostoli, V. Balzani, J. F. Stoddart, *Chem. Eur. J.* **2004**, *10*, 6375-6392; c) D. S. Marlin, D. González Cabrera, D. A. Leigh, A. M. Z. Slawin, *Angew. Chem. Int. Ed.* **2006**, *45*, 77-83; d) D. S. Marlin, D. González Cabrera, D. A. Leigh, A. M. Z. Slawin, *Angew. Chem. Int. Ed.* **2006**, *45*, 1385-1390.

[19] 'Co-conformation' refers to the relative positions of the mechanically interlocked components with respect to each other, see: M. C. T. Fyfe, P. T. Glink, S. Menzer, J. F. Stoddart, A. J. P. White, D. J. Williams, *Angew. Chem. Int. Ed. Engl.* **1997**, *36*, 2068-2070.

[20] Stimuli-induced shuttling has been used to control a number of different properties, for examples, see the following. Fluorescence switching: a) E. M. Pérez, D. T. F. Dryden, D. A. Leigh, G. Teobaldi, F. Zerbetto, *J. Am. Chem. Soc.* **2004**, *126*, 12210-12211; b) Q.-C. Wang, D.-H. Qu, J. Ren, K. Chen, H. Tian, *Angew. Chem. Int. Ed.* **2004**, *43*, 2661-2665; c) D.-H. Qu, Q.-C. Wang, J. Ren, H. Tian, *Org. Lett.* **2004**, *6*, 2085-2088; d) D.-H. Qu, Q.-C. Wang, H. Tian, *Mol. Cryst. Liquid Cryst.* **2005**, *430*, 59-65; e) D. A. Leigh, M. A. F. Morales, E. M. Pérez, J. K. Y. Wong, C. G. Saiz, A. M. Z. Slawin, A. J. Carmichael, D. M. Haddleton, A. M. Brouwer, W. J. Buma, G. W. H. Wurpel, S. León, F. Zerbetto, *Angew. Chem. Int. Ed.* **2005**, *44*, 3062-3067; f) D.-H. Qu, Q.-C. Wang, H. Tian, *Angew. Chem. Int. Ed.* **2005**, *44*, 5296-5299; g) D.-H. Qu, Q.-C. Wang, X. Ma, H. Tian, *Chem. Eur. J.* **2005**, *11*, 5929-5937; h) Y. Li, H. Li, Y. Li, H. Liu, S. Wang, X. He, N. Wang, D. Zhu, *Org. Lett.* **2005**, *7*, 4835-4838; i) H. Onagi, J. Rebek, *Chem. Commun.* **2005**, 4604-4606. Expression of chirality: j) G. Bottari, D. A. Leigh, E. M. Pérez, *J. Am. Chem. Soc.* **2003**, *125*, 13360-13361. Conductivity of solid-state electronic junctions: k) C. P. Collier, G. Mattersteig, E. W. Wong, Y. Luo, K. Beverly, J. Sampaio, F. M. Raymo, J. F. Stoddart, J. R. Heath, *Science* **2000**, *289*, 1172-1175; l) C. P. Collier, J. O. Jeppesen, Y. Luo, J. Perkins, E. W. Wong, J. R. Heath, J. F. Stoddart, *J. Am. Chem. Soc.* **2001**, *123*, 12632-12641; m) Y. Luo, C. P. Collier, J. O. Jeppesen, K. A. Nielsen, E. Delonno, G. Ho, J. Perkins, H.-R. Tseng, T. Yamamoto, J. F. Stoddart, J. R. Heath, *ChemPhysChem* **2002**, *3*, 519-525; n) M. R. Diehl, D. W. Steuerman, H.-R. Tseng, S. A. Vignon, A. Star, P. C. Celestre, J. F. Stoddart, J. R. Heath, *ChemPhysChem* **2003**, *4*, 1335-1339. Conductivity at electrode interfaces: o) I. Willner, V. Pardo-Yissar, E. Katz, K. T. Ranjit, *J. Electroanal. Chem.* **2001**, *497*, 172-177; p) L. Sheeney-Haj-Ichia, I. Willner, *J. Phys. Chem. B* **2002**, *106*, 13094-13097; q) E. Katz, L. Sheeney-Haj-Ichia, I. Willner, *Angew. Chem. Int. Ed.* **2004**, *43*, 3292-3300; r) E. Katz, O. Lioubashevsky, I. Willner, *J. Am. Chem. Soc.* **2004**, *126*, 15520-15532. Exertion of a mechanical force on a macroscopic object: s) T. J. Huang, B. Brough, C.-M. Ho, Y. Liu, A. H. Flood, P. A. Bonvallet, H.-R. Tseng, J. F. Stoddart, M. Baller, S. Magonov, *Appl. Phys. Lett.* **2004**, *85*, 5391-5393; t) Y. Liu, A. H. Flood, P. A. Bonvallet, S. A. Vignon, B. H. Northrop, H.-R. Tseng, J. O. Jeppesen, T. J. Huang, B. Brough, M. Baller, S. Magonov, S. D. Solares, W. A. Goddard, C.-M. Ho, J. F. Stoddart, *J. Am. Chem. Soc.* **2005**, *127*, 9745-9759. Access to a nanopore: u) T. D. Nguyen, H.-

R. Tseng, P. C. Celestre, A. H. Flood, Y. Liu, J. F. Stoddart, J. I. Zink, *Proc. Natl. Acad. Sci. USA* **2005**, *102*, 10029-10034. Surface wettability: ref. [20r] and v) J. Berná, D. A. Leigh, M. Lubomska, S. M. Mendoza, E. M. Pérez, P. Rudolf, G. Teobaldi, F. Zerbetto, *Nat. Mater.* **2005**, *4*, 704-710. The latter also demonstrates the macroscopic transport of a droplet of liquid across a surface using stimuli-responsive molecular shuttles.

[21] For an introduction to Brownian motors see: a) R. D. Astumian, *Sci. Am.* **2001**, *285* (1), 56-64; b) R. D. Astumian, P. Hänggi, *Phys. Today* **2002**, *55* (11), 33-39.

[22] For reviews of Brownian ratchet mechanisms, see: a) P. Hänggi, R. Bartussek in *Nonlinear Physics of Complex Systems – Current status and future trends: Lecture Notes in Physics, Vol. 476* (Eds.: J. Parisi, S. C. Müller, W. Zimmermann), Springer, Berlin, **1996**, pp. 294-308; b) R. D. Astumian, *Science* **1997**, *276*, 917-922; c) F. Jülicher, A. Ajdari, J. Prost, *Rev. Mod. Phys.* **1997**, *69*, 1269-1281; c) Special issue on "The constructive role of noise in fluctuation driven transport and stochastic resonance": *Chaos* **1998**, *8*, 533-664; d) P. Reimann, *Phys. Rep.* **2002**, *361*, 57-265; e) P. Reimann, P. Hänggi, *Appl. Phys. A* **2002**, *75*, 169-178; f) J. M. R. Parrondo, B. J. De Cisneros, *Appl. Phys. A* **2002**, *75*, 179-191; g) B. J. Gabryś, K. Pesz, S. J. Bartkiewicz, *Physica A* **2004**, *336*, 112-122; h) H. Linke, M. T. Downton, M. J. Zuckermann, *Chaos* **2005**, *15*, 026111.

[23] a) J. Rousselet, L. Salome, A. Ajdari, J. Prost, *Nature* **1994**, *370*, 446-448; b) L. P. Faucheux, L. S. Bourdieu, P. D. Kaplan, A. J. Libchaber, *Phys. Rev. Lett.* **1995**, *74*, 1504-1507; c) J. S. Bader, R. W. Hammond, S. A. Henck, M. W. Deem, G. A. McDermott, J. M. Bustillo, J. W. Simpson, G. T. Mulhern, J. M. Rothberg, *Proc. Natl. Acad. Sci. USA* **1999**, *96*, 13165-13169; d) H. Linke, T. E. Humphrey, A. Lofgren, A. O. Sushkov, R. Newbury, R. P. Taylor, P. Omling, *Science* **1999**, *286*, 2314-2317; e) S. Matthias, F. Müller, *Nature* **2003**, *424*, 53-57.

[24] Special issue on "Ratchets and Brownian motors: Basics, experiments and applications": *Appl. Phys. A* **2002**, *75*, 167-352.

[25] a) R. D. Astumian, M. Bier, *Biophys. J.* **1996**, *70*, 637-653; b) R. D. Astumian, I. Derényi, *Eur. Biophys. J.* **1998**, *27*, 474-489; c) R. Lipowsky in *Stochastic Processes in Physics, Chemistry and Biology: Lecture Notes in Physics, Vol. 557* (Eds.: J. A. Freund, T. Pöschel), Springer, Berlin, **2000**, pp. 21-31; d) C. Bustamante, D. Keller, G. Oster, *Acc. Chem. Res.* **2001**, *34*, 412-420; e) R. D. Astumian, *Appl. Phys. A* **2002**, *75*, 193-206; f) A. Mogilner, G. Oster, *Curr. Biol.* **2003**, *13*, R721-R733; g) G. Oster, H. Y. Wang, *Trends Cell Biol.* **2003**, *13*, 114-121; h) M. Kurzyński, P. Chelminiak, *Physica A* **2004**, *336*, 123-132.

[26] L. Onsager, *Phys. Rev.* **1931**, *37*, 405-426.

[27] The nomenclature used to denote individual rotaxane configurational and translational isomers follows conventions introduced in previous papers (e.g. ref. [8d]). Namely, a bolded compound number refers to a given structural

formula irrespective of functional group configuration or position of the macrocycle; a prefix *E* or *Z* describes the configuration of the olefin; a prefix *succ1*, *succ2*, *fum* or *mal* denotes the position of the macrocycle in a particular translational isomer.

[28] A. Itai, Y. Toriumi, S. Saito, H. Kagechika, K. Shudo, *J. Am. Chem. Soc.* **1992**, *114*, 10649-10650.

[29] Note that there is no indication of multiple tertiary amide rotamers in the ^{1}H NMR spectrum of **4** (Figure 2.2a). For example, only one signal is observed for H_q.

[30] D. A. Leigh, P. J. Nash, unpublished results.

[31] a) A. P. Krapcho, *Synthesis* **1982**, 805-822; b) A. P. Krapcho, *Synthesis* **1982**, 893-914.

[32] A. H. Parham, B. Windisch, F. Vögtle, *Eur. J. Org. Chem.* **1999**, 1233-1238.

[33] H. Sajiki, T. Ikawa, K. Hattori, K. Hirota, *Chem. Commun.* **2003**, 654-655.

[34] a) F. J. Britton, *Escapements: Their Actions Constructions and Proportion*, Arlington Book Co, Johnson City, TN, **1985**; b) W. J. Gazeley, *Clock and Watch Escapements*, Robert Hale & Co., London, **1992**.

[35] Some degradation of rotaxane **5** occurs upon irradiation at 254 nm, however, at 312 nm no degradation or side reactions are apparent and the photostationary state is 49:51 ± 2 *E*:*Z* by ^{1}H NMR spectroscopy.

[36] Note how the chemical shifts of some of the protons (e.g. H_d and H_e) in *fum-E*-**5** change among Figures 2.3b, 2.3c and 2.3d, illustrating the sensitivity of the hydrogen bonding between the macrocycle and thread to factors such as moisture, concentration and, possibly, impurities.

[37] This calculation assumes that both translational isomers of de-silylated *Z*-**5** are re-silylated at the same rate. If this is not true, if the position of the macrocycle on a station affects the rate of the unlinking reaction, then it is possible to produce a nonbalanced distribution of the macrocycle through just controlling kinetic energy barriers with the position of the ring – an 'information ratchet' (ref. [25b]).

[38] The pure single translational isomer *fum-E*-**5** cannot be regenerated by the operation of the machine but it can be separated from the reaction mixture at any stage using standard purification protocols.

[39] Starting from state **5A**, the linking and initial balance-breaking stimuli can be applied in either order (or simultaneously) in Scheme 2.8 for the task to be performed by the machine on the substrate, i.e. net transport of the macrocycle along the thread. In fact, any orthogonal transformations that transpire between two unlinking operations are commutative. Indeed, in a classic energy ratchet mechanism (e.g. ref. [25b]) – say using an oscillating electric field to

directionally transport a charged particle – the linking/unlinking and balance-breaking steps happen simultaneously which, of course, would have exactly the same effect as doing them sequentially as envisaged in Scheme 2.8. Balance-breaking and linking/unlinking steps also occur simultaneously during the operation of molecular shuttles containing cyclodextrins incorporated onto azobenzene or stilbene threads (refs. [13d, 13i, 13l, 13n, 20b- 20d, 20f, 20g]).

[40] Although escapement occurs during the operation of **5**, it is not escapement of a quantity that had been previously ratcheted by the operation of the motor. Prior to escapement, the macrocycles located on the olefin station in **5** have only been statistically unbalanced by the action of the motor, not ratcheted.

[41] Combinational logic circuits (NAND, NOR, OR, XOR, EOR, two- and three-input INH, etc.) are assembled by connecting combinations of AND, NOT and OR gates in various ways. These, in turn, are assembled by connecting simple 'on'–'off' switches in various ways. See: a) M. Ben-Ari, *Mathematical Logic for Computer Science*, Prentice-Hall, Hemel Hempstead, **1993**. For reviews on molecular-scale combinational logic systems, see: b) F. M. Raymo, *Adv. Mater.* **2002**, *14*, 401-414; c) A. P. de Silva, N. D. McClenaghan, *Chem. Eur. J.* **2004**, *10*, 574-586. For the sequential operation of combinational logic gates, see: d) A. P. de Silva, I. M. Dixon, H. Q. N. Gunaratne, T. Gunnlaugsson, P. R. S. Maxwell, T. E. Rice, *J. Am. Chem. Soc.* **1999**, *121*, 1393-1394; e) F. M. Raymo, S. Giordani, *Org. Lett.* **2001**, *3*, 3475-3478.

[42] a) A. P. Malvino, J. A. Brown, *Digital Computer Electronics*, 3rd ed., Glencoe, Lake Forest, **1993**; b) R. J. Mitchell, *Microprocessor Systems: An Introduction*, Macmillan, London, **1995**.

[43] A series of stimuli-responsive molecular shuttles have been shown to exhibit relatively long-lived nonequilibrium ('metastable') states when operating in self-assembled monolayers or a polymer electrolyte or at low temperatures (see refs. [15h-15j]). This may account for the junction hysteresis observed in solid-state electronic devices that utilize such rotaxanes (refs. [20k-20n]). Kinetically stable nonequilibrium co-conformations have also been observed in cyclodextrin-based shuttles, see refs. [13l, 16d].

[44] Since the method of operation of **5** involves varying the relative heights of energy minima and maxima irrespective of the position of the macrocycle, this is a partial 'energy ratchet' mechanism (ref. [25b]). Other types of mechanism are known (see ref. [22]), for example an 'information ratchet' which achieves directional transport of a Brownian substrate by varying the relative heights of energy maxima using information provided by the position of the substrate (ref. [25b]). See Chapter 4 for a molecular realization of an information ratchet.

[45] M. N. Chatterjee, S. Goldup, E. R. Kay, D. A. Leigh, unpublished results.

[46] Indeed, their branched topologies rule out rotaxanes as architectures for the particular examples of compartmentalized machines shown in Figure 2.7.

[47] a) Y. Hirai, M. Nagatsu, *Chem. Lett.* **1994**, 21-22; b) O. Okitsu, R. Suzuki, S. Kobayashi, *J. Org. Chem.* **2001**, *66*, 809-823.

[48] E. Boseggia, M. Gatos, L. Lucatello, F. Mancin, S. Moro, M. Palumbo, C. Sissi, P. Tecilla, U. Tonellato, G. Zagotto, *J. Am. Chem. Soc.* **2004**, *126*, 4543-4549.

CHAPTER THREE

A Reversible Synthetic Rotary Molecular Motor

Published in *Science* as "*A Reversible Synthetic Rotary Molecular Motor*":

J. V. Hernández, E. R. Kay, D. A. Leigh, *Science* **2004**, *306*, 1532-1537.

Acknowledgments and contributions

The synthetic tour de force that was synthesis and operation of [2]catenane **1** reported in this Chapter was entirely carried out by Dr José V. Hernández. The author analysed these results in the context of theoretical mechanisms from the literature, and wrote this Chapter and the paper it is based upon. The original design of **1** and overall guidance was provided by Prof. David A. Leigh.

Synopsis

Chapter 2 introduced the phenomenological terms necessary to describe the operation of a compartmentalized molecular machine, and explored how these features may be combined to create different categories of device. The simple rotaxane-based molecular machines used to exemplify these concepts operate on the basis of an olefin isomerization, which serves to alter the relative binding energies at stations on the thread, and alcohol protection–deprotection strategies to control the kinetics for movement of the Brownian substrate (the rotaxane macrocycle) between these stations. Here, we use these same design features to create a [2]catenane that is the first example of a reversible synthetic rotary molecular motor.

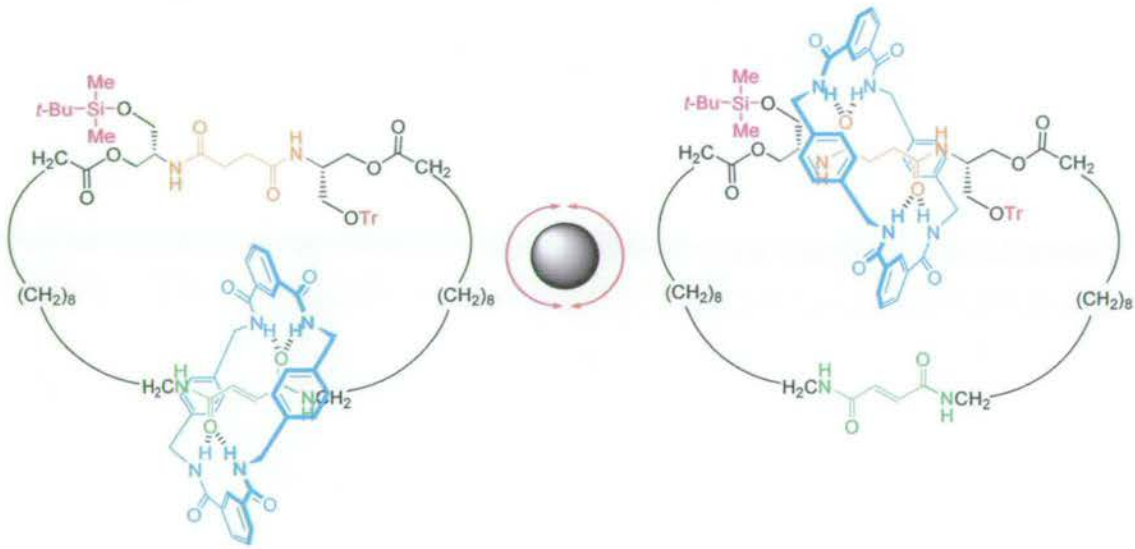

The movement of a small ring around a larger one occurs through positional displacements, arising from biased Brownian motion, and which are kinetically captured and then directionally released. The sense of rotation is governed solely by the order in which a series of orthogonal chemical transformations is performed. The minimalist nature of the [2]catenane flashing ratchet design permits certain mechanistic comparisons with the Smoluchowski–Feynman ratchet and pawl and further indicates how both informational and thermodynamic considerations govern directional Brownian rotation in molecular structures. Even when no work has to be done against an opposing force and no net energy is used to power the motion, a finite conversion of energy is intrinsically required for the molecular motor to undergo directional rotation. Non-directional rotation has no such requirement.

3.1 Introduction

Molecular-level motors differ from their macroscopic counterparts not only in scale, but in how environmental factors influence their operation. Macroscopic machines are generally unaffected by ambient thermal energy, and a directional force must be applied to cause movement of each component. For molecular-sized motors, however, inertia is negligible and the parts are subject to random and incessant Brownian motion.[1] Rather than fight this effect, biological motors use these random fluctuations in their mechanisms.[2] For example, in F_1F_0-adenosine triphosphatase (ATPase) – which spins the γ shaft counter-clockwise (viewing F_1 from above) as proton-motive force powers ATP production and clockwise if ATP is consumed to drive proton flow against a concentration gradient[3] – Brownian motion drives both the power and exhaust strokes.[2]

Inspired by such biological motors and by Feynman's celebrated discussion[4] of the miniature 'ratchet and pawl' concept first introduced by Smoluchowski,[5] efforts have been made to design molecules that exhibit directional control over submolecular rotary motion.[6–10] Unidirectional rotation about single,[11, 12] double,[13–16] and mechanical[17] bonds has been achieved, but unlike F_1F_0-ATPase, these artificial motor molecules are only able to rotate in one direction and not the other. We now report on a molecular structure in which a fragment can be circumrotated in either direction and probe features of the underlying mechanism.

3.2 Design

During the past decade, a number of remarkable theoretical formalisms have been developed using nonequilibrium statistical physics that explain how various types of fluctuation-driven transport can occur (see Chapter 1 for more details).[18, 19] Underlying each of these Brownian ratchet or motor mechanisms are three components:[20] (i) a randomizing element;[21] (ii) an energy input to avoid falling foul of the Second Law of Thermodynamics;[22] and (iii) asymmetry in the energy or information potential in the dimension in which the motion occurs. Such ratchet mechanisms not only account for the general principles behind biological motors[23–26] but have also been successfully applied to the development of transport and separation devices for mesoscopic particles and macromolecules, microfluidic pumping, the

photo-alignment of liquid crystals, and quantum and electronic applications.[25, 27–32] A flashing ratchet is a particular type of energy ratchet mechanism,[24] a classic example of which consists in physical terms (Figure 3.1) of an asymmetric potential energy surface (a periodic series of two different minima and two different maxima) along which a Brownian particle is directionally transported by sequentially raising and lowering each set of minima and maxima by changing the potential (for example, with an oscillating electric field and a charged particle).

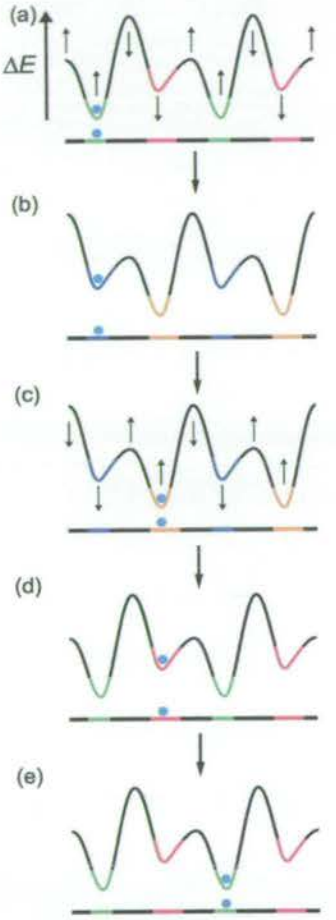

Figure 3.1 A flashing energy ratchet mechanism for Brownian particle transport along an oscillating potential energy surface.

Catenanes and rotaxanes, molecules in which components are physically linked together but not connected by covalent bonds, are excellent systems with which to study characteristics of submolecular motion.[8] The mechanical linkage inherently restricts certain degrees of freedom for the relative displacement of the interlocked components whilst simultaneously permitting large amplitude motion in the allowed vectors. The way in which the principles of an energy ratchet can be applied to a catenane architecture is not to consider the whole structure as a molecular machine,

but rather to view one macrocycle as a motor that transports a substrate – the other ring – directionally around itself. In its simplest manifestation this gives rise to a [2]catenane such as **1** (represented schematically in Figure 3.2) which should be able to unidirectionally rotate the smaller ring about the larger one in response to a series of chemical reactions.

There are several differences, however, between the flashing ratchet particle transport mechanism in Figure 3.1 and the one applied to catenane **1** in Figure 3.2: (i) the molecular system is cyclic so the translational transport along a periodic energy potential becomes a directional rotation around a two-minima-two-maxima loop; (ii) only one energy minimum is varied for **1**, not both (which is sufficient to ensure that the energy difference between the two minima changes twice); and (iii) the single steps that simultaneously change minima depth and maxima height in the classical energy ratchet mechanism are separated into their thermodynamic and kinetic constituents in the chemical system. Despite these differences, the physical principles behind the two mechanisms are the same.

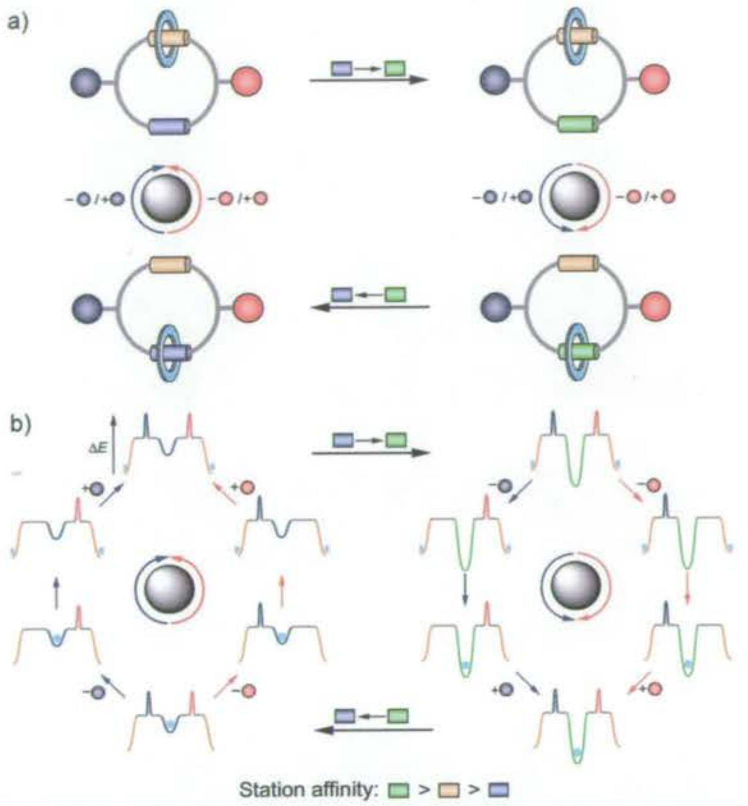

Figure 3.2 (a) Schematic illustration and (b) potential energy surface for the small light blue ring in a minimalist [2]catenane rotary molecular motor, **1**. The ring preferentially resides on one or other of the two binding sites (stations), represented by coloured cylinders. The coloured spheres are bulky groups, each of which sterically blocks one of the two tracks between the stations. The blue-to-green and green-to-blue transformations represent (balance-breaking) chemical reactions that change the binding affinity of a station for the small ring, providing a driving force for the ring to re-distribute itself between the stations if it is able to be exchanged between them. Removal of a red or purple sphere (linking reaction) allows the ring to move between stations by a particular route. Reattachment of the sphere (unlinking reaction) ratchets the net transported quantity of rings.

In chemical terms, catenane **1** is a stimuli-responsive molecular shuttle[8, 33] with two routes (each of which can be independently blocked) that connect the two binding sites or 'stations' for the small macrocycle (Scheme 3.1). To satisfy oneself that internal motion within a chemical structure can be described in terms of a stochastic transport mechanism, it is useful to consider how the net change of position occurs within a typical stimuli-responsive molecular shuttle.[33] At equilibrium, the small macrocycle is distributed between two different stations (an asymmetric track) according to a Boltzmann distribution. An external trigger (the energy input) chemically modifies one binding site in such a way that the initially disfavoured station becomes energetically more favourable for the macrocycle. Thermal fluctuations (the randomizing element) provide the energy required by the small

macrocycle to sever its interactions with a station and set off on a Brownian walk through which the new equilibrium position is established.

3.3 Operation of the molecular machine

Catenane **1** was prepared as the *fum-E*-**1** isomer[34] according to Scheme 3.1.[35] Net changes in the position or potential energy of the smaller ring were sequentially achieved by (a) photoisomerization to the maleamide (→*mal-Z*-**1**);[36, 37] (b) de-silylation/re-silylation (→*succ-Z*-**1**); (c) re-isomerization to the fumaramide (→*succ-E*-**1**); and finally, (d) de-tritylation/re-tritylation to regenerate *fum-E*-**1**, the whole reaction sequence producing a net clockwise (as drawn in Scheme 3.1) circumrotation of the small ring about the larger one. Exchanging the order of steps (b) and (d) generated the equivalent counter-clockwise rotation of the small ring. The time scales and number of reactions involved for directional rotation in **1** make it somewhat less practical than the methods previously developed for non-reversible synthetic rotary motors.[11–17] Nevertheless, the chemistry is surprisingly robust and can be carried out as a direct sequence of reactions without purification at each stage, using resins to neutralize or remove excess reagents and by-products, with only modest reductions in yields indicated by ^{1}H nuclear magnetic resonance (NMR) spectroscopy.

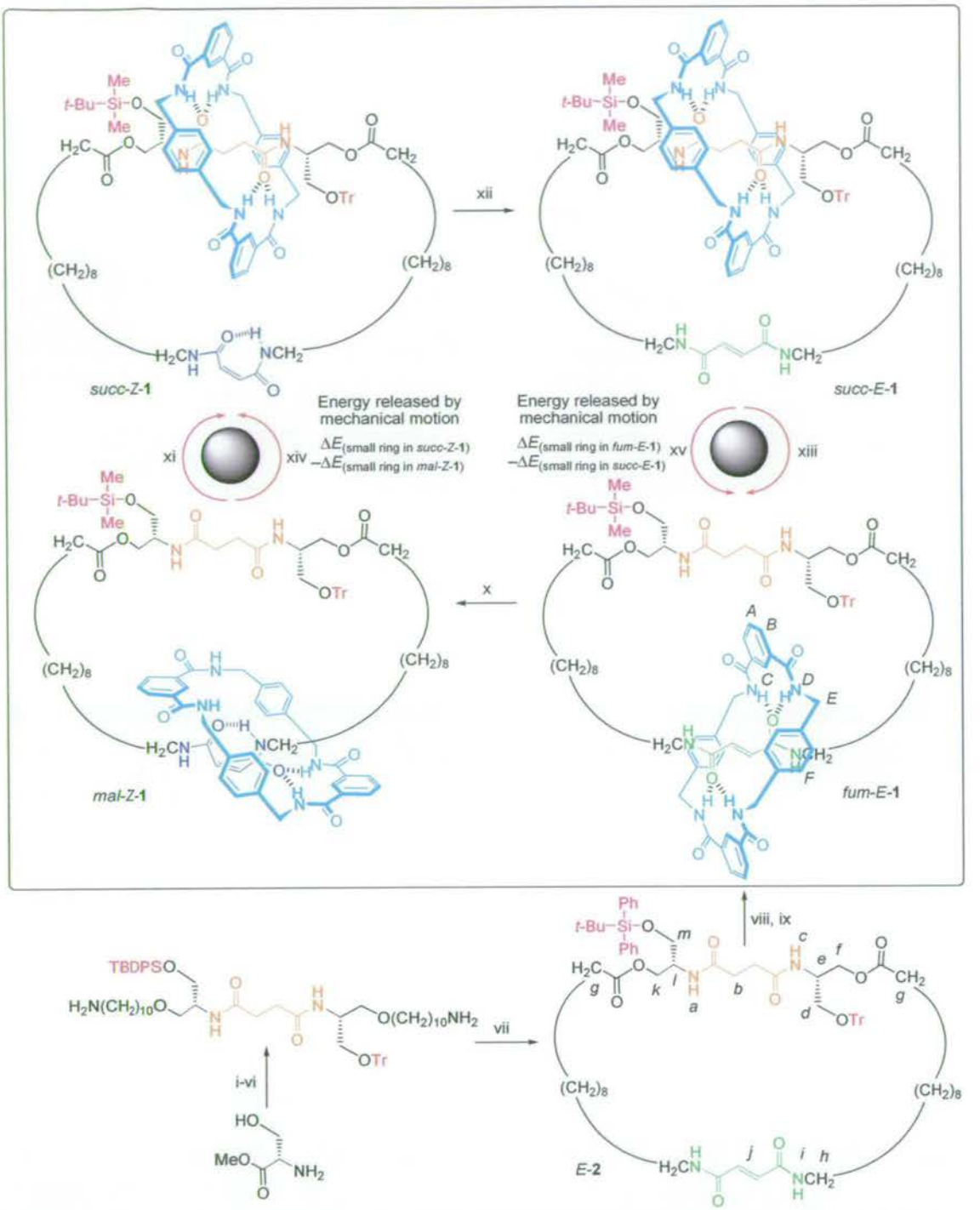

Scheme 3.1 Synthesis and operation of reversible rotary motor **1**. Reagents and conditions (unless otherwise stated, reactions were carried out at room temperature and in CH_2Cl_2): (i) succinyl chloride, Et_3N, DMF, 0 °C, 2 h, 80%; (ii) *tert*-butyldiphenylsilyl chloride (TBDPSCl), NH_4NO_3, DMF, 8 h, 30%; (iii) trityl chloride (TrCl), Bu_4NClO_4, 2,4,6-collidine, $CHCl_3$, 61 °C, 2 h, 86%; (iv) $NaBH_4$, LiCl, THF, EtOH, 8 h, 79%; (v) $FmocNH(CH_2)_{10}CO_2H$, dicyclohexylcarbodiimide (DCC), 1-hydroxybenzotriazole (HOBt), 4-(dimethylamino)pyridine, 8 h, 85%; (vi) Et_2NH, 8 h, 73%; (vii) fumaric acid, DCC, HOBt, $CHCl_3$, 8 h, 52%; (viii) isophthaloyl dichloride, *p*-xylylenediamine, Et_3N, $CHCl_3$, 3 h, 30%; (ix) tetrabutylammonium fluoride (TBAF), 20 min, cool to –10 °C and add 2,4,6-collidine, *tert*-butyldimethylsilyl triflate (TBDMSOTf), 40 min, overall 72%; (x) hν 254 nm, 5 min., 50%; (xi) TBAF, 20 min, cool to –78 °C and add 2,4,6-collidine, TBDMSOTf, 1 h, overall 61%; (xii) piperidine, 1 h, quantitative; (xiii) $Me_2S{\cdot}BCl_3$, –10 °C, 10 min, then TrCl, Bu_4NClO_4, 2,4,6-collidine, 16 h, overall 74%; (xiv) $Me_2S{\cdot}BCl_3$, –10 °C, 15 min, cool to –78 °C and add 2,4,6-collidine, TrOTf,

5 h, overall 63%; (xv) TBAF, 20 min, cool to –10 °C and add 2,4,6-collidine, TBDMSOTf, 40 min, overall 76%. The above refer to preparative yields of isolated compounds. Net clockwise circumrotation was also achieved in one pot through the successive addition of reagents to *fum-E*-**1** in the following sequence (^{1}H NMR-determined percentage conversions given in parentheses): (x) hν 254 nm, 5 min (50% *mal-Z*-**1** present); (xi) 4 equivalents of TBAF, 20 min, cool to –78 °C and add 30 equivalents of TBDMSOTf, 30 equivalents of 2,4,6-collidine, 30 min, then 60 equivalents of Wang resin, Dowex MR mixed bed ion-exchange resin and activated 4Å molecular sieves, decant (~33% *succ-Z*-**1** present); (xii) 20 equivalents of piperidine, 1 h, then Dowex MR mixed bed ion-exchange resin, decant (~33% *succ-E*-**1** present); (xiii) 1 equivalent of $Me_2S{\cdot}BCl_3$, –10 °C, 5 min, then 25 equivalents of 2,4,6-collidine, 20 equivalents of TrOTf, 1 h (~90% *fum-E*-**1** present; ~28% of the total molecules in the sample having undergone circumrotation). The chirality of **1** is present only for synthetic convenience.

Unlike the previously reported[17] [3]catenane rotor, which relied on the dynamics of model compounds to determine stimuli-induced unidirectional behaviour, the sense of rotation in **1** was demonstrated directly by isolation of samples of the [2]catenane after each synthetic step and the position of the small ring unambiguously determined by ^{1}H NMR spectroscopy (Figures 3.3 and 3.4). Shielding effects reveal the position of the small macrocycle in each of the four catenane isomers. Comparison of the spectrum of *fum-E*-**1** (Figure 3.3a) with that of the macrocycle *E*-**2** (Figure 3.3b) shows an upfield shift of the H_j protons of the fumaramide station but not the succinamide group (H_b) in the catenane. In contrast, *succ-E*-**1** (Figure 3.3c) features a –1.3 parts per million difference in the H_b protons but little change in the signals of the fumaramide residue. The macrocycle is similarly located over the succinamide residue in *succ-Z*-**1** (see, for example, the shifts of H_b in Figures 3.4c and 3.4b). Finally, although the small ring does not spend too much time actually over the poorly-binding maleamide station in *mal-Z*-**1** (as evidenced by the relatively small shift in H_j in Figure 3.4a as compared to Figure 3.4b), it is clearly trapped on the maleamide side of the silyl and trityl blocking groups because of the lack of shielding of the succinamide signals (H_b are unchanged between Figures 3.4a and 3.4b) and some significant shielding observed for H_h.

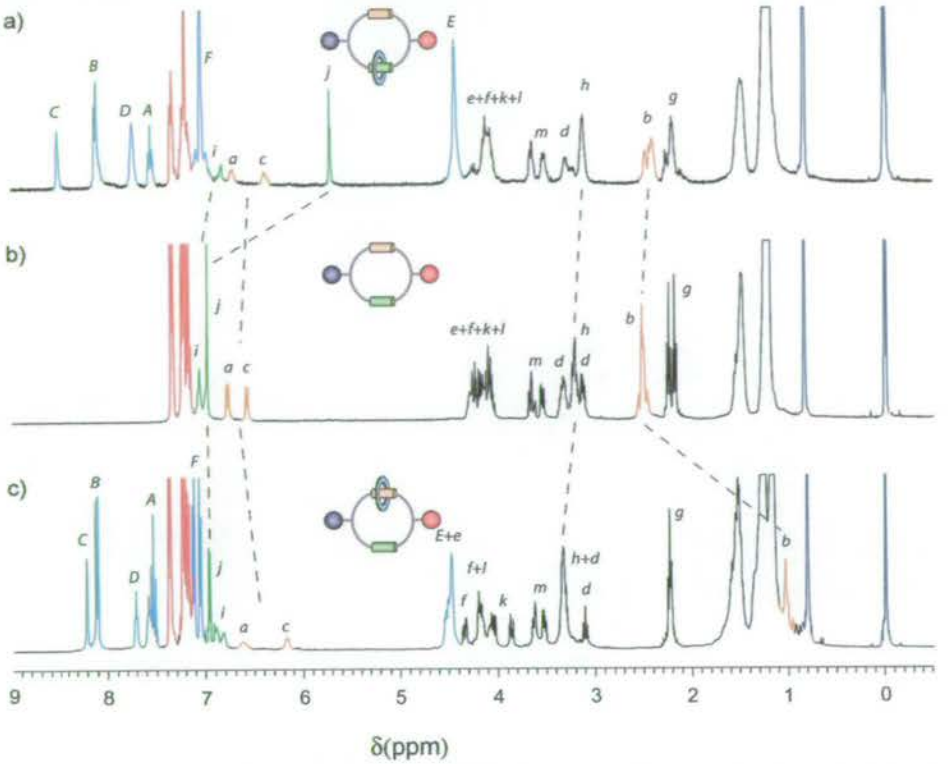

Figure 3.3 ^{1}H NMR spectra (400 MHz, $CDCl_3$, 298 K) of (a) [2]catenane *fum-E*-**1**; (b) macrocycle *E*-**2**; (c) [2]catenane *succ-E*-**1**. The colour coding and lettering correspond to the assignments shown in Scheme 3.1.

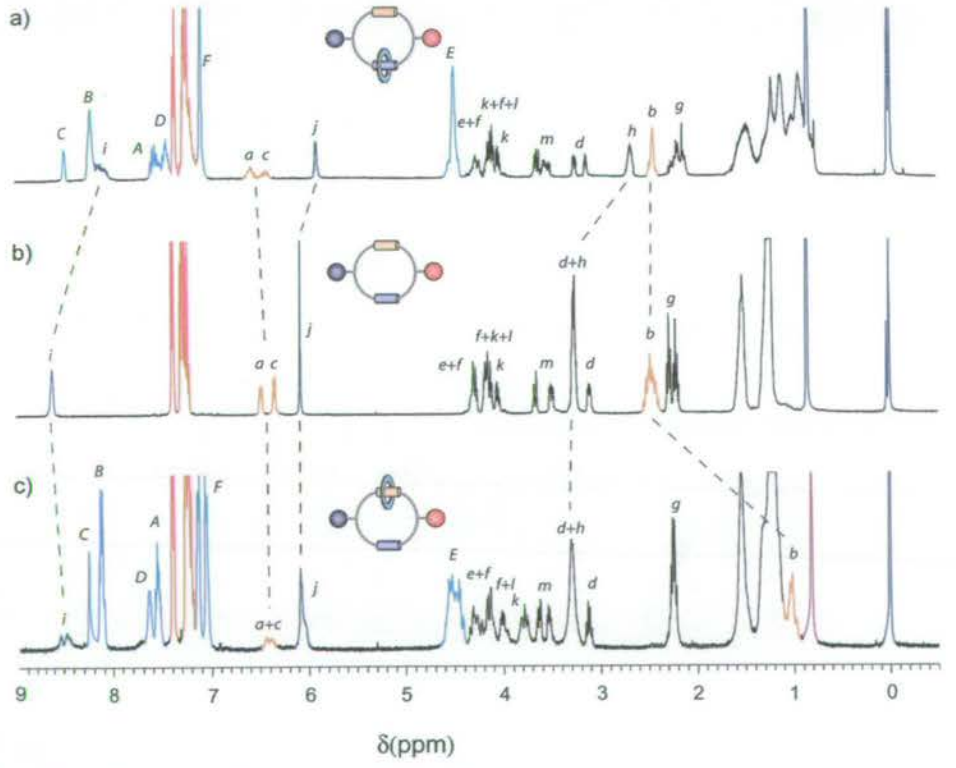

Figure 3.4 ^{1}H NMR spectra (400 MHz, $CDCl_3$, 298 K) of (a) [2]catenane *mal-Z*-**1**; (b) macrocycle *Z*-**2**; (c) [2]catenane *succ-Z*-**1**. The colour coding and lettering correspond to the assignments shown in Scheme 3.1.

3.4 Discussion

Biological motors are obviously too complex for the thermodynamic function of individual amino acid movements to be unravelled in detail. In contrast, the apparent simplicity of **1** and the minimalist nature of its design allow insight into the fundamental role that each part of the structure plays in the operation of the rotary machine.

The various chemical transformations perform two different functions: one pair [the linking/unlinking reactions – steps (xi) and (xiii), or (xiv) and (xv) in Scheme 3.1] modulates whether the small macrocycles can be exchanged between the two binding sites on the big ring (that is, allow the small macrocycle to become statistically balanced between the two binding sites according to a Boltzmann distribution); the second pair [balance-breaking reactions – steps (x) and (xii) in Scheme 3.1] isomerizes the olefin station (either $E \rightarrow Z$ or $Z \rightarrow E$), switching its binding affinity for the small macrocycle either 'on' or 'off'.[37] By changing the relative binding affinities of the two stations in the large ring, each balance-breaking stimulus provides a driving force for re-distribution of the small ring if it is able to move between the binding sites. In other words, the stations and blocking groups effectively disconnect the thermodynamic and kinetic components of detailed balance;[22] the balance-breaking reactions control the thermodynamics and impetus for net transport by biased Brownian motion, and the linking/unlinking reactions largely[38] control the relative kinetics and ability to exchange. Raising a kinetic barrier also 'ratchets' transportation, allowing the statistical balance of the small ring to be subsequently broken without reversing the preceding net transportation sequence. Lowering a kinetic barrier allows 'escapement' of a ratcheted quantity of rings in a particular direction.

To obtain 360° rotation of the small ring about the large ring, the four sets of reactions must be applied in one of two sequences, each taking the following form: first a balance-breaking reaction; then a linking/unlinking step; then the second balance-breaking reaction; finally, the second linking/unlinking step. The direction of net rotation is determined solely by the way in which the balance-breaking and linking/unlinking steps are paired – an external input of information. The efficiency or yields of the reactions – or the position of the ring at any stage (even if the machine

makes a 'mistake') – are immaterial to the direction in which net motion occurs as long as the reactions continue to be applied in the same sequence. Although changing the pairings rotates the small ring in the opposite direction, reversing the entire sequence of six chemical reactions does not, because linking/unlinking operations are not commutative.

We finish the circumrotation reaction sequence with the same molecule, *fum-E*-**1**, that we started with (although a 360° rotation of one fragment has occurred), and the light-fuelled balance-breaking reaction is reversed by a quantitative exergonic reaction so no net energy is consumed to fuel the rotation. This is in one sense obvious, because the movement of the small ring takes place through Brownian motion and does not have to be powered; and in another somewhat surprising, because directional circumrotation of the small ring has occurred which could be used to do external work – analogous to the hypothetical lifting of a flea by the Smoluchowski–Feynman ratchet and pawl.[4] Of course, if the [2]catenane does do work against an opposing force the energy required is taken from the balance-breaking reactions. However, in the absence of an opposing force, if the balance-breaking chemical reactions do not actually fuel the net rotation is it really necessary to carry them out? At first glance it seems that the small ring in a [2]catenane such as **3** might undergo directional circumrotation without them (Figure 3.5).

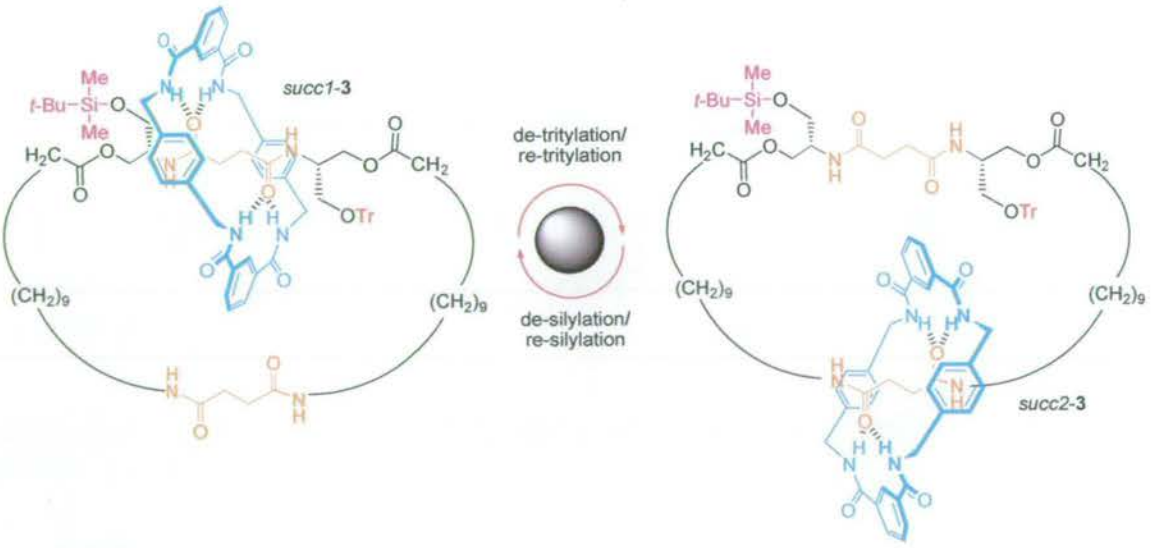

Figure 3.5 Positional isomerism in a [2]catenane, **3**, with stations of degenerate binding energies.

Let us consider the situation in which 100% of the small rings are initially located on the succinamide station closest to the blocking groups: 100% *succ1*-**3**. De-tritylation

followed by re-tritylation generates 50% *succ2*-**3** (and 50% remains as *succ1*-**3**). Treatment of this mixture with a de-silylation/re-silylation sequence leads to a final product mixture which again is 50% *succ1*-**3** and 50% *succ2*-**3**. However, half of the molecules that are now *succ1*-**3** (25% of the total molecules) have undergone a 360° clockwise circumrotation of the small ring, and all of the *succ2*-**3** structures (50% of the total molecules) have undergone a 180° rotation of the small ring (half clockwise; half counter-clockwise). The remaining 25% of total molecules have undergone no net positional change of the small ring, and so the average for the sample is a 90° clockwise rotation without applying any chemical reactions to change the relative values of the two stations' energy minima. When we apply the sequence of reactions for a second (or any subsequent) time, however, although 75% of the molecules again individually undergo partial or complete revolution of the small ring, no net rotation occurs in either direction over a bulk sample. The 50% of molecules that start as *succ1*-**3** give a net 90° clockwise rotation in response to the linking/unlinking sequence and the 50% that start as *succ2*-**3** rotate an equivalent amount in a counter-clockwise sense. A statistically significant number of catenane **3** molecules can only undergo net unidirectional rotation if the distribution of the small macrocycle between the binding sites is unbalanced at the start of the reaction sequence.

We can use some simple thermodynamic accountancy to calculate both the maximum amount of mechanical work that can be carried out by **1** and how much chemical energy has to be processed to cause directional motion of the small ring even if no work needs to be done against an opposing external force. The energy available to do work each time the small ring changes station equates to the macrocycle binding energy differences between the two sites.[33] The light-fuelled $E \rightarrow Z$ transformation allows up to $\Delta E_{(\text{small ring in } \textit{succ-Z}\text{-}\mathbf{1})} - \Delta E_{(\text{small ring in } \textit{mal-Z}\text{-}\mathbf{1})}$ to be performed during the subsequent linking step and the piperidine-catalysed $Z \rightarrow E$ reaction permits a further $\Delta E_{(\text{small ring in } \textit{fum-E}\text{-}\mathbf{1})} - \Delta E_{(\text{small ring in } \textit{succ-E}\text{-}\mathbf{1})}$ (Scheme 3.1). Because $\Delta E_{(\text{small ring in } \textit{succ-Z}\text{-}\mathbf{1})} \sim \Delta E_{(\text{small ring in } \textit{succ-E}\text{-}\mathbf{1})}$, the maximum total mechanical work that can be performed by circumrotation is $\Delta E_{(\text{small ring in } \textit{fum-E}\text{-}\mathbf{1})} - \Delta E_{(\text{small ring in } \textit{mal-Z}\text{-}\mathbf{1})}$; that is, the difference in small ring binding affinity between the fumaramide and maleamide stations. It is interesting to note that the binding affinity of the intermediate station is irrelevant to the amount of work that can be carried out by the molecular motor.

A quantitative thermodynamic requirement for unidirectional rotation of the small ring is provided by the difference between the free energies of the sequence of reactions (x), (xi), (xii), (xiii) carried out on *fum*-*E*-**1** and the same series of reactions applied to the macrocycle, *E*-**2**. The thermodynamics associated with the linking/unlinking steps cancel out.[39] However, the *E*→*Z* isomerization step (step x) for the catenane is inherently more endothermic than the analogous reaction on the macrocycle because of the additional energy necessary to disrupt the hydrogen-bond network of the small ring with the fumaramide station. The extra energy required to raise the potential energy of the transported particle (again, the difference in small ring binding energies of the fumaramide and maleamide stations) is returned to the thermal bath upon re-isomerization to fumaramide and subsequent re-positioning of the macrocycle. This requirement of extra energy to be processed by the system for the molecular machine to rotate directionally even when no work has to be done against an external force is once more reminiscent of the Smoluchowski–Feynman ratchet and pawl, which Feynman appreciated could be driven directionally by Brownian motion using heat flow between two thermal reservoirs; for example, by having the vanes attached to the shaft of the Feynman ratchet be hot and the wheel cold.[40] We note that the amount of additional chemical energy that must be processed for directional rotation to occur in the catenane is the sum of the energy differences that govern the Boltzmann distribution of the small ring between the binding sites at each stage; that is, the factor that determines the directional efficiency of the motor at constant temperature.

3.5 Conclusions

Mechanisms formulated from nonequilibrium statistical mechanics can be successfully used to design synthetic molecular motors such as **1**. In turn, the analysis of this deceptively simple molecule – particularly the separation of the kinetic and thermodynamic requirements for detailed balance – provides experimental insight into how and why an energy input is essential for directional rotation of a submolecular fragment by Brownian motion. Even though no net energy is used to power the motion, there has to be a particular amount of energy converted by the system for net rotation to be directional over a statistically significant number of molecules; a

requirement that is absent if the equivalent motion is non-directional (or, indeed, for directional rotation within a single molecule where balance is inherently broken). The quantity of energy conversion required to induce directionality has an intrinsic lower limit, corresponding exactly (and somewhat beautifully) to both the energy difference that determines the directional efficiency of rotation and the maximum amount of work that the motor can theoretically perform in a single cycle; there can be no perpetually unidirectionally rotating molecular structure of the second kind through such a mechanism. The factors that determine the sense of rotation in **1**, together with the requirement for finite energy conversion for directional rotation in circumstances when no work is done against an external force, illustrate how interplay between informational and thermodynamic laws governs directional Brownian rotation in molecular structures.

3.6 References and notes

[1] E. M. Purcell, *Am. J. Phys.* **1977**, *45*, 3-11.

[2] *Molecular Motors* (Ed.: M. Schliwa), Wiley-VCH, Weinheim, **2003**.

[3] P. D. Boyer, *Angew. Chem. Int. Ed.* **1998**, *37*, 2296-2307.

[4] R. P. Feynman, R. B. Leighton, M. Sands, *The Feynman Lectures on Physics, Vol. 1*, Addison-Wesley, Reading, MA, **1963**, Chapter 46.

[5] M. von Smoluchowski, *Physik. Z.* **1912**, *13*, 1069-1080.

[6] T. R. Kelly, I. Tellitu, J. P. Sestelo, *Angew. Chem. Int. Ed. Engl.* **1997**, *36*, 1866-1868.

[7] A. P. Davis, *Angew. Chem. Int. Ed.* **1998**, *37*, 909-910.

[8] V. Balzani, A. Credi, F. M. Raymo, J. F. Stoddart, *Angew. Chem. Int. Ed.* **2000**, *39*, 3349-3391.

[9] M. F. Hawthorne, J. I. Zink, J. M. Skelton, M. J. Bayer, C. Liu, E. Livshits, R. Baer, D. Neuhauser, *Science* **2004**, *303*, 1849-1851.

[10] C. P. Mandl, B. König, *Angew. Chem. Int. Ed.* **2004**, *43*, 1622-1624.

[11] T. R. Kelly, H. De Silva, R. A. Silva, *Nature* **1999**, *401*, 150-152.

[12] T. R. Kelly, R. A. Silva, H. De Silva, S. Jasmin, Y. J. Zhao, *J. Am. Chem. Soc.* **2000**, *122*, 6935-6949.

[13] N. Koumura, R. W. J. Zijlstra, R. A. van Delden, N. Harada, B. L. Feringa, *Nature* **1999**, *401*, 152-155.

[14] N. Koumura, E. M. Geertsema, A. Meetsma, B. L. Feringa, *J. Am. Chem. Soc.* **2000**, *122*, 12005-12006.

[15] N. Koumura, E. M. Geertsema, M. B. van Gelder, A. Meetsma, B. L. Feringa, *J. Am. Chem. Soc.* **2002**, *124*, 5037-5051.

[16] M. K. J. ter Wiel, R. A. van Delden, A. Meetsma, B. L. Feringa, *J. Am. Chem. Soc.* **2003**, *125*, 15076-15086.

[17] D. A. Leigh, J. K. Y. Wong, F. Dehez, F. Zerbetto, *Nature* **2003**, *424*, 174-179.

[18] P. Reimann, *Phys. Rep.* **2002**, *361*, 57-265.

[19] J. M. R. Parrondo, L. Dinís, *Contemp. Phys.* **2004**, *45*, 147-157.

[20] R. D. Astumian, *Science* **1997**, *276*, 917-922.

[21] Randomizing influences other than Brownian motion can be used in ratchet mechanisms. For example, in quantum ratchets, quantum effects such as tunnelling play this role.

[22] The principle of detailed balance (L. Onsager, *Phys. Rev.* **1931**, *37*, 405-426) tells us that no net task can be performed by the fluxional exchange of components at equilibrium because transitions take place at the same rate in opposite directions. The structure of catenane **1** is remarkable in that it separates the kinetic (ability to exchange) and thermodynamic (impetus for net transport) requirements for detailed balance.

[23] R. D. Astumian, P. Hänggi, *Phys. Today* **2002**, *55* (11), 33-39.

[24] R. D. Astumian, I. Derényi, *Eur. Biophys. J.* **1998**, *27*, 474-489.

[25] Special issue on "Ratchets and Brownian motors: Basics, experiments and applications": *Appl. Phys. A* **2002**, *75*, 167-352.

[26] G. Oster, H. Y. Wang, *Trends Cell Biol.* **2003**, *13*, 114-121.

[27] J. Rousselet, L. Salome, A. Ajdari, J. Prost, *Nature* **1994**, *370*, 446-448.

[28] L. P. Faucheux, L. S. Bourdieu, P. D. Kaplan, A. J. Libchaber, *Phys. Rev. Lett.* **1995**, *74*, 1504-1507.

[29] J. S. Bader, R. W. Hammond, S. A. Henck, M. W. Deem, G. A. McDermott, J. M. Bustillo, J. W. Simpson, G. T. Mulhern, J. M. Rothberg, *Proc. Natl. Acad. Sci. USA* **1999**, *96*, 13165-13169.

[30] A. van Oudenaarden, S. G. Boxer, *Science* **1999**, *285*, 1046-1048

[31] H. Linke, T. E. Humphrey, A. Lofgren, A. O. Sushkov, R. Newbury, R. P. Taylor, P. Omling, *Science* **1999**, *286*, 2314-2317

[32] S. Matthias, F. Müller, *Nature* **2003**, *424*, 53-57.

[33] A. Altieri, G. Bottari, F. Dehez, D. A. Leigh, J. K. Y. Wong, F. Zerbetto, *Angew. Chem. Int. Ed.* **2003**, *42*, 2296-2300.

[34] The prefix indicates the position of the smaller macrocycle on the larger one.

[35] Although catenane *fum-E*-**1** was originally prepared as its *O-tert*-butyldiphenylsilyl (TBDPS) derivative, the steric bulk caused low yields during the re-silylation protocol of step (xi), so it was replaced with the smaller TBDMS group for all the directional rotation studies.

[36] The photoisomerization reaction gives a 50:50 *E*:*Z* mixture in the photostationary state. No accompanying photodegradation or decomposition was detected.

[37] F. G. Gatti, S. León, J. K. Y. Wong, G. Bottari, A. Altieri, M. A. F. Morales, S. J. Teat, C. Frochot, D. A. Leigh, A. M. Brouwer, F. Zerbetto, *Proc. Natl. Acad. Sci. USA* **2003**, *100*, 10-14.

[38] By raising or lowering the energy minima, the balance-breaking reactions intrinsically affect the kinetic barriers as well.

[39] This is not quite as simple as the ΔG values of the forward and reverse covalent bond forming and breaking reactions cancelling each other out. When unlinking takes place, the restriction in freedom of movement reduces the entropy of the small macrocycle in addition to the ΔG change associated with the chemical reaction; however, when linking occurs the entropy increases by the same amount.

[40] Certain aspects of Feynman's discussion of the ratchet and pawl as a motor have been shown to be flawed, although this does not affect the general principles demonstrated. See: a) J. M. R. Parrondo, P. Español, *Am. J. Phys.* **1996**, *64*, 1125-1130; b) M. O. Magnasco, G. Stolovitzky, *J. Stat. Phys.* **1998**, *93*, 615-632.

CHAPTER FOUR

A Molecular Information Ratchet

A shortened version of this Chapter has been accepted for publication in the journal *Nature*:

V. Serreli, C.-F. Lee, E. R. Kay, D. A. Leigh, *Nature*, in press.

Acknowledgements and contributions

Synthesis and characterization of all new compounds and all photochemical experiments reported in this Chapter were carried out by Viviana Serreli and Dr Chin-Fa Lee, whose contributions are very gratefully acknowledged. I also thank Dr Philip Camp for the derivation of equation (1). In conjunction with Prof. David A. Leigh, the author devised the concept and structural design of the molecular information ratchet, its synthesis and the experiments required to characterize its operation, analysed the results and wrote this Chapter and the paper it is based upon.

Synopsis

The previous two Chapters have discussed molecular machines that operate by switching the relative energies of adjacent compartments in concert with altering the kinetics for transport between them. They employ 'energy ratchet' mechanisms, in which knowledge about the position of the Brownian particle is not required. In this Chapter, a compartmentalized molecular machine is reported, in which the distribution of a Brownian particle (the macrocycle in a rotaxane) is controlled by using the light-induced transmission of information to lower a kinetic barrier according to the location of the particle. For an ensemble of such machines the particle distribution is directionally driven further and further away from equilibrium, as envisaged for a Maxwellian pressure demon in molecular form. However, the nanomachine does not break the Second Law of Thermodynamics because the energy cost of the information transfer is met by externally supplied photons. As the behaviour of the molecular structure can be understood in clear chemical terms, it is possible in this experimental system to pin-point precisely how information is traded for energy. Intriguingly, the chemical mechanism can also be understood in terms of game theory. This is the first example of a synthetic molecular machine designed to operate via an information ratchet mechanism, where knowledge of a particle's position is used to control its transport away from equilibrium.

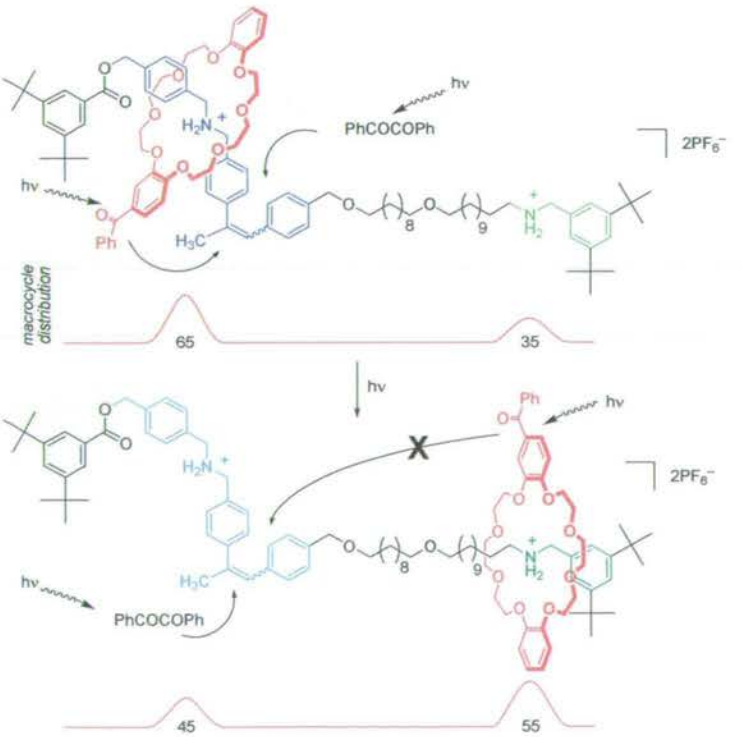

4.1 Introduction

The ability of nature's molecular motors and machines to drive chemical systems away from equilibrium is central to biology[1] but, despite recent advances,[2–15] remains rare[14] for the present-day early generations of artificial molecular machines. The concept of tiny machines capable of selectively transporting particles between two compartments by Brownian motion dates back to the 19th century when James Clerk Maxwell pondered the significance of a hypothetical 'sorting demon' being able to perform such a task adiabatically. Maxwell conceived his celebrated thought experiment,[16–19] which leads to a nonequilibrium distribution of thermal energy or Brownian particles (Figure 4.1), to illustrate the statistical nature of the Second Law of Thermodynamics, but modern synthetic chemistry allows us to consider his idea from a very different perspective. Rather than test the Second Law by attempting to drive an isolated system away from equilibrium, how can information transfer between a particle and a 'gate-keeper' be accomplished non-adiabatically to form a mechanism for a working Brownian motion nanomachine?

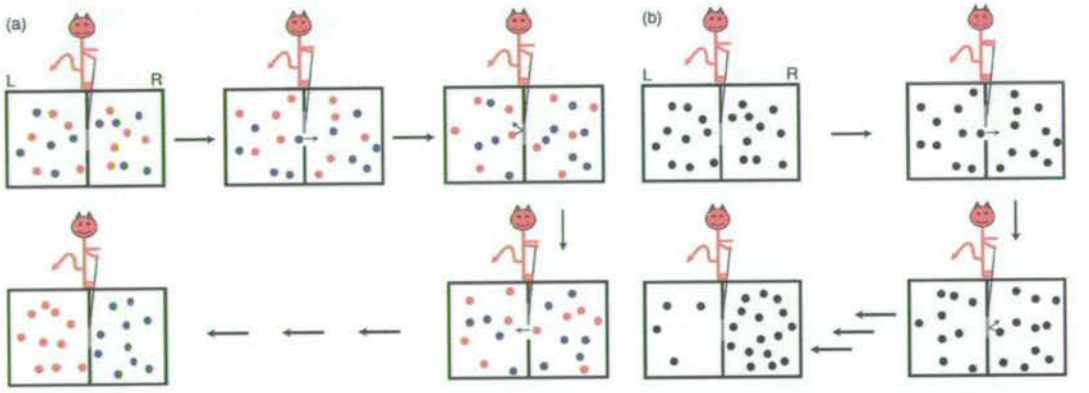

Figure 4.1 The 'Maxwell's Demon' thought experiments.[16–19] (a) Maxwell's 'temperature demon' in which a gas at uniform temperature is sorted into 'hot' (red) and 'cold' (blue) molecules.[16, 17] The demon opens the gate between the compartments when it detects a cold particle approaching the gate from the left or a hot particle coming from the right, thus separating the particles according to their thermal energy and creating a temperature differential between the compartments. (b) A Maxwellian 'pressure demon' in which a concentration gradient is established by the gate being opened only when a particle approaches it from the left. Maxwell introduced the concept of a pressure demon in a letter[18] to Peter Guthrie Tait: '*Concerning Demons...Is the production of an inequality of temperature their only occupation? No, for less intelligent demons can produce a difference in pressure as well as temperature by merely allowing all particles going in one direction while stopping all those going the other way. This reduces the demon to a valve.*'. In both versions of the thought experiment the idea is that the demon's actions involve no work being done, but as the end-result is a reduction in the entropy (i.e. an increase in free energy) of the gas, this is in conflict with the Second Law of Thermodynamics. Maxwell appreciated that the successful operation of the demon in the thought experiment somehow relied on its intelligence as an animate being. Subsequent analysis by several generations of scientists revealed a fundamental link between entropy and information, significantly influencing the development of statistical and quantum physics and chemistry, information theory and computer science.[19]

4.2 Design of a non-adiabatic molecular Maxwellian pressure demon

This question inspired the design of rotaxane **1** (Figure 4.2), which consists of a dibenzo-24-crown-8-based macrocycle mechanically locked onto a linear thread by bulky 3,5-di-*tert*-butylphenyl groups situated at either end and which was synthesized as outlined in Section 4.9.2 (25 steps in the longest linear sequence). An α-methyl stilbene unit divides the molecule into two 'compartments'. The *E*-stilbene isomer allows the macrocycle to move randomly along the full length of the thread by Brownian motion but the *Z*-form provides a non-traversable steric barrier,[20] trapping the ring in one or other of the compartments. The α-methyl stilbene 'gate' is asymmetrically positioned on the thread between two ammonium groups (monobenzyl ammonium, *mba*; dibenzyl ammonium, *dba*) which have somewhat similar noncovalent binding affinities for the crown ether ring[21–24] but are distinguishable for the purposes of monitoring the system. Photoinduced switching between the open (*E*-) and closed (*Z*-) forms of the gate can occur either through direct photon absorption by the α-methyl stilbene chromophore or indirectly via energy transfer from the excited state of a triplet photosensitizer. The former is a minor pathway under our experimental conditions (irradiation at 350 nm) because the triplet sensitizers employed absorb far more strongly at this wavelength than α-methyl stilbene.

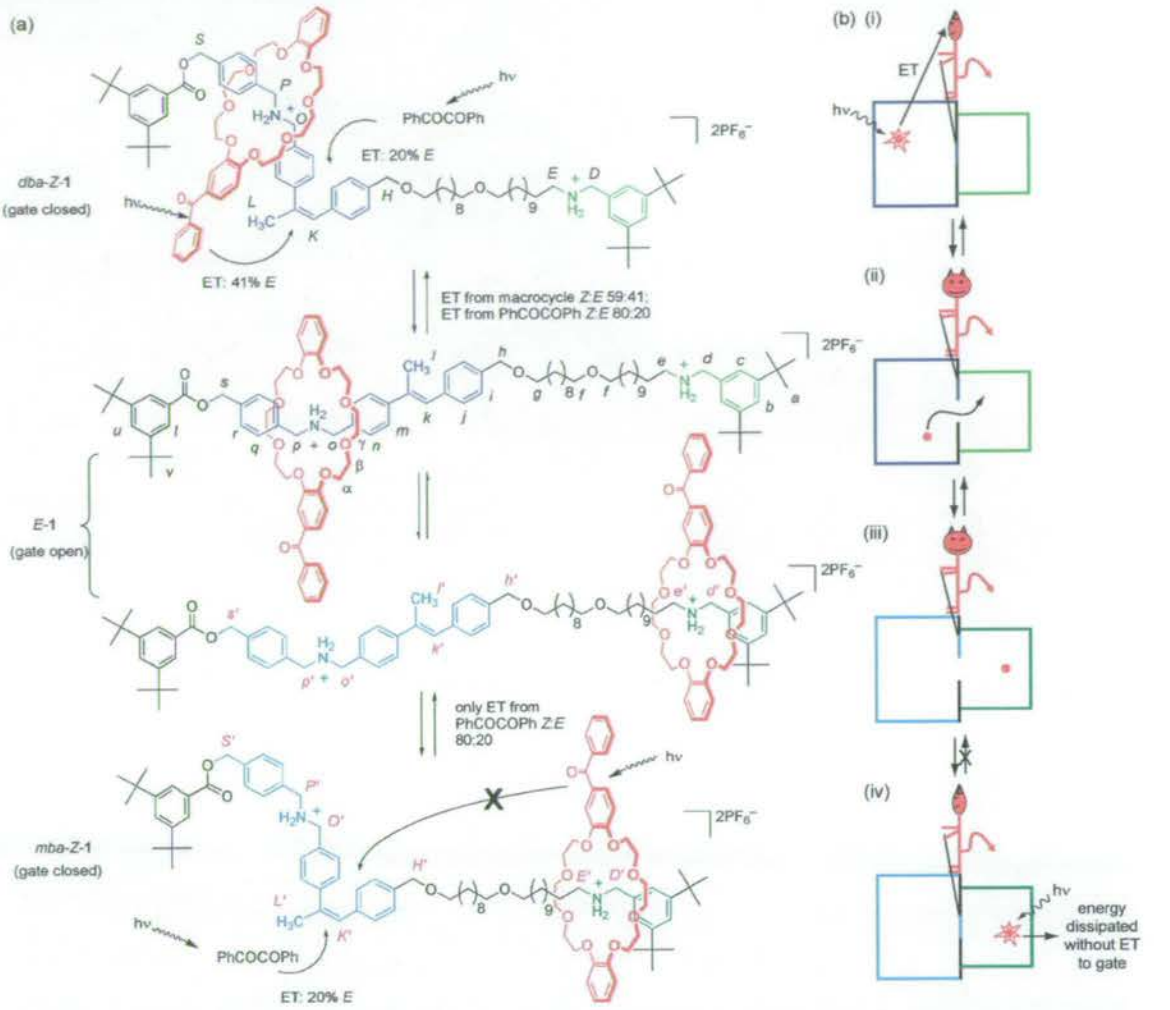

Figure 4.2 A photo-operated molecular information ratchet. (a) Irradiation of rotaxane **1** (1 mM) at 350 nm in CD_3OD at 298 K interconverts the three diastereomers of **1** and, in the presence of benzil (PhCOCOPh), drives the ring distribution away from the thermodynamic minimum, increasing the free energy of the system without ever changing the binding strengths of the macrocycle or ammonium binding sites. For clarity the photoinduced energy transfer (ET) pathways are only illustrated on the *Z*- (gate closed) forms of **1** although the same processes occur for the equivalent *E*- (gate open) translational isomers. When the macrocycle is on the *mba* binding site (green), intramolecular ET from the macrocycle is inefficient and intermolecular ET from benzil dominates (the cross on the intramolecular ET arrow is used to indicate that it is a rare event compared to other relaxation pathways). When the macrocycle is on the *dba* binding site (blue), both ET mechanisms can operate efficiently. The amount of benzil present determines the relative contributions of the two ET pathways and thus the nanomachine's effectiveness in pumping the macrocycle distribution away from equilibrium (see Figure 4.4). The mechanism requires the shuttling of the ring between the two ammonium groups in *E*-**1** to be slow with respect to the lifetime of the macrocycle-sensitizer triplet excited state. The greek and italicized lettering indicates the proton assignments for the ^{1}H NMR spectra shown in Figures 4.3 and 4.4. (b) Cartoon illustration of the operation of **1** in terms of a non-adiabatic Maxwellian pressure demon. (i) Photoinduced excitation of a particle signals its position in the blue compartment by energy transfer to the demon operating the gate (the demon uses information from the asymmetry in the compartments to distinguish where the excited particles are, here by their average distance from the gate). (ii) & (iii) The demon opens the gate and the particle shuttles incessantly between the two compartments by Brownian motion until the gate shuts trapping the particle at random in one of them. (iv) Photoinduced excitation of the particle in the green compartment is ignored by the demon and the energy of the excited state is dissipated as heat.

For a change in the distribution of the ring between the two binding sites of **1** to be established, the stilbene gate needs to be closed for much of the time. This is accomplished by operating the machine in the presence of benzil (PhCOCOPh); the benzil-sensitized photostationary state (PSS) of α-methyl stilbene is typically 82:18 *Z*:*E*[25] (model compounds used to design **1** all exhibited similar PSS ratios at 350 nm in various solvents, see Section 4.9.3). To open the gate preferentially when the macrocycle is in the left-hand (*dba*) compartment a different photosensitizer which produces a lower *Z*:*E* ratio for α-methyl stilbene than benzil must be associated with the macrocycle to 'signal' its position and open the gate. We chose benzophenone (PhCOPh) for this purpose, since it gives a 55:45 *Z*:*E* PSS ratio[25] for α-methyl stilbene and as a substructure it could readily be incorporated into a dibenzo-crown ether (see **1**). As energy transfer is distance dependent, the rates and efficiencies of the intramolecular photosensitized reaction of *dba*-*Z*-**1** to *E*-**1** should be very different to that of *mba*-*Z*-**1** to *E*-**1**, whereas the intermolecular photosensitized isomerization with benzil should be independent of the position of the macrocycle. Although it may seem counter-intuitive that one can drive the macrocycle distribution away from its equilibrium value without ever changing the binding properties of the ring or either ammonium group, if conditions are chosen so that the benzil-sensitized reaction dominates (gate closed) when the ring is in the *mba* compartment (i.e. held far from the gate) but benzophenone-sensitized isomerization is significant (gate open) when the ring is in the *dba* compartment (i.e. held near to the gate), then this is precisely what should happen.

4.3 Operation of the molecular machine

The system's operation is shown in Figure 4.2, with the results obtained reported in Figures 4.3 and 4.4 (see Section 4.9.4 for additional data). The macrocycle shuttles between the ammonium binding sites of the two co-conformers of *E*-**1** shown in Figure 4.2 slowly on the nuclear magnetic resonance (NMR) timescale and so two sets of signals, one for each translational form, are observed in the ^{1}H NMR spectrum of *E*-**1** (Figure 4.3b).[24] The relative integration of these peaks gives the distribution of the macrocycle between the compartments at equilibrium (gate open). The ratio is 65:35 *dba*:*mba* in CD_3OD at 298 K, as illustrated by the H_s (*dba* binding site

occupied) and $H_{s'}$ (*mba* binding site occupied) protons in the partial spectrum at point **I** shown in Figure 4.4. Irradiation (350 nm, CD_3OD, 298 K) of the rotaxane isomerizes the α-methyl stilbene unit, giving various amounts of the three diastereomers, *dba-Z*-**1**, *mba-Z*-**1** and *E*-**1**. As with the *dba*:*mba* distribution, the *Z*:*E* ratio can be readily established by the relative integration of various signals (e.g. $H_{K+K'}$ & $H_{k+k'}$ or $H_{L+L'}$ & $H_{l+l'}$ shown in Figures 4.3b, 4.3c and 4.3d; or $H_{S+S'}$ & $H_{s+s'}$ shown in **II-IV**, Figure 4.4c).

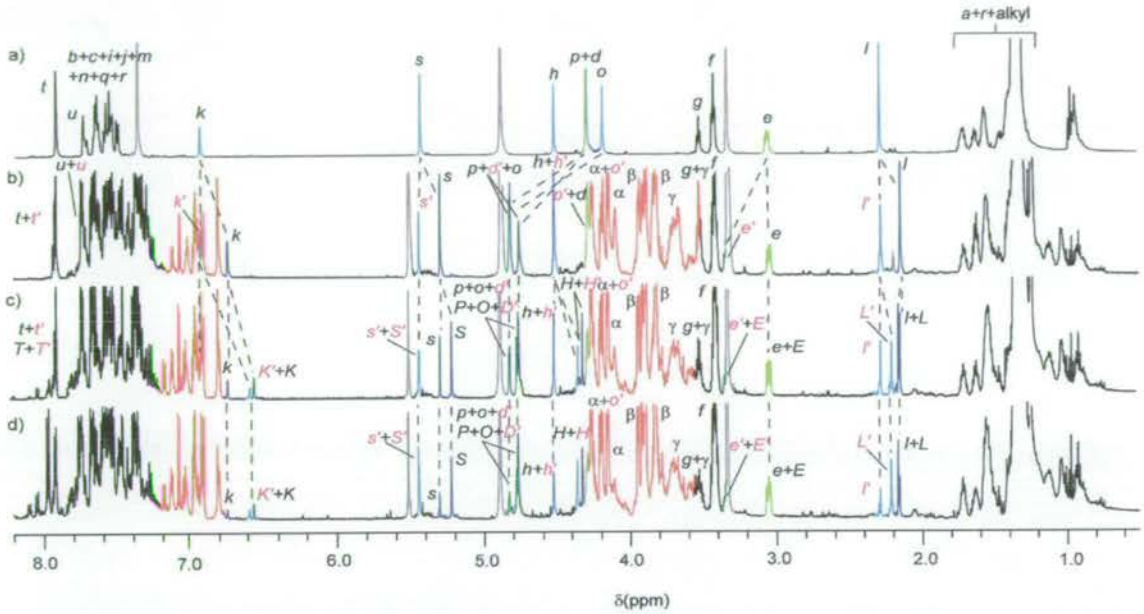

Figure 4.3 ^{1}H NMR spectra (600 MHz, CD_3OD, 298 K) of a working nanomachine. (a) Thread (*E*-diastereomer); (b) *E*-**1**; (c) **1** at the 350 nm photostationary state (*dba-Z*-**1**:*mba-Z*-**1**:*E*-**1** 38:21:41); (d) **1** + benzil (10 equivalents) at the 350 nm photostationary state (*dba-Z*-**1**:*mba-Z*-**1**:*E*-**1** 32:48:20). Resonances are coloured and the lettering assigned according to Figure 4.2: macrocycle, red; occupied *dba* binding site, dark blue; unoccupied *dba* binding site, light blue; occupied *mba* binding site, dark green; unoccupied *mba* binding site, light green. The overlapping aromatic ring signals above 7.2 ppm are not distinguished in this way. Residual non-deuterated solvents are shown in light grey (the signal at 5.5 ppm is CH_2Cl_2).

Starting from pristine *E*-**1** and with no benzil present (point **I**, Figure 4.4), irradiation at 350 nm (CD_3OD, 298 K) interconverts the three diastereomers of **1** ultimately leading to a 38:21:41 *dba-Z*-**1**:*mba-Z*-**1**:*E*-**1** photostationary state (i.e. point **II**, Figure 4.4). While the *Z*:*E* ratio of **1** changes from 0:100 to 59:41 during this part of the experiment, the *dba*:*mba* ratio remains almost invariant at 65:35 (see later for an explanation of the transient small increase in the population of the *dba* compartment during the first 5 minutes of irradiation, Figure 4.4b).

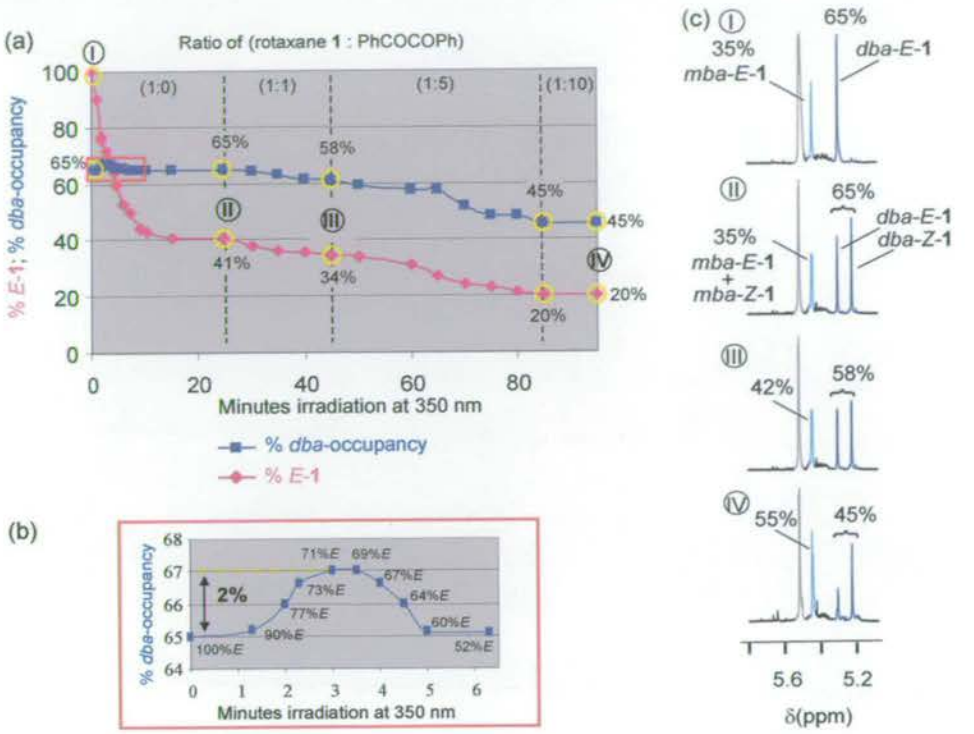

Figure 4.4 Operation of a molecular information ratchet. (a) Change in the *E*:*Z* ratio (% ***E*-1**, the amount of the 'open gate' form of the sample, shown by pink diamonds) and *dba*:*mba* ratio (% *dba*-occupancy shown by dark blue squares) that occurs during irradiation of **1** at 350 nm in CD_3OD, 298 K: **I** pristine *E*-**1**; **II** after 25 minutes (PSS), no added benzil; **III** after a further 20 minutes (PSS) with 1 equivalent of benzil; **IV** after a further 40 minutes with 5 equivalents of benzil plus a further 15 minutes (PSS) with 10 equivalents of benzil. A small amount of photodegradation (<2%) occurs over the course of the experiment and the error in the final *E*:*Z* and *dba*:*mba* ratios is ±2%. (b) Expansion showing the small increase in *dba* compartment occupancy that occurs during the first five minutes of irradiation in the absence of benzil. (c) ^{1}H NMR spectral window ($H_{s'+S'}$, H_s & H_S, 600 MHz, CD_3OD, 298 K) in which the changes in both the *E*:*Z* and *dba*:*mba* ratios can be seen during the photochemistry experiment.

After 25 minutes irradiation of **1** (point **II**, Figure 4.4), one equivalent of benzil was added and irradiation resumed. The 1:1 combination of the benzil and benzophenone-crown ether photosensitizers produces a higher *Z*:*E* α-methyl stilbene photostationary state ratio (63:34, point **III**, Figure 4.4) than the benzophenone-crown ether alone. This modest change is accompanied for the first time, however, by a *decrease* in the population of the *dba*-compartment (*dba*:*mba* 58:42). The amount of external sensitizer required for **1** to operate at greatest efficiency is determined by several factors, including the relative absorptions of the chromophores, the relative efficiencies of the energy transfers to the α-methyl stilbene and between the triplet sensitizers themselves, and the concentration of the external sensitizer. Five equivalents of benzil proved sufficient to increase the *Z*:*E* ratio of **1** at the PSS to 80:20, essentially the same as if no benzophenone was present. Addition of more benzil did not further increase the *Z*:*E* ratio (point **IV**, Figure 4.4). At this maximum

value the *dba*:*mba* ratio is 45:55 (*dba*-*Z*-**1**:*mba*-*Z*-**1**:*E*-**1** 32:48:20; ratios which are consistent with model studies, see Section 4.9.3); nearly one third of the macrocycles which occupied the more energetically favourable *dba* compartment at equilibrium (or the PSS obtained in the absence of benzil) have been pumped into the compartment with the less favourable *mba* binding site.

To confirm the mechanism by which the macrocycle distribution in **1** is driven away from its equilibrium value, the same photochemical experiment was performed on a rotaxane in which the crown ether does not contain a photosensitizer unit (Figure 4.5). Rotaxane **2** was irradiated (350 nm, CD_3OD, 298 K) in the presence of the unthreaded benzophenone-derivatized crown ether, **3**, both with and without benzil so that isomerization by each photosensitizer could only occur intermolecularly. The results are shown graphically in Figure 4.5. Although, like **1**, the *Z*:*E* ratio of **2** changes from 0:100 to 80:20 during the photochemical experiment, the distribution of the macrocycle between the two compartments in rotaxane **2** remains virtually unchanged from its equilibrium value of 52:48 *dba*:*mba* (the underivatized dibenzocrown ether in **2** is slightly less discriminatory for the different ammonium binding sites than the benzophenone-derivatized macrocycle in **1**). The 2% change in occupancy measured after 80 minutes irradiation is within experimental error but, if real, it could be caused by the dibenzocrown ether in **2** interacting with the α-methyl stilbene or one of the sensitizers and thus still modestly influencing the photochemistry as a function of its position on the thread.

A small, short-lived increase in the population of the *dba*-compartment is observed during the initial irradiation of *E*-**1** in the absence of benzil (Figure 4.4b). This occurs because the photosensitized isomerization reaction is a much more frequent occurrence when the photon is absorbed by the macrocycle on the *dba* binding site of *E*-**1** and so *dba*-*Z*-**1** is formed more rapidly from *E*-**1** than *mba*-*Z*-**1**. Equally, however, *dba*-*Z*-**1**, in which the photosensitizer is trapped close to the gate, is converted back to *E*-**1** much faster than is *mba*-*Z*-**1** and thus the statistical balance of the *dba*- and *mba*-compartments is quickly restored as the reaction proceeds. This is the equivalent of a Maxwellian pressure demon system in which the gate starts open and the demon opens or closes the gate at random whenever it detects a particle approaching from the left. After the demon has only operated the gate one or two times its actions are likely to have increased the time that the particle has spent in the left-hand compartment, but

this initial gradient is transient and falls away as the fraction of closed gate in the sample increases. The effect illustrates the fascinating interplay between the statistical balance of the position of the particle (*dba*/*mba* compartment) and the 'statistical balance' of the position of the gate (open *E*-stilbene/closed *Z*-stilbene) in the operation of **1**. Moving either one of these normally orthogonal chemical features away from its 'equilibrium' value moves the other one away too.

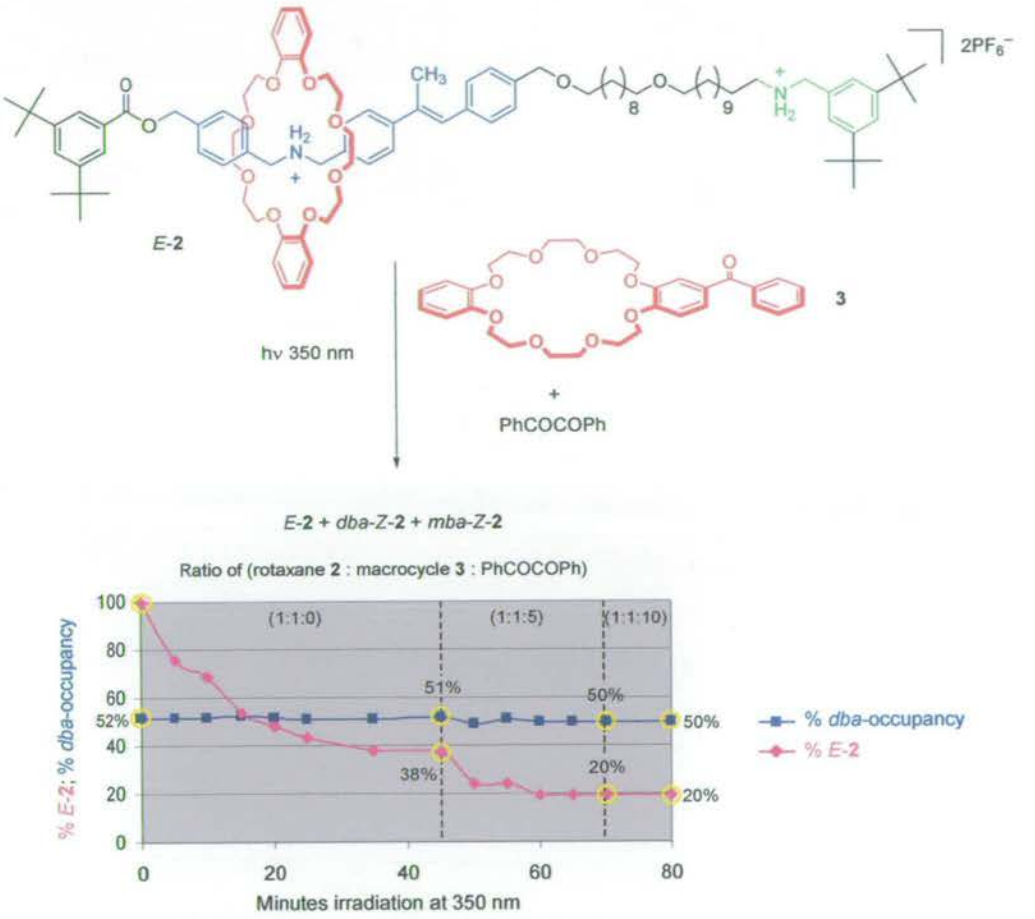

Figure 4.5 Operation of rotaxane **2**, featuring only intermolecular photosensitization of the α-methyl stilbene gate. The plot shows the change in the *E*:*Z* ratio (% *E*-**2** shown by pink diamonds) and *dba*:*mba* ratio (% *dba*-occupancy shown by dark blue squares) that occurs during irradiation of **2** + **3** (1:1) at 350 nm in CD_3OD, 298 K in the absence and presence (5 and 10 equivalents) of benzil. There is a small amount (<2%) of photodegradation over the course of the experiment and the error in the final *E*:*Z* and *dba*:*mba* ratios is ±2%.

4.4 The increase in free energy of the molecular machine

What is the work done on changing the ring distribution away from its equilibrium value? By relating the sorting of a macrocycle between the two compartments in an ensemble of **1**, to the sorting of a fixed number of ideal gas particles between two boxes of different volume, it can be shown (see Section 4.9.7) that the free-energy change on driving the distribution away from equilibrium is given by equation (1), where x_1 is the final mole fraction of particles in the *dba* compartment and y_1 the equilibrium mole fraction of particles in *dba*. Using the experimental values (Figure 4.4a) $x_1 = 0.45$ and $y_1 = 0.65$, this gives a free-energy change of $\Delta G = 0.083RT$ J mol^{-1} – the extent to which the molecular machine has been driven energetically uphill by movement of the macrocycle rings.

$$\Delta G = Nk_BT\left[x_1 \ln\frac{x_1}{y_1} + (1-x_1)\ln\frac{(1-x_1)}{(1-y_1)}\right] \quad (1)$$

4.5 Information, entropy and free energy

The molecular machine clearly acquires energy from absorbed photons. Yet the incident photons never bias particles in one compartment over the other by changing their relative energies; this nanomachine does not operate like any previous molecular machine that can move away from equilibrium.[2, 3, 5, 7, 8, 13, 14] Just like for Maxwell's thought experiment, the transfer of information about the location of the particle to a 'gate-keeper' can be used to perturb the particle distribution without energetically favouring one compartment over the other at any stage. In the current molecular system, information arising from asymmetry in the particle's position is transferred via photochemistry to selectively vary the height of a kinetic barrier. The effectiveness of this mechanism depends directly upon the efficiency of the ET to the closed gate from the excited state of a benzophenone-derivatized macrocycle located in the left-hand compartment (*dba*-*Z*-**1**/Figure 4.2b(i)), compared to that from one in the right-hand compartment (*mba*-*Z*-**1**/Figure 4.2b(iv)).

Maxwell's construct examines the simplest case, where not only are the energy levels of the two compartments invariant, but also equal in value. In this case, the only effect of driving the particle distribution away from equilibrium is an decrease in entropy of the system. As the macrocycle binding energies in the two compartments of rotaxane

1 are slightly different, however, enthalpic changes also occur, but the overall effect of moving away from the equilibrium distribution in either case, of course, is an increase in free energy as quantified in Section 4.4. Just as the demon discovered, no matter how the change in particle distribution is brought about, the Second Law of Thermodynamics demands that the energetic cost be repaid. In both the hypothetical construct and the real molecular system, it is the subtle requirement for energy dissipation during the transfer of information that meets this requirement.

There have been many insightful analyses of Maxwell's thought experiment and its variations over the past 130 years.[19, 26–33] Particularly important and influential have been those seeking to understand the nature of information acquisition, storage and erasure in terms of their intrinsic energetic cost. However, the current picture of the relationship between information and free energy (specifically, an increase in information equated to a reduction in entropy) is still incomplete and some of the conclusions drawn from these thought experiments are not universally accepted.[34–48]

One of the most fascinating features of the experimental realization of a non-adiabatic Maxwellian demon nanomachine is that its behaviour can be understood in well-defined chemical terms. How then does the increase in free energy of **1** arise from the input of light energy?

In practice, the conversion of photonic energy to heat occurs in several places during the various photochemical excitation, energy transfer and thermal relaxation processes that occur during the operation of **1**, meaning that the Second Law is easily satisfied in the face of the relatively modest increase in free energy of the system. However, the heat loss in most of these instances could theoretically be eliminated by changing details of the experimental design (for instance, benzil would be unnecessary if **1** could be modified so that the open form of the gate was able to exergonically relax to the closed form). The one part of the mechanism where loss of heat to the environment seems to be inevitable (without causing equivalent dissipation elsewhere in the mechanism) is during the isomerization of the gate by the sensitizer attached to the macrocycle. Photochemical excitation is an extremely rapid process and occurs without changes in molecular geometry. For olefin photoisomerization to occur, the initial 'vertically' excited state must relax to its preferred geometry (known as the 'perpendicular' state), which is usually intermediate between the *Z* and *E* forms. A further rearrangement of this nuclear configuration to the final *Z* or *E* product then

occurs following crossing onto the ground-state potential energy surface. Both of these nuclear rearrangements are necessarily energetically downhill processes (even if vibrational relaxation can be minimized) and they cannot be avoided. As the excited state of *dba-Z*-**1** is quenched by ET to open the gate, therefore, the information regarding the particle's (probable) location is erased on decay of the initial, vertically excited state to the perpendicular intermediate. Thus the part of the mechanism of **1** that intrinsically requires dissipation of energy is equivalent to the erasure of information known to a gate-operating demon, in agreement with Bennett's resolution[32] of the Maxwell demon paradox.

The link between information and entropy means that constraining the rings in **1** to sit in a specific compartment can, itself, be viewed as a form of information storage. The macrocycle's position in a particular compartment corresponds to the state of the switch and can be stored as one of the two kinetically stable *Z*-isomers. In recent years other stimuli-responsive rotaxanes have been investigated as prototypical positional switches for memories in molecular electronics.[39] These all rely on energy differences between two different macrocycle positions to achieve switching, which necessarily involves energy dissipation during thermal relaxation to the new state, and any intrinsic cost of computation is hidden. On the other hand, the architecture of switchable molecular shuttle **1** is the first in which the energies of the two switchable ring positions are invariant. This mechanism could therefore be applied to create a switch in which both states have identical energies. Rolf Landauer realized[40] that an ensemble of N such switches allows certain logic operations to be carried out reversibly (i.e. without dissipation), but not those processes that involve resetting or erasure. Such actions lose all information about the initial state and so must involve two steps: (i) randomization of the switch position; and then (ii) an identical resetting process for each switch, bringing them all to the same reference state. The first step may involve an increase in entropy (decrease in free energy) of the system depending on the nature of the initial state, but the second step corresponds to a reduction in entropy of the ensemble by $k_B N \ln 2$ (in the simplest case of degenerate switch states) and must therefore involve a corresponding release of heat to the surroundings. Hence, Landauer's Principle[40] states that erasure of one bit of information releases heat to the surroundings of at least $k_B T \ln 2$.

The operating mechanism of **1** is also suitable for performing useful work. For example, removing the stoppers of **1** could form the basis of a prototypical light-driven linear motor that, if inserted into a membrane, would be able to pump rings (and anything they are modified to carry) against a concentration gradient. Alternatively, replacing the *mba* binding site with a second *dba*-α-methyl stilbene unit and cyclizing would form a catenane in which, under irradiation at 350 nm, one ring should directionally rotate about the other. Interestingly, if **1** is used to do continuous work in such a rotating system, information regarding the macrocycle position is never physically stored and the mechanism no longer requires the extra 'wasted' photons shown in Figure 4.2b(iv) to dissipate their energy in an unproductive way.

4.6 Nanomachine mechanisms for operating far from equilibrium

Various methods for the net transport of macrocycles between the binding sites in rotaxanes have previously been demonstrated in the form of stimuli-responsive molecular shuttles.[4, 6, 9, 10, 12] However, these are simple switches,[41] the most basic and functionally limited type of molecular machine,[14] which can only change the ring distribution between equilibrium states. In contrast, biological motors and machines use mechanisms that operate far from equilibrium.[1] During the past decade, a number of theoretical mechanisms have been developed in statistical mechanics that explain how the transport of Brownian particles away from equilibrium can occur. These so-called 'Brownian ratchet' mechanisms fall into two general classes: energy ratchets,[42] in which the energy minima and maxima of the potential energy surface are varied irrespective of the particle's location; and information ratchets,[43–46] where the energy maxima (kinetic barriers to motion) change according to the position of the particle. The energy ratchet concept has recently been used to design some of the first synthetic molecular machines that are more complex than simple switches[7, 14] but rotaxane **1** is the first example of a synthetic molecular information ratchet. For an information ratchet to function it is unnecessary for the binding affinities of the two compartments to be identical as they are for Maxwell's demon, or even as similar as they are in **1** (although it affects the efficiency of the mechanism[46]), the point is to drive the particle distribution away from whatever its equilibrium value is. From the perspective of molecular machine

design the situation in which the two sites have significantly different binding affinities will probably prove more important because this corresponds to pumping the particles energetically uphill against an external force.

4.7 Chemical games

The chemistry which enables the ring distribution in **1** to be driven away from equilibrium can also be understood in terms of game theory. It has recently been shown that a theoretical Brownian ratchet mechanism can be related to two gambling games that, when played individually, tend to result in losses but, paradoxically, when played in an alternating fashion (either periodically or randomly), tend to result in winning.[47–51] For our purposes, let the outcome of a rotaxane 'game' be the ring position on the thread following each photochemical isomerization event or 'turn'. 'Winning' is when the ring is located in the *mba* compartment; 'losing' is when the ring is located in the *dba* compartment. Game ONE's 'rule' is that the outcome results from an intramolecular photoisomerization of the α-methyl stilbene gate on the asymmetric thread with benzophenone; Game TWO's rule is that the outcome is the product of intermolecular photoisomerization with benzil. When either Game ONE or TWO is played independently (i.e. irradiation of **1** in the absence of benzil – Game ONE; or irradiation of **2** in the presence of benzil – Game TWO), on average 65% of the rotaxane rings end up in the *dba* compartment – a net losing result. However, if we randomly alternate between the two 'games' with a molecule (i.e. irradiation of **1** in the presence of benzil) – the identity of the photosensitizer that happens to absorb the photon determines which set of rules are played each turn – then 55% of the rings end up in the *mba* compartment, a net winning result! This correlation between experimentally determined chemical behaviour and game theory may prove useful in both fields. The part of the mechanism in which the energetic cost of 'winning' is paid can be readily identified for the rotaxane 'game' – currently a puzzle in the game theory analysis of many such paradoxes.[48] In terms of chemistry, paradoxical games may provide the basis for mechanisms that enable other chemical reactions, not just those involving 'mechanical' molecular machines, to be driven away from equilibrium.

4.8 Discussion

Through the chemistry of **1**, a non-adiabatic version of Maxwell's thought experiment, we can see how the idea of a gate-keeper, gate operating system, signalling method and detector can be put into practice in a working nanomachine, utilizing an input of energy to drive a particle distribution away from equilibrium. In doing so, the way that information can be traded for free emergy can be observed in a well-defined experimental system and rationalized with the classic treatments of the demon paradox by Szilard,[26] von Smoluchowski,[27] von Neumann,[28] Brillouin,[29] Gabor,[30] Penrose,[31] Bennett,[32] and others[19]. The increase in free energy of **1** is compensated for by heat released to the surroundings during the sensitized gate-opening photoisomerization reaction, a step corresponding[32] to erasure of information known to the demon. Experimental systems never function perfectly, however, and the inefficiencies in the performance of **1** reveal other aspects of the interplay between information and free energy: the relationship between the 'statistical balance' of the gate position and the 'statistical balance' of the distribution of the particle; the circumstances in which it is possible to temporarily drive a particle distribution away from equilibrium in a system that returns to its equilibrium value at the photostationary state; and the effect on the operating mechanism of the nanomachine of whether it is required to store information or do useful work.

Most importantly, this nanomachine is the first example of a synthetic molecule designed to act as an information ratchet, a formalism identified[43–46] in theoretical statistical physics as a mechanism for driving Brownian particles away from equilibrium in a manner similar to biological motors and machines. The understanding of how to incorporate these and other Brownian ratchet mechanisms into synthetic molecular structures is the key to being able to move beyond simple switches to more sophisticated generations[14] of artificial nanomachines and, more generally, to discovering methodologies for controlling chemistry far from equilibrium.

4.9 Experimental section

4.9.1 Procedure for photochemical experiments

Photoisomerizations were carried out at 298 K using a multilamp photoreactor (model MLU18) manufactured by Photochemical Reactors Ltd, Reading, UK. In a typical experiment a sample of *E*-**1** was dissolved in CD_3OD at a concentration of 1 mM, placed in a quartz vessel, degassed by bubbling with nitrogen (20 min) and then irradiated at 350 nm. Once the photostationary state had been established (as determined by ^1H NMR), 1 equivalent of benzil was added to the solution, degassing repeated (N_2, 20 minutes), and irradiation resumed until the new photostationary state was reached. This process was repeated on the same sample, with totals of 5 equivalents and then 10 equivalents of benzil present.

The photoisomerization of *E*-**2** in the presence of 1 equivalent of macorcycle **3** was carried out in an identical fashion in the absence and then the presence of 5 equivalents and then 10 equivalents of benzil. Similarly, the photochemical studies on model compounds were carried out under the same conditions, using analogous procedures, for details see Section 4.9.3.

4.9.2 Synthetic sequence for the preparation of thread and rotaxane molecules

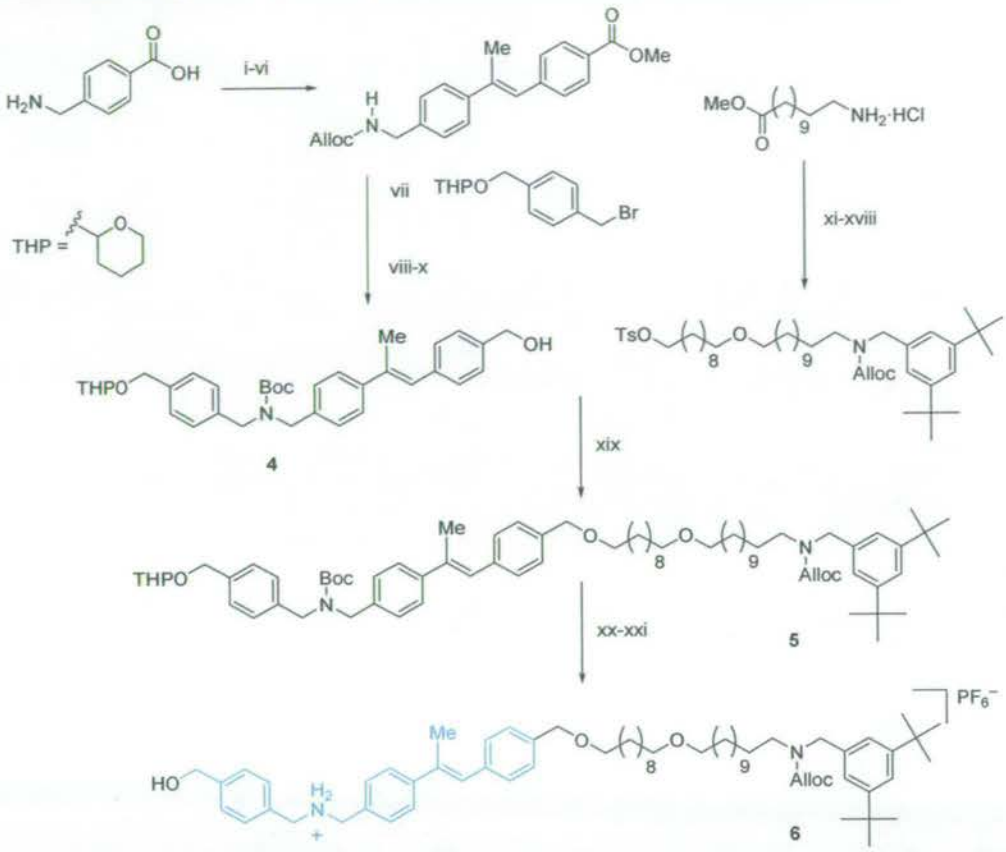

Scheme 4.1 Synthetic sequence for the preparation of thread precursors **4-6** (unless otherwise stated, reactions were carried out at room temperature): (i) di-*tert*-butyl dicarbonate (Boc_2O), NaOH, THF/H_2O (1:1), 0 °C to rt, 40 min, 81%; (ii) MeNHOMe, Et_3N, 1-(3-dimethylaminopropyl)-3-ethylcarbodiimide hydrochloride (EDCI·HCl), CH_2Cl_2, 16 h, 97%; (iii) MeMgBr (3.0 M in Et_2O), THF, 0 °C to rt, 15 h, 88%; (iv) diethyl-(4-methoxycarbonylbenzyl)phosphonate, NaH, THF, 0 °C, 1 h, 91% (*cis*:*trans* 2:1); (v) CF_3CO_2H, CH_2Cl_2, 20 h; (vi) allyl chloroformate, $NaHCO_3$, THF/H_2O (1:1), 0 °C to rt, 16 h, 65% (2 steps, based on *trans* isomer); (vii) NaH, DMF, 0 °C, 15 min, 85%; (viii) $PhSiH_3$, cat. $Pd(PPh_3)_4$, CH_2Cl_2, 1 h, 92%; (ix) $(Boc)_2O$, CH_2Cl_2, 2 h, 91%; (x) diisobutylaluminium hydride, THF, 0 °C, 4 h, 88%; (xi) 3,5-di-*tert*-butylbenzoic acid, Et_3N, EDCI·HCl, CH_2Cl_2, 48 h, quant.; (xii) $LiAlH_4$, THF, reflux, 2 h, 95%; (xiii) Boc_2O, CH_2Cl_2, 2 h, 91%; (xiv) $BnO(CH_2)_{10}OTf$, proton sponge, CH_2Cl_2, reflux, 48 h, 85%; (xv) H_2, 10% Pd/C, THF, 16 h, 92%; (xvi) CF_3CO_2H, CH_2Cl_2, 20 h; (xvii) allyl chloroformate, $NaHCO_3$, THF/H_2O (1:1), 0 °C to rt, 16 h, 62% (two steps); (xviii) p-toluenesulfonyl chloride (TsCl), Et_3N, CH_2Cl_2, 16 h, 54%; (xix) NaH, DMF, 48 h, 78%; (xx) HCl (1.0 M in Et_2O), MeOH, 18 h; (xxi) NH_4PF_6, acetone/H_2O (1:1), 1 h, 85% (two steps).

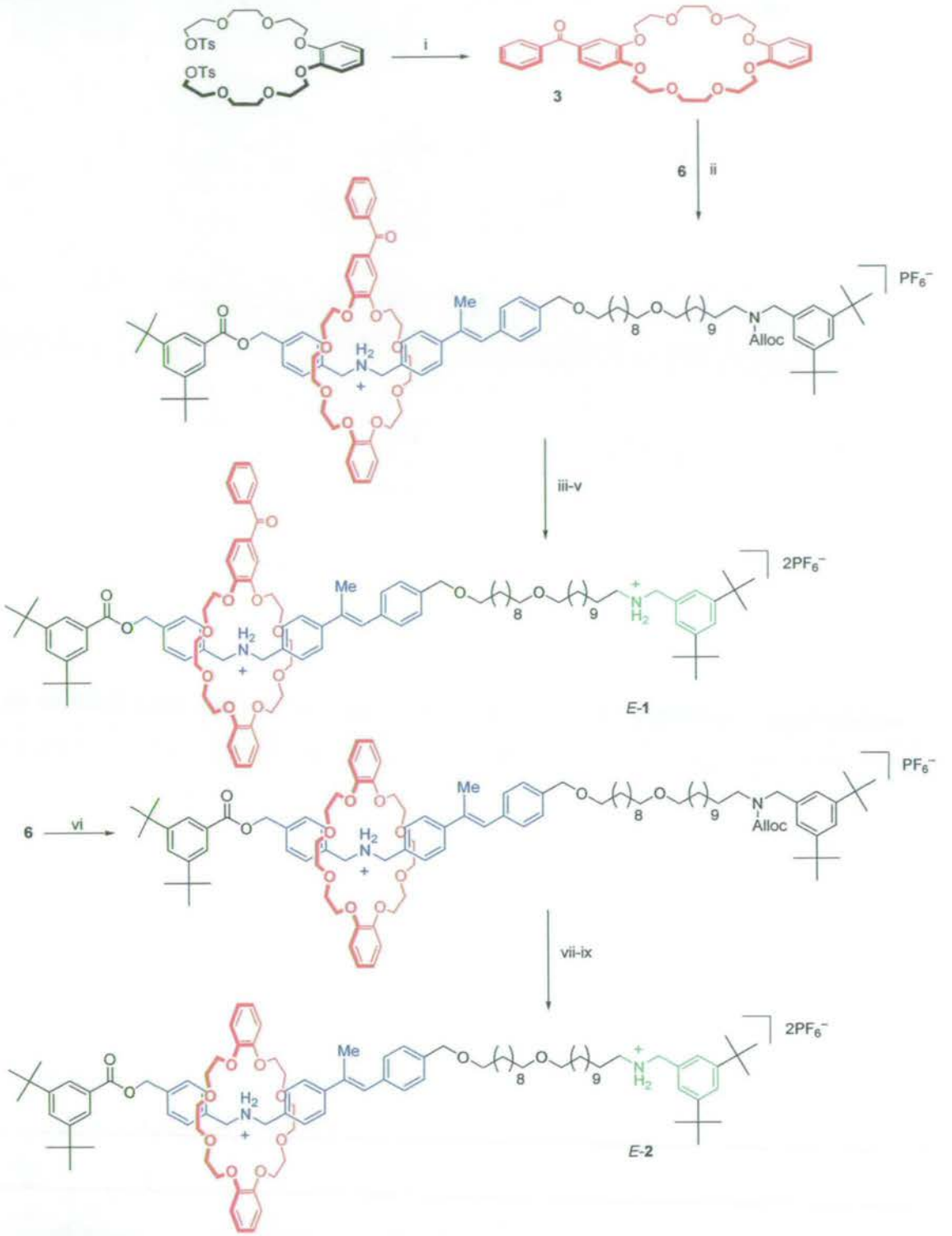

Scheme 4.2 Synthetic sequence for the preparation of macrocycle **3** and rotaxanes *E*-**1** and *E*-**2** (unless otherwise stated, reactions were carried out at room temperature): (i) 3,4-dihydroxybenzophenone, Cs_2CO_3, THF, reflux, 5 days, 54%; (ii) 3,5-di-*tert*-butylbenzoic anhydride, cat. PBu_3, CH_2Cl_2, 16 h, 91%; (iii) $PhSiH_3$, cat. $Pd(PPh_3)_4$, CH_2Cl_2, 2 h, 76%; (iv) HCl (1.0 M in Et_2O), CH_2Cl_2, 10 min; (v) NH_4PF_6, acetone/H_2O (1:1), 1 h, 88% (two steps); (vi) dibenzo-24-crown-8, cat. PBu_3, 3,5-di-*tert*-butylbenzoic anhydride, CH_2Cl_2, 16 h, 86%; (vii) $PhSiH_3$, cat. $Pd(PPh_3)_4$, CH_2Cl_2, 1 h; (viii) HCl (1.0 M in Et_2O), CH_2Cl_2, 10 min; (ix) NH_4PF_6, acetone/H_2O (1:1), 1 h, 58% (three steps).

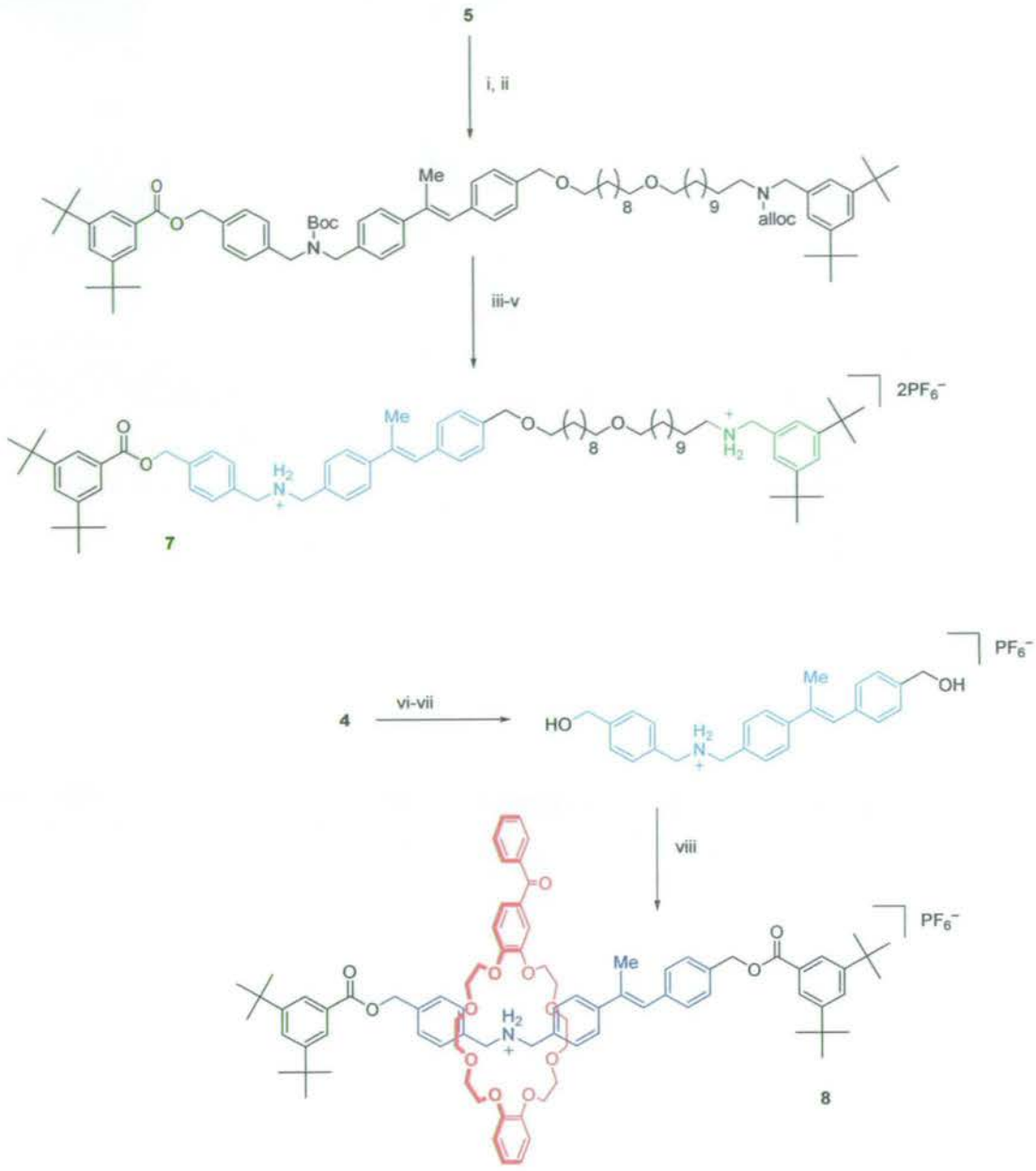

Scheme 4.3 Synthetic sequence for the preparation of thread **7** and model rotaxane **8** (unless otherwise stated, reactions were carried out at room temperature): (i) pyridinium *p*-toluensulfonate, EtOH, 60 °C, 7 h, 97%; (ii) 3,5-di-*tert*-butylbenzoyl chloride, Et_3N, CH_2Cl_2, 1 h, 77%; (iii) $PhSiH_3$, cat. $Pd(PPh_3)_4$, CH_2Cl_2, 1 h, 67%; (iv) HCl (1.0 M in Et_2O), CH_2Cl_2, 10 h; (v) NH_4PF_6, acetone/H_2O (1:1), 1 h, 89% (two steps); (vi) HCl (1 M in Et_2O), CH_2Cl_2, 1 h; (vii) NH_4PF_6, acetone/H_2O (1:1), 1 h, 79% (two steps); (viii) 3,5-di-*tert*-butylbenzoic anhydride, **3**, cat. PBu_3, CH_2Cl_2/CH_3CN (1:1), 16 h, 69%.

4.9.3 Photochemistry of model α-methyl stilbene derivatives

The results of photochemistry experiments carried out on various model compounds are summarised in Figure 4.6. Direct irradiation of model gate compound **9** (Figure 4.6a) gave a photostationary state (PSS) ratio of 55:45 *Z*:*E* after nearly 40 minutes. Irradiation of the same compound in the presence of 1 equivalent benzophenone-derivatized macrocycle **3** (Figure 4.6b) proved to be a faster process, reaching a PSS of 58:42 *Z*:*E* in 5 minutes. This is in close agreement with literature values for the benzophenone-sensitized photoisomerization of unsubstituted α-methyl stilbene.[25, 52] Irradiation of model rotaxane **8** (Figure 4.6c) results in an intramolecular benzophenone-sensitized process, giving a similar photostationary state (55:45 *Z*:*E*) to the intermolecular experiment, in a shorter time (< 1 minute). Irradiation of a model gate compound in the presence of benzil (1:1, not shown) gave a PSS ratio of 82:18 (*Z*:*E*) after 5 minutes, which is also in agreement with literature values for the benzil-sensitized photoisomerization of α-methyl stilbene.[25, 52]

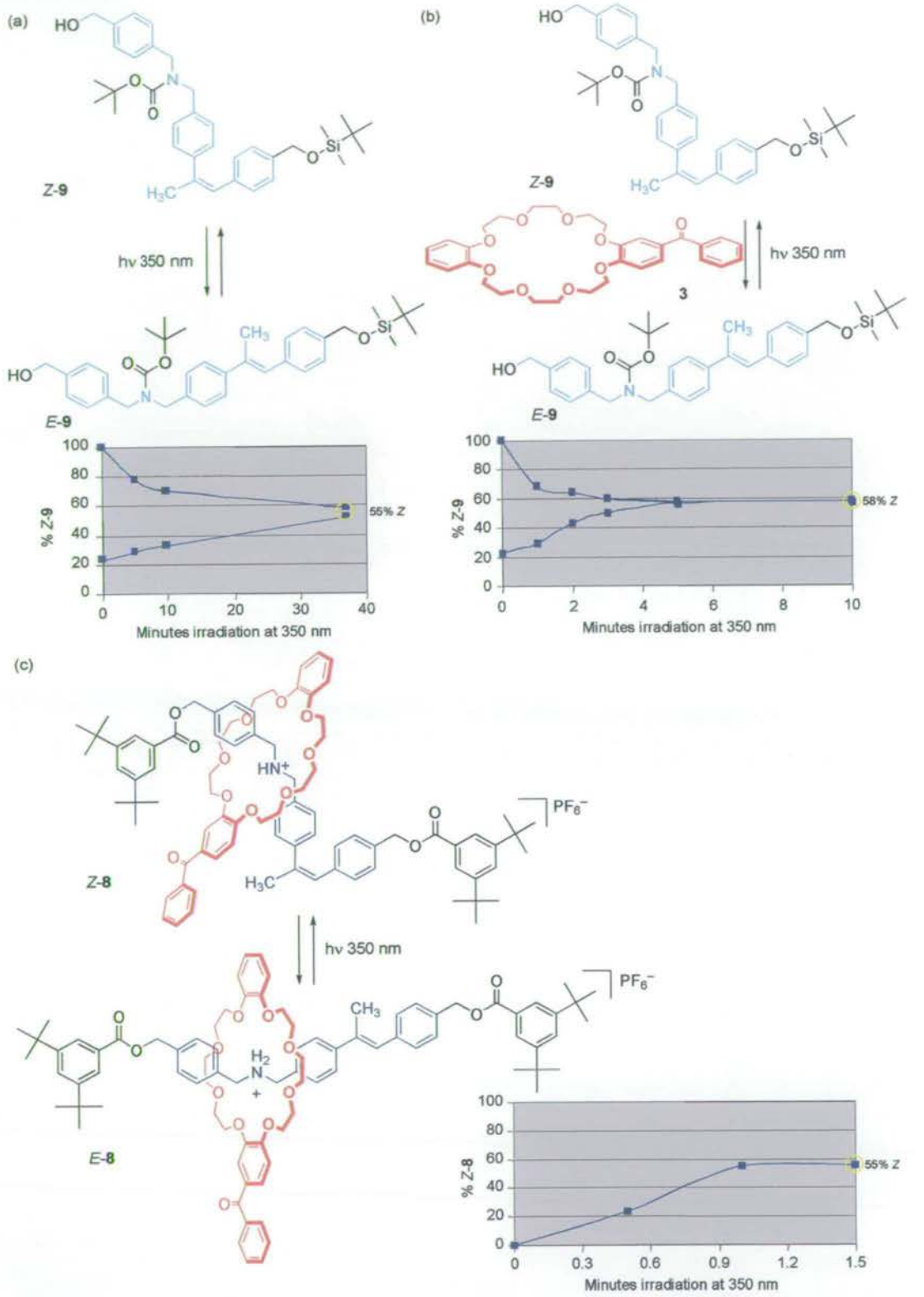

Figure 4.6 Summary of photochemistry experiments on model α-methyl stilbene derivatives. All experiments were carried out by irradiating 1 mM solutions in CH_2Cl_2 at 298 K with light at 350 nm. (a) Direct irradiation of gate model **9**. (b) Photoisomerization of gate model **9**, sensitized by benzophenone-derivatized crown ether macrocycle **3** (1:1 molar ratio). (c) Photoisomerization of single-station model [2]rotaxane **8**. The error in the measured diastereomer ratios is ±2%.

These results can be used to explain the behaviour of the two-station rotaxane system **1**. Although a number of photochemical processes will be occurring in this multi-component system, overall rate constants can be assigned to each of the interconversions of **1**, as shown in Figure 4.7. Thus, it can be shown that the steady-state (SS) ratio of station occupancies is given by equation (2).

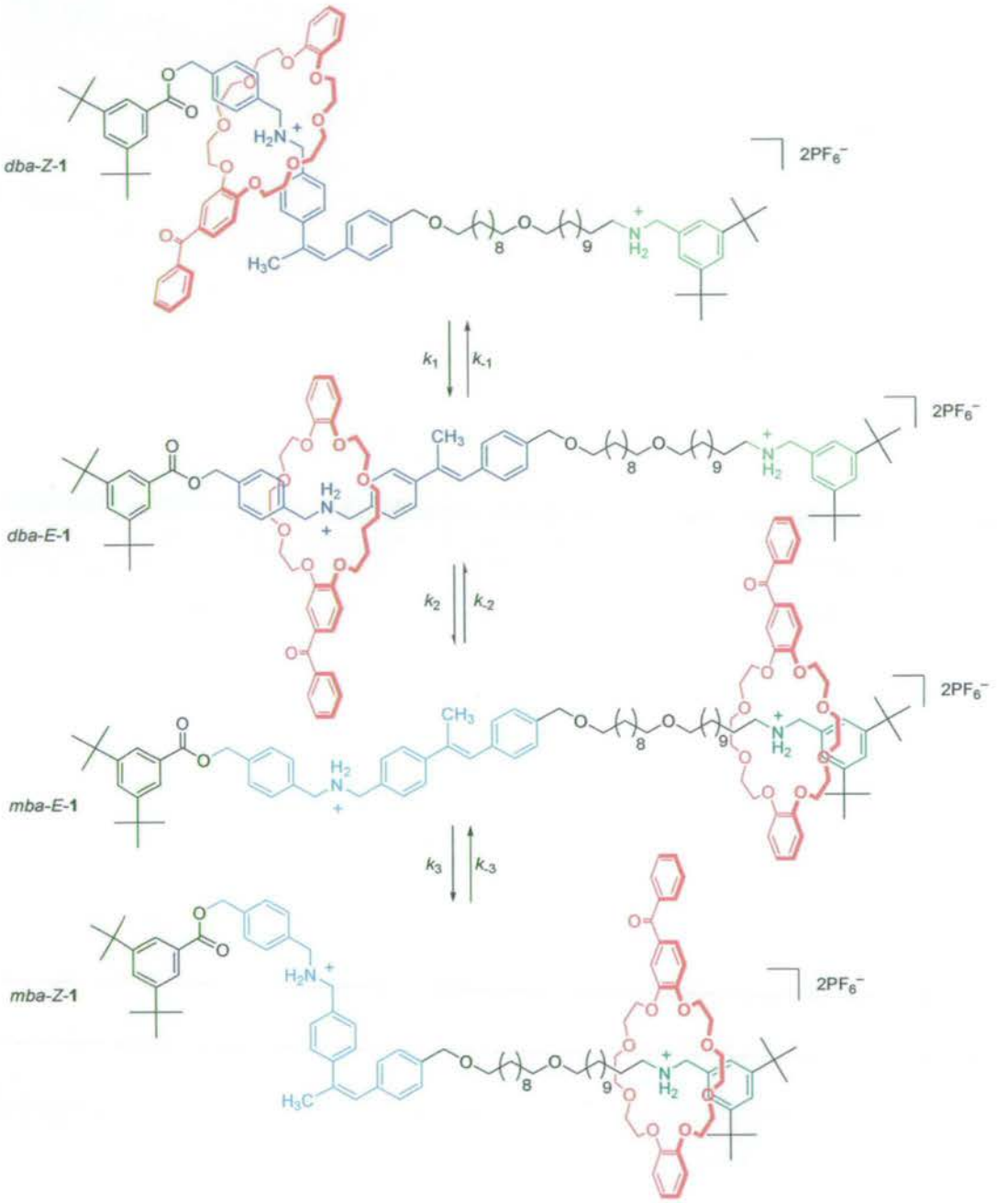

Figure 4.7. Assignment of overall rate constants to the interconversions between the four positional and configurational isomers of rotaxane **1**.

$$\frac{[mba]_{SS}}{[dba]_{SS}} = \frac{[mba-E-1]_{SS}+[mba-Z-1]_{SS}}{[dba-E-1]_{SS}+[dba-Z-1]_{SS}} = \frac{\left(1+{}^{k_3}/_{k_{-3}}\right)[mba-E-1]_{SS}}{\left(1+{}^{k_{-1}}/_{k_1}\right)[dba-E-1]_{SS}} \quad (2)$$

The steady-state ratio of *E*-**1** co-conformations can be equated to the equilibrium value observed for pure *E*-**1** (35:65 [*mba*]:[*dba*] in CD_3OD at 298 K). Although the processes described by k_1, k_{-1}, k_3, k_{-3} likely involve a combination of different pathways, we can discern three limiting situations in which their relative values should bear a simple relationship to the PSS ratios observed in the model studies (although it must be noted that these were carried out in CH_2Cl_2, not CD_3OD).

(i) When no benzil is added, the interconversion of *dba* isomers is effectively the same process as in the small rotaxane **8**, while interconversion between the *mba* forms must occur either by direct excitation of the olefin or by benzophenone-mediated sensitization in a slow, long-range intramolecular fashion or in an intermolecular process. The model studies show that the direct excitation is both inefficient and, coincidentally, gives a very similar PSS ratio to the benzophenone-sensitized process. It is clear from equation (2) that similar values for k_{-1}/k_1 and k_3/k_{-3} give a steady-state ratio of positional isomers which is close to the equilibrium value for *E*-**1**, in agreement with the experimental observations at point **II**, Figure 4.4.

Furthermore, the *relative* rates of the k_{-1}/k_1 (fast) and k_3/k_{-3} (slow) processes explain the origin of the transient decrease in [*mba*]:[*dba*] at the start of the experiment (illustrated in Figure 4.4b) as the PSS is approached more rapidly for the *dba* isomers than the *mba* forms, momentarily skewing the distribution in the *dba* direction.

(ii) For a moderate excess of benzil (~5 to >10 equivalents), the isomerization process for the *dba*-isomers can still be regarded as an unperturbed intramolecular benzophenone-sensitized process, similar to that observed in model rotaxane **8**. The value of k_{-1}/k_1 is therefore ~55:45. For the *mba*-isomers, however, the process is now largely intermolecular benzil-sensitized isomerization. A high concentration of benzil both increases the chance of an encounter with the α-methyl stilbene and, as benzil has a lower triplet excitation energy than benzophenone,[53] it helps to quench the macrocycle-based benzophenone excited state in competition with the long-range, slow interaction

with the gate. The value of k_3/k_{-3} is therefore ~82:18. Inserting these values into equation (2) gives a steady-state ratio of ~57:43 [*mba*]:[*dba*] which is in excellent agreement with the experimental results (point **IV**, Figure 4.4).

(iii) At large excesses of benzil (>> 10 equivalents) it might be expected that this may interfere with the interconversions of the *dba*-forms, eroding the difference between k_{-1}/k_1 and k_3/k_{-3} which would stop the demon from working. This has not been investigated experimentally, however.

4.9.4 Additional results on the operation of rotaxane 1

The operation of rotaxane **1** was reproducible over several runs. Results from a replicate of the experiment reported in Figure 4.4 are reproduced below in Figure 4.8. Fig. 4.8a shows the behaviour of the system in the absence of benzil. In a subsequent experiment, the resulting material was irradiated alone, then in the presence of 1, 5 and 10 equivalents of benzil (Figure 4.8b). Addition of benzil prior to irradiation had no effect on the station occupancies as observed by ^{1}H NMR, ruling out any intermolecular bonding interaction changing the relative binding affinities of the stations. It can be seen that the features reported in Figure 4.4 are reproduced here. It was observed, however, that the precise composition of photostationary state mixtures is sensitive to concentration and probably the presence of moisture and oxygen. In all experiments, no irreversible changes were observed (^{1}H NMR, TLC) beyond a small amount of photodegredation (< 2%).

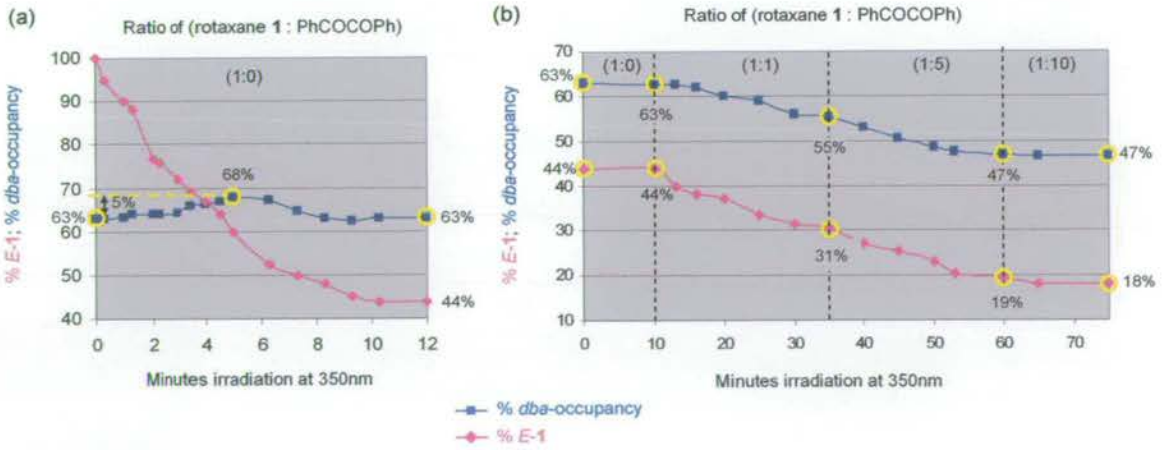

Figure 4.8 Operation of a molecular information ratchet – replicate experiment. (a) Change in the *E*:*Z* ratio (% *E*-**1**, the amount of the 'open gate' form of the sample, shown by pink diamonds) and *dba*:*mba* ratio (% *dba*-occupancy shown by dark blue squares) that occurs during irradiation of **1** alone at 350 nm in CD_3OD, 298 K. (b) Change in the *E*:*Z* ratio (% *E*-**1**) and *dba*:*mba* ratio (% *dba*-occupancy) that occurs on taking a sample of **1** already at the 350 nm PSS and irradiating at 350 nm alone, then in the presence of 1, 5 and 10 equivalents of benzil.

As the ratio of the two *E*- ('gate open') positional isomers must be constant, in addition to the overall distribution of rings between the two stations (% *dba*, plotted in Figures 4.4 and 4.8), the behaviour of **1** can also be described in terms of the ratio of *Z*- ('gate closed') positional isomers. For the experiment shown in Figure 4.4, this is plotted in Figure 4.9 as the percentage of *Z*-isomers in which the *dba* position is occupied – i.e. $\frac{[dba-Z-1]}{[dba-Z-1]+[mba-Z-1]}\times 100\%$.

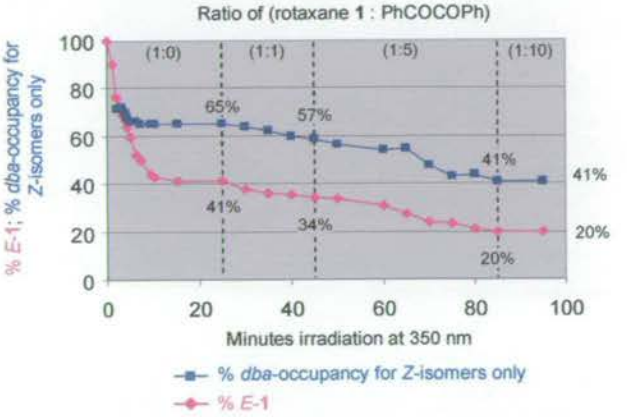

Figure 4.9 Results of the machine operation experiment shown in Figure 4.4, expressed in terms of the ratio of positional isomers in the *Z*-molecules only.

4.9.5 Does the stilbene isomerization affect macrocycle binding affinities?

The proximity of the stilbene gate to the *dba*-binding site raises the possibility that changing the olefin configuration could in fact alter the binding affinity for the ring at the *dba*-station. Mechanistically, this should not have any impact on the operation of the molecular machine, as exchange between the two binding sites can only occur in one of the two olefin configurational isomers (the *E*-isomer). Furthermore, it can be seen that for the two situations in which the information ratchet mechanism does *not* operate (rotaxane **1**, in the absence of benzil, or rotaxane **2**, under any conditions) the [*dba*]:[*mba*] ratio always approaches the equilibrium value for the pure *E*-rotaxane, irrespective of the *Z*:*E* ratio – any putative change in binding affinity at the *dba*-station does not affect the distribution of rings.

Obviously, it is not possible to directly measure the relative binding energies of the two stations in the *Z*-form. However, observations made during development of synthetic routes to **1** indicate that the configuration of the stilbene does not significantly affect the relative binding energies of the stations. Specifically, earlier synthetic attempts towards **1** focussed on threading and stoppering of fully

deprotected *cis*-thread precursor *Z*-**10** (Scheme 4.4a). Due to acylation of the free (*mba*) ammonium ion, this procedure yielded mixtures of rotaxane products and so was abandoned in favour of using the mono-protected *trans*-intermediate *E*-**6** (Scheme 4.4b). However, both routes lead to very similar overall yields (typically 75–85%) of rotaxane products, using virtually identical reaction conditions, suggesting that the binding affinity of the ammonium (*dba*) template is broadly similar irrespective of whether the stilbene unit is *E* or *Z*.

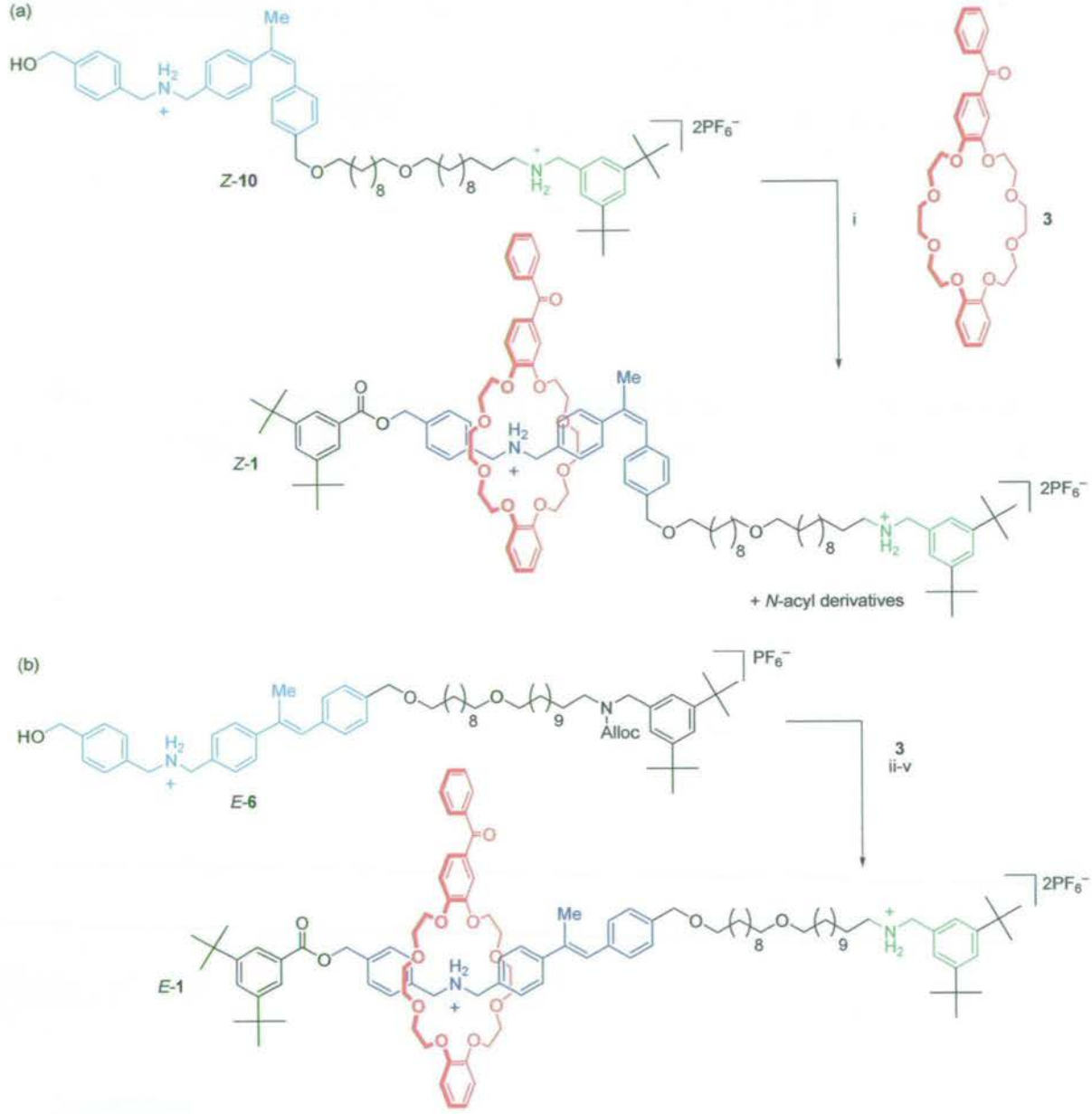

Scheme 4.4 Two synthetic routes to rotaxane **1**, employing (a) *Z*-stilbene and (b) *E*-stilbene *dba* templates (reactions were carried out at room temperature): i) 3,5-di-*tert*-butylbenzoic anhydride, cat. PBu_3, CH_2Cl_2/MeCN, 16 h; ii) 3,5-di-*tert*-butylbenzoic anhydride, cat. PBu_3, CH_2Cl_2, 16 h; iii) $PhSiH_3$, cat. $Pd(PPh_3)_4$, CH_2Cl_2, 2 h; iv) HCl (1.0 M in Et_2O), CH_2Cl_2, 10 min; v) NH_4PF_6, acetone/H_2O (1:1), 1 h.

4.9.6 Supplementary ^{1}H NMR spectra

^{1}H spectra relating to the control experiment illustrated in Figure 4.5

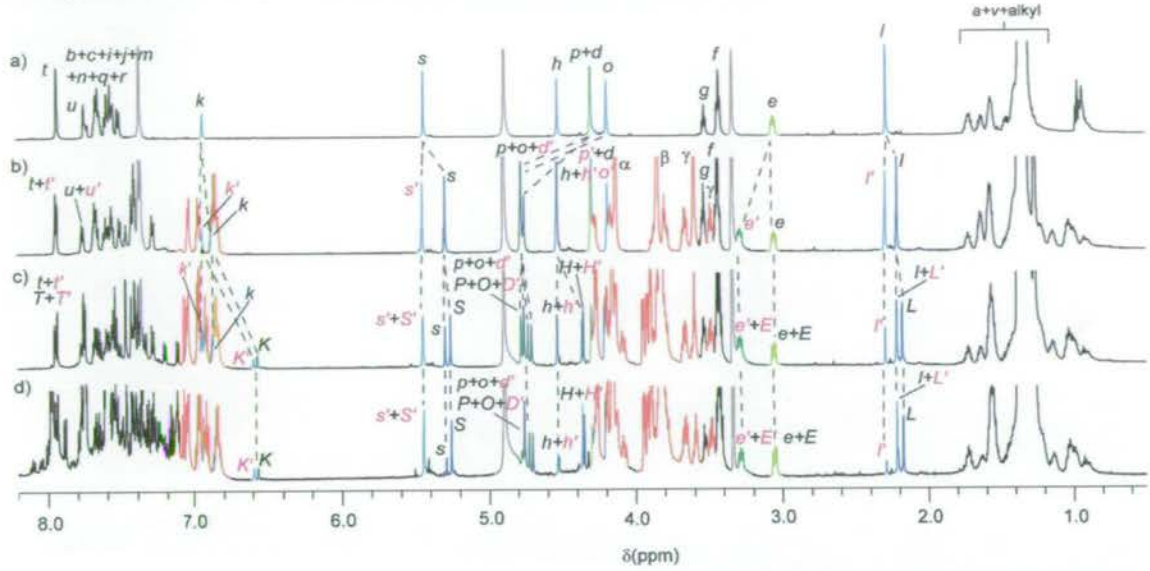

Figure 4.10 ^{1}H NMR spectra (600 MHz, CD_3OD, 298 K) of: (a) thread **7** (*E*-diastereoisomer); (b) rotaxane *E*-**2**; (c) rotaxane **2** + macrocycle **3** (1:1) at the 350 nm photostationary state (*dba*-*Z*-**2**:*mba*-*Z*-**2**:*E*-**2** 32:30:38); (d) **2** + **3** + benzil (1:1:10) at the 350 nm photostationary state (*dba*-*Z*-**2**:*mba*-*Z*-**2**:*E*-**2** 41:39:20). Resonances are coloured according to the conventions used throughout: macrocycle, red; occupied *dba* binding site, dark blue; unoccupied *dba* binding site, light blue; occupied *mba* binding site, dark green; unoccupied *mba* binding site, light green. Lettering corresponds to that used for the assignment of **1**, shown in Figure 4.2. The overlapping aromatic ring signals above 7.2 ppm are not distinguished in this way. Residual non-deuterated solvents are shown in light grey.

4.9.7 Calculation of the extent of deviation from statistical balance and the corresponding change in free energy

The natural statistical balance between the *dba* and *mba* stations follows a Boltzmann distribution based on the relative binding affinities of the two stations for the macrocycle. In *E*-**1**, at 298 K in CD_3OD the experimentally observed (Figure 4.3b) value is 65:35 *dba*:*mba*. Following irradiation of **1** in the presence of at least 5 equivalents benzil in CD_3OD, a *dba*:*mba* ratio of 45:55 is obtained. At point **IV** Figure 4.4a, in an ensemble of 100 molecules of **1**, a net number of 20 out of the 65 molecules (i.e. 31%) originally on the *dba* station have been moved onto the *mba* station.

The 45 molecules with the ring on the *dba* station, would be naturally balanced by 24 molecules with the ring on the *mba* station. Therefore, we have an excess of 55–24 = 31 molecules on the *mba* station. The 69 balanced molecules in our ensemble of 100 are clearly made up from the 20 *E*-**1** molecules which, by their gate-open nature, must be statistically balanced, together with 49 (of the 80 in total) *Z*-**1** molecules, obeying

the natural balance of 65:35 *dba*:*mba* (i.e. ~32 *dba*-Z-**1** molecules and ~17 *mba*-Z-**1** molecules).

In order to calculate the free-energy change on moving away from the equilibrium distribution of particles, consider N_1 (N_2) identical, non-interacting particles in box 1 (2) with volume V_1 (V_2). The total number of particles is $N = N_1 + N_2$ and the total volume is $V = V_1 + V_2$. The partition function is

$$Q = \frac{V_1^{N_1}}{N_1!\Lambda^{3N_1}} \times \frac{V_2^{N_2}}{N_2!\Lambda^{3N_2}} \tag{3}$$

where $\Lambda = \sqrt{h^2/2\pi m k_B T}$ is the de Broglie thermal wavelength (assumed identical for all N particles). The combinatorial factors $N_1!$ and $N_2!$ can be considered to arise form the number of ways of choosing N_1 particles from N ($N!/N_1!N_2!$) divided by the factor $N!$ arising from the particles being indistinguishable. The Helmholtz free energy of the combined system is

$$\begin{aligned} F &= -k_B T \ln Q \\ &= -k_B T\left[N_1 \ln\frac{V_1}{\Lambda^3} - \ln N_1! + N_2 \ln\frac{V_2}{\Lambda^3} - \ln N_2! \right] \\ &\approx -k_B T\left[N_1 \ln\frac{V_1}{\Lambda^3} - N_1 \ln N_1 + N_1 + N_2 \ln\frac{V_2}{\Lambda^3} - N_2 \ln N_2 + N_2 \right] \\ &= k_B T\left[N_1 \ln\frac{N_1\Lambda^3}{V_1} - N_1 + N_2 \ln\frac{N_2\Lambda^3}{V_2} - N_2 \right] \end{aligned} \tag{4}$$

where Stirling's approximation $\ln N! \approx N \ln N - N$ is used. Writing $N_i = x_i N$ and $V_i = y_i V$ where x_i and y_i are the particle-number fraction and box-volume fraction, respectively – equation (4) can be simplified as follows:

$$\frac{F}{N k_B T} = \left(\ln\frac{N\Lambda^3}{V} - 1 \right) + x_1 \ln\frac{x_1}{y_1} + x_2 \ln\frac{x_2}{y_2}. \tag{5}$$

The first term in brackets is recognised as the normal ideal-gas term, F_{id}/Nk_BT. For a fixed number of particles, the total free energy is minimized when $x_i = y_i$, which therefore represents the state of thermodynamic equilibrium:

$$\frac{d}{dx_1}\left(\frac{F}{Nk_BT}\right) = \frac{d}{dx_1}\left[x_1 \ln\frac{x_1}{y_1} + (1-x_1)\ln\frac{(1-x_1)}{(1-y_1)}\right]$$
$$= \ln\frac{x_1}{y_1} + 1 - \ln\frac{(1-x_1)}{(1-y_1)} - 1$$
$$= \ln\frac{x_1(1-y_1)}{y_1(1-x_1)}. \qquad (6)$$

This is equal to zero when $x_i = y_i$; at thermodynamic equilibrium $F = F_{id}$ [from equation (5)]. Hence, the *reversible* work required to make $x_i \neq y_i$ is

$$W = F - F_{id} = Nk_BT\left[x_1 \ln\frac{x_1}{y_1} + (1-x_1)\ln\frac{(1-x_1)}{(1-y_1)}\right]. \qquad (7)$$

This difference in Helmholtz free energies on perturbing the equilibrium distribution of gas particles between the two compartments can be equated to the difference in Gibbs free energies on perturbing the equilibrium distribution of rings between the *dba* and *mba* compartments in **1**. The final mole fraction of particles in the *dba* compartment is x_1, and y_1 is the equilibrium mole fraction of particles in *dba*, giving equation (1) from Section 4.4.

$$\Delta G = Nk_BT\left[x_1 \ln\frac{x_1}{y_1} + (1-x_1)\ln\frac{(1-x_1)}{(1-y_1)}\right] \qquad (1)$$

4.10 References and notes

[1] *Molecular Motors* (Ed.: M. Schliwa), Wiley-VCH, Weinheim, **2003**.

[2] T. R. Kelly, H. De Silva, R. A. Silva, *Nature* **1999**, *401*, 150-152.

[3] N. Koumura, R. W. J. Zijlstra, R. A. van Delden, N. Harada, B. L. Feringa, *Nature* **1999**, *401*, 152-155.

[4] A. M. Brouwer, C. Frochot, F. G. Gatti, D. A. Leigh, L. Mottier, F. Paolucci, S. Roffia, G. W. H. Wurpel, *Science* **2001**, *291*, 2124-2128.

[5] D. A. Leigh, J. K. Y. Wong, F. Dehez, F. Zerbetto, *Nature* **2003**, *424*, 174-179.

[6] J. D. Badjić, V. Balzani, A. Credi, S. Silvi, J. F. Stoddart, *Science* **2004**, *303*, 1845-1849.

[7] J. V. Hernández, E. R. Kay, D. A. Leigh, *Science* **2004**, *306*, 1532-1537 (reprinted, in full, in the Appendix and the basis for Chapter 3).

[8] S. P. Fletcher, F. Dumur, M. M. Pollard, B. L. Feringa, *Science* **2005**, *310*, 80-82.

[9] Y. Liu, A. H. Flood, P. A. Bonvallet, S. A. Vignon, B. H. Northrop, H.-R. Tseng, J. O. Jeppesen, T. J. Huang, B. Brough, M. Baller, S. Magonov, S. D. Solares, W. A. Goddard, C.-M. Ho, J. F. Stoddart, *J. Am. Chem. Soc.* **2005**, *127*, 9745-9759.

[10] J. Berná, D. A. Leigh, M. Lubomska, S. M. Mendoza, E. M. Pérez, P. Rudolf, G. Teobaldi, F. Zerbetto, *Nat. Mater.* **2005**, *4*, 704-710.

[11] Y. Shirai, A. J. Osgood, Y. Zhao, K. F. Kelly, J. M. Tour, *Nano Lett.* **2005**, *5*, 2330-2334.

[12] V. Balzani, M. Clemente-León, A. Credi, B. Ferrer, M. Venturi, A. H. Flood, J. F. Stoddart, *Proc. Natl. Acad. Sci. USA* **2006**, *103*, 1178-1183.

[13] R. Eelkema, M. M. Pollard, J. Vicario, N. Katsonis, B. S. Ramon, C. W. M. Bastiaansen, D. J. Broer, B. L. Feringa, *Nature* **2006**, *440*, 163.

[14] M. N. Chatterjee, E. R. Kay, D. A. Leigh, *J. Am. Chem. Soc.* **2006**, *128*, 4058-4073 (reprinted, in full, in the Appendix and the basis for Chapter 2).

[15] T. Muraoka, K. Kinbara, T. Aida, *Nature* **2006**, *440*, 512-515.

[16] J. C. Maxwell, *Letter to P. G. Tait, 11 December 1867*. Reproduced in *The Scientific Letters and Papers of James Clerk Maxwell Vol. II 1862-1873* (Ed.: P. M. Harman), Cambridge University Press, Cambridge, **1995**, pp. 331-332.

[17] J. C. Maxwell, *Theory of Heat*, Longmans, Green and Co., London, **1871**, Chapter 22.

[18] J. C. Maxwell, *Letter to P. G. Tait, circa. 1875*. Reproduced in *The Scientific Letters and Papers of James Clerk Maxwell Vol. III 1874-1879* (Ed.: P. M. Harman), Cambridge University Press, Cambridge, **2002**, pp. 185-187.

[19] *Maxwell's Demon 2. Entropy, Classical and Quantum Information, Computing* (Eds.: H. S. Leff, A. F. Rex), Institute of Physics Publishing, Bristol, **2003**.

[20] Y. Tokunaga, K. Akasaka, K. Hisada, Y. Shimomura, S. Kakuchi, *Chem. Commun.* **2003**, 2250-2251.

[21] P. R. Ashton, P. J. Campbell, E. J. T. Chrystal, P. T. Glink, S. Menzer, D. Philp, N. Spencer, J. F. Stoddart, P. A. Tasker, D. J. Williams, *Angew. Chem. Int. Ed. Engl.* **1995**, *34*, 1865-1869.

[22] A. G. Kolchinski, D. H. Busch, N. W. Alcock, *J. Chem. Soc. Chem. Commun.* **1995**, 1289-1291.

[23] P. T. Glink, C. Schiavo, J. F. Stoddart, D. J. Williams, *Chem. Commun.* **1996**, 1483-1490.

[24] S.-H. Chiu, A. M. Elizarov, P. T. Glink, J. F. Stoddart, *Org. Lett.* **2002**, *4*, 3561-3564.

[25] G. S. Hammond, J. Saltiel, A. A. Lamola, N. J. Turro, J. S. Bradshaw, D. W. Cowan, R. C. Counsell, V. Vogt, C. Dalton, *J. Am. Chem. Soc.* **1964**, *86*, 3197-3217.

[26] L. Szilard, *Z. Phys.* **1929**, *53*, 840-856.

[27] M. von Smoluchowski, *Physik. Z.* **1912**, *13*, 1069-1080.

[28] J. von Neumann, *Mathematische Grundlagen der Quanten Mechanik*, Springer-Verlag, Berlin, **1932**; English translation: *Mathematical Foundations of Quantum Mechanics*, Princeton University Press, Princeton, **1983**.

[29] L. Brillouin, *J. Appl. Phys.* **1951**, *22*, 334-337.

[30] D. Gabor in *Progress in Optics, Vol. 1* (Ed.: E. Wolf), North-Holland Publishing Co., Amsterdam, **1961**, pp. 111-153.

[31] O. Penrose, *Foundations of Statistical Mechanics*, Pergamon Press, Oxford, **1970**.

[32] C. H. Bennett, *Int. J. Theor. Phys.* **1982**, *21*, 905-940.

[33] W. H. Zurek in *Frontiers of Nonequilibrium Statistical Physics* (Eds.: G. T. Moore, M. O. Scully), Plenum Press, New York, **1984**, pp. 151-161.

[34] J. M. Jauch, J. G. Báron, *Helv. Phys. Acta* **1972**, *45*, 220-232.

[35] J. Earman, J. D. Norton, *Studies Hist. Phil. Mod. Phys.* **1998**, *29*, 435-471.

[36] J. Earman, J. D. Norton, *Studies Hist. Phil. Mod. Phys.* **1999**, *30*, 1-40.

[37] E. P. Gyftopoulos, *Physica A* **2002**, *307*, 405-420.

[38] E. P. Gyftopoulos, *Physica A* **2002**, *307*, 421-436.

[39] A. H. Flood, J. F. Stoddart, D. W. Steuerman, J. R. Heath, *Science* **2004**, *306*, 2055-2056.

[40] R. Landauer, *IBM J. Res. Dev.* **1961**, *5*, 183-191.

[41] E. R. Kay, D. A. Leigh, *Nature* **2006**, *440*, 286-287 (reprinted, in full, in the Appendix).

[42] P. Reimann, *Phys. Rep.* **2002**, *361*, 57-265.

[43] R. D. Astumian, I. Derényi, *Eur. Biophys. J.* **1998**, *27*, 474-489.

[44] I. Derényi, M. Bier, R. D. Astumian, *Phys. Rev. Lett.* **1999**, *83*, 903-906.

[45] A. Parmeggiani, F. Jülicher, A. Ajdari, J. Prost, *Phys. Rev. E* **1999**, *60*, 2127-2140.

[46] J. M. R. Parrondo, B. J. De Cisneros, *Appl. Phys. A* **2002**, *75*, 179-191.

[47] G. P. Harmer, D. Abbott, *Nature* **1999**, *402*, 864.

[48] G. P. Harmer, D. Abbott, P. G. Taylor, *Proc. R. Soc. Lond. A* **2000**, *456*, 247-259.

[49] R. D. Astumian, *Sci. Am.* **2001**, *285* (1), 56-64.

[50] J. M. R. Parrondo, L. Dinís, *Contemp. Phys.* **2004**, *45*, 147-157.

[51] R. D. Astumian, *Am. J. Phys*. **2005**, *73*, 178-183.

[52] W. G. Herkstroeter, G. S. Hammond, *J. Am. Chem. Soc.* **1966**, *88*, 4769-4777.

[53] W. G. Herkstroeter, A. A. Lamola, G. S. Hammond, *J. Am. Chem. Soc.* **1964**, *86*, 4537-4540.

CHAPTER FIVE

Electrochemically Switchable Hydrogen-Bonded Molecular Shuttles

Sections 5.1–5.6 of this Chapter have been published in *Journal of the American Chemical Society* as "*Electrochemically Switchable Hydrogen-Bonded Molecular Shuttles*":

A. Altieri, F. G. Gatti, E. R. Kay, D. A. Leigh, D. Martel, F. Paolucci, A. M. Z. Slawin, J. K. Y. Wong, *J. Am. Chem. Soc.* **2003**, *125*, 8644-8654.

Acknowledgements and contributions

A number of collaborators contributed to the work in this Chapter, as detailed below. Each of their efforts is gratefully acknowledged.

In our own group at the School of Chemistry, University of Edinburgh (and previously at the University of Warwick), synthesis and characterization of the original shuttle system – thread molecules **2**, **9**–**11** and rotaxanes **1**, **3**, **5**–**8** – was carried out by Dr Francesco G. Gatti, and rotaxane **4** was prepared by Dr Andrea Altieri.

Thread molecules **20**–**23** were synthesized by Dr Jacob Baggerman, under the supervision of Dr Albert M. Brouwer at the Institute of Molecular Chemistry, University of Amsterdam, The Netherlands, where photophysical studies are also presently underway.

Electrochemistry was carried out by Dr Alessio Altieri, Dr Giulia Fioravanti, Dr Natalia Haraszkiewicz, Dr Massimo Margotti and Dr David Martel, under the supervision of Prof. Francesco Paolucci at the Dipartimento di Chimica "G. Ciamician", Università delgi Studi di Bologna, Italy.

Thin film preparation and surface studies were carried out by Dr Monika Lubomska and Sandra M. Mendoza, under the supervision of Prof. Petra Rudolf at the Materials Science Centre, Rijksuniversiteit Groningen, The Netherlands.

X-Ray crystallography was carried out by Dr Jenny K. Y. Wong (**4**) at the University of Edinburgh and Prof. Alexandra M. Z. Slawin (**3**) at the Department of Chemistry, University of St. Andrews, UK.

The author synthesized and characterized the neutral state of rotaxanes **12**–**19** and **24**–**26**, collated the results from all collaborators and wrote this Chapter and the paper on which Sections 5.1–5.6 are based.

Synopsis

Chapters 2–4 have explored different mechanisms for molecular motors and machines, using rotaxanes and catenanes as ideal molecular architectures for investigating motion at the molecular level. Irrespective of the precise mechanism, the control of macrocycle motion in these systems depends on manipulating the binding affinities at specific stations on the thread (achieved by an olefin photoisomerization in Chapters 2 and 3) and controlling the kinetics for transport between these units (achieved by alcohol protection–deprotection strategies in Chapters 2 and 3, and by an olefin photoisomerization in Chapter 4). In order to support the ongoing investigation of increasingly complex molecular machines, and indeed, to meet the demands of any future application for such molecular devices, it is clearly desirable to develop a range of chemical structures which can demonstrate such abilities, controlled by various external stimuli and able to operate in different environments.

Returning to the classic concept of rotaxane-based molecular shuttles, a series of [2]rotaxanes containing succinamide and aromatic imide hydrogen-bonding stations for a benzylic amide macrocycle is described here. In the first example, electrochemical reduction and oxidation of a naphthalimide group alters its ability to form hydrogen bonds with the macrocycle to such a degree that redox processes can be used to switch the relative order of macrocycle-binding affinities of the two stations in the rotaxane. The structure of the neutral [2]rotaxane in solution is established by ^{1}H NMR spectroscopy and shows that the macrocycle exhibits remarkable positional integrity for the succinamide station in a variety of solvents. Cyclic voltammetry experiments allow the simultaneous stimulation and observation of a redox-induced dynamic process in the rotaxane, which is both reversible and cyclable. Model compounds, in which various conformational and co-conformational changes are prohibited, demonstrate unequivocally that the redox response is the result of shuttling of the macrocycle between the two stations. Furthermore, the electrochemical technique allows quantification of the kinetic parameters for shuttling: at room temperature in tetrahydrofuran the electrochemically induced movement of the macrocycle between the two stations takes ~50 μs.

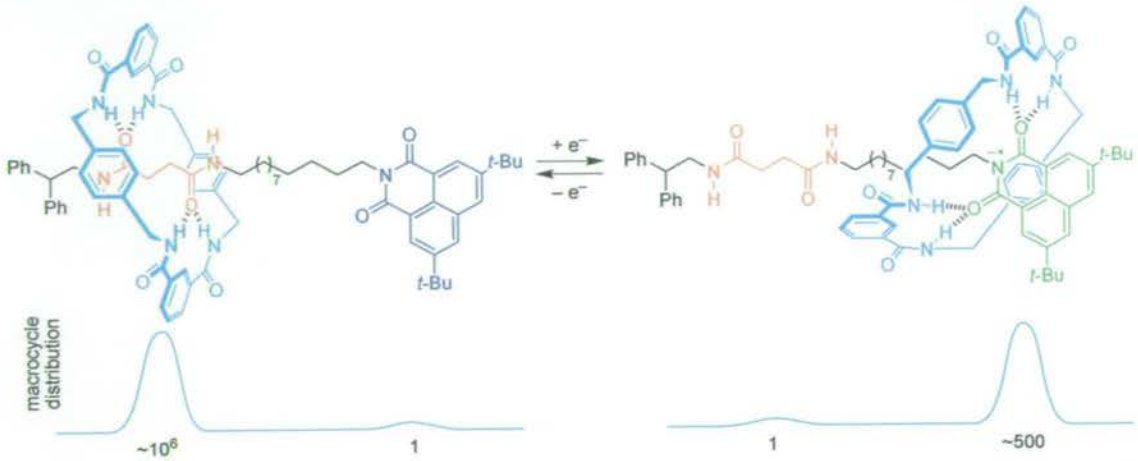

Having verified this redox-induced shuttling process, structural variation of the imide unit is investigated, with a view to tuning the thermodynamic and kinetic parameters for the dynamic process and probing redox-active units that exhibit more complex electrochemical and photochemical behaviours. Preliminary steps towards triggering and observing electrochemically induced shuttling in rotaxane molecules attached to surfaces is also reported.

5.1 Introduction

Natural[1] and artificial[2] devices that function through mechanical motion at the molecular level require a nanoscale structure that restricts the movement of the various components, coupled with a process – usually chemical – to power and control their motions. For the design of prototypical synthetic systems, chemists have started by taking inspiration from the structural elements of machinery from the macroscopic world.[3] Taking this analogy too far in terms of process must be cautioned, however, since the modes of action for useful movement at the molecular and macroscopic levels are very different. In the macroscopic world, objects do not move until provided with specific energy to do so. In a mechanical machine this is often through a directional stimulus (i.e. when work is done to move components in a particular way). At the molecular level, molecules – and their parts – are constantly moving above 0 K and it is the directional control of this motion which nature uses to perform useful mechanical tasks.[1]

'Molecular shuttles' provide a promising basis for molecular machines. Various types of rotaxane[4] structures permit large amplitude, largely independent, motions of the mechanically interlocked components and the noncovalent-bond-directed routes to their synthesis ultimately offer a process for controlling the relative positioning of the components through the interactions that 'live on' in the final products.[5] In a rotaxane with two different binding sites ('stations') in the thread, the macrocycle distributes itself between the stations according to the difference in the macrocycle-binding energies and the temperature. If a suitably large difference in macrocycle affinity between the two stations exists, the macrocycle resides overwhelmingly in one positional isomer or co-conformation.[6] In stimuli-responsive molecular shuttles,[7–11] an external trigger is used to chemically modify the system and alter the noncovalent intercomponent interactions such that the second macrocycle-binding site becomes energetically more favoured, causing translocation of the macrocycle along the thread to the second station (Figure 5.1). The system can be returned to its original state by using a second chemical modification to restore the initial order of station binding affinities. Performed consecutively, these two steps allow the 'machine' to carry out a complete cycle of shuttling motion. The movement of the macrocycle from station to station is thus caused by using chemical reactions to put the molecule into

nonequilibrium co-conformations and then allowing the background thermal energy to drive the macrocycle to the new global minimum (i.e. through biased Brownian motion).

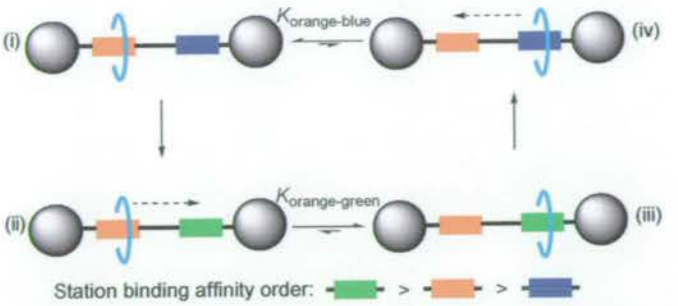

Figure 5.1 Translational submolecular motion in a stimuli-responsive molecular shuttle: (i) the macrocycle initially resides on the preferred (orange) station; (ii) a reaction occurs (blue→green) changing the relative binding potentials of the two stations such that, (iii), the macrocycle 'shuttles' to the now-preferred (green) station. If the reverse reaction (green→blue) now occurs, (iv), the components return to their original positions. The energy available to do mechanical work through shuttling in such a cycle is the sum of the difference in macrocycle binding energies of the two stations in each of the two states (i.e. $\Delta\Delta G_{orange\text{-}blue} + \Delta\Delta G_{green\text{-}orange}$).

We recently reported the real-time observation of macrocycle translocation in such a stimuli-responsive molecular shuttle following the photochemically induced reduction of the 1,8-naphthalimide unit in rotaxane **1**.[8g] In fact, we originally designed **1** as an electrochemically-switchable system.[12, 13] Electrochemistry is potentially an attractive method through which to modulate the behaviour of molecular devices because it can be easily and rapidly turned on and off, while also offering a reagent-free and waste-free procedure. Obviously, an important attribute of any molecular machine is that, for the submolecular motion to be useful, it must be detectable through some change in the system's properties. Electrochemistry is also advantageous in this regard since the same stimulus can simultaneously act as both effector and detector of the motion.

Here we report the cyclic voltammetry of **1** and a series of related rotaxanes and threads. The rates and energies obtained from the electrochemical redox experiments are consistent with those obtained photochemically. The spectroscopic and electrochemical behaviour of key model compounds is used to show unambiguously that the dynamics observed are a consequence of the position of the macrocycle on the thread changing upon reduction of the naphthalimide unit. Furthermore, structural variation of the redox-active unit is explored and preliminary steps are taken towards controlling and observing shuttling at surfaces.

Chart 5.1 Molecular Shuttle **1**, Shown as the *succ*-**1** Positional Isomer, and Thread **2**.[a]

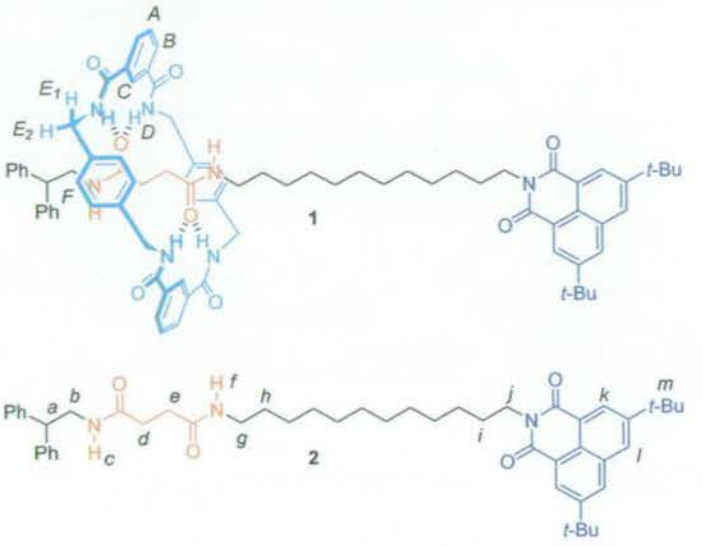

[a] The letters indicate selected non-equivalent ^{1}H environments.

5.2 Design

Hydrogen bonds are largely electrostatic in nature,[14] so changes in the electron charge density of a hydrogen-bonding group can have a dramatic effect on its binding ability – a phenomenon exploited in redox-switched molecular recognition[15] and the modulation of protein and peptide structure.[16] Molecular shuttle **1** consists of a benzylic amide macrocycle – a strong hydrogen-bond donor through the amide NH groups – mechanically linked onto a thread molecule, **2**, containing two potential hydrogen-bond acceptor moieties – a succinamide (*succ*) station and a redox-active 3,6-di-*tert*-butyl-1,8-naphthalimide[17] (*ni*) station – separated by a C_{12} aliphatic spacer (Chart 5.1). The ability of the *succ* station to template formation of the macrocycle by a five component 'clipping' reaction between isophthaloyl dichloride and *p*-xylylenediamine in apolar solvents is well established.[8g] X-ray crystal structures of model succinamide rotaxanes **3** and **4** (Figures 5.2 and 5.3) demonstrate an excellent fit between the thread and macrocycle, both in terms of steric interactions and the complementary positioning of the hydrogen-bonding amide groups on the two components. While the structure of **3** shows both intra- and intermolecular hydrogen bonding in the solid state, **4** has a solely intramolecularly hydrogen-bonded structure and is probably more representative of the hydrogen-bonding motifs adopted by 'isolated' molecules in solution. The macrocycle adopts a near-perfect chair conformation, driven by formation of two sets of bifurcated hydrogen bonds between

the amide protons of each isophthalamide moiety and the succinamide carbonyl oxygens.

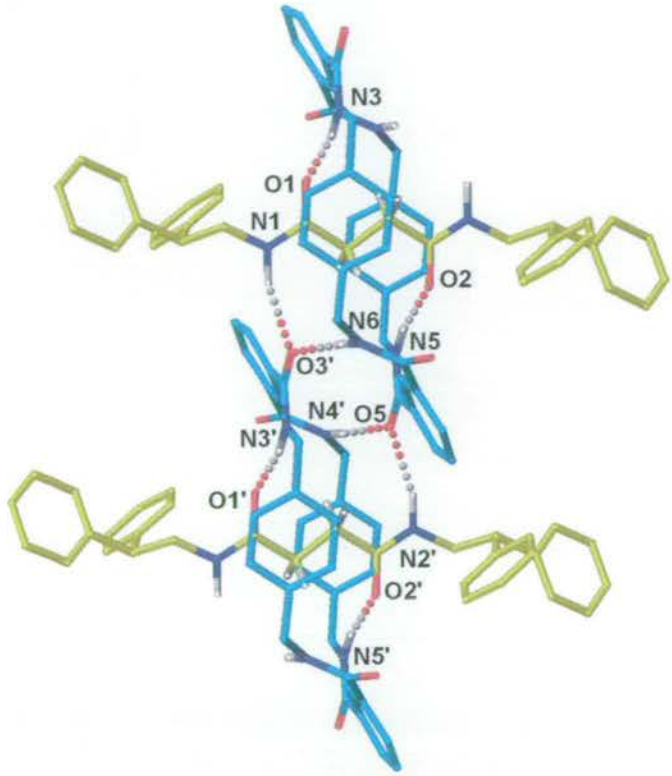

Figure 5.2 X-ray crystal structure of [2]rotaxane **3** (for clarity carbon atoms of the macrocycle are shown in blue and the carbon atoms of the thread are shown in yellow; oxygen atoms are depicted in red, nitrogen atoms in dark blue and amide protons in white). Intramolecular hydrogen-bond distances (Å): O1–HN3/O2–HN5 1.88. Intermolecular hydrogen-bond distances (Å): O5–HN4′/O3′–HN6 2.00, O3′–HN1/O5–HN2′ 2.21.

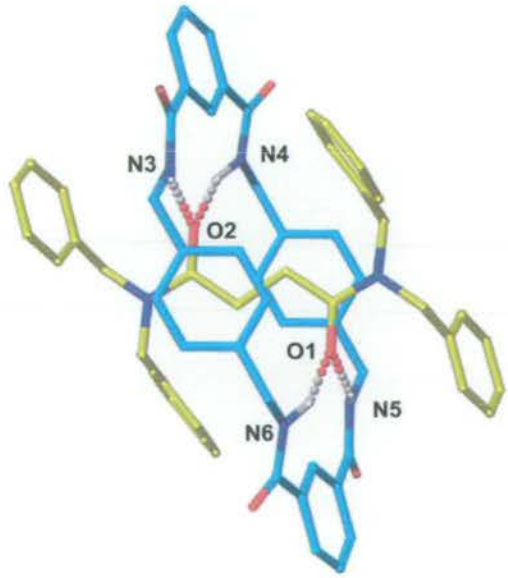

Figure 5.3 X-ray crystal structure of [2]rotaxane **4**. Intramolecular hydrogen-bond distances (Å): O2–HN3/O1–HN5 1.90, O2–HN4/O1–HN6 2.01.

The choice of a substituted naphthalimide unit as the redox-active station was inspired by the work of Smith[15b] and Rotello[15c, 15e, 15f]. Imides are comparatively poor hydrogen-bond acceptors,[18] indeed threads containing just the naphthalimide unit do not template formation of the benzylic amide macrocycle to give rotaxanes. In order to minimize its free energy, the macrocycle in **1** must therefore sit over the succinamide station in non-hydrogen-bonding solvents, so that co-conformation *succ*-**1** predominates (Figure 5.4). One-electron reduction of naphthalimides to the corresponding radical anion, however, results in a substantial increase in electron charge density on the imide carbonyls and a concomitant increase in hydrogen-bond accepting ability.[15b, 15c, 15e] In **1**, this change in oxidation state should reverse the relative hydrogen-bonding abilities of the two thread stations so that co-conformation *ni*-$\mathbf{1}^{-\bullet}$ is preferred in the reduced state. This dynamic process was studied in **1** through cyclic voltammetry experiments and ^{1}H NMR spectroscopy. In order to probe the nature of the stimulated motion we carried out similar studies on model rotaxanes **5**–**8** (Chart 5.2). Each of these analogues of **1** is designed to restrict a different type of conformational or co-conformational change so that the true origin of the effects seen for **1** could be unambiguously determined.

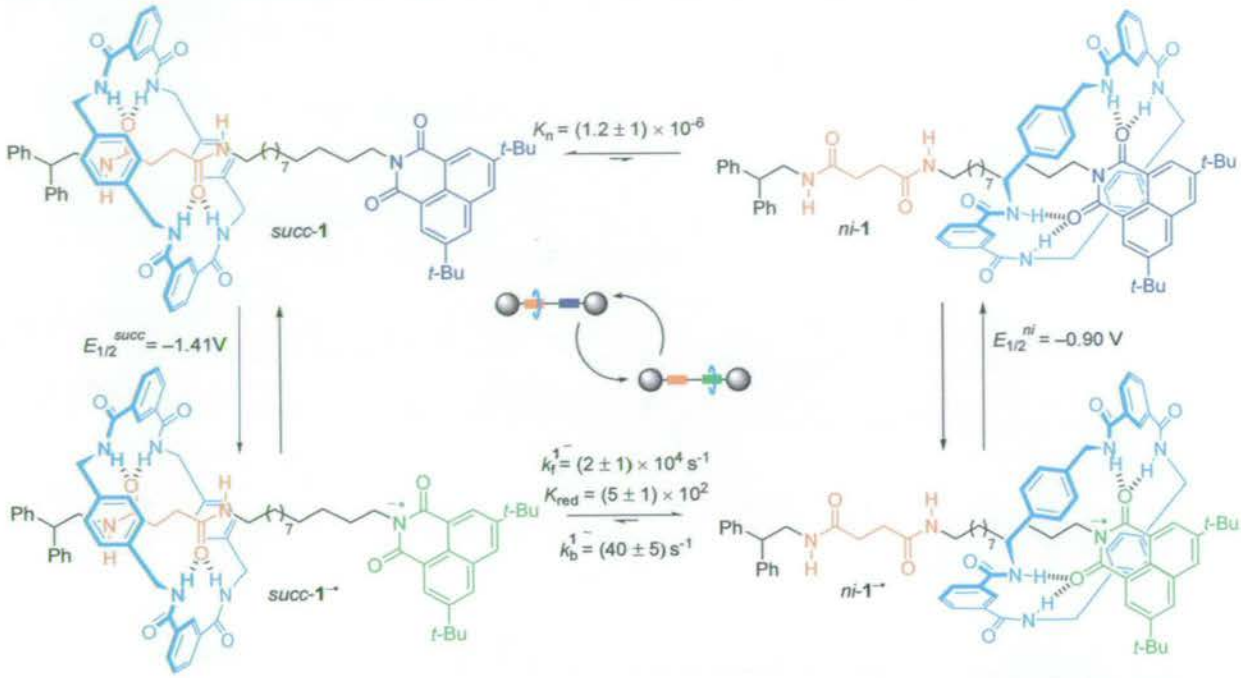

Figure 5.4 An electrochemically switchable, hydrogen-bonded molecular shuttle **1**. In the neutral state, the translational co-conformation *succ*-**1** is predominant as the *ni* station is a poor hydrogen-bond acceptor ($K_n = (1.2 \pm 1) \times 10^{-6}$). Upon reduction, the equilibrium between *succ*-**1**$^{-\bullet}$ and *ni*-**1**$^{-\bullet}$ is altered ($K_{red} = (5 \pm 1) \times 10^2$) because *ni*$^{-\bullet}$ is a powerful hydrogen-bond acceptor and the macrocycle moves through biased Brownian motion. Upon re-oxidation, the macrocycle shuttles back to its original position. Repeated reduction and oxidation causes the macrocycle to shuttle forwards and backwards between the two stations. All values were calculated by fitting experimental curves from experiments in anhydrous THF at 298 K with tetrabutylammonium hexafluorophosphate (TBHF) as the supporting electrolyte. For fitting parameters, see Tables 5.2 and 5.3 in Section 5.10.2.

Chart 5.2 Model Rotaxanes **3**–**8** Shown as the *succ*- Positional Isomers.[a]

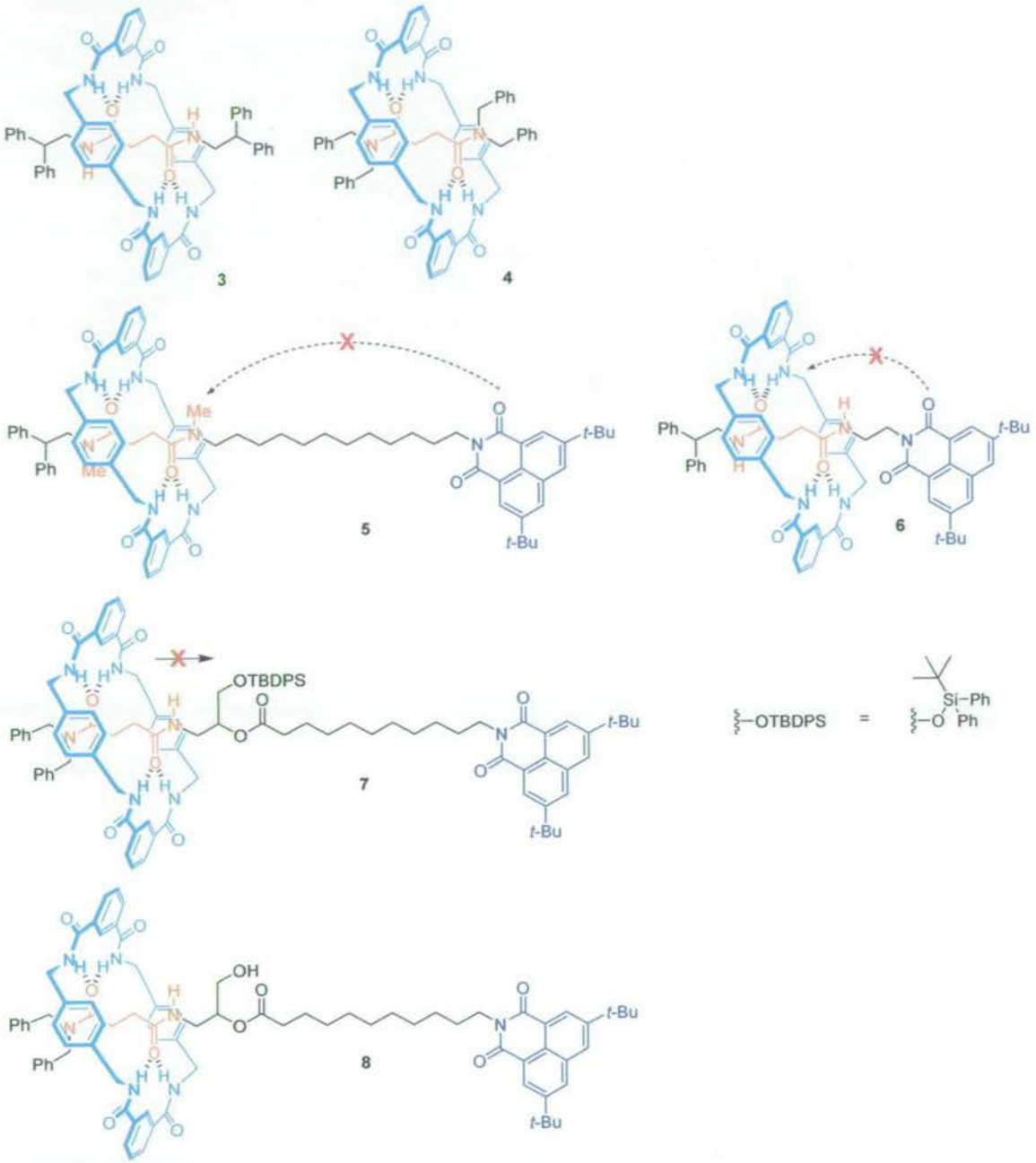

[a] The dashed lines show hydrogen-bond interactions possible in **1** but disallowed in the model compound. Solid lines show changes of co-conformation that require shuttling which are disallowed in the model compound.

5.3 Synthesis

Rotaxanes **1**, **5** and **6** were prepared according to Scheme 5.1. Treatment of threads **2**, **9** or **10** with 10 equivalents of each of *p*-xylylenediamine and isophthaloyl dichloride ($CHCl_3$, Et_3N, 4 hours, high dilution) provided [2]rotaxanes **1**, **5** and **6** in 59%, 33% and 62% yields, respectively. Scheme 5.2 shows the synthesis of 'gate-closed' thread

11 which, under similar rotaxane-forming conditions, furnished [2]rotaxane **7** in 23% yield. The 'gate-opened' rotaxane **8** was obtained by treatment of **7** with a stoichiometric amount of tetra-*n*-butylammonium fluoride in CH_2Cl_2.[19] Rotaxane **12**, an analogue of **1** in which the macrocycle contains two pyridyl moieties, was also prepared in a similar fashion to the others, but substituting pyridine-3,5-dicarbonyl dichloride for isophthaloyl dichloride, as shown in Scheme 5.1.

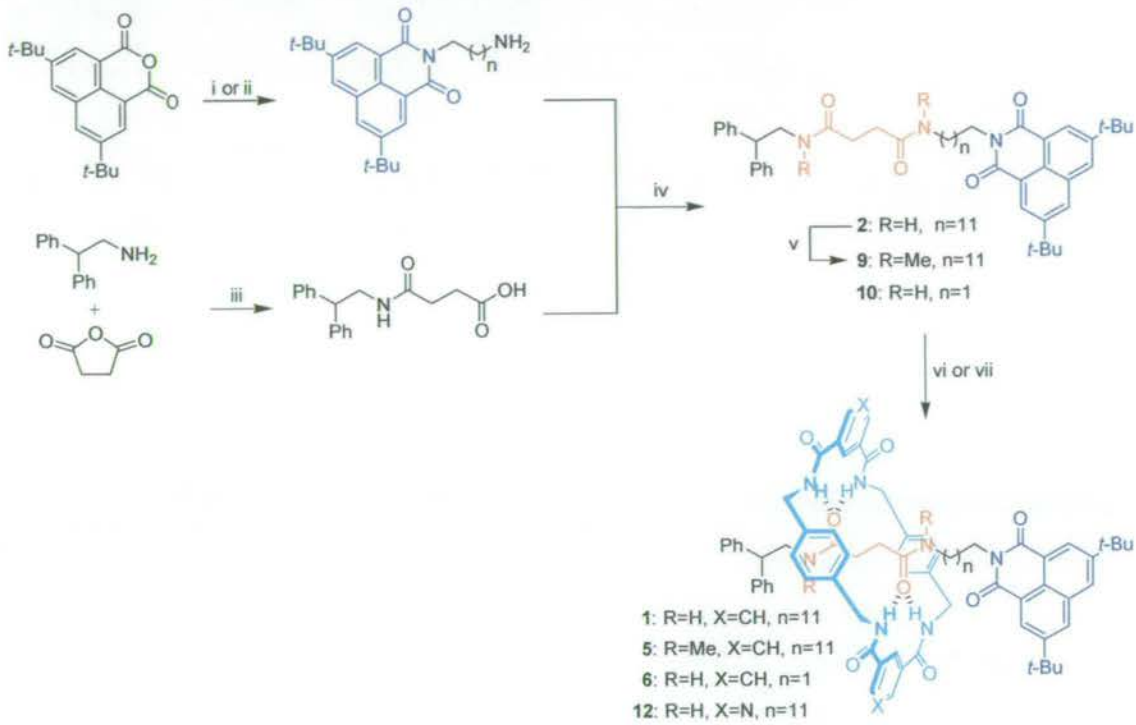

Scheme 5.1 Synthesis of rotaxanes **1**, **5**, **6** and **12**. Reagents and conditions (unless otherwise stated, reactions were carried out at room temperature): (i) 1,12-diaminododecane, Et_3N, EtOH, Δ, 2 h, 14%; (ii) 1,2-ethylenediamine, EtOH, Δ, 2 h, 78%; (iii) pyridine, 16 h, 90%; (iv) 1-[3-(dimethylamino)propyl]-3-ethylcarbodiimide hydrochloride (EDCI·HCl), 4-(dimethylamino)pyridine (DMAP), CH_2Cl_2, 0 °C to rt, 12 h, 98% (**2**), 93% (**10**); (v) MeI, NaH, THF, 0 °C to rt, 16 h, 94%; (vi) isophthaloyl dichloride, *p*-xylylenediamine, Et_3N, $CHCl_3$, 4 h, 59% (**1**), 33% (**5**), 62% (**6**); (vii) pyridine-3,5-dicarbonyl dichloride, *p*-xylylenediamine, Et_3N, $CHCl_3$, 4 h, 46% (**12**).

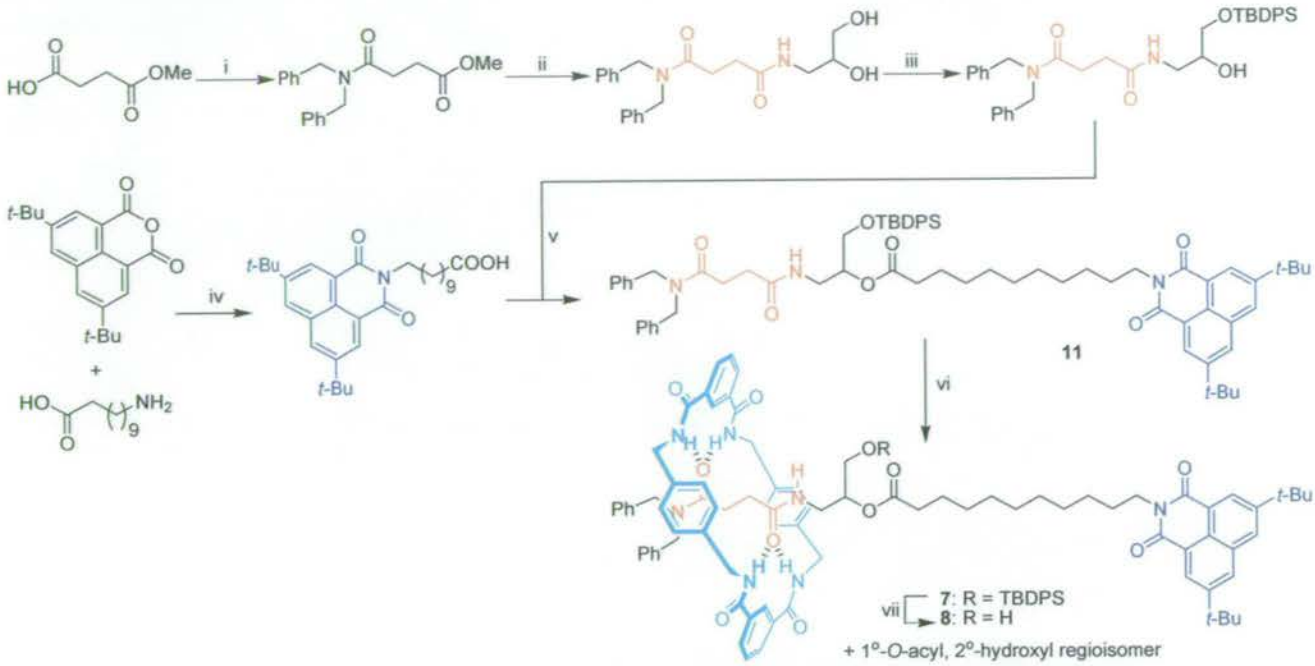

Scheme 5.2 Synthesis of rotaxanes **7** and **8**. Reagents and conditions (unless otherwise stated, reactions were carried out at room temperature): (i) $(PhCH_2)_2NH$, EDCI·HCl, DMAP, CH_2Cl_2, 0 °C to rt, 12 h, 94%; (ii) 3-amino-propane-1,2-diol, Δ, 3h, 84%; (iii) *tert*-butyldiphenylsilyl chloride (TBDPSCl), imidazole, DMAP, CH_2Cl_2, 24 h, 62%; (iv) pyridine, Δ, 18 h, 60%; (v) EDCI·HCl, DMAP, CH_2Cl_2, 0 °C to rt, 12 h, 90%; (vi) isophthaloyl dichloride, *p*-xylylenediamine, Et_3N, $CHCl_3$, 4 h, 23%; (vii) tetrabutylammonium fluoride, CH_2Cl_2, 2 h, 70%.

5.4 Co-conformation in the neutral state

^{1}H NMR spectroscopy is a useful tool for studying translational isomerism in rotaxanes. For benzylic amide macrocycle-containing rotaxanes, aromatic ring currents in the *p*-xylylene rings result in significant upfield shifting (typically $|\Delta\delta_H| > 1$ ppm) for protons on the portion of the thread covered by the macrocycle.[20] Comparison of the ^{1}H NMR spectra of rotaxane **1** and the corresponding thread **2** in $CDCl_3$ (Figure 5.5) shows such an upfield shift for succinic methylene protons H_d and H_e ($\Delta\delta_H = -1.45$ ppm).[21] Protons in close proximity to the *succ* station (H_a, H_b and H_g) are also shielded but to a lesser extent; all other thread protons, including those of the naphthalimide, are essentially unaffected by the presence of the macrocycle. The infrared spectrum of **1** in $CHCl_3$ also shows no changes in the CO stretching band of the naphthalimide moiety compared to the spectrum of **2** ($\overline{\nu}_{CO\,stretch} = 1780$ cm^{-1} in each case) suggesting no significant hydrogen bonding occurs to the naphthalimide subunit in the rotaxane.[8g] Clearly the *succ*-**1** translational isomer is the predominant structure in chloroform.

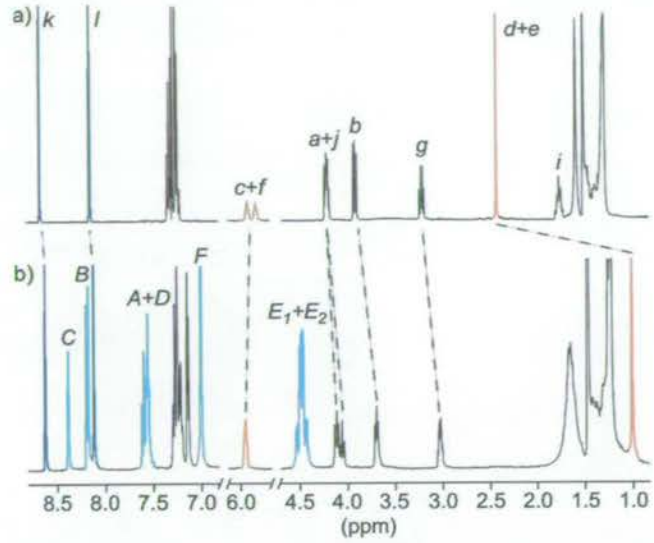

Figure 5.5 ^{1}H NMR spectra (400 MHz, $CDCl_3$, 298 K) of (a) **2** and (b) **1**. The letters correspond to the assignments shown in Chart 5.1.

In fact, unlike peptide-based molecular shuttles,[7a] the positional integrity of the macrocycle in **1** is remarkably independent of the nature of the solvent. The difference in chemical shifts for methylene protons H_d and H_e in **1** and **2**, as well as the shifts for succinamide amide protons H_c and H_f, in solvents of varying hydrogen-bonding ability are shown in Table 5.1. The increasing δ_H values for the amide protons illustrate the ability of these solvents to disrupt hydrogen bonding ($CDCl_3$ < $[D_3]$MeCN < $[D_8]$THF < $[D_6]$DMSO). It can be seen, however, that in $CDCl_3$, $[D_3]$MeCN and $[D_8]$THF, shielding of the *succ* methylene protons is virtually unchanged, indicating that positional integrity of the shuttle is maintained in all three solvents. Even in $[D_6]$DMSO the upfield shift for H_d and H_e is only reduced by ~50%, indicating that even in this strongly hydrogen-bond-disrupting solvent the macrocycle still spends a significant amount of time over the *succ* station.

Table 5.1 Solvent effects on chemical shifts (δ_H) and differential chemical shifts ($\Delta\delta_H$) for succinamide protons in **1** and **2**.

Solvent	NH_c and NH_f		H_d and H_e
	δ_H (**1**) / ppm	δ_H (**2**) / ppm	$\Delta\delta_H$ / ppm
$CDCl_3$	5.95	5.73; 5.61	–1.45
$[D_3]$MeCN[a]	6.47; 6.42	6.42; 6.22	–1.2
$[D_8]$THF	7.84; 7.63	7.20; 7.12	–1.2
$[D_6]$DMSO	7.92; 7.40	7.78; 7.60	–0.7

[a] Spectra collected at 329 K due to low solubility of **1** in $[D_3]$MeCN.

The energy barrier for pirouetting of the macrocycle around the thread provides a definitive measure of the strength of the intercomponent interactions.[22] Due to the complexity of the ^{1}H NMR spectra of **1** and its analogues, this process was studied in the simpler, C_2-symmetric, rotaxanes **3** and **4** as models for shuttles **1** and **5** respectively. Variable-temperature (VT) ^{1}H NMR experiments in $CDCl_3$ and $C_2D_2Cl_4$ (because of the wide temperature range involved) using both the coalescence method[23] and spin polarization transfer by selective inversion recovery (SPT-SIR)[24] were employed to calculate the rates of macrocycle pirouetting. The VT ^{1}H NMR plot for **4** (Figure 5.6) shows the signals for macrocycle benzylic methylene protons H_{E1} and H_{E2} are well separated at 243 K, while a single sharp peak is observed at 369 K.[25] SPT-SIR of **4** gives an energy barrier for macrocycle pirouetting at 298 K of 12.9 ± 0.1 kcal mol^{-1}. Similarly, the barrier for **3** was determined as 11.2 ± 0.1 kcal mol^{-1} at 298 K. Even when compared to the fumaramide template which holds the hydrogen-bond acceptor groups of the thread in a close-to-ideal arrangement for the donor groups in the macrocycle ($\Delta G^{\ddagger}_{298}$ for the fumaramide analogue of **3** = 13.4 ± 0.1 kcal mol^{-1})[22b] it can be seen that the succinic templates in **3** and **4** result in strong intercomponent hydrogen bonding. Clearly, dissociation from the succinamide station in a molecular shuttle will involve a significant energy barrier.

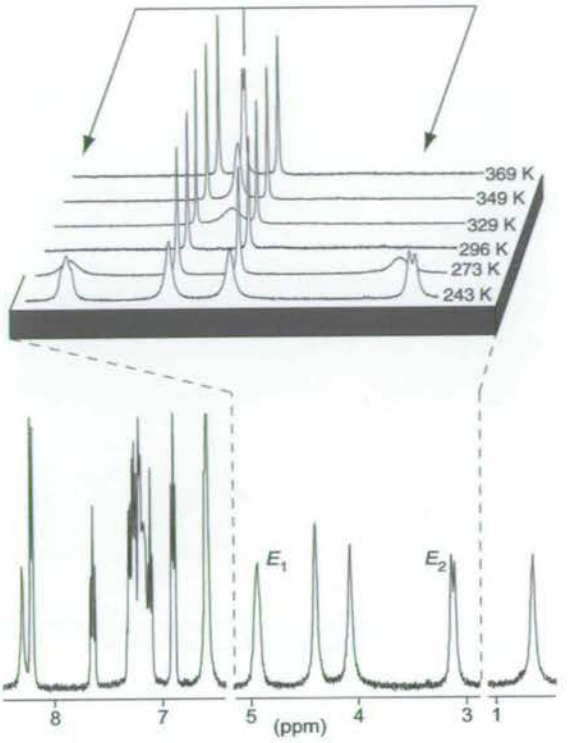

Figure 5.6 ^{1}H NMR spectrum of **4** (400 MHz, $CDCl_3$) at 243 K showing slow pirouetting of the macrocycle about the thread (H_{E1} and H_{E2} resolved). SPT-SIR between resolved signals gives the energy barrier for macrocycle pirouetting. Higher temperature spectra (expansion, 243-296 K ($CDCl_3$) and 329-369 K ($C_2D_2Cl_4$)) illustrate the wide temperature ranges that can exist between full resolution and coalescence of signals affected by the dynamic processes.

5.5 Redox-switched shuttling

Translocation of the macrocycle in **1** could be readily triggered by electrochemical reduction of the naphthalimide station to its radical anion. Since the changes in hydrogen-bonding pattern affect the electrochemical properties of the system, the shuttling process could be both effected and observed in cyclic voltammetry (CV) experiments of **1** and its analogues and components.[26] The CV response of **2** in anhydrous THF (Figure 5.7a) exhibits a reversible, one-electron reduction peak corresponding to reduction and re-oxidation of the naphthalimide group (**2**/**2**$^{-\bullet}$, $E_{1/2} = -1.41$ V).[17] Rotaxane **1** on the other hand, displays a similar cathodic signal, **I**, ($E_c = -1.40$ V, at 2 V s^{-1}), yet lacks the corresponding oxidation peak (Figure 5.7b). Rather, a new one-electron anodic peak, **II**, appears towards more positive potentials ($E_a = -0.89$ V, at 2 V s^{-1}). On subsequent scans, performed without renewal of the diffusion layer, it is only these two peaks that appear, indicating that the system returns to its original state after each cycle on this timescale.

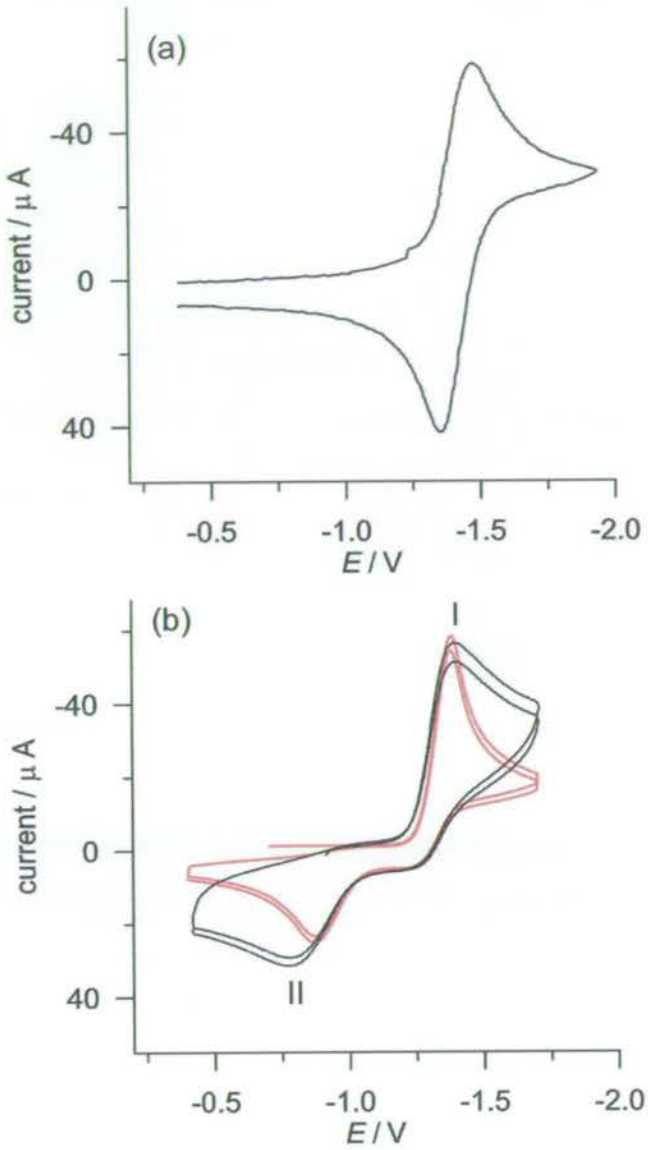

Figure 5.7 Cyclic voltammograms at 298 K of (a) **2** and (b) **1** showing both experimental (black line) and simulated (red line) results. Experiments carried out on 1 mmol L^{-1} solutions of substrate in anhydrous THF with TBHF (5×10^{-2} mol L^{-1}) as electrolyte and ferrocene as internal standard. Scan rate: 2 V s^{-1}. Working electrode: Pt.

These results can be interpreted in terms of a standard square scheme for a redox-switched binding process whereby the reversible translational isomerism equilibria for each oxidation state are connected *via* the electron transfer steps (Figure 5.4). As shown earlier, the shuttle in its neutral state overwhelmingly adopts co-conformation *succ*-**1**. Reduction of the naphthalimide group to give *succ*-$\mathbf{1}^{-\bullet}$ is therefore unaffected by the macrocycle. Due to the increased hydrogen-bonding ability of naphthalimide in its reduced state, the equilibrium between co-conformations in this oxidation state lies far towards the *ni*-$\mathbf{1}^{-\bullet}$ isomer so that shuttling of the macrocycle occurs. Resultant hydrogen bonding to the macrocycle amide protons stabilises the increased electron

density on the naphthalimide so that more positive potentials must be reached before the oxidation *ni*-**1**$^{-\bullet}$ → *ni*-**1** occurs (ΔE_p = 0.51 V). Once again in the neutral state, the macrocycle shuttles back to the preferred succinamide station therefore restoring the system to its original state as *succ*-**1**. The absence of any *succ*-**1**$^{-\bullet}$ → *succ*-**1** oxidation peak or *ni*-**1** → *ni*-**1**$^{-\bullet}$ reduction peak demonstrates the remarkable positional integrity of the shuttle in both oxidation states, while also indicating that the shuttling process is rapid on the timescale of the experiment.

The CV curve of **1** was simulated (Figure 5.7b). Fitting with the experimental results allowed calculation of the redox potential for the electron transfer process *ni*-**1**$^{-\bullet}$ ⇆ *ni*-**1** as $E_{1/2}^{ni}$ = –0.90 V. Also obtained were the rate constants in the reduced state for the forward shuttling process (*succ*-**1**$^{-\bullet}$ → *ni*-**1**$^{-\bullet}$; $k_f^{1^{--}} = (2 \pm 1) \times 10^4$ s^{-1}; T = 298 K, THF) and the backward process (*ni*-**1**$^{-\bullet}$ → *succ*-**1**$^{-\bullet}$; $k_b^{1^{--}} = (40 \pm 5)$ s^{-1}; T = 298 K, THF). These figures yield a co-conformational equilibrium constant for the reduced state of $K_{red} = (5 \pm 1) \times 10^2$ confirming that the *ni*-**1**$^{-\bullet}$ co-conformation is indeed strongly preferred. The *ni*-**1** → *succ*-**1** shuttling process occurs faster than the *ni*-**1**$^{-\bullet}$→ *ni*-**1** oxidative electron transfer step, so that it is not possible to calculate rate constants for this process.[27] The equilibrium constants in each oxidation state for any such redox-switched binding process are related by equation (1).[28] Accordingly, the constant for the neutral state co-conformational equilibrium was calculated as $K_n = (1.2 \pm 1) \times 10^{-6}$,[29] consistent with the predominance of the *succ*-**1** co-conformation shown by ^{1}H NMR and IR.

$$\Delta E^\circ = E_{1/2}^{ni} - E_{1/2}^{succ} = \frac{RT}{nF} \ln\left(\frac{K_{red}}{K_n}\right) \quad (1)$$

Given the fast rate constants for shuttling in the reduced state, a scan rate of the order of 10 kV s^{-1} would be required to observe the *succ*-**1**$^{-\bullet}$ → *succ*-**1** oxidation before shuttling to *ni*-**1**$^{-\bullet}$ occurs. Such high scan rates are not achievable with **1** due to the high resistivity of THF solutions. An alternative strategy is to run the experiments at low temperatures so as to slow the shuttling motion. Indeed, at 213 K, the cathodic peak, **I**, for reduction of the *succ*-**1** species exhibits an anodic counterpart, **III**, while the intensity of anodic peak **II** is correspondingly reduced (Figure 5.8). The even greater resistivity at this temperature prevents the use of higher scan rates to oxidize all *succ*-**1**$^{-\bullet}$ species before shuttling occurs.

Simulation of the low-temperature CV curve (Figure 5.8) indicated, as expected, that the rate constant for forwards shuttling in the reduced state is much lower than that at room temperature ($k_f^{I^{\bullet-}} \approx 1\ s^{-1}$; $T = 213$ K, THF). By repeating the simulation at various temperatures and subjecting the results to an Eyring plot analysis (see Figure 5.16, Section 5.10.3), the following activation parameters for the shuttling process in the reduced state were obtained: $\Delta H^{\ddagger} = 14.0 \pm 0.6$ kcal mol^{-1}, $\Delta S^{\ddagger} = 8.7 \pm 2$ cal K^{-1} mol^{-1} and $\Delta G^{\ddagger}_{298} = 11.4 \pm 1.2$ kcal mol^{-1}.

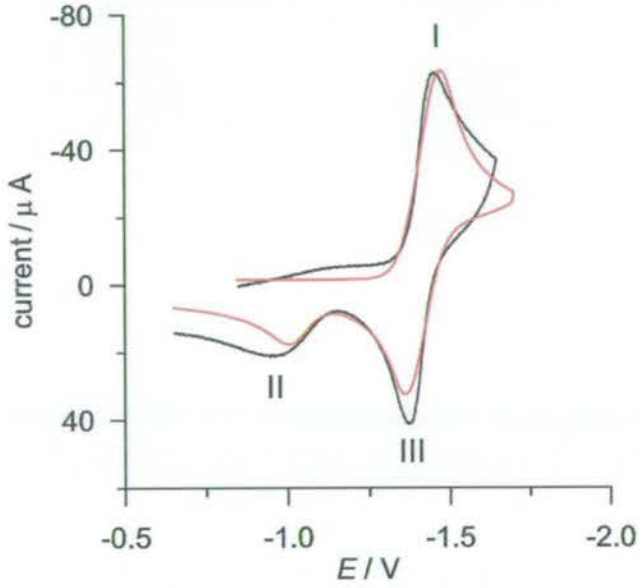

Figure 5.8 Cyclic voltammograms at 213 K of **1** showing both experimental (black line) and simulated (red line) results. Experiments carried out on 1 mmol L^{-1} solutions of substrate in anhydrous THF with TBHF (5×10^{-2} mol L^{-1}) as electrolyte and ferrocene as internal standard. Scan rate: 2 V s^{-1}. Working electrode: Pt.

The electrochemical results are consistent with the photochemically-induced shuttling experiments carried out in alkylnitrile solutions.[8g] Unfortunately, when carrying out the electrochemistry experiments in acetonitrile, adsorption phenomena at the electrodes prevented any analysis of the curves and therefore any direct comparison of the two stimuli in the same solvent. The electrochemical measurements were instead carried out on THF solutions and also repeated in DMF. Figure 5.9 compares the forward shuttling rates calculated from a range of experiments in different solvents using the two stimuli. An approximately linear relationship exists between the rate of shuttling ($k_f^{I^{\bullet-}}$) and polarity of the medium, suggesting that the nature of the solvent is the main variable affecting the shuttling rates in these experiments (the presence of the supporting electrolytes in the electrochemistry experiments might also play a role,

but see ref. [26]). Pleasingly, the shuttling process in this class of molecular shuttles is independent of the means – light or electrons – used to trigger it.

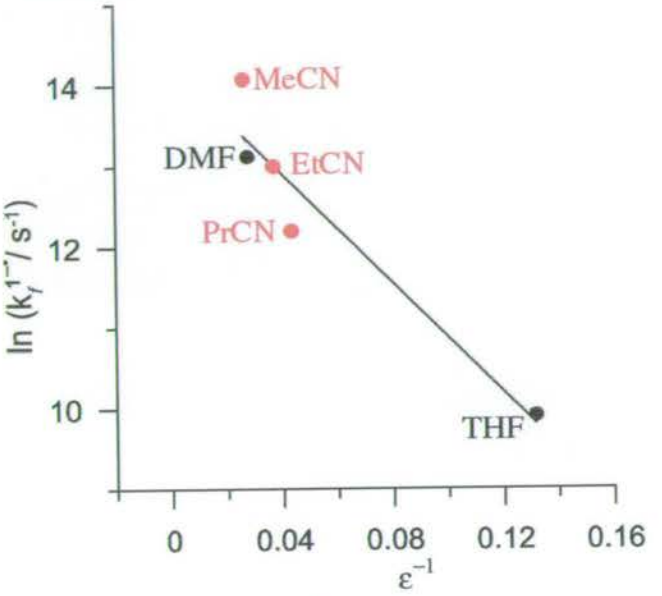

Figure 5.9 Variation of forward shuttling rate ($k_f^{1^{\bullet-}}$) with relative permittivity, ε, of solvent. Data points in black are calculated from experiments using an electrochemical stimulus; data points in red are calculated from experiments using a photochemical stimulus.[8g] All experiments were carried out at 298 K.

5.6 Is the redox-induced motion really shuttling?

It might be argued that hydrogen-bonding interactions between the *ni* station and either the *succ* station or the macrocycle in $\mathbf{1}^{\bullet-}$ could arise from folded conformations (e.g. *folded-succ*^{I}-$\mathbf{1}^{\bullet-}$ and *folded-succ*^{II}-$\mathbf{1}^{\bullet-}$, Figure 5.10), accounting for the experimental observations without requiring an actual change in the position of the macrocycle on the thread in the reduced rotaxane. In order to demonstrate unequivocally that the reduction of **1** does, in fact, result in shuttling of the macrocycle between the *succ* and *ni* stations, the electrochemical behaviour of model rotaxanes **5**–**8** (Chart 5.2) was investigated.

'Gate-closed' shuttle **7** incorporates a bulky silyl ether between the two stations which is large enough to preclude any shuttling, yet should not prevent the formation of a variety of folded conformations; removal of this group to give **8** restores the possibility of redox-switched shuttling, thus generating a system closely analogous to **1**.

Compared to **1**, rotaxane **6** has a reduced length of alkyl spacer (C_2 in place of C_{12}) thus disallowing folded conformations involving multipoint interactions between the naphthalimide carbonyls and macrocycle amide protons.

In model compound **5**, methylation of the succinamide nitrogens prevents a folded conformation involving hydrogen bonding to these units (i.e. the *succ* unit in **5** can only act as a hydrogen-bond acceptor).

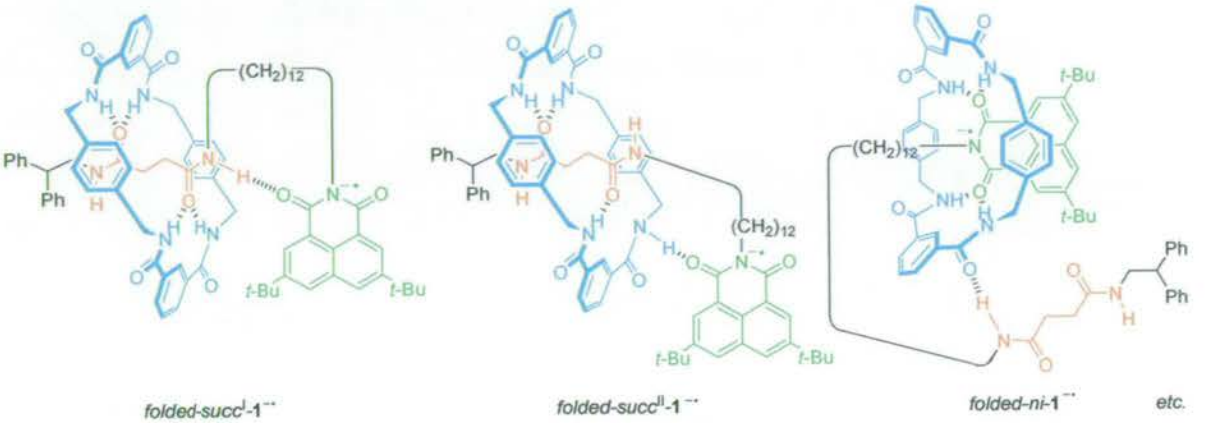

Figure 5.10 Possible folded co-conformations for reduced rotaxane $\mathbf{1}^{\bullet-}$.

^{1}H NMR spectra of each of **5**–**8** in $CDCl_3$ show that the macrocycle sits over the *succ* station in each case, exactly as observed for **1**. The behaviour of these model systems, together with other control experiments and observations, leads to a series of arguments showing that the observed CV effects in **1** are a result of the macrocycle shuttling along the thread.

(i) 'Gate-closed' rotaxane **7** (where shuttling is prohibited) shows a CV response (Figure 5.11a) identical to that of the thread **2** *not* rotaxane **1**, indicating that there is no hydrogen-bond stabilization of the naphthalimide radical anion as a result of folding in $\mathbf{7}^{\bullet-}$. However, the 'gate-opened' version **8** shows virtually identical CV behaviour (Figure 5.11b) to rotaxane **1**, the only difference being that the dynamics are over a slightly longer timescale presumably as a result of the branching in the thread providing a small steric barrier to macrocycle translation.

(ii) Model rotaxane **6**, which is too short and rigid to allow multiple hydrogen bonds between the macrocycle and the *ni* station, also shows very similar CV behaviour to **1** (see Figure 5.14, Section 5.10.2), although over a much shorter timescale, reflecting the smaller amplitude of shuttling that is required.

(iii) Removing the possibility of hydrogen bonding to the amide protons of the *succ* station in **5** does not affect the CV response, suggesting that *all* the hydrogen bonds to the $ni^{-\bullet}$ station come from the macrocycle.

(iv) Molecular modelling studies show that folded conformations of $\mathbf{1}^{-\bullet}$ can only be stabilized by one or two hydrogen bonds from the macrocycle to the *ni* station due to geometrical constraints. Molecular dynamics simulations on such structures indicate that the macrocycle would still shuttle along the thread in order to form multipoint hydrogen bonds to the naphthalimide unit.[30]

(v) The large anodic shift for re-oxidation of the naphthalimide in $\mathbf{1}^{-\bullet}$ indicates extensive stabilization of the radical anion (ΔE° = 0.51 V; corresponding to ΔG = –11.8 kcal mol^{-1}). This is equivalent to the formation of three or four strong hydrogen bonds which modelling shows can only arise in geometries where shuttling has occurred.[31]

(vi) If only one or two intramolecular hydrogen bonds were producing the shifts seen in the CV of **1**, a similar process could take place in the thread (**2**) using the succinamide amide protons as hydrogen-bond donors. This is clearly not the case as **2** exhibits an identical CV response to that of its *N*-methylated analogue (**9**).

(vii) For rotaxanes **1**, **5** and **8** (dynamics in **6** are too fast to measure) more polar solvents accelerate the speed of the process, suggesting that breaking of hydrogen bonds is the rate determining step, not formation of hydrogen bonds which one might expect in a folding mechanism.

(viii) It is known that alkyl chains fold several orders of magnitude faster than the dynamics observed in the current system.[32]

(ix) Folding a long alkyl chain is entropically unfavourable and cyclic, hydrogen-bonded conformations forming large rings of the type produced in the possible folded conformations of $\mathbf{1}^{-\bullet}$ are not often free energy minima.[33] In comparison, the entropy of activation calculated for shuttling in $\mathbf{1}^{-\bullet}$ ($\Delta S^{\ddagger}$ = 8.7 ± 2 cal K^{-1} mol^{-1}) is positive; the calculated enthalpy of activation ($\Delta H^{\ddagger}$ = 14.0 ± 0.6 kcal mol^{-1}) is also more consistent with a shuttling mechanism, where the rate determining step is breaking of hydrogen bonds as opposed to forming bonds in a folding mechanism.

(x) The energy barrier determined for shuttling in the reduced state ($\Delta G^{\ddagger}_{298}$ = 11.4 ± 0.6 kcal mol^{-1}) is consistent with known energy barriers for shuttling between two degenerate stations in similar molecular shuttles,[7a] and also with the energy barrier for pirouetting of the macrocycle in model rotaxane **3** (see Section 5.4, above).

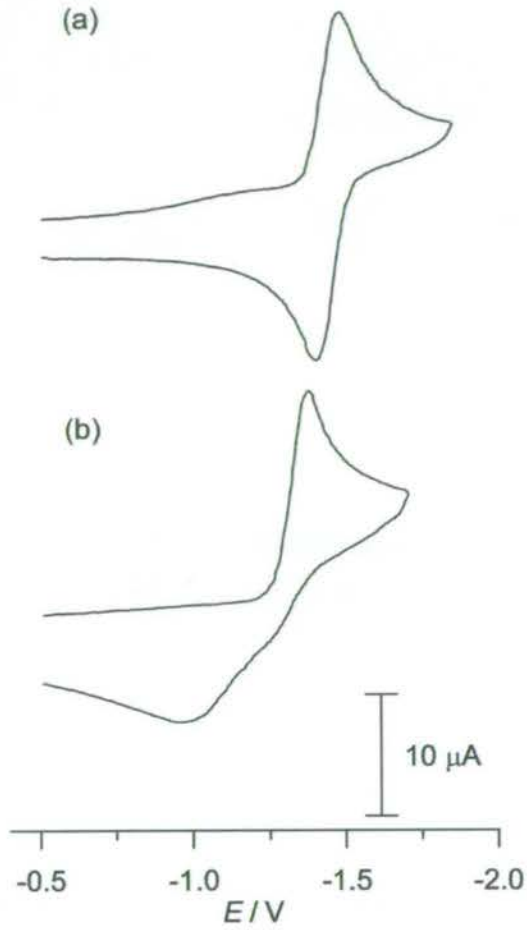

Figure 5.11 Cyclic voltammograms at 223 K of (a) **7** and (b) **8**. Experiments carried out on 0.5 mmol L^{-1} solutions in DMF with tetraethylammonium tetrafluoroborate (5 × 10^{-2} mol L^{-1}) as electrolyte. Scan rate: 0.5 V s^{-1}. Working electrode: Pt.

Given that folding cannot account for the multipoint hydrogen bonding that stabilizes the reduced naphthalimide in **1**$^{-\bullet}$, nor can it account for the behaviour of **8** mirroring that of **1** while that of **7** does not, the only process that satisfies the experimental behaviour for these molecules is shuttling. We do not exclude the likelihood that folding occurs in some of these systems to some degree (e.g. *folded-ni*-**1**$^{-\bullet}$, Figure 5.10). Indeed there is evidence to support this in a few of the low energy co-conformations identified in modelling studies (see above and ref. [30]). However, in

all these low energy co-conformations – folded or extended – the macrocycle has shuttled from the *succ* station to the $ni^{-\bullet}$ unit.

5.7 Variation of the redox-active station

Having verified and characterized the redox-induced shuttling mechanism in **1**, it was decided to explore the effects of structural variation at the imide unit on the dynamic process. Developing a range of related redox-switchable stations should both reveal aspects of the shuttling mechanism through trends across the series, while also providing a larger 'toolbox' of characterized units from which future device design can select. Rotaxanes **13–19** were therefore designed and prepared (Schemes 5.3 and 5.4). Each of these molecules contains a succinamide station separated from an imide-based redox-active moiety by a C_{12} alkyl chain. Shuttle **13** incorporates a 1,4,5,8-naphthalene diimide station in place of the 1,8-naphthalimide unit of **1**. The diimide station is able to undergo two reversible one-electron reduction processes, allowing comparison of the radical anion and dianion states, while the first reduction potential is expected to be significantly less negative than that of the naphthalimide.[13] The pyromellitic diimide moiety in **14** and **15** is a less extensive conjugated system, and so will not be as easily reduced as the naphthalene diimide, yet it too can accept two electrons.[13] Its smaller steric size should also allow the macrocycle free passage over the electroactive station, even at room temperature, a feature which may be of interest for the design of more complex molecular machines. The 3,3′,4,4′-benzophenone diimide in rotaxanes **16** and **17** is a three-electron acceptor – the keto-carbonyl providing the third site for reduction.[13] This central carbonyl, which is part of the delocalised system, may also present a different binding mode for the macrocycle. The 3,4,9,10-perylene diimide in **18** and **19** can also accept three electrons and should be the most easily reduced of all the redox centres here.[13]

These imide units have been shown to exhibit electrochromic behaviour, with each radical anion absorbing at longer wavelengths than the corresponding ground state or dianion. A linear relation exists between $E°_{1/2}$ for the first reduction and λ_{max} of the longest absorbance band of the radical anion, with bands well into the near IR region observed.[13] Photochemical excitation of the radical anions produces highly reducing excited states,[34] while electrogenerated chemiluminescence has also been observed

for the perylene radical anions, when generated in the presence of the corresponding radical cations.[35] The perylene ground state, however, also absorbs strongly in the visible region, leading to the brilliant purple colour of these materials, which has long made them of interest as vat dyes and pigments.[36] The naphthalene- and benzophenone-based derivatives show particularly efficient intersystem crossing to afford the triplet excited states which can be exploited to induce photoreduction of these systems;[8g, 37] the perylene chromophore on the other hand exhibits strong fluorescence in solution.[36] We therefore anticipate a range of interesting photophysical phenomena in these systems which may be used to initiate, probe or modify the shuttling process.

The symmetrical design of threads **21**–**23** – whereby each redox-active station is flanked by a succinamide unit on either side – brings synthetic advantages to the synthesis of the threads, but also allows preparation of both [2]- and [3]rotaxanes, and shuttling of two rings simultaneously onto the same unit can be investigated. Finally, pyridyl-containing analogues **24**–**26** were also prepared for the study of shuttling at surfaces (see Section 5.8, below).

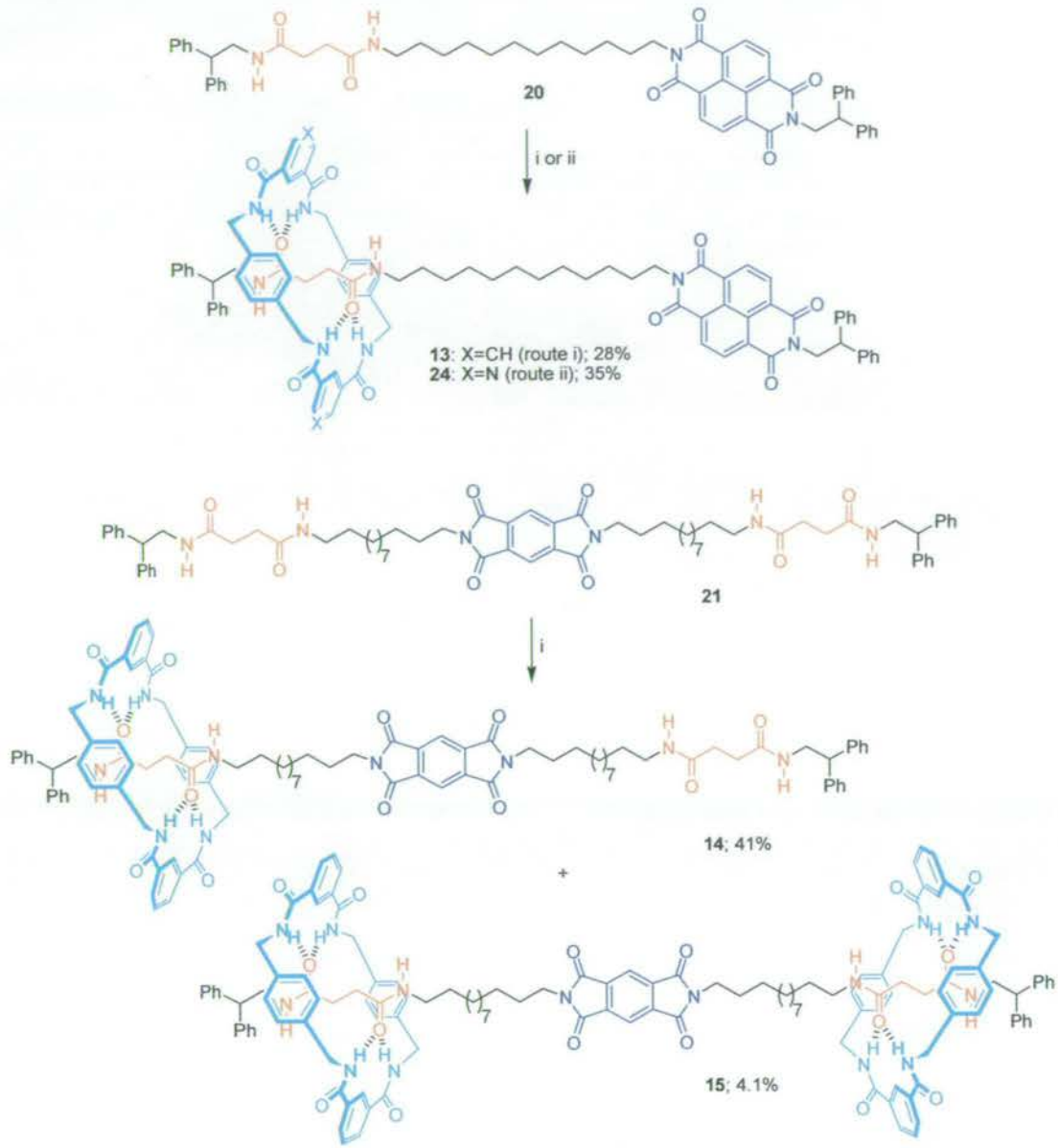

Scheme 5.3 Synthesis of rotaxanes **13**–**15** and **24**. Reagents and conditions: (i) isophthaloyl dichloride, *p*-xylyenediamine, Et_3N, $CHCl_3$, rt, 4 h; (ii) pyridine-3,5-dicarbonyl dichloride, *p*-xylyenediamine, Et_3N, $CHCl_3$, rt, 4 h.

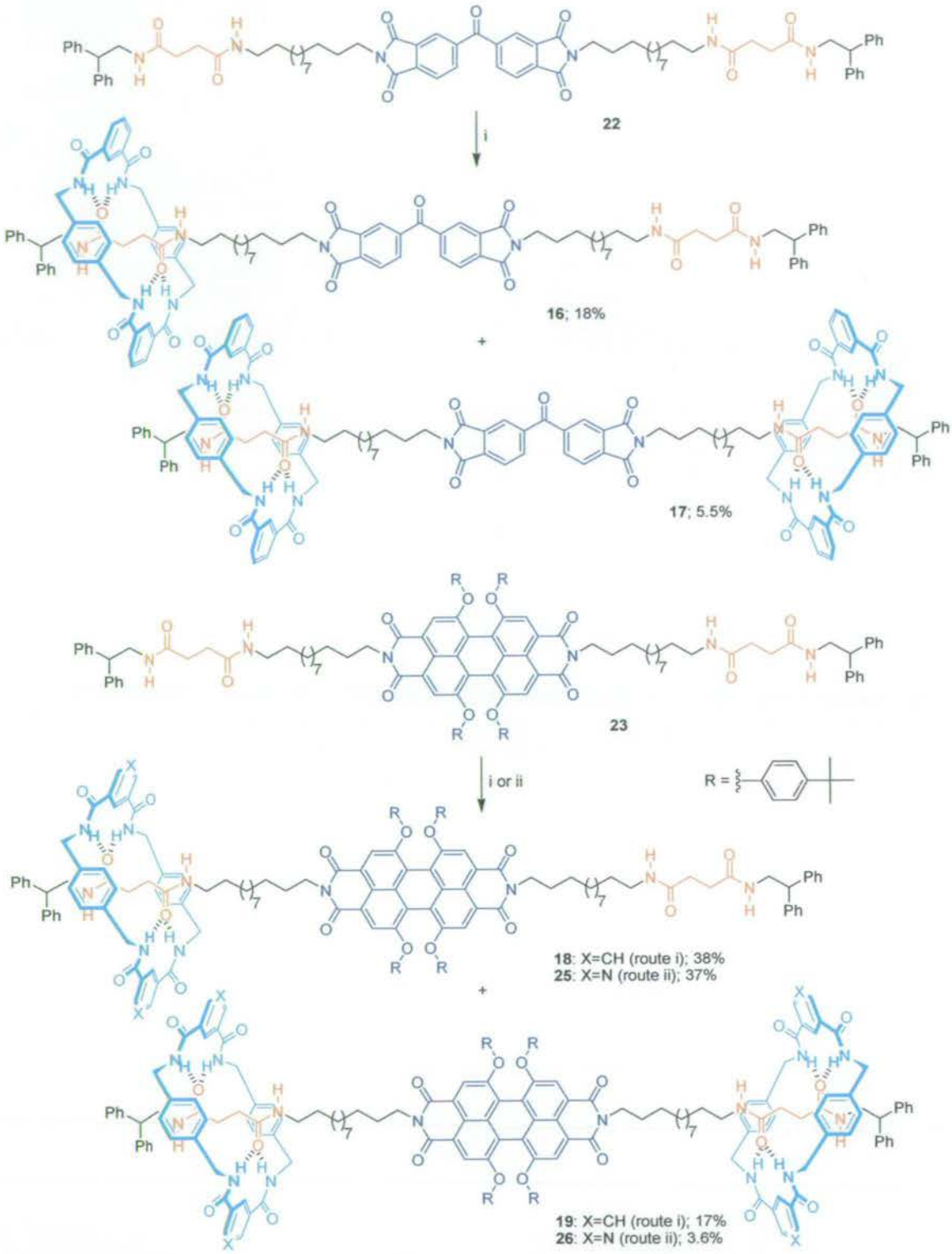

Scheme 5.4 Synthesis of rotaxanes **16**–**19**, **25** and **26**. Reagents and conditions: (i) isophthaloyl dichloride, *p*-xylyenediamine, Et_3N, $CHCl_3$, rt, 4 h; (ii) pyridine-3,5-dicarbonyl dichloride, *p*-xylyenediamine, Et_3N, $CHCl_3$, rt, 4 h.

^{1}H NMR spectroscopy in $CDCl_3$ indicates that for all the rotaxanes shown in Schemes 5.3 and 5.4, the co-conformation with the ring(s) residing over the succinamide station(s) is predominant, as expected ($\Delta\delta_H$ values for protons H_d and H_e in **13–19** compared to the respective threads are all in the range –1.39 to –1.42 ppm). Electrochemical and photophysical studies of these systems are ongoing, and preliminary results indicate that macrocycle shuttling can be induced in each of these second generation systems.

The electrochemically-induced processes occurring in **13** are summarised in Figure 5.12. Compared to **1**, the more extensive conjugated system in **13** is more easily reduced to give **13**$^{-\bullet}$. Again, the extra electron density is primarily located on the carbonyl oxygen atoms, but as there are four such groups in **13**, a smaller change in the hydrogen-bond basicity of the imide station is observed and the *succ*-**13**$^{-\bullet}$:*ni*-**13**$^{-\bullet}$ co-conformational ratio is ~50:50. On going to more negative potentials, however, the dianionic form can be accessed and in this state the co-conformational equilibrium now lies strongly in favour of *ni*-**13**$^{2-}$. As such, **13** represents one of the first examples of a molecular shuttle in which the affinity of one station for the macrocycle may be varied between more than two states by an external stimulus.[38]

The increased stability of the *ni*-co-conformation on increasing charge is reflected in the decreasing backward shuttling rates (k_b). However, it can be seen that on going from **13**$^{-\bullet}$ to **13**$^{2-}$, the forward shuttling rate (k_f) also increases by over two orders of magnitude. This may indicate that folded intermediates, which can form faster than macrocycle translocation,[32] play a role in the shuttling mechanism, particularly for the highly electron rich dianionic form. Shuttling in **13** has also been observed by transient absorption spectroscopy on photochemical generation of the radical anion.

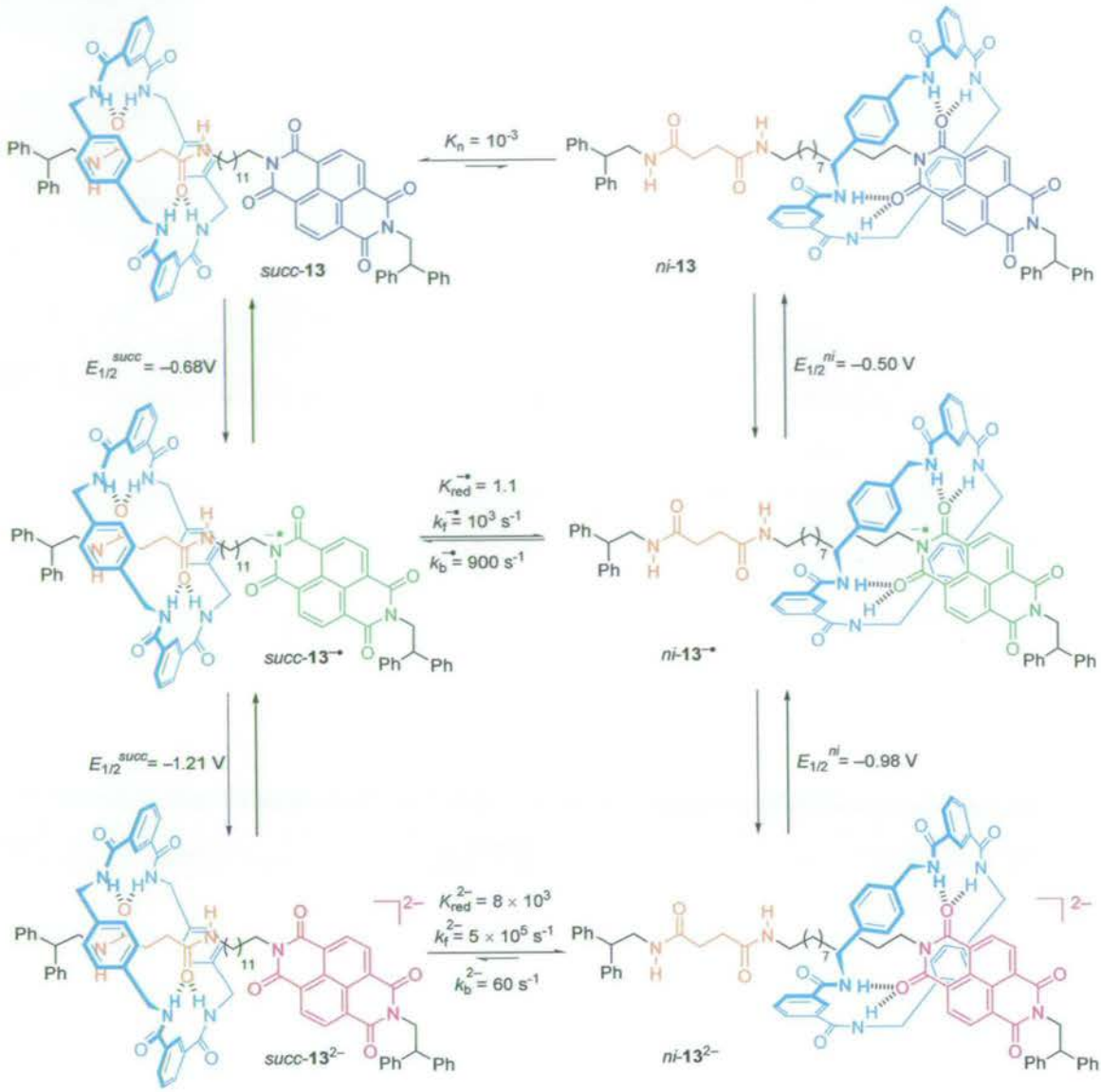

Figure 5.12 Square scheme describing the redox-switched shuttling in [2]rotaxane **13**. Data are calculated from fitting of simulated cyclic voltammetry curves to experimental data obtained on 0.5 mmol L^{-1} solutions of substrate in anhydrous THF, with TBHF (5×10^{-2} mol L^{-1}) as electrolyte and ferrocene as internal standard. Scan rate: 1 V s^{-1}, $T = 298$ K.

Electrochemically triggered shuttling in **14**, **16** and **18** has also been successfully observed, although these dynamic processes have yet to be fully characterized, while the [3]rotaxanes **15**, **17** and **19** await study, along with photophysical investigations of all these systems.

5.8 Towards observation of redox-switched shuttling at surfaces

Transposing working molecular machines from solution-phase environments onto surfaces and into the solid state will clearly be a key step in the development of many potential applications.[39] Molecular shuttles have been used to construct solid-state or

surface-based devices which exhibit switchable conductance,[2, 40] optical properties,[41] wettability,[42] porosity[43] and shape[44]. Although stimuli-induced shuttling is strongly implicated in the operation of each of these remarkable systems, reliable methods for anchoring shuttles in a way which preserves their dynamic properties and, moreover, strategies for *directly* observing their stimuli-induced motions in such environments are goals which have proven particularly challenging over nearly a decade of study.[45]

The vast majority of studies to date have involved attachment of the thread component in rotaxanes to surfaces, or its incorporation in a polymeric matrix.[46] Attachment of the macrocycle to a surface, however, should offer an alternative approach to creating functional shuttle-based devices. Rotaxane **12**, in which the macrocycle contains two pyridine-3,5-dicarboxamide moieties, has been successfully attached to a self-assembled monolayer (SAM) of 11-mercaptoundecanoic acid (11-MUA) and the surface characterized by X-ray photoelectron spectroscopy, electrochemical impedance spectroscopy and fluorescence spectroscopy.[47] In line with an earlier investigation on the attachment of a related pyridine-containing macrocycle to a SAM of 11-MUA,[48] it was determined that hydrogen bonds between the pyridines and alkanethiol carboxylates anchor the molecules with the macrocycle plane perpendicular to the SAM surface. In the case of the rotaxane, the thread is correspondingly oriented parallel to the surface and secondary hydrogen-bonding interactions occur between the imide carbonyls and 11-MUA carboxylates.[47] Overall surface coverage is very good, but the size and orientation of the molecules means that this corresponds to functionalization of ~3% of the 11-MUA molecules. Furthermore, the photophysical studies indicated that naphthalimide fluorescence is not completely quenched by the gold surface, suggesting that fluorescence spectroscopy may be useful for detecting stimuli-induced shuttling motions in this environment.

A different molecular shuttle (which operates on the basis of a photoisomerization) has since been grafted onto a SAM of 11-MUA in a similar fashion, creating surfaces exhibiting switchable wettability and across which a liquid droplet may be transported on application of the shuttling stimulus.[42] Direct observation of the shuttling motion, however, is yet to be achieved. Rotaxane **12** exhibits similar solution electrochemistry to the parent shuttle **1,** but the relatively large negative potential required to reduce the

naphthalimide station is incompatible with gold–thiolate SAMs, which are unstable at potentials below ca. –1.0 V.[49] The less negative reduction potential of the perylene diimide redox centre should be more suitable and so the pyridine-functionalized [2]rotaxane, **25**, was grafted onto surfaces in the manner described above. Double potential step chronoamperometry, which measures the rates of electron transfer processes, has revealed that oxidation of the radical anion has an additional, faster electron-transfer component, compared to the one-electron reduction process. This would be consistent with a model in which some of the reduced molecules have the macrocycle shuttled onto the imide station, thus providing a more direct through-bond route for electron transfer to the surface. However, although shuttling can be observed for **25** in solution (using fast scan rates and low temperatures), cyclic voltammetry at ambient temperature unexpectedly shows an irreversible chemical reaction of the radical anion form, which is unique to the rotaxane. It is therefore impossible to unequivocally assign the observations made on the surface as due to shuttling.

Attention has therefore now shifted to the naphthalene diimide redox centre, which exhibits reduction potentials very similar to the perylene diimde. The solution-phase electrochemistry of pyridine-containing rotaxane **24** is fully reversible and preparation and characterization of this shuttle on surfaces is currently under investigation.

5.9 Conclusions

The use of electrochemical stimuli to manipulate intercomponent interactions provides a powerful method for both controlling and observing submolecular motion in hydrogen-bonded molecular shuttles. In the present benzylic amide macrocycle-based rotaxane system, the motion resulting from reduction and re-oxidation of the naphthalimide station in **1** has been unequivocally shown to be reversible shuttling of the macrocycle along the thread. This constitutes a molecular shuttle which exhibits remarkable positional integrity of the macrocycle on the thread in both oxidation states and rapid dynamics of the triggered shuttling between them.

The simplicity of the structures involved and the process used to control and detect the intercomponent motion has readily allowed extension of this series to include a number of different imide-based electroactive stations. The results to date indicate that in all cases the redox-induced dynamics observed in **1** are conserved across the

series, while the parameters characterizing the shuttling process – redox potentials, rates, co-conformational equilibrium constants – can be tuned through these structural variations. Fully understanding the relationships between chemical structure and the shuttling characteristics should lead to an increasingly detailed understanding of the mechanisms by which translational motion in rotaxanes occurs.

Despite the successful operation of some remarkable devices in recent years, the investigation of large amplitude relative motions of interlocked molecular components in the solid state and at surfaces is currently an embryonic field. Surfaces created by physisorption of molecular shuttles onto an acid-terminated self-assembled monolayer on gold have been characterized and it is expected that by using a combination of electrochemical techniques and photophysical measurements it will be possible to observe stimuli-induced shuttling in such an environment and to characterize this process quantitatively.

5.10 Experimental section

5.10.1 Synthesis

[2]-(1,7,14,20-Tetraaza-2,6,15,19-tetraoxo-9,12,22,25-dibenzo-3,5,16,18-di[5-pyridyl]cyclohexacosane)-[*N*-(12-{[4-(2,2-diphenylethylamino)-4-oxobutanoyl]amino}dodecyl)-1,8-naphthalimide]-rotaxane (12)

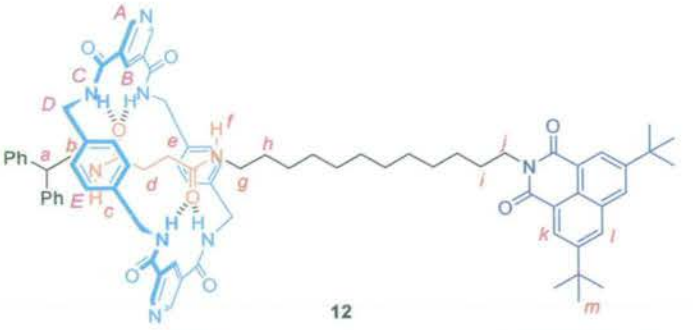

12

Solutions of freshly prepared pyridine-3,5-dicarbonyl dichloride (715 mg, 3.50 mmol) in chloroform (20 mL) and *p*-xylylenediamine (476 mg, 3.50 mmol) with triethylamine (983 μL, 7.01 mmol) in chloroform (20 mL) were simultaneously added using motor-driven syringe pumps over 4 h to a solution of thread **2** (338 mg, 0.438 mmol) in chloroform (50 mL). Following addition, the mixture was allowed to stir for a further 16 h before removal of the colourless precipitate by filtration. Solvent was removed from the resulting filtrate under reduced pressure to give a colourless solid. This material was purified by flash chromatography (SiO_2;

methanol/chloroform, 2:98 to 4:96) to provide [2]rotaxane **12** as a colourless solid (261 mg, 46%); mp > 200 °C (decomp.); ^{1}H NMR (400 MHz, $CDCl_3$): δ = 9.11 (br s, 4H, H_A), 8.68 (br s, 2H, H_B), 8.62 (d, J = 1.8 Hz, 2H, H_k), 8.25 (br t, 1H, H_c), 8.11 (d, J = 1.8 Hz, 2H, H_l), 8.07 (br t, 1H, H_f), 7.61 (br t, 4H, H_C), 7.32 (s, 8H, H_E), 7.28-7.14 (m, 10H, H_{Ph}), 4.57 (br s, 8H, H_D), 4.16-4.11 (m, 3H, H_a & H_j), 3.83 (br dd, 2H, H_b), 3.12 (br s, 2H, H_g), 1.69 (quint., J = 7.5 Hz, 2H, H_i), 1.46 (s, 20H, H_m & H_h), 1.41-1.22 (m, 16H, alkyl CH_2), 1.04 (s, 4H, H_d & H_e); ^{13}C NMR (100 MHz, $CDCl_3$): δ = 173.6 (succinamide C=O), 173.2 (succinamide C=O), 164.6 (imide C=O), 163.5 (macrocycle C=O), 151.1 ($ArCH_A$), 150.2 (naphthalene $ArC_qC(CH_3)_3$), 141.5 (phenyl ArC_q), 137.4 (xylyl ArC_q), 131.8 (naphthalene ArC_q), 131.8 ($ArCH_B$), 129.7 ($ArCH_E$), 129.2 (naphthalene ArCH), 129.1 (naphthalene ArCH), 128.8 (phenyl ArCH), 128.6 (pyridyl ArC_q), 127.7 (phenyl ArCH), 127.2 (phenyl ArCH), 124.8 (naphthalene ArC_q), 122.1 (naphthalene ArC_q), 50.6 (CH_a), 44.4 ($CH_{2(b)}$), 44.1 ($CH_{2(D)}$), 40.4 ($CH_{2(f)}$), 39.8 ($CH_{2(g)}$), 35.3 ($C_q(CH_3)_3$), 31.2 (CH_3), 29.6, 29.54, 29.50, 29.4, 29.32, 28.28, 28.2, 27.13, 27.06 (12 × CH_2); HRMS (FAB, 3-NOBA matrix): m/z = 1306.7044 [$(M+H)^+$] (anal. calcd for $C_{80}H_{92}N_9O_8^+$: m/z = 1306.7069).

[2]-(1,7,14,20-Tetraaza-2,6,15,19-tetraoxo-3,5,9,12,16,18,22,25-tetrabenzocyclohexacosane)-[*N*-(2,2-dipehnylethyl)-*N'*-(12-{[4-(2,2-diphenylethylamino)-4-oxobutanoyl]amino}dodecyl)-naphthalene-1,4,5,8-tetracarboxylic diimide]-rotaxane (13)

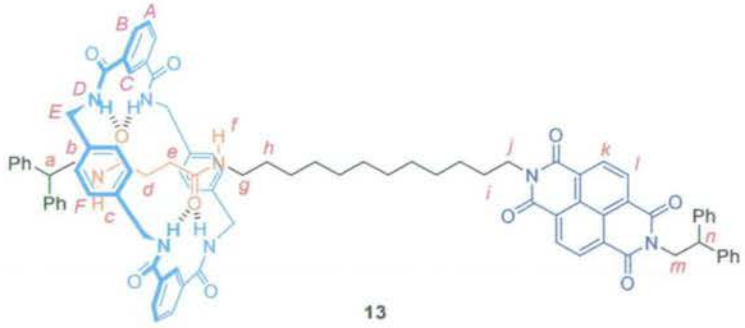

13

Solutions of isophthaloyl dichloride (354 mg, 1.74 mmol) in chloroform (10 mL) and *p*-xylylenediamine (237 mg, 1.74 mmol) with triethylamine (489 µL, 3.49 mmol) in chloroform (10 mL) were simultaneously added using motor-driven syringe pumps over 4 h to a solution of thread **20** (198 mg, 0.218 mmol) in chloroform (20 mL). Following addition, the mixture was allowed to stir for a further 2 h before removal of the off-white precipitate by filtration. The resulting filtrate was diluted with chloroform (40 mL) and washed with hydrochloric acid (1N, 3 × 80 mL), sodium

hydrogen carbonate (sat. aq., 3 × 100 mL) and brine (sat., 100 mL). The organics were then dried ($MgSO_4$) and evaporated to give a pale brown residue. This material was purified by flash chromatography (SiO_2; methanol/chloroform, 1:99), then the product-containing material was washed repeatedly in hot toluene to remove all traces of the thread starting material, affording the [2]rotaxane **13** as a pale yellow solid (88.0 mg, 28%); mp > 100 °C (decomp.); ^{1}H NMR (400 MHz, $CDCl_3$): δ = 8.68 (d, *J* = 7.6 Hz, 2H, H_k or H_l), 8.63 (d, *J* = 7.6 Hz, 2H, H_k or H_l), 8.33 (s, 2H, H_C), 8.13 (dd, *J* = 7.8 Hz and *J* = 1.3 Hz, 4H, H_B), 7.60-7.54 (m, 6H, H_A & H_D), 7.35-7.13 (m, 20H, H_{Ph}), 7.03 (s, 8H, H_F), 6.24 (t, *J* = 4.6 Hz, 1H, H_c), 6.19 (t, *J* = 5.3 Hz, 1H, H_f), 4.88 (d, *J* = 8.0 Hz, 2H, H_m), 4.78 (t, *J* = 7.8 Hz, 1H, H_n), 4.48 (d, *J* = 5.1 Hz, 8H, H_E), 4.14 (t, *J* = 7.6 Hz, 2H, H_j), 4.07 (t, *J* = 7.8 Hz, 1H, H_a), 3.70 (dd, *J* = 7.6 Hz and *J* = 5.8 Hz, 2H, H_b), 3.02 (q, *J* = 6.7 Hz, 2H, H_g), 1.68 (br s, 2H, H_i), 1.41-1.36 (m, 2H, H_h), 1.34-1.22 (m, 16H, alkyl CH_2), 0.98 (s, 4H, H_d & H_e); ^{13}C NMR (100 MHz, $CDCl_3$): δ = 173.0 (succinamide C=O), 172.8 (succinamide C=O), 166.4 (macrocycle C=O), 162.8 (2 × imide C=O), 141.4 (phenyl ArC_q), 141.2 (phenyl ArC_q), 137.7 (xylyl ArC_q), 133.8 (isophthaloyl ArC_q), 131.5 ($ArCH_B$), 130.9 (naphthalene ArCH), 130.8 (naphthalene ArCH), 129.14 ($ArCH_A$), 129.10 ($ArCH_F$), 128.9 (phenyl ArCH), 128.41 (phenyl ArCH), 128.37 (phenyl ArCH), 127.8 (phenyl ArCH), 127.2 (phenyl ArCH), 126.8 (phenyl ArCH), 126.57 (naphthalene ArC_q), 126.56 (naphthalene ArC_q), 126.5 (naphthalene ArC_q), 126.2 (naphthalene ArC_q), 123.9 ($ArCH_C$), 50.5 (CH_a), 48.6 (CH_n), 44.8 ($CH_{2(m)}$), 44.2 ($CH_{2(b)}$), 43.9 ($CH_{2(E)}$), 40.9 ($CH_{2(j)}$), 39.8 ($CH_{2(g)}$), 29.6, 29.54, 29.49, 29.43, 29.40, 29.3, 29.2, 28.0, 27.0, 26.9 (12 × CH_2); HRMS (FAB, 3-NOBA matrix): *m/z* = 1441.6759 [$(M+H)^+$] (anal. calcd for $^{12}C_{89}{}^{13}CH_{89}N_8O_{10}^+$: *m/z* = 1442.6735).

[2]-(1,7,14,20-Tetraaza-2,6,15,19-tetraoxo-3,5,9,12,16,18,22,25-tetrabenzocyclohexacosane)-[*N*,*N*′-bis(12-{[4-(2,2-diphenylethylamino)-4-oxobutanoyl]amino}dodecyl)-pyromellitic diimide]-rotaxane (14)

and

[3]-Bis(1,7,14,20-tetraaza-2,6,15,19-tetraoxo-3,5,9,12,16,18,22,25-tetrabenzocyclohexacosane)-[*N*,*N*′-bis(12-{[4-(2,2-diphenylethylamino)-4-oxobutanoyl]amino}dodecyl)-pyromellitic diimide]-rotaxane (15)

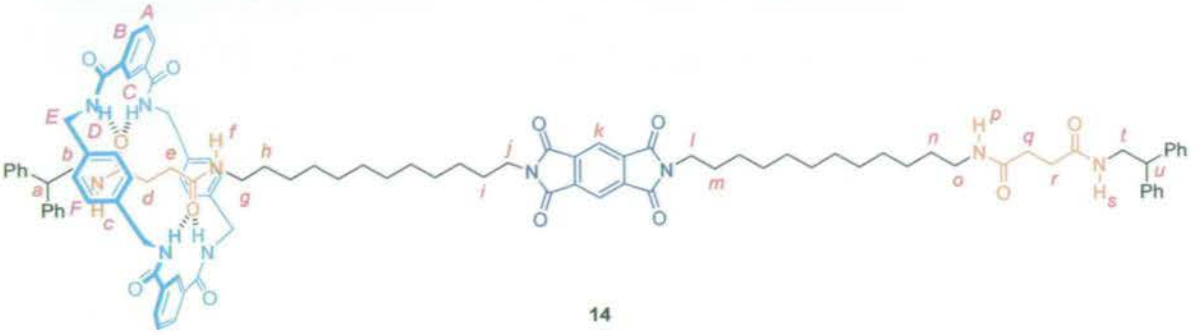

14

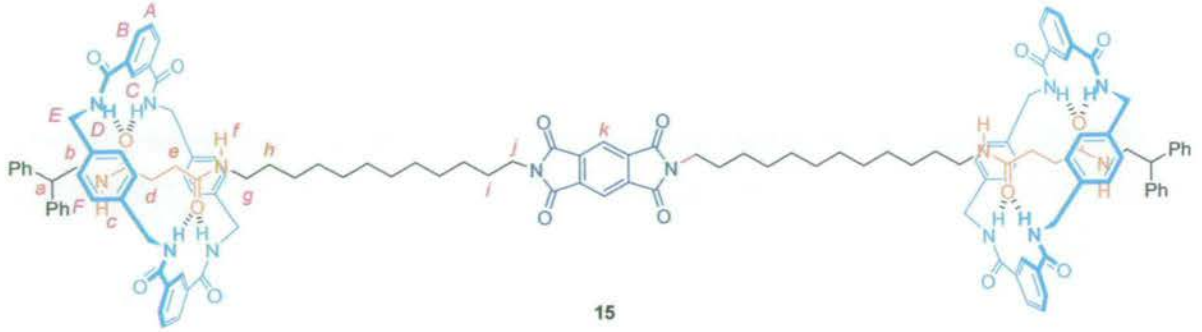

15

Solutions of isophthaloyl dichloride (271 mg, 1.34 mmol) in chloroform (10 mL) and *p*-xylylenediamine (182 mg, 1.34 mmol) with triethylamine (375 μL, 2.67 mmol) in chloroform (10 mL) were simultaneously added using motor-driven syringe pumps over 4 h to a solution of thread **21** (190 mg, 0.167 mmol) in chloroform (25 mL). Following addition, the mixture was allowed to stir for a further 16 h before removal of the off-white precipitate by filtration. The resulting filtrate was concentrated under reduced pressure and the crude product purified by repeated flash chromatography (SiO_2; 2:45:50 methanol/ethyl acetate/dichloromethane) to afford, in order of elution: [3]rotaxane **15** as a colourless solid (15.0 mg, 4.1%); mp > 140 °C (decomp.); ^{1}H NMR (400 MHz, $CDCl_3$): δ = 8.25 (s, 4H, H_C), 8.11 (s, 2H, H_k), 8.08 (d, J = 7.6 Hz, 8H, H_B), 7.63 (br s, 8H, H_D), 7.54 (t, J = 7.6 Hz, 4H, H_A), 7.30-7.15 (m, 20H, H_{Ph}), 7.07 (s, 16H, H_F), 6.70 (br t, 2H, H_f), 6.55 (br t, 2H, H_c), 4.51-4.43 (m, 16H, H_E), 4.11 (br t, 2H, H_a), 3.74-3.71 (m, 8H, H_b & H_j), 3.01 (br s, 4H, H_g), 1.68 (br s, 4H, H_i), 1.39 (br s, 4H, H_h), 1.28-1.16 (m, 32H, alkyl CH_2), 1.01-0.99 (m, 8H, H_d & H_e); ^{13}C

NMR (100 MHz, $CDCl_3$): δ = 173.1 (succinamide C=O), 172.9 (succinamide C=O), 166.42 (macrocycle or imide C=O), 166.40 (macrocycle or imide C=O), 141.5 (phenyl ArC_q), 137.5 (xylyl C_q), 137.1 (pyromellitic ArC_q), 133.7 (isophthaloyl ArC_q), 131.5 ($ArCH_B$), 129.2 ($ArCH_F$), 129.0 ($ArCH_A$), 128.9 (phenyl ArCH), 127.8 (phenyl ArCH), 127.1 (phenyl ArCH), 124.0 ($ArCH_C$), 117.8 ($ArCH_k$), 50.5 (CH_a), 44.8 ($CH_{2(b)}$), 44.0 ($CH_{2(E)}$), 39.8 ($CH_{2(g)}$), 38.9 ($CH_{2(j)}$), 29.7 (CH_2), 29.5 (CH_2), 29.4 (CH_2), 29.3 (CH_2), 29.22 (CH_2), 29.19 (CH_2), 29.1 (CH_2), 28.8 (CH_2), 28.1 (CH_2), 27.3 (CH_2), 26.9 (CH_2), 26.4 (CH_2); HRMS (FAB, THIOG matrix): *m/z* = 2207.1038 [$(M+H)^+$] (anal. calcd for $^{12}C_{133}{}^{13}CH_{145}N_{14}O_{16}^+$: *m/z* = 2207.0997);

[2]rotaxane **14** as a colourless solid (114 mg, 41%); mp > 120 °C (decomp.); ^1H NMR (400 MHz, $CDCl_3$): δ = 8.34 (s, 2H, H_C), 8.18 (s, 2H, H_k), 8.13 (d, *J* = 7.7 Hz, 4H, H_B), 7.63 (t, *J* = 5.0 Hz, 4H, H_D), 7.56 (t, *J* = 7.7 Hz, 2H, H_A), 7.31-7.13 (m, 20H, H_{Ph}), 7.03 (s, 8H, H_F), 6.41 (br t, 1H, H_f), 6.32 (br t, 1H, H_c), 6.10 (br s, 2H, H_p & H_s), 4.47 (d, *J* = 5.0 Hz, 8H, H_E), 4.16 (t, *J* = 7.9 Hz, 1H, H_u), 4.07 (t, *J* = 7.8 Hz, 1H, H_a), 3.85 (dd, *J* = 7.7 Hz and *J* = 5.9 Hz, 2H, H_t), 3.74-3.69 (m, 6H, H_b & H_j & H_l), 3.14 (q, *J* = 6.7 Hz, 2H, H_o), 3.00 (q, *J* = 6.5 Hz, 2H, H_g), 2.32 (s, 4H, H_q & H_r), 1.69-1.66 (m, 4H, H_i & H_m), 1.46-1.39 (m, 4H, H_h & H_n), 1.31-1.20 (m, 32H, alkyl CH_2), 0.98 (s, 4H, H_d & H_e); ^{13}C NMR (100 MHz, $CDCl_3$): δ = 173.1 (succinamide C=O), 172.9 (succinamide C=O), 172.4 (succinamide C=O), 172.1 (succinamide C=O), 166.4 (2 × imide C=O), 166.3 (macrocycle C=O), 141.7 (phenyl ArC_q), 141.5 (phenyl ArC_q), 137.7 (xylyl ArC_q), 137.1 (2 × pyromellitic ArC_q), 133.8 (isophthaloyl ArC_q), 131.5 ($ArCH_B$), 129.1 ($ArCH_F$), 129.0 ($ArCH_A$), 128.9 (phenyl ArCH), 128.7 (phenyl ArCH), 128.0 (phenyl ArCH), 127.8 (phenyl ArCH), 127.2 (phenyl ArCH), 126.8 (phenyl ArCH), 123.9 ($ArCH_C$), 117.9 ($ArCH_k$), 50.53 (CH_a), 50.49 (CH_u), 44.2 ($CH_{2(b)}$), 43.90 ($CH_{2(E)}$), 43.85 ($CH_{2(t)}$), 39.8 ($CH_{2(g)}$), 39.7 ($CH_{2(o)}$), 38.71 ($CH_{2(j\ or\ l)}$), 38.65 ($CH_{2(j\ or\ l)}$), 31.7 ($CH_{2(q\ or\ r)}$), 31.6 ($CH_{2(q\ or\ r)}$), 29.7, 29.6, 29.5, 29.44, 29.40, 29.30, 29.26, 29.2, 29.1, 28.9, 28.40, 28.37, 28.3, 26.9, 26.8, 26.6 (22 × CH_2); HRMS (FAB, 3-NOBA matrix): *m/z* = 1674.8875 [$(M+H)^+$] (anal. calcd for $^{12}C_{101}{}^{13}CH_{117}N_{10}O_{12}^+$: *m/z* = 1674.8886).

[2]-(1,7,14,20-Tetraaza-2,6,15,19-tetraoxo-3,5,9,12,16,18,22,25-tetrabenzocyclohexacosane)-[*N*,*N*′-bis(12-{[4-(2,2-diphenylethylamino)-4-oxobutanoyl]amino}dodecyl)-benzophenone-3,3′,4,4′-tetracarboxylic diimide]-rotaxane (16)

and

[3]-Bis(1,7,14,20-tetraaza-2,6,15,19-tetraoxo-3,5,9,12,16,18,22,25-tetrabenzocyclohexacosane)-[*N*,*N*′-bis(12-{[4-(2,2-diphenylethylamino)-4-oxobutanoyl]amino}dodecyl)-benzophenone-3,3′,4,4′-tetracarboxylic diimide]-rotaxane (17)

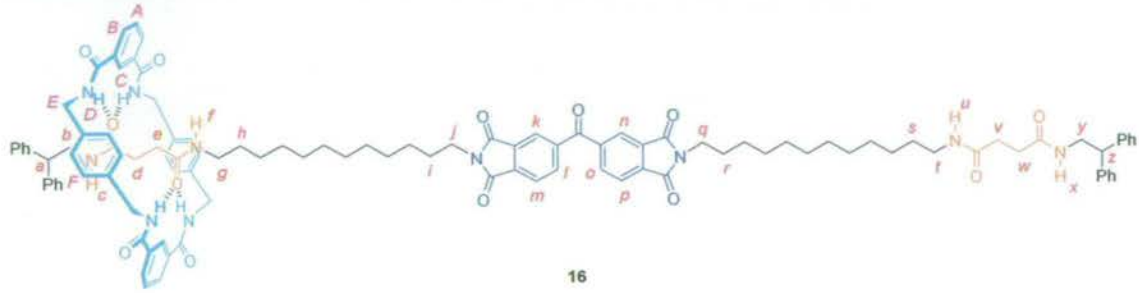

16

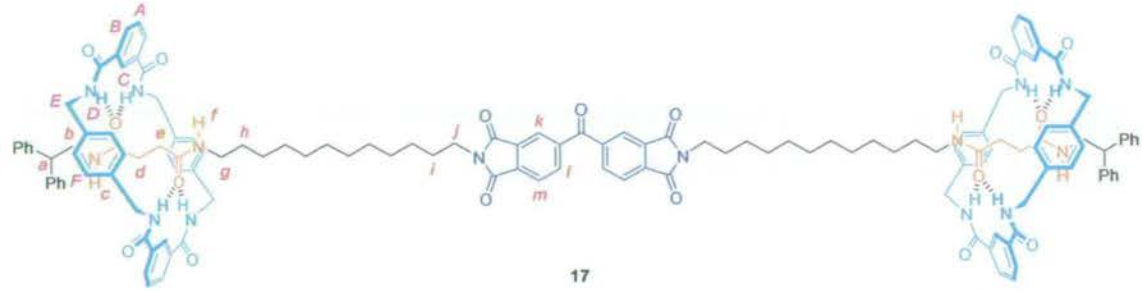

17

Solutions of isophthaloyl dichloride (629 mg, 3.10 mmol) in chloroform (20 mL) and *p*-xylylenediamine (422 mg, 3.10 mmol) with triethylamine (870 μL, 6.20 mmol) in chloroform (20 mL) were simultaneously added using motor-driven syringe pumps over 4 h to a solution of thread **22** (386 mg, 0.310 mmol) in chloroform (35 mL). Following addition, the mixture was allowed to stir for a further 16 h before removal of the off-white precipitate by filtration. The resulting filtrate was concentrated under reduced pressure and the crude product purified by repeated flash chromatography (SiO_2; methanol/ethyl acetate/dichloromethane, 2:38:50 to 2:48:50) to afford, in order of elution fractions of [3]rotaxane and [2]rotaxane which were further purified by recrystallization from a mixture of dichloromethane and toluene, giving:

[3]rotaxane **17** as a colourless solid (39.7 mg, 5.5%); mp 172-175 °C; ^{1}H NMR (400 MHz, $CDCl_3$): δ = 8.25 (s, 4H, H_C), 8.18-8.08 (m, 12H, H_k & H_m & H_B), 7.98 (d, J = 7.6 Hz, 2H, H_l), 7.63 (br t, 8H, H_D), 7.54 (t, J = 7.6 Hz, 4H, H_A), 7.29-7.13 (m, 20H, H_{Ph}), 7.05 (s, 16H, H_F), 6.60 (br s, 4H, H_c & H_f), 4.47 (br s, 16H, H_E), 4.09 (t, J

= 7.6 Hz, 2H, H_a), 3.71-3.68 (m, 8H, H_b & H_j), 3.01 (br q, 4H, H_g), 1.67 (br s, 4H, H_i), 1.40 (br s, 4H, H_h), 1.28-1.13 (m, 32H, alkyl CH_2), 0.99 (s, 8H, H_d & H_e); ^{13}C NMR (100 MHz, $CDCl_3$): δ = 193.2 (benzophenone C=O), 173.1 (succinamide C=O), 172.9 (succinamide C=O), 167.24 (imide C=O), 167.21 (imide C=O), 166.5 (macrocycle C=O), 141.52 (benzophenone ArC_q), 141.45 (phenyl ArC_q), 137.5 (xylyl ArC_q), 135.4 (benzophenone ArC_q), 135.4 (benzophenone ArCH), 133.7 (isophthaloyl ArC_q), 132.4 (benzophenone ArC_q), 131.5 ($ArCH_B$), 129.2 ($ArCH_F$), 129.0 ($ArCH_A$), 128.9 (phenyl ArCH), 127.8 (phenyl ArCH), 127.1 (phenyl ArCH), 124.1 (benzophenone ArCH), 124.0 ($ArCH_C$), 123.7 (benzophenone ArCH), 50.5 (CH_a), 44.0 ($CH_{2(b)}$ & $CH_{2(E)}$), 39.8 ($CH_{2(g)}$), 38.4 ($CH_{2(f)}$), 29.5 (CH_2), 29.43 (CH_2), 29.41 (CH_2), 29.38 (CH_2), 29.34 (CH_2), 29.27 (CH_2), 29.2 (CH_2), 29.02 (CH_2), 28.96 (CH_2), 27.0 (CH_2), 26.9 (CH_2), 26.7 (CH_2); HRMS (FAB, 3-NOBA matrix): *m/z* = 2311.1259 [$(M+H)^+$] (anal. calcd for $^{12}C_{140}{}^{13}CH_{149}N_{14}O_{17}{}^+$: *m/z* = 2311.1259);

[2]rotaxane **16** as a colourless solid (96.2 mg, 18%); mp 114-117 °C; ^1H NMR (400 MHz, $CDCl_3$): δ = 8.41 (s, 2H, H_C), 8.19-8.14 (m, 8H, H_k & H_m & H_n & H_p & H_B), 7.99 (d, *J* = 7.2 Hz, 2H, H_l & H_o), 7.61-7.56 (m, 6H, H_A & H_D), 7.31-7.14 (m, 20H, H_{Ph}), 7.01 (s, 8H, H_F), 6.05-5.94 (m, 4H, H_c & H_f & H_u & H_x), 4.47 (d, *J* = 5.1 Hz, 8H, H_E), 4.15 (t, *J* = 7.8 Hz, 1H, H_z), 4.06 (t, *J* = 7.4 Hz, 1H, H_a), 3.87-3.84 (m, 2H, H_y), 3.71 (br s, 6H, H_b & H_j & H_q), 3.14 (br q, 2H, H_t), 3.01 (br q, 2H, H_g), 2.32 (s, 4H, H_v & H_w), 1.68 (br s, 4H, H_i & H_r), 1.47-1.39 (m, 4H, H_h & H_s),1.31-1.23 (m, 32H, alkyl CH_2), 0.98 (s, 4H, H_d & H_e); ^{13}C NMR (100 MHz, $CDCl_3$): δ = 193.3 (benzophenone C=O), 173.0 (succinamide C=O), 172.9 (succinamide C=O), 172.2 (succinamide C=O), 171.9 (succinamide C=O), 167.2 (4 × imide C=O), 166.4 (macrocycle C=O), 141.8 (phenyl ArC_q), 141.5 (2 × benzophenone ArC_q), 141.4 (phenyl ArC_q), 137.8 (xylyl ArC_q), 135.4 (2 × benzophenone ArC_q), 135.3 (2 × benzophenone ArCH), 133.9 (isophthaloyl ArC_q), 132.5 (2 × benzophenone ArC_q), 131.6 ($ArCH_B$), 129.2 ($ArCH_A$), 129.1 ($ArCH_F$), 128.9 (phenyl ArCH), 128.7 (phenyl ArCH), 128.0 (phenyl ArCH), 127.8 (phenyl ArCH), 127.2 (phenyl ArCH), 126.8 (phenyl ArCH), 124.1 (2 × benzophenone ArCH), 123.9 ($ArCH_C$), 123.7 (2 × benzophenone ArCH), 50.6 (CH_z), 50.4 (CH_a), 44.0 ($CH_{2(b)}$), 43.9 ($CH_{2(E)}$), 43.8 ($CH_{2(y)}$), 39.70 ($CH_{2(g)}$), 39.65 ($CH_{2(t)}$), 38.5 ($CH_{2(f)}$ & $CH_{2(q)}$), 31.8 ($CH_{2(v \text{ or } w)}$), 31.7 ($CH_{2(v \text{ or } w)}$), 29.71, 29.69, 29.64, 29.61, 29.5, 29.4, 29.33, 29.27, 29.25, 29.23, 29.19, 29.11, 29.07, 28.5, 26.92, 26.89, 26.88, 26.79 (22 × CH_2); HRMS (FAB, 3-NOBA

matrix): m/z = 1778.9147 [$(M+H)^+$] (anal. calcd for $^{12}C_{108}{}^{13}CH_{121}N_{10}O_{13}^+$: m/z = 1778.9148).

[2]-(1,7,14,20-Tetraaza-2,6,15,19-tetraoxo-3,5,9,12,16,18,22,25-tetrabenzocyclohexacosane)-[*N*,*N*′-bis(12-{[4-(2,2-diphenylethylamino)-4-oxobutanoyl]amino}dodecyl)-1,6,7,12-tetra(4-*tert*-butylphenoxy)-perylene-3,4,9,10-tetracarboxylic diimide]-rotaxane (18)

and

[3]-Bis-(1,7,14,20-tetraaza-2,6,15,19-tetraoxo-3,5,9,12,16,18,22,25-tetrabenzocyclohexacosane)-[*N*,*N*′-bis(12-{[4-(2,2-diphenylethylamino)-4-oxobutanoyl]amino}dodecyl)-1,6,7,12-tetra(4-*tert*-butylphenoxy)-perylene-3,4,9,10-tetracarboxylic diimide]-rotaxane (19)

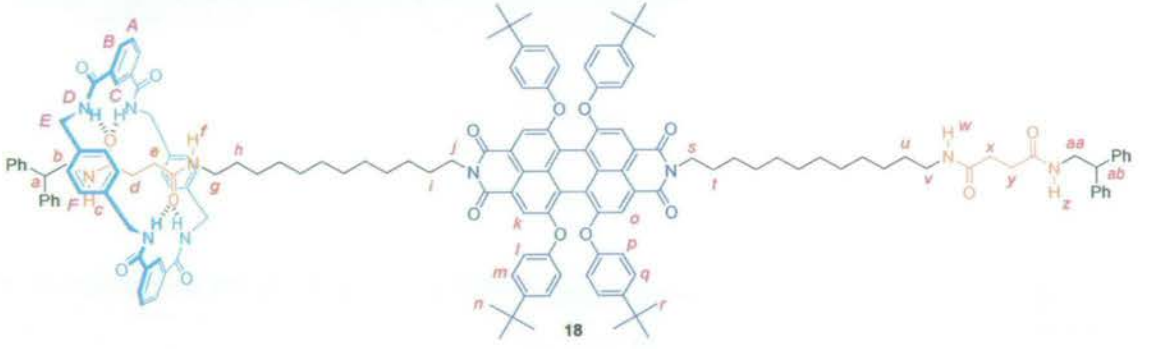

18

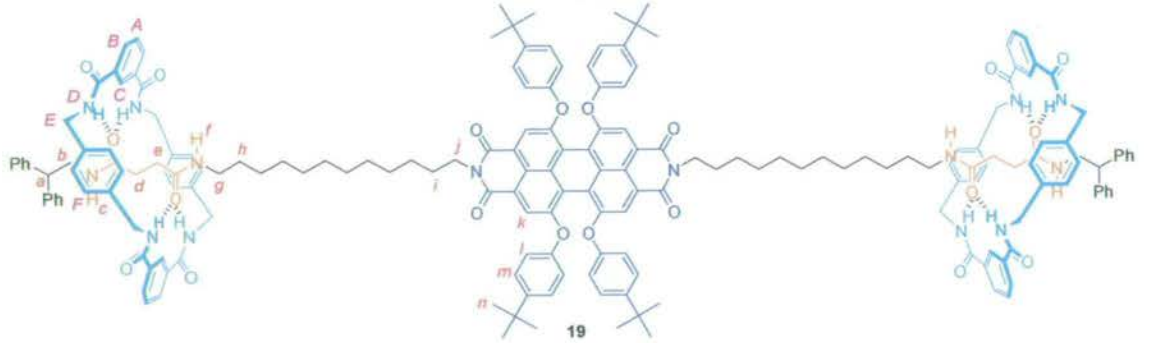

19

Solutions of isophthaloyl dichloride (77.5 mg, 0.382 mmol) in chloroform (5 mL) and *p*-xylylenediamine (52.0 mg, 0.382 mmol) with triethylamine (55.5 µL, 0.763 mmol) in chloroform (10 mL) were simultaneously added using motor-driven syringe pumps over 4 h to a solution of thread **23** (91.0 mg, 0.0477 mmol) in chloroform (10 mL). Following addition, the mixture was allowed to stir for a further 16 h before removal of the pale pink precipitate by filtration. The resulting filtrate was concentrated under reduced pressure and the crude product purified by preparative TLC (SiO_2; methanol/acetone/dichloromethane, 1:14:85) to afford, in order of elution:

[3]rotaxane **19** as a purple solid (17 mg, 12%); mp 158-160 °C; ^{1}H NMR (400 MHz, $CDCl_3$): δ = 8.36 (s, 4H, H_C), 8.21 (s, 4H, H_k), 8.17 (dd, J = 7.8 Hz and J = 1.0 Hz,

8H, H_B), 7.61-7.52 (m, 12H, H_A & H_D), 7.31-7.13 (m, 28H, H_m & H_{Ph}), 7.00 (s, 16H, H_F), 6.81 (d, J = 8.7 Hz, 8H, H_l), 6.02 (t, J = 5.4 Hz, 2H, H_c), 5.92 (t, J = 4.8 Hz, 2H, H_f), 4.47 (d, J = 5.1 Hz, 16H, H_E), 4.08-4.04 (m, 6H, H_a & H_j), 3.69 (dd, J = 7.7 Hz and J = 5.6 Hz, 4H, H_b), 2.99 (q, J = 6.5 Hz, 4H, H_g), 1.60 (br s, 4H, H_i), 1.43-1.37 (m, 4H, H_h), 1.33-1.19 (m, 68H, H_n & alkyl CH_2), 0.96 (s, 8H, H_d & H_e); ^{13}C NMR (100 MHz, $CDCl_3$): δ = 172.9 (succinamide C=O), 172.7 (succinamide C=O), 166.4 (macrocycle C=O), 163.4 (imide C=O), 155.9 (perylene ArC_q), 152.8 (ArC_qO–perylene), 147.2 ($ArC_qC(CH_3)_3$), 141.4 (phenyl ArC_q), 137.8 (xylyl ArC_q), 133.8 (isophthaloyl ArC_q), 132.8 (perylene ArC_q), 131.6 ($ArCH_B$), 129.2 ($ArCH_A$), 129.1 ($ArCH_F$), 128.9 (phenyl ArCH), 127.8 (phenyl ArCH), 127.2 (phenyl ArCH), 126.6 ($ArCH_m$), 123.9 ($ArCH_C$), 122.4 (perylene ArC_q), 120.5 (perylene ArC_q), 119.8 ($ArCH_k$), 119.4 (perylene ArC_q), 119.3 ($ArCH_l$), 50.5 (CH_a), 44.2 ($CH_{2(b)}$), 43.9 ($CH_{2(E)}$), 40.6 ($CH_{2(f)}$), 39.9 ($CH_{2(g)}$), 34.3 ($C_q(CH_3)_3$), 31.4 (CH_3), 29.7 (CH_2), 29.6 (CH_2), 29.52 (CH_2), 29.47 (CH_2), 29.4 (CH_2), 29.32 (CH_2), 29.29 (CH_2), 29.2 (CH_2), 28.1 (CH_2), 27.1 (CH_2), 26.9 (CH_2), 26.5 (CH_2); HRMS (FAB, 3-NOBA matrix): *m/z* = 2441.2897 [$(M+H)^+$] (anal. calcd for $^{12}C_{155}{}^{13}CH_{171}N_{10}O_{16}^+$: *m/z* = 2441.2908);

[2]rotaxane **18** as a purple solid (38 mg, 33%); mp 146-148 °C; ^{1}H NMR (400 MHz, $CDCl_3$): δ = 8.38 (s, 2H, H_C), 8.22 (s, 2H, H_o), 8.21 (s, 2H, H_k), 8.17 (d, J = 7.8 Hz, 4H, H_B), 7.61-7.57 (m, 6H, H_A & H_D), 7.31-7.13 (m, 28H, H_m & H_q & H_{Ph}), 7.00 (s, 8H, H_F), 6.82 (d, J = 8.7 Hz, 8H, H_l & H_p), 6.07-6.01 (m, 2H, H_c & H_f), 5.98 (t, J = 5.7 Hz, 1H, H_z), 5.91 (t, J = 5.4 Hz, 1H, H_w), 4.52-4.43 (m, 8H, H_E), 4.15 (t, J = 8.0 Hz, 1H, H_{ab}), 4.11-4.04 (m, 5H, H_a & H_j & H_s), 3.86 (dd, J = 7.9 Hz and J = 5.8 Hz, 2H, H_{aa}), 3.68 (dd, J = 8.3 Hz and J = 5.9 Hz, 2H, H_b), 3.14 (q, J = 6.8 Hz, 2H, H_v), 3.00 (q, J = 6.9 Hz, 2H, H_g), 2.35 (s, 4H, H_x & H_y), 1.69-1.60 (m, 4H, H_i & H_t), 1.46-1.37 (m, 4H, H_h & H_u), 1.33-1.22 (m, 68H, H_n & H_r & alkyl CH_2), 0.96 (s, 4H, H_d & H_e); ^{13}C NMR (100 MHz, $CDCl_3$): δ = 172.9 (succinamide C=O), 172.7 (succinamide C=O), 172.2 (succinamide C=O), 171.9 (succinamide C=O), 166.4 (macrocycle C=O), 163.4 (2 × imide C=O), 155.91 (perylene ArC_q), 155.88 (perylene ArC_q), 152.82 (ArC_qO–perylene), 152.81 (ArC_qO–perylene), 147.2 (2 × $ArC_qC(CH_3)_3$), 141.8 (phenyl ArC_q), 141.4 (phenyl ArC_q), 137.7 (xylyl ArC_q), 133.8 (isophthaloyl ArC_q), 132.8 (2 × perylene ArC_q), 131.6 ($ArCH_B$), 129.2 ($ArCH_A$), 129.1 ($ArCH_F$), 128.9 (phenyl ArCH), 128.7 (phenyl ArCH), 128.0 (phenyl ArCH), 127.8 (phenyl ArCH), 127.2 (phenyl ArCH), 126.8 (phenyl ArCH), 126.6 ($ArCH_m$ & $ArCH_q$), 123.9

($ArCH_C$), 122.42 (perylene ArC_q), 122.38 (perylene ArC_q), 120.5 (perylene ArC_q), 120.4 (perylene ArC_q), 119.83 ($ArCH_{(k \text{ or } o)}$), 119.81 ($ArCH_{(k \text{ or } o)}$), 119.4 (2 × perylene ArC_q), 119.29 ($ArCH_{(l \text{ or } p)}$), 119.28 ($ArCH_{(l \text{ or } p)}$), 50.6 (CH_{ab}), 50.5 (CH_a), 44.2 ($CH_{2(b)}$), 43.9 ($CH_{2(E)}$), 43.8 ($CH_{2(aa)}$), 40.6 ($CH_{2(j)}$ & $CH_{2(s)}$), 39.8 ($CH_{2(g)}$), 39.6 ($CH_{2(v)}$), 34.3 (2 × $C_q(CH_3)_3$), 31.8 ($CH_{2(x \text{ or } y)}$), 31.7 ($CH_{2(x \text{ or } y)}$), 31.4 (2 × CH_3), 29.7, 29.6, 29.51, 29.48, 29.4, 29.29, 29.26, 29.2, 28.1, 27.1, 26.9 (22 × CH_2); HRMS (FAB, 3-NOBA matrix): m/z = 2973.5083 [$(M+H)^+$] (anal. calcd for $^{12}C_{187}{}^{13}CH_{199}N_{14}O_{20}^+$: m/z = 2973.5019).

[2]-(1,7,14,20-Tetraaza-2,6,15,19-tetraoxo-9,12,22,25-dibenzo-3,5,16,18-di[5-pyridyl]cyclohexacosane)-[*N*-(2,2-dipehnylethyl)-*N'*-(12-{[4-(2,2-diphenylethylamino)-4-oxobutanoyl]amino}dodecyl)-naphthalene-1,4,5,8-tetracarboxylic diimide]-rotaxane (24)

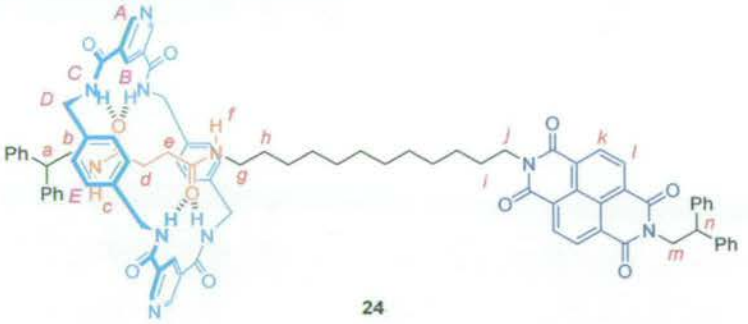

24

Solutions of freshly prepared pyridine-3,5-dicarbonyl dichloride (303 mg, 1.49 mmol) in chloroform (8 mL) and *p*-xylylenediamine (202 mg, 1.49 mmol) with triethylamine (417 μL, 2.98 mmol) in chloroform (8 mL) were simultaneously added using motor-driven syringe pumps over 4 h to a solution of thread **20** (169 mg, 0.186 mmol) in chloroform (20 mL). Following addition, the mixture was allowed to stir for a further 16 h before removal of the off-white precipitate by filtration. The resulting filtrate was diluted with chloroform (40 mL) and washed with hydrochloric acid (1N, 3 × 80 mL), sodium hydrogen carbonate (sat. aq., 3 × 100 mL) and brine (sat., 100 mL). The organics were then dried ($MgSO_4$) and evaporated to give a pale brown residue. This material was purified by flash chromatography (SiO_2; methanol/chloroform, 1:99 to 3:97), then the product-containing material was washed repeatedly in cold toluene to remove all traces of the thread starting material, affording the [2]rotaxane **24** as a pale brown solid (93.0 mg, 35%); mp 143-146 °C; ^{1}H NMR (400 MHz, $CDCl_3$): δ = 9.11 (s, 4H, H_A), 8.67-8.61 (m, 6H, H_B & H_k & H_l), 8.09 (s, 1H, H_c), 7.92 (s, 1H, H_f), 7.57 (s, 4H, H_C), 7.31-7.12 (m, 28H, H_E & H_{Ph}), 4.86 (d, J = 8.0 Hz, 2H, H_m), 4.77 (t, J =

7.5 Hz, 1H, H_n), 4.56 (s, 8H, H_D), 4.14-4.10 (m, 3H, H_a & H_j), 3.83 (br t, 2H, H_b), 3.11 (d, J = 4.5 Hz, 2H, H_g), 1.71 (br s, 2H, H_i), 1.44-1.43 (m, 2H, H_h), 1.41-1.22 (m, 16H, alkyl CH_2), 1.02 (s, 4H, H_d & H_e); ^{13}C NMR (100 MHz, $CDCl_3$): δ = 173.6 (succinamide C=O), 173.2 (succinamide C=O), 163.7 (macrocycle C=O), 162.7 (2 × imide C=O), 151.4 ($ArCH_A$), 141.5 (phenyl ArC_q), 141.2 (phenyl ArC_q), 137.4 (xylyl ArC_q), 131.6 ($ArCH_B$), 130.9 (naphthalene ArCH), 130.8 (naphthalene ArCH), 129.6 ($ArCH_E$), 128.9 (phenyl ArCH), 128.5 (pyridyl ArC_q), 128.4 (phenyl ArCH), 128.3 (phenyl ArCH), 127.8 (phenyl ArCH), 127.2 (phenyl ArCH), 126.8 (phenyl ArCH), 126.6 (2 × naphthalene ArC_q), 126.5 (naphthalene ArC_q), 126.2 (naphthalene ArC_q), 50.6 (CH_a), 48.6 (CH_n), 44.8 ($CH_{2(m)}$), 44.4 ($CH_{2(b)}$), 44.1 ($CH_{2(D)}$), 40.9 ($CH_{2(j)}$), 39.8 ($CH_{2(g)}$), 29.5, 29.4, 29.3, 29.2, 28.0, 27.1 (12 × CH_2); HRMS (FAB, 3-NOBA matrix): m/z = 1444.6687 [$(M+H)^+$] (anal. calcd for $^{13}C_{87}{}^{12}CH_{87}N_{10}O_{16}^+$: m/z = 1444.6640).

[2]-(1,7,14,20-Tetraaza-2,6,15,19-tetraoxo-9,12,22,25-dibenzo-3,5,16,18-di[5-pyridyl]cyclohexacosane)-[*N*,*N*′-bis(12-{[4-(2,2-diphenylethylamino)-4-oxobutanoyl]amino}dodecyl)-1,6,7,12-tetra(4-*tert*-butylphenoxy)-perylene-3,4,9,10-tetracarboxylic diimide]-rotaxane (25)

and

[3]-Bis-(1,7,14,20-tetraaza-2,6,15,19-tetraoxo-9,12,22,25-dibenzo-3,5,16,18-di[5-pyridyl]cyclohexacosane)-[*N*,*N*′-bis(12-{[4-(2,2-diphenylethylamino)-4-oxobutanoyl]amino}dodecyl)-1,6,7,12-tetra(4-*tert*-butylphenoxy)-perylene-3,4,9,10-tetracarboxylic diimide]-rotaxane (26)

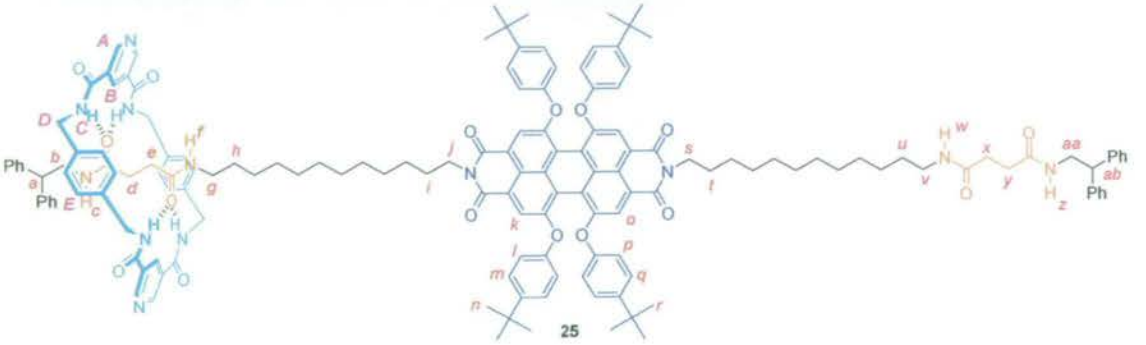

25

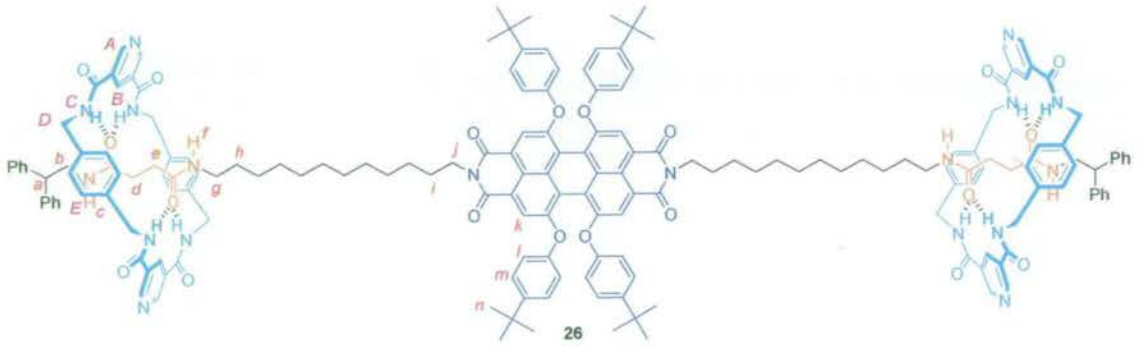

26

Solutions of freshly prepared pyridine-3,5-dicarbonyl dichloride (340 mg, 1.67 mmol) in chloroform (10 mL) and *p*-xylylenediamine (227 mg, 1.67 mmol) with triethylamine (468 µL, 3.34 mmol) in chloroform (10 mL) were simultaneously added using motor-driven syringe pumps over 4 h to a solution of thread **23** (265 mg, 0.139 mmol) in chloroform (20 mL). Following addition, the mixture was allowed to stir for a further 16 h before removal of the pale pink precipitate by filtration. The resulting filtrate was concentrated under reduced pressure and the crude product purified by flash chromatography (SiO_2; methanol/dichloromethane, 2:98 to 5:95) to afford, in order of elution, impure [2]rotaxane and impure [3]rotaxane. The contaminating salts were removed by re-dissolving each sample in turn in chloroform (20 mL) and washing with hydrochloric acid (1N, 3 × 30 mL), sodium hydrogen carbonate (sat. aq., 2 × 40 mL) and brine (sat., 40 mL) before drying ($MgSO_4$) the

organics and concentrating under reduced pressure. The resulting solids were further washed with hot diethylether and dried to give:

[2]rotaxane **25** as a purple solid (236 mg, 37%); mp > 220 °C (decomp.); ^{1}H NMR (400 MHz, $CDCl_3$): δ = 9.11 (s, 4H, H_A), 8.71 (br s, 2H, H_B), 8.21 (s, 2H, H_o), 8.20 (s, 2H, H_k), 7.71 (br s, 4H, H_C), 7.60 (br s, 1H, H_c), 7.48 (br s, 1H, H_f), 7.31-7.13 (m, 36H, H_E & H_m & H_q & H_{Ph}), 6.81 (d, J = 8.7 Hz, 8H, H_l & H_p), 5.98 (br t, 1H, H_z), 5.91 (br t, 1H, H_w), 4.60-4.48 (m, 8H, H_D), 4.15 (t, J = 8.0 Hz, 1H, H_{ab}), 4.10-4.04 (m, 5H, H_a & H_j & H_s), 3.86 (dd, J = 7.9 Hz and J = 5.9 Hz, 2H, H_{aa}), 3.77 (br dd, 2H, H_b), 3.15 (q, J = 6.7 Hz, 2H, H_v), 3.09-3.03 (m, 2H, H_g), 2.36 (s, 4H, H_x & H_y), 1.68-1.59 (m, 4H, H_i & H_t), 1.44-1.40 (m, 4H, H_h & H_u), 1.33-1.20 (m, 68H, H_n & H_r & alkyl CH_2), 1.00 (s, 4H, H_d & H_e); ^{13}C NMR (100 MHz, $CDCl_3$): δ = 173.3 (succinamide C=O), 173.0 (succinamide C=O), 172.2 (succinamide C=O), 171.9 (succinamide C=O), 163.8 (macrocycle C=O), 163.4 (2 × imide C=O), 155.91 (perylene ArC_q), 155.86 (perylene ArC_q), 152.81 (ArC_qO–perylene), 152.79 (ArC_qO–perylene), 151.7 ($ArCH_A$), 147.22 ($ArC_qC(CH_3)_3$), 147.19 ($ArC_qC(CH_3)_3$), 141.7 (phenyl ArC_q), 141.4 (phenyl ArC_q), 137.4 (xylyl ArC_q), 132.8 (2 × perylene ArC_q), 132.1 ($ArCH_B$), 129.5 ($ArCH_E$), 128.9 (phenyl ArCH), 128.8 (pyridyl ArC_q), 128.7 (phenyl ArCH), 128.0 (phenyl ArCH), 127.7 (phenyl ArCH), 127.2 (phenyl ArCH), 126.8 (phenyl ArCH), 126.6 ($ArCH_m$ & $ArCH_q$), 122.4 (perylene ArC_q), 122.3 (perylene ArC_q), 120.5 (perylene ArC_q), 120.4 (perylene ArC_q), 119.8 ($ArCH_k$ & $ArCH_o$), 119.4 (2 × perylene ArC_q), 119.29 ($ArCH_{(l \text{ or } p)}$), 119.27 ($ArCH_{(l \text{ or } p)}$), 50.6 ($CH_{(a \text{ or } ab)}$), 50.5 ($CH_{(a \text{ or } ab)}$), 44.03 ($CH_{2(b)}$), 44.01 ($CH_{2(D)}$), 43.8 ($CH_{2(aa)}$), 40.64 ($CH_{2(j \text{ or } s)}$), 40.61 ($CH_{2(j \text{ or } s)}$), 39.9 ($CH_{2(g)}$), 39.7 ($CH_{2(v)}$), 34.3 (2 × $C_q(CH_3)_3$), 31.8 ($CH_{2(x \text{ or } y)}$), 31.7 ($CH_{2(x \text{ or } y)}$), 31.4 (2 × CH_3), 29.52, 29.48, 29.4, 29.29, 29.27, 27.12, 27.11, 26.9 (22 × CH_2); HRMS (FAB, 3-NOBA matrix): m/z = 2443.2880 [$(M+H)^+$] (anal. calcd for $^{12}C_{153}{}^{13}CH_{169}N_{12}O_{16}^+$: m/z = 2443.2813);

[3]rotaxane **26** as a purple solid (15.0 mg, 3.6%); mp > 200 °C (decomp.); ^{1}H NMR (400 MHz, 5:95 $CD_3OD/CDCl_3$): δ = 9.21 (br s, 8H, H_A), 8.76 (s, 4H, H_B), 8.19 (s, 4H, H_k), 8.03 (br s, 8H, H_C), 7.30-7.14 (m, 32H, H_c & H_f & H_m & H_{Ph}), 7.07 (s, 16H, H_E), 6.81 (d, J = 8.7 Hz, 8H, H_l), 4.49 (d, J = 14.3 Hz, 8H, H_D), 4.43 (d, J = 14.2 Hz, 8H, $H_{D'}$), 4.07-4.04 (m, 6H, H_a & H_j), 3.66-3.64 (m, 4H, H_b), 2.93 (br s, 4H, H_g), 1.68-1.59 (m, 4H, H_i), 1.42-1.36 (m, 4H, H_h), 1.34-1.20 (m, 68H, H_n & alkyl CH_2), 0.95 (s, 8H, H_d & H_e); ^{13}C NMR (100 MHz, 5:95 $CD_3OD/CDCl_3$): δ = 172.9

(succinamide C=O), 172.7 (succinamide C=O), 164.7 (macrocycle C=O), 163.4 (imide C=O), 155.8 (perylene ArC_q), 152.7 (ArC_qO–perylene), 151.0 ($ArCH_A$), 147.2 ($ArC_qC(CH_3)_3$), 141.6 (phenyl ArC_q), 137.2 (xylyl ArC_q), 133.1 ($ArCH_B$), 132.7 (perylene ArC_q), 129.1 ($ArCH_E$), 128.9 (pyridyl ArC_q), 128.7 (phenyl ArCH), 127.7 (phenyl ArCH), 127.0 (phenyl ArCH), 126.5 ($ArCH_m$), 122.2 (perylene ArC_q), 120.4 (perylene ArC_q), 119.7 ($ArCH_k$), 119.3 (perylene ArC_q), 119.2 ($ArCH_l$), 50.3 (CH_a), 44.0 ($CH_{2(b)}$), 43.7 ($CH_{2(D)}$), 40.6 ($CH_{2(j)}$), 39.5 ($CH_{2(g)}$), 34.2 ($C_q(CH_3)_3$), 31.3 (CH_3), 29.44, 29.41, 29.2, 29.1, 28.0, 27.9, 27.0, 26.9 (12 × CH_2); HRMS (FAB, 3-NOBA matrix): *m/z* = 2977.4906 [$(M+H)^+$] (anal. calcd for $^{12}C_{183}{}^{13}CH_{195}N_{18}O_{20}^+$: *m/z* = 2977.4829).

5.10.2 Electrochemistry

Materials

All chemicals used were reagent grade. Tetrabutylammonium hexafluorophosphate (TBHF, FLUKA) was used as supporting electrolyte as received. Tetrahydrofuran (LiChrosolv) was treated according to a procedure described elsewhere.[50] For the electrochemical experiments, the solvent was distilled into the electrochemical cell, prior to use, by a trap-to-trap procedure.

Instrumentation and measurements

The one-compartment electrochemical cell was of airtight design, with high-vacuum glass stopcocks fitted with either Teflon or Kalrez (DuPont) O-rings, in order to prevent contamination by grease. The connections to the high-vacuum line and to the Schlenck flask containing the solvent were made by spherical joints fitted with Kalrez O-rings. The pressure measured in the electrochemical cell prior to performing the trap-to-trap distillation of the solvent was typically 1.0 to 2.0 × 10^{-5} mbar. The working electrode consisted either of a 0.6 mm diameter platinum wire (0.15 cm^2 approximately) sealed in glass or platinum disc ultramicroelectrodes (with radii from 5 to 62.5 μm) also sealed in glass. The counter electrode consisted of a platinum spiral and the quasi-reference electrode was a silver spiral. The quasi-reference electrode drift was negligible for the time required by a single experiment. Both the counter and the reference electrode were separated from the working electrode by ~0.5 cm. Potentials were measured with the ferrocene or decamethylferrocene standards and

are always referred to saturated calomel electrode (SCE). $E_{1/2}$ values correspond to $(E_c + E_a) / 2$ from CV. Ferrocene (decamethylferrocene) was also used as an internal standard for checking the electrochemical reversibility of a redox couple. The temperature dependence of the relevant internal standard redox couple potential was measured with respect to SCE by a nonisothermal arrangement.[51] Voltammograms were recorded with an AMEL Model 552 potentiostat or a custom made fast potentiostat controlled by either an AMEL Model 568 function generator or an ELCHEMA Model FG-206F. Data acquisition was performed by a Nicolet Model 3091 digital oscilloscope interfaced to a PC. Temperature control was accomplished within 0.1 °C with a Lauda thermostat. The minimization of ohmic drop was achieved through the positive feedback circuit implemented in the potentiostat. Digital simulations of cyclic voltammetric experiments were carried out by the DigiSim 3.0 software from Bioanalytical Systems Inc. All the fitting parameters (see below) were chosen so as to obtain a visual best fit over a 10^2–10^3-fold range of scan rates.

Parameters obtained by the best fitting of CV curves of 1

Table 5.2 Simulation parameters corresponding to the heterogeneous electron transfer processes of the square mechanism shown Figure 5.4.

Parameters	*succ*-**1**/*succ*-**1**$^{-\bullet}$	*ni*-**1**/*ni*-**1**$^{-\bullet}$
$E_{1/2}$ / V	–1.41	–0.90 (–1.00)[a]
$k°_{het}$ / cm s^{-1}	10	0.02
α	0.5	0.5
D /cm^2 s^{-1}	1×10^{-5}	1×10^{-5}

[a] At 213 K.

Table 5.3 Simulation parameters corresponding to the translational isomerizations of the square mechanism shown in Figure 5.4.

Reaction	Parameters	298 K	213 K
succ-**1** ⇆ *ni*-**1**	k_f^1 / s^{-1}	0.002	0.001
	k_b^1 / s^{-1}	1664	17
	K_n	1.2×10^{-6}	6×10^{-5} [a]
succ-**1**$^{-\bullet}$ ⇆ *ni*-**1**$^{-\bullet}$	$k_f^{1^{-\bullet}}$ /s^{-1}	2×10^4	1
	$k_b^{1^{-\bullet}}$ /s^{-1}	40	0.002
	K_{red}	500	500[a]

[a] Values not optimised.

Supplementary cyclic voltammetry studies

Additional cyclic voltammograms illustrating the effect of scan rate and of temperature on the electrochemical response of compounds **1**, **2**, **6**, **7** and **8** follow below.

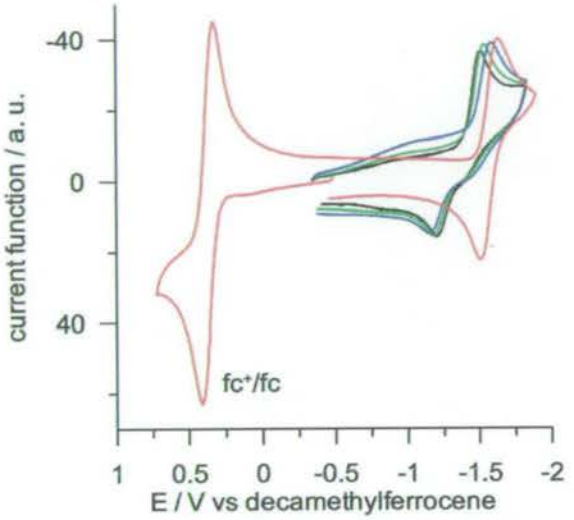

Figure 5.13 Cyclic voltammograms at 298 K of **1** at $v = 0.05$ V s^{-1} (black line); 0.2 V s^{-1} (green line); 1 V s^{-1} (blue line) and **2** at $v = 1$ V s^{-1} (red line), 1 mmol L^{-1} in anhydrous THF with TBHF (5×10^{-2} mol L^{-1}) as supporting electrolyte and ferrocene as internal standard. Working electrode: Pt.

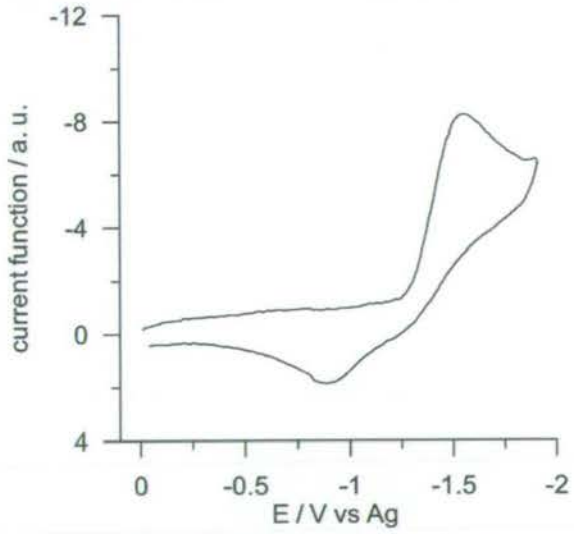

Figure 5.14 Cyclic voltammogram at 218 K of **6** at $v = 0.05$ V s^{-1}, 1 mmol L^{-1} in anhydrous THF with TBHF (5×10^{-1} mol L^{-1}) as supporting electrolyte and ferrocene as internal standard. Working electrode: Pt.

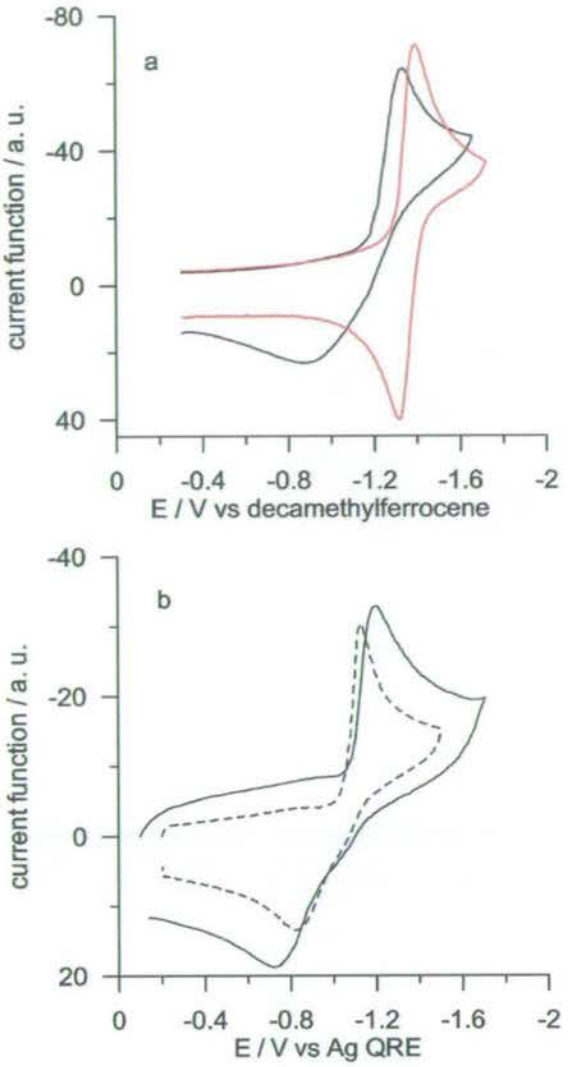

Figure 5.15 Cyclic voltammograms of 0.5 mmol L^{-1} **8** (black lines) or **7** (red line) in anhydrous DMF with tetraethylammonium hexafluorophosphate (5×10^{-2} mol L^{-1}) as supporting electrolyte and ferrocene as internal standard. (a) $T = 298$ K, $v = 5$ V s^{-1} (**8**, black line) and 1 V s^{-1} (**7**, red line). (b) $T = 223$ K, $v = 1$ V s^{-1} (dashed line) and 5 V s^{-1} (solid line).

5.10.3 Eyring plot for the variation of shuttling rates with temperature

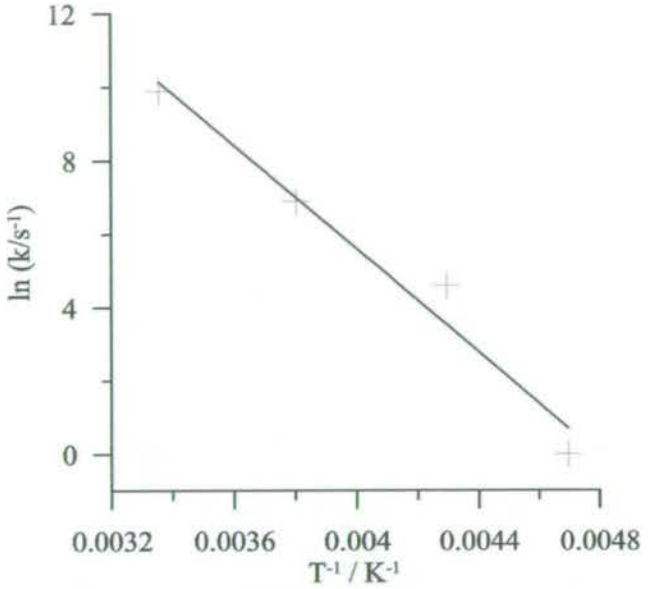

Figure 5.16 Eyring plot analysis of shuttling rates over a range of temperatures.

5.10.4 Crystallography

Crystallographic data for **3** and **4** (excluding structure factors) have been deposited with the Cambridge Crystallographic Data Centre as supplementary publication numbers CCDC-157381 (**3**) and CCDC-190628 (**4**). Copies of the data can be obtained free of charge via www.ccdc.cam.ac.uk/data_request/cif or on application to The Director, CCDC, 12 Union Road, Cambridge CB2 1EZ, UK (tel.: (+44)1443-336-408; fax: (+44)1223-336-033; e-mail: teched@chemcrys.cam.ac.uk).

5.11 References and notes

[1] *Molecular Motors* (Ed.: M. Schliwa), Wiley-VCH, Weinheim, **2003**.

[2] With the notable exception of liquid crystals, the first true artificial devices that rely on mechanical motion at the molecular level for a practical function are the catenanes and rotaxanes used to configure the remarkable solid-state switches and logic gates developed by Stoddart and Heath: a) C. P. Collier, E. W. Wong, M. Belohradský, F. M. Raymo, J. F. Stoddart, P. J. Kuekes, R. S. Williams, J. R. Heath, *Science* **1999**, *285*, 391-394; b) E. W. Wong, C. P. Collier, M. Běhloradský F. M. Raymo, J. F. Stoddart, J. R. Heath, *J. Am. Chem. Soc.* **2000**, *122*, 5831-5840; c) C. P. Collier, G. Mattersteig, E. W. Wong, Y. Luo, K. Beverly, J. Sampaio, F. M. Raymo, J. F. Stoddart, J. R. Heath, *Science* **2000**, *289*, 1172-1175; d) C. P. Collier, J. O. Jeppesen, Y. Luo, J. Perkins, E. W. Wong, J. R. Heath, J. F. Stoddart, *J. Am. Chem. Soc.* **2001**, *123*, 12632-12641; e) Y. Luo, C. P. Collier, J. O. Jeppesen, K. A. Nielsen, E. Delonno, G. Ho, J. Perkins, H.-R. Tseng, T. Yamamoto, J. F. Stoddart, J. R. Heath, *ChemPhysChem* **2002**, *3*, 519-525; f) M. R. Diehl, D. W. Steuerman,

H.-R. Tseng, S. A. Vignon, A. Star, P. C. Celestre, J. F. Stoddart, J. R. Heath, *ChemPhysChem* **2003**, *4*, 1335-1339.

[3] See, for example, analogic molecular versions of 'gears': a) H. Iwamura, K. Mislow, *Acc. Chem. Res.* **1988**, *21*, 175-182; 'turnstiles': b) T. C. Bedard, J. S. Moore, *J. Am. Chem. Soc.* **1995**, *117*, 10662-10671; 'brakes': c) T. R. Kelly, M. C. Bowyer, K. V. Bhaskar, D. Bebbington, A. Garcia, F. R. Lang, M. H. Kim, M. P. Jette, *J. Am. Chem. Soc.* **1994**, *116*, 3657-3658; d) A. M. Schoevaars, W. Kruizinga, R. W. J. Zijlstra, N. Veldman, A. L. Spek, B. L. Feringa, *J. Org. Chem.* **1997**, *62*, 4943-4948; 'ratchets': e) T. R. Kelly, I. Tellitu, J. P. Sestelo, *Angew. Chem. Int. Ed. Engl.* **1997**, *36*, 1866-1868; f) T. R. Kelly, J. P. Sestelo, I. Tellitu, *J. Org. Chem.* **1998**, *63*, 3655-3665; unidirectional spinning 'motors': g) T. R. Kelly, H. De Silva, R. A. Silva, *Nature* **1999**, *401*, 150-152; h) N. Koumura, R. W. J. Zijlstra, R. A. van Delden, N. Harada, B. L. Feringa, *Nature* **1999**, *401*, 152-155; i) T. R. Kelly, R. A. Silva, H. De Silva, S. Jasmin, Y. J. Zhao, *J. Am. Chem. Soc.* **2000**, *122*, 6935-6949; j) N. Koumura, E. M. Geertsema, A. Meetsma, B. L. Feringa, *J. Am. Chem. Soc.* **2000**, *122*, 12005-12006; k) N. Koumura, E. M. Geertsema, M. B. van Gelder, A. Meetsma, B. L. Feringa, *J. Am. Chem. Soc.* **2002**, *124*, 5037-5051; l) M. K. J. ter Wiel, R. A. van Delden, A. Meetsma, B. L. Feringa, *J. Am. Chem. Soc.* **2003**, *125*, 15076-15086.

[4] *Molecular Catenanes Rotaxanes and Knots* (Eds.: J.-P. Sauvage, C. Dietrich-Buchecker), Wiley-VCH, Weinheim, **1999**.

[5] For reviews on the development of interlocked molecules as molecular machines, see: a) A. C. Benniston, *Chem. Soc. Rev.* **1996**, *25*, 427-435; b) V. Balzani, M. Gómez-López, J. F. Stoddart, *Acc. Chem. Res.* **1998**, *31*, 405-414; c) J.-P. Sauvage, *Acc. Chem. Res.* **1998**, *31*, 611-619; d) J.-C. Chambron, J.-P. Sauvage, *Chem. Eur. J.* **1998**, *4*, 1362-1366; e) V. Balzani, A. Credi, F. M. Raymo, J. F. Stoddart, *Angew. Chem. Int. Ed.* **2000**, *39*, 3349-3391; f) A. R. Pease, J. O. Jeppesen, J. F. Stoddart, Y. Luo, C. P. Collier, J. R. Heath, *Acc. Chem. Res.* **2001**, *34*, 433-444; g) R. Ballardini, V. Balzani, A. Credi, M. T. Gandolfi, M. Venturi, *Acc. Chem. Res.* **2001**, *34*, 445-455; h) A. Harada, *Acc. Chem. Res.* **2001**, *34*, 456-464; i) C. A. Schalley, K. Beizai, F. Vögtle, *Acc. Chem. Res.* **2001**, *34*, 465-476; j) J.-P. Collin, C. Dietrich-Buchecker, P. Gaviña, M. C. Jimenez-Molero, J.-P. Sauvage, *Acc. Chem. Res.* **2001**, *34*, 477-487; k) L. Raehm, J.-P. Sauvage, *Struct. Bond.* **2001**, *99*, 55-78; l) R. Ballardini, V. Balzani, A. Credi, M. T. Gandolfi, M. Venturi, *Struct. Bond.* **2001**, *99*, 163-188; m) A. R. Pease, J. F. Stoddart, *Struct. Bond.* **2001**, *99*, 189-236; n) V. Balzani, M. Venturi, A. Credi, *Molecular Devices and Machines. A Journey into the Nanoworld*, Wiley-VCH, Weinheim, **2003**.

[6] 'Co-conformation' refers to the relative positions of the mechanically interlocked components with respect to each other, see: M. C. T. Fyfe, P. T. Glink, S. Menzer, J. F. Stoddart, A. J. P. White, D. J. Williams, *Angew. Chem. Int. Ed. Engl.* **1997**, *36*, 2068-2070. Energy differences between two translational isomers or co-conformations of greater than 1.18 kcal mol^{-1} imply > 90% station occupancy for the more favoured site at 298 K.

[7] For examples of chemically responsive molecular shuttles see: a) A. S. Lane, D. A. Leigh, A. Murphy, *J. Am. Chem. Soc.* **1997**, *119*, 11092-11093; b) M.-V. Martínez-Díaz, N. Spencer, J. F. Stoddart, *Angew. Chem. Int. Ed. Engl.* **1997**, *36*, 1904-1907; c) C. G. Gong, H. W. Gibson, *Angew. Chem. Int. Ed. Engl.* **1997**, *36*, 2331-2333; d) C. G. Gong, T. E. Glass, H. W. Gibson, *Macromolecules* **1998**, *31*, 308-313; e) P. R. Ashton, R. Ballardini, V. Balzani, I. Baxter, A. Credi, M. C. T. Fyfe, M. T. Gandolfi, M. Gómez-López, M.-V. Martínez-Díaz, A. Piersanti, N. Spencer, J. F. Stoddart, M. Venturi, A. J. P. White, D. J. Williams, *J. Am. Chem. Soc.* **1998**, *120*, 11932-11942; f) M. C. Jiménez, C. Dietrich-Buchecker, J.-P. Sauvage, *Angew. Chem. Int. Ed.* **2000**, *39*, 3284-3287; g) J. W. Lee, K. P. Kim, K. Kim, *Chem. Commun.* **2001**, 1042-1043; h) A. M. Elizarov, S.-H. Chiu, J. F. Stoddart, *J. Org. Chem.* **2002**, *67*, 9175-9181; i) M. C. Jimenez-Molero, C. Dietrich-Buchecker, J.-P. Sauvage, *Chem. Eur. J.* **2002**, *8*, 1456-1466; j) T. Da Ros, D. M. Guldi, A. F. Morales, D. A. Leigh, M. Prato, R. Turco, *Org. Lett.* **2003**, *5*, 689-691; k) H.-R. Tseng, S. A. Vignon, J. F. Stoddart, *Angew. Chem. Int. Ed.* **2003**, *42*, 1491-1495.

[8] For examples of photochemically responsive molecular shuttles see: a) A. C. Benniston, A. Harriman, *Angew. Chem. Int. Ed. Engl.* **1993**, *32*, 1459-1461; b) A. C. Benniston, A. Harriman, V. M. Lynch, *J. Am. Chem. Soc.* **1995**, *117*, 5275-5291; c) H. Murakami, A. Kawabuchi, K. Kotoo, M. Kunitake, N. Nakashima, *J. Am. Chem. Soc.* **1997**, *119*, 7605-7606; d) N. Armaroli, V. Balzani, J.-P. Collin, P. Gaviña, J.-P. Sauvage, B. Ventura, *J. Am. Chem. Soc.* **1999**, *121*, 4397-4408; e) P. R. Ashton, R. Ballardini, V. Balzani, A. Credi, K. R. Dress, E. Ishow, C. J. Kleverlaan, O. Kocian, J. A. Preece, N. Spencer, J. F. Stoddart, M. Venturi, S. Wenger, *Chem. Eur. J.* **2000**, *6*, 3558-3574; f) G. W. H. Wurpel, A. M. Brouwer, I. H. M. van Stokkum, A. Farran, D. A. Leigh, *J. Am. Chem. Soc.* **2001**, *123*, 11327-11328; g) A. M. Brouwer, C. Frochot, F. G. Gatti, D. A. Leigh, L. Mottier, F. Paolucci, S. Roffia, G. W. H. Wurpel, *Science* **2001**, *291*, 2124-2128; h) C. A. Stanier, S. J. Alderman, T. D. W. Claridge, H. L. Anderson, *Angew. Chem. Int. Ed.* **2002**, *41*, 1769-1772; i) A. Altieri, G. Bottari, F. Dehez, D. A. Leigh, J. K. Y. Wong, F. Zerbetto, *Angew. Chem. Int. Ed.* **2003**, *42*, 2296-2300.

[9] For examples of electrochemically responsive molecular shuttles see ref. [8d] and: a) R. A. Bissell, E. Córdova, A. E. Kaifer, J. F. Stoddart, *Nature* **1994**, *369*, 133-137; b) J.-P. Collin, P. Gaviña, J.-P. Sauvage, *New J. Chem.* **1997**, *21*, 525-528; c) R. Ballardini, V. Balzani, W. Dehaen, A. E. Dell'Erba, F. M. Raymo, J. F. Stoddart, M. Venturi, *Eur. J. Org. Chem.* **2000**, 591-602.

[10] For examples of the use of electrical and electrochemical stimuli to control ring rotation in catenanes, catenates and rotaxanes, see: a) D. B. Amabilino, C. O. Dietrich-Buchecker, A. Livoreil, L. Pérez-García, J.-P. Sauvage, J. F. Stoddart, *J. Am. Chem. Soc.* **1996**, *118*, 3905-3913; b) D. J. Cárdenas, A. Livoreil, J.-P. Sauvage, *J. Am. Chem. Soc.* **1996**, *118*, 11980-11981; c) A. Livoreil, J.-P. Sauvage, N. Armaroli, V. Balzani, L. Flamigni, B. Ventura, *J. Am. Chem. Soc.* **1997**, *119*, 12114-12124; d) M. Asakawa, P. R. Ashton, V. Balzani, A. Credi, C. Hamers, G. Mattersteig, M. Montalti, A. N. Shipway, N. Spencer, J. F. Stoddart, M. S. Tolley, M. Venturi, A. J. P. White, D. J. Williams, *Angew. Chem. Int. Ed.* **1998**, *37*, 333-337; e) L. Raehm, J.-M. Kern,

J.-P. Sauvage, *Chem. Eur. J.* **1999**, *5*, 3310-3317; f) M. Asakawa, M. Higuchi, G. Mattersteig, T. Nakamura, A. R. Pease, F. M. Raymo, T. Shimizu, J. F. Stoddart, *Adv. Mater.* **2000**, *12*, 1099-1102; g) V. Bermudez, N. Capron, T. Gase, F. G. Gatti, F. Kajzar, D. A. Leigh, F. Zerbetto, S. W. Zhang, *Nature* **2000**, *406*, 608-611; h) P. R. Ashton, V. Baldoni, V. Balzani, A. Credi, H. D. A. Hoffmann, M.-V. Martínez-Díaz, F. M. Raymo, J. F. Stoddart, M. Venturi, *Chem. Eur. J.* **2001**, *7*, 3482-3493.

[11] For examples of the use of electrochemical stimuli to control threading and de-threading in pseudorotaxanes and other host–guest systems see: a) A. R. Bernardo, J. F. Stoddart, A. E. Kaifer, *J. Am. Chem. Soc.* **1992**, *114*, 10624-10631; b) J.-P. Collin, P. Gaviña, J.-P. Sauvage, *Chem. Commun.* **1996**, 2005-2006; c) M. Asakawa, P. R. Ashton, V. Balzani, A. Credi, G. Mattersteig, O. A. Matthews, M. Montalti, N. Spencer, J. F. Stoddart, M. Venturi, *Chem. Eur. J.* **1997**, *3*, 1992-1996; d) W. Devonport, M. A. Blower, M. R. Bryce, L. M. Goldenberg, *J. Org. Chem.* **1997**, *62*, 885-887; e) A. Credi, M. Montalti, V. Balzani, S. J. Langford, F. M. Raymo, J. F. Stoddart, *New J. Chem.* **1998**, *22*, 1061-1065; f) M. Asakawa, P. R. Ashton, V. Balzani, S. E. Boyd, A. Credi, G. Mattersteig, S. Menzer, M. Montalti, F. M. Raymo, C. Ruffilli, J. F. Stoddart, M. Venturi, D. J. Williams, *Eur. J. Org. Chem.* **1999**, 985-994; g) P. R. Ashton, V. Balzani, J. Becher, A. Credi, M. C. T. Fyfe, G. Mattersteig, S. Menzer, M. B. Nielsen, F. M. Raymo, J. F. Stoddart, M. Venturi, D. J. Williams, *J. Am. Chem. Soc.* **1999**, *121*, 3951-3957; h) G. Cooke, F. M. A. Duclairoir, V. M. Rotello, J. F. Stoddart, *Tetrahedron Lett.* **2000**, *41*, 8163-8166; i) V. Balzani, A. Credi, G. Mattersteig, O. A. Matthews, F. M. Raymo, J. F. Stoddart, M. Venturi, A. J. P. White, D. J. Williams, *J. Org. Chem.* **2000**, *65*, 1924-1936; j) V. Balzani, J. Becher, A. Credi, M. B. Nielsen, F. M. Raymo, J. F. Stoddart, A. M. Talarico, M. Venturi, *J. Org. Chem.* **2000**, *65*, 1947-1956; k) M. Lahav, A. N. Shipway, I. Willner, M. B. Nielsen, J. F. Stoddart, *J. Electroanal. Chem.* **2000**, *482*, 217-221.

[12] Earlier attempts to make redox-active hydrogen-bonded molecular shuttles based on anthraquinone subunits were less successful [J. A. Dunnett, PhD Thesis, University of Manchester Institute of Science and Technology (UK), **2000**].

[13] The electrochemical behaviours of 1,8-naphthalimides and other related aromatic imides are well known. See, for example: A. Viehbeck, M. J. Goldberg, C. A. Kovac, *J. Electrochem. Soc.* **1990**, *137*, 1460-1466.

[14] K. Morokuma, *Acc. Chem. Res.* **1977**, *10*, 294-300.

[15] See, for example: a) P. A. Brooksby, C. A. Hunter, A. J. McQuillan, D. H. Purvis, A. E. Rowan, R. J. Shannon, R. Walsh, *Angew. Chem. Int. Ed. Engl.* **1994**, *33*, 2489-2491; b) Y. Ge, R. R. Lilienthal, D. K. Smith, *J. Am. Chem. Soc.* **1996**, *118*, 3976-3977; c) R. Deans, A. Niemz, E. C. Breinlinger, V. M. Rotello, *J. Am. Chem. Soc.* **1997**, *119*, 10863-10864; d) P. L. Boulas, M. Gómez-Kaifer, L. Echegoyen, *Angew. Chem. Int. Ed.* **1998**, *37*, 216-247; e) A. Niemz, V. M. Rotello, *Acc. Chem. Res.* **1999**, *32*, 44-52; f) A. K. Boal, V. M. Rotello, *J. Am. Chem. Soc.* **1999**, *121*, 4914-4915; g) Y. Ge, L. Miller, T.

Ouimet, D. K. Smith, *J. Org. Chem.* **2000**, *65*, 8831-8838; h) Y. Ge, D. K. Smith, *Anal. Chem.* **2000**, *72*, 1860-1865; i) J. D. Carr, S. J. Goles, M. B. Hursthouse, M. E. Light, J. H. R. Tucker, J. Westwood, *Angew. Chem. Int. Ed.* **2000**, *39*, 3296-3299; j) J. H. R. Tucker, S. R. Collinson, *Chem. Soc. Rev.* **2002**, *31*, 147-156; k) G. Cooke, V. M. Rotello, *Chem. Soc. Rev.* **2002**, *31*, 275-286.

[16] See, for example: a) H. L. Schenck, G. P. Dado, S. H. Gellman, *J. Am. Chem. Soc.* **1996**, *118*, 12487-12494; b) T. Pascher, J. P. Chesick, J. R. Winkler, H. B. Gray, *Science* **1996**, *271*, 1558-1560.

[17] The *tert*-butyl substituents provide the steric bulk necessary to stopper the rotaxane while only slightly altering the redox potential of the naphthalimide group ($E_{1/2}$ (**2**) = –1.41 V cf. $E_{1/2}$ (*N*-*n*-butyl naphthalimide) = –1.38 V), see ref. [13].

[18] G. A. Jeffrey, *An Introduction to Hydrogen Bonding*, Oxford University Press, New York, **1997**.

[19] 'Gate-opened' rotaxane **8** was obtained together with the 1°-*O*-acyl, 2°-hydroxyl regioisomer from which it was not separated.

[20] A. G. Johnston, D. A. Leigh, A. Murphy, J. P. Smart, M. D. Deegan, *J. Am. Chem. Soc.* **1996**, *118*, 10662-10663.

[21] Dilution experiments demonstrated that intermolecular hydrogen-bonding interactions were absent at concentrations of 10 mmol L^{-1} and below for the current rotaxanes and threads. All NMR spectra discussed were therefore collected at this standard concentration.

[22] For examples of macrocycle pirouetting in benzylic amide macrocycle-based [2]rotaxanes see ref. [10g] and: a) D. A. Leigh, A. Murphy, J. P. Smart, A. M. Z. Slawin, *Angew. Chem. Int. Ed. Engl.* **1997**, *36*, 728-732; b) F. G. Gatti, D. A. Leigh, S. A. Nepogodiev, A. M. Z. Slawin, S. J. Teat, J. K. Y. Wong, *J. Am. Chem. Soc.* **2001**, *123*, 5983-5989; c) F. G. Gatti, S. León, J. K. Y. Wong, G. Bottari, A. Altieri, M. A. F. Morales, S. J. Teat, C. Frochot, D. A. Leigh, A. M. Brouwer, F. Zerbetto, *Proc. Natl. Acad. Sci. USA* **2003**, *100*, 10-14.

[23] J. Sandström, *Dynamic NMR Spectroscopy*, Academic Press, London, **1982**.

[24] a) F. W. Dahlquist, K. J. Longmur, R. B. Du Vernet, *J. Magn. Reson.* **1975**, *17*, 406-413. For applications of SPT-SIR to dynamic processes in rotaxanes see, for example: b) W. Clegg, C. Gimenez-Saiz, D. A. Leigh, A. Murphy, A. M. Z. Slawin, S. J. Teat, *J. Am. Chem. Soc.* **1999**, *121*, 4124-4129.

[25] Due to the wide temperature range, spectra were collected in $CDCl_3$ from 243 K to 296 K and in $C_2D_2Cl_4$ from 329 K to 369 K.

[26] Cyclic voltammetry was carried out on 10^{-3} mol L^{-1} solutions of substrate in anhydrous THF with tetrabutylammonium hexafluorophosphate (TBHF, 5×10^{-2} mol L^{-1}) as electrolyte and ferrocene as internal standard. The invariance

of the chemical shift for amide protons of **1** and **2** in [D_8]THF in the presence of TBHF at 5×10^{-2} mol L^{-1} suggests that the electrolyte does not significantly affect amide–amide intramolecular hydrogen bonds at these concentrations.

[27] On increasing the scan rate from 20 mV s^{-1} to 250 V s^{-1} (selected experiments shown in Figure 5.13, Section 5.10.2), the anodic peak **II** shifts to higher potentials by ~60 mV / log unit of scan rate, indicating that the oxidation process is kinetically slow. Due to the non-Nernstian nature of the oxidation process the rate constants relative to the *ni*-**1**/*succ*-**1** shuttling process can therefore not be obtained by fitting of the CV curve. The absence of a cathodic counterpart for peak **II** at scan rates as high as 250 V s^{-1}, however, allows estimation of $k_b^1 \approx 1.6 \times 10^3$ s^{-1}, so that $k_f^1 \approx 2 \times 10^{-3}$ s^{-1}.

[28] A. E. Kaifer, M. Gómez-Kaifer, *Supramolecular Electrochemistry*, Wiley-VCH, Weinheim, **1999**.

[29] Assuming $E_{1/2}^{succ} = E_{1/2}$ (**2**) = –1.41 V.

[30] Indeed, recent molecular modelling studies by other groups reinforce this view: X. G. Zheng, K. Sohlberg, *J. Phys. Chem. A* **2003**, *107*, 1207-1215.

[31] In complexes with 2,6-diamidopyridines, three hydrogen bonds to a *ni* unit cause a stabilization of ~0.2 V: see refs. [15b, 15c].

[32] K. A. Zachariasse, A. L. Maçanita, W. Kühnle, *J. Phys. Chem. B* **1999**, *103*, 9356-9365.

[33] S. H. Gellman, G. P. Dado, G. B. Liang, B. R. Adams, *J. Am. Chem. Soc.* **1991**, *113*, 1164-1173.

[34] D. Gosztola, M. P. Niemczyk, W. Svec, A. S. Lukas, M. R. Wasielewski, *J. Phys. Chem. A* **2000**, *104*, 6545-6551.

[35] S. K. Lee, Y. B. Zu, A. Herrmann, Y. Geerts, K. Mullen, A. J. Bard, *J. Am. Chem. Soc.* **1999**, *121*, 3513-3520.

[36] H. Langhals, *Heterocycles* **1995**, *40*, 477-500, and references therein.

[37] a) J. C. Scaiano, A. F. Becknell, R. D. Small, *J. Photochem. Photobiol. A* **1988**, *44*, 99-110; b) B. M. Aveline, S. Matsugo, R. W. Redmond, *J. Am. Chem. Soc.* **1997**, *119*, 11785-11795; c) J. E. Rogers, L. A. Kelly, *J. Am. Chem. Soc.* **1999**, *121*, 3854-3861.

[38] In all hydrogen-bonded molecular shuttles the affinity of each station for the macrocycle may be varied almost infinitely by the effects of temperature or the hydrogen-bond-disrupting ability of the solvent. These stimuli however tend to indiscriminately affect all hydrogen bonds within the system.

[39] a) A. N. Shipway, E. Katz, I. Willner, *Struct. Bond.* **2001**, *99*, 237-281; b) A. H. Flood, R. J. A. Ramirez, W.-Q. Deng, R. P. Muller, W. A. Goddard, J. F. Stoddart, *Aust. J. Chem.* **2004**, *57*, 301-322; c) T. F. Magnera, J. Michl, *Top.*

Curr. Chem. **2005**, *262*, 63-97; d) S. D. Karlen, M. A. Garcia-Garibay, *Top. Curr. Chem.* **2005**, *262*, 179-227; e) P. M. Mendes, A. H. Flood, J. F. Stoddart, *Appl. Phys. A* **2005**, *80*, 1197-1209; f) A. B. Braunschweig, B. H. Northrop, J. F. Stoddart, *J. Mater. Chem.* **2006**, *16*, 32-44; g) T. A. V. Khuong, J. E. Nunez, C. E. Godinez, M. A. Garcia-Garibay, *Acc. Chem. Res.* **2006**, *39*, 413-422.

[40] a) L. Sheeney-Haj-Ichia, I. Willner, *J. Phys. Chem. B* **2002**, *106*, 13094-13097; b) E. Katz, L. Sheeney-Haj-Ichia, I. Willner, *Angew. Chem. Int. Ed.* **2004**, *43*, 3292-3300; c) E. Katz, O. Lioubashevsky, I. Willner, *J. Am. Chem. Soc.* **2004**, *126*, 15520-15532.

[41] a) D. W. Steuerman, H.-R. Tseng, A. J. Peters, A. H. Flood, J. O. Jeppesen, K. A. Nielsen, J. F. Stoddart, J. R. Heath, *Angew. Chem. Int. Ed.* **2004**, *43*, 6486-6491; b) D. A. Leigh, M. A. F. Morales, E. M. Pérez, J. K. Y. Wong, C. G. Saiz, A. M. Z. Slawin, A. J. Carmichael, D. M. Haddleton, A. M. Brouwer, W. J. Buma, G. W. H. Wurpel, S. León, F. Zerbetto, *Angew. Chem. Int. Ed.* **2005**, *44*, 3062-3067.

[42] J. Berná, D. A. Leigh, M. Lubomska, S. M. Mendoza, E. M. Pérez, P. Rudolf, G. Teobaldi, F. Zerbetto, *Nat. Mater.* **2005**, *4*, 704-710.

[43] T. D. Nguyen, H.-R. Tseng, P. C. Celestre, A. H. Flood, Y. Liu, J. F. Stoddart, J. I. Zink, *Proc. Natl. Acad. Sci. USA* **2005**, *102*, 10029-10034.

[44] a) T. J. Huang, B. Brough, C.-M. Ho, Y. Liu, A. H. Flood, P. A. Bonvallet, H.-R. Tseng, J. F. Stoddart, M. Baller, S. Magonov, *Appl. Phys. Lett.* **2004**, *85*, 5391-5393; b) Y. Liu, A. H. Flood, P. A. Bonvallet, S. A. Vignon, B. H. Northrop, H.-R. Tseng, J. O. Jeppesen, T. J. Huang, B. Brough, M. Baller, S. Magonov, S. D. Solares, W. A. Goddard, C.-M. Ho, J. F. Stoddart, *J. Am. Chem. Soc.* **2005**, *127*, 9745-9759.

[45] a) G. Bidan, M. Billon, B. Divisia-Blohorn, J.-M. Kern, L. Raehm, J.-P. Sauvage, *New J. Chem.* **1998**, *22*, 1139-1141; b) T. Gase, D. Grando, P. A. Chollet, F. Kajzar, A. Murphy, D. A. Leigh, *Adv. Mater.* **1999**, *11*, 1303-1305; c) L. Raehm, J.-M. Kern, J.-P. Sauvage, C. Hamann, S. Palacin, J. P. Bourgoin, *Chem. Eur. J.* **2002**, *8*, 2153-2162; d) B. Long, K. Nikitin, D. Fitzmaurice, *J. Am. Chem. Soc.* **2003**, *125*, 15490-15498; e) J. H. Huang, A. H. Flood, C.-W. Chu, S. Kang, T.-F. Guo, T. Yamamoto, H.-R. Tseng, B.-D. Yu, Y. Yang, J. F. Stoddart, C.-M. Ho, *IEEE Trans: Nanotechnology* **2003**, *2*, 698-701; f) H.-R. Tseng, D. M. Wu, N. X. L. Fang, X. Zhang, J. F. Stoddart, *ChemPhysChem* **2004**, *5*, 111-116; g) T. J. Huang, H.-R. Tseng, L. Sha, W. X. Lu, B. Brough, A. H. Flood, B.-D. Yu, P. C. Celestre, J. P. Chang, J. F. Stoddart, C.-M. Ho, *Nano Lett.* **2004**, *4*, 2065-2071; h) K. Nørgaard, B. W. Laursen, S. Nygaard, K. Kjaer, H.-R. Tseng, A. H. Flood, J. F. Stoddart, T. Bjørnholm, *Angew. Chem. Int. Ed.* **2005**, *44*, 7035-7039; i) M. Clemente-León, A. Credi, M. V. Martínez-Díaz, C. Mingotaud, J. F. Stoddart, *Adv. Mater.* **2006**, *18*, 1291-1296; j) G. Cooke, J. F. Garety, B. Jordan, N. Kryvokhyzha, A. Parkin, G. Rabani, V. M. Rotello, *Org. Lett.* **2006**, *8*, 2297-

2300; k) B. Brough, B. H. Northrop, J. J. Schmidt, H.-R. Tseng, K. N. Houk, J. F. Stoddart, C. M. Ho, *Proc. Natl. Acad. Sci. USA* **2006**, *103*, 8583-8588.

[46] Investigation of the motions possible in drop-casted or vacuum-evaporated thin films or polycrystalline samples of catenanes and rotaxanes is another emerging area of interest which may be important in the future. See, for example ref. [45b] and: a) M. Cavallini, R. Lazzaroni, R. Zamboni, F. Biscarini, D. Timpel, F. Zerbetto, G. J. Clarkson, D. A. Leigh, *J. Phys. Chem. B* **2001**, *105*, 10826-10830; b) G. Bottari, R. Caciuffo, M. Fanti, D. A. Leigh, S. F. Parker, F. Zerbetto, *ChemPhysChem* **2002**, *3*, 1038-1041; c) M. Cavallini, F. Biscarini, M. Massi, A. Farran-Morales, D. A. Leigh, F. Zerbetto, *Nano Lett.* **2002**, *2*, 635-639; d) M. Cavallini, F. Biscarini, S. León, F. Zerbetto, G. Bottari, D. A. Leigh, *Science* **2003**, *299*, 531-531; e) A. A. Farrell, T. Fukuma, T. Uchihashi, E. R. Kay, G. Bottari, D. A. Leigh, H. Yamada, S. P. Jarvis, *Phys. Rev. B* **2005**, *72*, 125430 (reprinted, in full, in the Appendix); f) S. M. Mendoza, C. M. Whelan, J. P. Jalkanen, F. Zerbetto, F. G. Gatti, E. R. Kay, D. A. Leigh, M. Lubomska, P. Rudolf, *J. Chem. Phys.* **2005**, *123*, 244708 (reprinted, in full, in the Appendix); g) J. F. Moulin, J. C. Kengne, R. Kshirsagar, M. Cavallini, F. Biscarini, S. Leon, F. Zerbetto, G. Bottari, D. A. Leigh, *J. Am. Chem. Soc.* **2006**, *128*, 526-532.

[47] F. Cecchet, P. Rudolf, S. Rapino, M. Margotti, F. Paolucci, J. Baggerman, A. M. Brouwer, E. R. Kay, J. K. Y. Wong, D. A. Leigh, *J. Phys. Chem. B* **2004**, *108*, 15192-15199 (reprinted, in full, in the Appendix).

[48] F. Cecchet, M. Pilling, L. Hevesi, S. Schergna, J. K. Y. Wong, G. J. Clarkson, D. A. Leigh, P. Rudolf, *J. Phys. Chem. B* **2003**, *107*, 10863-10872.

[49] In alkaline aqueous systems, this has been shown to be due to a partially reversible reductive desorption of the thiolates. The exact potential at which this occurs varies with certain structural features, and consequently this process has been widely studied as a method for probing the molecular structure of monolayers. See, for example: a) C. A. Widrig, C. Chung, M. D. Porter, *J. Electroanal. Chem.* **1991**, *310*, 335-359; b) M. M. Walczak, D. D. Popenoe, R. S. Deinhammer, B. D. Lamp, C. K. Chung, M. D. Porter, *Langmuir* **1991**, *7*, 2687-2693; c) T. Kakiuchi, H. Usui, D. Hobara, M. Yamamoto, *Langmuir* **2002**, *18*, 5231-5238. Even under neutral conditions, or in organic solvents where reductive desorption is not observed within the solvent window, alkanethiolate SAMs are still destroyed at negative potentials. The details of this complex, kinetically controlled process are less well understood. See, for example: d) W. R. Everett, T. L. Welch, L. Reed, I. Fritsch-Faules, *Anal. Chem.* **1995**, *67*, 292-298; e) W. R. Everett, I. Fritsch-Faules, *Anal. Chim. Acta* **1995**, *307*, 253-268; f) M. W. J. Beulen, M. I. Kastenberg, F. van Veggel, D. N. Reinhoudt, *Langmuir* **1998**, *14*, 7463-7467.

[50] F. Paolucci, M. Carano, P. Ceroni, L. Mottier, S. Roffia, *J. Electrochem. Soc.* **1999**, *146*, 3357-3360.

[51] E. L. Yee, R. J. Cave, K. L. Guyer, P. D. Tyma, M. J. Weaver, *J. Am. Chem. Soc.* **1979**, *101*, 1131-1137.

APPENDIX

Published Papers

Electrochemically switchable hydrogen-bonded molecular shuttles: A. Altieri, F. G. Gatti, E. R. Kay, D. A. Leigh, D. Martel, F. Paolucci, A. M. Z. Slawin, J. K. Y. Wong, *J. Am. Chem. Soc.* **2003**, *125*, 8644-8654.

Structural, electrochemical, and photophysical properties of a molecular shuttle attached to an acid-terminated self-assembled monolayer: F. Cecchet, P. Rudolf, S. Rapino, M. Margotti, F. Paolucci, J. Baggerman, A. M. Brouwer, E. R. Kay, J. K. Y. Wong, D. A. Leigh, *J. Phys. Chem. B* **2004**, *108*, 15192-15199.

A reversible synthetic rotary molecular motor: J. V. Hernández, E. R. Kay, D. A. Leigh, *Science* **2004**, *306*, 1532-1537.

Synthetic Molecular Machines: E. R. Kay, D. A. Leigh in *Functional Artificial Receptors* (Eds.: T. Schrader, A. D. Hamilton), Wiley-VCH, Weinheim, **2005**, pp. 333-406.

Conservative and dissipative force imaging of switchable rotaxanes with frequency-modulation atomic force microscopy: A. A. Farrell, T. Fukuma, T. Uchihashi, E. R. Kay, G. Bottari, D. A. Leigh, H. Yamada, S. P. Jarvis, *Phys. Rev. B* **2005**, *72*, 125430.

Experimental and theoretical study of the adsorption of fumaramide [2]rotaxane on Au(111) and Ag(111) surfaces: S. M. Mendoza, C. M. Whelan, J. P. Jalkanen, F. Zerbetto, F. G. Gatti, E. R. Kay, D. A. Leigh, M. Lubomska, P. Rudolf, *J. Chem. Phys.* **2005**, *123*, 244708.

Hydrogen bond-assembled synthetic molecular motors and machines: E. R. Kay, D. A. Leigh, *Top. Curr. Chem.* **2005**, *262*, 133-177.

Beyond switches: ratcheting a particle energetically uphill with a compartmentalized molecular machine: M. N. Chatterjee, E. R. Kay, D. A. Leigh, *J. Am. Chem. Soc.* **2006**, *128*, 4058-4073.

Lighting up nanomachines: E. R. Kay, D. A. Leigh, *Nature* **2006**, *440*, 286-287.

J|A|C|S
ARTICLES
Published on Web 06/18/2003

Electrochemically Switchable Hydrogen-Bonded Molecular Shuttles

Alessio Altieri,‡ Francesco G. Gatti,† Euan R. Kay,† David A. Leigh,*,† David Martel,‡ Francesco Paolucci,*,‡ Alexandra M. Z. Slawin,§ and Jenny K. Y. Wong†

Contribution from the School of Chemistry, University of Edinburgh, The King's Buildings, West Mains Road, Edinburgh EH9 3JJ, United Kingdom, Dipartimento di Chimica "G. Ciamician", Università degli Studi di Bologna, v. F. Selmi 2, 40126, Bologna, Italy, and Department of Chemistry, University of St. Andrews, St. Andrews KY16 9ST, United Kingdom

Received March 20, 2003; E-mail: david.leigh@ed.ac.uk; paolucci@ciam.unibo.it

Abstract: A series of [2]rotaxanes containing succinamide and naphthalimide hydrogen-bonding stations for a benzylic amide macrocycle is described. Electrochemical reduction and oxidation of the naphthalimide group alters its ability to form hydrogen bonds to the macrocycle to such a degree that redox processes can be used to switch the relative macrocycle-binding affinities of the two stations in a rotaxane by over 8 orders of magnitude. The structure of the neutral [2]rotaxane in solution is established by ^{1}H NMR spectroscopy and shows that the macrocycle exhibits remarkable positional integrity for the succinamide station in a variety of solvents. Cyclic voltammetry experiments allow the simultaneous stimulation and observation of a redox-induced dynamic process in the rotaxane which is both reversible and cyclable. Model compounds in which various conformational and co-conformational changes are prohibited demonstrate unequivocally that the redox response is the result of shuttling of the macrocycle between the two stations. At room temperature in tetrahydrofuran the electrochemically induced movement of the macrocycle between the two stations takes ~50 μs.

Introduction

Natural[1] and artificial[2] devices that function through mechanical motion at the molecular level require a nanoscale structure that restricts the freedom of movement of the various components coupled with a process—usually chemical—to power and control their motions. For the design of prototypical synthetic systems, chemists have taken inspiration from the structural elements of machinery from the macroscopic world.[3] Taking this analogy too far in terms of process must be cautioned, however, since the modes of action for useful movement at the molecular and macroscopic levels are very different. In the macroscopic world, objects do not move until provided with specific energy to do so. In a mechanical machine, this is often through a directional stimulus (i.e., when work is done to move components in a particular way). At the molecular level, molecules—and their parts—are constantly moving above 0 K and it is the directional control of this motion which Nature uses to perform useful mechanical tasks.[1]

'Molecular shuttles' provide a promising basis for artificial molecular machines. Various types of rotaxane[4] structures permit large amplitude, largely independent, motions of the mechanically interlocked components, and the noncovalent bond-directed routes to their synthesis offer a process for controlling the relative positioning of the components through the interactions that 'live on' in the final products.[5] In a rotaxane with two different binding sites ('stations') in the thread, the macrocycle distributes itself between the stations according to the difference in the macrocycle-binding energies and the temperature. If a suitably large difference in macrocycle affinity between the two stations exists, the macrocycle resides overwhelmingly in one

† University of Edinburgh.
‡ Università degli Studi di Bologna.
§ University of St. Andrews.

(1) *Molecular Motors*; Schliwa, M., Ed.; Wiley-VCH: Weinheim, 2003.
(2) With the notable exception of liquid crystals, the first artificial devices that rely on mechanical motion at the molecular level for a practical function are the catenanes and rotaxanes used to configure the remarkable solid-state switches and logic gates developed by Stoddart and Heath. (a) Collier, C. P.; Wong, E. W.; Bělohradský, M.; Raymo, F. M.; Stoddart, J. F.; Kuekes, P. J.; Williams, R. S.; Heath, J. R. *Science* **1999**, *285*, 391−394. (b) Wong, E. W.; Collier, C. P.; Bělohradský, M.; Raymo, F. M.; Stoddart, J. F.; Heath, J. R. *J. Am. Chem. Soc.* **2000**, *122*, 5831−5840. (c) Collier, C. P.; Jeppesen, J. O.; Luo, Y.; Perkins, J.; Wong, E. W.; Heath, J. R.; Stoddart, J. F. *J. Am. Chem. Soc.* **2001**, *123*, 12632−12641. (d) Luo, Y.; Collier, C. P.; Jeppesen, J. O.; Nielsen, K. A.; Delonno, E.; Ho, G.; Perkins, J.; Tseng, H.-R.; Yamamoto, T.; Stoddart, J. F.; Heath, J. R. *Chem. Phys. Chem.* **2002**, *3*, 519−525.
(3) See, for example, analogic molecular versions of gears: (a) Iwamura, H.; Mislow, K. *Acc. Chem. Res.* **1988**, *21*, 175−182. Turnstiles: (b) Bedard, T. C.; Moore, J. S. *J. Am. Chem. Soc.* **1995**, *117*, 10662−10671. Brakes: (c) Kelly, T. R.; Bowyer, M. C.; Bhaskar, K. V.; Bebbington, D.; Garcia, A.; Lang, F.; Kim, M. H.; Jette, M. P. *J. Am. Chem. Soc.* **1994**, *116*, 3657−3658. Ratchets: (d) Kelly, T. R.; Tellitu, I.; Sestelo, J. P. *Angew. Chem., Int. Ed. Engl.* **1997**, *36*, 1866−1868. (e) Kelly, T. R.; Sestelo, J. P.; Tellitu, I. *J. Org. Chem.* **1998**, *63*, 3655−3665. Rotors: (f) Schoevaars, A. M.; Kruizinga, W.; Zijlstra, R. W. J.; Veldman, N.; Spek, A. L.; Feringa, B. L. *J. Org. Chem.* **1997**, *62*, 4943−4948. Unidirectional spinning motors: (g) Kelly, T. R.; De Silva, H.; Silva, R. A. *Nature* **1999**, *401*, 150−152. (h) Koumura, N.; Zijlstra, R. W. J.; van Delden, R. A.; Harada, N.; Feringa, B. L. *Nature* **1999**, *401*, 152−155. (i) Kelly, T. R.; Silva, R. A.; De Silva, H.; Jasmin, S.; Zhao, Y. *J. Am. Chem. Soc.* **2000**, *122*, 6935−6949. (j) Koumura, N. L.; Geertsema, E. M.; van Gelder, M. B.; Meetsma, A.; Feringa, B. L. *J. Am. Chem. Soc.* **2002**, *124*, 5037−5051.
(4) *Molecular Catenanes, Rotaxanes and Knots*; Sauvage, J.-P., Dietrich-Buchecker, C., Eds.; Wiley-VCH: Weinheim, 1999.

10.1021/ja0352552 CCC: $25.00

positional isomer or co-conformation.[6] In stimuli-responsive molecular shuttles,[7−11] an external trigger is used to chemically modify the system and alter the noncovalent intercomponent interactions such that the second macrocycle-binding site becomes energetically more favored causing translocation of the macrocycle along the thread to the second station (Figure 1). The system can be returned to its original state by using a second chemical transformation to restore the initial order of station binding affinities. Performed consecutively, these two steps allow the 'machine' to carry out a complete cycle of shuttling motion. The movement of the macrocycle from station to station is thus caused by using chemical reactions to put the molecule into nonequilibrium co-conformations and then allowing the background thermal energy to drive the macrocycle to the new global minimum (i.e., through biased Brownian motion).

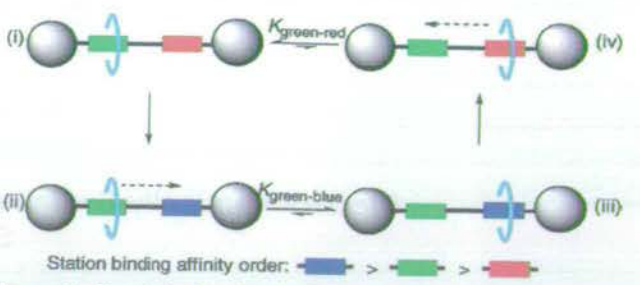

Figure 1. Translational submolecular motion in a stimuli-responsive molecular shuttle: (i) the macrocycle initially resides on the preferred (green) station; (ii) a reaction occurs (red → blue) changing the relative binding potentials of the two stations such that (iii) the macrocycle 'shuttles' to the now-preferred (blue) station. If the reverse reaction (blue → red) now occurs, (iv) the components return to their original positions. The energy available to do mechanical work through shuttling in such a cycle is the sum of the difference in macrocycle binding energies of the two stations in each of the two states (i.e., $\Delta\Delta G_{green-red} + \Delta\Delta G_{blue-green}$).

We recently reported the real-time observation of macrocycle translocation in such a stimuli-responsive molecular shuttle following the photochemically induced reduction of the naphthalimide unit in rotaxane **1**.[8f] In fact, we originally designed **1** as an electrochemically switchable system.[12] Electrochemistry is potentially an attractive method through which to modulate the behavior of molecular devices because it can be easily and rapidly turned on and off while also offering a reagent and waste-free procedure. Obviously, an important attribute of any 'molecular machine' is that for the submolecular motion to be useful it must be detectable through some change in the system's

(5) For reviews on the development of interlocked molecules as molecular machines, see: (a) Balzani, V.; Gómez-López, M.; Stoddart, J. F. *Acc. Chem. Res.* **1998**, *31*, 405−414. (b) Sauvage, J.-P. *Acc. Chem. Res.* **1998**, *31*, 611−619. (c) Chambron, J.-C.; Sauvage, J.-P. *Chem. Eur. J.* **1998**, *4*, 1362−1366. (d) Balzani, V.; Credi, A.; Raymo, F. M.; Stoddart, J. F. *Angew. Chem., Int. Ed.* **2000**, *39*, 3348−3391. (e) Asfari, Z.; Vicens, J. *J. Inclusion Phenom. Macro. Chem.* **2000**, *36*, 103−118. (f) Pease, A. R.; Jeppesen, J. O.; Stoddart, J. F.; Luo, Y.; Collier, C. P.; Heath, J. R. *Acc. Chem. Res.* **2001**, *34*, 433−444. (g) Ballardini, R.; Balzani, V.; Credi, A.; Gandolfi, M. T.; Venturi, M. *Acc. Chem. Res.* **2001**, *34*, 445−455. (h) Collin, J.-P.; Dietrich-Buchecker, C.; Gaviña, P.; Jimenez-Molero, M. C.; Sauvage, J.-P. *Acc. Chem. Res.* **2001**, *34*, 477−487. (i) *Molecular Machines and Motors*: *Structure and Bonding*; Sauvage, J.-P., Ed.; Springer: Berlin, 2001;Vol. 99. (j) Venturi, M.; Credi, A.; Balzani, V. *Molecular Devices and Machines—A Journey into the Nanoworld*, Wiley-VCH: Weinheim, 2003.

(6) "Co-conformation" refers to the relative positions of the mechanically interlocked components with respect to each other, see: Fyfe, M. C. T.; Glink, P. T.; Menzer, S.; Stoddart, J. F.; White, A. J. P.; Williams, D. J. *Angew. Chem., Int. Ed. Engl.* **1997**, *36*, 2068−2070. Energy differences between two translational isomers or co-conformations of greater than 1.18 kcal mol^{-1} imply >90% station occupancy for the more favored site at 298 K.

(7) For examples of chemically responsive molecular shuttles, see: (a) Lane, A. S.; Leigh, D. A.; Murphy, A. *J. Am. Chem. Soc.* **1997**, *119*, 11092−11093. (b) Martínez-Díaz, M.-V.; Spencer, N.; Stoddart, J. F. *Angew. Chem., Int. Ed. Engl.* **1997**, *36*, 1904−1907. (c) Gong, C.; Gibson, H. W. *Angew. Chem., Int. Ed. Engl.* **1997**, *36*, 2331−2333. (d) Ashton, P. R.; Ballardini, R.; Balzani, V.; Baxter, I.; Credi, A.; Fyfe, M. C. T.; Gandolfi, M. T.; Gómez-López, M.; Martínez-Díaz, M.-V.; Piersanti, A.; Spencer, N.; Stoddart, J. F.; Venturi, M.; White, A. J. P.; Williams, D. J. *J. Am. Chem. Soc.* **1998**, *120*, 11932−11942. (e) Jiménez, M. C.; Dietrich-Buchecker, C.; Sauvage, J.-P *Angew. Chem., Int. Ed.* **2000**, *39*, 3284−3287. (f) Lee, J. W.; Kim, K.; Kim, K. *Chem. Commun.* **2001**, 1042−1043. (g) Elizarov, A. M.; Chiu, S.-H.; Stoddart, J. F. *J. Org. Chem.* **2002**, *67*, 9175−9181. (h) Jimenez-Molero, M. C.; Dietrich-Buchecker, C.; Sauvage, J.-P. *Chem. Eur. J.* **2002**, *8*, 1456−1466. (i) Da Ross, T.; Guldi, D. M.; Farran Morales, A.; Leigh, D. A.; Prato, M.; Turco, R. *Org. Lett.* **2003**, *5*, 689−691. (j) Tseng, H.-R.; Vignon, S. A.; Stoddart, J. F. *Angew. Chem., Int. Ed.* **2003**, *42*, 1491−1495.

(8) For examples of photochemically responsive molecular shuttles, see: (a) Benniston, A. C. *Chem. Soc. Rev.* **1996**, *25*, 427−435. (b) Murakami, H.; Kawabuchi, A.; Kotoo, K.; Kunitake, M.; Nakashima, N. *J. Am. Chem. Soc.* **1997**, *119*, 7605−7606. (c) Blanco, M.-J.; Jiménez, M. C.; Chambron, J.-C.; Heitz, V.; Linke, M.; Sauvage, J.-P *Chem. Soc. Rev.* **1999**, *28*, 293−305. (d) Ashton, P. R.; Ballardini, R.; Balzani, V.; Credi, A.; Dress, K. R.; Ishow, E.; Kleverlaan, C. J.; Kocian, O.; Preece, J. A.; Spencer, N.; Stoddart, J. F.; Venturi, M.; Wenger, S. *Chem. Eur. J.* **2000**, *6*, 3558−3574. (e) Wurpel, G. W. H.; Brouwer, A. M.; van Stokkum, I. H. M.; Farran, A.; Leigh, D. A. *J. Am. Chem. Soc.* **2001**, *123*, 11327−11328. (f) Brouwer, A. M.; Frochot, C.; Gatti, F. G.; Leigh, D. A.; Mottier, L.; Paolucci, F.; Roffia, S.; Wurpel, G. W. H. *Science* **2001**, *291*, 2124−2128. (g) Stanier, C. A.; Alderman, S. J.; Claridge, T. D. W.; Anderson, H. L. *Angew. Chem., Int. Ed.* **2002**, *41*, 1769−1772. (h) Altieri, A.; Bottari, G.; Dehez, F.; Leigh, D. A.; Wong, J. K. Y.; Zerbetto, F. *Angew. Chem., Int. Ed.* **2003**, *42*, in press.

(9) For examples of electrochemically responsive molecular shuttles, see ref 8a and the following: (a) Bissell, R. A.; Córdova, E.; Kaifer, A. E.; Stoddart, J. F. *Nature* **1994**, *369*, 133−136. (b) Anelli, P.-L.; Asakawa, M.; Ashton, P. R.; Bissell, R. A.; Clavier, G.; Górski, R.; Kaifer, A. E.; Langford, S. J.; Mattersteig, G.; Menzer, S.; Philp, D.; Slawin, A. M. Z.; Spencer, N.; Stoddart, J. F.; Tolley, M. S.; Williams, D. J. *Chem. Eur. J.* **1997**, *3*, 1113−1135. (c) Collin, J.-P.; Gaviña, P.; Sauvage, J.-P. *New J. Chem.* **1997**, *21*, 525−528. (d) Armaroli, N.; Balzani, V.; Collin, J.-P.; Gaviña, P.; Sauvage, J.-P.; Ventura, B. *J. Am. Chem. Soc.* **1999**, *121*, 4397−4408. (e) Ballardini, R.; Balzani, V.; Dehaen, W.; Dell'Erba, A. E.; Raymo, F. M.; Stoddart, J. F.; Venturi, M. *Eur. J. Org. Chem.* **2000**, 591−602.

(10) For examples of the use of electrical and electrochemical stimuli to control ring rotation in catenanes, catenates, and rotaxanes, see: (a) Amabilino, D. B.; Dietrich-Buchecker, C. O.; Livoreil, A.; Pérez-García, L.; Sauvage, J.-P.; Stoddart, J. F. *J. Am. Chem. Soc.* **1996**, *118*, 3905−3913. (b) Cárdenas, D. J.; Livoreil, A.; Sauvage, J.-P. *J. Am. Chem. Soc.* **1996**, *118*, 11980−11981. (c) Livoreil, A.; Sauvage, J.-P.; Armaroli, N.; Balzani, V.; Flamigni, L.; Ventura, B. *J. Am. Chem. Soc.* **1997**, *119*, 12114−12124. (d) Asakawa, M.; Ashton, P. R.; Balzani, V.; Credi, A.; Hamers, C.; Mattersteig, G.; Montalti, M.; Shipway, A. N.; Spencer, N.; Stoddart, J. F.; Tolley, M. S.; Venturi, M.; White, A. J. P.; Williams, D. J. *Angew. Chem., Int. Ed. Engl.* **1998**, *37*, 333−337. (e) Raehm, L.; Kern, J.-M.; Sauvage, J.-P. *Chem. Eur. J.* **1999**, *5*, 3310−3317. (f) Collier, C. P.; Mattersteig, G.; Wong, E. W.; Luo, Y.; Beverly, K.; Sampaio, J.; Raymo, F. M.; Stoddart, J. F.; Heath, J. R. *Science* **2000**, *289*, 1172−1175. (g) Asakawa, M.; Higuchi, M.; Mattersteig, G.; Nakamura, T.; Pease, R.; Raymo, F. M.; Shimizu, T.; Stoddart, J. F. *Adv. Mater.* **2000**, *12*, 1099−1102. (h) Bermudez, V.; Capron, N.; Gase, T.; Gatti, F. G.; Kajzar, F.; Leigh, D. A.; Zerbetto, F.; Zhang, S. *Nature* **2000**, *406*, 608−611. (i) Ashton, P. R.; Baldoni, V.; Balzani, V.; Credi, A.; Hoffmann, H. D. A.; Martínez-Díaz, M.-V.; Raymo, F. M.; Stoddart, J. F.; Venturi, M. *Chem. Eur. J.* **2001**, *7*, 3482−3493.

(11) For examples of the use of electrochemical stimuli to control threading and dethreading in pseudorotaxanes and other host−guest systems, see: (a) Bernardo, A. R.; Stoddart, J. F.; Kaifer, A. E. *J. Am. Chem. Soc.* **1992**, *114*, 10624−10631. (b) Collin, J.-P.; Gaviña, P.; Sauvage, J.-P. *Chem. Commun.* **1996**, 2005−2006. (c) Asakawa, M.; Ashton, P. R.; Balzani, V.; Credi, A.; Mattersteig, G.; Matthews, O. A.; Montalti, M.; Spencer, N.; Stoddart, J. F.; Venturi, M. *Chem. Eur. J.* **1997**, *3*, 1992−1996. (d) Devonport, W.; Blower, M. A.; Bryce, M. R.; Goldenberg, L. M. *J. Org. Chem.* **1997**, *62*, 885−887. (e) Credi, A.; Montalti, M.; Balzani, V.; Langford, S. J.; Raymo, F. M.; Stoddart, J. F. *New. J. Chem.* **1998**, *22*, 1061−1065. (f) Asakawa, M.; Ashton, P. R.; Balzani, V.; Boyd, S. E.; Credi, A.; Mattersteig, G.; Menzer, S.; Montalti, M.; Raymo, F. M.; Ruffilli, C.; Stoddart, J. F.; Venturi, M.; Williams, D. J. *Eur. J. Org. Chem.* **1999**, 985−994. (g) Ashton, P. R.; Balzani, V.; Becher, J.; Credi, A.; Fyfe, M. C. T.; Mattersteig, G.; Menzer, S.; Nielsen, M. B.; Raymo, F. M.; Stoddart, J. F.; Venturi, M.; Williams, D. J. *J. Am. Chem. Soc.* **1999**, *121*, 3951−3957. (h) Cooke, G.; Duclairoir, F. M. A.; Rotello, V. M.; Stoddart, J. F. *Tetrahedron Lett.* **2000**, *41*, 8163−8166. (i) Balzani, V.; Credi, A.; Mattersteig, G.; Matthews, O. A.; Raymo, F. M.; Stoddart, J. F.; Venturi, M.; White, A. J. P.; Williams, D. J. *J. Org. Chem.* **2000**, *65*, 1924−1936. (j) Balzani, V.; Becher, J.; Credi, A.; Nielsen, M. B.; Raymo, F. M.; Stoddart, J. F.; Talarico, A. M.; Venturi, M. *J. Org. Chem.* **2000**, *65*, 1947−1956. (k) Lahav, M.; Shipway, A. N.; Willner, I.; Nielsen, M. B.; Stoddart, J. F. *J. Electroanal. Chem.* **2000**, *482*, 217−221.

(12) Earlier attempts to make redox-active hydrogen-bonded molecular shuttles based on anthraquinone subunits were unsuccessful (Dunnett, J. A. Ph.D. Thesis, University of Manchester Institute of Science and Technology, U.K., 2000).

Chart 1. Molecular Shuttle **1**, Shown as the *succ*-**1** Positional Isomer, and Thread **2**[a]

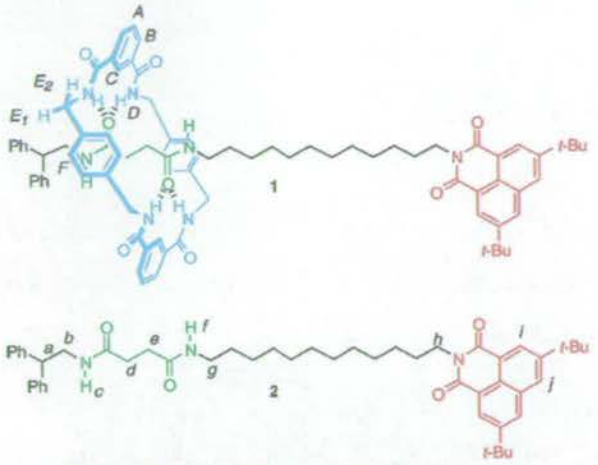

[a] The letters indicate selected nonequivalent ^{1}H environments.

properties. Electrochemistry is also advantageous in this regard since the same stimulus can simultaneously act as both effector and detector of the motion.

Here we report the cyclic voltammetry of **1** and a series of related rotaxanes and threads. The rates and energies obtained from the electrochemical redox experiments are consistent with those obtained photochemically. The spectroscopic and electrochemical behavior of key model compounds is used to show unambiguously that the dynamics observed is a consequence of the position of the macrocycle on the thread changing upon reduction of the naphthalimide unit.

Design

Hydrogen bonds are largely electrostatic in nature,[13] so changes in the electron charge density of a hydrogen-bonding group can have a dramatic effect on its binding ability—a phenomenon exploited in redox-switched molecular recognition[14] and the modulation of protein and peptide structure.[15] Molecular shuttle **1** consists of a benzylic amide macrocycle—a strong hydrogen-bond donor through the amide NH groups—mechanically linked onto a thread molecule, **2**, containing two potential hydrogen-bond acceptor moieties—a succinamide (*succ*) station and a redox-active 3,6-di-*tert*-butyl-1,8-naphthalimide[16] (*ni*) station—separated by a C_{12} aliphatic spacer (Chart 1). The ability of the *succ* station to template formation of the macrocycle by a five-component 'clipping' reaction between isophthaloyl dichloride and *p*-xylylene diamine in apolar solvents is well established.[8f] X-ray crystal structures of model succinamide rotaxanes **3** and **4** (Figures 2 and 3) demonstrate an excellent fit between the thread and macrocycle, both in terms of steric interactions and the complementary positioning of the hydrogen-bonding amide groups on the two components. While the structure of **3** shows both intra- and intermolecular hydrogen bonding in the solid state, **4** has a solely intramolecularly hydrogen-bonded structure and is presumably more representative of the hydrogen-bonding motifs adopted by 'isolated' molecules in solution. The macrocycle adopts a near-perfect chair conformation, driven by formation of two sets of bifurcated hydrogen bonds between the amide protons of each isophthalamide moiety and the succinamide carbonyl oxygens.

The choice of a substituted naphthalimide unit as the redox-active station was inspired by the work of Smith[14b] and Rotello.[14c,e,f] Imides are comparatively poor hydrogen-bond acceptors;[17] indeed, threads containing just the naphthalimide

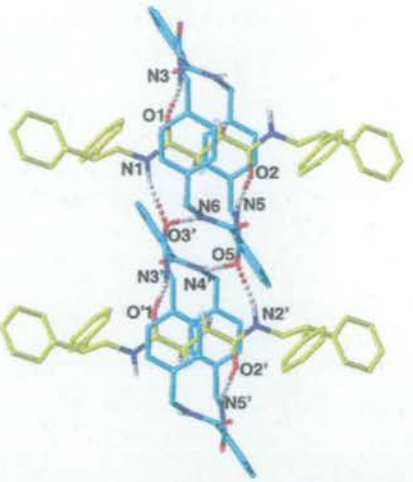

Figure 2. X-ray crystal structure of [2]rotaxane **3** (for clarity carbon atoms of the macrocycle are shown in blue and the carbon atoms of the thread are shown in yellow; oxygen atoms are depicted in red, nitrogen atoms in dark blue, and amide protons in white). Intramolecular hydrogen-bond distances (Å): O1−HN3/O2−HN5 1.88. Intermolecular hydrogen-bond distances (Å): O5−HN4′/ O3′-HN6 2.0, O3′-HN1/O5−HN2′ 2.21.

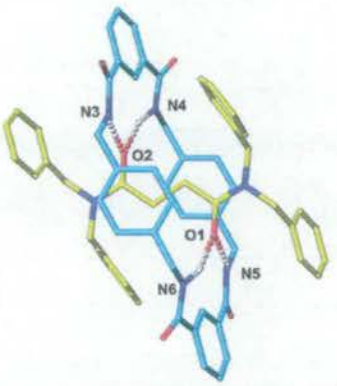

Figure 3. X-ray crystal structure of [2]rotaxane **4**. Intramolecular hydrogen-bond distances (Å): O2−HN3/O1−HN5 1.90, O2−HN4/O1−HN6 2.01.

(13) Morokuma, K. *Acc. Chem. Res.* **1977**, *10*, 294−300.
(14) See, for example: (a) Brooksby, P. A.; Hunter, C. A.; McQuillan, A. J.; Purvis, D. H.; Rowan, A. E.; Shannon, R. J.; Walsh, R. *Angew. Chem., Int. Ed. Engl.* **1994**, *33*, 2489−2491. (b) Ge, Y.; Lilienthal, R.; Smith, D. K. *J. Am. Chem. Soc.* **1996**, *118*, 3976−3977. (c) Deans, R.; Niemz, A.; Breinlinger, E. C.; Rotello, V. M. *J. Am. Chem. Soc.* **1997**, *119*, 10863−10864. (d) Boulas, P. L.; Gómez-Kaifer, M.; Echegoyen, L. *Angew. Chem., Int. Ed. Engl.* **1998**, *37*, 216−247. (e) Niemz, A.; Rotello, V. M. *Acc. Chem. Res.* **1999**, *32*, 44−52. (f) Boal, A. K.; Rotello, V. M. *J. Am. Chem. Soc.* **1999**, *121*, 4914−4915. (g) Ge, Y.; Miller, L.; Ouimet, T.; Smith, D. K *J. Org. Chem.* **2000**, *65*, 8831−8838. (h) Ge, Y.; Smith, D. K. *Anal. Chem.* **2000**, *72*, 1860−1865. (i) Carr, J. D.; Coles, S. J.; Hursthouse, M. B.; Light, M. E.; Tucker, J. H. R.; Westwood, J. *Angew. Chem., Int. Ed.* **2000**, *39*, 3296−3299. (j) Tucker, J. H. R.; Collinson, S. R. *Chem. Soc. Rev.* **2002**, *31*, 147−156. (k) Cooke, G.; Rotello, V. M. *Chem. Soc. Rev.* **2002**, *31*, 275−286.
(15) See, for example: (a) Schenck, H. L.; Dado, G. P.; Gellman, S. H. *J. Am. Chem. Soc.* **1996**, *118*, 12487−12494. (b) Pascher, T.; Chesick, J. P.; Winkler, J. R.; Gray, H. B. *Science* **1996**, *271*, 1558−1560.
(16) The *tert*-butyl substituents provide the steric bulk necessary to stopper the rotaxane while only slightly altering the redox potential of the naphthalimide group ($E_{1/2}$ (**2**) = −1.41 V cf. $E_{1/2}$ (*N*-methyl naphthalimide) = −1.31 V): Viehbeck, A.; Goldberg, M. J.; Kovac, C. A. *J. Electrochem. Soc.* **1990**, *137*, 1460−1466.
(17) Jeffrey, G. A. *An Introduction to Hydrogen Bonding*; Oxford University Press: New York, 1997.

Chart 2. Model Rotaxanes **3**–**8** Shown as the *succ*- Positional Isomers[a]

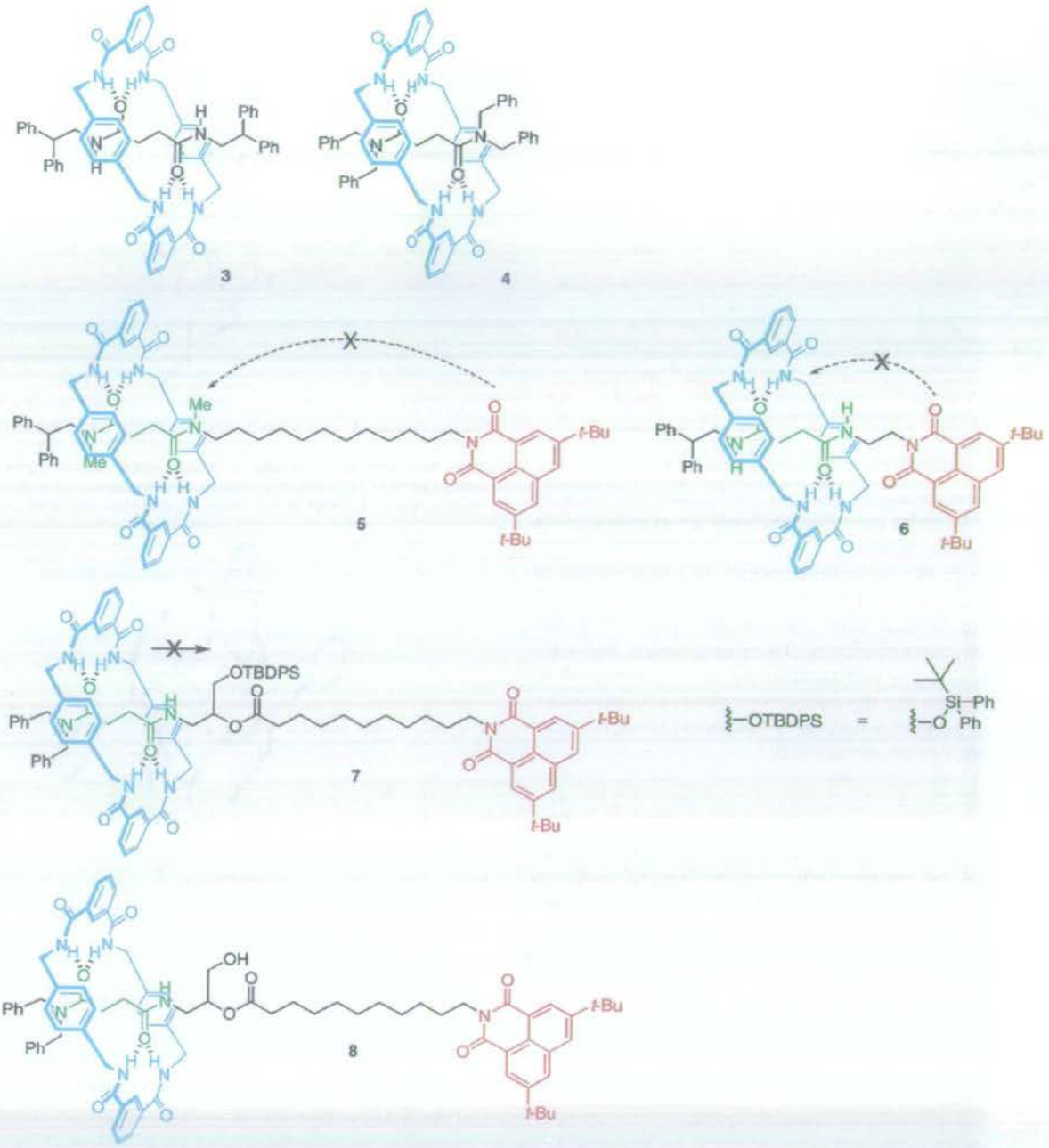

[a] The dashed lines show hydrogen-bond interactions possible in **1** but disallowed in the model compound. Solid lines show changes of co-conformation that require shuttling which are disallowed in the model compound.

unit do not template formation of the benzylic amide macrocycle to give rotaxanes. To minimize its free energy, the macrocycle in **1** must therefore sit over the succinamide station in non-hydrogen-bonding solvents, so that co-conformation *succ*-**1** predominates (Figure 4). One-electron reduction of naphthalimides to the corresponding radical anion, however, results in a substantial increase in electron charge density on the imide carbonyls and a concomitant increase in hydrogen-bond accepting ability.[14b,c,e] In **1**, this change in oxidation state should reverse the relative hydrogen-bonding abilities of the two thread stations so that co-conformation *ni*-$\mathbf{1}^{-\bullet}$ is preferred in the reduced state. This dynamic process was studied in **1** through cyclic voltammetry experiments and ^{1}H NMR spectroscopy. To probe the nature of the stimulated motion, we carried out similar studies on model rotaxanes **5**–**8** (Chart 2). Each of these analogues of **1** is designed to restrict a different type of conformational or co-conformational change so that the true origin of the effects seen for **1** could be unambiguously determined.

Synthesis

Rotaxanes **1**, **5**, and **6** were prepared according to Scheme 1. Treatment of threads **2**, **9**, or **10** with 10 equiv of each of *p*-xylylene diamine and isophthaloyl dichloride ($CHCl_3$, Et_3N,

Scheme 1. Synthesis of Rotaxanes **1**, **5**, and **6**[a]

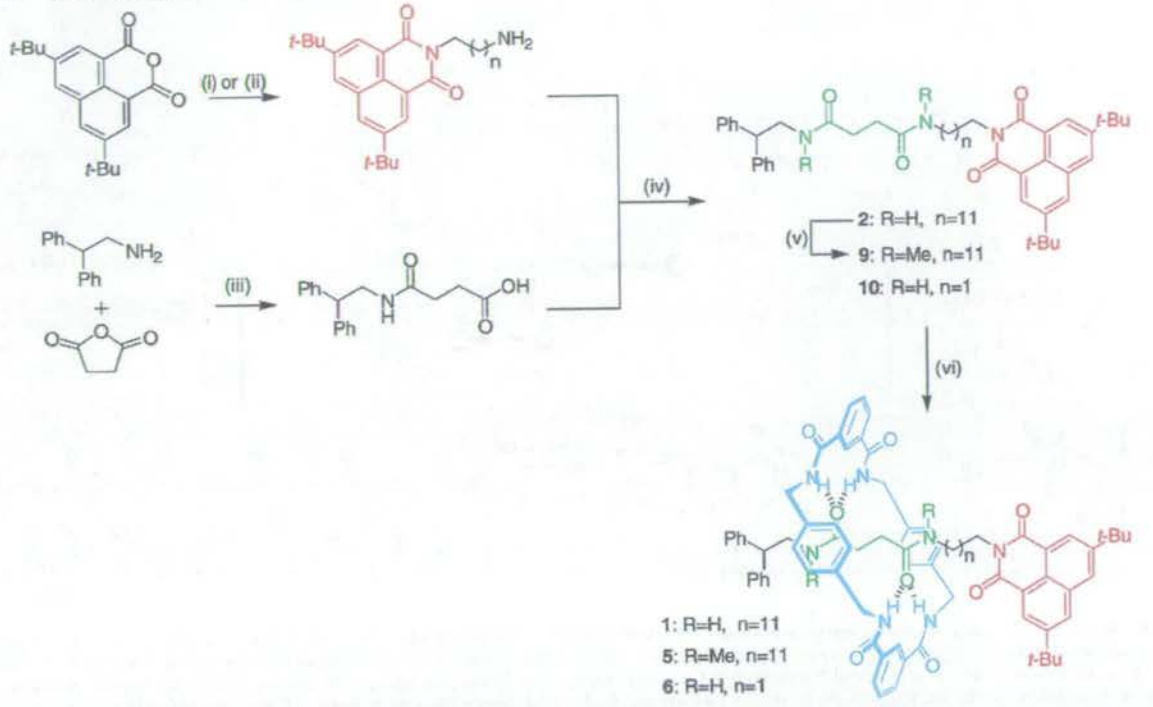

[a] (i) 1,12-Diaminododecane, Et_3N, EtOH, Δ, 14%; (ii) 1,2-ethylenediamine, EtOH, Δ, 78%; (iii) pyridine, AcOH, 90%; (iv) 1-[3-(dimethylamino)propyl]-3-ethylcarbodiimide hydrochloride (EDCI), 4-(dimethylamino)pyridine (DMAP), CH_2Cl_2, 0 °C to RT, 98% (**2**), 93% (**10**); (v) MeI, NaH, THF, 0 °C to RT, 94%; (vi) isophthaloyl dichloride, *p*-xylylene diamine, Et_3N, $CHCl_3$, 59% (**1**), 33% (**5**), 62% (**6**).

Scheme 2. Synthesis of Rotaxanes **7** and **8**[a]

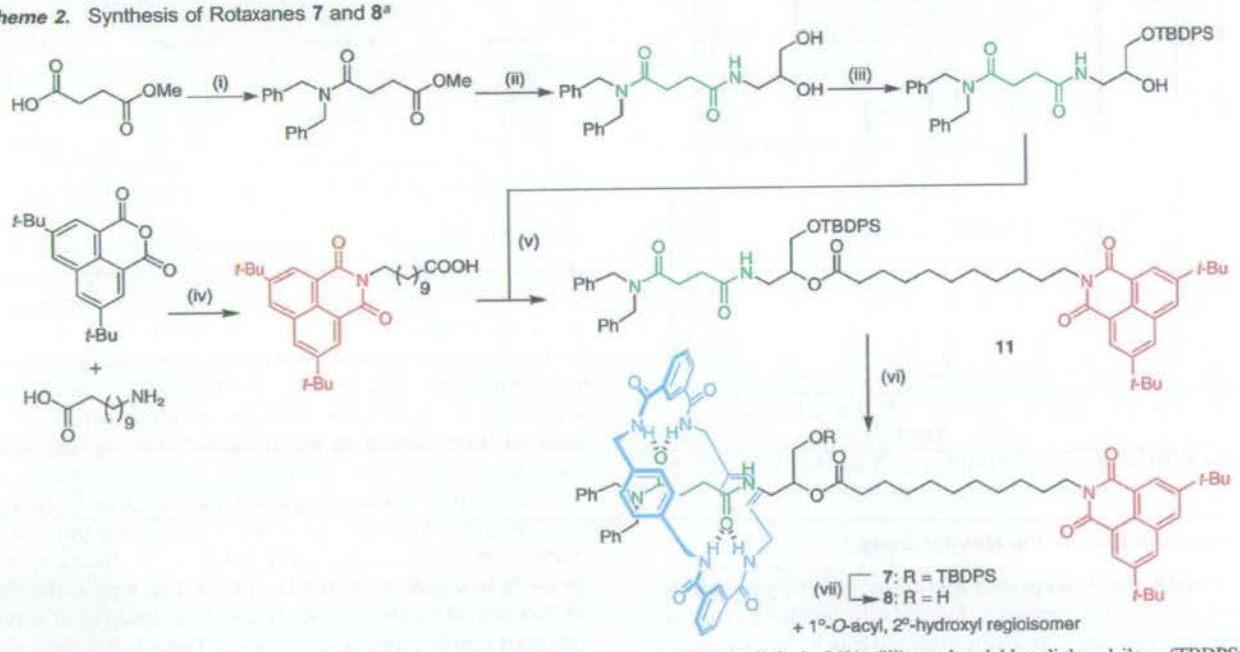

[a] (i) $(PhCH_2)_2NH$, EDCI, DMAP, CH_2Cl_2, 0 °C to RT, 94%; (ii) 3-amino-propane-1,2-diol, Δ, 84%; (iii) *tert*-butylchlorodiphenylsilane (TBDPSCl), imidazole, DMAP, CH_2Cl_2, 62%; (iv) pyridine, Δ, 60%; (v) EDCI, DMAP, CH_2Cl_2, 0 °C to RT, 90%; (vi) isophthaloyl dichloride, *p*-xylylene diamine, Et_3N, $CHCl_3$, 23%; (vii) CH_2Cl_2, tetrabutylammonium fluoride (TBAF), 70%.

4 h, high dilution) provided [2]rotaxanes **1**, **5**, and **6** in 59%, 33%, and 62% yields, respectively. Scheme 2 shows the synthesis of 'gate-closed' thread **11** which, under similar rotaxane-forming conditions, furnished [2]rotaxane **7** in 23% yield. The 'gate-opened' rotaxane **8** was obtained by treatment of **7** with a stoichiometric amount of tetra-*n*-butylammonium fluoride in CH_2Cl_2.[18]

(18) 'Gate-opened' rotaxane **8** was obtained together with the 1°-*O*-acyl, 2°-hydroxyl regioisomer from which it was not separated.

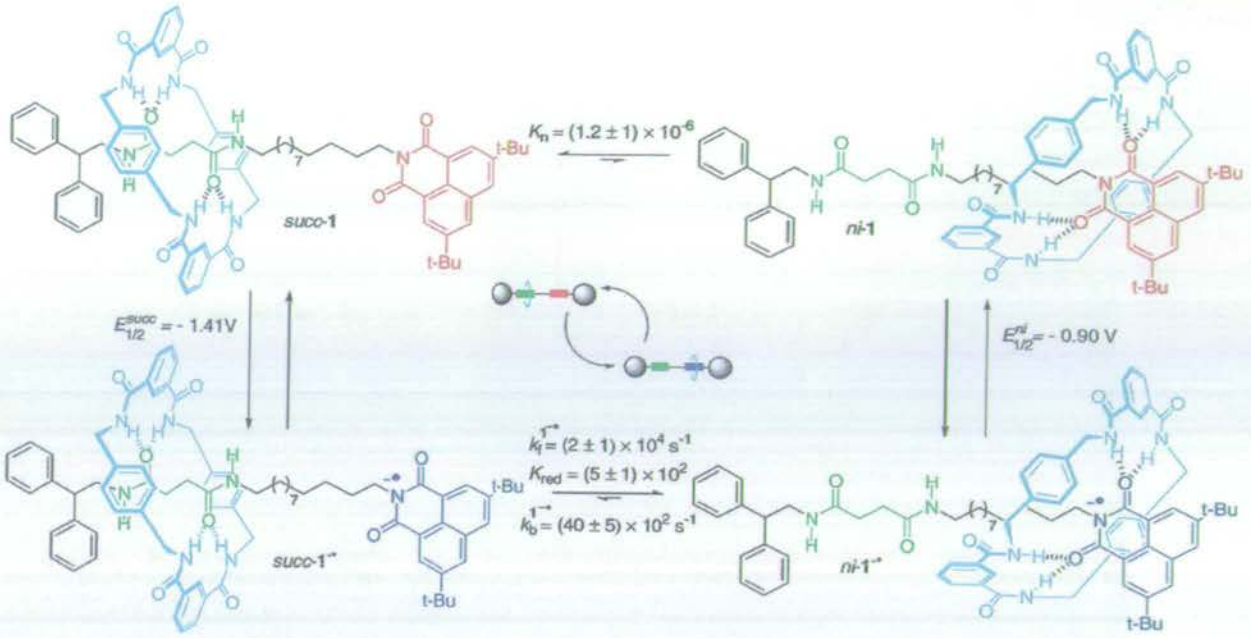

Figure 4. An electrochemically switchable, hydrogen-bonded molecular shuttle **1**. In the neutral state, the translational co-conformation *succ*-**1** is predominant as the *ni* station is a poor hydrogen-bond acceptor ($K_n = (1.2 \pm 1) \times 10^{-6}$). Upon reduction, the equilibrium between *succ*-**1**$^{\cdot-}$ and *ni*-**1**$^{\cdot-}$ is altered ($K_{red} = (5 \pm 1) \times 10^2$) because *ni*$^{\cdot-}$ is a powerful hydrogen-bond acceptor. Upon reoxidation, the macrocycle shuttles back to its original position. Repeated reduction and oxidation causes the macrocycle to shuttle forward and backward between the two stations. All the values shown refer to experiments in anhydrous THF at 298 K with tetrabutylammonium hexafluorophosphate as the supporting electrolyte.

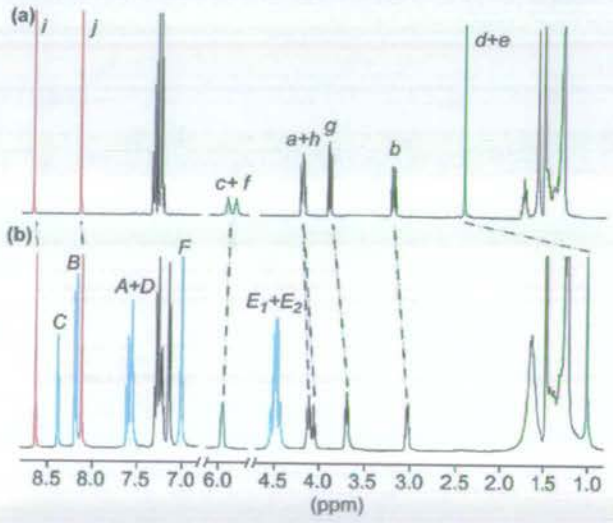

Figure 5. ^{1}H NMR spectra (400 MHz) of (a) **2** and (b) **1** in $CDCl_3$ at 298 K. The letters correspond to the assignments shown in Chart 1.

Co-conformation in the Neutral State

^{1}H NMR spectroscopy is a useful tool for studying translational isomerism in rotaxanes. For benzylic amide macrocycle-containing rotaxanes, aromatic ring currents in the *p*-xylylene rings result in significant upfield shifting (typically $\Delta\delta_H > 1$ ppm) for protons on the portion of the thread covered by the macrocycle.[19] Comparison of the ^{1}H NMR spectra of rotaxane **1** and the corresponding thread **2** in $CDCl_3$ (Figure 5) shows such an upfield shift for succinic methylene protons H_d and H_e ($\Delta\delta_H = -1.45$ ppm).[20] Protons in close proximity to the *succ* station (H_a, H_b, and H_g) are also shielded but to a lesser extent; all other thread protons, including those of the naphthalimide, are essentially unaffected by the presence of the macrocycle. The infrared spectrum of **1** in $CHCl_3$ also shows no changes in the CO stretching band of the naphthalimide moiety compared to the spectrum of **2** ($\nu_{CO_{stretch}} = 1780$ cm^{-1} in each case), suggesting no significant hydrogen bonding occurs to the naphthalimide subunit in the rotaxane.[8f] Clearly the *succ*-**1** translational isomer is the predominant structure in chloroform.

Table 1. Solvent Effects on Chemical Shifts (δ_H) and Differential Chemical Shifts ($\Delta\delta_H$) for Succinamide Protons in **1** and **2**

	NH_c and NH_f		H_d and H_e
solvent	δH (**1**)/ppm	δH (**2**)/ppm	$\Delta\delta$H/ppm
$CDCl_3$	5.95	5.73; 5.61	−1.45
d_3-MeCN[a]	6.47; 6.42	6.42; 4.22	−1.2
d_8-THF	7.84; 7.63	7.20; 7.12	−1.2
d_6-DMSO	7.92; 7.40	7.78; 7.60	−0.7

[a] Spectra collected at 329 K due to low solubility of **1** in d_3-MeCN.

In fact, unlike peptide-based molecular shuttles,[7a] the positional integrity of the macrocycle in **1** is remarkably independent of the nature of the solvent. The difference in chemical shifts for methylene protons H_d and H_e in **1** and **2** as well as the shifts for succinamide amide protons H_c and H_f in solvents of varying hydrogen-bonding ability are shown in Table 1. The increasing δ_H values for the amide protons illustrate the ability of these solvents to disrupt hydrogen bonding ($CDCl_3$ < d_3-MeCN < d_8-THF < d_6-DMSO). It can be seen, however, that in $CDCl_3$, d_3-MeCN, and d_8-THF, shielding of the *succ* methylene protons is virtually unchanged, indicating that positional integrity of the

(19) Johnston, A. G.; Leigh, D. A.; Murphy, A.; Smart, J. P.; Deegan, M. D. *J. Am. Chem. Soc.* **1996**, *118*, 10662−10663.

(20) Dilution experiments demonstrated that intermolecular hydrogen-bonding interactions were absent at concentrations of 10 mmol L^{-1} and below for the current rotaxanes and threads. All NMR spectra discussed were therefore collected at this standard concentration.

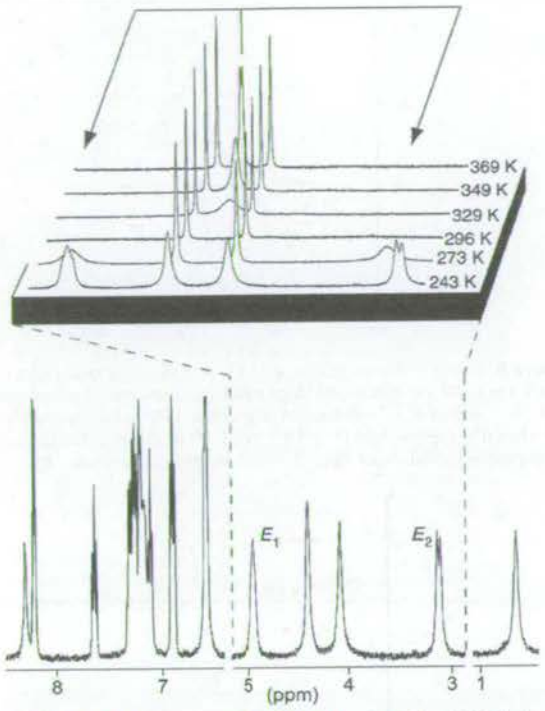

Figure 6. ^{1}H NMR spectrum of **4** (400 MHz, $CDCl_3$) at 243 K showing slow pirouetting of the macrocycle about the thread (H_{E1} and H_{E2} resolved). SPT-SIR between resolved signals gives the energy barrier for macrocycle pirouetting. Higher temperature spectra (expansion, 243−296 K ($CDCl_3$) and 329−369 K ($C_2D_2Cl_4$)) illustrate the wide temperature ranges that can exist between full resolution and coalescence of signals affected by the dynamic processes.

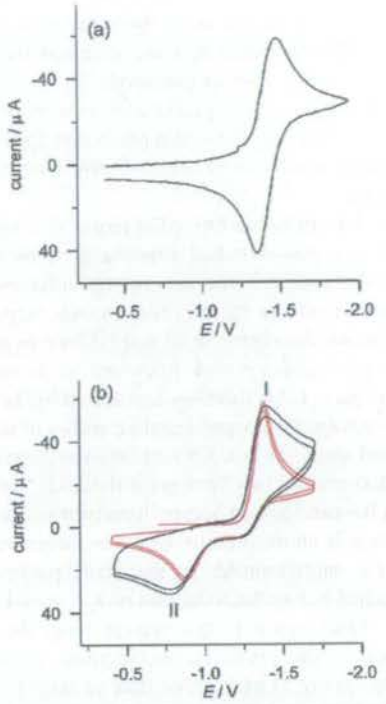

Figure 7. Cyclic voltammograms at 298 K of (a) **2** and (b) **1** showing both experimental (black line) and simulated (red line) results. Experiments carried out on 1 mmol L^{-1} solutions of substrate in anhydrous THF with tetrabutylammonium hexafluorophosphate (5×10^{-2} mol L^{-1}) as electrolyte and ferrocene as internal standard. Scan rate: 2 V s^{-1}. Working electrode: Pt.

shuttle is maintained in all three solvents. Even in d_6-DMSO the upfield shift for H_d and H_e is only reduced by ≈50%, indicating that even in this strongly hydrogen-bond-disrupting solvent the macrocycle still spends a significant amount of time over the *succ* station.

The energy barrier for pirouetting of the macrocycle around the thread provides a definitive measure of the strength of the intercomponent interactions.[21] Due to the complexity of the ^{1}H NMR spectra of **1** and its analogues, this process was studied in the simpler, C_2-symmetric, rotaxanes **3** and **4** as models for shuttles **1** and **5**, respectively. Variable-temperature (VT) ^{1}H NMR experiments in $CDCl_3$ and $C_2D_2Cl_4$ (because of the wide temperature range involved) using both the coalescence method[22] and spin polarization transfer by selective inversion recovery (SPT-SIR)[23] were employed to calculate the rates of macrocycle pirouetting. The VT ^{1}H NMR plot for **4** (Figure 6) shows the signals for macrocycle benzylic methylene protons E_1 and E_2 are well separated at 243 K, while a single sharp peak is observed at 369 K.[24] SPT-SIR of **4** gives an energy barrier for macrocycle pirouetting at 298 K of 12.9 ± 0.1 kcal mol^{-1}. Similarly, the barrier for **3** was determined as 11.2 ± 0.1 kcal mol^{-1} at 298 K. Even when compared to the fumaramide template which holds the hydrogen-bond acceptor groups of the thread in a close-to-ideal arrangement for the donor groups in the macrocycle ($\Delta G_{298}^{\ddagger}$ for the fumaramide analogue of **3** = 13.4 ± 0.1 kcal mol^{-1})[21b] it can be seen that the succinic templates in **3** and **4** result in strong intercomponent hydrogen bonding. Clearly, dissociation from the succinamide station in a molecular shuttle will involve a significant energy barrier.

Redox-Switched Shuttling

Translocation of the macrocycle in **1** could be readily triggered by electrochemical reduction of the naphthalimide station to its radical anion. Since the changes in hydrogen-bonding pattern affect the electrochemical properties of the system, the shuttling process could be both effected and observed in cyclic voltammetry (CV) experiments of **1** and its analogues and components.[25] The CV response of **2** in anhydrous THF (Figure 7a) exhibits a reversible, one-electron reduction peak corresponding to reduction and reoxidation of the naphthalimide group (**2**/**2**$^{-\bullet}$, $E_{1/2} = -1.41$ V).[16] Rotaxane **1**, on the other hand, displays a similar cathodic signal, **I** (E_c =

(21) For examples of macrocycle pirouetting in benzylic amide macrocycle-based [2]rotaxanes, see ref 10h and the following: (a) Leigh, D. A.; Murphy, A.; Smart, J. P.; Slawin, A. M. Z. *Angew. Chem., Int. Ed. Engl.* **1997**, *36*, 728−732. (b) Gatti, F. G.; Leigh, D. A.; Nepogodiev, S. A.; Slawin, A. M. Z.; Teat, S. J.; Wong, J. K. Y. *J. Am. Chem. Soc.* **2001**, *121*, 5983−5989. (c) Gatti, F. G.; León, S.; Wong, J. K. Y.; Bottari, G.; Altieri, A.; Farran Morales, A. M.; Teat, S. J.; Frochot, C.; Leigh, D. A.; Brouwer, A. M.; Zerbetto, F. *Proc. Natl. Acad. Sci. U.S.A.* **2003**, *100*, 10−14.

(22) Sandström, J. *Dynamic NMR Spectroscopy*; Academic Press: London, 1982.

(23) Dahlquist, F. W.; Longmur, K. J.; Du Vernet, R. B. *J. Magn. Reson.* **1975**, *17*, 406−413. For applications of SPT-SIR to dynamic processes in rotaxanes, see, for example: Clegg, W.; Gimenez-Saiz, C.; Leigh, D. A.; Murphy, A.; Slawin, A. M. Z.; Teat, S. J. *J. Am. Chem. Soc.* **1999**, *121*, 4124−4129. For an example of how the SPT-SIR experiments were performed for the current systems, see the Supporting Information.

(24) Due to the wide temperature range, spectra were collected in $CDCl_3$ from 243 to 296 K and in $C_2D_2Cl_4$ from 329 to 369 K.

(25) Cyclic voltammetry was carried out on 10^{-3} mol L^{-1} solutions of substrate in anhydrous THF with tetrabutylammonium hexafluorophosphate (TBHF, 5×10^{-2} mol L^{-1}) as electrolyte and ferrocene as internal standard. The invariance of the chemical shift for amide protons of **1** and **2** in d_8-THF in the presence of TBHF at 5×10^{-2} mol L^{-1} suggests that the electrolyte does not significantly affect amide−amide intramolecular hydrogen bonds at these concentrations.

−1.40 V, at 2 V s^{-1}), yet lacks the corresponding oxidation peak (Figure 7b). Rather, a new one-electron anodic peak, **II**, appears toward more positive potentials ($E_a = -0.89$ V, at 2 V s^{-1}). On subsequent scans, performed without renewal of the diffusion layer, it is only these two peaks that appear, indicating that the system returns to its original state after each cycle on this time scale.

These results can be interpreted in terms of a standard square scheme for a redox-switched binding process whereby the reversible translational isomerism equilibria for each oxidation state are connected via the electron-transfer steps (Figure 4). As shown earlier, the shuttle in its neutral state overwhelmingly adopts co-conformation *succ*-**1**. Reduction of the naphthalimide group to give *succ*-$\mathbf{1}^{-\bullet}$ is therefore unaffected by the macrocycle. Due to the increased hydrogen-bonding ability of naphthalimide in its reduced state, the equilibrium between co-conformations in this oxidation state lies far toward the *ni*-$\mathbf{1}^{-\bullet}$ isomer so that shuttling of the macrocycle occurs. Resultant hydrogen bonding to the macrocycle amide protons stabilizes the increased electron charge on the naphthalimide so that more positive potentials must be reached before the oxidation *ni*-$\mathbf{1}^{-\bullet} \rightarrow$ *ni*-**1** occurs ($\Delta E_p = 0.51$ V). Once again in the neutral state, the macrocycle shuttles back to the preferred succinamide station therefore restoring the system to its original state as *succ*-**1**. The absence of any *succ*-$\mathbf{1}^{-\bullet} \rightarrow$ *succ*-**1** oxidation peak or *ni*-**1** $\rightarrow$ *ni*-$\mathbf{1}^{-\bullet}$ reduction peak demonstrates the remarkable positional integrity of the shuttle in both oxidation states while also indicating that the shuttling process is rapid on the time scale of the experiment.

The CV curve of **1** was simulated (Figure 7b). Fitting with the experimental results allowed calculation of the redox potential for the electron-transfer process *ni*-$\mathbf{1}^{-\bullet} \rightleftharpoons$ *ni*-**1** as $E_{1/2}^{ni} = -0.90$ V. Also obtained were the rate constants in the reduced state for the forward shuttling process (*succ*-$\mathbf{1}^{-\bullet} \rightarrow$ *ni*-$\mathbf{1}^{-\bullet}$; $k_f^{\mathbf{1}-\bullet} = (2 \pm 1) \times 10^4$ s^{-1}; $T = 298$ K, THF) and the backward process (*ni*-$\mathbf{1}^{-\bullet} \rightarrow$ *succ*-$\mathbf{1}^{-\bullet}$; $k_b^{\mathbf{1}-\bullet} = (40 \pm 5) \times 10^2$ s^{-1}; $T = 298$ K, THF). These figures yield a co-conformational equilibrium constant for the reduced state of $K_{red} = (5 \pm 1) \times 10^2$ confirming that the *ni*-$\mathbf{1}^{-\bullet}$ co-conformation is indeed strongly preferred. The *ni*-**1** $\rightarrow$ *succ*-**1** shuttling process occurs faster than the *ni*-$\mathbf{1}^{-\bullet} \rightarrow$ *ni*-**1** oxidative electron-transfer step, so that it is not possible to calculate rate constants for this process.[26] The equilibrium constants in each oxidation state for any such redox-switched binding process are related by eq 1.[27] Accordingly, the constant for the neutral state co-conformational equilibrium was calculated as $K_n = (1.2 \pm 1) \times 10^{-6}$,[28] consistent with the predominance of the *succ*-**1** co-conformation shown by ^{1}H NMR and IR.

$$\Delta E^\circ = E_{1/2}^{\ ni} - E_{1/2}^{\ succ} = \frac{RT}{nF} \ln\left(\frac{K_{red}}{K_n}\right) \qquad (1)$$

Given the fast rate constants for shuttling in the reduced state, a scan rate on the order of 10 kV s^{-1} would be required to observe the *succ*-$\mathbf{1}^{-\bullet} \rightarrow$ *succ*-**1** oxidation before shuttling to *ni*-$\mathbf{1}^{-\bullet}$ occurs. Such high scan rates are not achievable with **1** due to the high resistivity of THF solutions. An alternative strategy is to run the experiments at low temperatures to slow the shuttling motion. Indeed, at 213 K, the cathodic peak, **I**, for reduction of the *succ*-**1** species exhibits an anodic counterpart, **III**, while the intensity of anodic peak **II** is correspondingly reduced (Figure 8). The even greater resistivity at this temperature prevents the use of higher scan rates to oxidize all *succ*-$\mathbf{1}^{-\bullet}$ species before shuttling occurs.

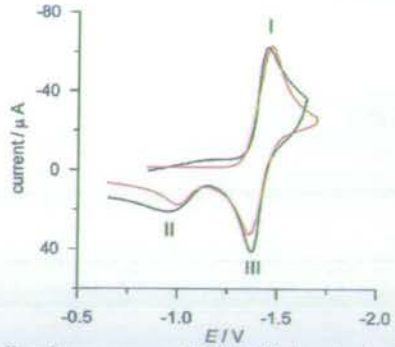

Figure 8. Cyclic voltammograms at 213 K of **1** showing both experimental (black line) and simulated (red line) results. Experiments carried out on 1 mmol L^{-1} solutions of substrate in anhydrous THF with tetrabutylammonium hexafluorophosphate (5×10^{-2} mol L^{-1}) as electrolyte and ferrocene as internal standard. Scan rate: 2 V s^{-1}. Working electrode: Pt.

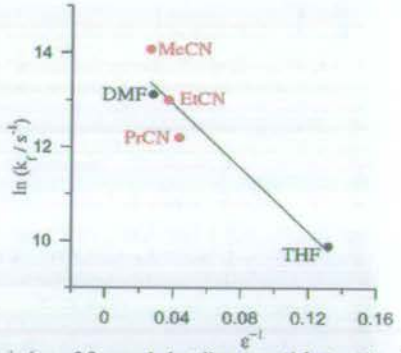

Figure 9. Variation of forward shuttling rate ($k_f^{\mathbf{1}-\bullet}$) with relative permittivity, ϵ, of solvent. Data points in black are calculated from experiments using an electrochemical stimulus; data points in red are calculated from experiments using a photochemical stimulus.[8f] All experiments were carried out at 298 K.

Simulation of the low-temperature CV curve (Figure 8) indicated, as expected, that the rate constant for forward shuttling in the reduced state is much lower than that at room temperature ($k_f^{\mathbf{1}-\bullet} \approx 1$ s^{-1}; $T = 213$ K, THF). By repeating the simulation at various temperatures and subjecting the results to an Eyring plot analysis, the following activation parameters for the shuttling process in the reduced state were obtained: $\Delta H^\ddagger = 14.0 \pm 0.6$ kcal mol^{-1}, $\Delta S^\ddagger = 8.7 \pm 2$ cal K^{-1} mol^{-1} and $\Delta G_{298}^{\ddagger} = 11.4 \pm 1.2$ kcal mol^{-1}.

The electrochemical results are consistent with the photochemically induced shuttling experiments carried out in alkylnitrile solutions.[8f] Unfortunately, when carrying out the electrochemistry experiments in acetonitrile, adsorption phenomena at the electrodes prevented any analysis of the curves and therefore any direct comparison of the two stimuli in the same solvent. The electrochemical measurements were instead repeated in DMF. Figure 9 compares the forward shuttling rates

(26) On increasing the scan rate from 20 mV s^{-1} to 250 V s^{-1}, the anodic peak II shifts to higher potentials by ≈60 mV/log unit of scan rate, indicating that the oxidation process is kinetically slow. Due to the non-Nernstian nature of the oxidation process, the rate constants relative to the *ni*-**1**/*succ*-**1** shuttling process can therefore not be obtained by fitting of the CV curve. The absence of a cathodic counterpart for peak II at scan rates as high as 250 V s^{-1}, however, allows estimation of $k_b^1 \approx 1.6 \times 10^3$ s^{-1}, so that $k_f^1 \approx 2 \times 10^{-3}$ s^{-1}.

(27) Kaifer, A.; Gómez-Kaifer, M. *Supramolecular Electrochemistry*; Wiley-VCH: Weinheim, 1999.

(28) Assuming $E_{1/2}^{succ} = E_{1/2}$ (**2**) = −1.41 V.

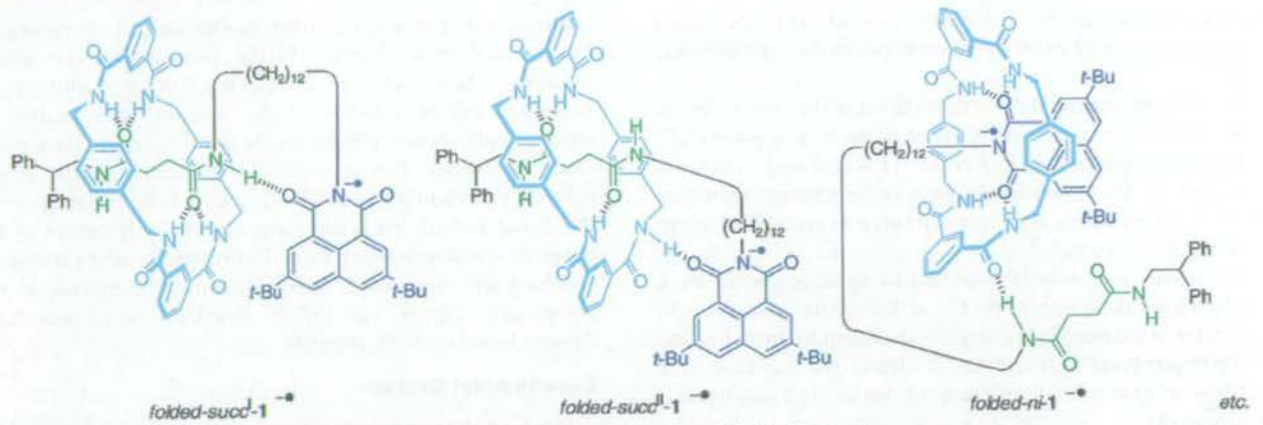

Figure 10. Possible folded co-conformations for reduced rotaxane $\mathbf{1}^{-\bullet}$. In fact, only *folded-ni*-$\mathbf{1}^{-\bullet}$ is a low-energy structure.

calculated from a range of experiments in different solvents using the two stimuli. An approximately linear relationship exists between the rate of shuttling ($k_t^{\mathbf{1}-\bullet}$) and polarity of the medium, suggesting that the nature of the solvent is the main variable affecting the shuttling rates in these experiments (the presence of the supporting electrolytes in the electrochemistry experiments could also play a role, but see ref 25). Pleasingly, the shuttling process in this class of molecular shuttles is independent of the means—light or electrons—used to trigger it.

Is the Redox-Induced Motion Really Shuttling?

It might be argued that hydrogen-bonding interactions between the *ni* station and either the *succ* station or the macrocycle in $\mathbf{1}^{-\bullet}$ could arise from folded conformations (e.g., *folded-succ*^{I}-$\mathbf{1}^{-\bullet}$ and *folded-succ*^{II}-$\mathbf{1}^{-\bullet}$, Figure 10), accounting for the experimental observations without requiring an actual change in the position of the macrocycle on the thread in the reduced rotaxane. To demonstrate unequivocally that the reduction of **1** does, in fact, result in shuttling of the macrocycle between the *succ* and *ni* stations, the electrochemical behavior of model rotaxanes **5**–**8** (Chart 2) was investigated.

'Gate-closed' shuttle **7** incorporates a bulky silyl ether between the two stations which is large enough to preclude any shuttling yet should not prevent the formation of a variety of folded conformations; removal of this group to give **8** restores the possibility of redox-switched shuttling, thus generating a system closely analogous to **1**.

Compared to **1**, rotaxane **6** has a reduced length of alkyl spacer (C_2 in place of C_{12}), thus disallowing folded conformations involving multipoint interactions between the naphthalimide carbonyls and macrocycle amide protons.

In model compound **5**, methylation of the succinamide nitrogens prevents a folded conformation involving hydrogen bonding to these units (i.e., the *succ* unit in **5** can only act as a hydrogen-bond acceptor).

^{1}H NMR spectra of each of **5**–**8** in $CDCl_3$ show that the macrocycle sits over the *succ* station in each case, exactly as observed for **1**. The behavior of these model systems, together with other control experiments and observations, leads to a series of arguments showing that the observed CV effects in **1** are a result of the macrocycle shuttling along the thread.

(i) 'Gate-closed' rotaxane **7** (where shuttling is prohibited) shows a CV response (Figure 11a) identical to that of the thread **2** *not* rotaxane **1**, indicating that there is no hydrogen-bond

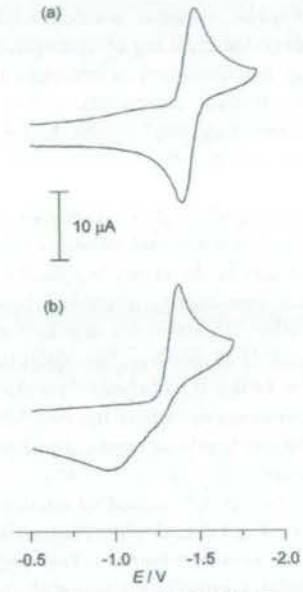

Figure 11. Cyclic voltammograms at 223 K of (a) **7** and (b) **8**. Experiments carried out on 0.5 mmol L^{-1} solutions in DMF with tetraethylammonium tetrafluoroborate (5×10^{-2} mol l^{-1}) as internal standard. Scan rate: 0.5 V s^{-1}. Working electrode: Pt.

stabilization of the naphthalimide radical anion as a result of folding in $\mathbf{7}^{-\bullet}$. However, the 'gate-opened' version **8** shows virtually identical CV behavior (Figure 11b) to rotaxane **1**, the only difference being that the dynamics are over a slightly longer time scale presumably as a result of the branching in the thread providing a small steric barrier to macrocycle translation.

(ii) Model rotaxane **6**, which is too short and rigid to allow multiple hydrogen bonds between the macrocycle and the *ni* station when the macrocycle is situated over the succinamide station, also shows very similar CV behavior to **1**, although over a much shorter time scale, reflecting the smaller amplitude of shuttling that is required.

(iii) Removing the possibility of hydrogen bonding to the amide protons of the *succ* station in **5** does not affect the CV response, suggesting that *all* the hydrogen bonds to the $ni^{-\bullet}$ station come from the macrocycle.

(iv) Molecular modeling studies show that folded conformations of $\mathbf{1}^{-\bullet}$ can only be stabilized by one or two hydrogen bonds from the macrocycle to the *ni* station due to geometrical constraints. Molecular dynamics simulations on such structures

indicate that the macrocycle would still shuttle along the thread in order to form multipoint hydrogen bonds to the naphthalimide unit.[29]

(v) The large anodic shift for reoxidation of the naphthalimide in $\mathbf{1}^{-\bullet}$ indicates extensive stabilization of the radical anion ($\Delta E^{\circ} = 0.51$ V; corresponding to $\Delta G = -11.8$ kcal mol^{-1}). This is equivalent to the formation of three or four strong hydrogen bonds which modeling shows can only arise in geometries where shuttling has occurred.[30]

(vi) If only one or two intramolecular hydrogen bonds were producing the shifts seen in the CV of **1**, a similar process could take place in the thread (**2**) using the succinamide amide protons as hydrogen-bond donors. This is clearly not the case as **2** exhibits an identical CV response to that of its *N*-methylated analogue (**9**).

(vii) For rotaxanes **1**, **5**, and **8** (dynamics in **6** are too fast to measure), more polar solvents accelerate the speed of the process, suggesting that breaking of hydrogen bonds is the rate-determining step, not formation of hydrogen bonds which one might expect in a folding mechanism.

(viii) It is known that alkyl chains fold several orders of magnitude faster than the dynamics observed in the current system.[31]

(ix) Folding a long alkyl chain is entropically unfavorable, and cyclic hydrogen-bonded conformations forming large rings of the type produced in the possible folded conformations of $\mathbf{1}^{-\bullet}$ are not often free energy minima.[32] In comparison, the entropy of activation calculated for shuttling in $\mathbf{1}^{-\bullet}$ ($\Delta S^{\ddagger} = 8.7 \pm 2$ cal K^{-1} mol^{-1}) is positive; the calculated enthalpy of activation ($\Delta H^{\ddagger} = 14.0 \pm 0.6$ kcal mol^{-1}) is also more consistent with a shuttling mechanism, where the rate-determining step is breaking of hydrogen bonds as opposed to forming bonds in a folding mechanism.

(x) The energy barrier determined for shuttling in the reduced state ($\Delta G_{298}^{\ddagger} = 11.4 \pm 1.2$ kcal mol^{-1}) is consistent with known energy barriers for shuttling between two degenerate stations in similar molecular shuttles[7a] and also with the energy barrier for pirouetting of the macrocycle in model rotaxane **3** (see above).

Given that folding cannot account for the multipoint hydrogen bonding that stabilizes the reduced naphthalimide in $\mathbf{1}^{-\bullet}$ nor can it account for the behavior of **8** mirroring that of **1** while that of **7** does not, the only process that satisfies the experimental behavior for these molecules is shuttling. We do not exclude the likelihood that folding occurs in some of these systems to some degree (e.g., *folded-ni*-$\mathbf{1}^{-\bullet}$, Figure 10). Indeed, there is evidence to support this in a few of the low-energy co-conformations identified in modeling studies (see above and ref 29). However, in all these low-energy co-conformations—folded or extended—the macrocycle has shuttled from the *succ* station to the $ni^{-\bullet}$ unit.

Conclusions

The use of electrochemical stimuli to manipulate intercomponent interactions provides a powerful method for both controlling and observing submolecular motion in hydrogen-bonded molecular shuttles. In the present benzylic amide macrocycle-based rotaxane system, the motion resulting from reduction and reoxidation of the naphthalimide station is unequivocally shown to be reversible shuttling of the macrocycle along the thread. This constitutes a molecular shuttle which exhibits remarkable positional integrity of the macrocycle on the thread in both oxidation states and rapid dynamics of the triggered shuttling between them. The simplicity of the structures involved and the process used to control the motion of the components augurs well for the development of molecular devices based on such systems.

Experimental Section

Synthesis. All synthetic procedures are reported in the Supporting Information.

Electrochemistry. Materials. All chemicals used were reagent grade. Tetrabutylammonium hexafluorophosphate (TBHF, Fluka) was used as supporting electrolyte as received. Tetrahydrofuran (LiChrosolv) was treated according to a procedure described elsewhere.[33] For the electrochemical experiments, the solvent was distilled into the electrochemical cell, prior to use, by a trap-to-trap procedure.

Instrumentation and Measurements. The one-compartment electrochemical cell was of airtight design, with high-vacuum glass stopcocks fitted with either Teflon or Kalrez (DuPont) O-rings to prevent contamination by grease. The connections to the high-vacuum line and to the Schlenck containing the solvent were made by spherical joints fitted with Kalrez O-rings. The pressure measured in the electrochemical cell prior to performing the trap-to-trap distillation of the solvent was typically 1.0 to 2.0 $\times$ 10^{-5} mbar. The working electrode consisted either of a 0.6 mm diameter platinum wire (0.15 cm^2 approximately) sealed in glass or platinum disk ultramicroelectrodes (with radii from 5 to 62.5 μm) also sealed in glass. The counter electrode consisted of a platinum spiral, and the quasi-reference electrode was a silver spiral. The quasi-reference electrode drift was negligible for the time required by a single experiment. Both the counter and reference electrodes were separated from the working electrode by ~0.5 cm. Potentials were measured with the ferrocene or decamethylferrocene standards and are always referred to saturated calomel electrode (SCE). $E_{1/2}$ values correspond to $(E_c + E_a)/2$ from CV. Ferrocene (decamethylferrocene) was also used as an internal standard for checking the electrochemical reversibility of a redox couple. The temperature dependence of the relevant internal standard redox couple potential was measured with respect to SCE by a nonisothermal arrangement.[34] Voltammograms were recorded with an AMEL Model 552 potentiostat or a custom-made fast potentiostat controlled by either an AMEL Model 568 function generator or an ELCHEMA Model FG-206F. Data acquisition was performed by a Nicolet Model 3091 digital oscilloscope interfaced to a PC. Temperature control was accomplished within 0.1 °C with a Lauda thermostat. The minimization of ohmic drop was achieved through the positive feedback circuit implemented in the potentiostat. Digital simulation of cyclic voltammetric experiments: The CV simulations were carried out by the DigiSim 3.0 software by Bioanalytical Systems Inc. All the fitting parameters (see Supporting Information) were chosen so as to obtain a visual best fit over a 10^2-10^3-fold range of scan rates.

Acknowledgment. We thank Andrea Altieri for the preparation of model rotaxane **4**. This work was supported through the EU TMR Network contract FMRX-CT96-0059, the EPSRC, the University of Bologna ("Funds for Selected Research

(29) Indeed, recent molecular modelling studies by other groups reinforce this view: Zheng, X.; Sohlberg, K. *J. Phys. Chem. A* **2003**, *107*, 1207–1215.
(30) In complexes with 2,6-diamidopyridines, three hydrogen bonds to a *ni* unit cause a stabilization of ~0.2 V: see refs 14b and 14c.
(31) Zachariasse, K. A.; Maçanita, A. L.; Kühnle, W. *J. Phys. Chem. B* **1999** *103*, 9356–9365.
(32) Gellman, S. H.; Dado, G. P.; Liang, G.-B.; Adams, B. R. *J. Am. Chem. Soc.* **1991**, *113*, 1164–1173.
(33) Carano, M.; Ceroni, P.; Mottier, L.; Paolucci, F.; Roffia, S. *J. Electrochem. Soc.* **1999**, *146*, 3357–3360.
(34) Yee, E. L.; Cave, R. J.; Guyer, K. L.; Tyma, P. D.; Weaver, M. J. *J. Am. Chem. Soc.* **1979**, *101*, 1131–1137.

Topics"), MIUR (PRIN 2002, prot. 2002035735), and CNR (Agenzia 2000). F.G.G. and D.A.L. are Marie Curie (FMBI-CT97-2834) and EPSRC Advanced (AF/982324) Research Fellows.

Supporting Information Available: Full synthetic procedures, crystallographic information, fitting parameters for the simulation of cyclic voltammetry curves, additional cyclic voltammograms illustrating the effect of scan rate and of temperature on the electrochemical response of compounds **1**, **2**, **6**, **7**, and **8**, procedure for spin polarization transfer by selective inversion recovery (SPT-SIR) experiments, and Eyring plot for the variation of shuttling rates with temperature (PDF and CIF). This material is available free of charge via the Internet at http://pubs.acs.org.

JA0352552

Structural, Electrochemical, and Photophysical Properties of a Molecular Shuttle Attached to an Acid-Terminated Self-Assembled Monolayer

Francesca Cecchet[†] and Petra Rudolf*[,‡]

Laboratoire Interdisciplinaire de Spectroscopie Electronique, Facultés Universitaires Notre-Dame de la Paix, 61 rue de Bruxelles, B-5000 Namur, Belgium, and Materials Science Centre, Rijksuniversiteit Groningen, Nijenborgh 4, NL-9747AG Groningen, The Netherlands

Stefania Rapino, Massimo Margotti, and Francesco Paolucci*

Department of Chemistry "G. Ciamician", University of Bologna, via F. Selmi 2, I-40126 Bologna, Italy

Jacob Baggerman and Albert M. Brouwer*

Institute of Molecular Chemistry, University of Amsterdam, Nieuwe Achtergracht 129, NL-1018 WS Amsterdam, The Netherlands

Euan R. Kay, Jenny K. Y. Wong, and David A. Leigh*

School of Chemistry, University of Edinburgh, West Mains Road, Edinburgh EH9 3JJ, United Kingdom

Received: March 30, 2004; In Final Form: July 6, 2004

A benzylic amide macrocycle containing a pyridine moiety (macrocycle **2**) and a related benzylic amide macrocycle-based molecular shuttle (naphthalimide rotaxane) with two pyridine moieties on the macrocyclic unit were grafted onto a self-assembled monolayer (SAM) of 11-mercaptoundecanoic acid (11-MUA) on gold. X-ray photoelectron spectroscopy (XPS) indicates that the molecules are linked to the SAM by hydrogen-bonding. Electrochemical investigations show that the self-assembled monolayer is densely packed and well ordered and allows the estimation of the average thickness of the SAM alone and of the SAM functionalized with either macrocycle **2** or with naphthalimide rotaxane. The estimated thickness values suggest that the 11-MUA chains in the SAM are tilted with respect to the surface normal, as expected for ordered and stable SAMs, whereas the rotaxane molecules are oriented with the thread parallel to the SAM surface and macrocycle plan preferentially perpendicular to the surface. The photophysical studies of the naphthalimide rotaxane grafted onto the SAM on gold demonstrated that fluorescence is partially quenched but still remains easily measurable because the presence of the SAM reduces the quenching effect of the metal substrate. Moreover, the photophysical analysis clearly indicates that the naphthalimide part of the rotaxane strongly interacts with the carboxylic groups of the SAM, in agreement with the orientation of the molecule obtained from the electrochemistry.

1. Introduction

The design and construction of new architectures for the purpose of developing innovative and promising multifunctional materials is one of the central themes of nanotechnology. Rotaxanes, a class of mechanically interlocked molecules, are proving popular prototypical systems for device applications, because of their unusual structural characteristics. In fact, they are composed of a macrocycle ring locked onto a thread by two bulky stoppers, and the mechanical bond holding together the components of the molecule allows large amplitude relative movements that can be used to modify the molecular properties by external stimuli.[1−4] Various molecular systems in which translational or rotational motion of submolecular components takes place after chemical, electrochemical, electrical or photochemical excitation, have been described previously.[5−14] Up to now, most rotaxane-based submolecular motions have been studied in solution where the large possibility of orientation and ample freedom of movements are allowed. However, the creation of a rotaxane-based device requires the incorporation of rotaxane molecules in bidimensional arrays onto a surface, in a way that preserves the dynamic properties of the molecule. This implies first that the anchoring of the molecules has to ensure that the mutual interactions and the link with the substrate do not affect the molecules' internal degrees of freedom necessary for their use as functional units. Second, the chemical or physical properties of molecules adsorbed on a surface can be slightly or strongly affected and modified, depending on the nature of the substrate and of the adsorbed species, on the distance between the two, and on the presence of an intermediate layer. In addition to these intrinsic difficulties, experimental problems also interfere with the characterization and understanding of the behavior of such surfaces because the number

* Corresponding authors. For thin film preparation and XPS characterization (P.R.): P.Rudolf@phys.rug.nl. For electrochemical measurements (F.P.): francesco.paolucci@unibo.it. For photophysics (A.M.B.): fred@science.uva.nl. For materials (D.A.L.): David.Leigh@ed.ac.uk.

[†] Universitaires Notre-Dame de la Paix.

[‡] Rijksuniversiteit Groningen.

10.1021/jp048621s CCC: $27.50
Published on Web 09/08/2004

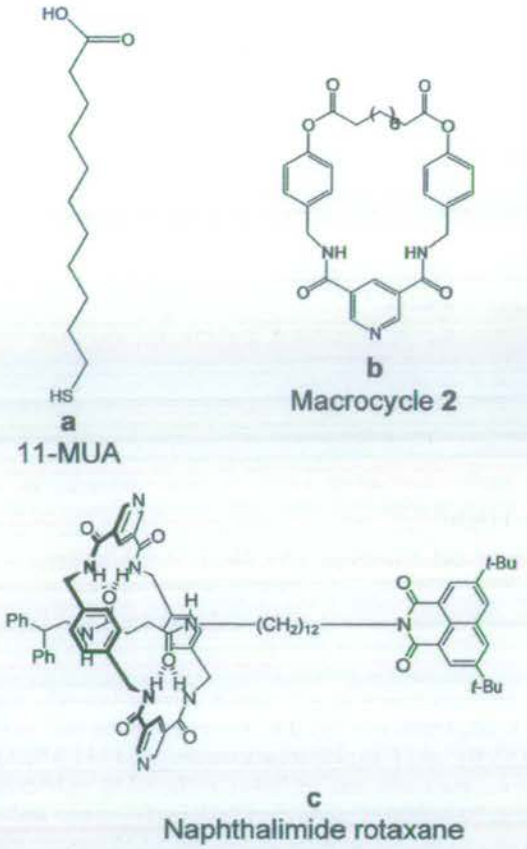

Figure 1. Simplified representation of (a) 11-mercaptoundecanoic acid (11-MUA), (b) macrocycle **2**, and (c) naphthalimide rotaxane.

of molecules adsorbed on the surface is often so low that it falls below the detection limits of many techniques.

A method often used to anchor macromolecular units, such as proteins or enzymes, onto a solid surface is the functionalization of a self-assembled monolayer (SAM) of alkanethiols [see, for example, refs 15−27]. The success of SAMs is due to the simplicity of the experimental procedure to prepare the films, their reproducibility, and the possibility of creating a wide range of surfaces via the incorporation of different groups at the end of the alkyl chains. These groups allow us to graft different types of molecules onto a surface and serve therefore as a starting point from which to build up more complex molecular architectures.

Here a functionalized benzylic amide macrocycle and molecular shuttle were anchored on the surface of an acid-terminated self-assembled monolayer on gold. Macrocycle **2** (Figure 1b) contains a pyridine function that allows grafting by hydrogen bonding with the acid groups of SAM, as already shown in a previous work.[28] Similarly, the naphthalimide rotaxane molecule (Figure 1c) contains two pyridine moieties localized on the macrocycle unit and is hence also expected to hydrogen-bond to the SAM. A similar rotaxane with two phenyl groups in the place of the two pyridine groups on the macrocycle already demonstrated behavior as a molecular shuttle in solution, either after excitation by a laser pulse[10] or after electron transfer at an electrode.[11]

The aim of this work has been to investigate the structural, electrical, and/or the photophysical properties of such surfaces, focusing the attention especially on the packing, the order, and the thickness of macrocycle and rotaxane films, and on the photoluminescent properties of the naphthalimide rotaxane films on gold.

2. Experimental Section

Materials. Macrocycle **2** and naphthalimide rotaxane (Figure 1b,c) were synthesized using methods analogous to those previously described in the literature.[29] 11-Mercaptoundecanoic acid (95%, Aldrich) (Figure 1a), chloroform, and dichloromethane (HPLC grade, Acros) were used as supplied.

Preparation of Monolayers. The substrates were evaporated gold films supported on Si(111) wafers (IMEC, Belgium). They were cleaned in an ozone discharge for 15 min, followed by sonication in ethanol for 20 min immediately before being employed. Carboxylic acid-terminated SAMs were prepared by immersion of the gold substrates in a 1 mM chloroform solution of 11-MUA for 21 h. The samples were rinsed in chloroform and dried under argon before contact angle measurements or introduction into ultrahigh vacuum for characterization by X-ray photoelectron spectroscopy (XPS).

Functionalization Using Macrocycle 2. Grafting of macrocycle **2** onto the SAM surface has been carried out after 98 h of immersion of the 11-MUA monolayer in a 1 mM solution of macrocycle **2** in dichloromethane, as described in the literature.[28]

Functionalization Using Naphthalimide Rotaxane. For grafting the rotaxane molecules, the carboxylic acid-terminated SAMs were immersed in a 0.1 mM solution of naphthalimide rotaxane in dichloromethane for 120 h.

The modified surfaces were each rinsed and sonicated for 30 s in pure dichloromethane and dried under a stream of argon and then characterized by XPS, cyclic voltammetry, impedance spectroscopy, and fluorescence spectroscopy.

X-ray Photoelectron Spectroscopy (XPS) Analysis. XPS measurements were performed using a SSX-100 (Surface Science Instruments) photoelectron spectrometer with a monochromatic Al Kα X-ray source ($h\nu$ = 1486.6 eV). The energy resolution was set to 0.92 eV to minimize data acquisition time and the photoelectron takeoff angle (TOA) was 90°. All binding energies were referenced to the Au $4f_{7/2}$ core level.[30] The base pressure in the spectrometer was in the low 10^{-10} Torr range.

Spectral analysis included a linear background subtraction and peak separation using mixed Gaussian−Lorentzian functions, in least squares curve-fitting program (Winspec) developed in the LISE laboratory of the Facultés Universitaires Notre-Dame de la Paix, Namur, Belgium. The photoemission peak areas of each element, used to estimate the amount of each species on the surface, were normalized by the sensitivity factors of each element tabulated for the spectrometer used.

Electrochemical Instrumentation and Measurements. The electrochemical experiments were performed in unbuffered 0.1 M KCl aqueous solutions using a two-compartment electrochemical cell fitted with a saturated calomel electrode (SCE) and a platinum spiral as counter electrode. Cyclic voltammetry (CV) and electrochemical impedance spectroscopy (EIS) experiments were carried out with an Autolab Model PGSTAT 30.

Fluorescence Spectroscopy. Steady-state spectra of the films were recorded on a Spex Fluorolog 3 spectrometer, equipped with two double grating monochromators in the excitation and emission channels. A front-face geometry was used, with an angle of 20° between excitation and detection directions. The detector was a Peltier cooled R636-10 (Hamamatsu) photomultiplier tube.

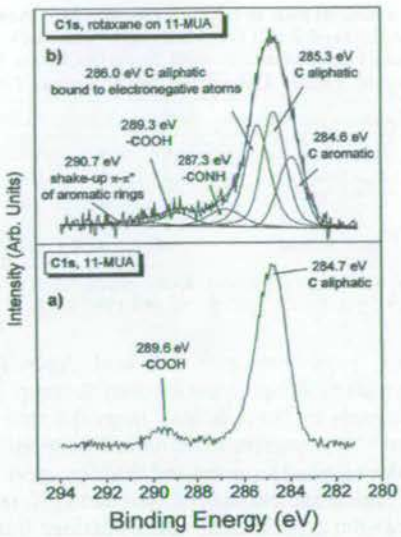

Figure 2. Photoemission spectra and fit of the C 1s core level region for (a) a film of 11-MUA and (b) a film of 11-MUA functionalized with naphthalimide rotaxane.

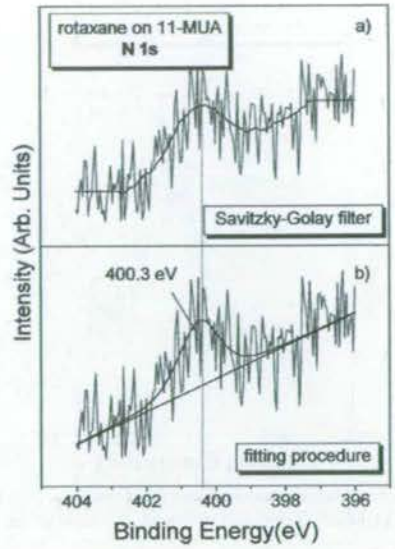

Figure 3. Photoemission spectra of the N 1s core level region for a film of 11-MUA functionalized with naphthalimide rotaxane: (a) experimental curve and fit; (b) experimental curve and Savitzky−Golay filtered curve.

Time-resolved fluorescence measurements were performed using a Hamamatsu streak camera system, consisting of a Chromex IS250 spectrograph, a M5677 slow-speed sweep unit, a C4792 trigger unit, a C5680 blanking unit, and a C4742-95 digital CCD camera.[31] The sample was excited using an LTB MSG400 nitrogen laser (337 nm, fwhm ≈ 0.9 ns, 10 Hz). Excitation and emission light were guided via optical fibers in a front-face geometry. For analysis the data were imported into the Igor Pro 4.0 data analysis package (Wavemetrics, Inc., Lake Oswega, OR). The system response (scattered laser light) was modeled as a Gaussian function, and the decay traces were fitted to the convolution of a Gaussian pulse and an exponential decay.

3. Results and Discussion

XPS Analysis. Figure 2, bottom panel, shows the carbon 1s core level photoemission spectrum for a monolayer of 11-MUA. As already discussed in a previous work for films of macrocycle **2**,[28] to analyze these data, we mathematically reconstruct the spectrum with a minimum number of peaks consistent with the raw data and the molecular structure of the film, with the simplification of assuming equivalent carbon atoms for chemical environments that are expected to give very close values of the binding energy. Following this procedure, the analysis of the carbon 1s core level region recorded for the monolayer provides the identification of three contributions to the experimental curve: a first main peak, at 284.7 eV, is assigned to the aliphatic carbons of the alkyl chains. The main peak is slightly asymmetric due to the contribution at higher binding energy (0.3−0.5 eV from the pure aliphatic carbons) of the carbon atom bound to the acid group and to a possible CO atmospheric contamination. The last peak at 289.6 eV corresponds to the carboxylic carbon.[28−35] The analysis of the carbon 1s core level region for a SAM of 11-MUA represents the starting point to characterize the functionalization process with macrocycle **2**[28] or with naphthalimide rotaxane.

Figure 2, top panel, shows the C 1s core level region for a monolayer functionalized with naphthalimide rotaxane molecules: as can be clearly seen, there are several differences between the spectrum recorded for the SAM alone and for the SAM modified with the rotaxane, confirming that they refer to different situations. If we compare these two spectra and rely on the characteristic peak energies for the different carbon species reported in the literature,[35−37] we can assign all fitted peaks to chemical species present in the SAM functionalized with rotaxane molecules. The peak at 284.6 eV is the signature of aromatic carbons, which occur only in the rotaxane. The peak at 285.3 eV can be assigned either to aliphatic carbon atoms or to aromatic carbons bound to electronegative groups. The peak at 286.0 eV corresponds to aliphatic carbons of the rotaxane bound to electronegative atoms such as N or O. At 287.3 eV binding energy we see the peak characteristic of amide and imide carbons of the rotaxane, and at 289.3 eV the contribution of carboxylate carbons. The shake-up feature associated with the aromatic rings of the rotaxane is found at 290.7 eV.

Figure 3 bottom panel shows the N 1s core level spectrum recorded for the SAM functionalized with naphthalimide rotaxane. The presence of a signal in this region is the most convincing evidence that rotaxane is grafted on the surface of the self-assembled monolayer because nitrogen occurs only in the rotaxane. The experimental curve is very weak and noisy because nitrogen has a small photoionization cross-section and because the molecule contains only 9 nitrogen atoms whereas the other 88 atoms are other elements (H is here not computed). However, the fitting procedure allowed us to evidence a single peak at 400.3 eV binding energy corresponding to the amide, imide, and pyridine nitrogen atoms of the naphthalimide rotaxane. To validate the peak assignment obtained from the fitting procedure, we treated the same experimental curve with a Savitzky−Golay filter method,[38] which has the peculiarity of preserving features of the data such as peak height and width. The result is shown in Figure 3, top panel: the experimental curve smoothed with this method shows a peak centered at 400.3 eV, i.e., at exactly the same energy as the peak obtained from the fitting procedure. As shown previously[28] for macrocycle **2** films, the fact that the nitrogen 1s experimental curve is fitted with a single peak gives information on the interaction between the macrocycle and SAM. In general, one expects the signature of the pyridine nitrogen at a binding energy between 399.0 and 399.5 eV depending on the chemical environment of the pyridine rings.[35] However, theoretical calculations investigating the

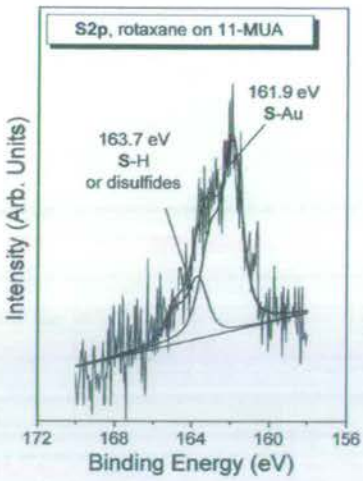

Figure 4. Photoemission spectrum and fit of the S 2p core level region for a film of 11-MUA functionalized with naphthalimide rotaxane.

effects of intra- and intermolecular interactions on the binding energy for similar molecules, i.e., benzylic amide catenanes, showed that hydrogen bonding interactions can produce shifts to a higher binding energy of up to 1 eV.[39] In addition, shifts up to 1.7 eV have been already observed for pyridine moieties interacting with acid groups by hydrogen bonding.[40] However, an electrostatic interaction between a protonated pyridine nitrogen and an anionic carboxylate function following the exchange of the proton of the carboxylic acid group, should give rise to a new component in the N 1s core level region between 401.0 and 402.0 eV.[35] The N1s signal is quite weak, and therefore we cannot easily identify a possible second contribution at higher binding energy, between 401 and 402 eV; however, the raw data indicate that such a contribution, if it exists, has to be sensibly weaker than the main component at 400.3 eV. We can therefore conclude that the majority of the rotaxane molecules links to the SAM by a hydrogen-bonding interaction between the pyridine nitrogen localized on the macrocycle unit of the naphthalimide rotaxane and the acid group of SAM, similarly to what was already evidenced for the macrocycle **2** alone grafted onto SAM.[28]

Figure 4 shows the S 2p core level region for the SAM functionalized with the naphthalimide rotaxane: the fitting of the experimental curve clearly shows two contributions, one where the S $2p_{3/2}$ is found at 161.9 eV and which is assigned to sulfur bonded to gold,[30,41] and the other component with the S $2p_{3/2}$ peak at 163.7 eV which could be due to a small amount of alkanethiols not covalently bonded to the substrate but only intercalated between 11-MUA molecules bound to Au or physisorbed as a double layer.[30,41] Alternatively, the second component might derive from disulfides formed under the influence of the X-rays during spectral acquisition.[42-44] No oxidized species of sulfur can be detected at binding energies of 164.8 and 168.5 eV.[45]

Quantitative analysis of XPS spectra allows us to determine the yield of functionalization of the SAM with naphthalimide rotaxane molecules: from the photoemission peak area of each element the amount of that species on the surface is obtained. We compared the experimentally determined atomic percentages with atomic ratios calculated for different functionalization yields of the acid groups of the SAM: in the calculation we considered a model surface of 100 thiol chains and computed the atomic percentages for C, O, S, and N (excluding hydrogen which cannot be detected by XPS) for coverages of 1, 3, 5, 10, 20, and up to 100 rotaxane molecules. The error on the photoemission peak areas was estimated depending on the signal/noise ratio in the spectrum for each element: the carbon and oxygen signals are better defined; hence the error was found to be 2% and 5%, respectively. Sulfur and nitrogen signals are weaker, producing noisier spectra, and therefore more substantial errors in the peak areas, estimated at 10% and 15%, respectively. Table 1 shows the experimental values obtained from our film and the theoretical ones computed for functionalization of 1%, 3%, 5%, and 10% of the acid groups. C and especially the O signal always contain a contribution of atmospheric contaminants, which affect all percentages. Namely, the percentages of C and O increase and consequently the percentages of S and N decrease. However, the N/S ratio, which is not affected by contaminants, and the comparison between theoretical and experimental data clearly indicate that the functionalization of the SAM by the rotaxane molecules is close to 3%, whereas the theoretical data assuming that 1%, 5%, or 10% of the acid groups are functionalized with rotaxane molecules strongly deviate from the experimental data.

TABLE 1: Comparison between Experimental Atomic Percentages Derived from the Photoemission Peak Areas of 11-MUA Film Functionalized with Naphthalimide Rotaxane and Theoretical Values Calculated for Different Coverages[a]

	exptl atomic percentages	th 1%	th 3%	th 5%	th 10%
% C	78.1 ± 1.6	78.9	79.3	79.7	80.3
% O	16.1 ± 0.8	13.9	13.2	12.7	11.7
% S	4.5 ± 0.5	6.7	5.9	5.3	4.2
% N	1.2 ± 0.2	0.6	1.6	2.4	3.8
N/S	0.27 ± 0.05	0.09	0.27	0.45	0.90

[a] The error on the experimental atomic percentages was estimated to be 2% for C, 5% for O, 10% for S, and 15% for N.

Electrochemistry. The electrochemical properties of 11-MUA SAMs, both pristine and functionalized with macrocycle **2** or with naphthalimide rotaxane, were investigated by cyclic voltammetry (CV) and electrochemical impedance spectroscopy (EIS). Both techniques have been widely used, in either the presence or the absence of a redox probe, on one hand to determine the size and number of defects in the SAM, and on the other to evaluate the double layer capacitance of the modified electrode and whence the average thickness of the organic layer.[46,47] Though in CV large potential sweeps (of the order of 0.1 to 1 V) are applied to the electrode/solution interface and the resulting dc current is measured, in EIS the interface is usually kept at its rest potential and probed by using a small-amplitude (typically ≤20 mV) sinusoidal voltage. Hence EIS is a much less disturbing technique than CV.[48,49] Excitation frequencies (f) ranging between 1 mHz and 1 MHz can be used, permitting the investigation of phenomena with time scales ranging over 9 decades, which may be resolved in principle according to their relaxation time.

Both CV and EIS confirmed the very low level of defects present in the 11-MUA monolayer. In particular, Figure 5 shows the CV curves relative to $[Fe(CN)_6]^{3-/4-}$ reduction/oxidation obtained at the unmodified gold electrode (dotted line) and at the gold electrode modified with 11-MUA (solid line). No microelectrode-type behavior, typical of the presence of pinholes in the film,[46] was observed in the CV curve associated with the 11-MUA modified gold surface, indicating that electron transfer occurs preferentially by through-film tunneling.[46,50-52] The very low level of defects in the film was also assessed by performing an EIS analysis under the conditions of Figure 6. [The presence of unbound or disulfide thiol species evidenced by XPS could introduce defect sites in the monolayer; however, the latter did not affect the electrochemical blocking behavior of the SAM,

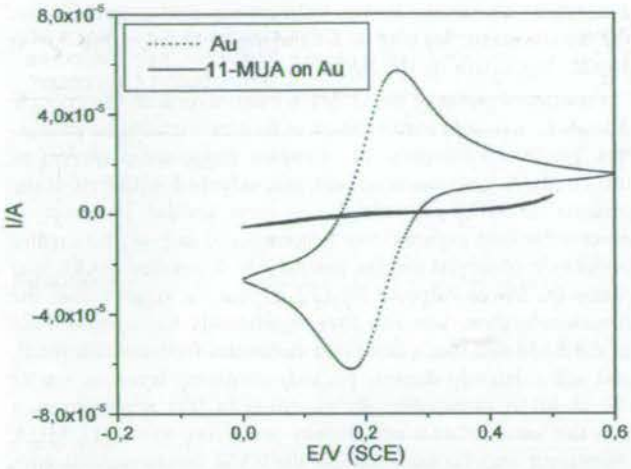

Figure 5. Cyclic voltammetry curves recorded for pure gold electrode (···) and for a SAM of 11-MUA (—) in a 0.1 M KCl aqueous solution, at 50 mV/s.

as evidenced by our electrochemical experiments.] In this figure the out-of-phase component of the impedance, Z'', is plotted vs the in-phase one, Z' where Z'' and Z' are the parametric functions of the frequency (Z plot or Nyquist plot).[47,48] Figure 6a shows the impedance spectra obtained at various potentials: the incomplete semicircles that rapidly shrink upon increasing overpotential (under the present conditions, the open circuit potential, E_{oc}, coincides with $E°_{[Fe(CN_6)]^{3-/4-}} = 0.18$ V) are associated with the slow electron transfer kinetics experienced by the redox probe at the modified electrode.[46-48] An alternative presentation of the impedance data is shown in Figure 6b where the complex capacitance C is displayed (C plot). C is defined as $1/j\omega Z$, where $j = -1^{1/2}$ and ω is the angular frequency ($=2\pi f$). The C plot emphasizes the interface response at higher frequencies with respect to the Z plot.[53,54] Notice that, in the framework of an equivalent circuit description of the electrochemical interface,[47,48] a semicircle in the Z plot corresponds to a parallel RC (resistor, capacitor) arrangement and a straight vertical line to a series RC arrangement, and vice versa in the case of C plot. The prominently blocking behavior of the 11-MUA monolayer is evidenced by the semicircle observed in the C plots in the medium-to-high frequency range, both in the presence of the redox couple and in its absence. A second (incomplete) semicircle occurring at relatively lower frequencies, is associated with a parallel charging path characterized by a higher time constant (likely associated with protonation/deprotonation and/or diffusion processes, vide infra), whereas only in the low-frequency range do slow processes associated with charge transfer involving $[Fe(CN)_6]^{3-/4-}$ or diffusion take place (compare, in Figure 6b, the two plots obtained in the presence and in the absence of the redox probe). The electrical response of the interface was described in terms of the equivalent circuit shown in Figure 6. R_Ω represents the solution resistance, C_{dl} the double layer capacitance, and R_{ct} the charge transfer resistance (related to the exchange current i_0[49] and clearly omitted in the case of data obtained in the absence of redox couple). The electrical parameters were evaluated by fitting procedures, using the CNLS method described by Boukamp.[55] In analogy with other equivalent circuits proposed for describing the electrical behavior of a thick SAM,[56] the branch comprising the element R_{SAM}, C_{SAM}, and the Warburg element Z_w, were introduced to reproduce the behavior at $f < 1$ Hz. Such elements are associated with physical processes occurring at the interface such as desorption/adsorption of protons at the terminal acid groups[46] and/or diffusion within the SAM at grain boundaries or other defects in the film.[53,57] The best-fit values of the various elements in the circuit of Figure 6, measured at the E_{oc}, are reported in Table 2. From the value of R_{ct} obtained at E_{oc} ($=E°$),

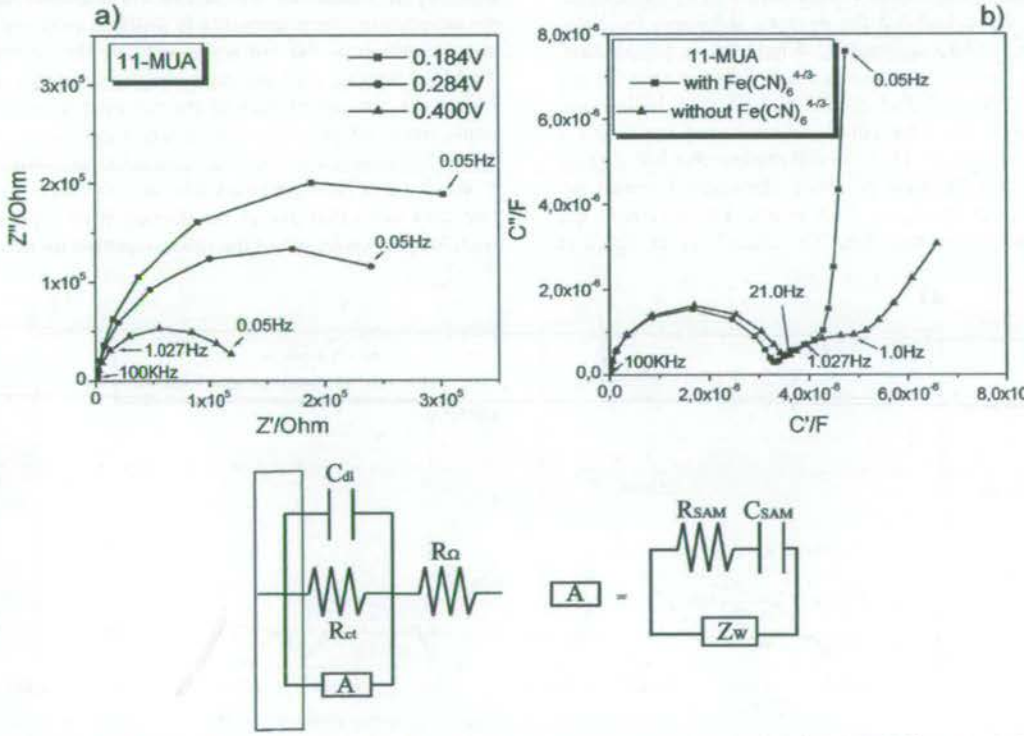

Figure 6. (a) Nyquist plots recorded for a film of 11-MUA in a 0.1 M KCl aqueous solution 1 mM of $Fe(CN)_6^{3-/4-}$: 0.1 M of KCl at 0.184 V (■), at 0.284 (●), and at 0.400 V (◆). (b) C plots recorded for a film of 11-MUA in a 0.1 M KCl aqueous solution (▲) and 1 mM of $Fe(CN)_6^{3-/4-}$ (■). (c) Representation of the equivalent circuit associated with the electrochemical interface solution/SAM/gold.

TABLE 2: Electrical Parameters Associated with the Solution/SAM/Gold Electrochemical Interface Obtained from Fitting of EIS Spectra of Figure 6 by Using the Equivalent Circuit Shown in Schematic Form in the Lower Part of Figure 6

potential, V	R_Ω, Ω	R_{SAM}, kΩ	R_{ct}, kΩ	C_{dl}, μF cm^{-2}	C_{SAM}, μF cm^{-2}	$10^{-6}W$
0.184	55.1	0.485	60.6	3.19	0.752	0.798
0.284	55.1	0.339	35.4	3.05	0.787	1.270
0.400	55.1	0.133	19.1	3.00	0.867	7.705

the standard heterogeneous constant, k^0, was estimated using the equation[48,49]

$$k^0 = (RT/n^2F^2AC_0)(1/R_{ct}) \quad (1)$$

and found to be equal to 1.1×10^{-6} cm s^{-1}. On the other hand, the value for k^0 at the clean gold surface is 0.031 cm s^{-1},[58] whence, according to the relationship for tunneling

$$k_{SAM} = k_{Au}e^{-(\beta d)} \quad (2)$$

an electronic tunneling factor $\beta = 0.93/CH_2$ was obtained. This is in very good agreement with reported values of β for alkanethiols[50,51,59] and confirms the highly blocking nature of the 11-MUA monolayer. Furthermore, the low value of C_{dl} (Table 2) is also typical of electrodes covered by a well-formed SAM of long-chain thiols.[46] Within the Helmholtz capacitor approximation of the double layer and assuming a dielectric constant of the organic layer $\epsilon = 4 \pm 1$,[46] we find from the best-fit value for C_{dl} that the average thickness of the SAM amounts to $t = \epsilon\epsilon_0/C_{dl} = 12.5 \pm 0.6$ Å^2. Taking into account the length of the 11-MUA molecule (16.1 Å), this value for t indicates that 11-MUA forms a close-packed SAM with molecules tilted between 35° and 40° from the surface normal.

[To validate the SAM thickness value obtained by capacitance measurements, we calculated the average thickness by XPS: following the procedure outlined by Whelan et al. (*Appl. Surf. Sci.* **1998**, *134*, 144), we calculated the layer thickness for the SAM from the data collected on the Au substrate before and after immersion in the alkanethiol solution, and we found a thickness value of ~10 Å. This value is comparable but slightly lower than the one obtained by electrochemistry because the gold surface was analyzed by XPS before immersion in the alkanethiol solution and therefore the "clean" Au 4f signal is necessarily attenuated by the hydrocarbon contaminants from the environment, leading to an underestimation of the Au 4f signal attenuation by the SAM.]

Functionalization of the 11-MUA monolayer with macrocycle **2** leads to a sizable modification of its electrochemical properties. Figure 7a compares the complex capacitance spectra of the 11-MUA functionalized with macrocycle **2** with that of the pristine 11-MUA monolayer. A very similar behavior is observed at both high and low frequencies. However, the smaller semicircle observed for the macrocycle **2** covered SAM, and hence the lower value of C_{dl} (2.1 μF cm^{-2}), suggest that the functionalization does not alter significantly the compactness of the SAM and that macrocycle molecules form an additional, and still relatively densely packed, insulating layer on top of the 11-MUA monolayer. By assuming in first approximation that the same relative permittivity pertaining to the 11-MUA monolayer may be used also for the SAM functionalized with macrocycle **2**, an increased Helmholtz capacitor thickness of 16.9 ± 0.9 Å is obtained.

Analogous results were obtained in the case of 11-MUA functionalized with naphthalimide rotaxane, as shown in Figure 7b, where the C plot relative to the pristine 11-MUA monolayer is compared to the C plot relative to 11-MUA functionalization with naphthalimide rotaxane. Apparently, only the capacitive properties of the film are affected by functionalization because the EIS spectra display the same high-frequency semicircle, but with a significant decrease of diameter. The corresponding C_{dl} value (2.4 μF cm^{-2}) is very close to that measured for the macrocycle **2** film: this suggests the rotaxane molecules are arranged with the thread parallel to the surface, in agreement with a grafting process in which the pyridine moieties, localized on the macrocycle are hydrogen-bound to the acid groups. In fact, if one considers the size of the naphthalimide molecular shuttle (the linear thread's length is about 35 Å and the macrocycle's diameter ~10 Å), the average thickness estimated by capacitance measurements is justified only on the basis of an orientation of the molecule with the thread parallel to the 11-MUA surface and the macrocycle plan perpendicular to it. Moreover, the orientation of the rotaxane molecules gives an explanation of the low functionalization yield estimated by XPS: by relating the size of a naphthalimide rotaxane molecule to the distance between two sulfur atoms (which is about 5 Å),[60] one concludes that 3% of functionalization represents a quite high level of coverage of the self-assembled monolayer surface.

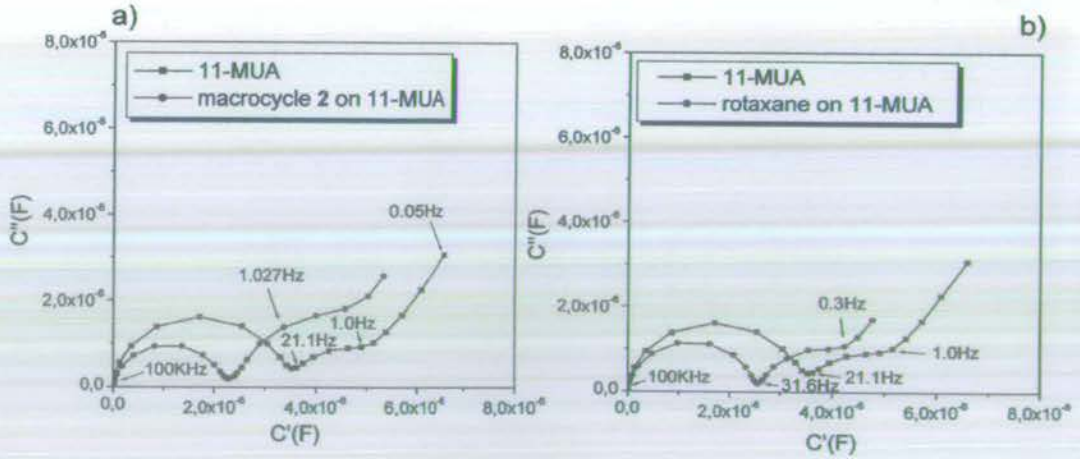

Figure 7. (a) C plots recorded for a SAM of 11-MUA (■) and for a SAM of 11-MUA functionalized with macrocycle **2** (●) in a 0.1 M KCl aqueous solution and (b) C plots recorded for a SAM of 11-MUA (■) and for a SAM of 11-MUA functionalized with rotaxane (●) in a 0.1 M KCl aqueous solution.

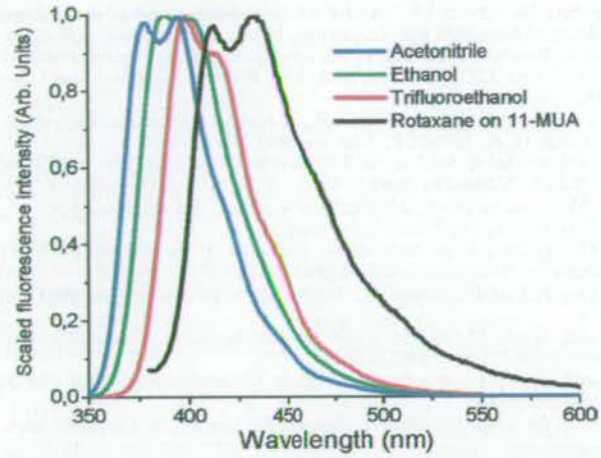

Figure 8. Fluorescence emission spectra of the rotaxane in acetonitrile (blue line), ethanol (green line), and trifluoroethanol (red line), and on 11-MUA (black line).

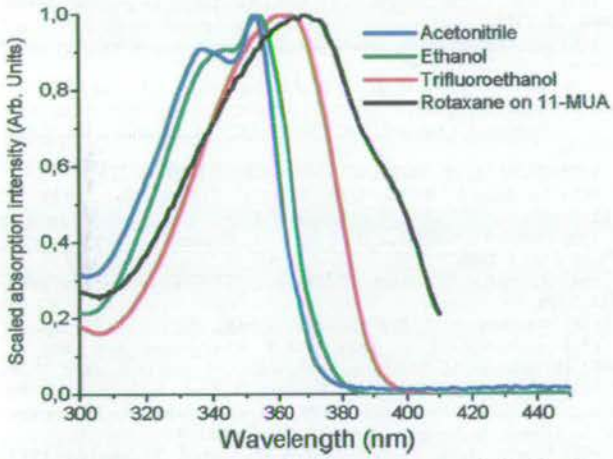

Figure 9. Absorption spectra of the rotaxane in acetonitrile (blue line), ethanol (green line), and trifluoroethanol (red line) and fluorescence excitation spectrum ($\lambda_{em} = 435$ nm) of the rotaxane on 11-MUA (black line).

Fluorescence Spectroscopy. The fluorescence emission spectra of the naphthalimide rotaxane on the SAM are shown in Figure 8 together with the spectra measured in acetonitrile, ethanol, and trifluoroethanol solutions. The fluorescence decay times in these solvents are 1.6, 2.3, and 3.3 ns, respectively. Unfortunately, the signal from the rotaxane on the SAM was too weak to permit a reliable lifetime measurement. The excitation spectrum of the naphthalimide rotaxane on the SAM is shown in Figure 9, together with the absorption spectra in solution. Both the excitation and the emission spectrum, which are due to the naphthalene imide chromophore, are substantially shifted to lower energy compared to the spectra in solution. The similar shapes of the emission spectra can be taken as an indication that the emissive species are not essentially different; i.e., strong intermolecular associations between the chromophores on the SAM can be ruled out.[61] The red shift of the spectra is likely to be due to hydrogen bonding between the imide carbonyl groups and the carboxylic acids in the SAM. It is known for naphthalimides that the fluorescence red shifts with increasing polarity and proticity of the solvent.[62] The systematic red shift of the bands in the series acetonitrile−ethanol−trifluoroethanol correlates with an increase in the hydrogen bond donating capacity of the solvents. In solution, the red shift is accompanied by a substantial increase of the excited-state lifetime.

The fluorescence results demonstrate that not only the pyridine rings, but also the naphthalimide part of the rotaxane is strongly interacting with the carboxylic groups of the SAM, confirming that the thread is oriented parallel to the surface. Strong interchromophore interaction is not apparent. Although the fluorescence of the naphthalimide rotaxane molecules is partially quenched by the nearby gold surface, it is still easily measurable. This implies that it should be possible to detect a shuttling process, induced by some external stimulus, by means of fluorescence spectroscopy. Design and synthesis of molecular systems in which this concept can be realized are in progress.

4. Conclusions

A benzylic amide macrocycle and rotaxane have been physisorbed onto an acid-terminated self-assembled monolayer on gold. XPS characterization suggests that the molecules are held in place by hydrogen-bonding between the pyridine moieties of the macrocycle and the acid functions of SAM. Electrochemical investigations indicate a well-packed and ordered self-assembled monolayer with a very low fraction of defects, giving reason to the adsorption of macrocycle and naphthalimide rotaxane molecules on top of SAM and not intercalated between the thiol chains. Moreover, by capacitance measurements it was possible to estimate the averaged thickness of SAM and SAM functionalized with macrocycle or rotaxane: the thickness found for SAM is in agreement with the molecular length of 11-MUA thiol assuming a tilting angle of 35−40° from the normal to the surface, as expected for the ordered and stable structure of SAM. The increase in film thickness for macrocycle **2** on SAM and naphthalimide rotaxane on SAM indirectly confirms the functionalization process. In addition, from the film thickness and from dimensional considerations the orientation of rotaxane molecules onto the SAM surface was inferred, with the thread parallel to the surface and the macrocycle plan preferentially perpendicular to the surface in the conformation useful for the interaction of one pyridine moiety with an acid group. The fluorescence properties of naphthalimide rotaxane adsorbed on the acid-terminated SAM on gold showed that fluorescence is partially quenched due to the gold substrate; however, it is still easily measurable because of the presence of the intermediate SAM reduces the quenching effect. Moreover, the photophysical analysis clearly indicated that also the naphthalimide part of the rotaxane is strongly interacting with the carboxylic groups of the SAM, which validates the orientation of the molecules with the thread parallel to the surface, as inferred from electrochemistry.

Acknowledgment. This work was performed within the EU RT network EMMMA contract no. HPRN-CT-2002-00168 and received additional support from the EU contract MECHMOL no. IST-2001-35504, from PAI P5/01, from MIUR the University of Bologna, from FOM (Netherlands) and from the Breedtestrategie program of the Rijksuniversiteit Groningen. This research was also supported in part by The Netherlands Organization for the Advancement of Research (NWO).

References and Notes

(1) Johnston, A. G.; Leigh, D. A.; Nezhat, L.; Smart, J. P.; Deegan, M. D. *Angew. Chem., Int. Ed. Engl.* **1995**, *34*, 1212.

(2) Leigh, D. A.; Moody, K.; Smart, J. P.; Watson, K. J.; Slawin, A. M. Z. *Angew. Chem., Int. Ed. Engl.* **1996**, *35*, 306.

(3) Leigh, D. A.; Murphy, A.; Smart, J. P.; Slawin, A. M. Z. *Angew. Chem., Int. Ed. Engl.* **1997**, *36*, 728.

(4) Johnston, A. G.; Leigh, D. A.; Murphy, A.; Smart, J. P.; Deegan, M. D. *J. Am. Chem. Soc.* **1996**, *118*, 10662.
(5) Dietrich-Buchcker, C.; Sauvage, J.-P. *Bioorg. Chem. Frontiers* **1991**, *2*, 195.
(6) Bissell, R. A.; Cordova, E.; Kaifer, A. E.; Stoddart, J. F. *Nature* **1994**, *369*, 133.
(7) Kelly, T. R.; Sestelo, J. P.; Telliu, I. *J. Org. Chem.* **1998**, *63*, 3655.
(8) Collier, C. P.; Wong, E. W. Belohradsky, M.; Raymo, F. M. Stoddart, J. F.; Kuekes, P. J.; Williams, R. S.; Heath, J. R. *Science* **1999**, *285*, 391.
(9) Bermudez, V.; Capron, N.; Gase, T.; Gatti, F. G.; Kazjar, F.; Leigh, D. A.; Zerbetto, F.; Zhang, S. *Nature* **2000**, *406*, 608.
(10) Brouwer, A. M.; Frochot, C.; Gatti, F. G.; Leigh, D. A.; Mottier, L.; Paolucci, F.; Roffia, S.; Wurpel, G. W. H. *Science* **2001**, *16*, 2124.
(11) Altieri, A.; Gatti, F. G.; Kay, E. R.; Leigh, D. A.; Paolucci, F.; Slawin, A. M. Z.; Wong, J. K. Y. *J. Am. Chem. Soc* **2003**, *125*, 8644.
(12) Cavallini, M.; Biscarini, F.; León, S.; Zerbetto, F.; Bottari, G.; Leigh, D. A. *Science* **2003**, *299*, 531.
(13) Leigh, D. A.; Wong, J. K. Y.; Dehez, F.; Zerbetto, F. *Nature* **2003**, *424*, 174−179.
(14) Bottari, G.; Leigh, D. A.; Pérez, E. M. *J. Am. Chem. Soc.* **2003**, *125*, 13360−13361.
(15) Azehara, H.; Mizutani, W.; Suzuki, Y.; Ishida, T.; Nagawa, Y.; Tokumoto, H.; Hiratani, K. *Langmuir* **2003**, *19*, 2115.
(16) Ferretti, S.; Paynter, S.; Russell, D. A.; Sapsford, K. E.; Richardson, D. J. *Trends Anal. Chem.* **2000**, *9*, 19.
(17) Allara, D. *Biosensor Bioelectron.* **1995**, *10*, 771.
(18) Higashi, N.; Takahashi, M.; Niwa, M. *Langmuir* **1999**, *15*, 111.
(19) Madoz, J.; Kuznztzov, B. A.; Medrano, F. J.; Garcia, J. L.; Fernandez, V. M. *J. Am. Chem. Soc.* **1997**, *119*, 1043.
(20) Blonder, R.; Willner, I.; Buckmann, F. *J. Am. Chem. Soc.* **1998**, *120*, 9335.
(21) Jordan, C. E.; Frey, B. L.; Kornguth, S.; Corn, R. M. *Langmuir* **1994**, *10*, 3642.
(22) Ostuni, E.; Yan, L.; Whitesides, G. M. *Colloids Surf. B: Biointerfaces* **1999**, *15*, 3.
(23) Gooding, J. J.; Hibbert, D. B. *Trends Anal. Chem.* **1999**, *8*, 18.
(24) Patel, N.; Davies, M. C.; Hartshorne, M.; Heaton, R. J.; Roberts, C. J.; Tendler, S. J. B.; Williams, P. M. *Langmuir* **1997**, *13*, 6485.
(25) Jiang, L.; Glidle, A.; Griffith, A.; McNeil, C. J.; Cooper, J. M. *Bioelectrochem. Bioenerg.* **1997**, *42*, 15.
(26) Yang, H. C.; Dermody, D. L.; Xu, C.; Ricco, A. J.; Crooks, R. M. *Langmuir* **1996**, *12*, 726.
(27) Strither, T.; Cai, W.; Zhao, X.; Hamers, R. J.; Smith, L. M. *J. Am. Chem. Soc.* **2000**, *122*, 1205.
(28) Cecchet, F.; Pilling, M.; Hevesi, L.; Schergna, S.; Wong, J. K. Y.; Clarkson, G. J.; Leigh, D. A.; Rudolf, P. *J. Phys. Chem. B* **2003**, *107*, 10863.
(29) Lane, A. S.; Leigh, D. A.; Murphy, A. *J. Am. Chem. Soc.* **1997**, *119*, 11092.
(30) Moulder, J. F.; Stickle, W. F.; Sobol, P. E.; Bomben, K. D. *Handbook of Photoelectron Spectroscopy*; Perkin-Elmer Corporation, Physical Electronics Division: Eden Prairie, MN, 1992.
(31) Lauteslager, X. Y.; van Stokkum, I. H. M.; van Ramesdonk, H. J.; Brouwer, A. M.; Verhoeven, J. W. *J. Phys. Chem. A* **1999**, *103*, 653.
(32) Czandema, A. W.; King, D. E.; Spauling, D. *J. Vac. Sci. Technol. A* **1995**, *9*−*5*, 2607.
(33) Vogt, A. D.; Han, T.; Beebe, T. B., Jr. *Langmuir* **1997**, *13*, 3397.
(34) Wagner, C. D.; Naumkin, A. V.; Kraut-Vass, A.; Allison, J. W.; Powell, C. J.; Rumble, J. R., Jr. NIST X-ray Photoelectron Spectroscopy Database 20, Version 3.4, Standard reference data program of the National Institute of Standards and Technology; NIST: Gaithersburg, MD, 2003.
(35) Beamson, G.; Briggs, D. *High-Resolution XPS of Organic Polymers − The Scienta ESCA Database*; John Wiley & Sons Ltd.: Chichester, U.K., 1992.
(36) Fustin, C. A.; Gouttebaron, R.; De Nadaï, C.; Caudano, R.; Zerbetto, F.; Leigh, D. A.; Rudolf, P. *Surf. Sci.* **2001**, *474*, 37.
(37) Whelan, C. M.; Cecchet, F.; Clarkson, G. J.; Leigh, D. A.; Caudano, R.; Rudolf, P. *Surf. Sci.* **2001**, *474*, 71.
(38) From Origin6.0, Microcal Software Inc., Nothampton, MA.
(39) Bureau, Ch. Private communication.
(40) O'Shea, J. N.; Schnadt, J.; Brühwiler, P. A.; Hillesheimer, H.; Mårtensson, N. *J. Phys. Chem. B* **2001**, *105*, 1917.
(41) Arnold, R.; Azzam, W.; Terfort, A.; Wöll, C. *Langmuir* **2002**, *18*, 3980.
(42) Wirde, M.; Gelius, U.; Dunbar, T.; Allara, D. L. *Nucl. Instrum. Methods Phys. Res. B* **1997**, *131*, 245.
(43) Heister, K.; Zharnikov, M.; Grunze, M.; Johansson, L. S. O.; Ulman, A. *Langmuir* **2001**, *17*, 8.
(44) Zharnikov, M.; Frey, S.; Heister, K.; Grunze, M. *Langmuir* **2000**, *16*, 2697.
(45) Mekhalif, Z.; Riga, J.; Pireaux, J.-J.; Delhalle, J. *Langmuir* **1997**, *13*, 2285.
(46) Finklea, H. O. In *Electroanalytical Chemistry*; Bard, A. J., Ed.; Marcel Dekker: New York, 1996; Vol. 19, p 109.
(47) Flink, S.; van Veggel, F. C. J. M.; Reinhoudt, D. N. *Adv. Mater.* **2000**, *12*, 1315.
(48) MacDonald, J. R. *Impedance Spectroscopy; Emphasizing Solid Materials and Systems*; Wiley: New York, 1987.
(49) Bard, A. J.; Faulkner, L. R. *Electrochemical Methods*, 2nd ed.; Wiley: New York, 2001.
(50) Amatore, C.; Saveant, J. M.; Tessier, D. *J. Electroanal. Chem.* **1983**, *147*, 39.
(51) Becka, A. M.; Miller, C. *J. Phys. Chem.* **1992**, *96*, 2657.
(52) Terrettaz, S.; Becka, A. M.; Miller, C. *J. Phys. Chem.* **1995**, *99*, 11216.
(53) Gafni, Y.; Weizman, H.; Libman, J.; Shanzer, A.; Rubinstein, I. *Chem. Eur. J.* **1996**, *2*, 759.
(54) Rubinstein, I.; Sabatani, E.; Rishpon, J. *J. Electrochem. Soc.* **1987**, *134*, 3078.
(55) Boukamp, B. A. *Solid State Ionics* **1986**, *20*, 31.
(56) (a) Protsailo, L. V.; Fawcett, W. R. *Electrochim. Acta* **2000**, *45*, 3497. (b) Dijksma, M.; Boukamp, B. A.; Kamp, B.; van Bennekom, W. P. *Langmuir* **2002**, *18*, 3105. (c) Cui, X.; Jiang, D.; Diao, P.; Li, J., Tong, R.; Wang, X. *J. Electroanal. Chem.* **1999**, *470*, 9. (d) Janek, R. P.; Fawcett, W. R.; Ulman, A. *J. Phys. Chem. B* **1997**, *101*, 8550.
(57) Finklea, H. O.; Avery, S.; Lynch, M.; Furtsch, T. *Langmuir* **1987**, *3*, 409.
(58) Diao, P.; Jiang, D.; Cui, X.; Gu, R.; Tong, D.; Zhong, B. *J. Electroanal. Chem.* **1999**, *464*, 61.
(59) Miller, C.; Cuendet, P.; Grätzel, M. *J. Phys. Chem.* **1991**, *95*, 877.
(60) Colton, R. J., Engel, A., Frommer, J. E., Gaub, H. E., Gewirth, A., Guckenberger, R., Heckl, W. M., Parkinson, B., Rabe, J., Eds. *Procedures in Scanning Probe Microscopies*; John Wiley & Sons Ltd.: New York, 1998.
(61) Barros, T. C.; Berci, P.; Toscano, V. G.; Politi, M. J. *J. Photochem. Photobiol. A: Chem.* **1995**, *89*, 141.
(62) Barros, T. C. *J. Photochem. Photobiol. A: Chem.* **1993**, *76*, 55.

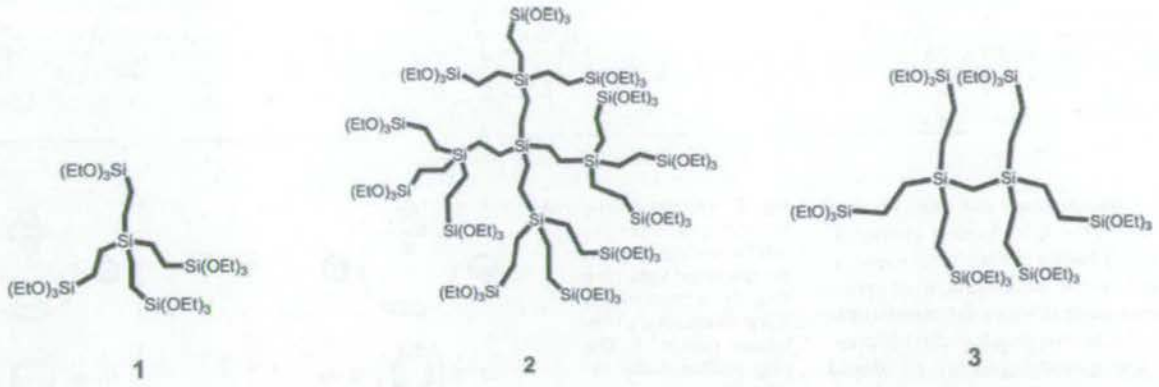

Scheme 1.

SiC_4 units. The integral ratios were reproducible, with varying pulse delay times between 3 and 30 s, indicating that the ^{29}Si nuclei were sufficiently relaxed to give accurate integrals. Nitrogen isotherms demonstrated the ordered mesoporous nature of both PMD-2 and PMD-3 by showing typical type-IV isotherms. The BET surface areas were 775 $m^2\ g^{-1}$ (PMD-2) and 767 $m^2\ g^{-1}$ (PMD-3). The BJH analysis revealed a narrow pore size distribution with average pore sizes of 9.1 nm (PMD-2) and 8.2 nm (PMD-3), which is consistent with the TEM data.

References and Notes

1. I. W. Hamley, *Angew. Chem. Int. Ed. Engl.* **42**, 1692 (2003).
2. G. J. de A. A. Soler-Illia, C. Sanchez, B. Lebeau, J. Patarin, *Chem. Rev.* **102**, 4093 (2002).
3. G. R. Newkome, E. He, C. N. Moorefield, *Chem. Rev.* **99**, 1689 (1999).
4. M. Fischer, F. Vögtle, *Angew. Chem. Int. Ed. Engl.* **38**, 884 (1999).
5. C. T. Kresge, M. Leonowicz, J. C. Vartuli, J. S. Beck, *Nature* **359**, 710 (1992).
6. A. W. Van der Made, P. W. N. M. Van Leeuwen, *Chem. Commun.* 1400 (1992).
7. M. J. Michalczyk, W. J. Simonsick Jr., K. G. Sharp, *J. Organomet. Chem.* **521**, 261 (1996).
8. D. Seyferth, D. Y. Son, A. L. Rheingold, R. L. Ostrander, *Organometallics* **13**, 2682 (1994).
9. Materials and methods are available as supporting material on *Science* Online.
10. S. Inagaki, S. Guan, Y. Fukushima, T. Ohsuna, O. Terasaki, *J. Am. Chem. Soc.* **121**, 9611 (1999).
11. The authors thank Dr. N. Coombs for the TEM imaging. G.A.O. is Government of Canada Research Chair in Materials Chemistry. He is indebted to the Natural Sciences and Engineering Research Council of Canada for support of this work.

Supporting Online Material
www.sciencemag.org/cgi/content/full/306/5701/1529/DC1
Materials and Methods

26 August 2004; accepted 13 October 2004

A Reversible Synthetic Rotary Molecular Motor

José V. Hernández, Euan R. Kay, David A. Leigh*

The circumrotation of a submolecular fragment in either direction in a synthetic molecular structure is described. The movement of a small ring around a larger one occurs through positional displacements arising from biased Brownian motion that are kinetically captured and then directionally released. The sense of rotation is governed solely by the order in which a series of orthogonal chemical transformations is performed. The minimalist nature of the [2]catenane flashing ratchet design permits certain mechanistic comparisons with the Smoluchowski-Feynman ratchet and pawl. Even when no work has to be done against an opposing force and no net energy is used to power the motion, a finite conversion of energy is intrinsically required for the molecular motor to undergo directional rotation. Nondirectional rotation has no such requirement.

Molecular-level motors differ from their macroscopic counterparts not only in scale but in how environmental factors influence their operation. Macroscopic machines are generally unaffected by ambient thermal energy, and a directional force must be applied to cause movement of each component. For molecular-sized motors, however, inertia is negligible and the parts are subject to random and incessant Brownian motion (*1*). Rather than fight this effect, biological motors use these random fluctuations in their mechanisms (*2*). For example, in F_1F_0–adenosine triphosphatase (ATPase), which spins the γ shaft counterclockwise (viewing F_1 from above) as proton-motive force powers ATP production and clockwise if ATP is consumed to drive proton flow against a concentration gradient (*3*), Brownian motion drives both the power and exhaust strokes (*2*). Inspired by such biological motors and by Feynman's celebrated discussion (*4*) of the miniature ratchet and pawl first introduced (*5*) by Smoluchowski, efforts have been made to design molecules that exhibit directional control over submolecular rotary motion (*6–10*). Unidirectional rotation about single (*11*, *12*), double (*13–16*), and mechanical (*17*) bonds has been achieved, but unlike F_1F_0-ATPase, these artificial motor molecules are only able to rotate in one direction but not the other. We now report on a molecular structure in which a fragment can be circumrotated in either direction, and we probe features of the underlying mechanism.

During the past decade, a number of remarkable theoretical formalisms have been developed using nonequilibrium statistical physics that explain how various types of fluctuation-driven transport can occur (*18*, *19*). Underlying each of these Brownian ratchet or motor mechanisms are three components (*20*): (i) a randomizing element (*21*), (ii) an energy input to avoid falling foul of the Second Law of Thermodynamics (*22*, *23*), and (iii) asymmetry in the energy or information potential in the dimension in which the motion occurs.

School of Chemistry, University of Edinburgh, The King's Buildings, West Mains Road, Edinburgh EH9 3JJ, UK.

*To whom correspondence should be addressed. E-mail: David.Leigh@ed.ac.uk

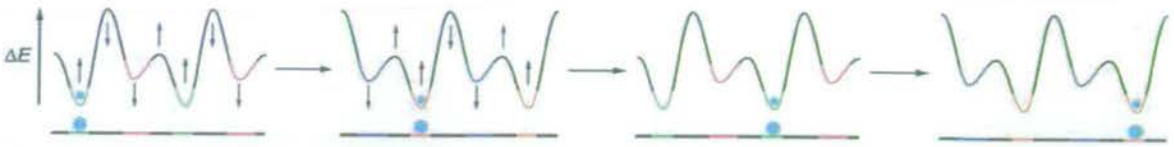

Fig. 1. A flashing energy ratchet mechanism for Brownian particle transport along an oscillating potential energy surface.

Such ratchet mechanisms not only account for the general principles behind biological motors (*24*–*27*) but have also been successfully applied to the development of transport and separation devices for mesoscopic particles and macromolecules, microfluidic pumping, the photoalignment of liquid crystals, and quantum and electronic applications (*26*, *28*–*31*).

A flashing ratchet is a particular type of energy ratchet mechanism (*25*), a classic example of which consists in physical terms (Fig. 1) of an asymmetric potential energy surface (a periodic series of two different minima and two different maxima) along which a Brownian particle is directionally transported by sequentially raising and lowering each set of minima and maxima by changing the potential (for example, with an oscillating electric field and a charged particle). Catenanes and rotaxanes, molecules in which components are physically linked together but not connected by covalent bonds, are excellent systems with which to study characteristics of submolecular motion (*8*). The mechanical linkage inherently restricts certain degrees of freedom for the relative displacement of the interlocked components while simultaneously permitting large-amplitude motion in the allowed vectors. The way in which the principles of an energy ratchet can be applied to a catenane architecture is not to consider the whole structure as a molecular machine, but rather to view one macrocycle as a motor that transports a substrate—the other ring—directionally around itself. In its simplest manifestation, this gives rise to a [2]catenane such as **1** (Fig. 2) that should be able to unidirectionally rotate the smaller ring about the larger one in response to a series of chemical reactions.

There are several differences, however, between the flashing ratchet particle transport mechanism in Fig. 1 and the one applied to catenane **1** in Fig. 2: (i) The molecular system is cyclic, so the translational transport along a periodic energy potential becomes a directional rotation around a two-minima–two-maxima loop; (ii) only one energy minimum is varied for **1**, not both (which is sufficient to ensure that the energy difference between the two minima changes twice); and (iii) the single steps that simultaneously change minima depth and maxima height in the classical energy ratchet mechanism are separated into their thermodynamic and kinetic constituents in the chemical system. Despite these differences, the physical principles behind the two mechanisms are the same.

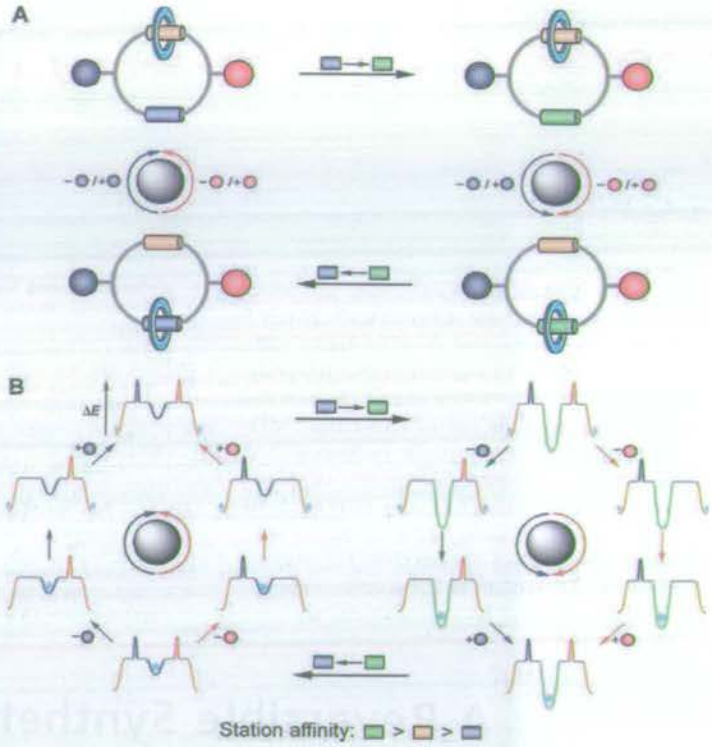

Fig. 2. (**A**) Schematic illustration and (**B**) potential energy surface for the small light blue ring in a minimalist [2]catenane rotary molecular motor, **1**. The ring preferentially resides on one or other of the two binding sites (stations), represented by colored cylinders. The colored spheres are bulky groups, each of which sterically blocks one of the two tracks between the stations. The blue-to-green and green-to-blue transformations represent (balance-breaking) chemical reactions that change the binding affinity of a station for the small ring, providing a driving force for the ring to redistribute itself between the stations if it is able to be exchanged between them. Removal of a red or purple sphere (linking reaction) allows the ring to move between stations by a particular route. Reattachment of the sphere (unlinking reaction) ratchets the net transported quantity of rings.

In chemical terms, catenane **1** is a stimuli-responsive molecular shuttle (*8*, *32*) with two routes (each of which can be independently blocked) that connect the two binding sites or "stations" for the small macrocycle (Fig. 3). To satisfy oneself that internal motion within a chemical structure can be described in terms of a stochastic transport mechanism, it is useful to consider how the net change of position occurs within a typical stimuli-responsive molecular shuttle (*32*). At equilibrium, the small macrocycle is distributed between two different stations (an asymmetric track) according to a Boltzmann distribution. An external trigger (the energy input) chemically modifies one binding site in such a way that the initially disfavored station becomes energetically more favorable for the macrocycle. Thermal fluctuations (the randomizing element) provide the energy required by the small macrocycle to sever its interactions with a station and set off on a Brownian walk through which the new equilibrium position is established.

Catenane **1** was prepared as the *fum*-*E*-**1** (*33*) isomer according to Fig. 3 (*34*, *35*). Net changes in the position or potential energy of the smaller ring were sequentially achieved by (i) photoisomerization to the maleamide (→*mal*-*Z*-**1**) (*36*, *37*); (ii) de-silylation/re-silylation (→*succ*-*Z*-**1**); (iii) reisomerization to the fumaramide (→*succ*-*E*-**1**); and finally, (iv) de-tritylation/re-tritylation to regenerate *fum*-*E*-**1**, the whole reaction sequence producing a net clockwise (as drawn in Fig. 3) circumrotation of the small ring about the larger one. Exchanging the order of steps (ii) and (iv) generated the equivalent counterclockwise rotation of the small ring. The time scales and number of reactions involved for directional rotation in **1** make it somewhat less practical than the methods previously developed for nonreversible synthetic rotary motors (*11*–*17*). Nevertheless, the chemistry is surprisingly robust and can be carried out as a direct sequence of reactions without purification at each stage, using resins to neutralize or remove excess re-

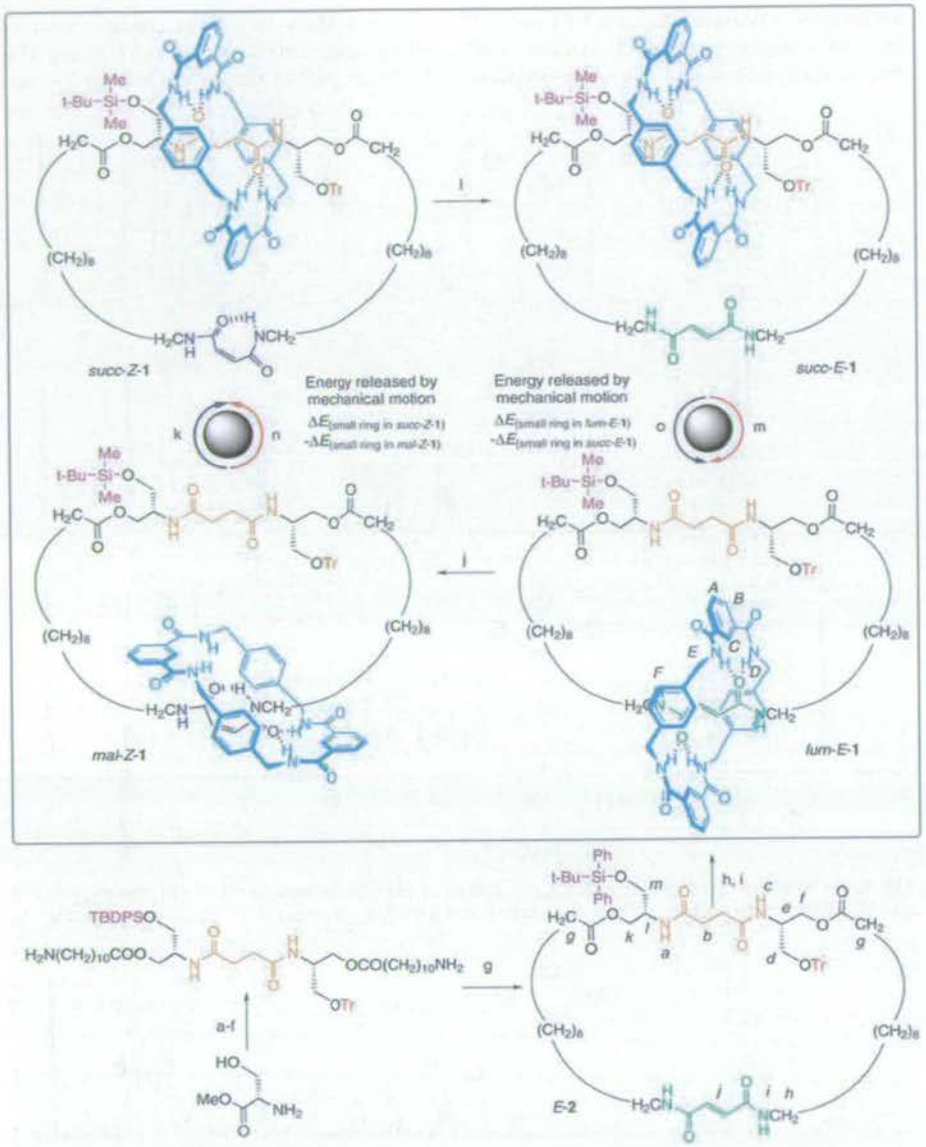

Fig. 3. Synthesis route and operation of reversible rotary motor **1**. Reagents and conditions (unless otherwise stated, reactions were carried out at room temperature and in CH_2Cl_2) were as follows: step a, succinyl chloride, triethylamine (Et_3N), and *N*,*N*-dimethyformamide (DMF) 0°C, 2 hours, 80%; step b, *t*-butyldiphenylsilyl chloride (TBDPSCl), NH_4NO_3, DMF, 8 hours, 30%; step c, trityl chloride (TrCl), Bu_4NClO_4, 2,4,6-collidine, $CHCl_3$, 61°C, 2 hours, 86%; step d, $NaBH_4$, LiCl, tetrahydrofuran and ethanol, 8 hours, 79%; step e, $FmocNH(CH_2)_{10}CO_2H$, dicyclohexylcarbodiimide (DCC), 1-hydroxybenzotriazole (HOBt), 4-(dimethylamino)pyridine, 8 hours, 85%; step f, Et_2NH, 8 hours, 73%; step g, fumaric acid, DCC, HOBt, $CHCl_3$, 8 hours, 52%; step h, 8 equivalents of isophthaloyl dichloride, 8 equivalents of *p*-xylylenediamine, Et_3N, $CHCl_3$, 3 hours, 30%; step i, tetrabutylammonium fluoride (TBAF), 20 min then cool to −10°C and add 2,4,6-collidine, *t*-butyldimethylsilyl triflate (TBDMSOTf), 40 min, overall 72%; step j, hν 254 nm, 5 min, 50%; step k, TBAF, 20 min then cool to −78°C and add 2,4,6-collidine, TBDMSOTf, 1 hour, overall 61%; step l, piperidine, 1 hour, ~100%; step m, $Me_2S{\cdot}BCl_3$, −10°C, 10 min, and then TrCl, Bu_4NClO_4, 2,4,6-collidine, 16 hours, overall 74%; step n, $Me_2S{\cdot}BCl_3$, −10°C, 15 min, then cool to −78°C and add 2,4,6-collidine, TrOTf, 5 hours, overall 63%; step o, TBAF, 20 min, then cool to −10°C and add 2,4,6-collidine, TBDMSOTf, 40 min, overall 76%. The above refer to preparative yields of isolated compounds. Net clockwise circumrotation was also achieved in one pot through the successive addition of reagents to *fum*-*E*-**1** in the following sequence (¹H NMR-determined percentage conversions are given in parentheses): step j, hν 254 nm, 5 min (50% *mal*-*Z*-**1** present); step k, 4 equivalents of TBAF, 20 min, cool to −78°C and add 30 equivalents of TBDMSOTf and 30 equivalents of 2,4,6-collidine, 30 min, then 60 equivalents of Wang resin, Dowex MR mixed bed ion-exchange resin and activated 4 Å molecular sieves, decant (~33% *succ*-*Z*-**1** present); step l, 20 equivalents of piperidine, 1 hour, then Dowex MR mixed bed ion-exchange resin, decant (~33% *succ*-*E*-**1** present); step m, 1 equivalent of $Me_2S{\cdot}BCl_3$, −10°C, 5 min, and then add 25 equivalents of 2,4,6-collidine and 20 equivalents of TrOTf, 1 hour (~90% *fum*-*E*-**1** present; ~28% of the total molecules in the sample having undergone circumrotation). The chirality of **1** is present only for synthetic convenience.

agents and byproducts, with only modest reductions in yields indicated by ¹H nuclear magnetic resonance (NMR) spectroscopy.

Unlike the previously reported (*17*) [3]catenane rotor, which relied on the dynamics of model compounds to determine stimuli-induced unidirectional behavior, the sense of rotation in **1** was demonstrated directly by isolation of samples of the [2]catenane after each synthetic step and the position of the small ring unambiguously determined by ¹H NMR (Figs. 4 and 5). Shielding effects reveal the position of the small macrocycle in each of the four catenane isomers. Comparison of the spectrum of *fum*-*E*-**1** (Fig. 4A) with that of the macrocycle *E*-**2** (Fig. 4B) shows a downfield shift of the H_j protons of the fumaramide station but not the succinamide group (H_b) in the catenane. In contrast, *succ*-*E*-**1** (Fig. 4C) features a −1.3 parts per million difference in the H_b protons but little change in the signals of the fumaramide residue. The macrocycle is similarly located over the succinamide residue in *succ*-*Z*-**1** (see, for example, the shifts of H_b in Fig. 5, B and C). Finally, although the small ring does not spend too much time actually over the poorly binding maleamide station in *mal*-*Z*-**1** (as evidenced by the relatively small shift in H_j in Fig. 5A as compared to Fig. 5B), it is clearly trapped on the maleamide side of the silyl and trityl blocking groups because of the lack of shielding of the succinamide signals (H_b are unchanged between Fig. 5A and Fig. 5B) and some significant shielding observed for H_h.

Biological motors are too complex for the thermodynamic function of individual amino acid movements to be unravelled in detail. In contrast, the apparent simplicity of **1** and the minimalist nature of its design allow insight into the fundamental role that each part of the structure plays in the operation of the rotary machine.

The various chemical transformations perform two different functions: One pair (the linking/unlinking reactions, steps k and m or n and o in Fig. 3) modulates whether the small macrocycles can be exchanged between the two binding sites on the big ring (that is, allow the small macrocycle to become statistically balanced between the two binding sites according to a Boltzmann distribution); the second pair (balance-breaking reactions, steps j and l in Fig. 3) isomerize the olefin station (either *E*→*Z* or *Z*→*E*), switching its binding affinity for the small macrocycle either on or off (*37*). By changing the relative binding affinities of the two stations in the large ring, each balance-breaking stimulus provides a driving force for redistribution of the small ring if it is able to move between the binding sites. In other words, the stations and blocking groups effectively disconnect the thermodynamic and kinetic components of detailed

balance (*22*, *23*); the balance-breaking reactions control the thermodynamics and impetus for net transport by biased Brownian motion, and the linking/unlinking reactions largely (*38*) control the relative kinetics and ability to exchange. Raising a kinetic barrier also "ratchets" transportation, allowing the statistical balance of the small ring to be subsequently broken without reversing the preceding net transportation sequence. Lowering a kinetic barrier allows "escapement" of a ratcheted quantity of rings in a particular direction.

To obtain 360° rotation of the small ring about the large ring, the four sets of reactions must be applied in one of two sequences, each taking the following form: first a balance-breaking reaction; then a linking/unlinking step; then the second balance-breaking reaction; finally, the second linking/unlinking step. The direction of net rotation is determined solely by the way in which the balance-breaking and linking/unlinking steps are paired: an external input of information. The efficiency or yields of the reactions or the position of the ring at any stage (even if the machine makes a "mistake") are immaterial to the direction in which net motion occurs, as long as the reactions continue to be applied in the same sequence. Although reversing the sequence of the four steps changes the pairings and so rotates the small ring in the opposite direction, reversing the entire sequence of six chemical reactions does not, because linking/unlinking operations are not commutative.

We finish the circumrotation reaction sequence with the same molecule, *fum-E*-**1**, that we started with (although a 360° rotation of one fragment has occurred), and the light-fueled balance-breaking reaction is reversed by a quantitative exoergic reaction, so no net energy is consumed to fuel the rotation. This is in one sense obvious, because the movement of the small ring takes place through Brownian motion and does not have to be powered; and in another somewhat surprising, because directional circumrotation of the small ring has occurred, which could be used to do external work—analogous to the hypothetical lifting of a flea by the Smoluchowski-Feynman ratchet and pawl (*4*). However, if the [2]catenane does do work against an opposing force, the energy required is taken from the balance-breaking reactions. If the balance-breaking chemical reactions do not actually fuel the net rotation, is it really necessary to carry them out? At first glance it seems that the small ring in a [2]catenane such as **3** might undergo directional circumrotation without them (Fig. 6).

Let us consider the situation in which 100% of the small rings are initially located on the succinamide station closest to the blocking groups: 100% *succ1*-**3**. De-tritylation followed by re-tritylation generates 50% *succ2*-**3** (and 50% remains as *succ1*-**3**). Treatment of this mixture with a de-silylation/re-silylation sequence leads to a final product mixture, which again is 50% *succ1*-**3** and 50% *succ2*-**3**. However, half of the molecules that are now

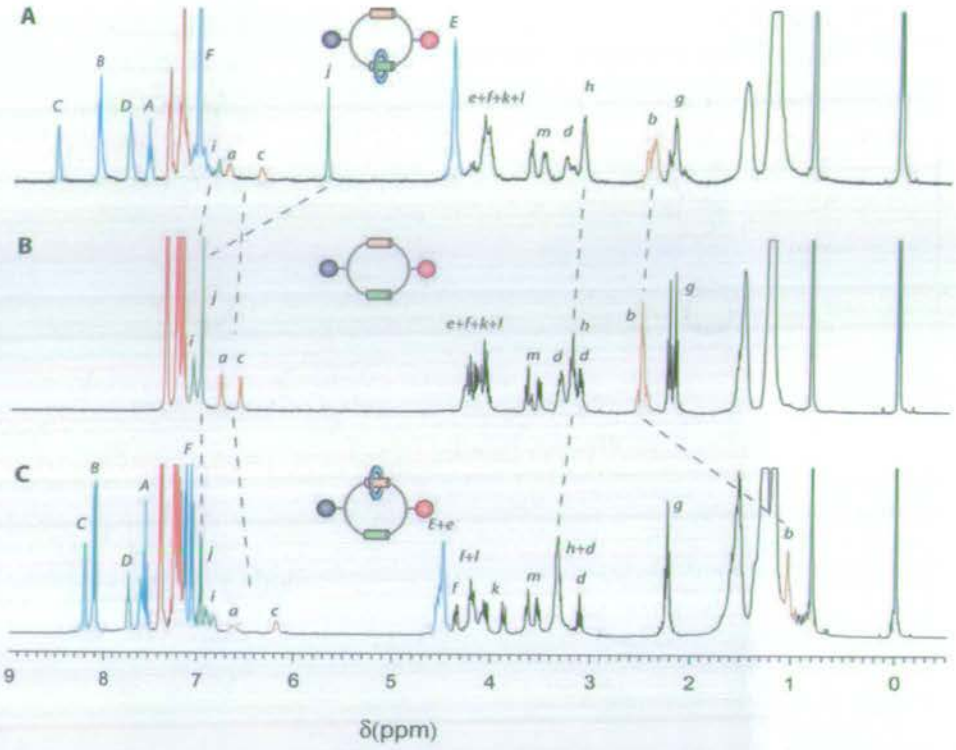

Fig. 4. ^{1}H NMR spectra (400 MHz, $CDCl_3$, at 298 K) of (A) [2]catenane *fum-E*-**1**, (B) macrocycle *E*-**2**, and (C) [2]catenane *succ-E*-**1**. The color coding and lettering correspond to those shown in Fig. 3.

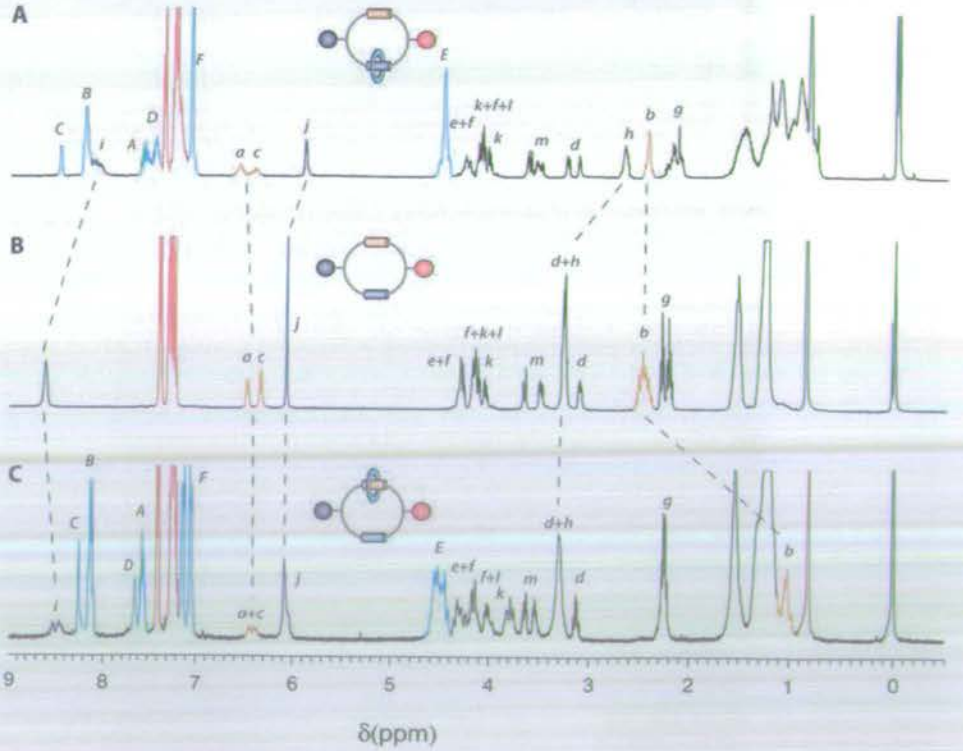

Fig. 5. ^{1}H NMR spectra (400 MHz, $CDCl_3$, at 298 K) of (A) [2]catenane *mal-Z*-**1**, (B) macrocycle *Z*-**2**, and (C) [2]catenane *succ-Z*-**1**.

succ1-**3** (25% of the total molecules) have undergone a 360° clockwise circumrotation of the small ring, and all of the *succ2*-**3** structures (50% of the total molecules) have undergone a 180° rotation of the small ring (half clockwise, half counterclockwise). The remaining 25% of total molecules have undergone no net positional change of the small ring, and so the average for the sample is a 90° clockwise rotation without applying any chemical reactions to change the relative values of the two stations' energy minima. When we apply the sequence of reactions for a second (or any subsequent) time, however, although 75% of the molecules again individually undergo partial or complete revolution of the small ring, no net rotation occurs in either direction over a bulk sample. The 50% of molecules that start as *succ1*-**3** give a net 90° clockwise rotation in response to the linking/unlinking sequence, and the 50% that start as *succ2*-**3** rotate an equivalent amount in a counterclockwise sense. A statistically significant number of catenane **3** molecules can only undergo net unidirectional rotation if the distribution of the small macrocycle between the binding sites is unbalanced at the start of the reaction sequence.

We can use some simple thermodynamic accountancy to calculate both the maximum amount of mechanical work that can be done by **1** and how much chemical energy has to be processed to cause directional motion of the small ring even if no work needs to be done against an opposing external force. The energy available to do work each time the small ring changes station equates to the macrocycle binding energy differences between the two sites (*32*). The light-fueled $E \rightarrow Z$ transformation allows up to $\Delta E_{(\text{small ring in } succ\text{-}Z\text{-}\mathbf{1})} - \Delta E_{(\text{small ring in } mal\text{-}Z\text{-}\mathbf{1})}$ to be performed during the subsequent linking step and the piperidine-catalyzed $Z \rightarrow E$ reaction permits a further $\Delta E_{(\text{small ring in } fum\text{-}E\text{-}\mathbf{1})} - \Delta E_{(\text{small ring in } succ\text{-}E\text{-}\mathbf{1})}$ (Fig. 3). Because $\Delta E_{(\text{small ring in } succ\text{-}Z\text{-}\mathbf{1})} \sim \Delta E_{(\text{small ring in } succ\text{-}E\text{-}\mathbf{1})}$, the maximum total mechanical work that can be performed by circumrotation is $\Delta E_{(\text{small ring in } fum\text{-}E\text{-}\mathbf{1})} - \Delta E_{(\text{small ring in } mal\text{-}Z\text{-}\mathbf{1})}$; that is, the difference in small ring binding affinity between the fumaramide and maleamide stations. It is interesting to note that the binding affinity of the intermediate station is irrelevant to the amount of work that can be carried out by the molecular motor.

A quantitative thermodynamic requirement for unidirectional rotation of the small ring is provided by the difference between the free energies of the sequence of reactions j, k, l, m carried out on *fum*-*E*-**1** and the same series of reactions applied to the macrocycle, *E*-**2**. The thermodynamics associated with the linking/unlinking steps cancel out (*39*). However, the $E \rightarrow Z$ isomerization step (step j) for the catenane is inherently more endothermic than the analogous reaction on the macrocycle because of the additional energy necessary to disrupt the hydrogen bond network of the small ring with the fumaramide station. The extra energy required to raise the potential energy of the transported particle (again, the difference in small ring binding energies of the fumaramide and maleamide stations) is returned to the thermal bath upon reisomerization to fumaramide and subsequent repositioning of the macrocycle. This requirement of extra energy to be processed by the system for the molecular machine to rotate directionally even when no work has to be done against an external force is once more reminiscent of the Smoluchowski-Feynman ratchet and pawl, which Feynman appreciated could be driven directionally by Brownian motion using heat flow between two thermal reservoirs; for example, by having the vanes attached to the shaft of the Feynman ratchet be hot and the wheel cold (*40*–*42*). We note that the amount of additional chemical energy that must be processed for directional rotation to occur in the catenane is the sum of the energy differences that govern the Boltzmann distribution of the small ring between the binding sites at each stage; that is, the factor that determines the directional efficiency of the motor at constant temperature.

Mechanisms formulated from nonequilibrium statistical mechanics can be successfully used to design synthetic molecular motors such as **1**. In turn, the analysis of this deceptively simple molecule, particularly the separation of the kinetic and thermodynamic requirements for detailed balance, provides experimental insight into how and why an energy input is essential for directional rotation of a submolecular fragment by Brownian motion. Even though no net energy is used to power the motion, there has to be a particular amount of energy conversion for net rotation to be directional over a statistically significant number of molecules; a requirement that is absent if the equivalent motion is nondirectional (or, indeed, for directional rotation within a single molecule where balance is inherently broken). The quantity of energy conversion required to induce directionality has an intrinsic lower limit, corresponding exactly (and somewhat beautifully) to both the energy difference that determines the directional efficiency of rotation and the maximum amount of work that the motor can theoretically perform in a single cycle; there can be no perpetually unidirectionally rotating molecular structure of the second kind through such a mechanism. The factors that determine the sense of rotation in **1**, together with the requirement for finite energy conversion for directional rotation in circumstances when no work is done against an external force, illustrate how interplay between informational and thermodynamic laws governs directional Brownian rotation in molecular structures.

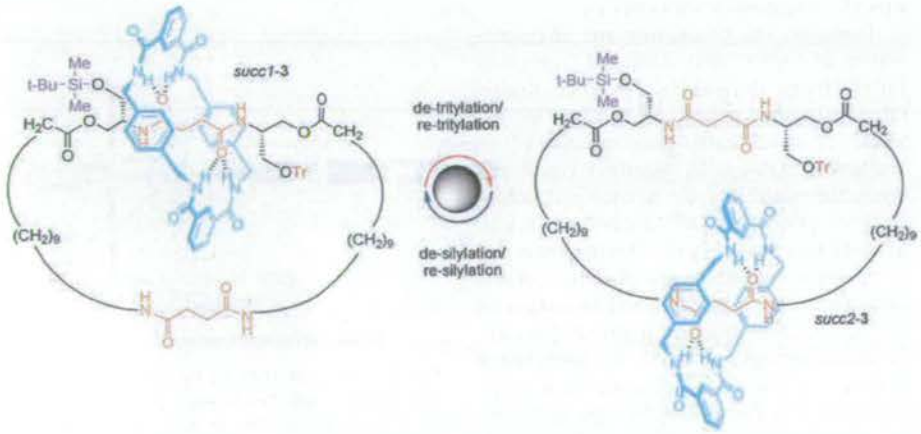

Fig. 6. Positional isomerism in a [2]catenane, **3**, with stations of degenerate binding energies.

References and Notes

1. E. M. Purcell, *Am. J. Phys.* **45**, 3 (1977).
2. M. Schliwa, Ed., *Molecular Motors* (Wiley-VCH, Weinheim, Germany, 2003).
3. P. D. Boyer, *Angew. Chem. Int. Ed.* **37**, 2296 (1998).
4. R. P. Feynman, R. B. Leighton, M. Sands, *The Feynman Lectures on Physics* (Addison-Wesley, Reading, MA, 1963), vol. 1, chap. 46.
5. M. von Smoluchowski, *Physik. Zeitschr.* **13**, 1069 (1912).
6. T. R. Kelly, I. Tellitu, J. P. Sestelo, *Angew. Chem. Int. Ed. Engl.* **36**, 1866 (1997).
7. A. P. Davis, *Angew. Chem. Int. Ed.* **37**, 909 (1998).
8. V. Balzani, A. Credi, F. M. Raymo, J. F. Stoddart, *Angew. Chem. Int. Ed.* **39**, 3349 (2000).
9. M. F. Hawthorne *et al.*, *Science* **303**, 1849 (2004).
10. C. P. Mandl, B. König, *Angew. Chem. Int. Ed.* **43**, 1622 (2004).
11. T. R. Kelly, H. De Silva, R. A. Silva, *Nature* **401**, 150 (1999).
12. T. R. Kelly, R. A. Silva, H. De Silva, S. Jasmin, Y. J. Zhao, *J. Am. Chem. Soc.* **122**, 6935 (2000).
13. N. Koumura, R. W. J. Zijlstra, R. A. van Delden, N. Harada, B. L. Feringa, *Nature* **401**, 152 (1999).
14. N. Koumura, E. M. Geertsema, M. B. van Gelder, A. Meetsma, B. L. Feringa, *J. Am. Chem. Soc.* **124**, 5037 (2002).

15. M. K. J. ter Wiel, R. A. van Delden, A. Meetsma, B. L. Feringa, *J. Am. Chem. Soc.* **125**, 15076 (2003).
16. R. A. van Delden, M. K. J. ter Wiel, H. De Jong, A. Meetsma, B. L. Feringa, *Org. Biomol. Chem.* **2**, 1531 (2004).
17. D. A. Leigh, J. K. Y. Wong, F. Dehez, F. Zerbetto, *Nature* **424**, 174 (2003).
18. P. Reimann, *Phys. Rep.* **361**, 57 (2002).
19. J. M. R. Parrondo, L. Dinis, *Contemp. Phys.* **45**, 147 (2004).
20. R. D. Astumian, *Science* **276**, 917 (1997).
21. Randomizing influences other than Brownian motion can be used in ratchet mechanisms. For example, in quantum ratchets, quantum effects such as tunneling play this role.
22. The principle of detailed balance (*23*) tells us that no net task can be performed by the fluxional exchange of components at equilibrium, because transitions take place at the same rate in opposite directions. The structure of catenane 1 is remarkable in that it separates the kinetic (ability to exchange) and thermodynamic (impetus for net transport) requirements for detailed balance.
23. L. Onsager, *Phys. Rev.* **37**, 405 (1931).
24. R. D. Astumian, P. Hänggi, *Phys. Today* **55**, 33 (November 2002).
25. R. D. Astumian, I. Derényi, *Eur. Biophys. J.* **27**, 474 (1998).
26. Special issue on "Ratchets and Brownian Motors: Basics, Experiments and Applications," H. Linke, Ed., *Appl. Phys. A* **75**, 167 (2002).
27. G. Oster, H. Y. Wang, *Trends Cell Biol.* **13**, 114 (2003).
28. J. Rousselet, L. Salome, A. Ajdari, J. Prost, *Nature* **370**, 446 (1994).
29. L. P. Faucheux, L. S. Bourdieu, P. D. Kaplan, A. J. Libchaber, *Phys. Rev. Lett.* **74**, 1504 (1995).
30. J. S. Bader *et al.*, *Proc. Natl. Acad. Sci. U.S.A.* **96**, 13165 (1999).
31. S. Matthias, F. Müller, *Nature* **424**, 53 (2003).
32. A. Altieri *et al.*, *Angew. Chem. Int. Ed.* **42**, 2296 (2003).
33. The prefix indicates the position of the smaller macrocycle on the larger one.
34. Although catenane *fum-E*-1 was originally prepared as its *O-t*-butyldiphenylsilyl (TBDPS) derivative, the steric bulk caused low yields during the re-silylation protocol of step k, so it was replaced with the smaller TBDMS group for all the directional rotation studies.
35. Materials and methods are available as supporting material on *Science* Online.
36. The photoisomerization reaction gives a 50:50 *E:Z* mixture in the photostationary state. No accompanying photodegradation or decomposition was detected (*37*).
37. F. G. Gatti *et al.*, *Proc. Natl. Acad. Sci. U.S.A.* **100**, 10 (2003).
38. By raising or lowering the energy minima, the balance-breaking reactions intrinsically affect the kinetic barriers as well.
39. This is not quite as simple as the ΔG values of the forward and reverse covalent bond forming and breaking reactions canceling each other out. When unlinking takes place, the restriction in freedom of movement reduces the entropy of the small macrocycle in addition to the ΔG change associated with the chemical reaction; however, when linking occurs, the entropy increases by the same amount.
40. Certain aspects of Feynman's discussion of the ratchet and pawl as a motor have been shown to be flawed (*41*, *42*).
41. J. M. R. Parrondo, P. Español, *Am. J. Phys.* **64**, 1125 (1996).
42. M. O. Magnasco, G. Stolovitzky, *J. Stat. Phys.* **93**, 615 (1998).
43. This work was supported by the Carnegie Trust (a scholarship to E.R.K.) and the European Union (a Marie Curie Fellowship to J.V.H.).

Supporting Online Material
www.sciencemag.org/cgi/content/full/306/5701/1532/DC1
Materials and Methods
Scheme S1

11 August 2004; accepted 8 October 2004

Three-Dimensional Hydrogen Microscopy in Diamond

P. Reichart,[1]*† G. Datzmann,[1] A. Hauptner,[1] R. Hertenberger,[2] C. Wild,[3] G. Dollinger[1]‡

A microprobe of protons with an energy of 17 million electron volts is used to quantitatively image three-dimensional hydrogen distributions at a lateral resolution better than 1 micrometer with high sensitivity. Hydrogen images of a <110>-textured undoped polycrystalline diamond film show that most of the hydrogen is located at grain boundaries. The average amount of hydrogen atoms along the grain boundaries is $(8.1 \pm 1.5) \times 10^{14}$ per square centimeter, corresponding to about a third of a monolayer. The hydrogen content within the grain is below the experimental sensitivity of 1.4×10^{16} atoms per cubic centimeter (0.08 atomic parts per million). The data prove a low hydrogen content within chemical vapor deposition–grown diamond and the importance of hydrogen at grain boundaries, for example, with respect to electronic properties of polycrystalline diamond.

Diamond is a promising material for various applications. Although its chemical and mechanical properties have led already to widespread applications, its potential for electronic or optical application remains limited because of imperfections (*1*). The recently demonstrated high carrier mobility in single-crystal chemical vapor–deposited diamond (*2*) opens perspectives for electronic devices in hostile, high-voltage, or high-temperature environments (*3*); diamond optics (*4*); radiation sensors (*5*); and particle detectors (*6*).

However, the production and characterization of high-quality diamond, especially for electronic devices, is a great challenge. Chemical vapor deposition (CVD), for example, is a well-established method (*7*) to synthesize high-quality diamond layers and opens the possibility for hetero- and homoepitaxial growth of CVD diamond layers up to some mm thickness (*8*, *9*). One main aim is to understand the origin of structural imperfections and impurities and to reduce or control these in order to improve the electronic and optical properties. The presence of hydrogen is known to influence these properties (*10*, *11*). Depending on type and quality, average hydrogen concentrations were found from below the detection limits of 10^{17} atoms/cm^3 up to about 10^{19} atoms/cm^3 in the bulk of polycrystalline diamond layers (*12*). Also, several hydrogen-related complexes were identified (*13*–*15*). However, there is insufficient information about the quantity and the spatial distribution of these, and perhaps as-yet-unidentified, types of hydrogen-related defects. It is even unknown whether most of the hydrogen being detected in diamond is concentrated at grain boundaries, inclusions, and other extended defects or whether hydrogen is distributed homogeneously throughout the bulk at defects of atomic dimensions. The decrease of the hydrogen content with increasing size of the crystallites inside polycrystalline CVD diamond layers, as well as infrared (*15*) or electron spin resonance studies (*16*), indirectly indicate that most of the hydrogen is situated at grain boundaries. Another explanation, however, is that there is reduced defect density within the grains with growing film thickness. Information about the absolute quantity of hydrogen inside the grain compared with

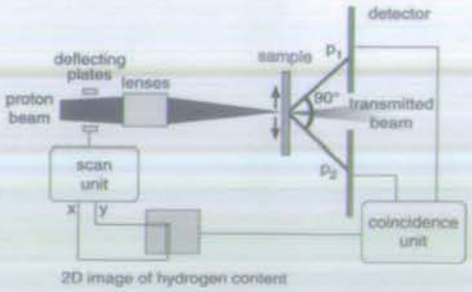

Fig. 1. Hydrogen analysis by pp scattering. The two protons emitted from a proton scattered at a hydrogen nuclei of the sample are detected in coincidence by a suitable detection system (*25*).

[1]Physik Department E12, Technische Universität (TU) München, 85748 Garching, Germany. [2]Department für Physik, Ludwig-Maximilians-Universität (LMU) München, 85748 Garching, Germany. [3]Fraunhofer Institut für Angewandte Festköperphysik, 79108 Freiburg, Germany.

*Present address: Microanalytical Research Centre, School of Physics, University of Melbourne, Victoria, 3010, Australia.
†To whom correspondence should be addressed. E-mail: p.reichart@ph.unimelb.edu.au
‡Present address: Angewandte Physik und Messtechnik, Universität der Bundeswehr München, 85577 Neubiberg, Germany.

7
Synthetic Molecular Machines

Euan R. Kay and David A. Leigh

7.1
Introduction

The widespread use of molecular-level motion in key natural processes suggests that great rewards could come from bridging the gap between the present generation of synthetic molecular systems – which usually rely on electronic and chemical effects to perform their functions – and the machines of the macroscopic world, which utilize the synchronized movements of smaller parts to perform particular tasks. In recent years it has proved relatively straightforward to design synthetic molecular systems in which positional changes of submolecular components occur by moving energetically downhill, but what are the structural features necessary for molecules to use directional displacements to do work? How can we make a synthetic molecular machine that pumps ions against a gradient, for example, or moves itself energetically uphill along a track? Artificial compounds that can do such things have yet to be realized; the field of synthetic molecular machines is still in its infancy and only the most basic systems – mechanical switches and slightly more sophisticated, but still rudimentary, molecular rotors – have been made thus far. In this chapter we outline the early successes in taming molecular-level motion and the progress made toward utilizing synthetic molecular structures to perform mechanical tasks. We also highlight some of the challenges and problems that must still be overcome.

The path toward synthetic molecular machines starts nearly two centuries ago, with the discovery of the random nature of molecular-level motion. In 1827, the Scottish botanist Robert Brown noted through his microscope the incessant, haphazard motion of tiny particles within translucent pollen grains suspended in water. Subsequent investigations of both biological and inorganic materials led to the realization that all objects are subject to constant buffeting by their surroundings, as a result of the motions which intrinsically occur at the molecular level. A complete explanation of the phenomenon – now known as Brownian motion or movement – had to wait for Einstein nearly 80 years later, but ever since scientists have been fascinated by the stochastic nature of molecular-level motion and its implications. In exciting develop-

Functional Synthetic Receptors. Edited by T. Schrader, A. D. Hamilton

ISBN: 3-527-30655-2

ments over the past decade, theoretical physics has explained how random, directionless fluctuations can cause directed motion of particles [1, 2] which successfully accounts for the general principles behind biological motors [3]. The chemist's interest in the creation, behavior, and control of molecular structures means that an understanding of the physics involved can now help him/her to design artificial structures which perform mechanical operations at the molecular-level and transpose those effects to the macroscopic world. Nature provides proof that such an approach is possible in the form of ion pumps, motor proteins, photoactive proteins, retinal, and many other natural products [4]. Indeed, biological structures have already been incorporated into semi-synthetic biomaterials which can perform "unnatural" mechanical tasks [5]; now the synthetic chemist is trying to create functional molecular machines from scratch. Initially, such systems will probably be simpler and less effective than their biological counterparts, yet there is no reason to suggest that one day they might not be just as powerful or ubiquitous.

7.1.1 Molecular-level Machines and the Language Used to Describe Them

It has been suggested that problems arise as soon as a scientific definition is established. In fact, of course, language scholars tell us that precisely the opposite is true. Language – especially scientific language – must be suitably defined and correctly used to accurately convey concepts in a field. Nowhere is the need for accurate scientific language more apparent than in the discussion of the ideas and mechanisms by which nanoscale machines could – and do – operate. Much of the terminology used comes from phenomena observed by physicists and biologists, but unfortunately their findings and descriptions have sometimes been misunderstood and misapplied by chemists. Perhaps inevitably in a newly emerging field, there is not even clear agreement in the literature about what constitutes molecular machines and what differentiates them from other molecular devices [6]. Initially, categorization of molecules as machines was purely iconic – the structures "looked" like pieces of machinery – or they were so-called because they carried out a function that in the macroscopic world would require a machine to perform it. Many of the chemical systems first likened to pistons and other machines were simply host–guest complexes in which the binding could be switched "on" or "off" by external stimuli such as light. Although these early studies were unquestionably the key to popularizing the field, with hindsight consideration of the effects of scale tells us that supramolecular decomplexation events have little in common with the motion of a piston (the analogy is better within a rotaxane architecture, because the components are still kinetically associated after decomplexation) and that a photosensitizer is not phenomenologically related to a "light-fuelled motor". In fact, it is probably most useful differentiate "device" and "machine" on the basis that the etymology and meaning of "machine" implies mechanical movement – i.e. at the molecular level a net nuclear displacement – which causes something useful to happen. This leads to the definition that "molecular machines" are a subset of molecular devices (functional molecular systems) in which a stimulus triggers the controlled, large-amplitude mechanical motion of

one component relative to another (or of a substrate relative to the machine) which results in a net task being performed. In this chapter we shall not discuss the larger field of supramolecular devices but will limit our discussion to approaches to machines, systems that actually feature some control over molecular-level motion. The examples given illustrate this point and help demonstrate the requirements for mechanical task performance at the molecular-level.

7.1.2 Principles of Motion at the Molecular Level – the Effects of Scale

The random thermal fluctuations experienced by molecules dominate mechanical behavior in the molecular world. Even the most efficient nanoscale machines – the motor proteins found in Nature – are swamped by its effect. A typical motor protein consumes ATP fuel at a rate of 100–1000 molecules every second, corresponding to a maximum possible power output in the region 10^{-16} to 10^{-17} W per molecule. When compared with the random environmental buffeting of ~10^{-8} W experienced by molecules in solution at room temperature, it seems remarkable that *any* form of controlled motion is possible [1].

The constant presence of Brownian motion is not the only distinction between motion at the molecular-level and in the macroscopic world. Because the physics which govern mechanical dynamic processes in the two regimes are completely different, vastly different mechanisms are required for controlled transport or propulsion. In the macroscopic world the equations of motion are governed by inertial terms (dependent on mass). Viscous forces (dependent on surface areas) dampen motion by converting kinetic energy into heat and objects do not move until provided with specific energy to do so. In a macroscopic machine this is often provided through a directional force when work is done to move mechanical components in a particular way. As objects become less massive and smaller in dimension, inertial terms decrease in importance and viscous terms begin to dominate. A parameter which quantifies this effect is Reynolds number – essentially the ratio of inertial to viscous forces – given by Eq. (1) for a particle of length dimension a, moving at velocity v, in a medium with viscosity η and density ρ [7]:

$$R = \frac{a v \rho}{\eta} \tag{1}$$

Size affects modes of motion long before we reach the nanoscale. Even at the mesoscopic level of bacteria (length dimensions ~10^{-5} m), viscous forces dominate. At the molecular level, Reynolds number is extremely low (except at low pressures in the gas phase) and the result is that molecules, or their components, cannot be given a one-off "push" in the macroscopic sense – momentum has become irrelevant. The motion of a molecular-level object is determined entirely by the forces acting on it at that particular instant – whether they be externally applied forces, viscosity or random thermal perturbations and Brownian motion. In more general terms, this analysis points to a central tenet – although the macroscopic machines we encounter in every-

day life may provide the inspiration for what we might like molecular machines to achieve, drawing too close an analogy for their modes of operation is a poor design strategy. The "rules of the game" at different length scales are simply too different. Two basic principles *must* be followed for any molecular device to be able to carry out a mechanical function:

- First, the movement of the kinetically-associated molecules or their components must be controlled by employing interactions which restrict the natural tendency for three-dimensional random motion and, somehow, bias, rectify, or direct the motion along the required vectors.
- Second, the Second Law of Thermodynamics tells us that no machine can continually operate solely using energy drawn from the thermal bath, so an external input of energy is required to perform a mechanical task with any synthetic molecular machine.

Learning how to make successful designs based on these two principles is the subject of the rest of the chapter.

7.2
Controlling Conformational Changes

Consideration of the restriction of thermal motion in chemistry first arose in regard to a fundamental question of molecular stereochemistry [8]. The rotational triple energy minima about C–C single bonds follows directly from the tetrahedral geometry of saturated carbon centers, yet it was not proven experimentally until 1936 [9]. In the 1960s and 70s sterically crowded systems were synthesized which included examples of different atropisomers of constitutionally identical chemical structures and characterization of rotamerization about sp^2–sp^3 and sp^3–sp^3 linkages, elegantly illustrated by the triptycenes investigated by Ōki and coworkers (for example **1**, Fig. 7.1) [10].

These studies inspired the first molecular analogs of macroscopic machine parts – propellers and gears [11]. Linking 9-triptycyl units through an sp^3 linker, Iwamura and Mislow independently created "molecular gears" such as **2** in the early 1980s. In **2**, the blades of each triptycyl group are tightly intermeshed so that rotation of one unit is inextricably linked to the other – if **A** rotates clockwise, **B** must rotate counter-

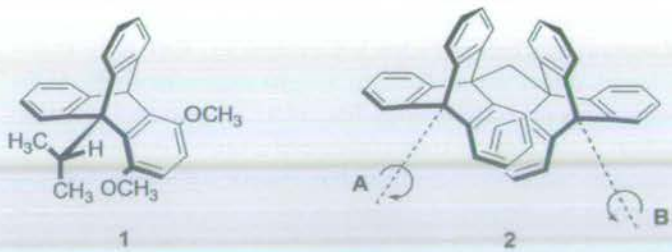

1 2

Figure 7.1 Triptycene derivatives **1** and **2** with hindered and correlated rotation around C–C bonds.

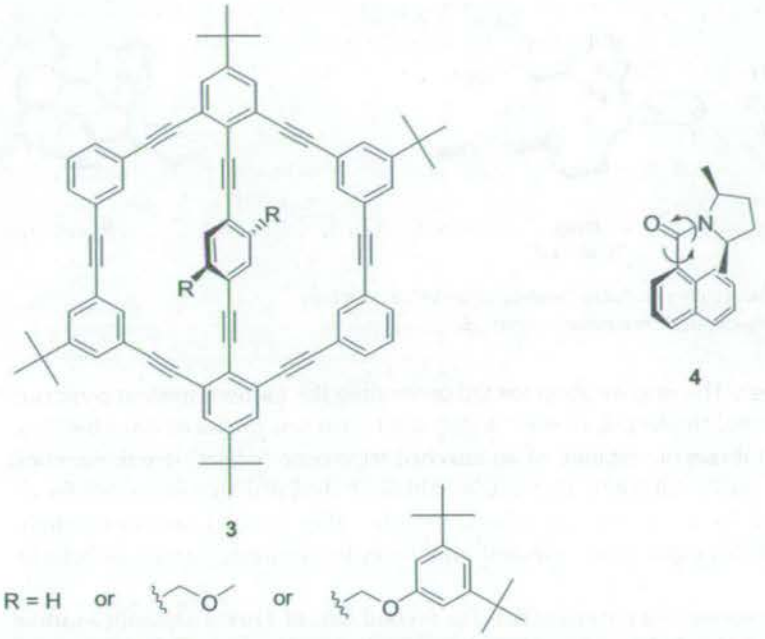

Figure 7.2 Molecular structures of **3** and **4** in which restricted rotation around single bonds has been observed.

clockwise and vice versa. The disrotatory correlated motion mirrors the operation of a macroscopic bevel gear. Experimental and theoretical studies confirm that the barrier to the conrotatory process – analogous to gear slippage – is large. Significantly, barriers to net disrotatory motion are negligible (0.2 kcal mol^{-1} for **2**), indicating that such motion encounters almost no friction – an early illustration of the differences between motion at the molecular and macroscopic levels.

Later, a "molecular turnstile", **3**, (which subsequently inspired "molecular gyroscopes") was created in which the rate of rotation of the central phenyl ring could be tuned by varying substitutions [12]; correlated rotational motion has also been observed around hindered amides such as **4** (Fig. 7.2) [13].

Although these studies clearly demonstrate the role steric interactions can play, the submolecular motions are, of course, non-directional even within a partial rotational event. Simply restricting the thermal rotary motion of one unit by a larger blocking group or by the similarly random motion of another unit cannot, in itself, lead to directionality. A molecular machine requires some form of external modulation over the dynamic processes.

As a first step toward achieving controlled and externally initiated rotation around C–C single bonds, Kelly combined triptycene structures (Fig. 7.1) with a molecular recognition event [14]. In the resulting "molecular brake", **5** (Fig. 7.3) [15], free rotation of a triptycyl group could be halted on application of Hg^{2+} ions which caused a conformational change in the appended bipyridyl unit – effectively putting a "stick"

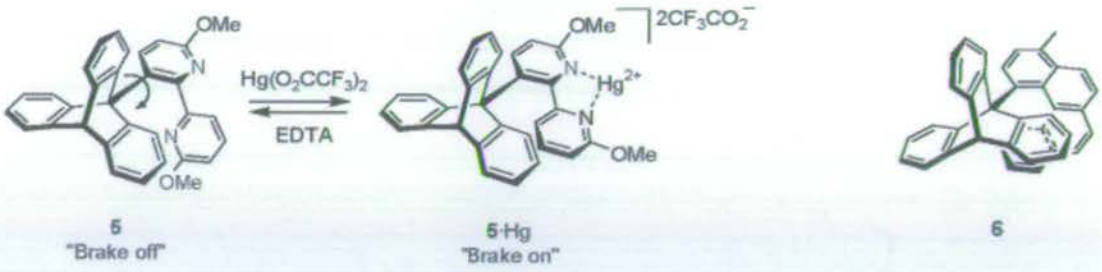

Figure 7.3 A chemically switchable "molecular brake", **5**, and the design of an unsuccessful "molecular ratchet", **6**.

in the "spokes". The next iteration toward controlling the motion involved construction of a potential "molecular ratchet", **6** [16], in which it was proposed that a helicene "pawl" might direct the rotation of an attached triptycene "wheel" in one direction owing to the pawl's chiral helical structure. Although the calculated energetics for rotation showed the energy barrier to be asymmetric (Fig. 7.4), ^{1}H nuclear magnetic resonance (NMR) experiments showed rotation to be occurring equally in both directions.

This result serves as a reminder that the Second Law of Thermodynamics cannot be escaped – although thermal motion can be used to move a system toward its equilibrium state, it cannot be used to power work [17]. The rate of any chemical transformation – clockwise and anticlockwise rotation in **6** included – depends on the energy of the transition state passed over and the temperature. However, state functions such as enthalpy and free energy do not depend on a system's history [18]. Thus, the energy of the transition state in Fig. 7.4, $\Delta H^{\ddagger}$, is independent of whether it is approached from the left (clockwise rotation of the triptycene as drawn) or the right (anticlockwise rotation) and the rates of rotation are constrained to be equal in either direction.

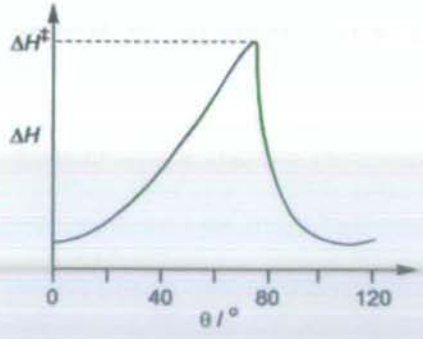

Figure 7.4 Schematic representation of the calculated enthalpy changes for rotation around the single degree of internal rotational freedom in proposed ratchet **6**.

The temptation to relate **6** to a macroscopic ratchet and pawl, which does use an asymmetric energy-profile to produce unidirectional motion from a randomly fluctuating input force, is clear – what is different about the molecular-level system? Smoluchowski and, more famously, Feynman have considered the problem of a molecular-level ratchet, showing that the effect of thermal fluctuations on the molecular-level "pawl" would cause it to disengage and the overall result would be random motion in either direction – the Second Law survives [19]. Feynman went on to show that for directional motion to occur energy must be added to the system in some way, to remove it from equilibrium [20]. The requirements for unidirectional motion at the molecular-level therefore are: (1) a randomizing force which enables the system to seek its equilibrium position; (2) some form of asymmetry in the structure, surroundings, or information within the system which differentiates two potential directions of travel; and, crucially, (3) an energy input which drives the system away from equilibrium.

In **6**, criteria 1 and 2 are clearly already present in the form of thermally powered random fluctuations around the single degree of internal rotational freedom and the helical chirality of the structure, respectively. Yet to achieve *unidirectional* motion the system must be driven away from equilibrium – to break "detailed balance" – so that the Second Law of Thermodynamics is not contravened. Kelly therefore proposed **7a** (Fig. 7.5), a modified version of the ratchet structure in which a chemical reaction is

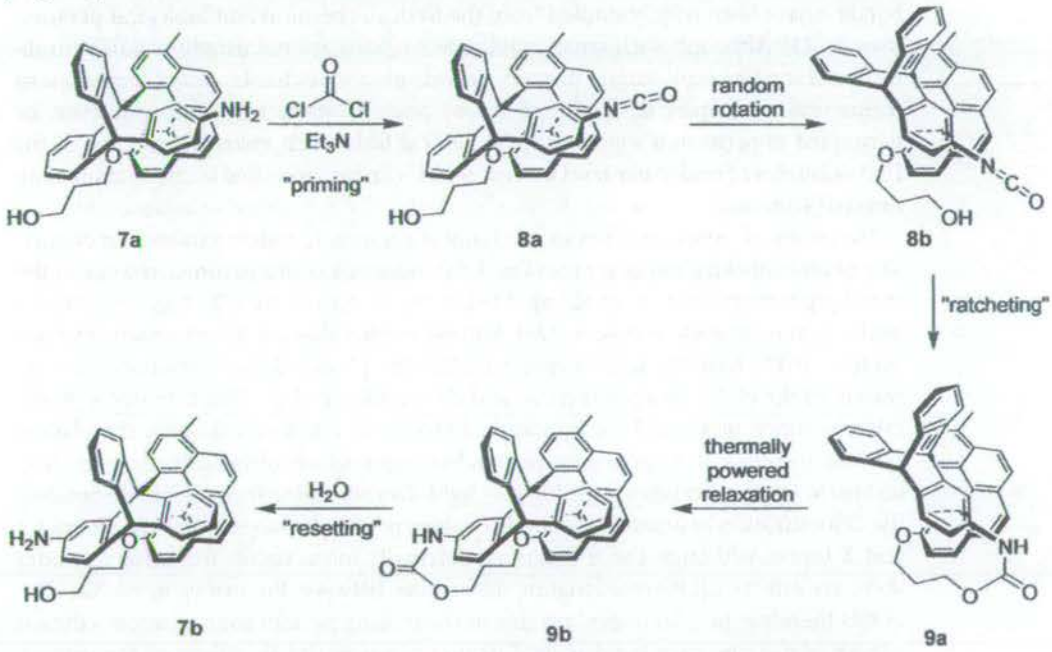

Figure 7.5 A chemically powered unidirectional rotary motor in action. Priming of the motor in its initial state with phosgene (**7a** → **8a**) enables a chemical reaction to occur when the helicene rotates far enough up its potential well toward the blocking triptycene arm (**8b**). This gives a tethered state **9a** for which rotation over the barrier to **9b** is an exoergic process and occurs under thermal control. Finally, the urethane linker can be cleaved to give the original rotor rotated by 120° (**7b**).

used as a source of energy [21]. Ignoring the amino group, all three possible positions for the helicene relative to the triptycene "spokes" are identical – the energy profile for 360° rotation would appear as three equal energy minima, separated by equal barriers. As the helicene oscillates back and forth in a trough, however, sometimes it will come close enough to the amine for chemical reaction to occur (as in **8b**). Priming the system with chemical "fuel" (phosgene in this example to give the isocyanate **8a**) results in "ratcheting" of the motion some way up the energy barrier (**9a**). Continuation of the rotation in the same direction, over the energy barrier, can occur under thermal control and is now an exoergic process (giving **9b**) before cleavage of the urethane gives the 120° rotated system (**7b**). Although the current system can only perform one third of a full rotation, it demonstrates the principles required for a fully operating and cyclable rotary system under chemical control and is a significant advance from the original restricted C–C bond-rotation systems.

7.3 Controlling Configurational Changes

Changes in configuration [22] – in particular cis–trans isomerization of double bonds – have been widely studied from theoretical, chemical and biological perspectives [8, 23]. Although such small-amplitude motions are not usually suitable for direct machine-like exploitation, they can provide photoswitchable control mechanisms within more complex devices (see below) and, in some instances, can even be harnessed to perform a significant mechanical task. Such systems are some of the first examples of molecular-level motion which can be controlled by application of an external stimulus.

The utility of isomerizations in mechanical systems is widely exploited in Nature. The photoisomerization of retinal (Fig. 7.6a) induces a conformational change in the visual pigment rhodopsin, enabling it to bind to protein-G, thereby triggering the visual signal-transduction process [24]. Equally remarkable are the photoactive yellow proteins (PYP) found in some eubacteria [25]. The photoinduced trans-to-cis isomerization of the olefin in a *p*-coumaric acid chromophore (Fig. 7.6b) activates a photocycle in which this small configurational change is amplified through the protein scaffold resulting in large conformational changes which ultimately cause the bacterium to swim away from harmful blue light. Despite being formally single bonded, the delocalization in amide C–N bonds enables peptide linkages to exist in distinct *Z* and *E* forms. Although the *E* forms are normally more stable, for tertiary amides there are only small thermodynamic differences between the two isomers. Xaa–Pro bonds therefore play an important role in controlling protein conformation – the existence of just one such bond as its *Z* isomer can have drastic effects on the secondary structure of the protein. Enzymes which catalyze *E* to *Z* isomerization – peptidyl–prolyl cis–trans isomerases (PPIases) – play important roles in directing protein folding and controlling the subsequent biological activity of many proline-containing proteins [26].

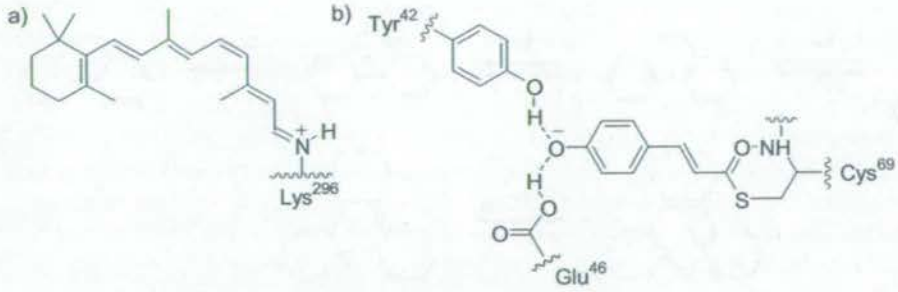

Figure 7.6 (a) Chemical structure of the rhodopsin chromophore – an iminium derivative of 11-*cis*-retinal. (b) Chemical structure of the PYP chromophore – a thioester of *p*-coumaric acid.

As a prototypical example of the reaction class, the photoisomerization of stilbenes has been extensively studied theoretically and preparatively for well over 50 years [27]. As organic photochemistry began to develop, other important photochromic systems were discovered (Fig. 7.7) [28]: the photoisomerization of azobenzenes [29], the interconversion of spiropyrans with merocyanine (and the associated spirooxazine/merocyanine system) [30], the photochromic reactions of fulgides [31], and chiroptical systems such as overcrowded alkenes (for example **10**, Fig. 7.9) [32]. All these processes are accompanied by marked changes in both physical and chemical properties, for example color, charge, and stereochemistry, and a wide range of switching applications have both been proposed and realized, from liquid-crystal display technology to variable-tint spectacles and optical recording media [33].

Although photochromism in modern diarylethene systems [34] and in fulgides is based on a photocyclization process (rendering the configurational cis–trans isomerization an undesirable side-reaction), most applications of these photochromic systems simply rely on the intrinsic electronic and spectroscopic changes on interconversion between the two species. As such, these systems do not normally fit our definition of molecular machines. There are some systems, however, which harness small configurational changes in a more mechanical fashion so that the resulting devices can, indeed, be described as machine-like.

A variety of configurational changes (but in particular azobenzene photoisomerization) have been used to alter peptide structures, creating semi-synthetic biomaterials whose activity can be controlled photonically [35]. These systems, which amplify the small configurational change of the synthetic unit to cause a significant change in the peptide secondary structure, to some extent mimic the combined role of proline and PPIases in controlling protein activity in the cell.

Combining photochromism with liquid crystal systems can lead to a variety of photoswitched changes in the properties of the liquid crystal [36]. The trans → cis photoisomerization of stilbene or azobenzene dopants, for example, can lead to reversible disruption of the nematic mesophase, effectively turning off liquid crystalline properties. More subtle control over the alignment of liquid crystals can also be achieved in systems in which the mesophase structure is maintained throughout.

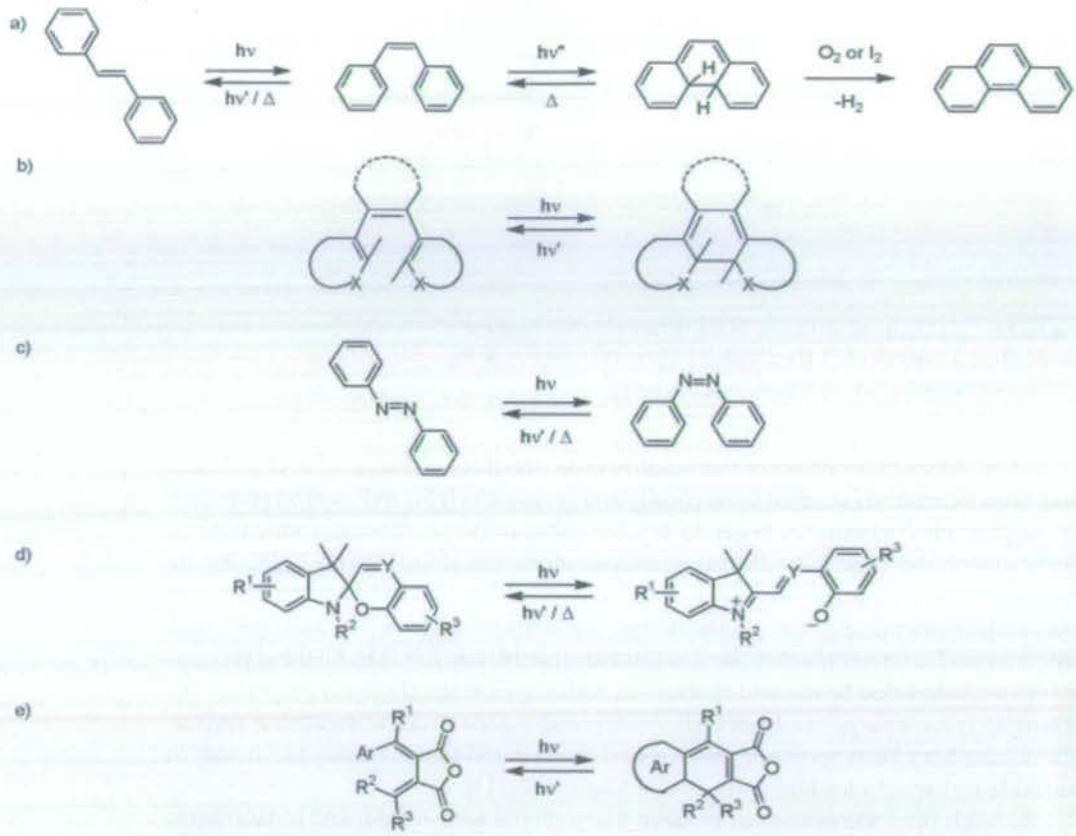

Figure 7.7 Some photochromic systems which can potentially give rise to a mechanical response. (a) The cis–trans isomerization of stilbene can be accomplished photochemically. A competing process is the 6π-electron cyclization to give dihydrophenanthrene, which reverts to cis-stilbene in the dark or, in the presence of a suitable oxidant, irreversibly loses H_2 to give phenanthrene. (b) Other diarylethene systems exploit the photocyclization process by blocking the cis → trans and hydrogen-elimination processes through substitution, while replacing the phenyl rings with heteroaromatics stabilizes the cyclized form (X = C, NH, O, S). (c) The cis–trans isomerization of azobenzene. (d) The interconversion of spiropyrans (Y = C) or spirooxazines (Y = N) with their merocyanine forms. (e) The interconversion of ring-open and cyclized forms of fulgides, both of which are thermally stable (cis–trans isomerization around either bond can occur, but is undesirable).

Use of plane-polarized light to stimulate repetitive cis–trans isomerization of photochromic dopant molecules can lead to photoorientation of these species by axis-selective photoconversion. This directional orientation triggers concomitant alignment of the whole liquid crystal phase. A second vector of polarization can then produce a different aligned state. Potential applications of this photo-induced mechanical molecular-level motion include optical recording media and light-addressable displays [36].

In such systems, quite remarkable amplification of a relatively small photoinduced configurational change causes a global change in orientation in the bulk. It is even possible to create surface-controlled systems in which a monolayer of photochromic species (a so-called "command surface") controls the alignment of a whole liquid-crystal layer in contact with it. The same principles can be applied to the photonic control of the organization in other systems such as gels and Langmuir–Blodgett films [37].

Photoinduced mechanical changes have also been observed at the single-molecule level by use of atomic-force microscopy (AFM) [38]. One end of a polyazopeptide (a polymer of azobenzene units linked by dipeptide spacers) was isolated on a glass slide while the other was attached to a gold-coated AFM tip via a thioether–Au bond (Fig. 7.8). At zero applied force, repeated shortening and lengthening of the polymer was observed on photoisomerization of the azobenzene units to cis and trans respectively. This experimental arrangement was, furthermore, used to demonstrate the transduction of light energy into mechanical work. A "load" was applied to one of the polyazopeptides – in its fully trans form – by increasing the force applied by the AFM tip from 80 pN to 200 pN, resulting in stretching of the polymer. Photoisomerization, to yield what is assumed to be the fully cis polymer, resulted in contraction even against this external force ("raising the load"). Removal of the "load" by reducing the applied force, followed by re-isomerization to the trans form, restored the polymer to its original length – ready to lift another load. The work done by this single molecule device is $\sim 5 \times 10^{-20}$ J.

While investigating the use of overcrowded alkenes as chiroptical molecular switches, Feringa and coworkers created molecular brake **10** in which the speed of rotation around an arene–arene bond can be varied by changing the alkene configuration (Fig. 7.9) [39]. Counter-intuitively from the two-dimensional structures in Fig. 7.9, the rate of rotation around the indicated bond is faster in *cis*-**10** than in *trans*-**10** (demonstrated by the respective free energies of activation, $\Delta G^{\ddagger}$, for the process). Unfortunately, the photochemical interconversion between cis and trans could not be accomplished efficiently for this molecule, yet the system stands as proof that a change in configuration can alter not just optical properties or bulk orientations, but can also control large-amplitude submolecular motions.

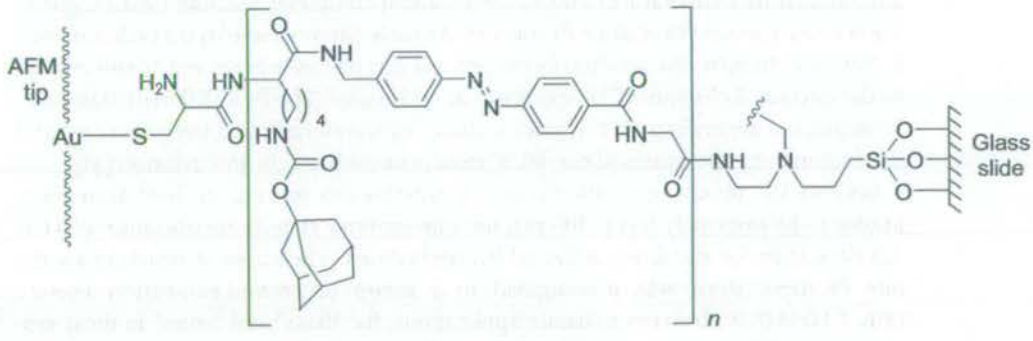

Figure 7.8 Experimental arrangement for observation of single-molecule extension and contraction using AFM (azobenzene unit shown as the extended *Z* isomer).

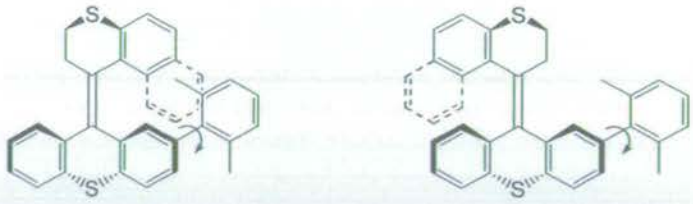

cis-**10**
$\Delta G^{\ddagger}_{303} = 19.0 \pm 0.2$ kcal mol^{-1}

trans-**10**
$\Delta G^{\ddagger}_{303} = 19.7 \pm 0.2$ kcal mol^{-1}

Figure 7.9 Counterintuitive variation of kinetic barrier to rotation around an aryl-aryl bond by isomerization of the double bond in an overcrowded alkene. Values for the free energy of activation ($\Delta G^{\ddagger}$) for the rotary motion in each configuration are shown.

The chiral helicity of molecules such as **10** causes the photochemically induced trans–cis isomerization to occur unidirectionally according to the handedness of the helix. Accordingly, these systems already have many of the requirements necessary for a unidirectional molecular rotor and, indeed, the incorporation of another stereogenic center enabled realization of this potential and creation of the first synthetic molecular rotor capable of achieving a full and repetitive 360° unidirectional rotation (Fig. 7.10) [40]. Irradiation ($\lambda > 250$ nm) of this extraordinary molecule, (3*R*,3'*R*)-(*P*,*P*)-*trans*-**11**, causes chiral helicity-directed clockwise rotation of the upper half relative to the lower portion (as drawn), at the same time switching the configuration of the double bond and inverting the helicity to give (3*R*,3'*R*)-(*M*,*M*)-*cis*-**11**. Unlike previously investigated systems however [32b], this form is not stable at temperatures above –55 °C, because the cyclohexyl ring methyl substituents are placed in an unfavorable equatorial position. At ambient temperatures, therefore, the system relaxes via a second, thermally activated helix inversion thus continuing to rotate in the same direction, giving (3*R*,3'*R*)-(*P*,*P*)-*cis*-**11**. Irradiation of this new species ($\lambda > 250$ nm) results again in photoisomerization and helix inversion to give (3*R*,3'*R*)-(*M*,*M*)-*trans*-**11**. Once more the methyl substituents are in an equatorial position and thermal relaxation (this time temperatures >60 °C are required) completes the 360° rotation giving the starting species (3*R*,3'*R*)-(*P*,*P*)-*trans*-**11**. As each different step in the cycle involves a change in helicity, the unidirectional process can be easily observed by the change in the circular dichroism (CD) spectrum at each stage. The four different states can be populated depending on the precise choice of wavelength and temperatures, and irradiation at temperatures above 60 °C results in continuous 360° rotation [41].

Because the photochemically induced isomerization process in these systems is known to be extremely fast (<300 ps), the rate-limiting step in the operation of **11** is the slowest of the thermally activated isomerizations. The effect of structure on the rate of these steps was investigated in a series of second-generation motors (Fig. 7.11) [42]. With a view to future applications, the "base" and "rotor" in these systems were differentiated, so that only one directing methyl group is present. This, however, is still sufficient for unidirectional rotation. For all examples in Fig. 7.11, the slowest thermal isomerization step has a lower kinetic barrier than that in **11**. It was,

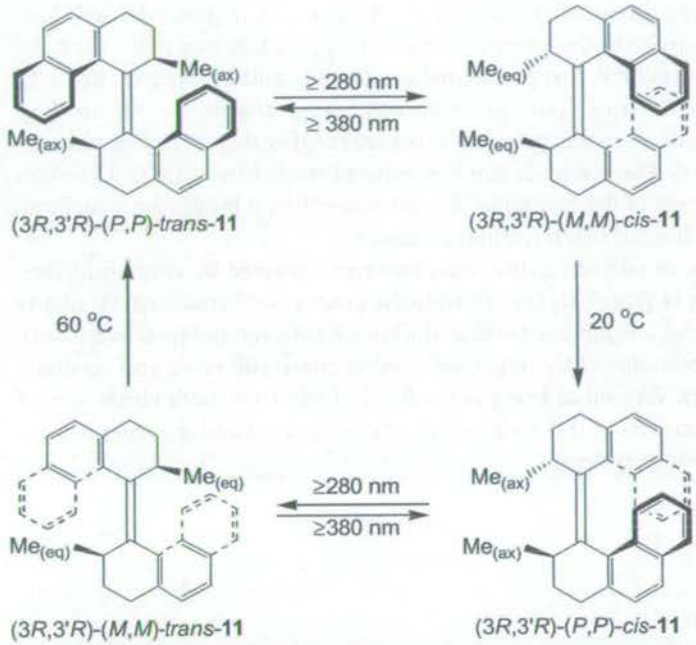

Figure 7.10 Operation of the first, continuously operating, unidirectional 360° rotor, (3*R*,3'*R*)-**11**.

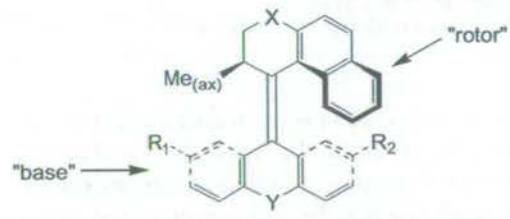

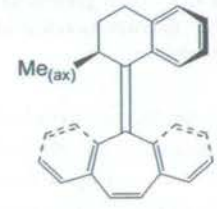

13

	X	Y	R_1	R_2
12a	S	S	OMe	H
12b	S	S	H	OMe
12c	S	S	H	H
12d	S	S	OMe	OMe
12e	S	O	H	H
12f	S	$C(CH_3)_2$	H	H
12g	CH_2	S	H	H
12h	CH_2	$C(CH_3)_2$	H	H
12i	CH_2	CH=CH	H	H

Figure 7.11 Second-generation light-driven unidirectional rotors **12a–i** and **13**.

furthermore, observed that smaller bridging groups at Y and, in particular, at X lowered the activation barrier to this process so that $\Delta G^{\ddagger}_{293} = 21.90$ kcal mol^{-1} for compound **12g**. Not all structural changes turned out to be intuitive, however. Rotor **13** contains an even smaller upper portion yet the free energy of activation for the thermal isomerization process in this molecule is actually higher than that of its phenanthrene analog **12i** [43]. The reason is that the reduced steric hindrance in **13** lowers the ground-state energy of the "unstable" isomer more than it lowers the transition-state energy for the thermal isomerization process.

A further increase in rate of rotation was, however, achieved by creation of five-membered homolog **14** (Fig. 7.12) [44]. Despite the greater conformational flexibility of the cyclopentyl ring, a significant energy difference between the pseudoequatorial and pseudoaxial positions of the appended methyl group still exists and unidirectional rotation occurs. As well as being accessible in higher synthetic yields, one of the thermal isomerizations in this molecule is extremely rapid and the other is competitive with the previous systems.

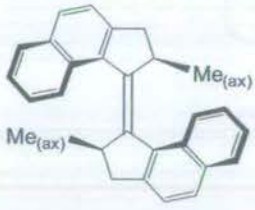

(2*R*,2'*R*)-(*P*,*P*)-*trans*-**14**

Figure 7.12 Third-generation unidirectional rotor, **14**. In this structure "ax" denotes pseudoaxial orientation of substituents on the cyclopentyl ring.

A potential drawback of third-generation molecule **14** is the reduced extent of isomerization at the photostationary states. Yet, owing to the "ratcheted" mechanism which does not allow backwards movement of the rotor, this does not reduce the integrity of the unidirectional process, it simply reduces the photoisomerization quantum yield.

7.4 Controlling Motion in Supramolecular Systems

We have seen how, by judicial choice of structure, it is possible to restrict submolecular motion such as bond rotation whereas configurational changes can provide an external control element for molecular geometry, orientation, and submolecular motion. Yet these generally enable only relatively crude control over molecular-level motion (the Feringa "motors" are an obvious exception to this caveat). Molecular recognition [45] and the control of noncovalent interactions provides the opportunity to *selectively*, *specifically*, and *strongly* position one molecule or molecular component relative to another.

Furthermore, a wide range of recognition systems are now known which can be modulated in strength – or even effectively switched "on" or "off" – using a range of external stimuli. We must be careful to remember, however, that a net mechanical task requires control of molecular-level motion. This means that the putative "machine" assembly must be *kinetically associated* (i.e. it cannot exchange with the bulk) over the timeframe of operation of the machine and that a stimulus-induced molecular recognition event is neither a sufficient nor necessary condition for construction of such a machine.

7.4.1 Switchable Host–Guest Systems

Using an external stimulus to modulate the binding affinity of a host for a guest is the simplest expression of controllable molecular recognition. A wide variety of stimuli can be used to precipitate changes – not just in geometric configuration but also electronic arrangement and environmental influences – which modulate noncovalent interactions. Switchable host–guest systems teach us much about the nature of noncovalent interactions and their manipulation, yet the requirement for kinetic association of components in a molecular machine rules out simple host–guest complexation where binding does not bring about a change in the conformation of either species or where transport of the guest between sites within the host is slow relative to exchange with the bulk. Although all complexation events clearly involve movement of the components relative to each other, the physics of complexation depend only on binding affinity and concentration, not factors associated with mechanical task performance (net position, mass, etc.). This is why myosin must move along a track to which it is kinetically associated over a series of sequential binding events to bring about muscle contraction; no mechanical task occurs through simple "on"/"off" binding to the track by myosin molecules from the bulk [46]. In other words, simple host–guest/supramolecular systems cannot function as nanoscale mechanical machines unless restrictions on the motion of the unbound species apply or the binding event brings about a mechanical (i.e. conformational) change in one of the molecular components.

Whilst this means that many switchable host–guest systems do not have the potential to act as mechanical machines, many still do. A good example of a molecular system on the borderline of machine-like behavior is given by the "tail-biting" crown ethers *E*/*Z*-**15**•H$^+$ (Fig. 7.13) developed by Shinkai and coworkers [47]. Nominally

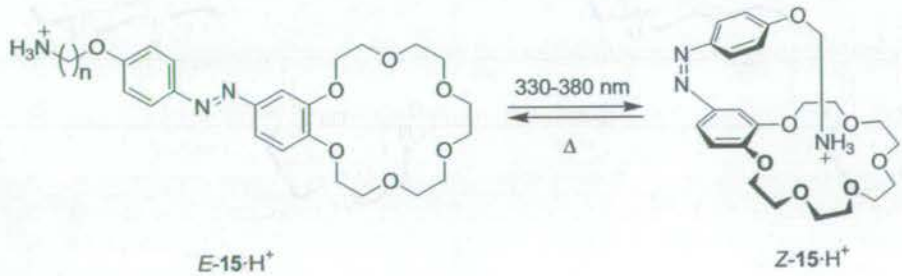

E-**15**·H$^+$ *Z*-**15**·H$^+$

Figure 7.13 Isomerization of "tail-biting" crown ethers.

these systems are simply switched molecular receptors, not molecular machines. In the *Z*-**15**•H^+ forms, intramolecular binding of the ammonium ion to the crown ether prevents recognition of other cations in the medium whereas thermal isomerization to give *E*-**15**•H^+ restores the alkali metal cation binding properties of the crown ether. It is observed, however, that the rate of $Z \rightarrow E$ isomerization is lowered (by 1.6 to 2.2 fold) for *Z*-**15**•H^+ when compared with the deprotonated control *Z*-**15**. Crucially, the rate of this reaction increases with increasing concentration of K^+ ions in solution, so that the system can indeed be viewed as a primitive molecular machine in which a binding event at the crown ether affects the $Z \rightarrow E$ isomerization process of the azobenzene moiety *with which it is kinetically associated.*

7.4.2
Intramolecular Ion Translocation

Metal–ligand binding interactions are often kinetically stable and careful structural design can produce systems in which intramolecular motion is significantly favored over intermolecular exchange [48]. System $\mathbf{16}^{4+}$ (Fig. 7.14) consists of a coordinatively unsaturated Cu^{II} center covalently linked to a redox-active Ni^{II}-cyclam unit [49]. In this form chloride anions bind strongly to the copper, filling the vacant coordination site ($[\mathbf{16}\bullet Cl]^{3+}$). Electrochemical oxidation of the nickel center to Ni^{III} dramatically increases its affinity for anions so that the chloride translocates to this new, more energetically favorable site. The motion is completely reversible on reduction of the nickel. There is, of course, the distinct possibility that the switching of anion position is an intermolecular process involving either free anion in solution or more than one molecule of **16**. However, the process was demonstrated not to be concentration-dependent, in contrast with the analogous noncovalently linked three-component system (Cu receptor + Ni receptor + Cl^-) for which the behavior is strongly concentration dependent. Further thermodynamic comparisons of the two systems suggest that the dominant mechanism in **16** is intramolecular translocation, brought about by folding of the ditopic receptor so that the motion pathway of the chloride ion is defined.

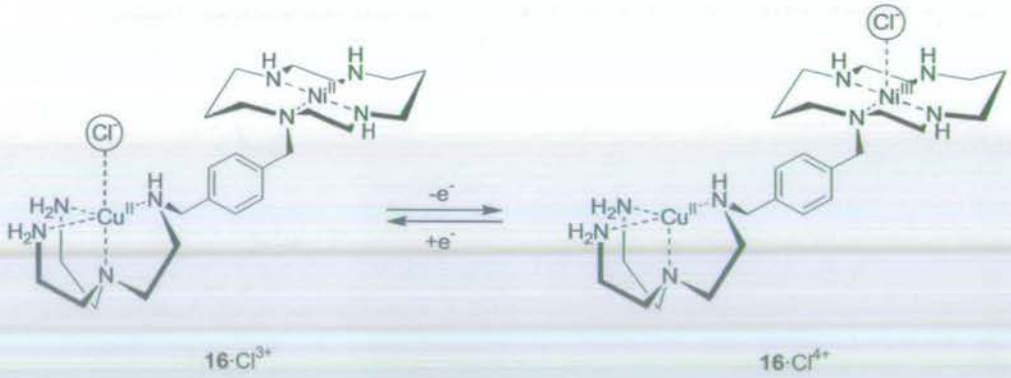

16·Cl^{3+} **16**·Cl^{4+}

Figure 7.14 Redox-driven intramolecular anion translocation.

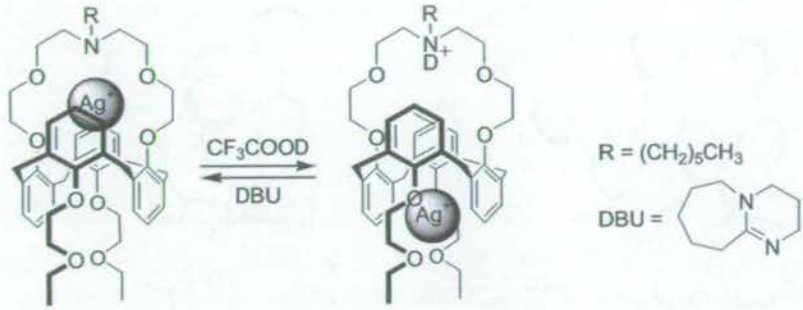

Figure 7.15 Translocation of a silver cation between two sites in a calix[4]arene cavity – a "molecular syringe".

Calix[4]arene **17** performs reversible translocation of metal cations by protonation of the tertiary nitrogen. Dynamic ^{1}H NMR experiments indicate a high kinetic barrier to dissociation of the metal from the deprotonated receptor, suggesting that on protonation, translocation occurs in an intramolecular fashion through the cavity defined by the aromatic rings, in a manner resembling the operation of a syringe. In the protonated form, however, intermolecular exchange of the cation is much faster, so the return stroke, at least, can involve a significant amount of undefined intermolecular motion (Fig. 7.15) [50].

The first redox-driven cation translocation process was reported by Shanzer and coworkers in a helical complex [**18**•Fe^{III}] for which there is strong evidence for a fully intramolecular process [51]. The system works by exploiting the preference of Fe^{III} for hard ligands and Fe^{II} for a softer coordination sphere. Chemical reduction of [**18**•Fe^{III}] with ascorbic acid gives [**18**•Fe^{II}•3H]$^{2+}$ which has spectral properties characteristic of the Fe^{II}(bipyridyl)$_3$ coordination sphere (Fig. 7.16). Subsequent re-oxidation (ammonium persulfate) returns the system to its original state. The equivalent intermolecular process between two monotopic ligands failed to occur under the same conditions, and even the translocation in **18** is relatively kinetically slow, suggesting an intramolecular process.

Pseudorotaxanes – supramolecular complexes in which a macrocyclic host encapsulates a linear, thread-like guest – are subject to the same issues with regard to kinetic stability as other host–guest complexes [52–54]. While these complexes are model systems for kinetically associated systems such as interlocked rotaxanes (see Sect. 7.5), their basic structure is similar to that of other supramolecular systems. Many interesting pseudorotaxane devices have been created with functions including reversible formation and de-threading of the interlocked species using a number of stimuli [55], switching between different preferred guests [56], and control of intramolecular electron transfer reactions [57]. Only for kinetically stable pseudorotaxanes, however – systems in which the components do not exchange with the bulk over the operation of the machine – are there sufficient restrictions on the motions of the unbound species for them to feature controlled mechanical behavior and otherwise they are best considered supramolecular devices not mechanical machines [58].

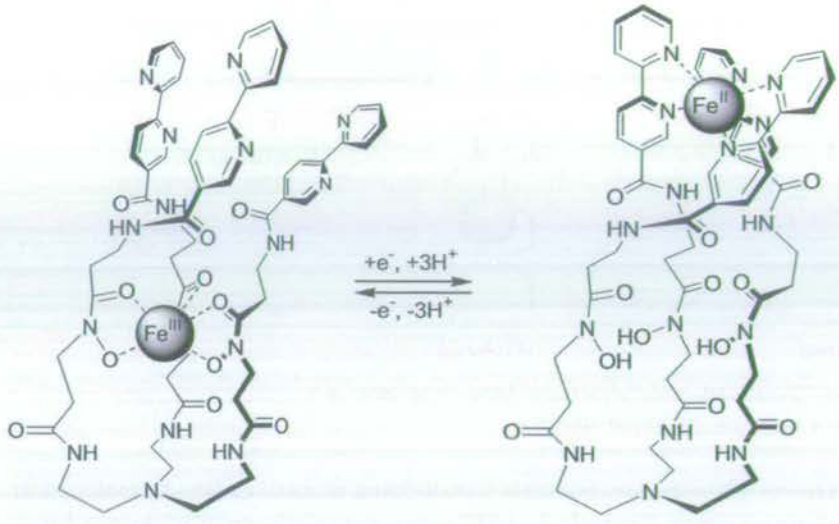

Figure 7.16 Redox-switched intramolecular cation translocation in a triple-stranded helical complex. The reductant is ascorbic acid and the oxidant $(NH_4)_2S_2O_8$.

7.5
Controlling Motion in Interlocked Systems

7.5.1
Basic Features

Catenanes are chemical structures in which two or more macrocycles are interlocked; in rotaxanes one or more macrocycles are mechanically prevented from de-threading from linear chains by bulky "stoppers" (Fig. 7.17) [59]. Although the components are not covalently connected, catenanes and rotaxanes are molecules – not supramolecular complexes – because covalent bonds must be broken to separate the constituent parts. In these kinetically associated species [60, 61] the mechanical bond restricts the degrees of freedom for relative movement of the components while often permitting extraordinarily large amplitude motion in the allowed vectors. This is directly analogous to the restriction of movement imposed on biological motors by a structural track [46] and is one reason interlocked structures have played a central role in the development of synthetic molecular machines [62].

Large-amplitude submolecular motion in catenanes and rotaxanes can be divided into two classes (Fig. 7.17) – pirouetting of the macrocycle around the thread (rotaxanes) or the other ring (catenanes), and translation of the macrocycle along the thread (rotaxanes) or around the other ring (catenanes). By analogy with conformational changes within classical molecules, the relative movements between interlocked species are termed co-conformational changes [22]. Motion in these systems is most

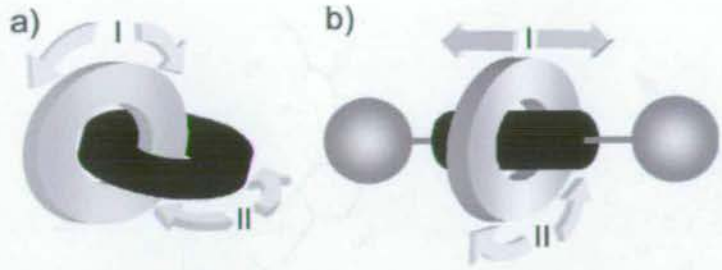

Figure 7.17 Cartoon representations of (a) a [2]catenane and (b) a [2]rotaxane [63]. Arrows show possible large-amplitude modes of movement for one component relative to another.

easily described by assuming one component to be a stationary frame of reference around or along which the other units move. Often the choice of this frame of reference is based on the relative size or complexity of the components. The distinction can become ambiguous, however, as discussed below.

For a long time these non-classical architectures were no more than academic curiosities, particularly as synthetic approaches relied on inefficient statistical or time-consuming covalently-directed approaches [64]. Introduction of supramolecular chemistry, however, enabled chemists to apply an understanding of noncovalent interactions to synthesis, resulting in various template methods to catenanes and rotaxanes [65]. In such syntheses noncovalent binding interactions between the components often "live-on" in the interlocked products. These interactions enable restriction of the relative motion of components, further to that defined by their architecture, and they can ultimately be manipulated to affect positional displacements. Much attention has been devoted both to intrinsic submolecular motion within these structures and control of this motion by manipulation of recognition events.

7.5.2
Inherent Dynamics: Ring Pirouetting in Rotaxanes

Pirouetting is the random rotation of the macrocycle about the axis defined by the thread. While this motion is often observed to be occurring, it can be difficult to study in detail because of the symmetry of the components. Benzylic amide macrocycle-based rotaxanes possess a useful characteristic in this respect. In many examples of these molecules, the benzylic amide macrocycle adopts a chair-like conformation meaning that for each pair of benzylic protons (H_E, Fig. 7.18), one is in an equatorial environment, while the other is axial [66]. For a macrocycle on a symmetric thread, two ^1H NMR signals would therefore be expected for the 8 benzylic protons in the molecule. Rotation of the macrocycle around the axis shown by 180° must, however, result in a chair-chair flip so as to maintain the hydrogen bonding network between the macrocyclic amide protons and carbonyl oxygen atoms on the thread. This co-conformational change therefore interconverts the axial and equatorial sets of protons twice during a full 360° revolution. It is possible to study chemical exchange process-

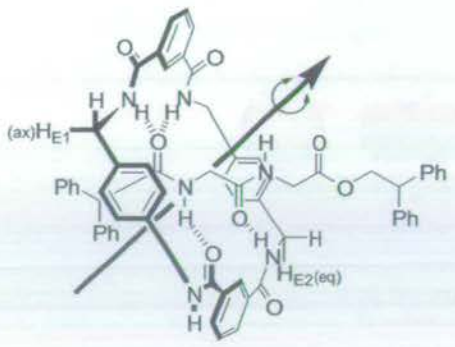

19

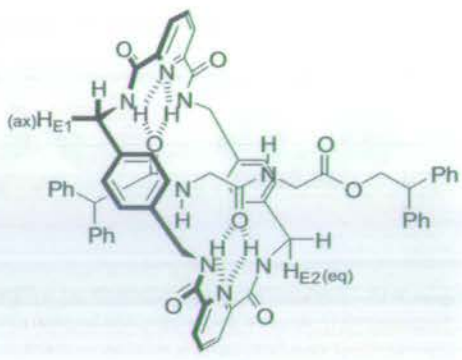

20

Figure 7.18 Peptidorotaxanes **19** and **20**. The arrow on **19** indicates the axis about which macrocycle pirouetting occurs.

es such as this by variable temperature (VT) NMR techniques, including the coalescence method [67], or spin polarization transfer by selective inversion recovery (SPT-SIR) [68].

For example, the room temperature ^{1}H NMR spectrum in $CDCl_3$ of the glycylglycine-based [2]rotaxane **19** contains the fewest possible signals for the macrocycle protons, indicating rapid pirouetting (820 s^{-1}) of the ring at ambient temperature [66]. The pyridyl-2,6-dicarbonyl-based macrocycle in **20** has a different, overall slightly stronger, hydrogen-bonding network between the components, producing a concomitant reduction in pirouetting rate to 100 s^{-1}.

As the rate of pirouetting is directly related to the strength with which the macrocycle is held to the thread, this motion can be a useful probe for evaluating the effect of structural changes on the strength of intercomponent interactions in rotaxanes. For the series of fumaric acid-based [2]rotaxanes shown in Fig. 7.19, yields of the rotaxane forming process (a five-component clipping reaction in which formation of the benzylic amide macrocycle is templated by the fumaric acid residue) increase in the order **23** < **22** < **21** [69]. As expected, the rates of macrocycle pirouetting in the products were shown to follow exactly the opposite order (Fig. 7.19), confirmation that the efficiency of the templated synthesis is directly related to the hydrogen-bonding ability of the thread templates.

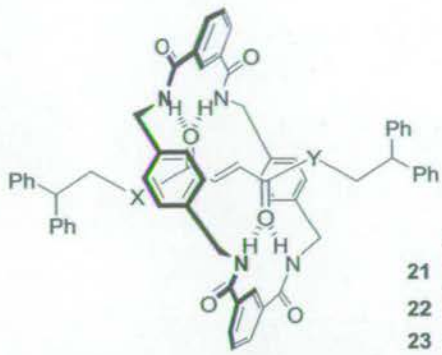

	X	Y	Yield	$\Delta G^{\ddagger}_{298}$ / kcal mol^{-1}
21	NH	NH	97%	11.5
22	NH	O	35%	9.3
23	O	O	3%	7.2

Figure 7.19 Variation of yield in rotaxane-forming reactions for a series of simple fumaric acid based templates is correlated with the strength of intercomponent interactions in the products, as evidenced by $\Delta G^{\ddagger}_{298}$, the energy barrier to pirouetting in CD_2Cl_2.

7.5.3
Inherent Dynamics: Ring Pirouetting in Catenanes

Pirouetting in catenanes is not quite so easily defined. Spinning of one macrocycle around an axis defined by its interlocked partner is directly analogous to the pirouetting motion in rotaxanes – the "thread" is simply cyclic in this case (e.g. motion I, Fig. 7.17a is pirouetting of the gray ring around the "stationary" black one). This same motion could, on the other hand, be regarded as rotation of the second macrocycle around the first in a manner analogous to shuttling in rotaxanes (i.e. motion I, Fig. 7.17a could also be regarded as rotation of the black ring around the "stationary" gray ring). Likewise, motion II can be considered to be pirouetting or rotation depending on which ring is taken as the stationary frame of reference. In practice, for the simplest case of homocircuit catenanes (when gray = black), the distinction is unnecessary, as motions I and II are identical, the overall result often being termed circumvolution (also called "circumrotation") if a full 360° rotation is involved.

7.5.3.1 Metal-based Homocircuit Catenates and Catenands

As a result of the degeneracy of the pirouetting and rotational motions, homocircuit catenanes are the simplest systems in which the intrinsic dynamics of interlocked architectures can be studied. The transition metal templated [2]catenates produced by the Sauvage group (e.g. **24**, Fig. 7.20) were the first interlocked molecules to be produced by template synthesis [70–72]. The catenates have both rings coordinated to a metal ion and so are co-conformationally locked and no large-amplitude submolecular motion is observed. Removal of the metal template forms the corresponding catenand. The lack of intercomponent interactions in catenands usually means that the relative motion of the two rings is extremely fast and are difficult to study.

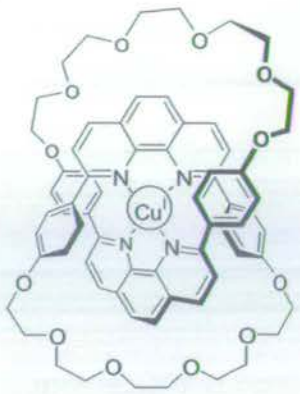

24

Figure 7.20 Chemical structure of the first transition metal templated catenate, **24**.

7.5.3.2 Amide-based Homocircuit Catenanes

Amide-based catenanes, in which hydrogen bonds template interlocking of the two rings, were first reported in 1992 by Hunter (**25**) [73], prompting the publication of similar work by Vögtle (**26**) (Fig. 7.21) [74]. In these systems, the steric bulk of the cyclohexyl groups prevents full circumvolution of the macrocycles. A 90° rotational motion which exchanges the non-equivalent isophthaloyl rings (labeled "1" and "2" in

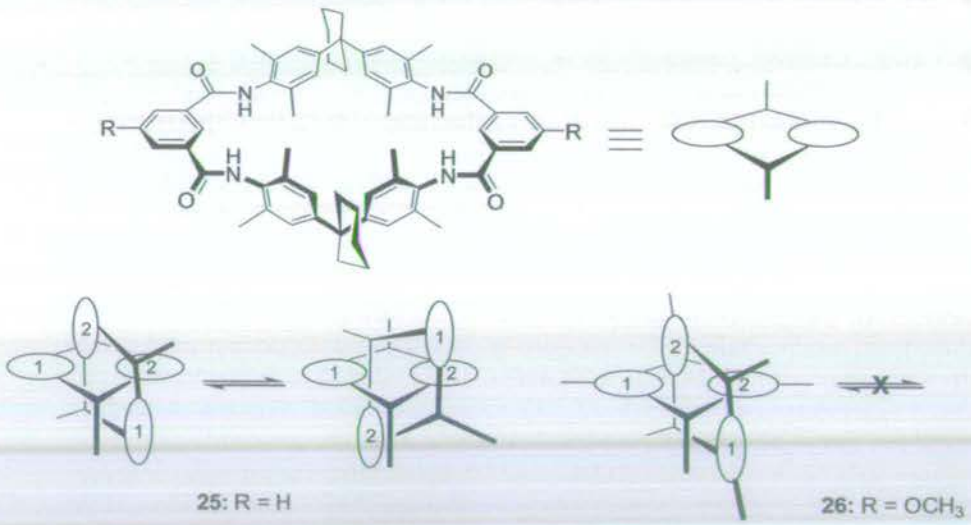

25: R = H

26: R = OCH_3

Figure 7.21 Hydrogen bond-assembled [2]catenanes **25** and **26** reported by Hunter and Vögtle respectively, showing the large-amplitude motion possible in **25**, but not in **26**.

Fig. 7.21) is possible, but even this is blocked on substitution at the 5-position of the isophthaloyl ring (e.g. in **26**).

The amide-based homocircuit catenane **27** (Fig. 7.22), discovered by chance in 1995, has more interesting and versatile dynamics [75]. The catenane has the simplest possible ^{1}H NMR spectrum for this kind of structure, only the six different constitutional types of proton are apparent in DMSO-d_6, the same number seen for the parent macrocycle [76]. Despite the smaller macrocycle cavity size of **27** compared with **25** and **26**, both the isophthaloyl and *p*-xylylene components can rotate through the cavity of the other macrocycle and the circumvolution process is rapid on the NMR timescale in polar solvents at room temperature. The catenane-formation process tolerates a number of aromatic 1,3-dicarbonyl and benzylic amide precursors, so a diverse range of analogs could be prepared and the effect of structure on the dynamic processes assessed [77].

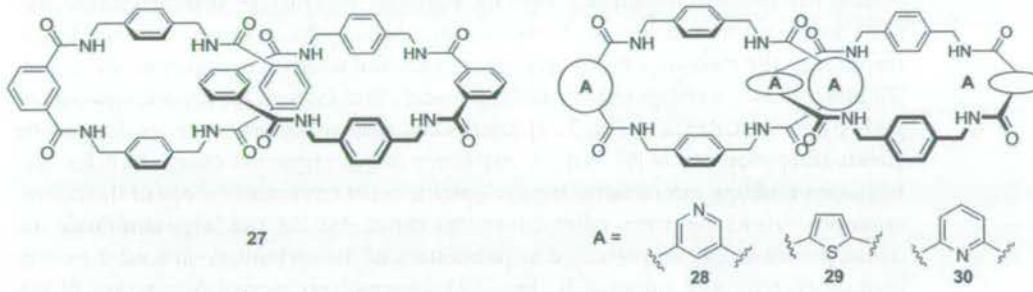

Figure 7.22 The original hydrogen bond-assembled benzylic amide [2]catenane **27** and structural analogs **28–30** with different aromatic-1,3-dicarbonyl units.

Any substitution on the isophthaloyl ring (at either the 5- or 4-position) prevents complete circumvolution of the macrocycles, thereby destroying the plane of symmetry bisecting the isophthaloyl units in each ring. A series of coalescence temperature measurements and SPT-SIR NMR experiments [77, 78] revealed circumvolution to be slow on the NMR timescale for the pyridine-2,6-dicarbonyl derivative (**30**) – just as its pirouetting rates are slower than other macrocycles in rotaxanes (Sect. 7.5.2). The thiophene derivative (**29**) was shown to rotate the fastest – in fact 3.2 million times faster than **30** in $C_2D_2Cl_4$ at room temperature.

This quite remarkable variation in dynamic behavior resulting from relatively simple structural changes can also be allied to the more subtle effects on rate of solvent composition. Hydrogen-bond-disrupting solvents such as CD_3OD and, to an even greater extent, $(CD_3)_2SO$ increase the rate of circumvolution by competing for the hydrogen bonding groups in the macrocycle. This has the effect of weakening the ground-state interactions and stabilizing the intermediate co-conformations during circumvolution, thus lowering the energy barriers for the process. Variation of solvent composition enables fine-tuning of the circumvolution rate after selection of the approximate value by appropriate choice of structure [77, 78].

Both these solvent and structural effects on rate suggest that a key process in the circumvolution mechanism is rupture and formation of intercomponent hydrogen bonds. An isolated molecule molecular mechanics approach has been used to simulate the dynamics in these catenane systems, enabling simulation of the molecular shape at the transition states [78, 79]. Together with a full low-dimensional quantum-mechanical description of circumvolution [80], these studies enable the theoretical and practical understanding of the intrinsic motion in a catenane system necessary for development of molecular devices and materials in which the frequency of motion is a key characteristic.

7.5.3.3 Heterocircuit Catenanes

The very first catenanes in which dynamic processes were studied were not homocircuit systems but rather molecules comprising two different interlocked rings. Most heterocircuit catenanes (gray ≠ black in Fig. 7.17a) consist of a larger ring containing two or more recognition sites for a smaller macrocycle. It is, therefore, usually convenient to consider such systems analogously to rotaxanes with the larger component the stationary frame of reference around which the smaller unit(s) move. [2]Catenane $\mathbf{31}^{4+}$ is composed of a π-electron-deficient cyclophane (cyclobis(paraquat-*p*-phenylene or $CBPQT^{4+}$, Fig. 7.23) interlocked with an electron-rich bis-dioxyarene crown-ether macrocycle [81, 82]. To maximize intercomponent charge-transfer and hydrogen-bonding interactions, the cyclophane must circumscribe one of the hydroquinone units in the crown ether. Given this constraint, the two large-amplitude dynamic processes can be portrayed as pirouetting of the cyclophane around the occupied dioxyarene unit (process II, Fig. 7.23, alternatively viewed as rotation of the crown ether around the cyclophane) and rotation of the cyclophane around the crown ether from one dioxyarene station to another (process I, Fig. 7.23, alternatively viewed as pirouetting of the crown ether through the cyclophane). Both processes are observable in ^{1}H and ^{13}C VT NMR studies, enabling calculation of activation barriers for the two processes; process I is the higher in energy.

Enlargement of the electron-rich macrocycle in $\mathbf{32}^{4+}$, which contains four dioxybenzene stations, renders the distinction between pirouetting and rotation less equivocal; the larger ring is intuitively regarded as stationary with the smaller one moving around it. By employing high pressure methods the related [3]catenane $\mathbf{33}^{8+}$ can also be obtained [83]. Interestingly, two non-degenerate translational isomers are now possible for the rotational motion of the two cyclophanes – the two tetracations occupying adjacent stations (*proximal* isomer) or opposite stations (*distal* isomer, shown). The former situation is not observed [84], with the tetracationic cyclophanes preferring to minimize electrostatic repulsion by maximizing the distance between themselves at all times. More recently, the Stoddart group have reported an analogous, hydrogen bonded, [3]catenane which contains four secondary ammonium recognition sites in the large macrocycle as stations for two uncharged polyether macrocycles [85]. In this case, both translational isomers *are* observed, in approximately equal proportions. Given that, statistically, a 2:1 ratio of *proximal*:*distal* isomers would be expected, the observed ratio suggests that while clearly no large electrostatic repulsion exists, there is still some small (probably steric) interaction destabilizing the *proximal* isomer [86].

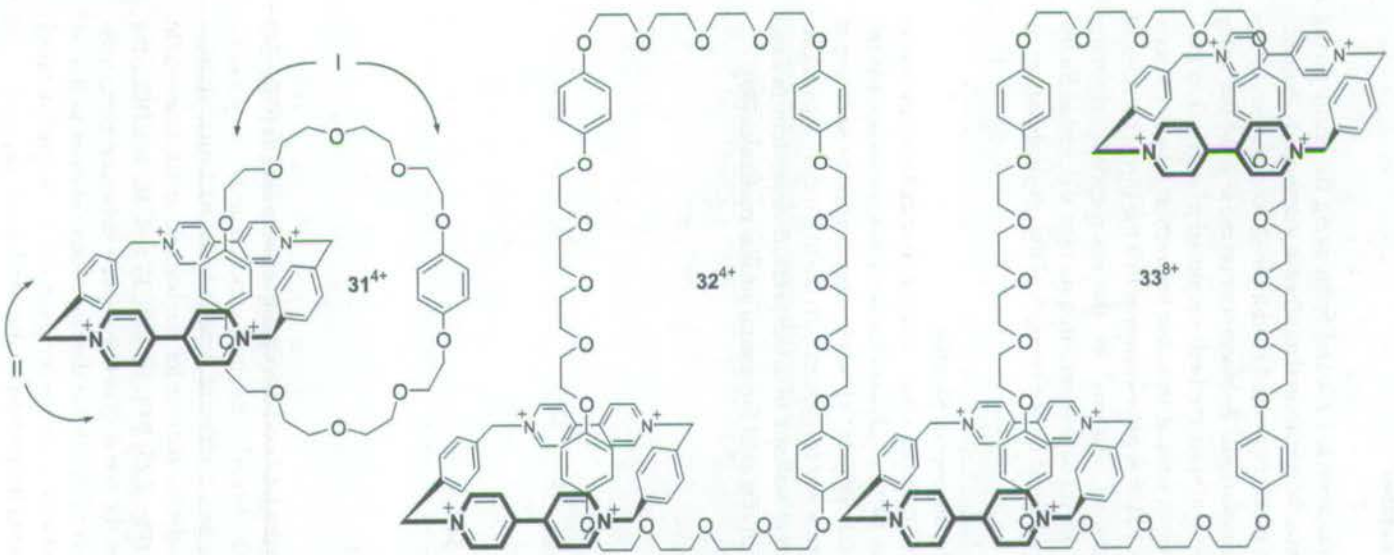

Figure 7.23 Examples of the first catenanes in which dynamic processes were studied. [3]Catenane $\mathbf{33}^{8+}$ is shown in the preferred *distal* translational isomer.

7.5.4
Inherent Dynamics: Shuttling in Rotaxanes

Shuttling is the movement of a macrocycle back and forth along the linear thread component of a rotaxane (or one macrocycle around another in a catenane). This motion takes the form of a Brownian motion-powered random walk, constrained to one dimension by the thread and to translational displacement boundaries by the bulky stoppers. By virtue of the template synthesis methods employed in interlocked molecule synthesis [65], rotaxanes without sites of attractive interaction between macrocycle and thread are relatively rare [87]. It is more common that the thread consists of one or more recognition elements, or "stations" for the macrocycle(s); shuttling therefore becomes the movement on, off or between such stations and, just as for the pirouetting motions, the dynamics depend on the strength of the intercomponent interactions.

7.5.4.1 Observation of Shuttling in Degenerate Shuttles

In the first [2]rotaxane for which the dynamics were studied, Stoddart and coworkers demonstrated shuttling behavior in $\mathbf{34}^{4+}$ (which uses the same π–π interactions as the catenanes discussed in Sect. 7.5.3.3) [88]. In ^{1}H NMR experiments the behavior of proton signals from both components was consistent with the macrocycle moving between the two identical hydroquinol stations in a temperature-dependent fashion (Fig. 7.24). Directly analogous situations exist for several similar molecules [89].

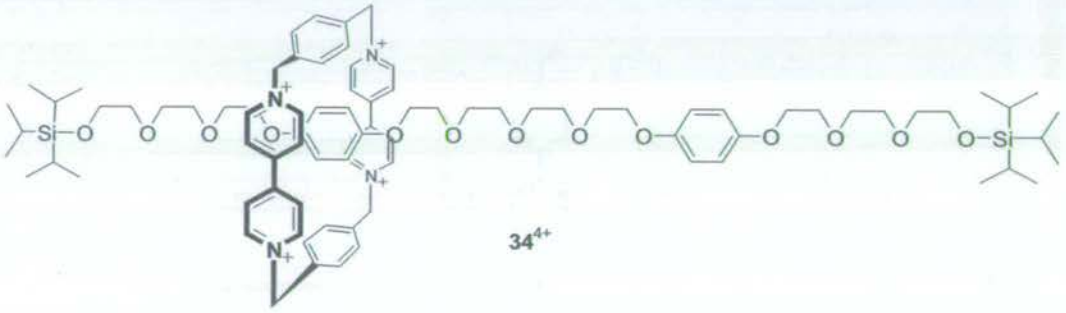

Figure 7.24 The first "molecular shuttle".

Following the observation that hydrogen-bond-disrupting solvents such as $(CD_3)_2SO$ destroy the interactions between the benzylic amide macrocycle and a glycylglycine thread in [2]rotaxane **19** (Fig. 7.18) [66], a series of peptide-based molecular shuttles were described in which two glycylglycine stations for the benzylic amide macrocycle are separated by aliphatic linkers (Fig. 7.25) [90]. In both **35** and **36**, in $CDCl_3$, the macrocycle shuttles rapidly between the two degenerate peptide stations at room temperature, evidenced by the single set of signals for the two peptide stations in the ^{1}H NMR spectrum being resolved into two sets (for the occupied and unoccupied stations) on cooling the sample and freezing out the motion on the NMR timescale.

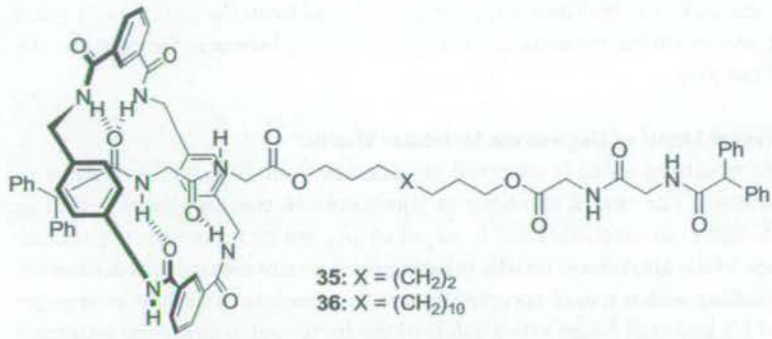

Figure 7.25 Peptide-based degenerate molecular shuttles **35** and **36**.

Just as for the pirouetting motions, the shuttling mechanism must require at least partial rupture of the intercomponent interactions at one station before formation of new interactions at the new station. The thermodynamics of the degenerate process in each of **34**–**36** therefore involves passage over an activation barrier from one energy well to another, identical, minimum (Fig. 7.26). Just as for the analogous benzylic amide catenanes, solvent composition has a profound effect on the shuttling rate in **35** and **36** – as little as 5 % CD_3OD in halogenated solutions of peptide-based rotaxanes leads to rate increases in excess of two orders of magnitude. The hydrogen-bond-disrupting methanol weakens the intercomponent interactions, effectively loosening the macrocycle from its station (i.e. reducing $\Delta G^{\ddagger}$) with a concomitant increase in the shuttling rate [90].

This increase in rate does not, however, continue indefinitely with increasing solvent hydrogen bond basicity. An additional feature of the rotaxanes compared with the analogous benzylic amide catenanes discussed in Sect. 7.5.3.2 is that a major change in solvent polarity (changing from halogenated solvents to $(CD_3)_2SO$) stops the macrocycle shuttling between the peptide stations and causes it to preferentially

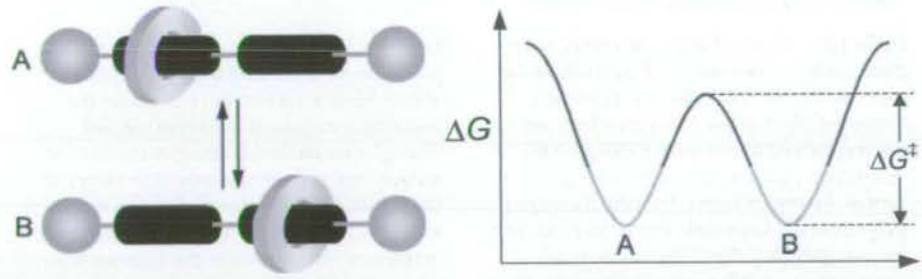

Figure 7.26 Idealized free-energy profile for movement between two identical stations in a degenerate molecular shuttle. The height of the barrier $\Delta G^{\ddagger}$ contains two components – the energy required to break the noncovalent interactions holding it to the station and a distance-dependent diffusional component.

sit over the hydrophobic thread instead, hiding the thread from the unfavorably polar environment and enabling maximum hydrogen bonding between the peptide stations and solvent [90].

7.5.4.2 A Physical Model of Degenerate Molecular Shuttles

An interesting structural effect is observed on increasing the length of the spacer in degenerate shuttles. The rate of shuttling in [2]rotaxane **36** was compared to that in **35** (Fig. 7.25). Although ostensibly not involved in any interactions with the macrocycle, extension of the alkyl chain results in an experimentally measured reduction in the rate of shuttling which would correspond to an increase in activation energy for the process of 1.2 kcal mol^{-1} – an effect solely of the increased distance the macrocycle must travel [80].

All these effects are most clearly understood by considering the macrocycle as a particle moving along a one-dimensional potential energy (rather than free energy) surface (Fig. 7.27). At any point on the potential energy surface the gradient of the line gives the force exerted on the macrocycle by the thread. When the macrocycle is in the vicinity of a station, hydrogen bonds and/or other attractive noncovalent inter-

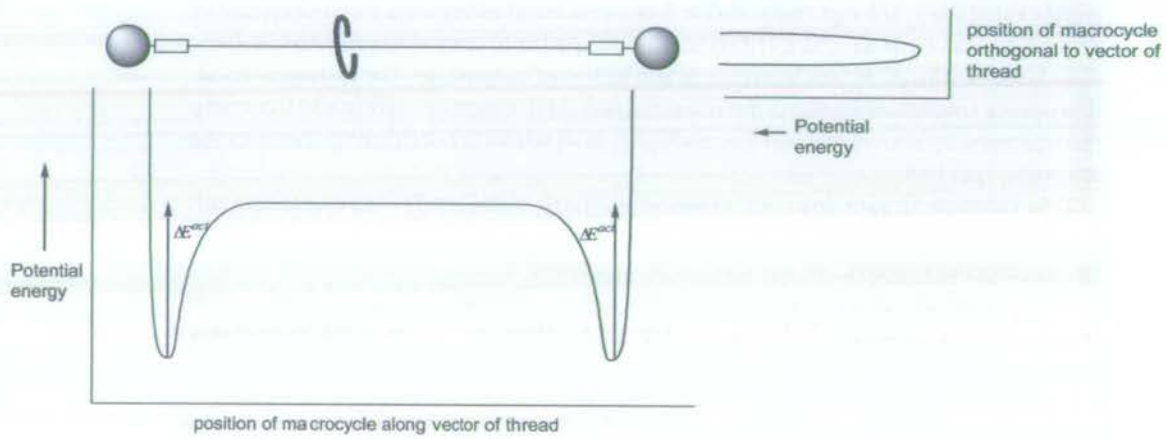

Figure 7.27 Idealized potential energy of the macrocycle in a two-station degenerate molecular shuttle. The potential energy surface shows the effect of the interaction between macrocycle and thread on the energy of the macrocycle (ignoring any complicating factors such as folding). Chemical potential energies (ΔE) usually follow trends similar to those of free energies (ΔG, Fig. 7.26) but there are some important differences; for example, the activation free energy of shuttling, $\Delta G^{\ddagger}$, corresponds to the energy required for the macrocycle to move all the way to the new binding site (i.e. includes a contribution for the distance the ring has to move along the track to reach the other station) whereas the $\Delta E^{\ddagger}$, shown here, is the energy required for the macrocycle to escape the forces exerted through noncovalent binding interactions at a station. The main plot shows ΔE in terms of the position of the macrocycle along the vector of the thread; the minor plot shows the ΔE in terms of the position of the macrocycle orthogonal to the vector of the thread, illustrating that the thread genuinely behaves as a one-dimensional potential-energy surface for the macrocycle.

actions exert large forces (typically varying as a high power of the inverse distance, r^{-n}) on the macrocycle, opposing its motion. When the macrocycle is on the thread *between* the stations, the hydrogen bonds and other noncovalent binding interactions are broken and no forces are exerted on the macrocycle by the thread (i.e. the gradient of the line is zero).

It is thermal energy which enables the macrocycle to escape these energy wells and explore the full length of the thread. For a population of shuttles at equilibrium, therefore, the macrocycles reside on the different stations and the thread according to a Boltzmann distribution and for a single molecule these populations correspond to the amount of time the macrocycle spends on each site. In a degenerate shuttle, in which the binding energy to each station is the same, and no significant interaction with the thread occurs, the macrocycle spends a negligible amount of time on the thread and splits its time equally between the two stations.

The rate at which the macrocycles escape from each station is given by a standard Arrhenius equation, depending on the depth of the energy well and the temperature. This is not the only factor involved in determining the rate at which macrocycles move between the two stations, however, there must also be some distance-dependent diffusional factor in the function describing rate of shuttling – easily understood from consideration of Fig. 7.27.

This phenomenon has been studied further in an attempt to link the experimentally determined values of $\Delta G^{\ddagger}$ with a quantum-mechanical description of the shuttling mechanism [91]. Calculation of the wavefunctions for the system shows that an increase in distance between the stations does not, of course, change the activation energy for cleavage of hydrogen bonds but rather, the effect is to widen the free energy potential well (Fig. 7.26). As this well widens, it has a higher density of states per unit energy (just like the simple "particle in a box" model). The closer to one another the levels are, the more readily thermally populated they are or, in other words, the larger is the partition function and hence $\Delta G^{\ddagger}$.

The nature of the wavefunctions at energies close to the top of the barrier is intriguing, because under this energy regime the maximum probability of finding the macrocycle is, in fact, over the aliphatic spacer. The shuttling process can therefore be thought of in terms of a function of free energy (Fig. 7.26) as long as we remember that the height of the $\Delta G^{\ddagger}$ barrier is affected by *both* binding strength and distance between the stations. The behavior of the macrocycle is similar to a cart moving along a roller coaster track shaped like the double potential in Fig. 7.26. At low temperatures, the cart mostly resides on the stations (oscillating with small amplitude in the troughs). As energy approaches the value of the barrier, the cart spends most of its time passing over the barrier. At higher energies still, the cart is most likely to be found at the extremes of its translational motion.

7.5.5
Controlling Translational Motion: Molecular Shuttles

With increasing understanding of the nature of the inherent restriction in degrees of freedom in interlocked architectures came the realization that control of intercomponent positioning was achievable [92]. Switching on and off degenerate shut-

tling in a rotaxane or varying the frequency of circumvolution in a catenane by solvent effects, structural effects or temperature demonstrates control of motion at the most basic level and only hints at the possibilities which have now been realized.

In shuttles such as 34^{4+}, considered in Sect. 7.5.4.1, there are two identical recognition sites (stations) for the macrocycle so that it is equally likely to reside on either – they are degenerate. As we have seen, the rate at which the macrocycle moves between the stations can be regulated by the temperature or, occasionally, solvent composition. A different kind of control, however, can be achieved in stimulus-responsive shuttles, in which the net location of the macrocycle can be varied by applying an external stimulus.

7.5.5.1 Single-station Switchable Shuttles

A limited amount of control over shuttling can be introduced into single-station rotaxanes if the affinity of the macrocycle recognition site can be affected by a stimulus. [2]Rotaxane 37^{4+} (Fig. 7.28) is closely related to those produced by the Stoddart group and features attractive interactions between a cyclobis(paraquat-*p*-phenylene) cyclophane and an electron-rich dialkoxybenzene station in the thread to template its formation [93]. In 37^{4+}, however, the bulky stoppers are redox-active ferrocenyl residues. A laser flash photolysis pulse within the charge-transfer band of 37^{4+} induces electron transfer between the two interacting components, giving an intimate radical–ion pair (RIP). In closely related systems, decay of the RIP by charge recombination is rapid compared with any competing processes such as solvent penetration or spatial separation of the radical ions. The flexible thread, however, enables close contact of the electron rich ferrocenyl stoppers with the cyclophane by means of a secondary π-stacking interaction. This electronic coupling enables some of the radical ion pairs (~25 %) to undergo a secondary electron transfer step in which the hole on the hydroquinone residue is transferred to one of the ferrocenyl stoppers. This transfer simultaneously breaks the interactions between the cyclophane and both the stopper and dialkoxybenzene, so the system is free to undergo conformational changes involving unraveling of the thread and shuttling of the cyclophane away from the oxidized stopper to reduce electrostatic repulsion. The lifetime of this "long-lived" species is approximately 550 ns – a timescale on which some shuttling of the cyclophane could occur before charge recombination restores the initial state; there is,

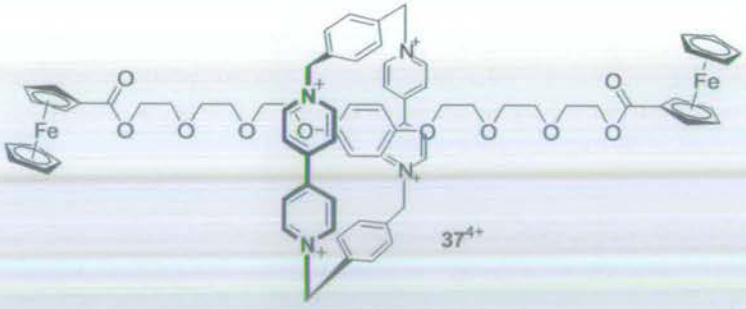

Figure 7.28 [2]Rotaxane 37^{4+} – a "single station" molecular shuttle.

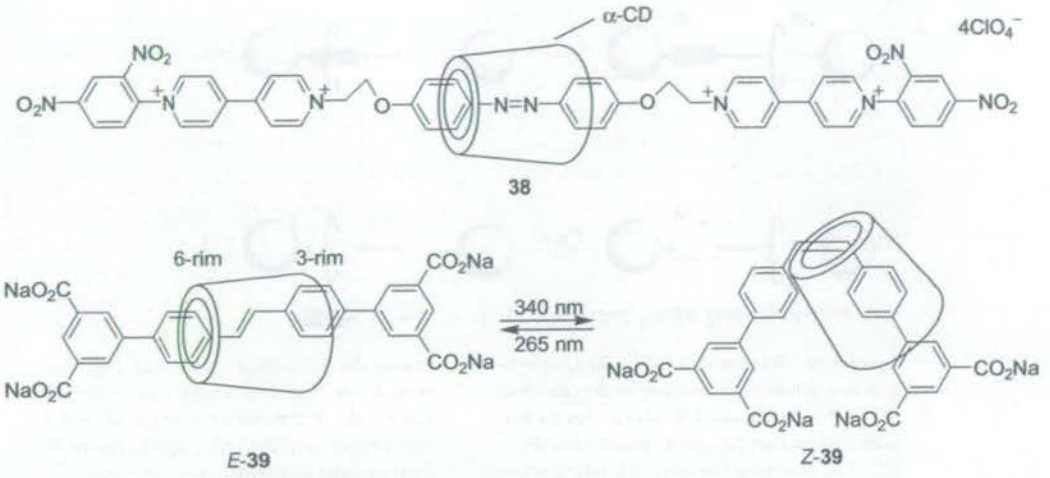

Figure 7.29 Photo-responsive single station shuttles **38** and **39**, based on azobenzene and stilbene units, respectively.

however, no direct evidence for this transient shuttling, nor means to control the position of the cyclophane in the spatially-remote charge-separated state.

It has also been possible to control the position of a cyclodextrin (CD) "macrocycle" on azobenzene and stilbene containing threads in two related systems [94, 95]. In the *E* isomers of [2]rotaxanes **38** and **39** (Fig. 7.29) in aqueous media the cyclodextrin spends most of its time over the central aromatic units. Irradiation at suitable wavelengths results in photoisomerization of the N=N and C=C double bonds in **38** and **39**, respectively, to the *Z* forms. The steric requirements of this "kinking" in the thread demands shuttling of the cyclodextrin away from the central units. Interestingly, in **39** [95], this motion is unidirectional, with the narrower 6-rim of the cyclodextrin always closest to the *Z* olefin. It was also demonstrated, however, that even in the *E* isomers the cyclodextrin only spends approximately two-thirds of its time over the central unit, and it is probably during its vacation of this site that photoisomerization occurs.

7.5.5.2 A Physical Model of Two-station, Stimuli-responsive, Molecular Shuttles

Rotaxanes in which the macrocycle can be translocated between two or more well-separated stations in response to an external signal should, in principle, provide a greater level of control for machines. As we have seen (Sect. 7.5.4), in any rotaxane the macrocycle distributes itself between the available binding sites according to the difference between the macrocycle binding energies and the temperature. If a suitably large difference in macrocycle affinity between two stations exists, the macrocycle resides overwhelmingly in one positional isomer or co-conformation [22]. In stimuli-responsive molecular shuttles, an external trigger is used to chemically modify the system and alter the noncovalent intercomponent interactions such that the second macrocycle binding site becomes energetically more favored, causing translocation of the macrocycle along the thread to the second station (Fig. 7.30). This might be

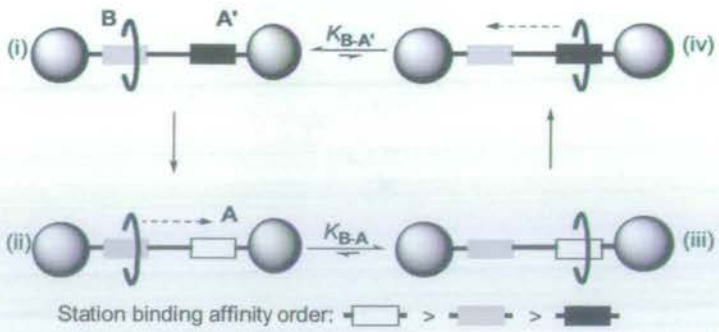

Figure 7.30 Translational submolecular motion in a stimulus-responsive molecular shuttle: (i) the macrocycle initially resides on the preferred station (B); (ii) a reaction occurs (A' → A) changing the relative binding potentials of the two stations such that, (iii), the macrocycle "shuttles" to the now-preferred station (A). If the reverse reaction (A → A') now occurs, (iv), the components return to their original positions.

achieved by addressing either of the stations (destabilizing the initially preferred site or increasing the binding affinity of the originally weaker station). The system can be returned to its original state by using a second chemical modification to restore the initial order of station-binding affinities. Performed consecutively these two steps enable the "machine" to perform a complete cycle of shuttling motion.

The physical basis for this motion is again best understood by consideration of the potential energy of the macrocycle as a function of its position along the thread (Fig. 7.31). It is important to appreciate that the external stimulus does not induce directional motion of the macrocycle *per se*, rather, by increasing the binding strength of the less populated station and/or destabilizing the initially preferred binding site, the system is put out of co-conformational equilibrium [96]. Relaxation towards the new global energy minimum subsequently occurs by *thermally activated* motion of the components, a phenomenon which we recognize as biased Brownian motion. In other words, biased Brownian motion arises from a difference in the activation energies for movement in different directions, *not* from the difference in energy minima. This results in net directional transport (a directional flux) of macrocycles when these barriers are suddenly changed, putting the system out of equilibrium.

Given this mode of action, a key requirement is finding ways of generating sufficiently large, long-lived binding energy differences between pairs of positional isomers. A Boltzmann distribution at 298 K requires a $\Delta\Delta E$ (or $\Delta\Delta G$) between translational co-conformers of ~2 kcal mol^{-1} for 95 % occupancy of one station. Achieving such discrimination in *two* states to form a positionally bistable shuttle (i.e. both $\Delta\Delta E_{B\text{-}A'}$ and $\Delta\Delta E_{B\text{-}A} \geq 2$ kcal mol^{-1}) by modifying only intrinsically weak, noncovalent binding modes is thus a significant challenge.

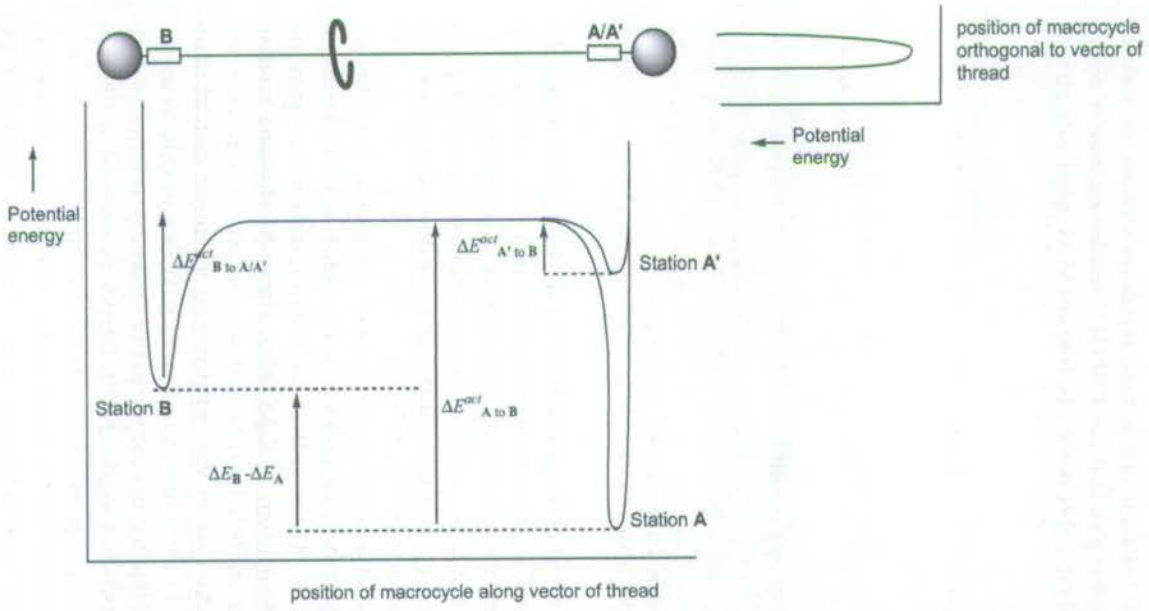

Figure 7.31 Idealized potential energy of the macrocycle in a stimulus-responsive molecular shuttle in which one station changes (A' → A) in response to the stimulus, and complicating factors such as folding are ignored. As before (Fig. 7.27), the potential energy surface shows the effect of the interaction between macrocycle and thread on the energy of the macrocycle. The main plot shows ΔE in terms of the position of the macrocycle along the vector of the thread; the minor plot shows ΔE in terms of the position of the macrocycle orthogonal to the vector of the thread.

7.5.5.3 Adding and Removing Protons to Control Shuttling

In fact, the very first bistable switchable molecular shuttle, reported by Stoddart and Kaifer in 1994, was a two-station design of this type [97]. The biphenol and benzidine units in the thread of [2]rotaxane 40^{4+} (Fig. 7.32) are both potential π-electron donor stations for the $CBPQT^{4+}$ cyclophane, and at room temperature rapid shuttling of the macrocycle occurs, as in the related degenerate shuttles described above (Sect. 7.5.4.1). Cooling the sample to 229 K enables observation (by NMR and UV–visible absorption spectroscopy) of the two non-degenerate translational isomers in a ratio of 21:4 in favor of encapsulation of the benzidine station. Protonation of the basic benzidine residue with CF_3CO_2D results in electrostatic repulsion between the positively charged station and cyclophane so that the $CBPQT^{4+}$ resides exclusively on the biphenol station. The system can subsequently be restored to its initial state on neutralization with pyridine-d_5.

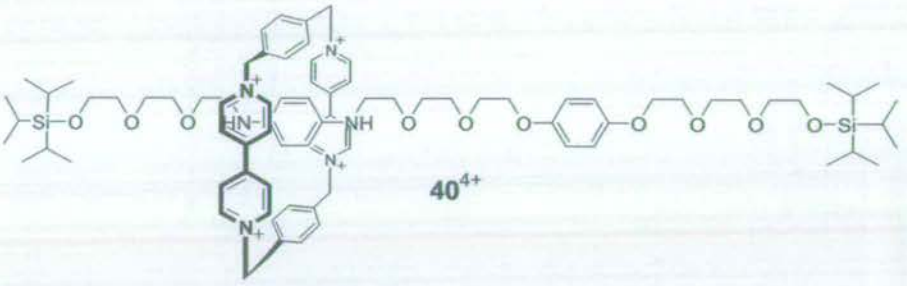

Figure 7.32 The first switchable molecular shuttle 40^{4+}, shown in the preferred co-conformation in the neutral state.

Although this system has many of the attributes of a fully controllable molecular shuttle, it has modest positional integrity in the non-protonated state – a much larger binding difference between the two stations was required. Inspired by the complexation of ammonium ions by crown ethers, Stoddart and coworkers developed a new series of systems based on threads containing secondary alkylammonium species and crown ether macrocycles [98]. [2]Rotaxane $41{\cdot}H^{3+}$ (Fig. 7.33) was the first switchable molecular shuttle reported using these units [99]. The dibenzo-crown ether is bound to the ammonium cation by means of $[N^+–H\cdots O]$ hydrogen bonds and well as weaker $[C–H\cdots O]$ bonds from methylene groups in the α-position to the nitrogen. ^1H NMR spectroscopy in CD_3COCD_3 shows no shuttling motion, with the crown ether sitting overwhelmingly (but *not* exclusively [113]) over the cation, to the limits of detection set by this experimental technique even at room temperature. Deprotonation of the ammonium center with diisopropylethylamine turns off the interactions holding the macrocycle to this station, so it is free to shuttle on to the alternative bipyridinium station (41^{2+}). Despite no observation of binding between the crown ether and bipyridinium units in a non-interlocked pseudorotaxane model system, NMR studies on the deprotonated rotaxane show the system again adopting a co-conformation with high of positional integrity, sitting over the

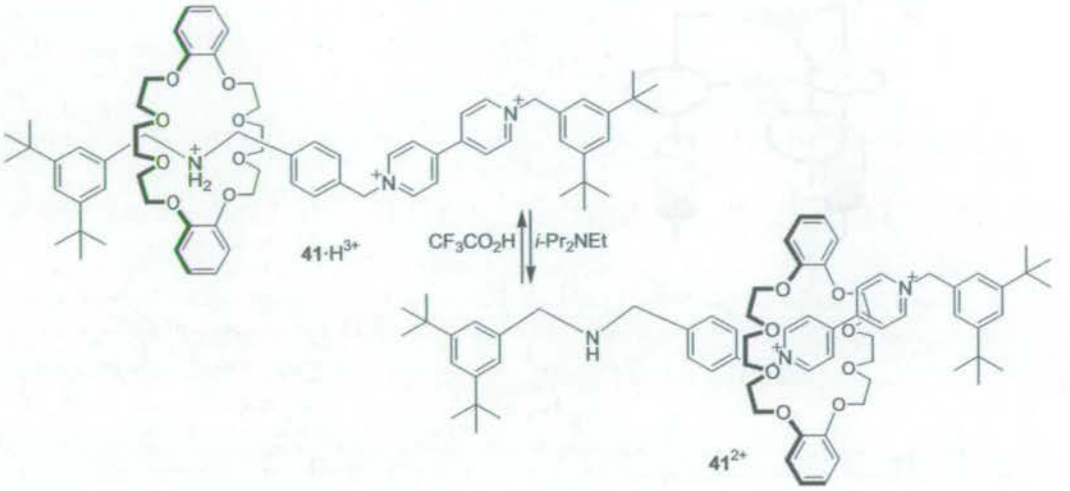

Figure 7.33 A pH-responsive bistable molecular shuttle with excellent positional integrity in both chemical states.

bipyridinium unit in an asymmetric fashion; a corresponding yellow charge-transfer interaction between the catechol rings and bipyridinium station is observed [100].

Although excellent macrocycle positional integrity in both chemical states is observed for this example, the low binding constant between the crown ether and bipyridinium moieties in the deprotonated state might be a limitation in more complex systems, especially if the macrocycle is afforded a greater degree of translational freedom (the distance between the stations in the current system is ~7 Å). Accordingly, Stoddart and coworkers have prepared a combination of three shuttle units in parallel using this system [101]. The molecule (**42**•3H^{9+}) consists of three thread-like components connected at one end and encircled by three catechol–polyether macrocycles connected in a platform-like fashion (Fig. 7.34). Essentially, the shuttling action works precisely as in **41**, just over three equivalents of base are required to move the platform from ammonium ("top") to bipyridinium ("bottom") positions. The combined effect of three binding sites is excellent positional integrity in both positions.

The first pH switched shuttle to exploit [N-H···anion] hydrogen bonding interactions has also been reported [102]. In [2]rotaxane **43**•H (Fig. 7.35), formation of the benzylic amide macrocycle is templated by a succinamide station in the thread. The thread however also contains a cinnamate derivative (related to the *p*-coumaric acid chromophore of PYP, see Sect. 7.3). In the neutral form, the cinnamate phenol is a relatively poor hydrogen-bonding group and the macrocycle resides on the succinamide station >95 % of the time. Deprotonation to give **43**$^-$, however, results in the macrocycle binding to the phenolate anion. Reprotonation of the phenol returns the system to its original state. Although a wide range of bases (with a variety of counterions) proved efficacious, shuttling was found to be extremely solvent-dependent. Hydrogen-bond-mediated systems usually perform best in "non-competing" solvents – those with low hydrogen bond basicity. Yet when deprotonation of **43**•H is con-

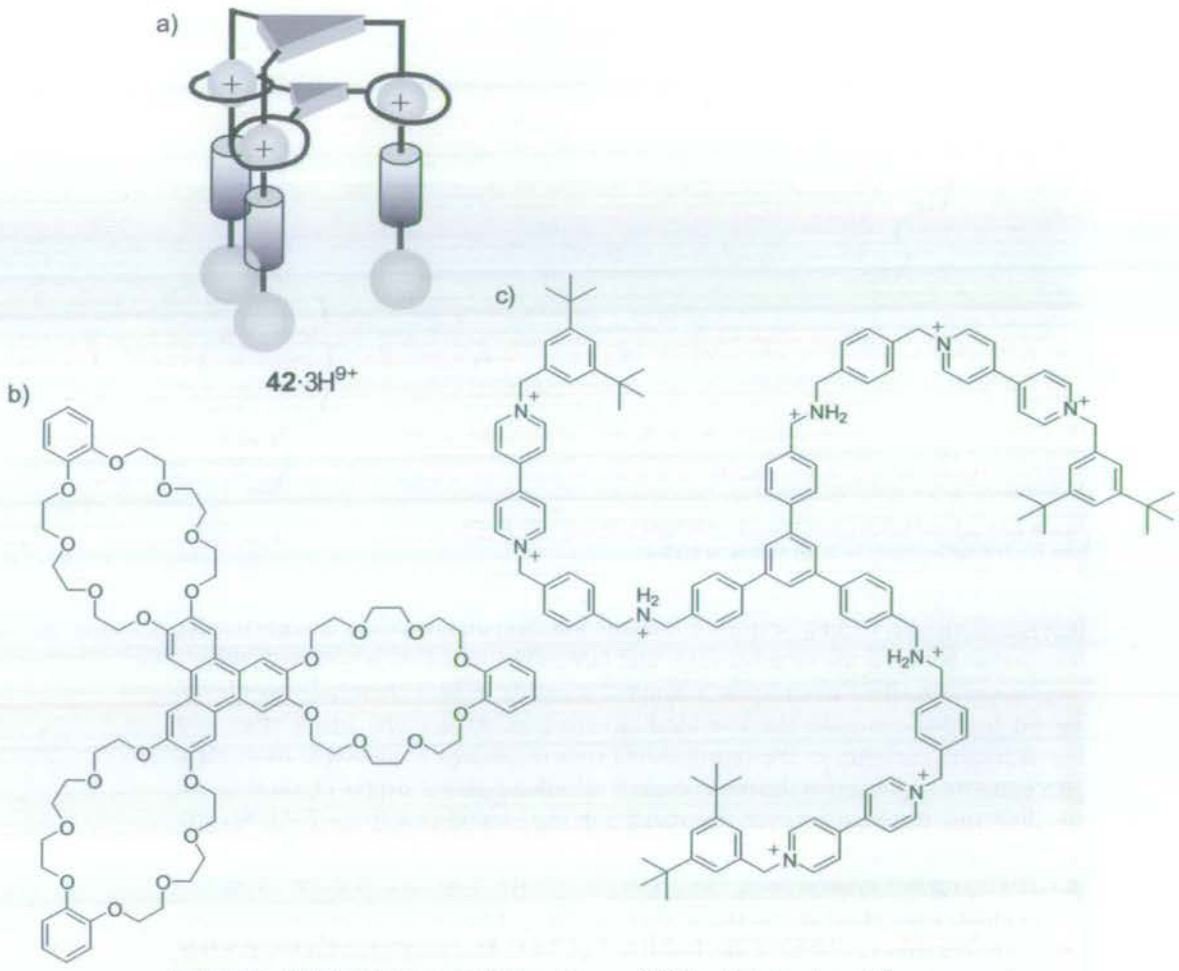

Figure 7.34 (a) Schematic representation of a "molecular elevator" **42**•$3H^{9+}$, with the "platform" on the "top" dialkylammonium station. (b) Chemical structure of the macrocyclic "platform" component of **42**. (c) Chemical structure of "rig" component of **42**.

ducted in $CDCl_3$ or CD_2Cl_2, a change of position of the macrocycle does not occur. Rather an intramolecular folding event occurs to enable the phenolate to hydrogen bond with the macrocycle while it remains on the succinamide station. The interaction between macrocycle and succinamide station in **43**•H is so strong, however, that even in DMF-d_7 the excellent positional integrity is maintained. On deprotonation in this solvent, shuttling does indeed occur and in $\mathbf{43}^-$ the only co-conformation detectable by NMR has the succinamide station vacated with the macrocycle hydrogen-bonding to the phenolate. This solvent dependence can be understood when we consider that the phenolate can only satisfy the hydrogen-bonding requirements of one isophthalamide unit in the macrocycle. The presence of a hydrogen-bond-accepting solvent such as DMF can therefore compensate for this loss of stabilization. The

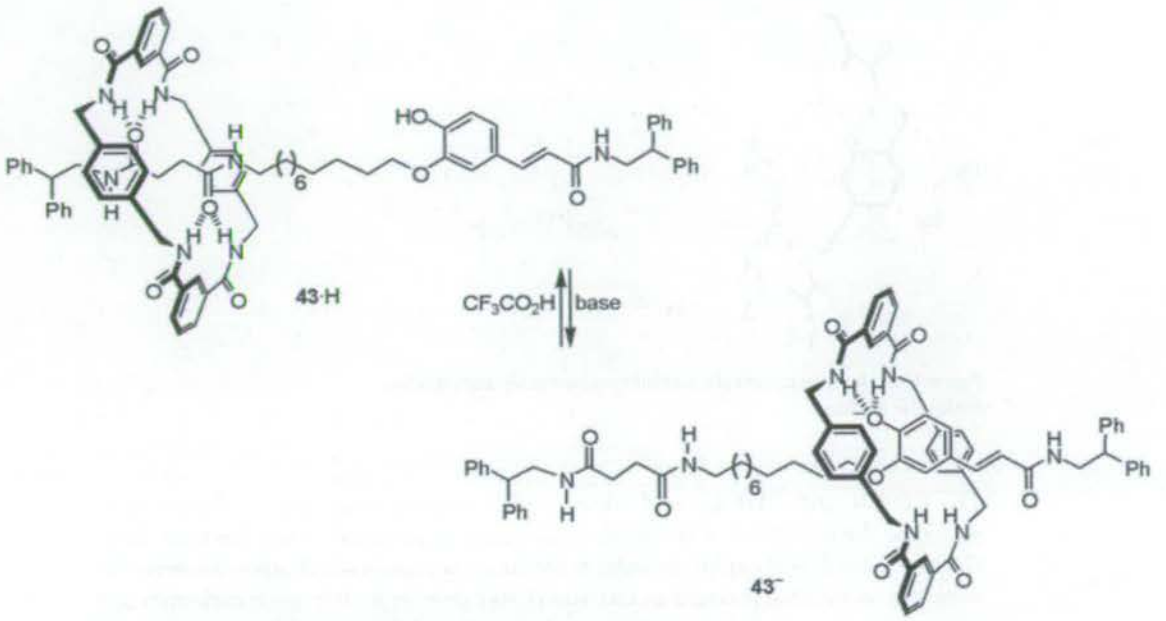

Figure 7.35 pH-switched anion shuttling in a hydrogen bonded [2]rotaxane. Bases used: LiOH, NaOH, KOH, CsOH, Bu_4NOH, *t*BuOK, DBU, Schwesinger's phosphazine P_1 base.

strength of binding to the anion is illustrated by the fact that the shuttling process continues to occur even in CD_3CN – only a moderate hydrogen-bond acceptor and weaker than the amide groups of the thread.

7.5.5.4 Adding and Removing Electrons to Control Shuttling

With the original switchable shuttle 40^{4+} it was found that the change of position could be achieved in a reagent-free manner by electrochemical oxidation of the benzidine station – shuttling away from this station occurring after oxidation to the radical cation. Unfortunately, several attempts to create analogous redox-switched shuttles with improved positional integrity failed to give the desired distribution of translational isomers in the ground state [103] and intrinsic shuttling at ambient temperatures always remained rapid [104, 105].

[2]Rotaxane **44** contains two potential hydrogen-bonding stations for the benzylic amide macrocycle – a succinamide (*succ*) station and a redox-active 3,6-di-*tert*-butyl-1,8-naphthalimide(*ni*) station – separated by a C_{12} aliphatic spacer (Fig. 7.36) [106].

While the ability of the *succ* station to template formation of the macrocycle is well established, the neutral naphthalimide moiety is a poor hydrogen-bond acceptor. To minimize its free energy the macrocycle in **44** must therefore sit over the succinamide station in non-hydrogen-bonding solvents, so that co-conformation *succ*-**44** predominates (Fig. 7.37). In fact the difference between macrocycle-binding affinity is so great that *succ*-**44** is the only translational isomer detectable by ^1H NMR in CD-

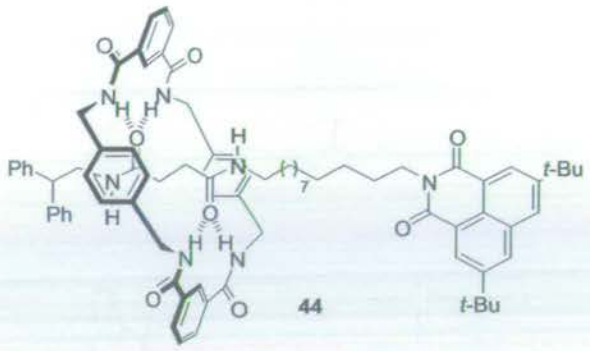

Figure 7.36 A photochemically and electrochemically addressable molecular shuttle.

Cl_3, CD_3CN and THF-d_8, and even in the strongly hydrogen-bond-disrupting $(CD_3)_2SO$ the macrocycle sits over the *succ* station approximately half the time. One-electron reduction of naphthalimides to the corresponding radical anion, however, results in a substantial increase in electron charge density on the imide carbonyls and a concomitant increase in hydrogen-bond-accepting ability. In **44**, this change in oxidation state reverses the relative hydrogen bonding abilities of the two thread stations so that co-conformation *ni*-**44**$^{\bullet-}$ is preferred in the reduced state. Subsequent re-oxidation to the neutral state restores the original order of binding site affinities and the shuttle returns to its initial state as co-conformation *succ*-**44**. This process can be stimulated and observed in cyclic voltammetry experiments [106b] or, alternatively, photochemistry can be employed to initiate (through excitation of the naphthalimide group by a nanosecond laser pulse at 355 nm followed by electron transfer from a regenerable external electron donor) and observe (using transient absorption spectroscopy) the change of position [106a]. A number of control experiments were able to prove unequivocally that the dynamic process observed is reversible shuttling of the macrocycle between the stations rather than any other conformational or co-conformational change [106b].

Although many metal–ligand interactions can be rather kinetically stable, the availability of different oxidation states with different properties can be harnessed to control intercomponent motion in transition metal-based systems. [2]Rotaxane **45** (Fig. 7.38) exploits the unique properties (among the first row transition metals at least) of copper – in particular, the strong stereoelectronic requirements for the mono- and divalent cations [107]. The preference of Cu^{I} for four-coordinate tetrahedral complexes has been widely exploited to synthesize interlocked architectures (see Sect. 7.5.3.1), because it enforces the orthogonal arrangement of two bidentate ligands which can subsequently be cyclized to give interlocked species. In **45-I-N$_4$**, a macrocyclic ring containing a bidentate 2,9-diphenyl-1,10-phenanthroline (dpp) unit, is locked around a thread component which also contains one phenanthroline as well as one tridentate 2,2':6',2''-terpyridine (terpy) unit. The preference of Cu^{I} for tetrahedral geometries requires that the ring sits around the phenanthroline station in the

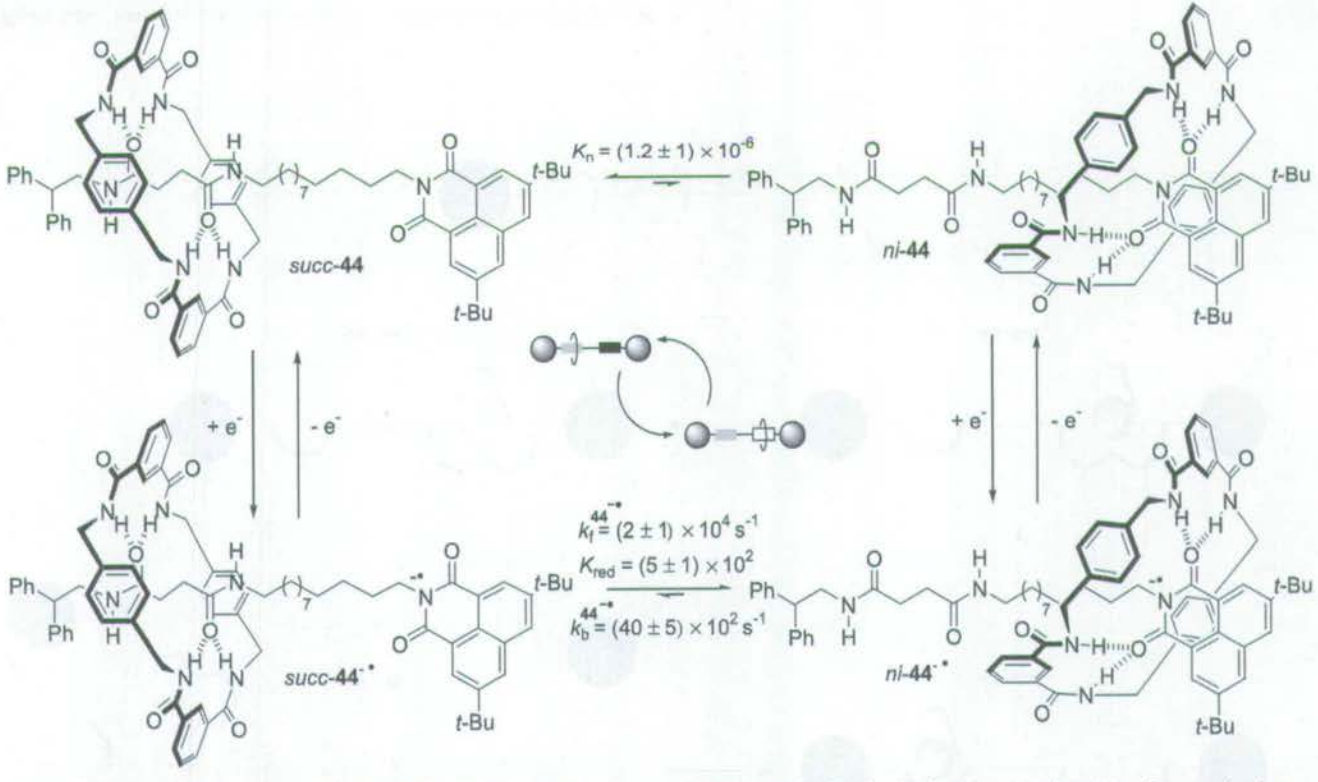

Figure 7.37 The photochemically and electrochemically switchable, hydrogen-bonded molecular shuttle **44**. In the neutral state, the translational co-conformation *succ*-**44** is predominant because the *ni* station is a poor hydrogen-bond acceptor ($K_n = (1.2 \pm 1) \times 10^{-6}$). On reduction, the equilibrium between *succ*-$\mathbf{44}^{-\bullet}$ and *ni*-$\mathbf{44}^{-\bullet}$ is altered ($K_{red} = (5 \pm 1) \times 10^2$) because *ni*$^{-\bullet}$ is a powerful hydrogen-bond acceptor and the macrocycle moves through biased Brownian motion. On reoxidation the macrocycle shuttles back to its original position. Repeated reduction and oxidation causes the macrocycle to shuttle forwards and backwards between the two stations. All the values shown refer to cyclic voltammetry experiments in anhydrous THF at 298 K with tetrabutylammonium hexafluorophosphate as the supporting electrolyte. Similar values were determined on photoexcitation and reduction of the ensuing triplet excited state by an external electron donor.

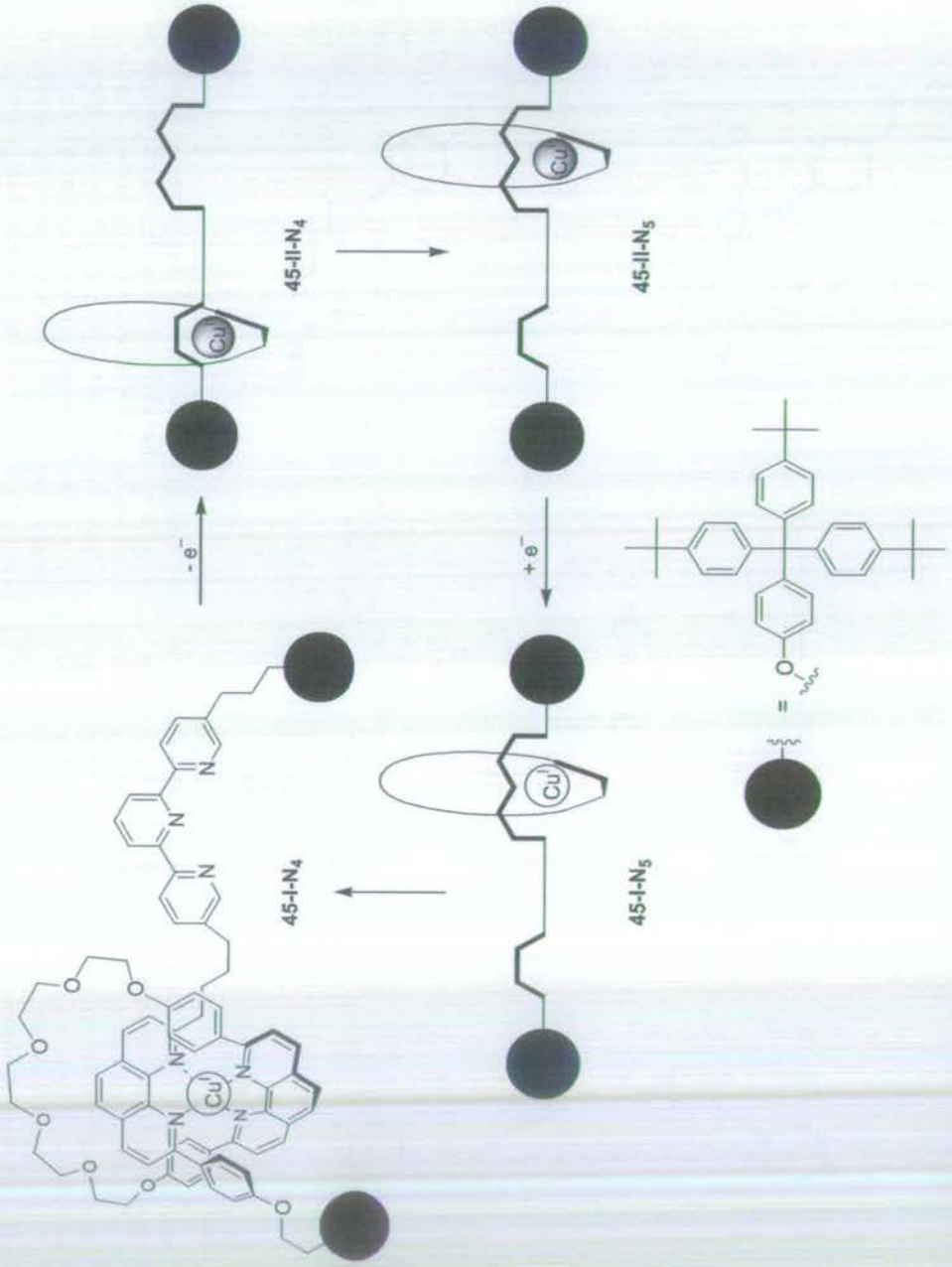

Figure 7.38 Redox-switched shuttling in a metal-templated [2]rotaxane, **45**.

thread with the metal ion coordinated between the two components. Electrochemical reduction gives **45-II-N_4**. As Cu^{II} prefers higher coordination numbers, thermally activated relaxation to the thermodynamically preferred **45-II-N_5** product occurs. Even the metastable **45-II-N_4** state is relatively kinetically inert, however, and this shuttling step takes several hours ($k = 1.5 \times 10^{-4}\ s^{-1}$). Electrochemical reduction of the divalent species gives **45-I-N_5** which slowly converts to the starting material **45-I-N_4** ($10^{-4} \leq k \leq 10^{-2}\ s^{-1}$). The shuttling process can also be accomplished by a photochemically-triggered oxidation. The reverse reductive step cannot be performed photochemically but proceeds successfully with a chemical reductant (ascorbic acid).

7.5.5.5 Changing Configuration to Control Shuttling

As with the control of submolecular motion in covalently bound systems, isomerization processes are an attractive means of controlling shuttling in rotaxanes. Shuttle *E/Z*-**46** (Fig. 7.39) employs the interconversion between fumaramide (trans) and maleamide (cis) isomers of the olefinic unit [108]. Fumaramide moieties are excellent binding sites for benzylic amide macrocycles – the trans olefin fixes the two strongly hydrogen-bond-accepting amide carbonyls in a close-to-ideal spatial arrangement for interaction with the amide protons from the macrocycle. Strong interactions between macrocycle and thread, in the guise of two sets of bifurcated hydrogen bonds, are the result. Although a similar hydrogen-bonding surface is presented to the macrocycle, binding to the succinamide station results in both a loss in entropy (because of loss of bond rotation) and also one less intracomponent hydrogen bond which cannot be reproduced in the rigid fumaramide station. The result is that only one positional isomer of *E*-**46** is observed in NMR studies at room temperature. Photoisomerization of the fumaramide station by irradiation at 254 nm reduces the number of possible intercomponent hydrogen bonds at this station from four to two so that a new co-conformational energy minimum now exists; the macrocycle now sits overwhelmingly on the succinamide station. Unlike the succinamide/naphthalimide system (Fig. 7.36, Sect. 7.5.5.4), this new state is indefinitely stable until a further

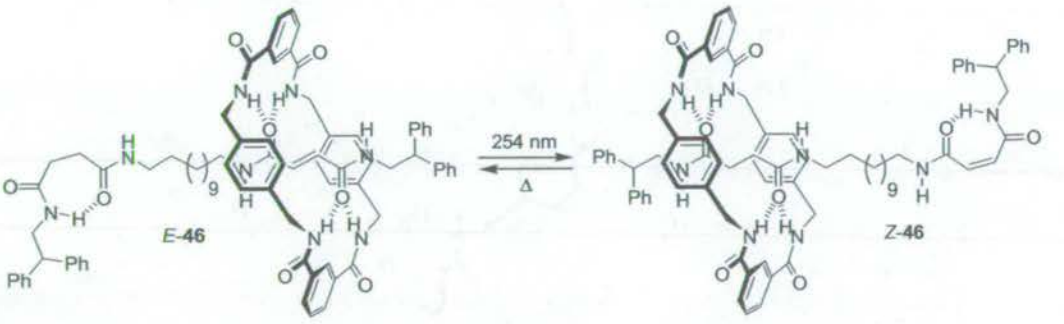

Figure 7.39 Bistable molecular shuttle *E/Z*-**46** in which self-binding of the "low affinity" station in each state is a major factor in producing excellent positional discrimination.

stimulus is applied – namely thermal or chemical re-isomerization of the maleamide unit back to fumaramide, thus restoring the shuttle to its initial state [109].

7.5.5.6 Entropy-driven Shuttling

Most of the shuttles which exhibit excellent positional discrimination can be switched using stimuli such as pH, light, polarity of the environment or electrochemistry to modify the enthalpy of macrocycle binding to one or both stations. In general the effect of temperature is simply to alter the extent of discrimination the macrocycle expresses for the different stations, not to alter the station preference [110]. In [2]rotaxane **47**, however, the macrocycle can be switched between stations simply by changing the temperature. In fact, **47** is a *tristable* molecular shuttle – a rotaxane in which the ring can be switched between three different positions on the thread (Fig. 7.40).

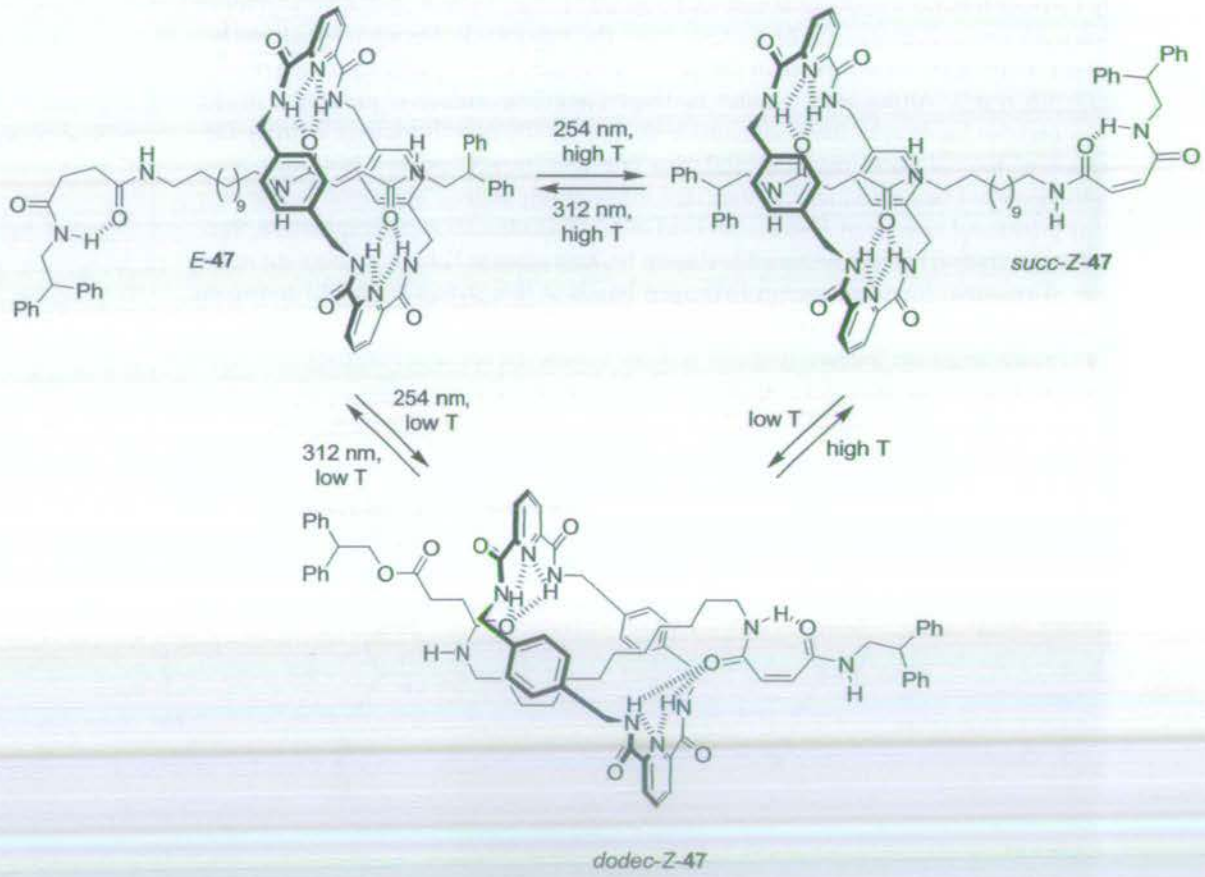

Figure 7.40 A tristable molecular shuttle **47**.

Structurally, **47** is closely related to **46**, the difference being substitution of the isophthaloyl unit in the macrocycle for a pyridine-2,6-dicarbonyl moiety. In the *E*-**47** form, the macrocycle resides over the strong fumaramide station at all temperatures investigated, as expected. Photoisomerization of *E*-**47** gave the maleamide *Z*-**47** isomer. The ^{1}H NMR spectra of this product showed clearly that shuttling away from the maleamide station had occurred, but the nature of the product was highly temperature-dependent. At elevated temperatures (308 K) the expected *succ-Z*-**47** co-conformation was observed; the macrocycle spends nearly all its time over the succinamide station. At lower temperatures, however, the macrocycle occupies neither the succinamide nor the maleamide units – the alkyl chain exhibits spectroscopic shifts indicative of encapsulation by the ring. This suggests that the thread adopts an S-shaped conformation with the macrocycle binding to one amide of each station (*dodec-Z*-**42**, Fig. 7.40). Unlike [2]rotaxane **46**, photochemical cis → trans isomerization was effective (irradiation of *Z*-**47** at 312 nm gave a photostationary state of >95:5 *E*:*Z* compared with ~45:55 under the same conditions for **46**) so no heating is necessary for this step and all the interconversions shown in Fig. 7.40 are possible.

The origin of this temperature-switchable effect is presumably the large difference in entropy of binding ($\Delta S_{binding}$) to the succinamide and alkyl chain stations, which enables the $T\Delta S_{binding}$ term to have a significant overall impact on $\Delta G_{binding}$ as temperature is varied. In the *succ-Z*-**47** co-conformation, the macrocycle forms two strong hydrogen bonds with an amide carbonyl and two, significantly weaker, bonds to the ester carbonyl. The *dodec-Z*-**47** co-conformation, however, enables formation of four strong hydrogen bonds to amide carbonyls making it enthalpically favored by ~2 kcal mol^{-1}. At low temperatures, when the effects of the entropy term are less significant, the molecule therefore adopts the *dodec-Z*-**42** co-conformation. At higher temperatures, the increased contribution from the $T\Delta S_{binding}$ term requires that the molecule adopts the more entropically favorable *succ-Z*-**42** co-conformation to minimize its energy [111].

This effect seems to be quite structure specific – no other shuttles in this series have shown temperature-dependent co-conformational preference. If suitable systems can be successfully designed, however, entropy-driven temperature control of positional isomerism could prove a useful addition to the expanding strategies for controlling submolecular motions [112].

Many of the shuttling examples described show remarkable degrees of control over submolecular fragment positioning and dynamics. They utilize a number of different stimuli-induced processes to effect macrocycle shuttling over large amplitudes (up to ~15 Å in **43**, **46**, and **47**) and operate over a range of timescales (a complete shuttling cycle in **44** is over in ~100 μs whereas in **46** both states are indefinitely stable and the time for a full cycle is infinitely variable). It must, however, be remembered that all such shuttles exist as an equilibrium of co-conformations and it is simply the position of the equilibrium that is varied [113].

7.5.6
Controlling the Motion: Ring Pirouetting in Rotaxanes

Control of macrocycle pirouetting in rotaxanes presents two challenges – frequency of random pirouetting and directionality (Fig. 7.41). The former has been achieved by means of the effects of temperature, structure, electric fields, light, and solvent; the latter has not yet been demonstrated.

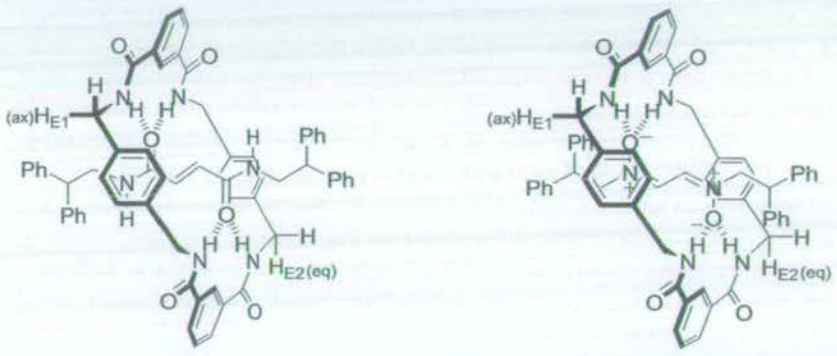

Figure 7.41 [2]Rotaxanes **21** and **48** in which the rate of pirouetting can be controlled by application of an alternating current electric field.

Alternating-current (a.c.) electric fields would be an ideal stimulus for control of submolecular dynamics in many applications. In two of the benzylic amide-based, hydrogen-bonded [2]rotaxanes (**21** and **48**), it was observed that application of a.c fields of approximately 50 Hz resulted in unusual Kerr-effect responses unique to the interlocked architecture (i.e. not observed for either of the components alone) [114]. Reducing the field strength had the same effect as increasing temperature – enhancement of the response – indicating that the underlying phenomenon is addressable by these two stimuli. Both VT NMR experiments and molecular modeling confirmed that macrocycle pirouetting is the only possible dynamic process on this timescale in these structures. The experimental and theoretical studies also predict the slightly more complex Kerr effect response observed experimentally for **21** compared with **48**. Application of an a.c. electric field therefore attenuates macrocycle pirouetting in **21** and **48**. The extent of the dampening can be varied with the strength of the applied field – even modest fields of ~1 V cm^{-1} produce rate reductions a large as 2–3 orders of magnitude.

An alternative strategy for affecting pirouetting rates would be to apply some stimulus which directly alters the structure or electronics of the thread or macrocycle, to adjust the strength of intercomponent interactions. This has been achieved for the fumaramide-based [2]rotaxanes **49–51** (Fig. 7.42), which are closely analogous to **21** above [115]. The decrease in intercomponent binding affinity on photoisomerization

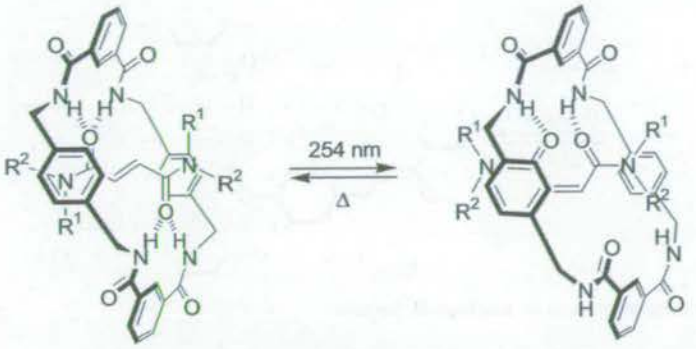

E-**49** $R^1 = R^2 = CH_2CO_2CH_2Ph$ *Z*-**49**
E-**50** R^1 Me, $R_2 = CH_2CHPh_2$ *Z*-**50**
E-**51** $R^1 = H$, $R^2 = CH_2CHPh_2$ *Z*-**51**

Figure 7.42 Photoisomerization of [2]rotaxanes **49–51** which results in pirouetting rate enhancements of up to six orders of magnitude. The reverse process Z → E isomerization can be effected by heating a 0.02 M solution of the Z rotaxanes at 400 K or generating bromine radicals (cat. Br_2, *hν* 400 nm) or by reversible Michael addition of piperidine (RT, 1 h).

of the fumaramide units in **49–51**, to the *cis*-maleamide isomers, gives a huge increase in rate of pirouetting of more than six orders of magnitude. The switching process is also reversible; subjecting the maleamide rotaxanes to heat or a variety of chemical stimuli results in re-isomerization to the more thermally stable trans olefin isomers, with accompanying reinstatement of the strong hydrogen-bonding network [116, 117].

7.5.7
Controlling the Motion: Switchable Catenanes – the Issue of Directionality

The fundamental principles of controlling shuttling in rotaxanes and rotation in catenanes are the same. For example, homocircuit [2]catenane **52**, acts somewhat like the two-station degenerate shuttle **35** (Sect. 7.5.4.1) [118]. In halogenated solvents such as $CDCl_3$ the two macrocycles interact by hydrogen bonding between their aromatic 1,3-diamide groups, resulting in a "host–guest" relationship in which each (constitutionally identical) ring adopts a different conformation and exists in a different chemical environment (**52**-a, Fig. 7.43, also the structure observed in the solid state). Pirouetting of the two rings interconverts this host–guest relationship and is fast on the NMR timescale. In a hydrogen bond-disrupting solvent such as $(CD_3)_2SO$, however, the preferred co-conformation has the amides exposed on the surface, where they can interact with the surrounding medium, while the hydrophobic alkyl chains are buried in the middle of the molecule (**52**-b, Fig. 7.43). Of course, with disruption of the main noncovalent interactions between the two rings, the frequency of movements is also greatly increased in polar media.

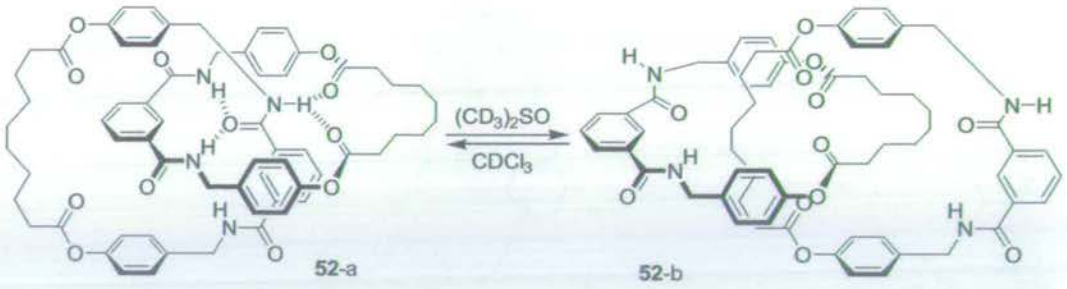

Figure 7.43 Translational isomerism in an amphiphilic benzylic amide [2]catenane **52**.

Heterocircuit [2]catenane 53^{4+} (Fig. 7.44) behaves similarly to analogous two-station non-degenerate [2]rotaxanes [119]. Initially the tetracationic cyclophane encircles the more electron-rich tetrathiafulvalene station (TTF), as evidenced by ^{1}H NMR and UV–visible absorption spectroscopy studies. Oxidation of the TTF to either its radical cation or dication can be achieved chemically or electrochemically. This oxidation results in complete movement of the cyclophane away from the cationic residue to the hydroxynaphthalene unit. This process has been observed using cyclic voltammetry measurements and ^{1}H NMR and UV–visible absorption spectroscopy and is accompanied by a green to maroon color change. The process can be reversed by either chemical or electrochemical reduction of the TTF unit back to its neutral state. There is, however, no control over which direction the motion occurs; the cyclophane has a choice of two identical routes between the stations and half the molecules will rotate one way, the other half the other way [120].

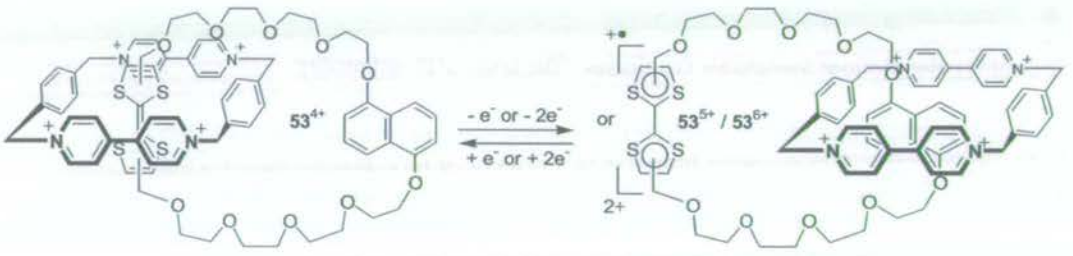

Figure 7.44 Chemically and electrochemically driven translational isomer switching of [2]catenane **53**.

Sauvage has demonstrated both electrochemical and photochemical control over ring motion in hetero-[2]catenate **54** (Fig. 7.45) which is directly related to [2]rotaxane **45** (Sect. 7.5.5.4) [121]. The observed behavior of the catenate is essentially the same as that of the rotaxane analog, although the 4-coordinate to 5-coordinate (dpp → terpy) shuttling process is slower in the catenate and the reverse terpy → dpp step is faster. These discrepancies are explained by the easier access to the metal for solvent

54-I-N_4

Figure 7.45 Heterocircuit switchable catenate **54**.

or ionic species in the rotaxane, thus stabilizing transition states on the way to higher-coordination-number species [122].

The behavior of the related homocircuit [2]catenate **55** (Fig. 7.46) – in which each ring now contains a bidentate dpp unit and tridentate terpy site – is more complicated [123]. In **55-I-N_4**, the Cu^{I} template coordinates to the two dpp units in the expected tetrahedral arrangement. Oxidation of the metal center to its divalent state (by either chemical or electrochemical means) reverses the order of preference for coordination numbers: CN = 6 > 5 > 4 is the preferred order for Cu^{II}. The result is circumvolution of the rings to give the preferred hexacoordinated species. It was demonstrated that this process occurs by revolution of one ring to give an intermediate five-coordinate species (**55-II-N_5**). In comparison with the other metal templated systems, this process is relatively fast, the translational process being on the timescale of tens of seconds. The process is completely reversible, via the same five-coordinate geometry, on reduction to Cu^{I} (i.e. via **55-I-N_5**).

As such, this catenate can exist as three translational "isomers" (six different states when the oxidation state of the metal ion is considered). The intermediate five-coordinate states are, however, only transient and cannot be isolated. A system which does have three distinct, stable states is [2]catenane **56**. Furthermore, **56** – and the related [3]catenane **57** – extends the fumaramide photoisomerization strategy seen in [2]rotaxanes **46**, **47** and **49**–**51** to create the first examples of stimuli-driven sequential and unidirectional rotation in interlocked molecules, thereby illustrating the key difference between shuttling in two-station rotaxanes and rotation in catenanes – the issue of directionality [124].

Sequential movement of one macrocycle between three stations on another ring requires independent switching of the affinity for two of the units to change the relative order of binding affinity, as shown schematically in Fig. 7.47.

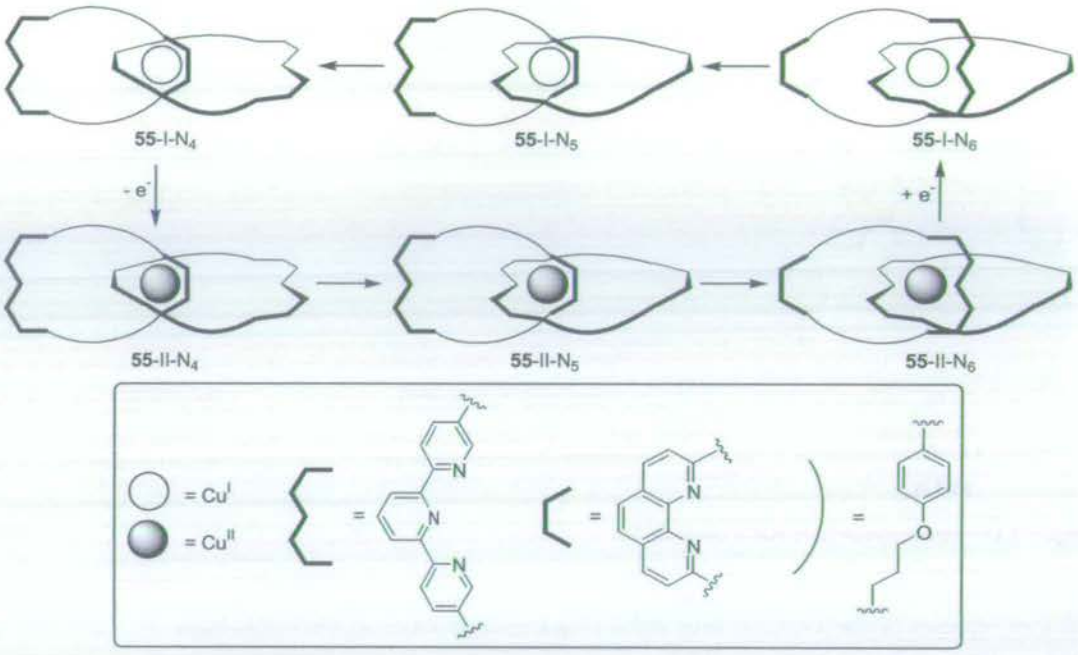

Figure 7.46 Oxidation state-controlled switching of [2]catenate **55** between three distinct co-conformations.

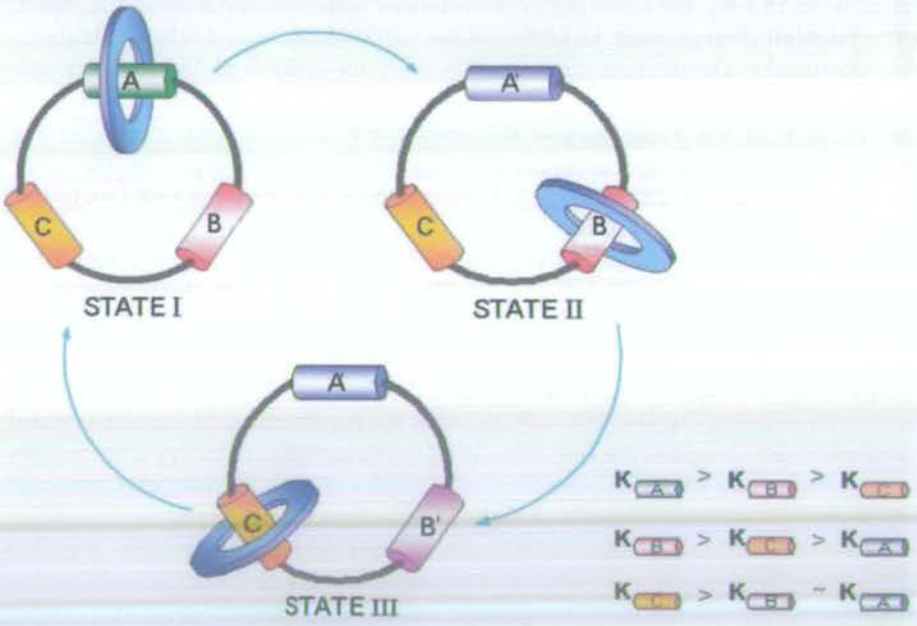

Figure 7.47 Stimulus-induced sequential movement of a macrocycle between three different binding sites in a [2]catenane.

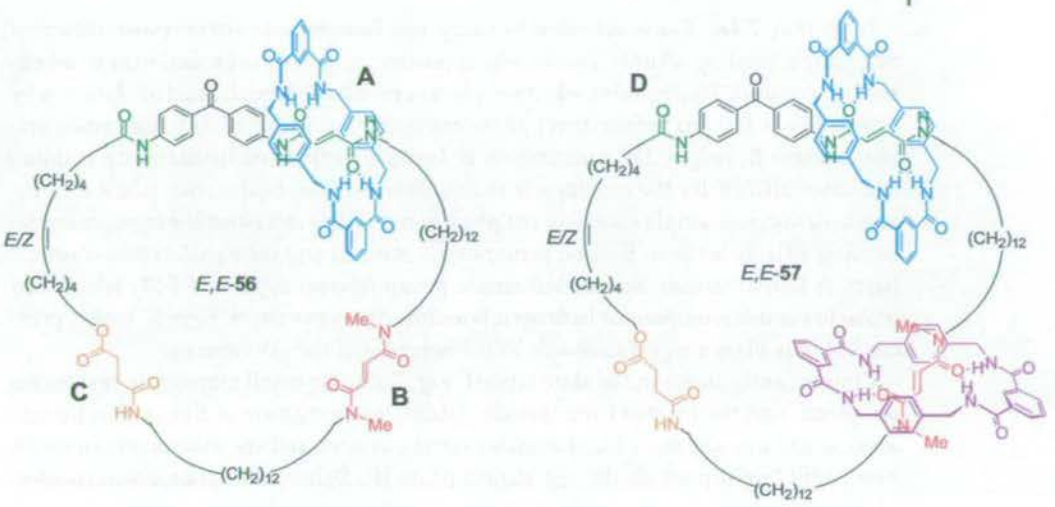

Figure 7.48 [2]Catenane **56** and [3]catenane **57**, shown as their *E,E* isomers.

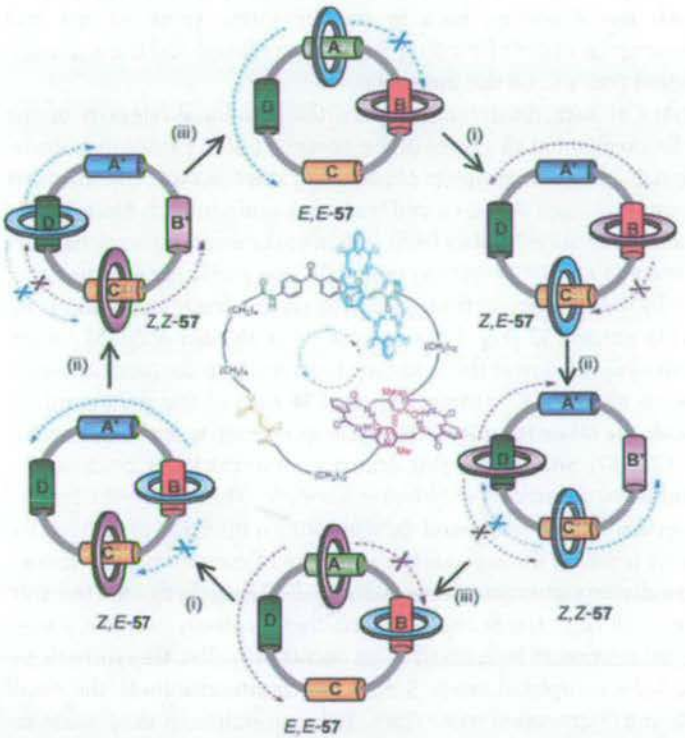

Figure 7.49 Stimulus-induced unidirectional rotation in a four station [3]catenane, **57**. (i) 350 nm, CH_2Cl_2, 5 min, 67 %; (ii) 254 nm, CH_2Cl_2, 20 min, 50 %; (iii) Δ, 100 °C, $C_2H_2Cl_4$, 24 h, ~100 %, or catalytic ethylenediamine, 50 °C, 48 h, 65 %; or catalytic Br_2, 400–670 nm, CH_2Cl_2, −78 °C, 10 min. ~100 %.

In **56** (Fig. 7.48), this is achieved by using two fumaramide stations with different macrocycle binding affinity, one of which (station A, green) is located next to a benzophenone unit. This enables selective, photosensitized isomerization of station A by irradiation at 350 nm before direct photoisomerization of the other fumaramide station (station B, red) at 254 nm. Station B, being a methylated fumaramide residue, has lower affinity for the macrocycle than station A. The third station (station C, orange) – a succinic amide ester – is not photoactive and is intermediate in macrocycle-binding affinity between the two fumaramide stations and their maleamide counterparts. A fourth station, an isolated amide group (shown as D in *E,E*-**57**) which can make fewer intercomponent hydrogen bonding contacts than A, B, or C, is also present but only plays a significant role in the behavior of the [3]catenane.

Consequently, in the initial state (state I, Fig. 7.47), the small macrocycle resides on the green, non-methylated fumaramide station. Isomerization of this station (irradiation at 350 nm, green → blue) destabilizes the system and the macrocycle finds its new energy minimum on the red station (state II). Subsequent photoisomerization of this station (irradiation at 254 nm, red → pink) means the macrocycle must now move on to the succinic amide ester unit (orange, state III). Finally, heating the catenane (or treating it with photo-generated bromine radicals or piperidine) results in isomerization of both the *Z* olefins back to their *E* forms (pink → red and blue → green) so the original order of binding affinity is restored and the macrocycle returns to its original position on the green station.

The ^{1}H NMR spectra of each diastereomer show the positional integrity of the small macrocycle to be excellent at all stages of the process, but the rotation is undeniably not unidirectional – over the complete sequence of reactions an equal number of macrocycles go from A, though B and C, and back to A again in each direction.

To bias the direction the macrocycle takes from station to station, temporary barriers are required at each stage to restrict Brownian motion in one particular direction and so bias the path taken by the macrocycle from station to station. Such a situation is intrinsically present in [3]catenane **57** (Fig. 7.48). Irradiation at 350 nm of *E,E*-**57** causes counterclockwise (as drawn) rotation of the light blue macrocycle to the succinic amide ester (orange) station to give *Z,E*-**57**. Isomerization (254 nm) of the remaining fumaramide group causes the other (purple) macrocycle to relocate to the single amide (dark green) station (*Z,Z*-**57**) and, again, this occurs counterclockwise because the clockwise route is blocked by the other (light blue) macrocycle. This "follow-the-leader" process, each macrocycle in turn moving and then blocking a direction of passage for the other macrocycle, is repeated throughout the sequence of transformations shown in Fig. 7.49. After three diastereomer interconversions, *E,E*-**57** is again formed but 360° rotation of each of the small rings has not yet occurred, they have only swapped places. Complete unidirectional rotation of both small rings occurs only after the synthetic sequence (i) to (iii) has been completed twice. Somewhat counterintuitively, the small macrocycles in the [2]- and [3]catenanes move from station to station in an opposite sequence in response to the same series of chemical reactions.

7.6
From Laboratory to Technology: Toward Useful Molecular Machines

7.6.1
Current Challenges

The creation of novel molecular architectures – both classical covalent and mechanically interlocked structures – which in some way restrict the thermally-powered movements of their constituent parts has been central to developing control over motion at the molecular level. These structural constraints have been successfully combined with external switching of molecular structure and/or electronics to create systems with a remarkable level of control over both the relative position of units and the frequency of their motion. Whatever the application, it is clear that the machine and its components must be able to interact with the macroscopic world, either directly or through further interactions with other molecular-scale devices. This problem of "wiring" molecular machines also has implications for the physical construction of molecular devices which might very probably also require the creation of ordered arrays of functional molecules. In the following sections, we shall briefly examine some of these challenges and current progress towards surmounting them.

7.6.2
Reporting Motion: Switches and Memories

In direct analogy to the more established molecular switches which do not employ (significant) submolecular motion, any change in properties accompanied by the submolecular motion in a molecular machine could be applied to some sort of switching or information storage device. The fundamental requirements for such systems are the same as their non-mechanical counterparts and include: (1) a useful and detectable difference between two states; (2) fatigue resistance; (3) stability of each state under the operating conditions; (4) rapid response times; and particularly for memory applications, (5) non-destructive read-out [32a, 33].

7.6.2.1 Solid-state Molecular Electronic Devices

In a series of ground-breaking experiments, molecular shuttles (Sect. 7.5.5) have been employed as the active molecular component in solid-state molecular electronic devices. In the first example of such devices to utilize interlocked molecules, a monolayer of redox-active, degenerate two-station rotaxanes (58^{4+}, Fig. 7.50) was sandwiched between electrodes made from titanium and aluminum oxide [125]. The molecules were aligned during the manufacturing process, due to designed hydrophobic and hydrophilic regions in the thread portions. On application of a negative voltage to the resulting junctions (up to –2 V), a current flows, owing to resonant tunneling through the single-molecule layer, and the variation of current with increasing voltage is strongly non-linear. Application of a small, oxidizing voltage (typically +0.7 V, for several minutes) irreversibly reduces the current response by a factor of 60 to 80. It was shown, however, that the observed response is characteristic of

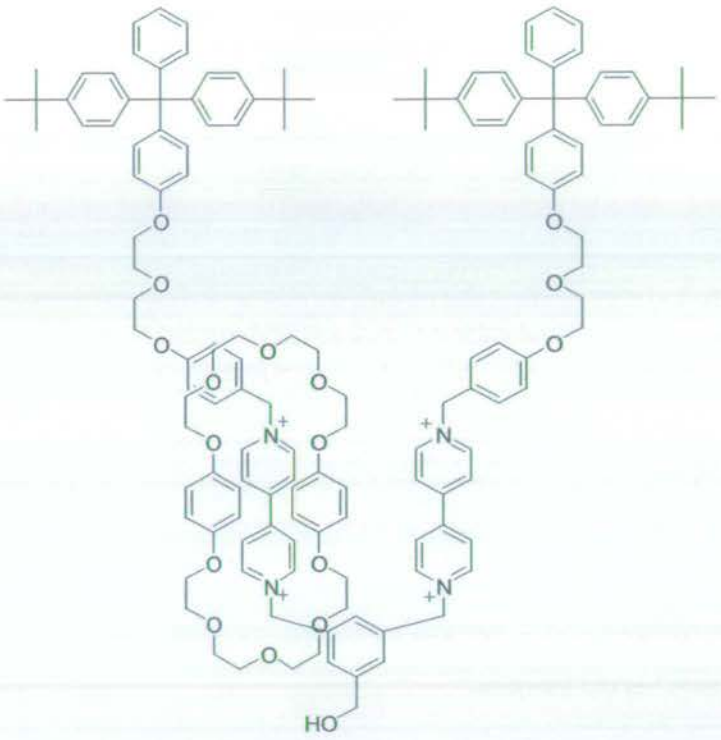

58^{4+}

Figure 7.50 Chemical structure of amphiphilic [2]rotaxane 58^{4+} used in the first interlocked-molecule-based electronic switches. Alignment of the molecules was achieved by exploiting to the hydrophobic and hydrophilic portions, respectively, at the top and bottom of the molecule as drawn.

the thread portion, being essentially the same for monolayers of [2]rotaxane 58^{4+} and its related thread and [3]rotaxane analogs, so that for this species mechanical interlocking and motion do not seem to play a significant role. Although these devices each contained several million rotaxane or thread molecules, the electronic properties of the organic molecules in the solid state correlated well with the known solution-state characteristics, suggesting that scaling down toward single-molecule dimensions would not change the mode of operation. Furthermore, connection of such switches in linear arrays enabled creation of wired-logic gates performing OR and AND functions and with much more pronounced voltage responses compared with resistor-based circuits.

In a second generation of devices, bistable interlocked molecules were employed and reversible switching was achieved. Such a *molecular switchable tunnel junction* (MSTJ) was first demonstrated using a monolayer of bistable [2]catenanes 53^{4+} (Sect. 7.5.7) sandwiched between silicon and titanium/aluminum electrodes [126]. With these devices a moderate (a factor of ~2) but reversible change in resistance is ob-

served on application of oxidizing (opening the switch) and reducing (closing the switch) voltages. The "read" voltage was in the region 0.1 to 0.3 V, and so did not interfere with switch configuration, while the devices withstood many switching cycles. A rational design process then led to devices made from a related [2]pseudorotaxane ($\mathbf{59}^{4+}$, Fig. 7.51), for which the on/off current ratio was much larger ($\sim 10^2$) and the "on" currents larger than for the [2]catenane-based system [127]. The output currents and switching voltages were, however, found to vary widely between both cycles and devices. On further investigation, these problems were attributed to the formation of molecular domains, with the result that device characteristics were no longer determined by single-molecule properties.

This led to further refinement of shuttle structure, producing kinetically stable pseudo[2]rotaxanes $\mathbf{60}^{4+}$ and, ultimately, $\mathbf{61}^{4+}$. MSTJ comprising these rotaxanes had stable switching voltages of approximately –2 and +2 V with reasonable on/off ratios and switch-closed currents [128]. Such favorable characteristics enabled preparation of nanometer-scale devices with properties similar to those of the original micrometer analogs, demonstrating that operation is occurring on the molecular level. Furthermore, these devices were successfully connected in a circuit architecture known as a 2D crossbar. The resulting circuit could be used as a reliable 64-bit random access memory (RAM). The even more demanding task of creating a logic circuit could also be demonstrated by hard-wiring 1D circuits. A true 2D MSTJ-based crossbar logic circuit, however, will require junctions with features yet to be achieved, for example diode character and gain.

Throughout these investigations several control molecules were tested to probe the origin of the switching effect [126–128]. These have demonstrated that some form of bistability, together with the presence of *both* interlocked components, is necessary for the switching properties. It is not clear, however, whether relative motions of the components are responsible. In particular, resistance switching is still observed for devices made from a related single-station [2]rotaxane, albeit with an on/off ratio significantly lower than for the two station analogs $\mathbf{60}^{4+}$ and $\mathbf{61}^{4+}$. It has also been demonstrated that the switching process is thermally activated – at lower temperatures, higher voltages are required to operate the switch. Although this might suggest that some form of submolecular motion is required for operation of the device, it can also be understood in terms of reduced polarizability of the silicon electrode at reduced temperatures [127].

Although these devices have high potential as possible components for truly single-molecule electronic devices, a significant barrier to achieving this goal will be the physical connections used to wire the device. At very small dimensions it is expected that metal wires will have the best conductance characteristics but, unfortunately, devices similar to those described above, but with two metal electrodes, did not have switching properties dependent on the nature of the organic monolayer [129]. Devices which use single-walled carbon nanotubes in place of the silicon electrode have, however, been successfully created and this might provide a valuable alternative in the creation of real-world devices [130].

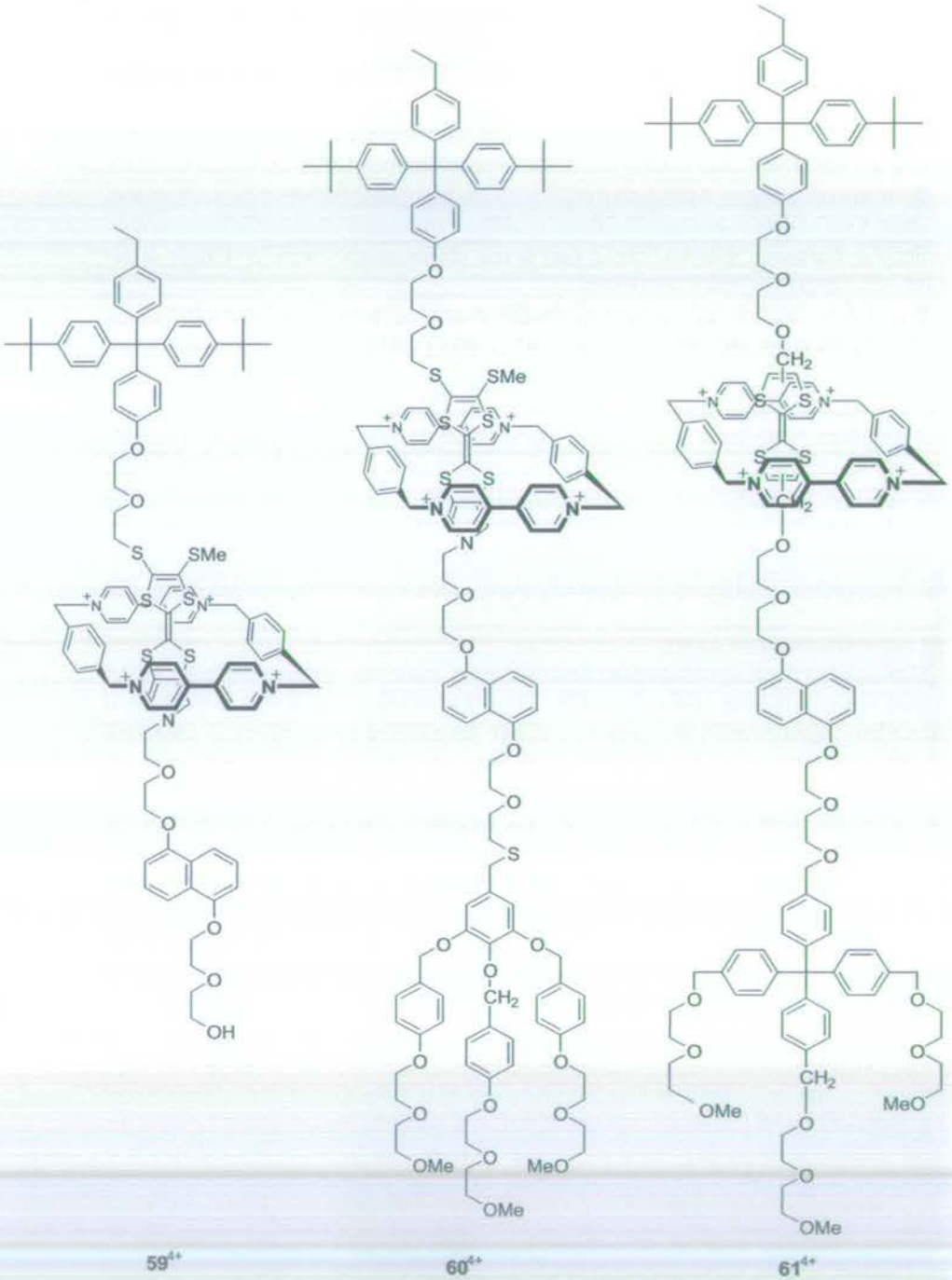

59^{4+} 60^{4+} 61^{4+}

Figure 7.51 Chemical structures of [2]pseudorotaxane 59^{4+} and [2]rotaxanes 60^{4+} and 61^{4+} used as the active components in molecular switched tunnel junctions (MSTJ).

7.6.2.2 A Molecular Muscle

The principles of shuttling in metal-templated rotaxanes have been extended to create a dimeric system in which the submolecular motion results in lengthening and contraction of the molecule in a manner reminiscent of the operation of the actin-myosin complex which is the basis of natural muscle [131]. Each monomer unit for the construction of the rotaxane dimer (Fig. 7.52) consists of a bidentate dpp site embedded in a macrocyclic ring, as in **45** (see Sect. 7.5.5.4), but this ring is now connected to a thread portion which also contains a phenanthroline (a 2,9-dimethylphenanthroline, dmp) ligand and a tridentate terpyridine site. The Cu^{I} ions used to template formation of the dimer coordinate preferentially – once again in a tetrahedral geometry – to the dpp of one unit and the dmp of another component, resulting in the threaded dimer structure $[\mathbf{62}\bullet 2Cu]^{2+}$ (Fig. 7.53). Unfortunately, in this example electrochemical oxidation to the Cu^{II} species did not trigger motion – even this unfavorable geometry for divalent copper is kinetically too stable. Instead, demetallation (excess KCN, room temperature, 3 h) to give the free ligand system **62**, followed by insertion of Zn^{II} ions ($Zn(NO_3)_2$, room temperature, 1 h) gives the contracted form $[\mathbf{62}\bullet 2Zn]^{4+}$, as evidenced by ^1H NMR studies. The molecule can then be returned to its original length simply by treatment with excess $[Cu(CH_3CN)_4]\bullet PF_6$.

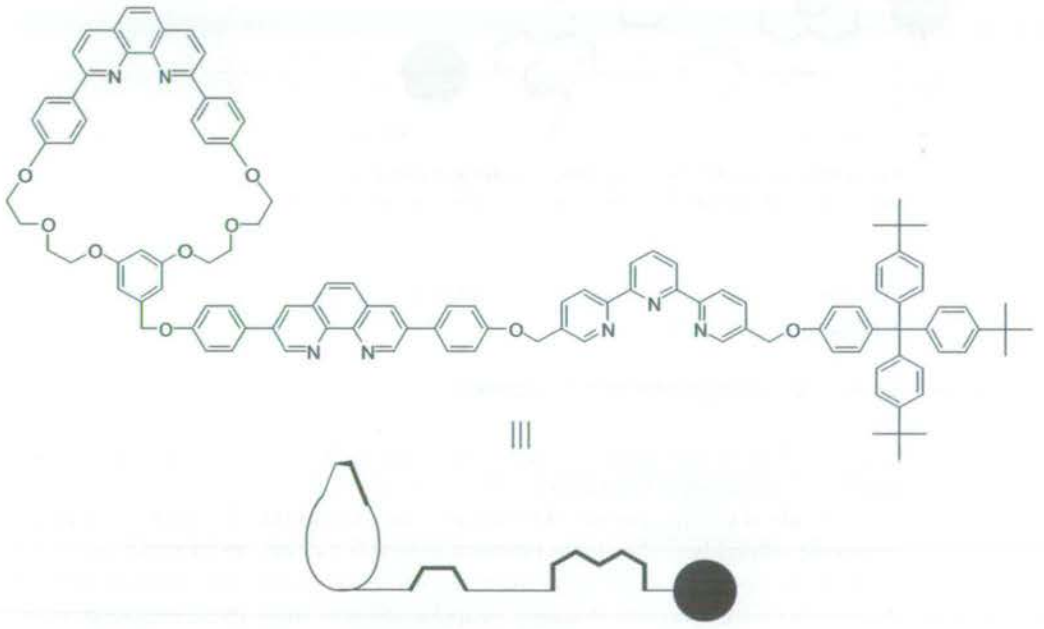

Figure 7.52 Monomer unit for the construction of artificial molecular muscle rotaxane dimer **62**.

In this molecule, therefore, the shuttling of metal templates between two sites on the linear portions results in the filaments gliding over each other – as the distance between the metal centers is increased, the overall length of the molecule decreases.

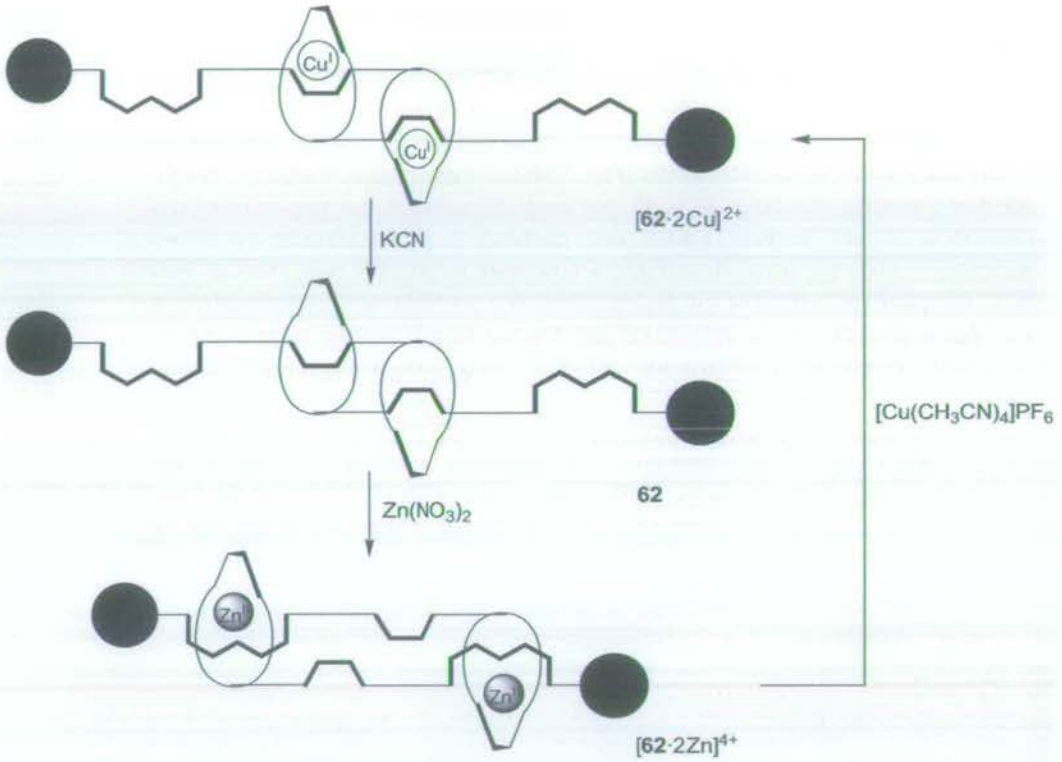

Figure 7.53 Reversible switching between extended ([**62**•2Cu]$^{2+}$) and contracted ([**62**•2Zn]$^{4+}$) forms in a chemically-switched artificial molecular muscle.

During this process, the length of the molecule changes from approximately 85 Å to 65 Å, a reduction of 24 %.

7.6.2.3 Shuttle-based Mechanical Switches

The coupling of submolecular motion in a shuttle with a change in molecular properties can lead to mechanical switches operating at the molecular level and which could perform a range of functions.

In a study of chiral dipeptide [2]rotaxanes it was found that the presence of an intrinsically achiral benzylic amide macrocycle near the chiral center could induce an asymmetric response in the aromatic ring absorption bands. This induced circular dichroism (ICD) effect was strongest in apolar solvents when intercomponent interactions are maximized and it was shown that the chirality is transmitted from the amino acid asymmetric center on the thread, via the achiral macrocycle to the aromatic rings of the achiral C-terminal stopper on the thread [132]. These observations led to the design of chiroptical switch *E*/*Z*-**63** which utilizes the same fumaramide–maleamide function as [2]rotaxane shuttles **46** and **47** in Sect. 7.5.5, above (Fig. 7.54) [133]. Unlike chiroptical switches in which the presence of or handedness

of chirality is intrinsically altered [32], *E*/*Z*-**63** remains chiral and non-racemic, with the same handedness throughout; it is the *expression* of chirality that is altered. In the *E*-**63** form, the macrocycle is held over the excellent fumaramide template and thus far from the chiral center in the peptidic station. Correspondingly, the CD response is flat, as observed for the free thread. In the *Z*-**63** isomer, in which the macrocycle resides on the peptide station, close to the L-Leu residue, a strong ($-13k$ deg cm^2 dmol^{-1}), negative CD response is observed. Preparatively, the $E \rightarrow Z$ isomerization is most efficiently carried out by irradiation at 312 nm in the presence of a benzophenone sensitizer (photostationary state 70:30 *Z*:*E*), while the $Z \rightarrow E$ transformation can be achieved almost quantitatively by irradiation at 400–670 nm in the presence of catalytic Br_2. In the context of any switching application, however, addition of any external reagent is obviously undesirable and a more modest difference between photostationary states can be achieved by irradiation at 254 nm (photostationary state 56:44 *Z*:*E*) and 312 nm (photostationary state 49:51 *Z*:*E*). Even under these conditions a large net change (>1500 deg cm^2 dmol^{-1}) in the elliptical polarization response is observed and this is reproducible over several cycles.

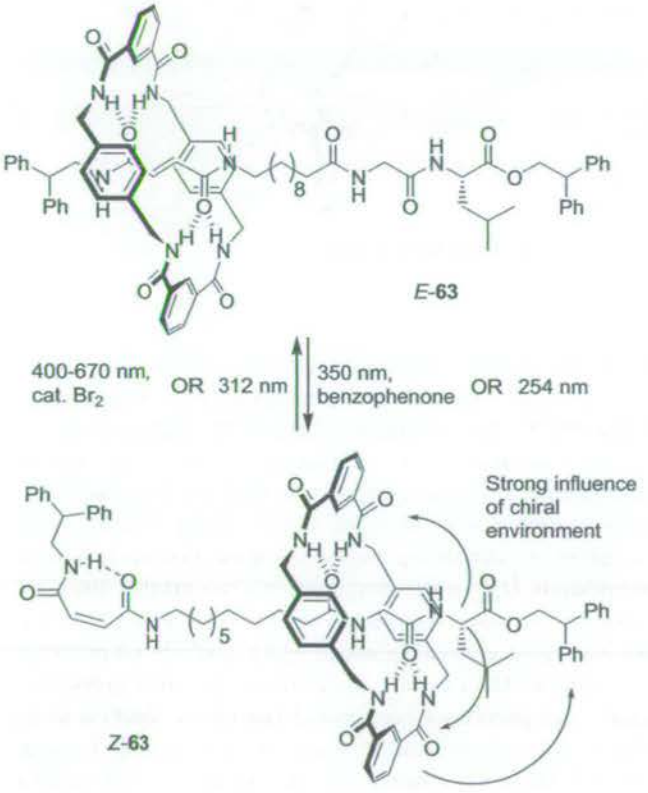

Figure 7.54 Chiroptical switching in [2]rotaxane-based molecular shuttle *E*/*Z*-**63**.

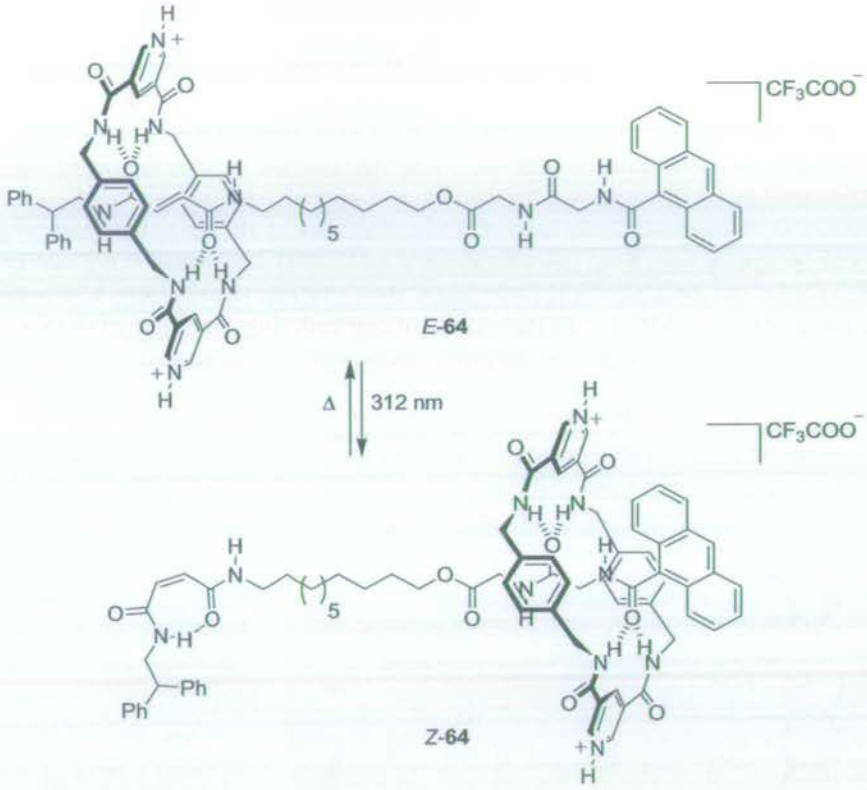

Figure 7.55 A fluorescent molecular switch based on [2]rotaxane molecular shuttle *E*/*Z*-**64**.

Encouraged by these results, bistable molecular shuttle *E*/*Z*-**64** was created (Fig. 7.55) [134]. This system also relies on the photoswitchable fumaramide/maleamide station, but attached to the intermediate, dipeptide station is an anthracene fluorophore, and the macrocycle now contains pyridinium units – known to quench anthracene fluorescence by electron transfer. In both the free thread and *E*-**64**, strong fluorescence (λ_{exc} = 365 nm) is observed, and shuttling of the macrocycle on to the glycylglycine station in *Z*-**64** almost completely quenches this emission. At the maximum of *E*-**64** emission (λ_{max} = 417 nm) there is a remarkable 200:1 difference in intensity between the two states – strikingly visible to the naked eye.

These two examples demonstrate a generic approach which could be taken to create mechanical molecular switches for a variety of distance-dependent properties. The fumaramide/maleamide unit provides a means of changing the position of the macrocycle using a number of olefin isomerization procedures (the strategy is equally relevant for any other bistable stimuli-responsive shuttle system for which there is good macrocycle positional integrity between the two stations in both states). The glycylglycine is a non-reactive station of intermediate affinity and the alkyl spacer can be

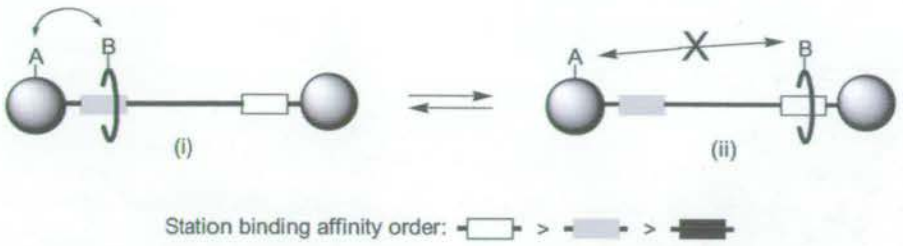

Figure 7.56 Exploiting a well-defined, large amplitude positional change to trigger property changes. (i) A and B interact to produce a physical response (fluorescence quenching, specific dipole, or magnetic moment, NLO properties, color, creation/concealment of a binding site or reactive/catalytic group, hydrophobic/hydrophilic region, etc.); (ii) moving A and B far apart mechanically switches off the interaction and the corresponding property effect.

varied in length to suit the distance dependency of the property in question. Suitable functionalization of the macrocycle and one end of the thread should therefore lead to molecular switches that could perform several functions (Fig. 7.56).

A similar strategy has been used to achieve fluorescence switching in [2]rotaxane *E*/*Z*-**65** (Fig. 7.57) [135]. In *E*-**65**•2H, the α-cyclodextrin ring sits preferentially over the *trans*-stilbene unit and this co-conformation is further stabilized by strong hydrogen-bonding interactions between hydroxyl groups on the 3-rim of the cyclodextrin and the isophthaloyl stopper group. As for the previous α-CD based systems (Fig. 7.29, Sect. 7.5.5.1), photoisomerization of the stilbene unit can occur only when thermal motion has moved the ring away from the binding site. The strength of the combined hydrophobic and hydrogen-bonding interactions (even in water) for *E*-**65**•2H, however, means that the shuttle is conformationally *locked* – irradiation at 355 nm, which should isomerize the stilbene moiety, results in no change to the system. Formation of the disodium salt of the isophthaloyl group (giving *E*-**65**•2Na) breaks the hydrogen-bonding network and although NMR studies show that the cyclodextrin continues to sit over the stilbene station, enough thermal motion is now present to enable photoisomerization, to give *Z*-**65**•2Na (photostationary state 63:37 *Z*:*E*). In this state, the cyclodextrin ring is forced to reside over the biphenyl group. The shuttling motion is accompanied by an increase of approximately 46 % in the fluorescence intensity of the 4-aminonaphthalimide stopper (λ_{max} = 530 nm). This change is attributed to restriction of vibrational and rotational movement of the methylene and biaryl linkages thus disfavoring non-radiative relaxation processes. The shuttling and fluorescence changes are completely reversible on re-isomerization to *E*-**65**•2Na at 280 nm.

The same researchers have elaborated this concept in [2]rotaxane *E*/*Z*-**66** (Fig. 7.58) which contains two fluorophores; the intensity of each of these can be selectively enhanced depending on the position of the ring [136]. In this instance the configurational switch is an azobenzene group but the operation is essentially the same as above. In *E*-**66**, the α-CD sits over the azobenzene moiety, thus enhancing the fluorescence of the adjacent 4-aminonaphthalimide stopper (λ_{max} = 520 nm). Photoiso-

Figure 7.57 Photoswitched shuttling in [2]rotaxane *E*/*Z*-**65**•2Na which results in fluorescence enhancement of the 4-aminonaphthalimide group. The photoisomerization process is prevented when the free carboxylic acids of the isophthaloyl stopper are present (*E*-**65**•2H).

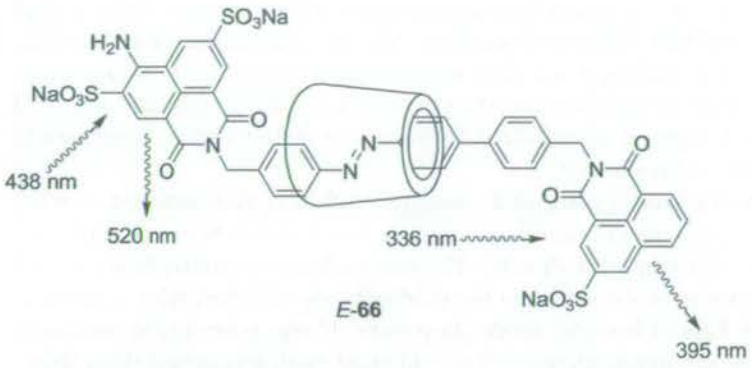

Figure 7.58 [2]Rotaxane *E*-**66** in which the F_{520} band is selectively enhanced. Photoisomerization of the azobenzene unit (360 nm) results in shuttling of the α-cyclodextrin ring to the biaryl site and concomitant reduction of the F_{520} emission together with enhancement of the F_{395} band.

merization to *Z*-**66** (irradiation at 360 nm; photostationary state 59:41 *Z*:*E*) results in shuttling of the ring to the biaryl station, simultaneously reducing the intensity of the F_{520} emission while enhancing the fluorescence of the right-hand fluorophore (λ_{max} = 395 nm). The original state (100 % *E*-**66**) can be achieved on irradiation at 430 nm and the process can be repeated over several cycles.

7.6.3 The Interface with Real-world Technology

It has already been mentioned that the implementation of a technology based on molecular machines faces several problems with regard to the actual engineering of devices and their interconnection with each other and with the macroscopic world. Although light-operated systems such as those discussed in Sect. 7.6.2.3 might have potential in some respects, the generally non-directional nature of emission processes would make specific communication between nanoscale devices difficult, and the focus resolution of laser light that might be used to address such systems is limited by the wavelength. On the other hand, systems designed to perform mechanical tasks, for example rotaxane dimer **62** described in Sect. 7.6.2.2, might require anchoring to a massive object, and correlation of the efforts of many molecular machines will probably be required to produce a desired macroscopic effect. The devices and circuits outlined in Sect. 7.6.2.1 highlight the utility of electrical signals for selective addressing of small-scale devices which seem to operate at the single-molecule level, yet the device dimensions are limited by the nature of the electrodes required.

It is recognized that transfer of molecular machine technology to solid substrates might be a key step in the development of many potential applications. There are already several examples of switchable molecular recognition events (including threading and de-threading of pseudorotaxanes) which occur at surfaces functionalized with either host or guest components [137]. In one example the reversible recognition

event is also observed in a nanoporous silicate matrix [137f]. The state of the art has been demonstrated by Stoddart and coworkers who have harnessed the photochemically triggered de-threading of a surface-mounted pseudorotaxane to release molecules trapped in nanoscopic pores on the same surface [138]. In addition, switched conformational motions of immobilized, fully-covalent molecules have been used to alter the properties of surfaces [139].

The problem of achieving controlled movement within surface-mounted or solid-state interlocked molecules is more demanding, however, with both components constrained by the solid support at all times. The first evidence for externally stimulated submolecular motion of a catenane in the solid state was observed when a vacuum-evaporated thin film of benzylic amide [2]catenane **27** was subjected to oscillating electric fields, producing an unexpected second-order nonlinear optical effect [140].

Electrochemically-induced shuttling has been observed in self-assembled monolayers (SAM) on gold wire of an alkanethiol derivative of [2]rotaxane $\mathbf{61}^{4+}$ [141]. Shuttling of the macrocycle on oxidation and subsequent reduction of the TTF unit was observed by voltammetry measurements in an analogous fashion to solution-state studies. Although this motion is occurring at the solid–liquid interface, the characteristics of the shuttling process, which involves a relatively long-lived metastable state, provides some backing for the occurrence of similar submolecular motion in the solid-state devices discussed in Sect. 7.6.2.1.

A different redox-active molecular shuttle could be orientated perpendicular to the surface of a titanium dioxide nanoparticle, by attachment of a tripodal phosphonate unit at one end of the thread [142]. The use of nanoparticles enabled characterization of the dynamic processes in the surface-mounted species by both ^{1}H NMR and cyclic voltammetry. Redox-triggered shuttling of the macrocycle was indeed observed, although in this example, positional integrity was found to be poor.

A potentially useful way of detecting and subsequently communicating the state of any type of molecular switch is to translate its state into an electrical signal [143]. This has been accomplished for a molecular shuttle attached to the surface of a gold electrode [144]. In this case, photochemically induced shuttling of a cyclodextrin ring closer to the electrode surface was detectable as an increase in the rate of oxidation of a redox-active ferrocene unit attached to the mobile ring.

Probe microscopy techniques such as scanning–tunnelling microscopy (STM) and AFM have been instrumental in the development of many fields over the last two decades, in particular where atomic-level movements are to be effected or observed [145], yet their use in the study and operation of synthetic molecular machines is still relatively underdeveloped. Recently, however, this technology has been used to move components in interlocked molecules. In one report, an STM tip was used to reversibly move one or two adjacent cyclodextrin rings along the poly(ethylene glycol)-derived thread in a polyrotaxane [146]. It has also been demonstrated that an AFM tip can be used to create a regular array of deformations on thin films of benzylic amide-based rotaxanes [147]. This effect is unique to films made from interlocked molecules (compared with their non-interlocked components) and is a result of coupled nucleation recrystallization being favored by the ease of intercomponent mobility (even in the solid state) for these molecules. The characteristics of these fea-

tures are readily variable with the nature of the film and show potential for application in information-storage technology.

The high resolution achievable with atomically sharp microscope probes, together with the range of possible functions (e.g. mechanical, electrical, or thermal perturbations and observations are all possible) suggests that such techniques may prove key in the future development of useful devices based on synthetic molecular machines.

7.7 Summary and Outlook

The last few years have witnessed dramatic advances in the ability to control submolecular motion in synthetic systems. Although these new-found skills continue to be refined, attention is now turning to the application of synthetic structures to perform useful tasks and create true molecular machines. Inspiration and assistance is continually offered as a result of the accumulating understanding of biological motor proteins and information processing, and the fantastic achievements of modern-day microelectronics and mechanical engineering, yet we must be sure to remember that the devices created by the synthetic chemist will have fundamentally different characteristics, strengths, and weaknesses to their counterparts from other regimes. Consequently, it is difficult to predict what the eventual applications of molecular machines will be. In the short term, changing surface properties, switching, and memory devices look particularly attractive. A greater challenge, however, would be to harness the motion of submolecular components to perform useful work at the molecular-level – that is, to transduce the energy input from an external stimulus into directed motion of some cargo or motion against an energy gradient. In each of Sects. 7.2, 7.3, and 7.5.7 we have seen the first examples of unidirectional rotors based on rotation around single, double, and mechanical bonds respectively. Although the physical principles underlying unidirectional motion at the molecular-level were perhaps not fully appreciated by chemists before the creation of this first wave of systems, these molecules demonstrate the basic principles required to perform work at the molecular level. The development of molecular-level systems which perform functions by responding to stimuli as a result of Boolean logic operations [148] has clear relevance to the future development of compartmentalized molecular machines which are more sophisticated than this current generation of mechanical switches and simple motors. Although current efforts in molecular logic have concentrated largely on photonic supramolecular systems and have not been applied to systems which rely on mechanical motion, their successful operation suggests a way in which existing but relatively simple molecular machine components might be connected to produce useful devices at the next level of complexity.

As with many areas of chemistry, mimicry of biological systems continues to be an important driving-force in this field. There is a synergistic relationship between the two subject areas, with biology providing the inspiration and operating principles while the comparatively simplistic synthetic systems provide fully characterizable

models for the more complicated natural processes. An elegant example is the toroidal, processive epoxidation catalyst described by Rowan, Nolte, and coworkers [149]. Although, one day, such systems might provide catalysts for post-polymerization modification of polymers, the mechanically linked nature of the catalyst–substrate complex should also provide important insights into the operation of the processive enzymes which are so central to fundamental processes in the cell.

Traditional covalent and noncovalent synthetic chemistry techniques are not the only route to molecular-level devices and machines. The unusual mechanical and electrical properties of nanotubes and other fullerenes constructed from boron nitride or carbon has enabled the downwards extension of current-day microelectromechanical systems (MEMS; the current state of the art, and perhaps limit, of silicon-based devices) toward true nanometer-scale electromechanical systems (NEMS) [150]. This is an example of "hard nanotechnology", but another area of intense interest involves so-called "soft" nanomaterials. This area encompasses functional materials created by self-assembly processes giving organized arrays of molecules on "hard" templates. Smaller length-scales and milder conditions are achievable compared with silicon-based lithography techniques [151]. Such processes might prove useful in the organization of synthetic molecular machines to create useful devices. Also included in this area however are several materials, for example polymers and gels, in which macroscopic mechanical motion can be generated in response to an external stimulus. Traditionally, these effects have been non-specific processes such as the uptake or expulsion of counterions during redox processes [152], yet there has been a recent move toward the creation of polymeric materials which stretch and contract as a result of specific molecular interactions [153] or nuclear arrangements [154].

Yet another field of interest turns to biology for the components to construct "artificial" molecular devices. Although some impressive successes have been achieved by harnessing biological motors to power motion outside the cell [155], others have borrowed one of Nature's most useful construction materials – nucleic acids – to build novel constructs capable of molecular-level motion [156].

Although the field is in its infancy, it is clear that the concept of harnessing molecular-level motion to perform useful tasks is exciting researchers in many disciplines. Creating entirely synthetic molecular machines should enable us to exploit the full potential of synthesis to create systems with currently unrealized characteristics – to use controlled mechanical motion to drive chemical reactions, make artificial machines which can "sort" ions into different types, or drive themselves and their cargo energetically uphill along tracks. Equally important will be the experimentally-derived insight into motion at the molecular level which will tell us how biological systems work. For synthetic molecular machines, the best is yet to come.

References

1 For an introduction to Brownian motors, see: R. D. Astumian, P. Hänggi, *Phys. Today* **2002**, *55 (11)*, 33–39.

2 For reviews on Brownian ratchet mechanisms, see: (a) F. Jülicher, A. Ajdari, J. Prost, *Rev. Mod. Phys.* **1997**, *69*, 1269–1281; (b) P. Reimann, *Phys. Rep.* **2002**, *361*, 57–265; (c) *Appl. Phys. A* **2002**, *75*, 167–352 (special issue on Ratchets and Brownian motors: basics, experiments and applications); (d) B. J. Gabrys, K. Pesz, S. J. Bartkiewicz, *Physica A* **2004**, *336*, 112–122.

3 For selected examples, see ref. [2c] and: (a) R. D. Astumian, M. Bier, *Eur. Biophys. J.* **1996**, *70*, 637–653; (b) R. D. Astumian, *Science* **1997**, *276*, 917–922; (c) R. D. Astumian, I. Derényi, *Eur. Biophys. J. Biophys. Lett.* **1998**, *27*, 474–489; (d) I. Derényi, T. Vicsek, *Physica A* **1998**, *249*, 397–406; (e) R. F. Fox, *Phys. Rev. E* **1998**, *57*, 2177–2203; (f) F. Jülicher, *arXiv:physics* **1999**, /9908054; (g) R. D. Astumian, I. Derényi, *Biophys. J.* **1999**, *77*, 993–1002; (h) R. D. Astumian, *Philos. Trans. R. Soc. Lond. Ser. B* **2000**, *355*, 511–522; (i) M. Kurzynski, P. Chełminiak, *Physica A* **2004**, *336*, 123–132.

4 *Molecular Motors* (Ed.: M. Schliwa), Wiley-VCH, Weinheim, **2003**.

5 H. Hess, G. D. Bachand, V. Vogel, *Chem. Eur. J.* **2004**, *10*, 2110–2116.

6 (a) V. Balzani, A. Credi, F. M. Raymo, J. F. Stoddart, *Angew. Chem. Int. Ed.* **2000**, *39*, 3349–3391; (b) J. F. Stoddart, *Acc. Chem. Res.* **2001**, *34*, 410–411; (c) R. Ballardini, V. Balzani, A. Credi, M. T. Gandolfi, M. Venturi, *Acc. Chem. Res.* **2001**, *34*, 445–455; (d) V. Balzani, A. Credi, M. Venturi, *Chem. Eur. J.* **2002**, *8*, 5524–5532; (e) V. Balzani, A. Credi, M. Venturi, *Molecular Devices and Machines. A Journey into the Nanoworld*, Wiley–VCH, Weinheim, **2003**; (f) J. D. Crowley, A. J. Goshe, I. M. Steele, B. Bosnich, *Chem. Eur. J.* **2004**, *10*, 1944–1955; (g) C. J. Easton, S. F. Lincoln, L. Barr, H. Onagi, *Chem. Eur. J.* **2004**, *10*, 3120–3128.

7 E. M. Purcell, *Am. J. Phys.* **1977**, *45*, 3–11.

8 E. L. Eliel, S. H. Wilen, *Stereochemistry of Organic Compounds*, Wiley–Interscience, New York, **1994**.

9 J. D. Kemp, K. S. Pitzer, *J. Chem. Phys.* **1936**, *4*, 749.

10 M. Öki, *Angew. Chem. Int. Ed. Engl.* **1976**, *15*, 87–93.

11 (a) H. Iwamura, K. Mislow, *Acc. Chem. Res.* **1988**, *21*, 175–182; (b) K. Mislow, *Chemtracts: Org. Chem.* **1989**, *2*, 151–174; (c) J. Vacek, J. Michl, *New J. Chem.* **1997**, *21*, 1259–1268.

12 T. C. Bedard, J. S. Moore, *J. Am. Chem. Soc.* **1995**, *117*, 10662–10671.

13 (a) J. Clayden, J. H. Pink, *Angew. Chem. Int. Ed.* **1998**, *37*, 1937–1939; (b) A. Ahmed, R. A. Bragg, J. Clayden, L. W. Lai, C. McCarthy, J. H. Pink, N. Westlund, S. A. Yasin, *Tetrahedron* **1998**, *54*, 13277–13294; (c) R. A. Bragg, J. Clayden, *Org. Lett.* **2000**, *2*, 3351–3354; (d) R. A. Bragg, J. Clayden, G. A. Morris, J. H. Pink, *Chem. Eur. J.* **2002**, *8*, 1279–1289.

14 (a) T. R. Kelly, *Acc. Chem. Res.* **2001**, *34*, 514–522; (b) J. P. Sestelo, T. R. Kelly, *Appl. Phys. A* **2002**, *75*, 337–343.

15 T. R. Kelly, M. C. Bowyer, K. V. Bhaskar, D. Bebbington, A. Garcia, F. R. Lang, M. H. Kim, M. P. Jette, *J. Am. Chem. Soc.* **1994**, *116*, 3657–3658.

16 (a) T. R. Kelly, I. Tellitu, J. P. Sestelo, *Angew. Chem. Int. Ed. Engl.* **1997**, *36*, 1866–1868; (b) T. R. Kelly, J. P. Sestelo, I. Tellitu, *J. Org. Chem.* **1998**, *63*, 3655–3665.

17 (a) A. P. Davis, *Angew. Chem. Int. Ed.* **1998**, *37*, 909–910; (b) G. Musser, *Sci. Am.* **1999**, *280* (2), 24.

18 P. W. Atkins, *Physical Chemistry*, 6th ed., Oxford University Press, Oxford, **1998**.

19 (a) M. von Smoluchowski, *Physik. Z.* **1912**, *13*, 1069–1080; (b) R. P. Feynman, R. B. Leighton, M. Sands, *The Feynman Lectures on Physics, Vol. 1 (Chap. 46)*, Addison–Wesley, Reading, MA, **1963**.

20 (a) For a modern critique of Feynman's analysis, see: J. M. R. Parrondo, P. Espanol, *Am. J. Phys.* **1996**, *64*, 1125–1130; (b) M. O. Magnasco, G. Stolovitzky, *J. Stat. Phys.* **1998**, *93*, 615–632.

21 (a) T. R. Kelly, H. De Silva, R. A. Silva, *Nature* **1999**, *401*, 150–152; (b) T. R. Kelly, R. A. Silva, H. De Silva, S. Jasmin, Y. J. Zhao, *J. Am. Chem. Soc.* **2000**, *122*, 6935–6949.

22 There are differences between the technical definition of the terms "configuration" and "conformation" and their common usage. While formally configurational differences involve differences in bond angles and conformational differences suggest changes in torsion angles, here "configuration" is applied to *cis–trans* isomerism around double bonds as convention suggests. The same categorization can be extended to include isomerism around the C–N bond of amides, although this is often considered as a conformational change around a formal single bond as in **4**. For further discussion, see ref. [8].
The arrangement in space of the components of interlocked molecules and supramolecular complexes requires definition of another stereochemical term; "coconformation". This refers to the relative positions of the noncovalently linked components with respect to each other, see: M. C. T. Fyfe, P. T. Glink, S. Menzer, J. F. Stoddart, A. J. P. White, D. J. Williams, *Angew. Chem. Int. Ed. Engl.* **1997**, *36*, 2068–2070.

23 For a comprehensive review, see: C. Dugave, L. Demange, *Chem. Rev.* **2003**, *103*, 2475–2532.

24 (a) T. Yoshizawa in *CRC Handbook of Organic Photochemistry and Photobiology* (Eds.: W. M. Horspool, P.-S. Song), CRC Press, Boca Raton, **1995**, pp. 1493–1499; (b) R. Needleman, *ibid.*, pp. 1508–1515; (c) T. G. Ebrey, J. Liang, *ibid.* pp. 1500–1507; (d) B. Borhan, M. L. Souto, H. Imai, Y. Shichida, K. Nakanishi, *Science* **2000**, *288*, 2209–2212.

25 (a) B. Perman, V. Srajer, Z. Ren, T. Y. Teng, C. Pradervand, T. Ursby, D. Bourgeois, F. Schotte, M. Wulff, R. Kort, K. Hellingwerf, K. Moffat, *Science* **1998**, *279*, 1946–1950; (b) I. Antes, W. Thiel, W. F. van Gunsteren, *Eur. Biophys. J.* **2002**, *31*, 504–520; (c) K. J. Hellingwerf, J. Hendriks, T. Gensch, *J. Phys. Chem. A* **2003**, *107*, 1082–1094.

26 (a) G. Fischer, *Angew. Chem. Int. Ed. Engl.* **1994**, *33*, 1415–1436; (b) G. Fischer, *Chem. Soc. Rev.* **2000**, *29*, 119–127; (c) J. Balbach, F. X. Schmid in *Mechanisms of Protein Folding: Frontiers in Molecular Biology, Vol. 32*, 2nd ed. (Ed.: R. H. Pain), Oxford University Press, Oxford, **2000**, pp. 212–249.

27 (a) D. H. Waldeck, *Chem. Rev.* **1991**, *91*, 415–436; (b) H. Meier, *Angew. Chem. Int. Ed. Engl.* **1992**, *31*, 1399–1420; (c) J. Saltiel, D. F. Sears Jr., D.-H. Ko, K.-M. Park in *CRC Handbook of Organic Photochemistry and Photobiology* (Eds.: W. M. Horspool, P.-S. Song), CRC Press, Boca Raton, **1995**, pp. 3–15.

28 A photochromic process is one in which a light-induced interconversion between two species results in a change in its absorption spectrum.

29 H. Suginome in *CRC Handbook of Organic Photochemistry and Photobiology* (Eds.: W. M. Horspool, P.-S. Song), CRC Press, Boca Raton, **1995**, pp. 824–840.

30 G. Berkovic, V. Krongauz, V. Weiss, *Chem. Rev.* **2000**, *100*, 1741–1753.

31 (a) H. G. Heller in *CRC Handbook of Organic Photochemistry and Photobiology* (Eds.: W. M. Horspool, P.-S. Song), CRC Press, Boca Raton, **1995**, pp. 173–183; (b) Y. Yokoyama, *Chem. Rev.* **2000**, *100*, 1717–1739; (c) Y. Yokoyama in *Molecular Switches* (Ed.: B. L. Feringa), Wiley–VCH, Weinheim, **2001**, pp. 107–121.

32 (a) B. L. Feringa, N. P. M. Huck, A. M. Schoevaars, *Adv. Mater.* **1996**, *8*, 681–684; (b) B. L. Feringa, R. A. van Delden, N. Koumura, E. M. Geertsema, *Chem. Rev.* **2000**, *100*, 1789–1816; (c) B. L. Feringa, R. A. van Delden, M. K. J. ter Wiel in *Molecular Switches* (Ed.: B. L. Feringa), Wiley–VCH, Weinheim, **2001**, pp. 123–163.

33 For reviews, see: (a) B. L. Feringa, W. F. Jager, B. Delange, *Tetrahedron* **1993**, *49*, 8267–8310; (b) *Chem. Rev.* **2000**, *100*, 1683–1890 (special issue on Photochromism: Memories and Switches); (c) *Molecular Switches* (Ed.: B. L. Feringa), Wiley–VCH, Weinheim, **2001**.

34 M. Irie, *Chem. Rev.* **2000**, *100*, 1685–1716.

35 (a) I. Willner, *Acc. Chem. Res.* **1997**, *30*, 347–356; (b) I. Willner, B. Willner in *Molecular Switches* (Ed.: B. L. Feringa), Wiley–VCH, Weinheim, **2001**, pp. 165–218.

36 (a) K. Ichimura, *Chem. Rev.* **2000**, *100*, 1847–1873; (b) N. Tamaoki, *Adv. Mater.* **2001**, *13*, 1135–1147; (c) T. Ikeda, A. Kanazawa in *Molecular Switches* (Ed.: B. L. Feringa), Wiley–VCH, Weinheim, **2001**, pp. 363–397.

37 See, for example: (a) G. S. Kumar, D. C. Neckers, *Chem. Rev.* **1989**, *89*, 1915–1925; (b) J. A. Delaire, K. Nakatani, *Chem. Rev.* **2000**, *100*, 1817–1845; (c) F. Ciardelli, O. Pieroni in *Molecular Switches* (Ed.: B. L. Feringa), Wiley-VCH, Weinheim, **2001**, pp. 399–441.

38 T. Hugel, N. B. Holland, A. Cattani, L. Moroder, M. Seitz, H. E. Gaub, *Science* **2002**, *296*, 1103–1106.

39 A. M. Schoevaars, W. Kruizinga, R. W. J. Zijlstra, N. Veldman, A. L. Spek, B. L. Feringa, *J. Org. Chem.* **1997**, *62*, 4943–4948.

40 (a) B. L. Feringa, N. Koumura, R. A. van Delden, M. K. J. ter Wiel, *Appl. Phys. A* **2002**, *75*, 301–308; (b) B. L. Feringa, *Acc. Chem. Res.* **2001**, *34*, 504–513.

41 N. Koumura, R. W. J. Zijlstra, R. A. van Delden, N. Harada, B. L. Feringa, *Nature* **1999**, *401*, 152–155.

42 N. Koumura, E. M. Geertsema, M. B. van Gelder, A. Meetsma, B. L. Feringa, *J. Am. Chem. Soc.* **2002**, *124*, 5037–5051.

43 E. M. Geertsema, N. Koumura, M. K. J. ter Wiel, A. Meetsma, B. L. Feringa, *Chem. Commun.* **2002**, 2962–2963.

44 M. K. J. ter Wiel, R. A. van Delden, A. Meetsma, B. L. Feringa, *J. Am. Chem. Soc.* **2003**, *125*, 15076–15086.

45 (a) J.-M. Lehn, *Supramolecular Chemistry: Concepts and Perspectives*, VCH, Weinheim, **1995**; (b) *Comprehensive Supramolecular Chemistry* (Eds.: J.-M. Lehn, J. L. Atwood, J. E. D. Davies, D. D. MacNicol, F. Vögtle), Pergamon, Oxford, **1996**.

46 Myosin requires an actin track to move along: (a) S. M. Block, *Cell* **1996**, *87*, 151–157; while kinesin processes along the pathway provided by microtubule filaments: (b) S. M. Block, *Cell* **1998**, *93*, 5–8; even ion pumps operate through precisely defined structural channels: (c) J. C. Skou, *Angew. Chem. Int. Ed.* **1998**, *37*, 2321–2328.

47 S. Shinkai, M. Ishihara, K. Ueda, O. Manabe, *J. Chem. Soc.–Perkin Trans. 2* **1985**, 511–518.

48 V. Amendola, L. Fabbrizzi, C. Mangano, P. Pallavicini, *Acc. Chem. Res.* **2001**, *34*, 488–493.

49 L. Fabbrizzi, F. Gatti, P. Pallavicini, E. Zambarbieri, *Chem. Eur. J.* **1999**, *5*, 682–690.

50 A. Ikeda, T. Tsudera, S. Shinkai, *J. Org. Chem.* **1997**, *62*, 3568–3574.

51 L. Zelikovich, J. Libman, A. Shanzer, *Nature* **1995**, *374*, 790–792.

52 For representative examples of pseudorotaxane architectures based on dialkylammonium linear components and polyether macrocycles, see: (a) P. R. Ashton, P. J. Campbell, E. J. T. Chrystal, P. T. Glink, S. Menzer, D. Philp, N. Spencer, J. F. Stoddart, P. A. Tasker, D. J. Williams, *Angew. Chem. Int. Ed. Engl.* **1995**, *34*, 1865–1869; (b) P. R. Ashton, E. J. T. Chrystal, P. T. Glink, S. Menzer, C. Schiavo, J. F. Stoddart, P. A. Tasker, D. J. Williams, *Angew. Chem. Int. Ed. Engl.* **1995**, *34*, 1869–1871; (c) P. R. Ashton, E. J. T. Chrystal, P. T. Glink, S. Menzer, C. Schiavo, N. Spencer, J. F. Stoddart, P. A. Tasker, A. J. P. White, D. J. Williams, *Chem. Eur. J.* **1996**, *2*, 709–728; (d) P. R. Ashton, M. C. T. Fyfe, P. T. Glink, S. Menzer, J. F. Stoddart, A. J. P. White, D. J. Williams, *J. Am. Chem. Soc.* **1997**, *119*, 12514–12524; (e) P. R. Ashton, I. Baxter, M. C. T. Fyfe, F. M. Raymo, N. Spencer, J. F. Stoddart, A. J. P. White, D. J. Williams, *J. Am. Chem. Soc.* **1998**, *120*, 2297–2307; (f) P. R. Ashton, M. C. T. Fyfe, M. V. Martinez-Diaz, S. Menzer, C. Schiavo, J. F. Stoddart, A. J. P. White, D. J. Williams, *Chem. Eur. J.* **1998**, *4*, 1523–1534; (g) T. Clifford, A. Abushamleh, D. H. Busch, *Proc. Natl. Acad. Sci. USA* **2002**, *99*, 4830–4836; (h) H. W. Gibson, N. Yamaguchi, J. W. Jones, *J. Am. Chem. Soc.* **2003**, *125*, 3522–3533.

53 For an example of a pseudorotaxane architecture based on π-donor guest and π-acceptor cyclophane interactions, see: P. L. Anelli, P. R. Ashton, N. Spencer, A. M. Z. Slawin, J. F. Stoddart, D. J. Williams, *Angew. Chem. Int. Ed. Engl.* **1991**, *30*, 1036–1039.

54 For examples of other types of pseudorotaxane architectures, see: (a) A. Mirzoian, A. E. Kaifer, *Chem. Eur. J.* **1997**, *3*, 1052–1058; (b) K. M. Huh, T. Ooya, S. Sasaki, N. Yui, *Macromolecules* **2001**, *34*, 2402–2404; (c) J. A. Wisner, P. D. Beer, N. G. Berry, B. Tomapatanaget, *Proc. Natl. Acad. Sci. USA* **2002**, *99*, 4983–4986; (d) F. H. Huang, F. R. Fronczek, H. W. Gibson, *J. Am. Chem. Soc.* **2003**, *125*, 9272–9273; (e) F. H. Huang, H. W. Gib-

son, W. S. Bryant, D. S. Nagvekar, F. R. Fronczek, *J. Am. Chem. Soc.* **2003**, *125*, 9367–9371; (f) Y. Inoue, T. Kanbara, T. Yamamoto, *Tetrahedron Lett.* **2004**, *45*, 4603–4606.

55 (a) R. Ballardini, V. Balzani, M. T. Gandolfi, L. Prodi, M. Venturi, D. Philp, H. G. Ricketts, J. F. Stoddart, *Angew. Chem. Int. Ed. Engl.* **1993**, *32*, 1301–1303; (b) R. Ballardini, V. Balzani, A. Credi, M. T. Gandolfi, S. J. Langford, S. Menzer, L. Prodi, J. F. Stoddart, M. Venturi, D. J. Williams, *Angew. Chem. Int. Ed. Engl.* **1996**, *35*, 978–981; (c) P. R. Ashton, R. Ballardini, V. Balzani, S. E. Boyd, A. Credi, M. T. Gandolfi, M. GomezLopez, S. Iqbal, D. Philp, J. A. Preece, L. Prodi, H. G. Ricketts, J. F. Stoddart, M. S. Tolley, M. Venturi, A. J. P. White, D. J. Williams, *Chem. Eur. J.* **1997**, *3*, 152–170; (d) M. Asakawa, P. R. Ashton, V. Balzani, A. Credi, G. Mattersteig, O. A. Matthews, M. Montalti, N. Spencer, J. F. Stoddart, M. Venturi, *Chem. Eur. J.* **1997**, *3*, 1992–1996; (e) A. Credi, V. Balzani, S. J. Langford, J. F. Stoddart, *J. Am. Chem. Soc.* **1997**, *119*, 2679–2681; (f) P. R. Ashton, R. Ballardini, V. Balzani, M. GomezLopez, S. E. Lawrence, M. V. Martinez-Diaz, M. Montalti, A. Piersanti, L. Prodi, J. F. Stoddart, D. J. Williams, *J. Am. Chem. Soc.* **1997**, *119*, 10641–10651; (g) M. Montalti, L. Prodi, *Chem. Commun.* **1998**, 1461–1462; (h) P. R. Ashton, V. Balzani, O. Kocian, L. Prodi, N. Spencer, J. F. Stoddart, *J. Am. Chem. Soc.* **1998**, *120*, 11190–11191; (i) V. Balzani, A. Credi, F. Marchioni, J. F. Stoddart, *Chem. Commun.* **2001**, 1860–1861; (j) T. Fujimoto, A. Nakamura, Y. Inoue, Y. Sakata, T. Kaneda, *Tetrahedron Lett.* **2001**, *42*, 7987–7989.

56 A. Credi, M. Montalti, V. Balzani, S. J. Langford, F. M. Raymo, J. F. Stoddart, *New J. Chem.* **1998**, *22*, 1061–1065.

57 (a) E. Ishow, A. Credi, V. Balzani, F. Spadola, L. Mandolini, *Chem. Eur. J.* **1999**, *5*, 984–989; (b) R. Ballardini, V. Balzani, M. Clemente-Leon, A. Credi, M. T. Gandolfi, E. Ishow, J. Perkins, J. F. Stoddart, H. R. Tseng, S. Wenger, *J. Am. Chem. Soc.* **2002**, *124*, 12786–12795.

58 For examples of kinetically stable pseudorotaxane systems, see: (a) J.-P. Collin, P. Gaviña, J.-P. Sauvage, *Chem. Commun.* **1996**, 2005–2006; (b) J. W. Lee, K. P. Kim, K. Kim, *Chem. Commun.* **2001**, 1042–1043.

59 (a) G. Schill, *Catenanes, Rotaxanes and Knots*, Academic Press, New York, **1971**; (b) D. M. Walba, *Tetrahedron* **1985**, *41*, 3161–3212; (c) D. B. Amabilino, J. F. Stoddart, *Chem. Rev.* **1995**, *95*, 2725–2828; (d) D. A. Leigh, A. Murphy, *Chem. Ind.* **1999**, 178–183; (e) G. A. Breault, C. A. Hunter, P. C. Mayers, *Tetrahedron* **1999**, *55*, 5265–5293; (f) *Molecular Catenanes Rotaxanes and Knots* (Eds.: J.-P. Sauvage, C. O. Dietrich-Buchecker), Wiley–VCH, Weinheim, **1999**.

60 There are some examples of catenanes and rotaxanes constructed under thermodynamic control using dynamic processes such as olefin metathesis or imine bond formation (see for example: J. S. Hannam, T. J. Kidd, D. A. Leigh, A. J. Wilson, *Org. Lett.* **2003**, *5*, 1907–1910 and references therein). Such systems cannot act as molecular machines if they exchange components with the bulk quicker than the timescale of their stimuli-induced motion.

61 Another synthetic strategy, 'slippage', theoretically provides a route to rotaxanes under thermodynamic control. However, the chemical assemblies thus far prepared by this route are misclassified in the literature. They do not satisfy the structural requirements of a rotaxane since the components can be separated from each other without breaking covalent bonds. Rather they are pseudo-rotaxanes – threaded host–guest complexes which are kinetically stable at room temperature. This incorrect classification is not normally an issue because the physical behavior of kinetically stable pseudo-rotaxanes generally mirrors that of rotaxanes. However, it increasingly appears to be confusing non-specialists into thinking that rotaxanes are supramolecular species or that pseudo-rotaxanes that are not kinetically stable can act as molecular machines. Slippage *could* be used as a strategy to form rotaxanes if the stabilization gained from the ring binding on the thread was sufficient to mean that covalent bond breaking is less energetically demanding than de-threading of the rings over the stoppers. To date no structures of this type have been reported.

62 For reviews on the development of interlocked molecules as molecular machines, see refs. [6a, 6c, 6e] and: (a) V. Balzani, M. Gomez-Lopez, J. F. Stoddart, *Acc. Chem. Res.* **1998**, *31*, 405–414; (b) J.-P. Sauvage, *Acc. Chem. Res.* **1998**, *31*, 611–619; (c) J.-C. Chambron, J.-P. Sauvage, *Chem. Eur. J.* **1998**, *4*, 1362–1366; (d) J.-P. Collin, P. Gaviña, V. Heitz, J.-P. Sauvage, *Eur. J. Inorg. Chem.* **1998**, 1–14; (e) M.-J. Blanco, M. C. Jimenez, J.-C. Chambron, V. Heitz, M. Linke, J.-P. Sauvage, *Chem. Soc. Rev.* **1999**, *28*, 293–305; (f) Z. Asfari, J. Vicens, *J. Inclusion Phenom. Macro. Chem.* **2000**, *36*, 103–118; (g) *Molecular Machines and Motors: Structure and Bonding, Vol. 99* (Ed.: J.-P. Sauvage), Springer, Berlin, **2001**; (h) A. R. Pease, J. O. Jeppesen, J. F. Stoddart, Y. Luo, C. P. Collier, J. R. Heath, *Acc. Chem. Res.* **2001**, *34*, 433–444; (i) C. A. Schalley, K. Beizai, F. Vögtle, *Acc. Chem. Res.* **2001**, *34*, 465–476; (j) J.-P. Collin, C. Dietrich-Buchecker, P. Gaviña, M. C. Jimenez-Molero, J.-P. Sauvage, *Acc. Chem. Res.* **2001**, *34*, 477–487; (k) B. X. Colasson, C. Dietrich-Buchecker, M. C. Jimenez-Molero, J.-P. Sauvage, *J. Phys. Org. Chem.* **2002**, *15*, 476–483.

63 Numbers in square brackets preceding the names of interlocked compounds indicate the number of mechanically interlocked species, e.g. a [2]rotaxane consists of one macrocycle and one thread component mechanically interlocked; two macrocycles both locked around the same thread would constitute a [3]rotaxane.

64 The concept of constructing a molecular catenane was first postulated by Willstätters before 1912 (see refs. [59a, 59b]). The first statistical synthesis of a catenane was achieved by Wasserman in 1960: (a) E. Wasserman, *J. Am. Chem. Soc.* **1960**, *82*, 4433–4434; and the first directed synthesis by Lüttringhaus and Schill in 1964: (b) G. Schill, A. Lüttringhaus, *Angew. Chem. Int. Ed. Engl.* **1964**, *3*, 546–547. The first rotaxane was synthesized by Harrison and Harrison in 1967: (c) I. T. Harrison, S. Harrison, *J. Am. Chem. Soc.* **1967**, *89*, 5723–5724; (d) I. T. Harrison, *J. Chem. Soc. Perkin Trans. 1* **1974**, 301–304.

65 For reviews on templated synthesis, see: (a) C. O. Dietrich-Buchecker, J.-P. Sauvage, *Chem. Rev.* **1987**, *87*, 795–810; (b) D. H. Busch, N. A. Stephenson, *Coord. Chem. Rev.* **1990**, *100*, 119–154; (c) D. Philp, J. F. Stoddart, *Synlett* **1991**, 445–458; (d) S. Anderson, H. L. Anderson, J. K. M. Sanders, *Acc. Chem. Res.* **1993**, *26*, 469–475; (e) R. Cacciapaglia, L. Mandolini, *Chem. Soc. Rev.* **1993**, *22*, 221–231; (f) R. Hoss, F. Vögtle, *Angew. Chem. Int. Ed. Engl.* **1994**, *33*, 375–384; (g) M. Fujita, K. Ogura, *Coord. Chem. Rev.* **1996**, *148*, 249–264; (h) M. C. T. Fyfe, J. F. Stoddart, *Acc. Chem. Res.* **1997**, *30*, 393–401; (i) R. Jager, F. Vögtle, *Angew. Chem. Int. Ed. Engl.* **1997**, *36*, 930–944; (j) *Templated Organic Synthesis* (Eds.: F. Diederich, P. J. Strang), Wiley–VCH, Weinheim, **1999**; (k) M. Fujita, *Acc. Chem. Res.* **1999**, *32*, 53–61; (l) T. J. Hubin, D. H. Busch, *Coord. Chem. Rev.* **2000**, *200*, 5–52; (m) J. F. Stoddart, H. R. Tseng, *Proc. Natl. Acad. Sci. USA* **2002**, *99*, 4797–4800; (n) R. Vilar, *Angew. Chem. Int. Ed.* **2003**, *42*, 1460–1477.

66 D. A. Leigh, A. Murphy, J. P. Smart, A. M. Z. Slawin, *Angew. Chem. Int. Ed. Engl.* **1997**, *36*, 728–732.

67 J. Sandström, *Dynamic NMR Spectroscopy*, Academic Press, London, **1982**.

68 F. W. Dahlquist, K. J. Longmur, R. B. Du Vernet, *J. Magn. Reson.* **1975**, *17*, 406–413.

69 F. G. Gatti, D. A. Leigh, S. A. Nepogodiev, A. M. Z. Slawin, S. J. Teat, J. K. Y. Wong, *J. Am. Chem. Soc.* **2001**, *123*, 5983–5989.

70 (a) C. O. Dietrich-Buchecker, J.-P. Sauvage, J. P. Kintzinger, *Tetrahedron Lett.* **1983**, *24*, 5095–5098; (b) C. O. Dietrich-Buchecker, J.-P. Sauvage, J.-M. Kern, *J. Am. Chem. Soc.* **1984**, *106*, 3043–3045; (c) C. Dietrich-Buchecker, J.-P. Sauvage, *Tetrahedron* **1990**, *46*, 503–512.

71 For reviews, see ref. [65a] and: (a) J.-P. Sauvage, *Acc. Chem. Res.* **1990**, *23*, 319–327; (b) J. C. Chambron, J. P. Collin, V. Heitz, D. Jouvenot, J. M. Kern, P. Mobian, D. Pomeranc, J. P. Sauvage, *Eur. J. Org. Chem.* **2004**, 1627–1638.

72 Metal-coordinated catenanes are sometimes known as catenates. Demetallation to give the uncomplexed, but still interlocked, ligands gives a catenand. No similar nomenclature is used for metal-coordinated rotaxane-like structures however, which are named as their organic counterparts. In recent times, the use of the terms

"catenate" and "catenand" has largely been superseded in the literature by the more general "catenane".

73 C. A. Hunter, *J. Am. Chem. Soc.* **1992**, *114*, 5303–5311.

74 F. Vögtle, S. Meier, R. Hoss, *Angew. Chem. Int. Ed. Engl.* **1992**, *31*, 1619–1622.

75 A. G. Johnston, D. A. Leigh, R. J. Pritchard, M. D. Deegan, *Angew. Chem. Int. Ed. Engl.* **1995**, *34*, 1209–1212.

76 This previously inaccessible species was obtained by trapping round an acyclic, stoppered benzylic amide thread to create a [2]rotaxane, followed by controlled cleavage of the thread and resultant de-threading: A. G. Johnston, D. A. Leigh, A. Murphy, J. P. Smart, M. D. Deegan, *J. Am. Chem. Soc.* **1996**, *118*, 10662–10663.

77 A. G. Johnston, D. A. Leigh, L. Nezhat, J. P. Smart, M. D. Deegan, *Angew. Chem. Int. Ed. Engl.* **1995**, *34*, 1212–1216.

78 D. A. Leigh, A. Murphy, J. P. Smart, M. S. Deleuze, F. Zerbetto, *J. Am. Chem. Soc.* **1998**, *120*, 6458–6467.

79 M. S. Deleuze, D. A. Leigh, F. Zerbetto, *J. Am. Chem. Soc.* **1999**, *121*, 2364–2379.

80 D. A. Leigh, A. Troisi, F. Zerbetto, *Chem. Eur. J.* **2001**, *7*, 1450–1454.

81 P. L. Anelli, P. R. Ashton, R. Ballardini, V. Balzani, M. Delgado, M. T. Gandolfi, T. T. Goodnow, A. E. Kaifer, D. Philp, M. Pietraszkiewicz, L. Prodi, M. V. Reddington, A. M. Z. Slawin, N. Spencer, J. F. Stoddart, C. Vicent, D. J. Williams, *J. Am. Chem. Soc.* **1992**, *114*, 193–218.

82 P. R. Ashton, T. T. Goodnow, A. E. Kaifer, M. V. Reddington, A. M. Z. Slawin, N. Spencer, J. F. Stoddart, C. Vicent, D. J. Williams, *Angew. Chem. Int. Ed. Engl.* **1989**, *28*, 1396–1399.

83 P. R. Ashton, C. L. Brown, E. J. T. Chrystal, K. P. Parry, M. Pietraszkiewicz, N. Spencer, J. F. Stoddart, *Angew. Chem. Int. Ed. Engl.* **1991**, *30*, 1042–1045.

84 The distal isomer may still be involved transiently in the circumvolution mechanism.

85 S.-H. Chiu, A. M. Elizarov, P. T. Glink, J. F. Stoddart, *Org. Lett.* **2002**, *4*, 3561–3564.

86 For further studies on the effect of structure on the dynamic properties of similar catenanes, see: (a) D. B. Amabilino, P. R. Ashton, M. S. Tolley, J. F. Stoddart, D. J. Williams, *Angew. Chem. Int. Ed. Engl.* **1993**, *32*, 1297–1301; (b) P. R. Ashton, M. A. Blower, S. Iqbal, C. H. McLean, J. F. Stoddart, M. S. Tolley, D. J. Williams, *Synlett* **1994**, 1059–1062; (c) D. B. Amabilino, P. R. Ashton, G. R. Brown, W. Hayes, J. F. Stoddart, M. S. Tolley, D. J. Williams, *J. Chem. Soc. Chem. Commun.* **1994**, 2479–2482; (d) D. B. Amabilino, P. L. Anelli, P. R. Ashton, G. R. Brown, E. Cordova, L. A. Godinez, W. Hayes, A. E. Kaifer, D. Philp, A. M. Z. Slawin, N. Spencer, J. F. Stoddart, M. S. Tolley, D. J. Williams, *J. Am. Chem. Soc.* **1995**, *117*, 11142–11170; (e) M. Asakawa, P. R. Ashton, S. E. Boyd, C. L. Brown, R. E. Gillard, O. Kocian, F. M. Raymo, J. F. Stoddart, M. S. Tolley, A. J. P. White, D. J. Williams, *J. Org. Chem.* **1997**, *62*, 26–37; (f) R. Ballardini, V. Balzani, A. Credi, C. L. Brown, R. E. Gillard, M. Montalti, D. Philp, J. F. Stoddart, M. Venturi, A. J. P. White, B. J. Williams, D. J. Williams, *J. Am. Chem. Soc.* **1997**, *119*, 12503–12513; (g) B. Cabezon, J. G. Cao, F. M. Raymo, J. F. Stoddart, A. J. P. White, D. J. Williams, *Angew. Chem. Int. Ed.* **2000**, *39*, 148–151.

87 With the notable exception of the earliest statistically constructed [2]rotaxanes (see refs. [64c, 64d]), there are very few examples of rotaxanes without any recognition elements in the thread, see however: (a) C. Heim, A. Affeld, M. Nieger, F. Vögtle, *Helv. Chim. Acta* **1999**, *82*, 746–759; (b) J. S. Hannam, S. M. Lacy, D. A. Leigh, C. G. Saiz, A. M. Z. Slawin, S. Stitchell, *Angew. Chem. Int. Ed.* **2004**, *43*, 3260–3264.

88 P. L. Anelli, N. Spencer, J. F. Stoddart, *J. Am. Chem. Soc.* **1991**, *113*, 5131–5133.

89 (a) P. R. Ashton, D. Philp, N. Spencer, J. F. Stoddart, *J. Chem. Soc. Chem. Commun.* **1992**, 1124–1128; (b) P. R. Ashton, M. R. Johnston, J. F. Stoddart, M. S. Tolley, J. W. Wheeler, *J. Chem. Soc. Chem. Commun.* **1992**, 1128–1131.

90 A. S. Lane, D. A. Leigh, A. Murphy, *J. Am. Chem. Soc.* **1997**, *119*, 11092–11093.

91 D. A. Leigh, A. Troisi, F. Zerbetto, *Angew. Chem. Int. Ed.* **2000**, *39*, 350–353.

92 Even in 1991, when reporting the first degenerate molecular shuttle (see ref. [88]), Stoddart noted that: "The opportunity now exists to desymmetrize the molecular shuttle by inserting nonidentical 'stations' along the polyether 'thread' in such a

manner that these different 'stations' can be addressed selectively by chemical, electrochemical, or photochemical means and so provide a mechanism to drive the 'bead' to and fro between 'stations' along the 'thread'.

93 (a) A. C. Benniston, A. Harriman, *Angew. Chem. Int. Ed. Engl.* **1993**, *32*, 1459–1461; (b) A. C. Benniston, A. Harriman, V. M. Lynch, *J. Am. Chem. Soc.* **1995**, *117*, 5275–5291.

94 H. Murakami, A. Kawabuchi, K. Kotoo, M. Kunitake, N. Nakashima, *J. Am. Chem. Soc.* **1997**, *119*, 7605–7606.

95 C. A. Stanier, S. J. Alderman, T. D. W. Claridge, H. L. Anderson, *Angew. Chem. Int. Ed.* **2002**, *41*, 1769–1772.

96 As long as the chemical reaction is fast with respect to the movement of the macrocycle.

97 R. A. Bissell, E. Cordova, A. E. Kaifer, J. F. Stoddart, *Nature* **1994**, *369*, 133–137.

98 See ref. [52] and: (a) A. G. Kolchinski, D. H. Busch, N. W. Alcock, *J. Chem. Soc. Chem. Commun.* **1995**, 1289–1291; (b) P. T. Glink, C. Schiavo, J. F. Stoddart, D. J. Williams, *Chem. Commun.* **1996**, 1483–1490; (c) P. R. Ashton, P. T. Glink, J. F. Stoddart, P. A. Tasker, A. J. P. White, D. J. Williams, *Chem. Eur. J.* **1996**, *2*, 729–736.

99 (a) M. V. Martinez-Diaz, N. Spencer, J. F. Stoddart, *Angew. Chem. Int. Ed. Engl.* **1997**, *36*, 1904–1907; (b) P. R. Ashton, R. Ballardini, V. Balzani, I. Baxter, A. Credi, M. C. T. Fyfe, M. T. Gandolfi, M. Gomez-Lopez, M. V. Martinez-Diaz, A. Piersanti, N. Spencer, J. F. Stoddart, M. Venturi, A. J. P. White, D. J. Williams, *J. Am. Chem. Soc.* **1998**, *120*, 11932–11942.

100 For an example of another pH switched shuttle from the Stoddart group, see: A. M. Elizarov, S.-H. Chiu, J. F. Stoddart, *J. Org. Chem.* **2002**, *67*, 9175–9181.

101 J. D. Badjić, V. Balzani, A. Credi, S. Silvi, J. F. Stoddart, *Science* **2004**, *303*, 1845–1849.

102 C. M. Keaveney, D. A. Leigh, *Angew. Chem. Int. Ed.* **2004**, *43*, 1222–1224.

103 (a) P. R. Ashton, R. A. Bissell, N. Spencer, J. F. Stoddart, M. S. Tolley, *Synlett* **1992**, 914–918; (b) P. R. Ashton, R. A. Bissell, R. Gorski, D. Philp, N. Spencer, J. F. Stoddart, M. S. Tolley, *Synlett* **1992**, 919–922; (c) P. R. Ashton, R. A. Bissell, N. Spencer, J. F. Stoddart, M. S. Tolley, *Synlett* **1992**, 923–926; (d) P. L. Anelli, M. Asakawa, P. R. Ashton, R. A. Bissell, G. Clavier, R. Gorski, A. E. Kaifer, S. J. Langford, G. Mattersteig, S. Menzer, D. Philp, A. M. Z. Slawin, N. Spencer, J. F. Stoddart, M. S. Tolley, D. J. Williams, *Chem. Eur. J.* **1997**, *3*, 1113–1135; (e) D. B. Amabilino, P. R. Ashton, S. E. Boyd, M. GomezLopez, W. Hayes, J. F. Stoddart, *J. Org. Chem.* **1997**, *62*, 3062–3075.

104 Shuttle **41** also shows a certain degree of electrochemical switching in the deprotonated state when electrochemical reduction of the bipyridinium unit causes movement of the macrocycle back towards the amine moiety. In this state however, the electron-rich macrocycle has no significant favorable interactions with the thread and its position is not well-defined, see ref. [99a].

105 For more recent examples of electrochemically switched shuttles from the Stoddart group, see: H. R. Tseng, S. A. Vignon, P. C. Celestre, J. Perkins, J. O. Jeppesen, A. Di Fabio, R. Ballardini, M. T. Gandolfi, M. Venturi, V. Balzani, J. F. Stoddart, *Chem. Eur. J.* **2004**, *10*, 155–172; and for an example of light- and electrochemically-triggered shuttling from the same group, see: P. R. Ashton, R. Ballardini, V. Balzani, A. Credi, K. R. Dress, E. Ishow, C. J. Kleverlaan, O. Kocian, J. A. Preece, N. Spencer, J. F. Stoddart, M. Venturi, S. Wenger, *Chem. Eur. J.* **2000**, *6*, 3558–3574.

106 (a) A. M. Brouwer, C. Frochot, F. G. Gatti, D. A. Leigh, L. Mottier, F. Paolucci, S. Roffia, G. W. H. Wurpel, *Science* **2001**, *291*, 2124–2128; (b) A. Altieri, F. G. Gatti, E. R. Kay, D. A. Leigh, D. Martel, F. Paolucci, A. M. Z. Slawin, J. K. Y. Wong, *J. Am. Chem. Soc.* **2003**, *125*, 8644–8654.

107 N. Armaroli, V. Balzani, J.-P. Collin, P. Gaviña, J.-P. Sauvage, B. Ventura, *J. Am. Chem. Soc.* **1999**, *121*, 4397–4408.

108 A. Altieri, G. Bottari, F. Dehez, D. A. Leigh, J. K. Y. Wong, F. Zerbetto, *Angew. Chem. Int. Ed.* **2003**, *42*, 2296–2300.

109 For an example of shuttling triggered by azobenzene photoisomerisation, see: M. Asakawa, P. R. Ashton, V. Balzani, C. L. Brown, A. Credi, O. A. Matthews, S. P.

Newton, F. M. Raymo, A. N. Shipway, N. Spencer, A. Quick, J. F. Stoddart, A. J. P. White, D. J. Williams, *Chem. Eur. J.* **1999**, *5*, 860–875.

110 Heat has been used to effect cis–trans isomerization in **46** resulting in a concomitant net change of position of the ring (see ref. [108]), while a temperature increase has also been used to overcome a significant kinetic barrier to shuttling, following a chemical change in a kinetically stable pseudorotaxane (see Ref. [58b]). In neither of these cases is the process reversible on cooling the material without some other stimulus being applied.

111 A C_{12} chain has >500 000 (3^{12}) possible C–C rotamers and a significant number of these degrees of freedom must be lost upon forming the *dodec-Z-***47** structure.

112 A series of theoretical designs for entropy-driven mechanical motion in mechanically interlocked molecules have been suggested, see: A. Hanke, R. Metzler, *Chem. Phys. Lett.* **2002**, *359*, 22–26.

113 The use of terms such as "all or nothing" or "quantitative" are inappropriate descriptions of an equilibrium.

114 V. Bermudez, N. Capron, T. Gase, F. G. Gatti, F. Kajzar, D. A. Leigh, F. Zerbetto, S. W. Zhang, *Nature* **2000**, *406*, 608–611.

115 F. G. Gatti, S. Leon, J. K. Y. Wong, G. Bottari, A. Altieri, M. A. F. Morales, S. J. Teat, C. Frochot, D. A. Leigh, A. M. Brouwer, F. Zerbetto, *Proc. Natl. Acad. Sci. USA* **2003**, *100*, 10–14.

116 For examples where the ring in a rotaxane is pirouetted between two distinct orientations, using the same principles as molecular shuttling (Section 7.5.5), see: (a) L. Raehm, J.-M. Kern, J.-P. Sauvage, *Chem. Eur. J.* **1999**, *5*, 3310–3317; (b) I. Poleschak, J.-M. Kern, J.-P. Sauvage, *Chem. Commun.* **2004**, 474–476.

117 It has recently been suggested that unidirectional pirouetting could result from simply derivatizing rotaxanes with chiral or knotted stoppers (see: O. Lukin, T. Kubota, Y. Okamoto, F. Schelhase, A. Yoneva, W. M. Müller, U. Müller, F. Vögtle, *Angew. Chem. Int. Ed.* **2003**, *42*, 4542–4545). As discussed in Section 7.2, this is incorrect. Directional rotation can only result from an external energy source being used to drive the system temporarily away from equilibrium.

118 D. A. Leigh, K. Moody, J. P. Smart, K. J. Watson, A. M. Z. Slawin, *Angew. Chem. Int. Ed. Engl.* **1996**, *35*, 306–310.

119 M. Asakawa, P. R. Ashton, V. Balzani, A. Credi, C. Hamers, G. Mattersteig, M. Montalti, A. N. Shipway, N. Spencer, J. F. Stoddart, M. S. Tolley, M. Venturi, A. J. P. White, D. J. Williams, *Angew. Chem. Int. Ed.* **1998**, *37*, 333–337.

120 For other examples of switchable motion in [2]catenanes from the Stoddart group, see ref. [109] and: (a) P. R. Ashton, L. Perezgarcia, J. F. Stoddart, A. J. P. White, D. J. Williams, *Angew. Chem. Int. Ed. Engl.* **1995**, *34*, 571–574; (b) P. R. Ashton, R. Ballardini, V. Balzani, A. Credi, M. T. Gandolfi, S. Menzer, L. Perezgarcia, L. Prodi, J. F. Stoddart, M. Venturi, A. J. P. White, D. J. Williams, *J. Am. Chem. Soc.* **1995**, *117*, 11171–11197; (c) M. Asakawa, P. R. Ashton, V. Balzani, S. E. Boyd, A. Credi, G. Mattersteig, S. Menzer, M. Montalti, F. M. Raymo, C. Ruffilli, J. F. Stoddart, M. Venturi, D. J. Williams, *Eur. J. Org. Chem.* **1999**, 985–994; (d) V. Balzani, A. Credi, G. Mattersteig, O. A. Matthews, F. M. Raymo, J. F. Stoddart, M. Venturi, A. J. P. White, D. J. Williams, *J. Org. Chem.* **2000**, *65*, 1924–1936; (e) P. R. Ashton, V. Baldoni, V. Balzani, A. Credi, H. D. A. Hoffmann, M. V. Martinez-Diaz, F. M. Raymo, J. F. Stoddart, M. Venturi, *Chem. Eur. J.* **2001**, *7*, 3482–3493.

121 (a) A. Livoreil, C. O. Dietrich-Buchecker, J.-P. Sauvage, *J. Am. Chem. Soc.* **1994**, *116*, 9399–9400; (b) F. Baumann, A. Livoreil, W. Kaim, J.-P. Sauvage, *Chem. Commun.* **1997**, 35–36; (c) A. Livoreil, J.-P. Sauvage, N. Armaroli, V. Balzani, L. Flamigni, B. Ventura, *J. Am. Chem. Soc.* **1997**, *119*, 12114–12124.

122 For an example of an electrochemically switched [2]catenane based on the redox reactions of metal centers embedded in one of the rings, see: B. Korybut-Daszkiewicz, A. Wieckowska, R. Bilewicz, S. Domagala, K. Woźniak, *Angew. Chem. Int. Ed.* **2004**, *43*, 1668–1672.

123 D. J. Cardenas, A. Livoreil, J.-P. Sauvage, *J. Am. Chem. Soc.* **1996**, *118*, 11980–11981.

124 D. A. Leigh, J. K. Y. Wong, F. Dehez, F. Zerbetto, *Nature* **2003**, *424*, 174–179.

125 (a) C. P. Collier, E. W. Wong, M. Bĕhloradský, F. M. Raymo, J. F. Stoddart, P. J. Kuekes, R. S. Williams, J. R. Heath, *Science* **1999**, *285*, 391–394; (b) E. W. Wong, C. P. Collier, M. Bĕhloradský, F. M. Raymo, J. F. Stoddart, J. R. Heath, *J. Am. Chem. Soc.* **2000**, *122*, 5831–5840.

126 C. P. Collier, G. Mattersteig, E. W. Wong, Y. Luo, K. Beverly, J. Sampaio, F. M. Raymo, J. F. Stoddart, J. R. Heath, *Science* **2000**, *289*, 1172–1175.

127 C. P. Collier, J. O. Jeppesen, Y. Luo, J. Perkins, E. W. Wong, J. R. Heath, J. F. Stoddart, *J. Am. Chem. Soc.* **2001**, *123*, 12632–12641.

128 Y. Luo, C. P. Collier, J. O. Jeppesen, K. A. Nielsen, E. Delonno, G. Ho, J. Perkins, H. R. Tseng, T. Yamamoto, J. F. Stoddart, J. R. Heath, *ChemPhysChem* **2002**, *3*, 519–525.

129 (a) Y. Chen, D. A. A. Ohlberg, X. M. Li, D. R. Stewart, R. S. Williams, J. O. Jeppesen, K. A. Nielsen, J. F. Stoddart, D. L. Olynick, E. Anderson, *Appl. Phys. Lett.* **2003**, *82*, 1610–1612; (b) Y. Chen, G. Y. Jung, D. A. A. Ohlberg, X. M. Li, D. R. Stewart, J. O. Jeppesen, K. A. Nielsen, J. F. Stoddart, R. S. Williams, *Nanotechnology* **2003**, *14*, 462–468; (c) D. R. Stewart, D. A. A. Ohlberg, P. A. Beck, Y. Chen, R. S. Williams, J. O. Jeppesen, K. A. Nielsen, J. F. Stoddart, *Nano Lett.* **2004**, *4*, 133–136.

130 M. R. Diehl, D. W. Steuerman, H. R. Tseng, S. A. Vignon, A. Star, P. C. Celestre, J. F. Stoddart, J. R. Heath, *ChemPhysChem* **2003**, *4*, 1335–1339.

131 (a) M. C. Jimenez, C. Dietrich-Buchecker, J.-P. Sauvage, *Angew. Chem. Int. Ed.* **2000**, *39*, 3284–3287; (b) M. C. Jimenez-Molero, C. Dietrich-Buchecker, J.-P. Sauvage, *Chem. Eur. J.* **2002**, *8*, 1456–1466; (c) M. C. Jimenez-Molero, C. Dietrich-Buchecker, J.-P. Sauvage, *Chem. Commun.* **2003**, 1613–1616.

132 M. Asakawa, G. Brancato, M. Fanti, D. A. Leigh, T. Shimizu, A. M. Z. Slawin, J. K. Y. Wong, F. Zerbetto, S. W. Zhang, *J. Am. Chem. Soc.* **2002**, *124*, 2939–2950.

133 G. Bottari, D. A. Leigh, E. M. Pérez, *J. Am. Chem. Soc.* **2003**, *125*, 13360–13361.

134 E. M. Pérez, D. T. F. Dryden, D. A. Leigh, G. Teobaldi, F. Zerbetto, **2004**, *J. Am. Chem. Soc.*, **2004**, *126*, 12210–12211.

135 Q.-C. Wang, D.-H. Qu, J. Ren, K. Chen, H. Tian, *Angew. Chem. Int. Ed.* **2004**, *43*, 2661–2665.

136 D.-H. Qu, Q.-C. Wang, J. Ren, H. Tian, *Org. Lett.* **2004**, *6*, 2085–2088.

137 See, for example: (a) A. K. Boal, V. M. Rotello, *J. Am. Chem. Soc.* **1999**, *121*, 4914–4915; (b) Y. Ge, D. K. Smith, *Anal. Chem.* **2000**, *72*, 1860–1865; (c) G. Cooke, F. M. A. Duclairoir, V. M. Rotello, J. F. Stoddart, *Tetrahedron Lett.* **2000**, *41*, 8163–8166; (d) A. Labande, D. Astruc, *Chem. Commun.* **2000**, 1007–1008; (e) M. C. Daniel, J. Ruiz, S. Nlate, J. Palumbo, J. C. Blais, D. Astruc, *Chem. Commun.* **2001**, 2000–2001; (f) S. Y. Chia, J. G. Cao, J. F. Stoddart, J. I. Zink, *Angew. Chem. Int. Ed.* **2001**, *40*, 2447–2451; (g) M. R. Bryce, G. Cooke, F. M. A. Duclairoir, P. John, D. F. Perepichka, N. Polwart, V. M. Rotello, J. F. Stoddart, H. R. Tseng, *J. Mater. Chem.* **2003**, *13*, 2111–2117; (h) K. Kim, W. S. Jeon, J.-K. Kang, J. W. Lee, S. Y. Jon, T. Kim, K. Kim, *Angew. Chem. Int. Ed.* **2003**, *42*, 2293–2296.

138 R. Hernandez, H. R. Tseng, J. W. Wong, J. F. Stoddart, J. I. Zink, *J. Am. Chem. Soc.* **2004**, *126*, 3370–3371.

139 (a) J. Lahann, S. Mitragotri, T. N. Tran, H. Kaido, J. Sundaram, I. S. Choi, S. Hoffer, G. A. Somorjai, R. Langer, *Science* **2003**, *299*, 371–374; (b) X. M. Wang, A. B. Kharitonov, E. Katz, I. Willner, *Chem. Commun.* **2003**, 1542–1543.

140 T. Gase, D. Grando, P. A. Chollet, F. Kajzar, A. Murphy, D. A. Leigh, *Adv. Mater.* **1999**, *11*, 1303–1305.

141 H. R. Tseng, D. M. Wu, N. X. L. Fang, X. Zhang, J. F. Stoddart, *ChemPhysChem* **2004**, *5*, 111–116.

142 B. Long, K. Nikitin, D. Fitzmaurice, *J. Am. Chem. Soc.* **2003**, *125*, 15490–15498.

143 (a) I. Willner, B. Willner, *J. Mater. Chem.* **1998**, *8*, 2543–2556; (b) A. N. Shipway, I. Willner, *Acc. Chem. Res.* **2001**, *34*, 421–432.

144 I. Willner, V. Pardo-Yissar, E. Katz, K. T. Ranjit, *J. Electroanal. Chem.* **2001**, *497*, 172–177.

145 See for example the observation of single-molecule stretching and contraction described in Section 7.2 and ref. [38], and additionally: (a) D. M. Eigler, C. P. Lutz, W. E. Rudge, *Nature* **1991**, *352*, 600–603; (b) T. A. Jung, R. R. Schlittler, J. K. Gimzewski, H. Tang, C. Joachim, *Science* **1996**, *271*, 181–184; (c) J. K. Gimzewski, C. Joachim, R. R. Schlittler, V. Langlais, H. Tang, I. Johannsen, *Science* **1998**, *281*, 531–533.

146 H. Shigekawa, K. Miyake, J. Sumaoka, A. Harada, M. Komiyama, *J. Am. Chem. Soc.* **2000**, *122*, 5411–5412.

147 M. Cavallini, F. Biscarini, S. Leon, F. Zerbetto, G. Bottari, D. A. Leigh, *Science* **2003**, *299*, 531–531.

148 (a) P. Ball, *Nature* **2000**, *406*, 118–120; (b) A. P. de Silva, N. D. McClenaghan, C. P. McCoy in *Molecular Switches* (Ed.: B. L. Feringa), Wiley–VCH, Weinheim, **2001**, pp. 339–361; (c) F. M. Raymo, *Adv. Mater.* **2002**, *14*, 401–414; (d) G. J. Brown, A. P. de Silva, S. Pagliari, *Chem. Commun.* **2002**, 2461–2463.

149 (a) P. Thordarson, E. J. A. Bijsterveld, A. E. Rowan, R. J. M. Nolte, *Nature* **2003**, *424*, 915–918; (b) P. Thordarson, R. J. M. Nolte, A. E. Rowan, *Aust. J. Chem.* **2004**, *57*, 323–327; (c) P. R. Carlier, *Angew. Chem. Int. Ed.* **2004**, *43*, 2602–2605.

150 See, for example: (a) S. J. Tans, A. R. M. Verschueren, C. Dekker, *Nature* **1998**, *393*, 49–52; (b) H. Park, J. Park, A. K. L. Lim, E. H. Anderson, A. P. Alivisatos, P. L. McEuen, *Nature* **2000**, *407*, 57–60 (nanoscale transistors); (c) A. M. Fennimore, T. D. Yuzvinsky, W. Q. Han, M. S. Fuhrer, J. Cumings, A. Zettl, *Nature* **2003**, *424*, 408–410 (nanoscale rotational actuator).

151 For reviews, see: (a) G. M. Whitesides, M. Boncheva, *Proc. Natl. Acad. Sci. USA* **2002**, *99*, 4769–4774; (b) I. W. Hamley, *Angew. Chem. Int. Ed.* **2003**, *42*, 1692–1712.

152 T. F. Otero, J. M. Sansinena, *Adv. Mater.* **1998**, *10*, 491–494 and references therein.

153 (a) M. Barboiu, J.-M. Lehn, *Proc. Natl. Acad. Sci. USA* **2002**, *99*, 5201–5206; (b) H. J. Schneider, T. J. Liu, N. Lomadze, *Angew. Chem. Int. Ed.* **2003**, *42*, 3544–3546.

154 M. J. Marsella, R. J. Reid, S. Estassi, L. S. Wang, *J. Am. Chem. Soc.* **2002**, *124*, 12507–12510.

155 See ref. [5] and, for example: (a) G. Steinberg-Yfrach, J. L. Rigaud, E. N. Durantini, A. L. Moore, D. Gust, T. A. Moore, *Nature* **1998**, *392*, 479–482; (b) C. Montemagno, G. Bachand, *Nanotechnology* **1999**, *10*, 225–231; (c) R. K. Soong, G. D. Bachand, H. P. Neves, A. G. Olkhovets, H. G. Craighead, C. D. Montemagno, *Science* **2000**, *290*, 1555–1558.

156 (a) B. Yurke, A. J. Turberfield, A. P. Mills, F. C. Simmel, J. L. Neumann, *Nature* **2000**, *406*, 605–608; (b) D. S. Liu, S. Balasubramanian, *Angew. Chem. Int. Ed.* **2003**, *42*, 5734–5736; (c) W. U. Dittmer, A. Reuter, F. C. Simmel, *Angew. Chem. Int. Ed.* **2004**, *43*, 3550–3553; (d) Y. Chen, M. Wang, C. Mao, *Angew. Chem. Int. Ed.* **2004**, *43*, 3554–3557.

Conservative and dissipative force imaging of switchable rotaxanes with frequency-modulation atomic force microscopy

Alan A. Farrell,[1,*] Takeshi Fukuma,[2] Takayuki Uchihashi,[1] Euan R. Kay,[3] Giovanni Bottari,[3] David A. Leigh,[3,†] Hirofumi Yamada,[2] and Suzanne P. Jarvis[1]

[1]*Nanoscale Function Group, Centre for Research on Adaptive Nanostructures and Nanodevices, University of Dublin, Trinity College, Dublin 2, Ireland*

[2]*Department of Electronic Science and Engineering, Kyoto University A1-326, Katsura, Nishikyo, Kyoto 615-8510, Japan*

[3]*School of Chemistry, University of Edinburgh, The King's Buildings, West Mains Road, Edinburgh EH9 3JJ, UK*

(Received 27 May 2005; published 23 September 2005)

We compare constant amplitude frequency modulation atomic force microscopy (FM-AFM) in ambient conditions to ultrahigh vacuum (UHV) experiments by analysis of thin films of rotaxane molecules. Working in ambient conditions is important for the development of real-world molecular devices. We show that the FM-AFM technique allows quantitative measurement of conservative and dissipative forces without instabilities caused by any native water layer. Molecular resolution is achieved despite the low Q-factor in the air. Furthermore, contrast in the energy dissipation is observed even at the molecular level. This should allow investigations into stimuli-induced sub-molecular motion of organic films.

DOI: 10.1103/PhysRevB.72.125430 PACS number(s): 68.37.Ps, 81.16.Fg, 81.07.Nb, 68.43.Fg

I. INTRODUCTION

In Frequency Modulation Atomic Force Microscopy (FM-AFM) a cantilever with a nanometer-sized probe is self-oscillated at its resonant frequency. Small changes in the resonance can be readily detected corresponding to a force interaction between tip and sample. In an ultrahigh vacuum (UHV) environment the technique is capable of imaging surfaces with true atomic resolution regardless of conductivity.[1–3] This is important for organic material applications, since most organic materials have poor conductivity. Indeed, molecularly resolved images of organic adsorbates in UHV have been presented.[4–7] In addition the entire distance range of the force interaction can be unambiguously quantified without instabilities.[1,8–10] The FM-AFM technique can also distinguish between conservative and dissipative forces, see, for example, Ref. 11. The conservative tip-sample force interaction results in a reversible change with distance in the cantilever resonance, without any loss of cantilever vibrational energy. On the other hand, the dissipative force interaction results in the loss of the cantilever vibrational energy. In the constant amplitude FM-AFM mode a feedback loop keeps the oscillation amplitude constant. The energy dissipation caused by the tip-sample interaction in FM-AFM is manifested as an increase in the excitation amplitude. This dissipation can be quite large, anywhere from 0.1 to a few eV depending on the sample, the interaction area, and the environment,[12,13] and moreover can be imaged at a single molecular or even atomic scale.[12,14] In the context of molecular thin films, dissipation is thought to be related to the local mechanical properties of the sample.

Real world chemical and biological applications require operation in air or liquid environments. In the liquid environment, where meniscus forces are not present, the FM-AFM technique is being adopted.[15–19] In ambient conditions the presence of any native water layer limits the imaging resolution and resolution of the full range of the force interaction. Some FM-AFM experiments in air have also been presented.[20] Recently Sasahara *et al.* imaged oxygen-atom vacancies as depressions in oxygen atom rows in a controlled dry N_2 environment after back-filling of a UHV chamber.[21] Fukuma *et al.* also imaged a hydrophobic alkanethiol SAM with true-molecular resolution.[22] Hölscher *et al.* used the constant excitation FM-AFM method to quantify the force in ambient conditions valid for large cantilever oscillation amplitudes.[23,24] Using the related dynamic technique of amplitude modulation AFM (AM-AFM) with ~1 nm cantilever oscillation amplitudes in the attractive force regime, Anselmetti *et al.* reported single molecular resolution of a hexagonal packed intermediate protein layer.[25] By monitoring the Q-factor of the cantilever as a function of tip-sample distance an indication of the energy dissipation was provided. For realistic future applications including molecular sensors the constant amplitude FM-AFM technique should be important for molecular-scale investigations; the advantages of the technique make it useful for the imaging of soft and easily damaged samples without the high loading forces associated with contact mode AFM, while offering high spatial resolution and the possibility for single molecule sensing, and with the capability of distinguishing the conservative and dissipative force interaction. In this study we consider an FM-AFM experiment carried out in UHV and show comparable results in air. We discuss the important information that can be obtained with the technique in relation to a specific system of rotaxane molecules. This information includes qualitative imaging, high-resolution imaging, exact determination of the force irrespective of the oscillation amplitude, and quantitative energy dissipation imaging at different length scales.

Rotaxanes are molecules with two parts—the "thread" (a chain-like section with two bulky stoppers) and the macrocycle—that are mechanically interlocked but not covalently linked. The macrocycle is situated most of the time at stable low energy sites on the thread, where optimal noncovalent inter-component interactions are achieved. Relative

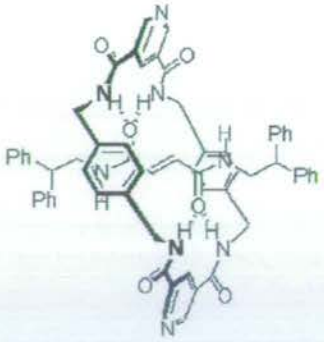

FIG. 1. Molecular structure of exopyridyl fumaramide rotaxane (EFR).

motion of the two components is driven by Brownian motion and can be controlled by altering the binding affinity between the macrocycle and different parts of the thread.[26] Since organic molecules show characteristic electrical and/or optical properties that are greatly sensitive to the molecular structure and conformation, rotaxane molecules have attracted a lot of attention as possible future molecular devices.[27–29] The molecules in this study are constructed from a fumaramide-containing thread, around which a benzylic amide macrocycle is assembled in a hydrogen-bond directed process.[30] In solution, the macrocycles exhibit continuous rotational ("pirouetting") motion with respect to the thread. Upon irradiation at 254 nm, the fumaramide (*trans*-double bond) unit is switched to a maleamide (*cis*-double bond) unit and in solution it is found that this results in an increase in the rate of macrocyle pirouetting by a factor of 10^6.[31] Other similar benzylic amide rotaxanes can have different kinds of switching behavior,[32–34] and from the results of the simple molecule used in this paper we may predict some of their behavior on a surface. In the solid-state such molecules are usually immobilized in a fixed conformation due to intermolecular hydrogen bonding.[35] The extra degrees of freedom associated with surface immobilization however, have been shown to permit sub-molecular motions and switching processes in a number of interlocked architectures.[36–45] Light switching of the properties of other types of organic thin films has also been demonstrated.[46–50] Using single-molecule force spectroscopy, where a long polymer chain was stretched between tip and sample, light-induced switching of an azobenzene polymer was directly observed on a molecular scale.[51] If we can develop dissipation imaging in ambient conditions on this model rotaxane system this technique may provide the opportunity to study externally stimulated sub-molecular motion at the local molecular level simultaneously with topography in this practical environment.

II. EXPERIMENT

The synthesis of fumaramide rotaxane molecules has been described elsewhere and the exopyridyl version used in this study (as shown in Fig. 1) was prepared by an analogous method.[30] Samples were prepared by dropping from acetone solution (HPLC grade, Aldrich). 0.005 mM solutions of exopyridyl fumaramide rotaxane were dropped (14 μl/cm^2) onto a freshly cleaved HOPG surface (ZYA quality, NT-MDT) to give approximately one monolayer surface coverage. To achieve homogeneous evaporation of the solvent the evaporation speed was reduced by reducing the temperature of the dropped solvent to approximately five degrees by refrigeration. Furthermore, during evaporation the sample was in a closed 500 cm^3 container in the presence of desiccant to prohibit condensation of water on the cold acetone.

FIG. 2. Meso-scale FM-AFM images of an EFR thin film on HOPG (a) in UHV before annealing (464 nm$\times$558 nm, cantilever: Nanosensors NCH, Δf=−15 Hz, a=8 nm), (b) in UHV after annealing (500 nm$\times$500 nm, cantilever: NCH, Δf=−20 Hz, a=8 nm), (c) in ambient conditions no annealing (500 nm$\times$500 nm, cantilever: Nanosensors EFM, Δf=−25 Hz, a=9.6 nm, Q=154).

A commercially available FM-AFM (JEOL JSPM-4500) with some modifications was used for UHV imaging (base pressure: About 1×10^{-7} Pa). The original frequency shift detector was replaced with a newly developed frequency modulation detector.[52] A highly doped n-Si cantilever (Nanosensors: NCH) with a resonance frequency of about 300 kHz and a nominal spring constant of 40 N/m was used for FM-AFM imaging. The Q factor measured under UHV conditions was about 30 000. After preparation the sample was immediately placed into the UHV chamber. For annealing, the sample was removed and annealed in air at 150 °C for two hours and re-introduced to the UHV chamber.

An Asylum MFP-3D with some modifications was used for imaging in ambient conditions, operated in FM-AFM mode with piezo activation or magnetically activated cantilevers (MAD-Mode).[53] In the latter method the lever is oscillated by the magnetic field of a current-carrying coil. Using the same Nanosensors NCH cantilevers as above a magnetic particle of NdFeB (with dimensions around 20 microns) was attached with epoxy to the end of the backside of the cantilever. After attachment the resonance of the lever was typically reduced to about 50 kHz. The Q-factor in ambient conditions was around 500. A home-built piezo tube scanner was used for high resolution imaging.

All measurements were performed in the constant frequency shift mode, where the negative frequency shift of the cantilever resonance frequency (Δf) induced by the tip-sample interaction was kept constant during FM-AFM imaging. The cantilever is vibrated at constant amplitude, where the vibration amplitude of the cantilever (a) was kept constant by adjusting the amplitude of a cantilever excitation signal A_{exc}. In this excitation mode, energy dissipation caused by the tip-sample interaction can be estimated from the additional increase of A_{exc}.[54] Thus, the dissipation image was obtained as a two-dimensional map of A_{exc}.

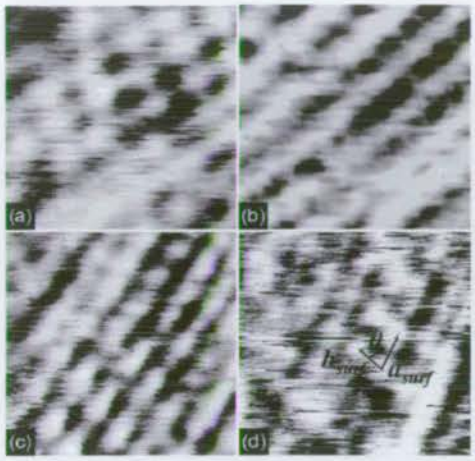

FIG. 3. Molecular-scale UHV FM-AFM images of an EFR thin film on HOPG. (a)–(c) Before annealing and (d) annealed sample, {(a): 9 nm×9 nm, $\Delta f=-150$ Hz, $a=6.5$ nm, (b): 9 nm×9 nm, $\Delta f=-150$ Hz, $a=6.5$ nm, (c): 9 nm×9 nm, $\Delta f=-170$ Hz, $a=6.5$ nm, (d): 9 nm×9 nm, $\Delta f=-180$ Hz, $a=5.9$ nm; measured lattice parameters: $a_{surf}=1.65$ nm±0.1 nm, $b_{surf}=1.35\pm0.1$ nm, $\theta=70°\pm2°$}.

III. RESULTS AND DISCUSSION

Figure 2(a) shows an FM-AFM image of a thin film of expyridyl fumaramide rotaxane on HOPG. The orientation of the domains according to the lattice direction of the substrate shows that the molecule grows epitaxially on graphite. After annealing [Fig. 2(b)] it can be seen that the domain edges are straight and that domains are more clearly defined. The increased uniformity of the surface indicates that the energy provided by the annealing process has resulted in rearrangement of the molecules in a lower energy configuration. Figure 2(c) demonstrates that the shape of the domains can also be evaluated by FM-AFM imaging in air.

Molecular-scale topographic images of the un-annealed sample are shown in Figs. 3(a)–3(c). Individual molecules in the rows can often be resolved, however, no periodic intermolecular distance is found along the rows (stripes in the image) and the rows are also unevenly spaced. The molecules are in a somewhat disordered nonequilibrium arrangement. In the case of the annealed sample [Fig. 3(d)], there is strong periodicity in both directions. This increase in long and short-range order is typical of the annealing process. Heating the sample gives the molecules the extra energy required to move from their local energy minimum and break up the nonequilibrium packing structure. In fact, the measured dimensions of $a_{surf}=1.65\pm0.1$ nm and $b_{surf}=1.35\pm0.1$ nm with $\theta=70°$ strongly suggests a commensurate molecular reconstruction of the form: $\begin{bmatrix} a_{surf} \\ b_{surf} \end{bmatrix}=M\begin{bmatrix} a \\ b \end{bmatrix}$, where $M=\begin{bmatrix} 7 & 0 \\ -1 & 6 \end{bmatrix}$ as illustrated in Fig. 4.

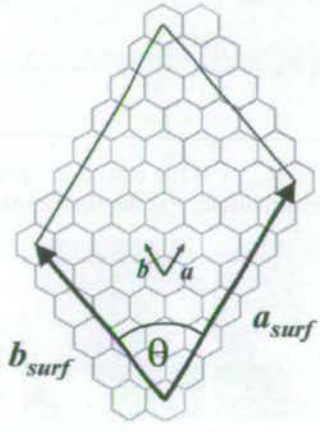

FIG. 4. Apparent equilibrium reconstruction of the EFR film on HOPG after annealing with parameters: $a_{surf}=1.65$ nm, $b_{surf}=1.37$, $\theta=68°$.

FIG. 5. Molecular-scale ambient FM-AFM topography image of EFR thin film on HOPG (70 nm×70 nm, cantilever: Nanosensors NCHR+magnet, $a=10.8$ nm, $\Delta f=-35$ Hz).

Strong intermolecular interactions in a closely packed film are restrictive to sub-molecular motion so it is not necessarily a good thing that the film is well ordered and it is useful that we are able to access the many nonequilibrium film-structures shown in Figs. 3(a)–3(c).

Figure 5 is a large image taken in ambient conditions, which shows clear molecular-scale features and has been chosen because it shows two neighboring domains and, therefore, true structure, as opposed to periodic noise. The

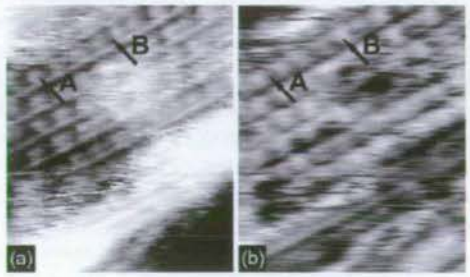

FIG. 6. Molecular-scale UHV FM-AFM images of an EFR thin film on HOPG. Simultaneous topography (a) and dissipation (b) images (23.2 nm×27.9 nm, cantilever: NCH, $\Delta f=-100$ Hz, $a=8.9$ nm).

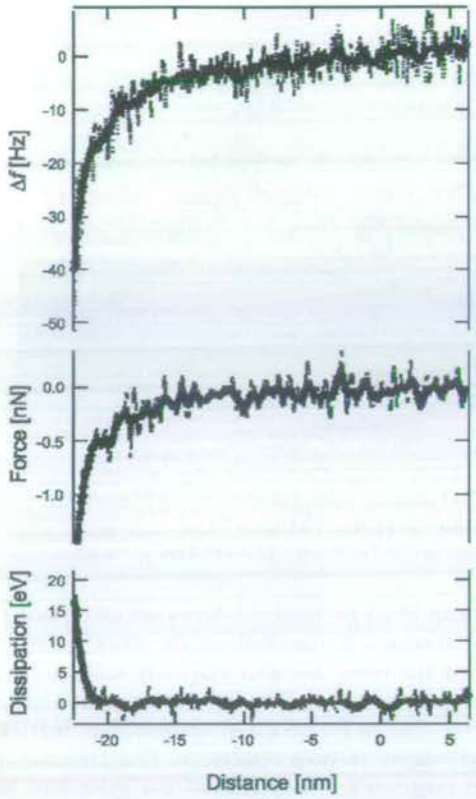

FIG. 7. Typical frequency, force and dissipation vs tip-sample distance curves in ambient conditions, dots: Raw data, line: Smoothed data (Cantilever: NCHR+magnet, $Q=510$, $a=8.9$ nm).

film structure dimensions are consistent with those measured in UHV for the un-annealed sample. Despite the lower Q-factor of the cantilever in air (500) compared to vacuum (~30 000), the presence of a liquid layer and contamination from long-chain hydrocarbons always present in ambient conditions, the resolution is still very high. The tip can move through the liquid layer while imaging the film, and any surface contamination must only be loosely bound and does not affect the imaging. The FM-AFM technique should thus be useful for the many kinds of study where high resolution is desirable.

The disordered or loose packing commonly found in organic thin films (and hence their stability against the tip-sample interaction force) has a strong influence on the contrast formation in energy dissipation images. Dissipation is increased on less ordered, less well-packed surfaces, both at the molecular scale and the meso scale.[55,56] Fukuma *et al.* showed that the contrasts are probably related to the number of molecules interacting with the tip—the more molecules interacting with the tip the greater the energy transfer; thus at the molecular scale the dissipation image shows inverted contrast relative to the topographic image.[7] Figure 6 shows a molecular-scale topographic image [Fig. 6(a)] of a nonequilibrium arrangement of the rotaxanes and the corresponding map of A_{exc} (dissipation image) [Fig. 6(b)], taken in UHV conditions. The dissipation image displays essentially inverted contrast with respect to the corresponding topographic

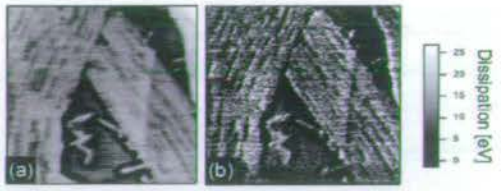

FIG. 8. Meso-scale ambient FM-AFM simultaneous topography (a) and dissipation (b) images of an EFR thin film on HOPG (500 nm×500 nm, $\Delta f=-26$ Hz, $a=11.8$ nm).

image. Arrows A and B mark the same points on each image. Position A corresponds to a tip position directly above a molecule. The internal motion of the molecule provides a coupling pathway and energy is dissipated into the sample. At position B the tip is over an intermolecular space and more than one molecule is involved in the dissipation process and thus the relative contrast is increased in these places. This explains the contrast inversion between the two image types. Images of A_{exc} such as these are easily converted to quantitative images of the average dissipated energy per oscillation.[54]

In ambient conditions the native layer of water adsorbates is often a problem for AFM techniques. "Contact mode," while allowing exact determination of the force, suffers from "jump-to-contact" instabilities (caused when the force gradient is higher than the cantilever stiffness) and adhesion instabilities (caused by a water meniscus between the tip and the local sample area). "Intermittent-contact mode" can overcome these obstacles with large amplitudes and stiffer cantilevers, however, unambiguous determination of the force is difficult with this technique.[57] The FM method with a constant amplitude has the same advantages but allows recovery of the force, which has been demonstrated in liquid and UHV environments.[58,59] Furthermore, in the FM method the attractive and repulsive force regions are easily distinguished which allows for exact control of the force. A portion of the attractive part of the force versus distance curve for a tip with a magnetically activated cantilever in ambient conditions is shown in Fig. 7. Force is calculated from the frequency shift using the method of Sader and Jarvis via the equation:

$$F(z)=2k\int_z^\infty \left(1+\frac{a^{1/2}}{8\sqrt{\pi(t-z)}}\right)\Omega(t)-\frac{a^{3/2}}{\sqrt{2(t-z)}}\frac{d\Omega(t)}{dt}dt \tag{1}$$

where $\Omega(z)=\Delta f(z)/f_{res}$, k is the cantilever spring constant, a is the oscillation amplitude, z is the tip-sample separation, f

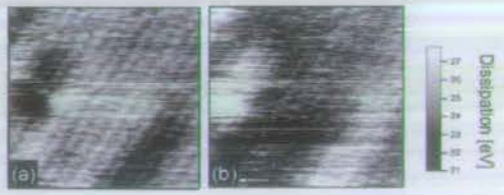

FIG. 9. Molecular-scale ambient FM-AFM simultaneous topography (a) and dissipation (b) images of an EFR thin film on HOPG (30 nm×30 nm, $\Delta f=-52$ Hz, $a=8.9$ nm).

is the resonance frequency of the cantilever, and f_{res} is the unperturbed resonance frequency.[10] This formula is valid for all oscillation amplitudes. The dissipation is calculated from the formula:

$$E = \frac{\pi k a^2}{Q}\left(\frac{A_{exc}}{A_{exc0}} - 1\right) \quad (2)$$

where Q is the quality factor, A_{exc} is the excitation voltage, and A_{exc0} is the excitation voltage away from the surface. Jump-to-contact instabilities do not occur and the retract curve (not shown) follows the approach exactly (i.e., no adhesion from the water layer occurs) and, therefore, we have shown that with this technique we can stably measure the force even in ambient conditions.

Figure 8(a) shows a 500 nm scan with the same cantilever with the corresponding quantified dissipation image [Fig. 8(b)] in units of eV per oscillation. The dissipated energy is greater on the rotaxane monolayer. The contrast in this large-scale image is essentially the same as in the height trace, the sub-molecular motion of the film providing more dissipation channels than the graphite. The molecular-scale dissipation contrast, however, [Fig. 9(b)], captured using the same tip is, by contrast, inverted with respect to the height trace [Fig. 9(a)]. In this image the presence of a defect in the film indicates that the image shows true structure. For the higher resolution image a smaller amplitude, but also a greater frequency shift set point (−52 Hz) is used. The optimum force is probably similar in both cases. Unstable imaging conditions occur if this force is exceeded, presumably because the tip enters the repulsive force region where the feedback polarity is reversed. The inversion of the dissipation image at the molecular scale compared to the meso-scale supports our proposed mechanism of increased dissipation when the number of energy transfer pathways is increased (by increased internal molecular motion), as opposed to a simple tip artefact. If this contrast difference were, for example, due to contact potential differences between graphite and the molecules, then this would imply that at a molecular scale the contrast would not be inverted as in Figs. 6 and 9, but would show similar contrast to topography—i.e., higher above the molecules and lower above the molecular spaces. Observation of increased molecular motion (and hence increased dissipation) as a result of externally induced molecular switching would seem possible, therefore, by dissipation imaging.

Observing switching of material properties of organic films is a specific potential usefulness of the FM-AFM technique in ambient conditions, especially if this is performed at the molecular level.

IV. CONCLUSIONS

We have demonstrated the stable imaging capabilities of the constant amplitude FM-AFM outside of UHV and the high resolution imaging of a soft organic film despite low Q-factor and the native water layer. Accurate determination of the interaction force was also achieved. The energy dissipation was quantitatively measured even at the molecular level, by which means induced sub-molecular motion may be observed in the future. These experiments help to demonstrate the increasing accessibility FM-AFM technique outside of UHV and the potential usefulness of the technique for the development of practical chemical and biological applications, which should help make this important technique more attractive to a wider audience.

ACKLOWLEDGMENT

This research was supported by Science Foundation Ireland Research Grant No. 01/PI.2/C033.

*Author to whom correspondence should be addressed. Email address: farrelaa@tcd.ie
†Email address: David.Leigh@ed.ac.uk

[1] F. J. Giessibl, Science **267**, 68 (1995).
[2] S. Kitamura and M. Iwatsuki, Jpn. J. Appl. Phys., Part 2 **34**, L145 (1995).
[3] M. Bammerlin and R. Luthi, Probe Microsc. **1**, 3 (1997).
[4] K. Kobayashi, H. Yamada, T. Horiuchi, and K. Matsushige, Appl. Surf. Sci. **140**, 281 (1999).
[5] T. Uchihashi, T. Ishida, M. Komiyama, M. Ashino, Y. Sugawara, W. Mizutani, K. Yokoyama, S. Morita, H. Tokumoto, and M. Ishikawa, Appl. Surf. Sci. **157**, 244 (2000).
[6] H. Onishi, A. Sasahara, H. Uetsuka, and T. Ishibashi, Appl. Surf. Sci. **188**, 257 (2002).
[7] T. Fukuma, K. Kobayashi, H. Yamada, and K. Matsushige, J. Appl. Phys. **95**, 4742 (2004).
[8] T. R. Albrecht, P. Grutter, D. Horne, and D. Rugar, J. Appl. Phys. **69**, 668 (1991).
[9] U. Durig, Appl. Phys. Lett. **75**, 433 (1999).
[10] J. E. Sader and S. P. Jarvis, Appl. Phys. Lett. **84**, 1801 (2004).
[11] J. E. Sader, T. Uchihashi, M. J. Higgins, A. Farrell, Y. Nakayama, and S. P. Jarvis, Nanotechnology **16**, S94 (2005).
[12] C. Loppacher, R. Bennewitz, O. Pfeiffer, M. Guggisberg, M. Bammerlin, S. Schär, V. Barwich, A. Baratoff, and E. Meyer, Phys. Rev. B **62**, 13674 (2000).
[13] T. Fukuma, K. Umeda, K. Kobayashi, H. Yamada, and K. Matsushige, Jpn. J. Appl. Phys., Part 1 **41**, 4903 (2002).
[14] C. Loppacher, M. Guggisberg, O. Pfeiffer, E. Meyer, M. Bammerlin, R. Lüthi, R. Schlittler, J. K. Gimzewski, H. Tang, and C. Joachim, Phys. Rev. Lett. **90**, 066107 (2003).
[15] S. P. Jarvis, T. Uchihashi, T. Ishida, H. Tokumoto, and Y. Nakayama, J. Phys. Chem. B **104**, 6091 (2000).
[16] R. Nishi, I. Houda, K. Kitano, Y. Sugawara, and S. Morita, Appl. Phys. A: Mater. Sci. Process. **72**, S93 (2001).
[17] M. Kageshima, H. Jensenius, M. Dienwiebel, Y. Nakayama, H. Tokumoto, S. P. Jarvis, and T. H. Oosterkamp, Appl. Phys. Lett. **188**, 440 (2002).
[18] H. Sekiguchi, T. Okajima, H. Arakawa, S. Maeda, A. Takashima, and A. Ikai, Appl. Surf. Sci. **210**, 61 (2003).
[19] T. Okajima and H. Tokumoto, Jpn. J. Appl. Phys., Part 1 **43**, 4634

(2004).
[20] K. Kobayashi, H. Yamada, and K. Matsushige, Appl. Surf. Sci. **188**, 430 (2002).
[21] A. Sasahara, S. Kitamura, H. Uetsuka, and H. Onishi, J. Phys. Chem. B **108**, 15735 (2004).
[22] T. Fukuma, T. Ichi, K. Kobayashi, H. Yamada, and K. Matsushige, Appl. Phys. Lett. **86**, 134103 (2005).
[23] H. Hölscher, B. Gotsmann, and A. Schirmeisen, Phys. Rev. B **68**, 153401 (2003).
[24] H. Hölscher and B. Anczykowski, Surf. Sci. **579**, 201 (2005).
[25] D. Anselmetti, M. Dreier, R. Lüthi, T. Richmond, E. Meyer, J. Frommer, and H.-J. Güntherodt, J. Vac. Sci. Technol. B **12**, 1500 (1994).
[26] *Molecular Catenanes, Rotaxanes and Knots*, edited by J.-P. Sauvage and C. Dietrich-Buchecker (Wiley-VCH, Weinheim, 1999).
[27] V. Balzani, A. Credi, F. M. Raymo, and J. F. Stoddart, Angew. Chem., Int. Ed. **39**, 3348 (2000).
[28] Special Issue on Molecular Machines: Acc. Chem. Res. **34**, 409 (2001).
[29] M. Venturi, A. Credi, and V. Balzani, *Molecular Devices and Machines-A Journey into the Nanoworld* (Wiley-VCH, Weinheim, 2003).
[30] F. G. Gatti, D. A. Leigh, S. A. Nepogodiev, A. M. Z. Slawin, S. J. Teat, and J. K. Y. Wong, J. Am. Chem. Soc. **123**, 5983 (2001).
[31] F. G. Gatti, S. Leòn, J. K. Y. Wong, G. Bottari, A. Altieri, M. A. Farran Morales, S. J. Teat, C. Frochot, D. A. Leigh, A. M. Brouwer, and F. Zerbetto, Proc. Natl. Acad. Sci. U.S.A. **100**, 10 (2003).
[32] A. Altieri, G. Bottari, F. Dehez, D. A. Leigh, J. K. Y. Wong, and F. Zerbetto, Angew. Chem., Int. Ed. **42**, 2296 (2003).
[33] A. Altieri, F. G. Gatti, E. R. Kay, D. A. Leigh, F. Paolucci, A. M. Z. Slawin, and J. K. Y. Wong, J. Am. Chem. Soc. **125**, 8644 (2003).
[34] D. A. Leigh and E. M. Pérez, Chem. Commun. (Cambridge) **2004**, 2262.
[35] F. Biscarini, M. Cavallini, D. A. Leigh, S. León, S. J. Teat, J. K. Y. Wong, and F. Zerbetto, J. Am. Chem. Soc. **124**, 225 (2002).
[36] T. Gase, D. Grando, P.-A. Chollet, F. Kajzar, A. Murphy, and D. A. Leigh, Adv. Mater. (Weinheim, Ger.) **11**, 1303 (1999).
[37] I. Willner, V. Pardo-Yissar, E. Katz, and K. T. Ranjit, J. Electroanal. Chem. **497**, 172 (2001).
[38] S. Chia, J. Cao, J. F. Stoddart, and J. I. Zink, Angew. Chem., Int. Ed. **40**, 2447 (2001).
[39] M. Cavallini, R. Lazzaroni, R. Zamboni, F. Biscarini, D. Timpel, F. Zerbetto, G. J. Clarkson, and D. A. Leigh, J. Phys. Chem. B **105**, 10826 (2001).
[40] B. Long, K. Nikitin, and D. Fitzmaurice, J. Am. Chem. Soc. **125**, 5152 (2003).
[41] B. Long, K. Nikitin, and D. Fitzmaurice, J. Am. Chem. Soc. **125**, 15490 (2003).
[42] H.-R. Tseng, D. Wu, N. X. Fang, X. Zhang, and J. F. Stoddart, Bandaoti Xuebao **5**, 111 (2004).
[43] T. Jun Huang, H.-R. Tseng, L. Sha, W. Lu, B. Brough, A. H. Flood, B.-D. Yu, P. C. Celestre, J. P. Chang, J. F. Stoddart, and C.-M. Ho, Nano Lett. **4**, 2065 (2004).
[44] E. Katz, L. Sheeney-Haj-Ichia, and I. Willner, Angew. Chem., Int. Ed. **43**, 3292 (2004).
[45] E. Katz, O. Lioubashevsky, and I. Willner, J. Am. Chem. Soc. **126**, 15520 (2004).
[46] K. Kobayashi, H. Yamada, K. Umeda, T. Horiuchi, S. Watanabe, T. Fujii, S. Hotta, and K. Matsushige, Appl. Phys. A: Mater. Sci. Process. **72**, S97 (2001).
[47] H. Yamada, T. Fukuma, K. Umeda, K. Kobayashi, and K. Matsushige, Appl. Surf. Sci. **188**, 391 (2002).
[48] K. Tamada, H. Akiyama, T.-X. Wei, and S.-A. Kim, Langmuir **19**, 2306 (2003).
[49] Z. Wang, M. J. Cook, A.-M. Nygård, and D. A. Russell, Langmuir **19**, 3779 (2003).
[50] Z. Wang, A.-M. Nygård, M. J. Cook, and D. A. Russell, Langmuir **20**, 5850 (2004).
[51] T. Hugel, N. B. Holland, A. Cattani, L. Moroder, M. Seitz, and H. E. Gaub, Science **296**, 1103 (2002).
[52] K. Kobayashi, H. Yamada, H. Itoh, T. Horiuchi, and K. Matsushige, Rev. Sci. Instrum. **72**, 4383 (2001).
[53] S. P. Jarvis, T. Ishida, T. Uchihashi, Y. Nakayama, and H. Tokumoto, Appl. Phys. A: Mater. Sci. Process. **72**, S129 (2001).
[54] B. Gotsmann, C. Seidel, B. Anczykowski, and H. Fuchs, Phys. Rev. B **60**, 11051 (1999).
[55] T. Ichii, T. Fukuma, K. Kobayashi, H. Yamada, and K. Matsushige, Appl. Surf. Sci. **210**, 99 (2003).
[56] T. Fukuma, T. Ichi, K. Kobayashi, H. Yamada, and K. Matsushige, J. Appl. Phys. **95**, 1222 (2004).
[57] R. García and R. Pérez, Surf. Sci. Rep. **47**, 197 (2002).
[58] M. A. Lantz, H. J. Hug, R. Horrmann, P. J. A. van Schendel, P. Kappenberger, S. Martin, A. Baratoff, and H.-J. Guntherodt, Science **291**, 2580 (2001).
[59] T. Uchihashi, M. J. Higgins, S. Yasuda, S. P. Jarvis, S. Akita, Y. Nakayama, and J. E. Sader, Appl. Phys. Lett. **85**, 3575 (2004).

Experimental and theoretical study of the adsorption of fumaramide [2]rotaxane on Au(111) and Ag(111) surfaces

Sandra M. Mendoza
Materials Science Centre, University of Groningen, Nijenborgh 4, 9747 AG Groningen, The Netherlands

Caroline M. Whelan[a)]
Laboratoire Interdisciplinaire de Spectroscopie Electronique, Facultés Universitaires Notre-Dame de la Paix, 61 Rue de Bruxelles, B-5000 Namur, Belgium

Jukka-Pekka Jalkanen and Francesco Zerbetto[b)]
Dipartimento di Chimica "G. Ciamician," Università degli Studi di Bologna, via F. Selmi 2, 40126 Bologna, Itaty

Francesco G. Gatti, Euan R. Kay, and David A. Leigh[c)]
School of Chemistry, The University of Edinburgh, Kings Buildings, Edinburgh EH9 3JJ, United Kingdom

Monika Lubomska and Petra Rudolf[d)]
Materials Science Centre, University of Groningen, Nijenborgh 4, 9747 AG Groningen, The Netherlands

(Received 14 July 2005; accepted 20 October 2005; published online 30 December 2005)

Thin films of fumaramide [2]rotaxane, a mechanically interlocked molecule composed of a macrocycle and a thread in a "bead and thread" configuration, were prepared by vapor deposition on both Ag(111) and Au(111) substrates. X-ray photoelectron spectroscopy (XPS) and high-resolution electron-energy-loss spectroscopy were used to characterize monolayer and bulklike multilayer films. XPS determination of the relative amounts of carbon, nitrogen, and oxygen indicates that the molecule adsorbs intact. On both metal surfaces, molecules in the first adsorbed layer show an additional component in the C 1*s* XPS line attributed to chemisorption via amide groups. Molecular-dynamics simulation indicates that the molecule orients two of its eight phenyl rings, one from the macrocycle and one from the thread, in a parallel bonding geometry with respect to the metal surfaces, leaving three amide groups very close to the substrate. In the case of fumaramide [2]rotaxane adsorption on Au(111), the presence of certain out-of-plane phenyl ring and Au–O vibrational modes points to such bonding and a preferential molecular orientation. The theoretical and experimental results imply that the three-dimensional intermolecular configuration permits chemisorption at low coverage to be driven by interactions between the three amide functions of fumaramide [2]rotaxane and the Ag(111) or Au(111) surface. © *2005 American Institute of Physics*. [DOI: 10.1063/1.2137694]

I. INTRODUCTION

Rotaxanes[1] are mechanically interlocked molecules in which one or more macrocycles are locked onto a molecular thread with bulky stoppers at both ends. The "mechanical bond" that holds the components of the molecule together is dynamic, and can therefore be used to modify a molecule's properties through external stimuli, as has been demonstrated using an electric field and light.[2–4] Hence, rotaxanes are considered as key elements for the development of nanoscale devices with mechanical effects in the macroscopic world. To date, most studies have focused on the behavior of such molecules in solution.[5–10] It is, however, through controlling their properties in the solid state that rotaxanes offer the greatest potential as versatile building blocks for the development of advanced materials.[10] Recent studies have shown that rotaxane thin films can be patterned in a controlled way at the nanoscale, an essential feature for information storage applications.[11] Rotaxanes have also been proposed as novel photonic molecules, useful for electronic and optical purposes.[3]

In the present work we investigate the nucleation and growth of fumaramide [2]rotaxane thin films on Ag(111) and Au(111) surfaces. The fumaramide [2]rotaxane comprises a benzylic amide macrocycle mechanically interlocked on a fumaramide thread.[5] Ag(111) and Au(111) substrates were chosen because for noble metals one expects that molecule-substrate interactions and molecule-molecule interactions are similarly strong so that one does not dominate the other.

This paper focuses on the characterization of fumaramide [2]rotaxane films with monolayer and bulklike coverages, prepared by sublimation in ultrahigh vacuum onto Ag(111) and Au(111) substrates and studied by x-ray photoelectron spectroscopy (XPS) and high-resolution electron-

[a)]Present address: IMEC, Kapeldreef 75, B-3001 Leuven, Belgium.
[b)]Author to whom correspondence should be addressed. Electronic mail: francesco.zerbetto@unibo.it
[c)]Author to whom correspondence should be addressed. Electronic mail: David.Leigh@ed.ac.uk
[d)]Author to whom correspondence should be addressed. Electronic mail: p.rudolf@rug.nl

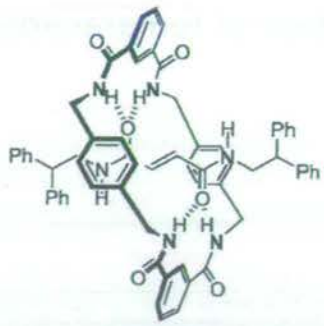

FIG. 1. Schematic drawing showing the chemical structure of fumaramide [2]rotaxane.

energy-loss spectroscopy (HREELS). Molecular-mechanics simulations were used to visualize the behavior and three-dimensional configuration of the adsorbed fumaramide [2]rotaxane.

II. EXPERIMENTAL DETAILS

The synthesis of fumaramide [2]rotaxane ([2]-(1,7,14,20-tetraaza-2,6,15,19-tetraoxo -3,5,9,12,16,18,22,25-tetrabenzocyclohexacosane)- (*E*)-(*N*,*N*′-bis(2′,2′-diphenyl -ethyl)-2′-butanediamide)rotaxane) has been described elsewhere.[5] The chemical structure is depicted in Fig. 1.

Ag substrates were prepared by vacuum sublimation onto freshly cleaved mica. The silver layer thickness was 400 nm as determined by a quartz microbalance mounted next to the growing film. The gold substrate was a Au(111) single crystal. Prior to fumaramide [2]rotaxane deposition, the Ag or Au substrate was cleaned in an UHV system (base pressure of 2×10^{-10} Torr) by cycles of argon ion bombardment and annealing until no contaminants could be detected by XPS or HREELS.

Fumaramide [2]rotaxane was sublimed *in situ* onto the substrates kept at 300 K using a custom-built cell which consisted of a Pyrex crucible topped with a 2 mm stainless-steel collimator. The crucible was heated resistively to 470 K with the temperature being measured by a chromel-alumel junction fixed at the tube exit. Exposures were monitored using an uncalibrated Bayard-Alpert ionization gauge. The organic film thickness was such that any interfacial interaction with the substrate is obscured, to the extent that the Ag 3*d* or Au 4*f* signal was totally attenuated, and hence we can consider that the photoemission features observed are representative of bulklike solid-state samples. In order to prepare a monolayer film, we first deposited a bulklike film and then annealed it *in situ* to induce desorption of multilayers, leaving a chemisorbed monolayer. This method has been used elsewhere for similar molecules.[12–14]

The XPS measurements were performed in two different laboratories. The films deposited on silver were analyzed using an X-probe Surface Science Laboratories photoelectron spectrometer with an Al $K\alpha$ monochromatic x-ray source ($h\nu$=1486.6 eV). The energy resolution was set to 1.1 eV and the photoelectron take-off angle was 37°. The films deposited on gold were analyzed using a Scienta ESCA 300 photoelectron spectrometer, also with an Al $K\alpha$ monochromatic x-ray source. The energy resolution was set to 0.8 eV and the photoelectron take-off angle was 90°. The binding energies were referenced to the Ag 3*d* or Au 4*f* core levels. The base pressure in the spectrometers was in the low 10^{-10} Torr range. Spectral analysis included a Shirley background subtraction for C 1*s*, linear background subtraction for N 1*s* and O 1*s* (see endnote[15]), and peak separation using mixed Gaussian-Lorentzian functions in a least-squares curve-fitting program (WINSPEC) developed at Laboratoire Interdisciplinaire de Spectroscopie Electronique, Facultés Universitaires Notre-Dame de la Paix, Belgium. The photoemission peak areas of each element, used to estimate the amount of each species on the surface, were normalized by the sensitivity factors of each element, including analyzer transmission. Three different points of each sample were analyzed to check for homogeneity. Within the error bars quoted, we found the same atomic percentages for all points of the same sample and therefore concluded that all samples can be considered homogeneous.

HREELS data were collected with a Riber Sedra spectrometer equipped with sample preparation and main analyser chambers operated at base pressures in the low 10^{-9} and 10^{-10} Torr, respectively. The analysis chamber consisted of 180° hemispherical monochromator and analyzer ensemble described in more detail elsewhere.[16] HREELS spectra were recorded with an incident beam energy of 6.0 eV and collected in specular ($\theta_i=\theta_r=45°$) scattering geometry. The spectra presented here were normalized to the specular elastic peak intensity. The instrumental resolution, defined by the full width at half maximum (FWHM) of the elastic peak, was 13 meV for these measurements.

For the molecular-dynamics simulations, we used the same model we employed recently to investigate a variety of other molecular adsorbates on Au(111), where the experimental adsorption energies were reproduced within 1 kcal mol^{-1}. Examples of past applications include (i) the adsorption of alkanes and 1-alkenes on Au(111),[17] where the adsorption energies of short chains, up to C_{10}, were reproduced with an average error of less than 1 kcal mol^{-1}, and the unexpected transition to disorder that occurs for the deposition of alkyl chains between 18 and 26 carbon atoms was explained; (ii) the apparent symmetry breaking of the present macrocyle on the Au surface;[12] (iii) the substitution kinetics of thiols on self-assembled monolayers;[18] (iv) the existence of two surface reconstructions for C_{60} adsorbed on Au(110),[19] and the adsorption and dynamics of DNA bases on Au(111) where the energies of adsorption were also within 1 kcal mol^{-1} from the experimental values.[20] The model does not require *a priori* definitions of bonds between the atoms of the molecules and those of the metal. The molecules are therefore free to drift on the surface, which can, in turn, reconstruct. The relative simplicity of the approach, which, however, requires the inversion of large matrices, allows the investigation of rather large unit cells. Under the same conditions, the use of modern density-functional-theory-based programs would be too demanding for the present computer hardware, especially for applications where large unit cells are necessary in conjunction with long dynamic runs.

TABLE I. Comparison between the experimental atomic percentages derived from the photoemission peak areas of fumaramide [2]rotaxane and the theoretical values calculated from the stoichiometry of the rotaxane.

Atomic (%)	Theoretical stoichiometry	Multilayer	Monolayer on Au	Monolayer on Ag
Carbon	84.2	84.8±1.7	84.3±1.7	83.1±1.7
Oxygen	7.9	7.5±0.8	7.2±0.8	8.2±0.8
Nitrogen	7.9	7.7±0.8	8.5±0.8	8.7±0.8

The calculations were performed for a single molecule of rotaxane deposited on Au(111) and Ag(111) surfaces. Its structure was minimized using the TINKER molecular-mechanics/dynamics software package.[21–23] The embedded atom model was used in describing the metal-metal interactions, a MM3 force field for the organic-organic part, and a modified Morse potential [Eq. (1)] in the description of metal-organic interactions.

$$U(r_{ij}) = -\epsilon^*(1-\{1-\exp[-A(r_{ij}-r_{ij}^*)]\}^2). \quad (1)$$

In addition, the charge equilibration scheme of Rappe and Goddard[21] was applied throughout the whole system. This method can be used to study the evolution of partial charges when the chemical environment or molecular geometry changes. The metal-organic interaction model was calibrated to produce experimental desorption geometries and energies of small organic fragments consisting of similar chemical groups that can be found in fumaramide [2]rotaxane. A (111) metal surface model consisting of five layers of 20×20 atoms was used and the lowest layer of metal atoms was kept fixed during the calculations. The top four layers of the surface model were allowed to relax or reconstruct to achieve the lowest energy. Details of the Ag-organic adsorption model will be discussed elsewhere.[24]

III. RESULTS AND DISCUSSION

A. X-ray photoelectron spectroscopy

Although fumaramide [2]rotaxane is stable at room temperature in air,[5] it is important to verify that the molecule remains intact when sublimed in vacuum. Photoemission spectra of the C 1*s*, O 1*s*, N 1*s*, Au 4*f*, and Ag 3*d* regions were measured for both monolayer and multilayer rotaxane films. In the case of C 1*s*, O 1*s*, and N 1*s* core levels, we observed binding energies and line shapes consistent with the chemical structure and the stoichiometry expected if fumaramide [2]rotaxane adsorbs intact. A quantitative analysis of the fumaramide [2]rotaxane XPS spectra allows us to determine the amount of C, N, and O (excluding hydrogen, which cannot be detected by XPS) on the surface from the photoemission peak area of each element. The error on the photoemission peak areas was estimated depending on the signal/noise ratio in the spectrum for each element. The carbon signal is better defined; thus the error was found to be 2%. The nitrogen and oxygen signals are weaker, producing noisier spectra, and therefore a more substantial error of 10% was estimated in the peak area. The experimental data presented in Table I show good agreement with theoretically calculated values. Hence, we conclude that fumaramide [2]rotaxane remains intact following sublimation in vacuum.

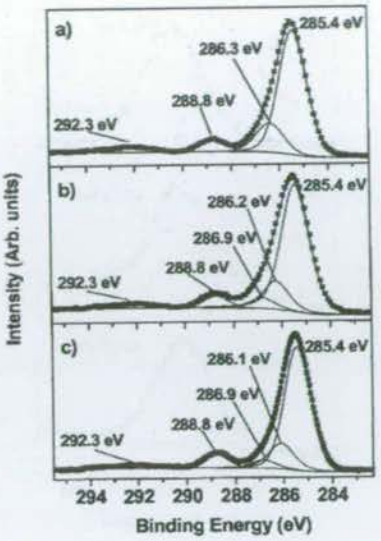

FIG. 2. X-ray photoemission spectra of the C 1*s* core levels for: a fumaramide [2]rotaxane (a) multilayer on Ag(111), (b) monolayer on Ag(111), and (c) monolayer on Au(111). Raw data (■) and fit to the experimental data (—).

We also checked the stability of the fumaramide [2]rotaxane upon exposure to the x-ray beam and the secondary electrons produced by photoemission in the underlying metal. Upon monitoring the line shape and relative intensity of the C 1*s*, N 1*s*, and O 1*s* core levels as a function of irradiation time, we found no evidence of a charging effect or structural degradation.

Figure 2 shows the C 1*s* photoemission lines and their mathematical reconstruction for a fumaramide [2]rotaxane multilayer on Ag(111), a monolayer on Ag(111) and a monolayer on Au(111). While rigorously there are sixteen chemically distinct carbon environments in the fumaramide [2]rotaxane, in practice XPS may not distinguish between the various types of phenyl ring carbon. Hence, the mathematical decomposition procedure consists of fitting a minimum number of peaks consistent with the raw data and the molecular structure of the adsorbate with the simplification of assuming equivalent aromatic carbon atoms. In Fig. 2(a), the fit was carried out assuming a molecule with three distinct chemically shifted C 1*s* core-level emissions occurring at 285.4, 286.3, and 288.8 eV attributed to the aromatic, aliphatic, and carbonyl components. The shake-up structure associated with π-π^* transitions of the phenyl rings can be observed at 292.3 eV and it represents around 5% of the C 1*s* signal originated by the phenyl rings, in agreement with the data found for compounds with a similar chemical structure.[25] The area ratio for the three distinct components is ~2:3:15, which is in agreement with the stoichiometry of the molecule. The 1.1 eV binding-energy shift relative to benzene (284.3 eV) (Ref. 26) is understandable given that 17% of the phenyl ring carbon are bound to CH_2NH or NHCO moieties which themselves display C 1*s* binding energies well within the range reported in literature.[25,27]

Comparing the multilayer spectrum with the monolayer

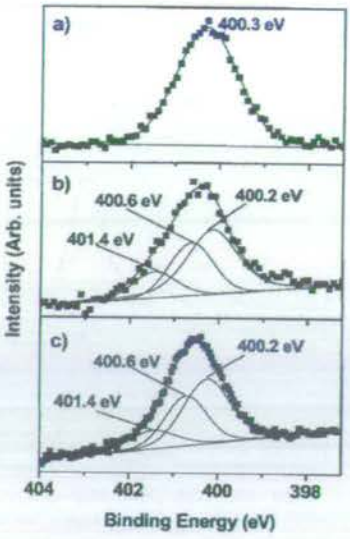

FIG. 3. X-ray photoemission spectra of the N 1*s* core levels for: a fumaramide [2]rotaxane (a) multilayer on Ag(111), (b) monolayer on Ag(111), and (c) monolayer on Au(111). Raw data (■) and fit to the experimental data (—).

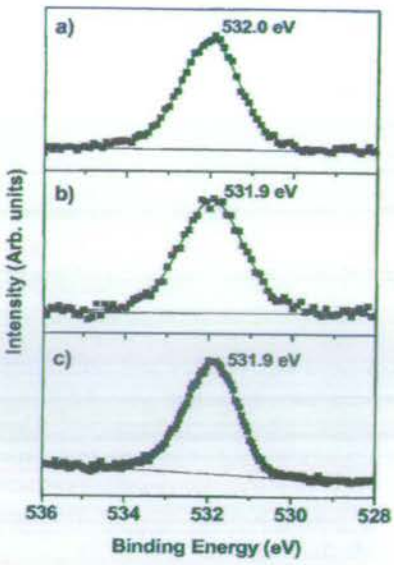

FIG. 4. X-ray photoemission spectra of the O 1*s* core levels for: a fumaramide [2]rotaxane (a) multilayer on Ag(111), (b) monolayer on Ag(111), and (c) monolayer on Au(111). Raw data (■) and fit to the experimental data (—).

spectra in Figs. 2(a) and 2(b), an additional feature can be distinguished at 286.9 eV. Taking into account the area ratio of the C 1*s* components (~1:1:3:15), the stoichiometry of fumaramide [2]rotaxane and previous studies,[12] we conclude that the carbonyl contribution splits into two peaks at 288.8 and 286.9 eV, suggesting that three amide groups interact with the substrate. Thus, the additional component is reasonably assigned to the carbonyl group involved in Ag–O or Au–O bonding, in agreement with the molecular rearrangement found by the molecular-dynamics simulations (see below). Chemisorption of the oxygen atom to the substrate surface gives rise to charge redistribution in the amide function and, in particular, alters the amount of electronic charge contributed to the C=O bond. The presence of the π-π^* shake-up transition at 292.3 eV indicates that the interfacial bonding does not disrupt the electron conjugation of the phenyl rings; hence, any interactions between the surface and the aromatic groups are weak. There is no difference between the C 1*s* core level of the monolayer deposited on Au(111) and the one deposited on Ag(111).

In Fig. 3(a) we present the N 1*s* photoemission line for a multilayer film of fumaramide [2]rotaxane on Ag. The symmetric peak is centered at 400.3 eV and is therefore shifted by 0.5 eV to higher binding energy relative to the reference moiety CH_2CONH (399.8 eV).[26,27] Presumably, this is a consequence of additional bonding to CH_2 and aromatic groups and perhaps, to a lesser extent, of the involvement in intermolecular hydrogen bonding interactions. Again XPS cannot distinguish between all the different types of nitrogen present in the N 1*s* spectra; however, their existence is reflected in the FWHM of 1.6 eV, which is larger than the experimental resolution (1.1 eV). Figures 3(b) and 3(c) show the N 1*s* core-level region for the fumaramide [2]rotaxane monolayer on Ag(111) and on Au(111), respectively. Closer inspection reveals an asymmetry in the N 1*s* region associated with the amide function. Decomposition of the raw data suggests that the N 1*s* signal of the monolayer films could be fitted by two peaks occurring at 400.3 and 401.4 eV (not shown). However, the peak at 400.3 eV obtained in this way is very broad (~1.4–1.3 eV). Thus, we tried to fit the N 1*s* with three components, as shown in the figure, with maxima at 400.2, 400.6, and 401.4 eV. The area ratio of the three components in both monolayers is 3:2:1. This is in agreement with the three-dimensional molecular configuration that arises from the simulations of fumaramide [2]rotaxane adsorbed on the substrate (see discussion below) and allows us to assign the three components with confidence. The peak at 400.2 eV has almost the same binding energy found for the multilayer film and corresponds to unperturbed amide functions. Indeed, fumaramide [2]rotaxane presents three amide groups located far from the substrate, two from the macrocycle and one from the thread. The other two N 1*s* components correspond to amide groups in close proximity with the substrate, and their difference in chemical shift originates from hydrogen bonds that produce shifts to higher binding energies:[28] the spectral feature at 400.6 eV can be attributed to amide groups close to the substrate, one from the macrocycle and one from the thread, which are not involved in hydrogen bonds, and the component at higher binding energy (401.4 eV) corresponds to an amide group from the macrocycle which does form a hydrogen bond.

The O 1*s* core-level spectra of monolayer and multilayer fumaramide [2]rotaxane coverages on Au(111) and Ag(111) are presented in Fig. 4. The multilayer spectrum [Fig. 4(a)] presents a maximum at 532.0 eV, and its FWHM of 1.6 eV, larger than the experimental resolution, reflects the presence of oxygen atoms in different chemical environments. The symmetrical shape of the peak does not allow the decomposition of the O 1*s* line shape with confidence. The results for a monolayer on Ag [Fig. 4(a)] and on Au [Fig. 4(b)] are very similar: both monolayer spectra are centered at 531.9 eV and

their FWHM are about 10% larger than that for the multilayer spectrum collected with the same experimental resolution. The latter indicates greater differences in chemical environment for oxygen in the monolayer than in the multilayer. However, from XPS analysis and in contrast with HREELS data discussed below, there is no clear evidence for oxygen interaction with the substrate. Since the entire amide group would feel the loss of charge, it is not possible to discriminate between the situation where only the carbonyl group is bound to Ag or Au and the situation where both oxygen and nitrogen interact with the substrate via their lone pairs.[13] In fact, in the first case the bonding involves probably the lone pairs of the oxygen and the empty orbital of the metallic surface as seen for the adsorption of acetone on Pt(111).[29]

B. Molecular-dynamics simulations

The static picture given by the geometry optimization is modified when the effect of temperature is included. Indeed, even short-time molecular-dynamics (MD) simulations (5 ps) for fumaramide [2]rotaxane on both Au(111) and Ag(111) show that the largest changes on partial charges of atoms occur on carbonyl oxygens, on the first-layer metal atoms directly below them and on the hydrogen atoms contributing to the intramolecular hydrogen bonds. On both surfaces, the carbonyl oxygens gain electron density from the surface and become more negative, whereas the closest metal atoms show a loss of electrons. In all cases, the average charge changes on the atoms of the rotaxane are less than $0.1e$, including the hydrogens involved in hydrogen bonds between the thread and the macrocycle. The metal charge changes seem to be of equal magnitude on both surfaces, ranging from $-0.06e$ to $0.115e$ and showing only negligible differences between Ag and Au. The "footprint" of the rotaxane, i.e., how the charge is distributed among the surface atoms, however, is different. On Ag(111), most of the first-layer surface atoms are positively charged, whereas on Au(111) negatively charged metal atoms are also observed. This leads to a smaller electric field on Au(111) than on Ag(111), which was recently found to be in good accordance with surface-enhanced second-harmonic generation (SHG) measurements. The details of this experiment can be found in the work of Arfaoui *et al.*[30] In this method the system is bombarded with a Nd:YAG (yttrium aluminum garnet) laser, and frequencies twice the original radiation can be observed due to a lack of symmetry on the surface. Electrical properties such as the field strength and the $\chi^{(2)}(-2\omega;\omega,\omega)$ susceptibility close to the surface can be calculated. The charges of the molecular model system, obtained with the method described in Sec. II, were used to calculate the electric field with the Poisson-Boltzmann algorithms in the DELPHI4 program.[31,32] This approach yielded an electric field of ~15 MV/cm for silver and ~7 MV/cm for gold. For silver, this leads to a $\chi^{(2)}(-2\omega;\omega,\omega)$ susceptibility of 23.4 pm/V and is in good agreement with the experimental value of 24.2 pm/V. The resulting field is inhomogeneous, reflecting the charge distribution on the surface atoms. The field is strongest on top of the metal atoms that are directly below

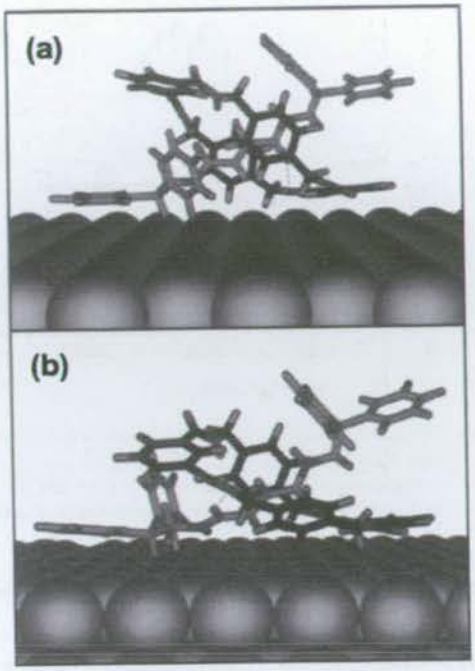

FIG. 5. The average structure of fumaramide [2]rotaxane on (a) Ag(111) and (b) Au(111). The structures were obtained by averaging atom locations of a 5 ps molecular-dynamics run at 298 K. The average structure from the MD runs resembles a collapsed letter X. Color code: carbon=green/black, nitrogen=blue, oxygen=red, and hydrogen=gray.

the carbonyl groups of the rotaxane, and it is unlikely that this feature is strongly dependent on adsorption coverage since it would require a close proximity of carbonyl groups of two adjacent fumaramide [2]rotaxane molecules on the surface. This is hardly the case due to lateral repulsion between the molecules. According to the model, the binding energy of fumaramide [2]rotaxane on Ag(111) is roughly 59 kcal mol^{-1} compared with 86 kcal mol^{-1} on Au(111). The shortest surface normal to the closest nitrogen atom on the fumaramide [2]rotaxane is 2.89 Å, and the benzene rings are 2.7–2.8 Å above the Ag(111) surface. The corresponding distances on Au(111) are 2.76 and 2.8 Å. The fumaramide [2]rotaxane orients itself in such a way that there are two or three benzene rings parallel to the surface. The comparison between the optimized structure and the MD simulations reveal that on Ag(111), one of the benzene rings of the macrocycle and one on the thread are parallel to the surface, as shown in Fig. 5(a).This can also be observed on Au(111) where, in addition to the aromatic ring on the thread, there are two benzene rings on the macrocycle that are almost parallel to the surface [Fig. 5(b)]. The macrocycle prefers to lie close to the surface, collapsing the X-like orientation of the molecule that is observed during the geometry optimization. The orientation of the rings is in accordance with the HREELS measurements (discussed below), suggesting that some of the rings are parallel to the surface. These figures also show that there are three amide groups close to the (111) surface, but the charge changes on nitrogen atoms are negligible ($|\Delta q| < 0.01e$). A metal surface reconstruction at 298 K was not observed when averaging the movement of atoms undergoing thermal motion.

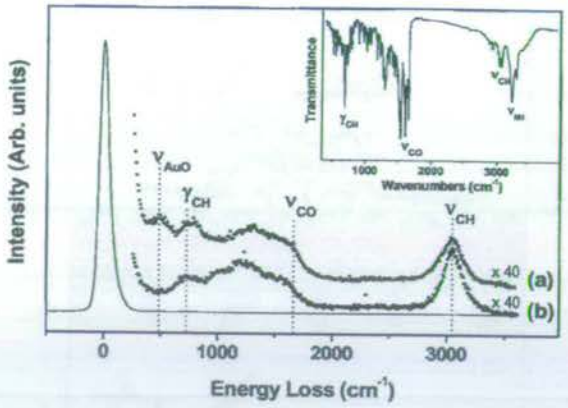

FIG. 6. HREELS spectra collected in specular scattering geometry ($\theta_i = \theta_r = 45°$) at a primary beam energy of 6.0 eV from fumaramide [2]rotaxane monolayer (a) and multilayer (b) adsorbed on Au(111) at 300 K. FWHM =13 meV. Inset: solid-state infrared spectrum of fumaramide [2]rotaxane.

C. High-resolution electron-energy-loss spectroscopy

Since the results obtained by XPS and molecular-mechanics simulations are very similar for both systems, fumaramide [2]rotaxane deposited on Au(111) and on Ag(111), we have chosen to study only one of them by HREELS. Figure 6 shows the HREELS data from monolayer (a) and multilayer (b) fumaramide [2]rotaxane films adsorbed on Au(111). The solid-state infrared data is presented as an inset for comparison. Previous HREELS studies of benzylic amide macrocycle[33] and benzylic amide [2]catenane adsorbed on Au(111)[34] and infrared reflection absorption spectroscopy data for benzylic amide [2]catenane adsorbed on Au(111)[35] are also taken into account for the assignment of the energy losses.

The expected main vibrational bands can be recognized in the monolayer spectrum. Bands at 730 and 3050 cm^{-1} signal the presence of aliphatic and aromatic groups. The first band is unambiguously assigned to out-of-plane C–H deformations (γ_{CH}) of the phenyl rings, while the second one corresponds to C–H in-plane stretching (ν_{CH}). Additionally, there is a complex group of unresolved low-intensity bands extending from 800 to 1600 cm^{-1} that originate from C–H in-plane bending, ring breathing, and stretching vibrations. Of particular interest in the assignment of adsorbate-substrate bonding is the clearly resolved peak superimposed on the tailing elastic peak at 480 cm^{-1}. This band is attributed to a Au–O stretching mode (ν_{AuO}) and can be only explained by the chemisorption of the rotaxane on the Au surface via amide functions, as already inferred from XPS results. A frustrated z transition, i.e., vibration of the entire molecule against the surface, would also appear in this region. However, such an energy loss is usually observed with low intensity, and hence the band at 480 cm^{-1} is assigned predominantly to Au–O stretching, in agreement with previous studies.[36,37] The relative intensities of the γ_{CH} and ν_{AuO} bands (compared with the ν_{CH} band) decrease at higher coverage, consistent with the increased disorder and the absence of Au–O bonding in the multilayer film. The N–H stretching mode (~3330 cm^{-1})[38,39] is not detected in monolayer and multilayer spectra. The absence of this band is expected, given that its predicted intensity is very low and occurs close to the ν_{CH} region.[35,40,41]

Information concerning the molecular orientation of the rotaxane with respect to the substrate surface can be achieved by applying the metal surface selection rule (MSSR) in specular scattering geometry. This selection rule specifies that only those vibrations with a component of the dipole moment change normal to the surface may be detected.[42] In a detailed HREELS study of fumaramide [2]rotaxane adsorption on Au(111) from submonolayer to multilayer coverages that will be reported in detail elsewhere,[43] we could identify the γ_{CH}, ν_{CH}, and ν_{AuO} bands as having strong normal dipole components, evidenced by a significant decrease in intensity in measuring in off-specular scattering geometry. For the monolayer coverage, of relevance to this present report, the γ_{CH} and ν_{AuO} bands disappear in the off-specular measuring mode, implying a preferred molecular orientation of phenyl rings and Au–O bonding via the carbonyl moieties of the amide functionalities. The fact that the out-of-pane γ_{CH} band, which has its dipole moment perpendicular to the phenyl ring and hence should be maximum for phenyl rings parallel to the surface, is observed indicates that at least some of the phenyl rings are oriented parallel to the Au(111) surface in agreement with the molecular-mechanics simulation results. In such an adsorption geometry, it is understandable that the carbonyl moieties can bond to the substrate, thus explaining the observation of the ν_{AuO} band in the monolayer spectrum.

IV. CONCLUSIONS

The present study shows that it is possible to sublime fumaramide [2]rotaxane without decomposition. The C 1*s* photoemission line of monolayer films reveals that fumaramide [2]rotaxane chemisorbs via three amide functions on Ag(111) and Au(111). XPS results are consistent with the picture proposed by theoretical simulations showing that, on Au(111) and Ag(111) surfaces, fumaramide [2]rotaxane prefers to orient the macrocycle part of the molecule as close to the surface as possible, leading to a "collapsed X-like" structure. According to the molecular-dynamics simulations, fumaramide [2]rotaxane adopts a three-dimensional conformation where two phenyl rings are parallel to the substrate and three amide groups are within bonding distance of it. From HREELS characterization of fumaramide [2]rotaxane adsorption on Au(111), monolayer chemisorption via carbonyl groups of the amide moieties is confirmed by the presence of the Au–O stretching vibration. Furthermore, by comparison of specular and off-specular intensities for out-of-plane C–H deformations, an orientation of the rotaxane with some of the phenyl rings lying parallel to the substrate is revealed.

ACKNOWLEDGMENTS

This work has been carried out within the DRUM TMR and EMMMA RT networks supported by the European Commission, Contracts No. FMRX-CT97-0097 and No. HPRN-CT2002-00168, respectively. Additional support was provided by the Dutch Foundation for Fundamental Research on

Matter (FOM) and the Breedtestrategie program of the University of Groningen.

[1] *Molecular Catenanes, Rotaxanes and Knots*, edited by J.-P. Sauvage and C. Dietrich-Buchecker (Wiley-VCH, Weinheim, 1999).
[2] J.-P. Collin, D. Jouvenot, M. Koizumi, and J.-P. Sauvage, Eur. J. Inorg. Chem. **10**, 1850 (2005).
[3] V. Bermudez, N. Capron, T. Gase, F. G. Gatti, F. Kajzar, D. A. Leigh, F. Zerbetto, and S. Zhang, Nature (London) **406**, 608 (2000).
[4] D.-H. Qu, Q.-C. Wang, J. Ren, and H. Tian, Org. Lett. **6**, 2085 (2004).
[5] F. G. Gatti, D. A. Leigh, S. A. Nepogodiev, A. M. Z. Slawin, S. J. Teat, and J. K. Y. Wong, J. Am. Chem. Soc. **123**, 5983 (2001).
[6] A. M. Brouwer, C. Frochot, F. G. Gatti, D. A. Leigh, L. Mottier, F. Paolucci, S. Roffia, and G. W. H. Wurpel, Science **291**, 2114 (2001).
[7] F. G. Gatti, S. León, J. K. Y. Wong, G. Bottari, A. Altieri, M. A. Farran Morales, S. J. Teat, C. Frochot, D. A. Leigh, and A. M. Brouwer, Proc. Natl. Acad. Sci. U.S.A. **100**, 10 (2003).
[8] A. Altieri, G. Bottari, F. Dehez, D. A. Leigh, J. K. Y. Wong, and F. Zerbetto, Angew. Chem., Int. Ed. **42**, 2296 (2003).
[9] C. M. Keaveney and D. A. Leigh, Angew. Chem., Int. Ed. **43**, 1222 (2004).
[10] V. Balzani, A. Credi, F. M. Raymo, and J. F. Stoddart, Angew. Chem., Int. Ed. **39**, 3348 (2000).
[11] M. Cavallini, F. Biscarini, S. León, F. Zerbetto, G. Bottari, and D. A. Leigh, Science **299**, 531 (2003).
[12] C. M. Whelan, F. Cecchet, R. Baxter, F. Zerbetto, G. J. Clarkson, D. A. Leigh, and P. Rudolf, J. Phys. Chem. B **106**, 8739 (2002).
[13] C.-A. Fustin, R. Gouttebaron, C. De Nadaï, R. Caudano, P. Rudolf, F. Zerbetto, and D. A. Leigh, Surf. Sci. **474**, 37 (2001).
[14] J. W. Ponder and F. J. Richards, J. Comput. Chem. **8**, 1016 (1987).
[15] The Shirley background could not be applied to the O 1*s* and N 1*s* signals of the monolayer spectra because on gold the O 1*s* peak appears at the onset of the Au 4*p* line and the N 1*s* line is situated on the secondary electron background of the Au 4*d* signal, while on silver the N 1*s* is affected by the secondary electrons of the Ag 3*d* peaks and the plasmon shake-up.
[16] P. A. Thiry, J.-J. Pireaux, and R. Caudano, Phys. Mag. **4**, 35 (1981).
[17] R. Baxter, G. Teobaldi, and F. Zerbetto, Langmuir **19**, 7335 (2003).
[18] M. Montalti, L. Prodi, N. Zaccheroni, R. J. Baxter, G. Teobaldi, and F. Zerbetto, Langmuir **19**, 5172 (2003).
[19] R. J. Baxter, P. Rudolf, G. Teobaldi, and F. Zerbetto, ChemPhysChem **5**, 245 (2004).
[20] S. Rapino and F. Zerbetto, Langmuir **21**, 2512 (2005).
[21] A. K. Rappe and W. A. Goddard III, J. Phys. Chem. **95**, 3358 (1991).
[22] C. Kundrot, J. W. Ponder, and F. J. Richards, J. Comput. Chem. **12**, 402 (1991).
[23] M. J. Dudek and J. W. Ponder, J. Comput. Chem. **16**, 791 (1995).
[24] J.-P. Jalkanen *et al.* (unpublished).
[25] G. Beamson and D. Briggs, *High-Resolution XPS of Organic Polymers-The Scienta ESCA300 Database* (Wiley, Chichester, 1992).
[26] J. Riga, J.-J. Pireaux, and J. Verbist, Mol. Phys. **34**, 131 (1977).
[27] J. K. Moulder, W. F. Stickle, P. E. Sobol, and K. D. Bomben, *Handbook of X-Ray Photoelectron Spectroscopy* (Physical Electronics, Eden Prairie, Minnesota, 1995).
[28] M. J. Ariza, E. Rodríguez-Castellón, R. Rico, J. Benavente, M. Muñoz, and M. Oleinikova, J. Colloid Interface Sci. **226**, 151 (2000).
[29] N. R. Avery, A. B. Anton, B. H. Toby, and W. H. Weinberg, J. Electron Spectrosc. Relat. Phenom. **29**, 233 (1983).
[30] I. Arfaoui, V. Bermudez, C. De Nadaï *et al.*, Proc. SPIE **5724**, 139 (2005).
[31] W. Rocchia, E. Alexoy, and B. Honig, J. Phys. Chem. B **105**, 6507 (2001).
[32] W. Rocchia, S. Sridharan, A. Nicholls, E. Alexoy, A. Chiabrera, and B. Honig, J. Comput. Chem. **23**, 128 (2002).
[33] C. M. Whelan, F. Cecchet, G. J. Clarkson, D. A. Leigh, R. Caudano, and P. Rudolf, Surf. Sci. **474**, 71 (2001).
[34] C.-A. Fustin, P. Rudolf, A. F. Taminiaux, F. Zerbetto, D. A. Leigh, and R. Caudano, Thin Solid Films **327–329**, 321 (1998).
[35] C.-A. Fustin, S. Haq, A. Wingen, C. Grégoire, R. Raval, P. Dumas, J. S. Hannam, D. A. Leigh, and P. Rudolf, Surf. Sci. **580**, 57 (2005).
[36] M. Chtaïb, P. A. Thiry, J. -J. Pireaux, J. P. Delrue, and R. Caudano, Surf. Sci. **162**, 245 (1985).
[37] M. Chtaïb, P. A. Thiry, J. P. Delrue, J.-J. Pireaux, and R. Caudano, J. Electron Spectrosc. Relat. Phenom. **29**, 293 (1983).
[38] L. J. Bellamy, *The Infrared Spectra of Complex Molecules* (Methuen, London, 1996).
[39] G. Socrates, *Infrared Characteristic Group Frequencies* (Wiley, Chichester, 1980).
[40] K. K. Lee, J. M. Vohs, and N. J. Di Nardo, Surf. Sci. **420**, L115 (1999).
[41] C. R. Flores, Q. Gao, and J. C. Hemminger, Surf. Sci. **239**, 156 (1990).
[42] H. Ibach and D. L. Mills, *Electron Energy Loss Spectroscopy and Surface Vibrations* (Academic, London, 1982).
[43] C. M. Whelan, F. Gatti, D. A. Leigh, and P. Rudolf (unpublished).

Top Curr Chem (2005) 262: 133–177
DOI 10.1007/128_011

Published online: 13 October 2005

Hydrogen Bond-Assembled Synthetic Molecular Motors and Machines

Euan R. Kay · David A. Leigh (✉)

School of Chemistry, The University of Edinburgh, West Mains Road,
Edinburgh EH9 3JJ, UK
David.Leigh@ed.ac.uk

Abstract Nature uses molecular motors and machines in virtually every significant biological process but learning how to design and assemble simpler artificial structures that function through controlled molecular-level motion is a major challenge for contemporary physical science. In this review we discuss some of the principles behind synthetic molecular motors and machines and examine a class of molecular architectures, benzylic amide catenanes and rotaxanes, that are proving promising in this area. The movement of the components in these systems can be controlled by light, electrons, chemical reactions, pH, temperature and the nature of the environment leading to both simple switches (molecular shuttles) and more complex molecular motors. They operate through biasing random thermal motion and can be understood through an appreciation of physical fluxional transport mechanisms. Remarkably simple examples of stimuli-responsive molecular shuttles can be interfaced with—and even perform physical tasks in—the macroscopic world.

Keywords Catenane · Molecular machine · Molecular motor · Molecular shuttle · Rotaxane

Abbreviations

a.c.	alternating current
ICD	induced circular dichroism
NMR	nuclear magnetic resonance
NTs	*N*-tosyl
SPT-SIR	spin polarization transfer by selective inversion recovery
VT	variable temperature

1 Design Principles for Molecular-Level Motors and Machines

The widespread use of molecular-level motion in key natural processes suggests that great rewards could come from bridging the gap between the present generation of synthetic molecular systems—which by and large rely upon electronic and chemical effects to carry out their functions—and the machines of the macroscopic world, which utilize the synchronized movements of smaller parts to perform particular tasks. In recent years it has proved relatively straightforward to design synthetic molecular systems where positional changes of submolecular components occur by moving energetically downhill, but what are the structural features necessary for molecules to use directional displacements to do work? How can we make a synthetic molecular machine that pumps ions against a gradient, say, or moves itself energetically uphill along a track? Artificial compounds that can do such things have yet to be realized; the field of synthetic molecular ma-

chines is still in its infancy and only the most basic systems—mechanical switches and slightly more sophisticated, but still rudimentary, molecular rotary motors—have been made thus far [1–6]. Here we outline some early successes in taming molecular-level movement using a particular type of molecular architecture, benzylic amide catenanes and rotaxanes.

1.1 Molecular-Level Machines and the Language Used to Describe Them

Language—especially scientific language—has to be suitably defined and correctly used in order to accurately convey concepts in a field. Nowhere is the need for accurate scientific language more apparent than in the discussion of the ideas and mechanisms by which nanoscale machines could—and do—operate. Much of the terminology used to describe molecular-level machines comes from the systems observed by physicists and biologists, but unfortunately their findings and descriptions have sometimes been misunderstood or unappreciated by chemists. Perhaps inevitably in a newly emerging field, there is not even a clear consensus as to what constitutes a molecular machine and what differentiates them from other molecular devices [1–6]. Initially, the categorization of molecules as machines by chemists was purely iconic—the structures "looked" like pieces of machinery—or they were so-called because they carried out a function that in the macroscopic world would require a machine to perform it. Many of the chemical systems first likened to pistons and other machines were simply host-guest complexes in which the binding could be switched "on" or "off" by external stimuli such as light. Whilst these early studies were the key to popularizing the field, with hindsight a consideration of the effects of scale tells us that supramolecular decomplexation events have little in common with the motion of a piston (the analogy is better within a rotaxane architecture because the components are still kinetically associated after decomplexation but the implication of imparting momentum is still unfortunate) and that a photosensitizer is not phenomenologically related to a "light-fueled motor". In fact, it is probably most useful to differentiate "device" and "machine" on the basis that the etymology and meaning of machine implies mechanical movement—i.e. a net nuclear displacement in the molecular world—which causes something useful to happen. This leads to the definition that "molecular machines" are a subset of "molecular devices" (functional molecular systems) in which some stimulus triggers the controlled, large amplitude or directional mechanical motion of one component relative to another (or of a substrate relative to the machine) which results in a net task being performed.

When developing the terminology necessary to describe molecular behavior or systems scientifically, the standard dictionary definitions meant for everyday use are not always appropriate in regimes that the definitions were never intended to cover. The difference between a "molecular motor" and

a "molecular switch", for example, is crucial because they are different phenomenological descriptors, not iconic classifications of molecular shapes: In physical terms a "switch" influences a system as a function of state; a "motor" influences a system as a function of its trajectory. Returning a switch to its original position undoes its effect on an external system, whereas when a motor returns to its original position through a different pathway to the one it left by (say, a 360° directional rotation in the case of a rotary motor), it does not. This difference is profound and the terms really should not be used interchangeably as sometimes happens in the chemistry (but not physics or biology) literature. Switches cannot use chemical energy to progressively drive a system away from equilibrium whereas a motor can.

The examples of amide-based catenanes and rotaxanes in this Chapter are chosen to help demonstrate some of the requirements for mechanical task performance at the molecular level.

1.2 The Effects of Scale

The path towards synthetic molecular machines starts nearly two centuries ago with the observation of effects that pointed to the random motion inherently experienced by all molecular-scale structures. In 1827, the Scottish botanist Robert Brown noted through his microscope the incessant, haphazard motion of tiny particles within translucent pollen grains suspended in water. An explanation of the phenomenon—now known as Brownian motion or movement—was provided by Einstein in one of his three extraordinary papers of 1905 and was proved experimentally by Perrin over the next decade. Ever since, scientists have been fascinated by the stochastic nature of molecular-level motion and its implications. The random thermal fluctuations experienced by molecules dominate mechanical behavior in the molecular world. Even the most efficient nanoscale machines are swamped by its effect. A typical motor protein consumes ATP fuel at a rate of 100–1000 molecules every second, corresponding to a maximum possible power output in the region 10^{-16} to 10^{-17} W per molecule. When compared with the random environmental buffeting of $\sim 10^{-8}$ W experienced by molecules in solution at room temperature, it seems remarkable that *any* form of controlled motion is possible [7]. When designing molecular machines it is important to remember that the presence of Brownian motion is a consequence of scale, not of the nature of the surroundings. It cannot be avoided by putting a molecular-level structure in a near-vacuum for example. Although there would be few random collisions to set such a Brownian particle in motion, equally there would be little viscosity to slow it down. These effects always cancel each other out and as long as a temperature for an object can be defined, it will undergo Brownian motion appropriate to that temperature (which determines the kinetic energy of the particle). In the absence of

any other molecules, heat would still be transmitted from the hot walls of the container to the particle by electromagnetic radiation, the random emission and absorption of the photons producing the Brownian motion. In fact, even temperature is not a very effective modulator of the background Brownian motion since the velocity of the particles depends on the square root of the temperature. So to reduce Brownian motion to 10% of the amount present at room temperature, one would have to drop the temperature from 300 K to 3 K [7, 8].

It seems sensible, therefore, to try to utilize Brownian motion when designing molecular machines rather than make structures that have to fight against it. In exciting developments over the past decade, theoretical physics has explained how random, *directionless* fluctuations can cause the *directional* transport of particles [7, 9–14] successfully accounting for the general principles behind biological motors [15–18]. An appreciation of the physics involved is crucial for the design of artificial structures which perform mechanical operations at the molecular level and transpose those effects to the macroscopic world. Nature provides examples of successful designs in the form of ion pumps, motor proteins, photoactive proteins, retinal, and many other systems [19]. Indeed, biological structures have already been incorporated into semi-synthetic biomaterials which can carry out "unnatural" mechanical tasks [20, 21].

The constant presence of Brownian motion is not the only distinction between motion at the molecular level and in the macroscopic world. The physics which govern mechanical dynamic processes in the two regimes are completely different, therefore requiring fundamentally different mechanisms for controlled transport or propulsion. In the macroscopic world, the equations of motion are governed by inertial terms (dependent on mass). Viscous forces (dependent on surface areas) dampen motion by converting kinetic energy into heat, and objects do not move until provided with specific energy to do so. In a macroscopic machine this is often provided through a directional force when work is done to move mechanical components in a particular way. As objects become less massive and smaller in dimension, inertial terms decrease in importance and viscosity begins to dominate. A parameter which quantifies this effect is Reynolds number (R)—essentially the ratio of inertial to viscous forces—given by Eq. 1 for a particle of length dimension a, moving at velocity v, in a medium with viscosity η and density ρ [22].

$$R = \frac{av\rho}{\eta} \tag{1}$$

Size affects modes of motion long before we reach the nanoscale. Even at the mesoscopic level of bacteria (length dimensions $\sim 10^{-5}$ m), viscous forces dominate. At the molecular level, Reynolds number is extremely low (except at low pressures in the gas phase) and the result is that molecules, or their

components, cannot be given a one-off "push" in the macroscopic sense—momentum is irrelevant. The motion of a molecular-level object is determined entirely by the forces acting on it at that particular instant—whether they be externally applied forces, viscosity, or random thermal perturbations and Brownian motion. In more general terms, this analysis leads to a central tenet: while the macroscopic machines we encounter in everyday life may provide the inspiration for what we might like molecular machines to achieve, drawing too close an analogy for their modes of operation is a poor design strategy. The "rules of the game" at different length scales are simply too different. Two basic principles must be followed for any molecular device to be able to carry out a mechanical function: First, the movement of the kinetically-associated molecules or their components must be controlled by employing interactions which restrict the natural tendency for three-dimensional random motion and somehow bias, rectify or direct the motion along the required vectors. Secondly, the Second Law of Thermodynamics tells us that no machine can continually operate solely using energy drawn from the thermal bath, so an external input of energy is required to perform a mechanical task with any synthetic molecular machine.

1.3 Lessons to Learn from Biological Motors and Machines

That the miniaturization of mechanical motors and machines to the molecular level is feasible is demonstrated by the fact that they are already all around us. Nature has developed an exquisite molecular nanotechnology that it employs to astonishing effect in virtually every significant biological process. Appreciating how Nature has overcome the issues of scale, environment, Brownian motion, and viscosity is extremely useful for learning how to design synthetic molecular systems that have to do the same.

There are many important differences between biological molecular machines and the man-made machines of the macroscopic world: Biological machines are soft, not rigid; they work at ambient temperatures (heat is dissipated almost instantaneously at small length scales so one cannot exploit temperature gradients); biological motors utilize chemical energy, often in the form of ATP hydrolysis or chemical gradients; they work in solution or at surfaces and operate under conditions of intrinsically high viscosity; they rely on and utilize—rather than oppose—Brownian motion; biomolecular machines need not use chemical energy to initiate movement—their components are constantly in motion—rather, they must control the directionality of that movement; the molecular machine and the substrate(s) it is acting upon are kinetically associated during the operation of the machine; biological machines are made by a combination of multiple parallel synthesis and self-assembly; their operation is governed by non-covalent interactions; and, finally, they utilize architectures (e.g. tracks) which restrict most of the de-

grees of freedom of the machine components and/or the substrate(s) it is acting upon. It is these last points, in particular, that have encouraged the study of catenanes and rotaxanes as potential structures for synthetic molecular motors and machines.

2
Mechanically Interlocked Molecular Architectures

2.1
Basic Features of Catenanes and Rotaxanes

Catenanes are chemical structures in which two or more macrocycles are interlocked, while in rotaxanes, one or more macrocycles are mechanically prevented from de-threading from linear chains by bulky "stoppers" (Fig. 1) [23–28]. Even though the components are not covalently connected, catenanes and rotaxanes are molecules—not supramolecular complexes—as covalent bonds must be broken in order to separate the constituent parts. In these kinetically associated species [29], the mechanical bond imparts a restriction in the degrees of freedom for relative movement of the components while often permitting extraordinarily large amplitude motion in the allowed vectors. This is in many ways analogous to the restriction of movement imposed on biological motors by a structural track [30–32].

Large-amplitude submolecular motions in catenanes and rotaxanes can be divided into two classes (Fig. 1): pirouetting of the macrocycle around the thread (rotaxanes) or another ring (catenanes); and translation of the macrocycle along the thread (rotaxanes) or around another ring (catenanes). By analogy to conformational changes within classical molecules, the relative movements between interlocked species are termed "co-conformational" changes [33]. Motions in these systems are most easily described by taking one component as a frame of reference, around or along which the other parts

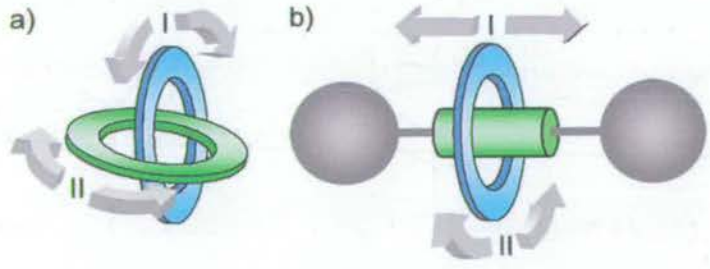

Fig. 1 Schematic representation of **a** a [2]catenane and **b** a [2]rotaxane. *Arrows* show possible large amplitude modes of movement of one component relative to another

move. Often the choice of this frame of reference is based on the relative size or complexity of the components, although this distinction can become blurred.

For a long time synthetic approaches to such structures relied on statistical or relatively inefficient covalently-directed approaches [34–37]. The development of supramolecular chemistry, however, allowed chemists to apply their increasing appreciation of non-covalent interactions to synthesis, resulting in numerous, often extremely elegant, template methods to catenanes and rotaxanes [38–51]. In such syntheses, non-covalent binding interactions between the components often "live-on" in the interlocked products. These interactions restrict the relative motions of components further to that defined by their architecture and can ultimately be manipulated to effect positional displacements. Much attention has been given to both intrinsic submolecular motions within these structures and the control of the relative positioning of the interlocked components through manipulation of recognition events.

2.2
Amide-Based Catenanes and Rotaxanes

Amide-based catenanes, in which hydrogen bonds template interlocking of the two rings, were first reported in 1992 by Hunter (**1**, Fig. 2) [52]. The steric bulk of the cyclohexyl groups prevents circumrotation of the macrocyclic rings in **1**, a feature which allowed Hunter to suggest the mechanically interlocked archi-

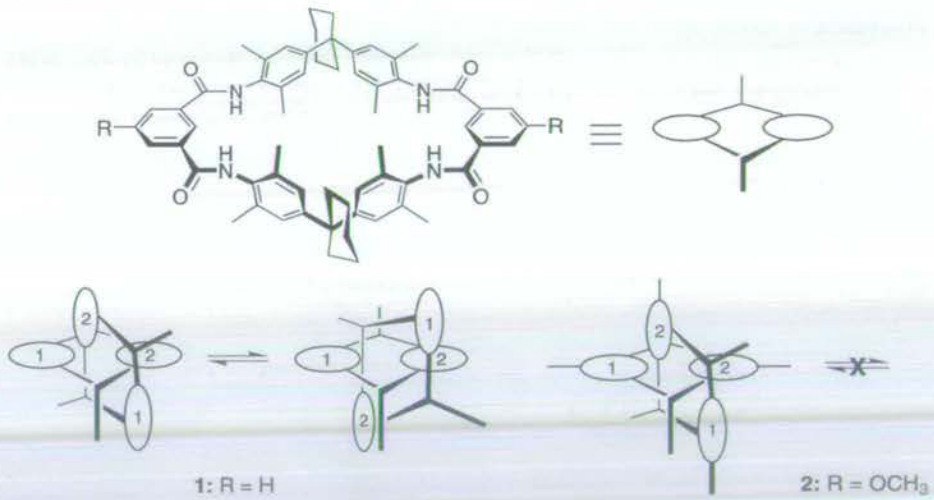

Fig. 2 Hydrogen bond-assembled [2]catenanes **1** and **2** reported by Hunter and Vögtle respectively, showing the limited component rotation possible in **1** but not in **2**, which is essentially completely locked in conformational terms

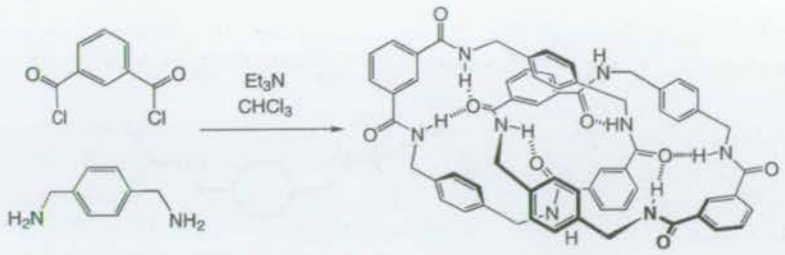

3

Scheme 1 The original hydrogen bond-assembled benzylic amide [2]catenane **3**, made in one step (20% yield) from isophthaloyl dichloride and *p*-xylylene diamine

tecture through a quite brilliant analysis of the complex 1D and 2D ^{1}H NMR data. Hunter's discovery prompted the publication of similar compounds by Vögtle (**2**) [53]. In the Hunter catenane (**1**), a 90° rotational motion which exchanges the non-equivalent isophthaloyl rings (labeled "1" and "2" in Fig. 2) is possible, but even this is blocked on substitution at the 5-position of the isophthaloyl ring (e.g. in **2**). Despite the accumulation of a large body of work over the subsequent decade, the fundamental problem that these systems exist in a rigidly locked co-conformation has never been overcome.

Fortunately, the benzylic amide catenane **3** (Scheme 1) discovered by chance in 1995 exhibits far more versatile dynamics than the Hunter–Vögtle system [54]. Catenane **3** has the simplest possible ^{1}H NMR spectrum, with only the six different constitutional types of protons apparent in [D_6]DMSO, the same number seen for the parent macrocycle [55]. Despite the smaller macrocycle cavity size of **3** compared to **1** and **2**, both the isophthaloyl and *p*-xylylene components are able to rotate through the cavity of the other macrocycle and the circumvolution process is fast on the NMR timescale in polar solvents at room temperature. The catenane formation process tolerates a number of aromatic 1,3-dicarbonyl and benzylic amide precursors so that a diverse range of analogues could be prepared (e.g. **4**, Fig. 3) and the effect of structure on the dynamic processes determined [56].

The hydrogen bonding patterns in the X-ray crystal structures of the benzylic amide catenanes suggested that modification of the synthetic procedure might allow rotaxanes to be synthesized. Sure enough, if the catenane-forming reaction was carried out in the presence of a suitable stoppered benzylic 1,3-diamide thread (e.g. **5**) rotaxanes such as **6** were also formed (Scheme 2) [55].

The rotaxane architecture brings about significant changes in the chemical and physical properties of the components; for example, the rotaxane **6** is 10^5 times more soluble in non-polar organic solvents than the parent macrocycle [55].

The wealth of structural data obtained on the benzylic amide catenane and rotaxane system showed that the mechanism for the formation of the

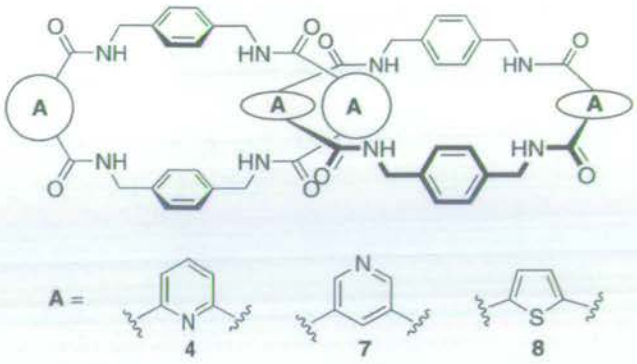

Fig. 3 Benzylic amide catenanes 4, 7 and 8 with differing aromatic-1,3-dicarbonyl units and differing dynamic properties

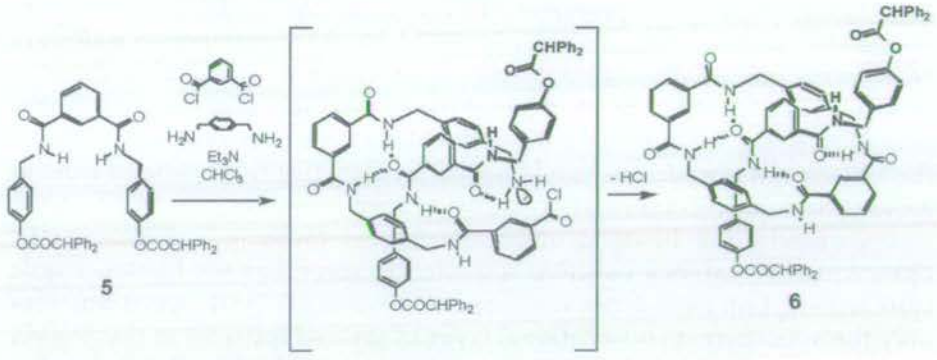

Scheme 2 Hydrogen bond-directed benzylic amide rotaxane formation

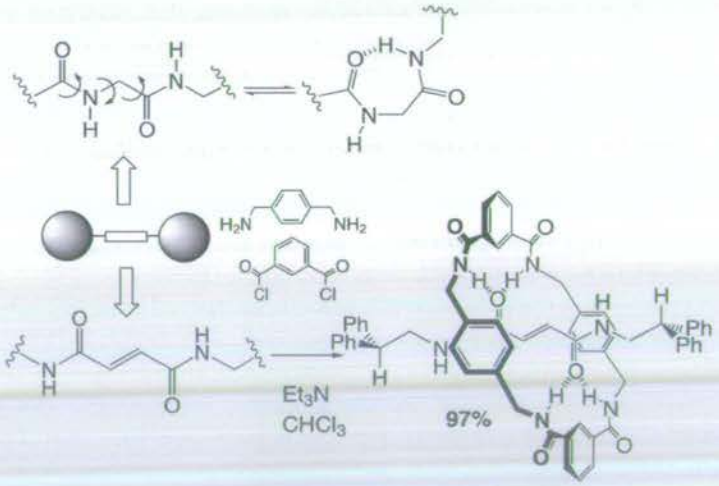

Scheme 3 The dramatic effect of preorganizing binding sites on the efficiency of rotaxane synthesis [60]

interlocked products was primarily the templated assembly of the macrocycle around two amide bonds [57]. Divergent hydrogen bonding sites in a similar spatial arrangement occur in adjacent amino acid residues in peptide chains and, indeed, it was found that simple peptides are also able to template the cyclization of benzylic amide macrocycles to give peptide rotaxanes [58, 59]. However, the inherent flexibility of the peptide backbone is not optimal for rotaxane formation. Replacing the peptide motif with a fumaramide unit maintains the required hydrogen bonding groups but with a rigidified backbone. This results in a remarkable 97% yield for a rotaxane, from a five component assembly process in just two steps from commercial starting materials (Scheme 3) [60].

3
Controlling Motion in Amide-Based Catenanes and Rotaxanes

3.1
Inherent Dynamics: Pirouetting in Benzylic Amide Catenanes

Any alkyl substitution on the isophthaloyl ring (at either the 5- or 4-positions) prevents complete circumvolution of the macrocycles in benzylic amide catenanes, thereby destroying the plane of symmetry bisecting the isophthaloyl units in each ring. A series of coalescence temperature measurements and spin polarization transfer by selective inversion recovery (SPT-SIR) NMR experiments [56, 61], revealed that the pyridine-2,6-dicarbonyl derivative (**4**) exhibits slow circumvolution on the NMR timescale. The thiophene derivative (**8**) was shown to rotate the fastest—in fact 3.2 million times faster than **4** in $C_2D_2Cl_4$ at room temperature.

This remarkable variation in dynamic behavior resulting from relatively simple structural changes can be allied to more subtle effects on rate using the solvent composition. Hydrogen bond-disrupting solvents such as CD_3OD and, to an even greater degree, [D_6]DMSO increase the rate of circumvolution by competing for the hydrogen bonding groups in the macrocycle. This has the effect of weakening the ground-state interactions and stabilizing the intermediate co-conformations during circumvolution, therefore lowering the energy barriers for the process. Variation of solvent composition allows fine-tuning of the circumvolution rate following selection of the gross "ball-park" value through structure choice [56, 61].

Both these solvent and structural effects on rate suggest that a key process in the circumvolution mechanism is rupture and formation of intercomponent hydrogen bonds. An isolated molecule molecular mechanics approach has been used to simulate the dynamics in these catenane systems, allowing simulation of the molecular shape at the transition states [61, 62]. Together with a full low-dimensional quantum-mechanical description of circumvolu-

tion [63], these studies provide the necessary theoretical and practical understanding of the intrinsic motions in a catenane system important for the development of molecular devices in which the frequency of motions may be a key characteristic.

3.2
Inherent Dynamics: Ring Pirouetting in Benzylic Amide Rotaxanes

Pirouetting is the random Brownian rotation of the macrocycle about the axis defined by the thread in a rotaxane. While this motion is often clearly occurring, it can be difficult to study in detail because of the symmetry of the components. Benzylic amide macrocycle-based rotaxanes possess a useful characteristic in this respect. In many examples, the benzylic amide macrocycle adopts a chair-like conformation meaning that for each pair of benzylic protons (H_E, Fig. 4), one is in an equatorial environment, while the other is axial [58]. For a macrocycle on a symmetric thread, two ^{1}H NMR signals would therefore be expected for the 8 benzylic protons in the molecule. Rotation of the macrocycle around the axis shown by 180° must, however, result in a chair-chair flip so as to maintain the hydrogen bonding network between the macrocyclic amide protons and carbonyl oxygens on the thread. This co-conformational change therefore interconverts the axial and equatorial sets of protons twice during a full 360° revolution. It is possible to study chemical exchange processes such as this by variable temperature (VT) NMR techniques, including the coalescence method [64], or spin polarization transfer by selective inversion recovery (SPT-SIR) [65].

For example, the room temperature ^{1}H NMR spectrum in $CDCl_3$ of the glycylglycine-based [2]rotaxane **9** displays the fewest possible signals for the macrocycle protons, indicating rapid pirouetting (820 s^{-1}) of the ring at ambient temperature [58]. The pyridyl-2,6-dicarbonyl-based macrocycle in **10**

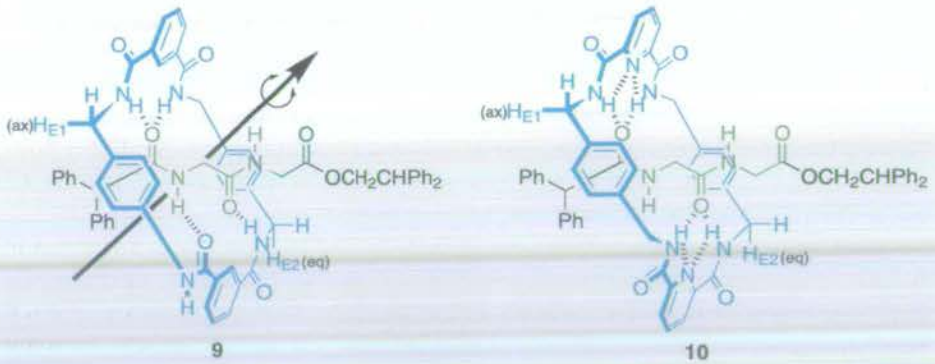

9 10

Fig. 4 Peptidorotaxanes **9** and **10**. The *arrow* on **9** indicates the axis about which macrocycle pirouetting occurs

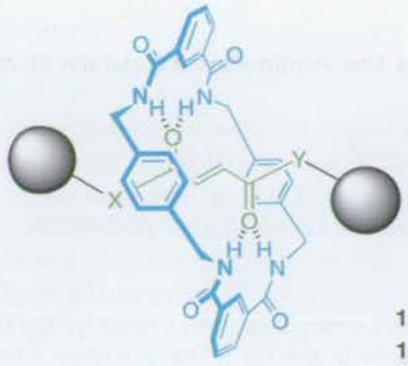

	X	Y	Yield	$\Delta G^{\ddagger}_{298}$ / kcal mol^{-1}
11	NH	NH	97%	11.5
12	NH	O	35%	9.3
13	O	O	3%	7.2

Fig. 5 Variation of yield in the rotaxane forming reactions for a series of simple fumaric acid based templates is correlated with the strength of intercomponent interactions in the products, as evidenced by $\Delta G^{\ddagger}_{298}$, the energy barrier to pirouetting in CD_2Cl_2

possesses a different, overall slightly stronger, hydrogen bonding network between the components, producing a concomitant reduction in pirouetting rate to 100 s^{-1} in $CDCl_3$ at rt.

As the rate of pirouetting is directly related to the strength with which the macrocycle is held to the thread, this motion can be a useful probe to evaluate the effect of structural changes on the strength of intercomponent interactions in rotaxanes. For the series of fumaric acid based [2]rotaxanes shown in Fig. 5, yields of the rotaxane forming process (a five-component clipping reaction in which formation of the benzylic amide macrocycle is templated by the fumaric acid residue) increase in the order **13** < **12** < **11** [60]. As expected, the rates of macrocycle pirouetting in the products were shown to follow exactly the opposite trend (Fig. 5), confirming that the efficiency of the templated synthesis is directly related to the hydrogen bonding ability of the thread templates.

3.3 Inherent Dynamics: Shuttling in Benzylic Amide Rotaxanes

Shuttling is the movement of a macrocycle back and forth along the thread component of a rotaxane. This motion takes the form of a Brownian motion-powered random walk, constrained to one dimension by the thread and to translational displacement boundaries by the bulky stoppers. By virtue of the template methods employed in their synthesis, the threads of amide-based rotaxanes consist of one or more recognition elements, or "stations" for the macrocycle(s); shuttling therefore becomes the movement on, off, or between such stations and just as for pirouetting motions, the dynamics depend on the strength of the intercomponent interactions.

3.3.1
Shuttling in Degenerate, Two Binding Site, Peptide-Based Molecular Shuttles

Following the observation that hydrogen bond-disrupting solvents such as [D_6]DMSO destroy the interactions between the benzylic amide macrocycle and a glycylglycine thread in [2]rotaxane **9** (Fig. 4) [58], a series of peptide-based molecular shuttles were reported in which two glycylglycine stations for the benzylic amide macrocycle are separated by aliphatic linkers [59]. In **14–16** (Fig. 6), in $CDCl_3$, the macrocycle shuttles between the two degenerate peptide stations rapidly at room temperature, evidenced by the single set of signals for the two peptide stations in the ^{1}H NMR spectrum which is resolved into two sets (for the occupied and unoccupied stations) on cooling the sample and freezing out the motion on the NMR timescale.

Just as for the pirouetting motions, the shuttling mechanism requires at least partial rupture of the intercomponent interactions at one station, before formation of new interactions at the new station. The thermodynamics of the degenerate process in each of **14–16** therefore involves passage over some activation barrier from one energy well to another identical minimum (Fig. 7). Of course, if the kinetic barrier is significantly larger than the thermal energy, shuttling ceases to occur. This can be achieved in **17** by introduction of a bulky *N*-tosyl (NTs) moiety (Fig. 6). Shuttling is restored on removal of this bulky barrier. Just as for the analogous benzylic amide catenanes, solvent composition has a profound effect on the shuttling rate in **14–16**—as little as 5% CD_3OD in halogenated solutions of peptide-based rotaxanes provides rate increases in excess of two orders of magnitude. The hydrogen bond-disrupting methanol weakens the intercomponent interactions, effectively loosening the macrocycle from its station (i.e. reducing $\Delta G^{\ddagger}$) with a concomitant increase in the shuttling rate [59].

This increase in rate does not, however, continue indefinitely with increasing solvent hydrogen bond basicity. An additional feature of these rotaxanes is

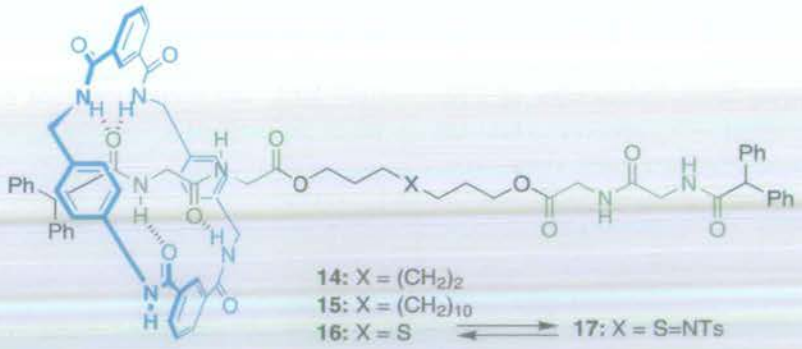

Fig. 6 Shuttling in peptide-based degenerate station molecular shuttles **14–17**

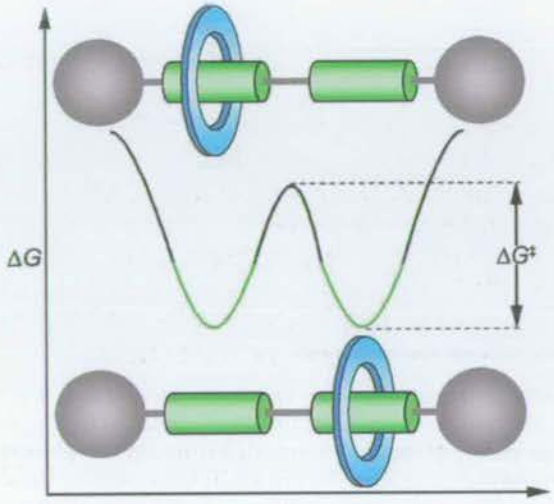

Fig. 7 Idealized free energy profile for movement between two identical stations in a degenerate molecular shuttle. The height of the barrier $\Delta G^{\ddagger}$ contains two components: the energy required to break the non-covalent interactions holding it to the station; and a distance-dependent diffusional component

that a major change in solvent polarity (changing from halogenated solvents to [D_6]DMSO) stops the macrocycle shuttling between the peptide stations and causes it to preferentially reside over the hydrophobic thread instead, hiding the thread from the unfavorably polar environment and allowing maximum hydrogen bonding between the peptide stations and solvent [59].

3.3.2 A Physical Model of Degenerate, Two Binding Site, Molecular Shuttles

An interesting structural effect is observed on increasing the length of the spacer in degenerate shuttles. The rate of shuttling in [2]rotaxane **14** was compared to that of **15** (Fig. 6). Although ostensibly not involved in any interactions with the macrocycle, extension of the alkyl chain results in an experimentally measured reduction in the rate of shuttling which corresponds to an increase in activation energy for the process of 1.2 kcal mol^{-1} at rt—an effect solely of the increased distance the macrocycle must travel [59].

These effects are most easily understood by considering the macrocycle as a particle moving along a one-dimensional potential energy (rather than free energy) surface (Fig. 8). At any point on the potential energy surface, the gradient of the line gives the force exerted on the macrocycle by the thread. When the macrocycle is in the vicinity of a station, hydrogen bonds and/or other attractive non-covalent interactions exert large forces (typically varying as a high power of the inverse distance, r^{-n}) on the macrocycle, opposing its mo-

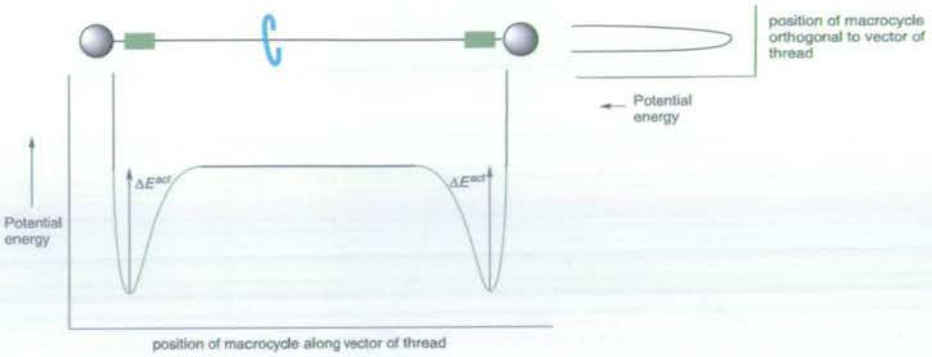

Fig. 8 Idealized potential energy of the macrocycle in a two-station degenerate molecular shuttle. The potential energy surface shows the effect of the interaction between macrocycle and thread on the energy of the macrocycle (ignoring any complicating factors such as folding). Chemical potential energies (ΔE's) generally follow similar trends to free energies (ΔG's, Fig. 7) but there are some important differences; for example, the activation free energy of shuttling, $\Delta G^{\ddagger}$, corresponds to the energy required for the macrocycle to move all the way to the new binding site (i.e. includes a contribution for the distance the ring has to move along the track to reach the other station) whereas the $\Delta E^{\ddagger}$, shown here, represents the energy required for the macrocycle to escape the forces exerted through non-covalent binding interactions at a station. The main plot shows the ΔE in terms of the position of the macrocycle along the vector of the thread; the minor plot shows the ΔE in terms of the position of the macrocycle orthogonal to the vector of the thread, illustrating that the thread genuinely behaves as a one-dimensional potential energy surface for the macrocycle

tion. When the macrocycle is on the thread *between* the stations, the hydrogen bonds and other non-covalent binding interactions are broken and no forces are exerted on the macrocycle by the thread (i.e. the gradient of the line is zero).

It is thermal energy which allows the macrocycle to escape these energy wells and explore the full length of the thread. For a population of shuttles at equilibrium, therefore, the macrocycles reside on the different stations and the thread according to a Boltzmann distribution and for a single molecule, these populations correspond to the amount of time the macrocycle spends on each site. In a degenerate shuttle, where the binding energy to each station is the same, while no significant interaction with the thread occurs, the macrocycle spends a negligible amount of time on the thread and splits its time equally between the two stations.

The rate at which the macrocycles escape from each station is given by a standard Arrhenius equation, depending on the depth of the energy well and the temperature. This is not the only factor involved in determining the rate at which macrocycles move between the two stations, however, there must also be some distance-dependent diffusional factor in the function describing the rate of shuttling (Fig. 8).

This phenomenon has been studied in an attempt to link the experimentally determined values of $\Delta G^{\ddagger}$ with a quantum-mechanical description of

the shuttling mechanism [66]. Calculation of the wavefunctions for the system shows that an increase in distance between the stations widens the free energy potential well (Fig. 7). As the well widens, it possesses a higher density of states per unit energy (just like the simple "particle in a box" model). The closer to one another the levels are, the more readily thermally populated they are or, in other words, the larger is the partition function and hence $\Delta G^{\ddagger}$.

The nature of the wavefunctions at energies close to the top of the barrier is intriguing, as under this energy regime the maximum probability of finding the macrocycle is in fact over the aliphatic spacer! The shuttling process can therefore be thought of in terms of a function of free energy (Fig. 7) as long as it is remembered that the height of the $\Delta G^{\ddagger}$ barrier is affected by *both* binding strength and distance between the stations. The behavior of the macrocycle is similar to a cart moving along a roller coaster track shaped like the double potential in Fig. 7. At low temperatures, the cart mostly resides on the stations (oscillating with small amplitude in the troughs). As energy approaches the value of the barrier, the cart spends most of its time passing over the barrier. At higher energies still, the cart is most likely to be found at the extremes of its translational motion.

3.4 Translational Molecular Switches: Stimuli-Responsive Molecular Shuttles

With increasing understanding of the nature of the inherent restriction in degrees of freedom in interlocked architectures, came the realization that control of intercomponent positioning was achievable. In shuttles such as **14–16** there are two identical recognition sites (stations) for the macrocycle so that it is equally likely to reside on either—they are degenerate. As we have seen, the rate at which the macrocycle moves between the stations can be regulated by the temperature or, in some cases, solvent composition. A different kind of control, however, can be achieved in stimuli responsive shuttles in which the net location of the macrocycle can be varied using an applied external stimulus. Indeed, as early as 1991 when reporting the first degenerate molecular shuttle [67], Stoddart noted that: "*The opportunity now exists to desymmetrize the molecular shuttle by inserting nonidentical 'stations' along the polyether 'thread' in such a manner that these different 'stations' can be addressed selectively by chemical, electrochemical, or photochemical means and so provide a mechanism to drive the 'bead' to and fro between 'stations' along the 'thread'.*"

3.4.1 A Physical Model of Two Binding Site, Stimuli-Responsive Molecular Shuttles

Rotaxanes in which the macrocycle can be translocated between two or more well-separated stations in response to an external signal can, in principle,

act as molecular-level mechanical switches. As we have seen, in any rotaxane the macrocycle distributes itself between the available binding sites according to the difference in the macrocycle binding energies and the temperature. If a suitably large difference in macrocycle affinity between two stations exists, the macrocycle resides overwhelmingly in one positional isomer or co-conformation. In stimuli-responsive molecular shuttles, an external trigger is used to chemically modify the system and alter the non-covalent intercomponent interactions such that the second macrocycle binding site becomes energetically more favored, causing translocation of the macrocycle along the thread to the second station (Fig. 9). This may be achieved by addressing either of the stations (destabilizing the initially preferred site or increasing the binding affinity of the originally weaker station). The system can be returned to its original state by using a second chemical modification to restore the initial order of station binding affinities. Performed consecutively these two steps allow the machine to carry out a complete cycle of shuttling motion.

The physical basis for this motion is again best understood by consideration of the potential energy of the macrocycle as a function of its position along the thread (Fig. 10). It is important to appreciate that the external stimulus does not induce directional motion of the macrocycle per se, rather by increasing the binding strength of the less-populated station and/or destabilizing the initially preferred binding site, the system is put out of co-conformational equilibrium. Relaxation towards the new global energy minimum subsequently occurs by *thermally activated* motion of the components, a phenomenon which we recognize as biased Brownian motion. In other words, biased Brownian motion arises from a difference in the activation energies for movement in different directions, *not* from the difference in energy minima. This results in net di-

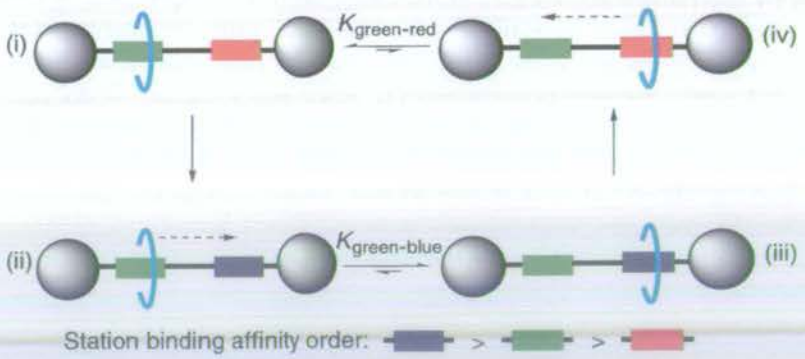

Fig. 9 Translational submolecular motion in a stimuli-responsive molecular shuttle: (i) the macrocycle initially resides on the preferred station (*green*); (ii) a reaction occurs (*red* → *blue*) changing the relative binding potentials of the two stations such that, (iii), the macrocycle "shuttles" to the now-preferred station (*blue*). If the reverse reaction (*blue* → *red*) now occurs, (iv), the components return to their original positions

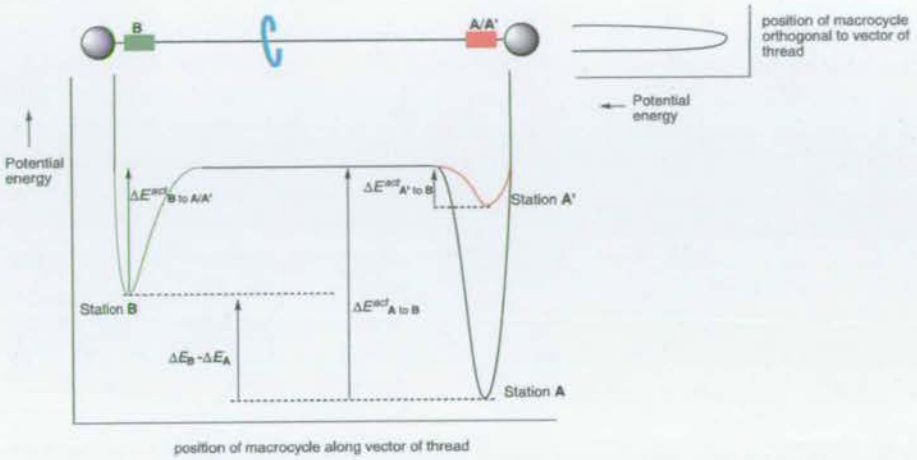

Fig. 10 Idealized potential energy of the macrocycle in a stimuli-responsive molecular shuttle in which one station changes (A′ → A) in response to the stimulus and complicating factors such as folding are ignored. As before (Fig. 8), the potential energy surface shows the effect of the interaction between macrocycle and thread on the energy of the macrocycle. The main plot shows the ΔE in terms of the position of the macrocycle along the vector of the thread; the minor plot shows the ΔE in terms of the position of the macrocycle orthogonal to the vector of the thread

rectional transport (a directional flux) of macrocycles when these barriers are suddenly changed putting the system out of equilibrium.

Given this mode of action, a key requirement is finding ways of generating sufficiently large, long-lived binding energy differences between pairs of positional isomers. A Boltzmann distribution at 298 K requires a $\Delta\Delta E$ (or $\Delta\Delta G$) between translational co-conformers of ~ 2 kcal mol^{-1} for 95% occupancy of one station. Achieving such discrimination in *two* states to form a positionally bistable shuttle (i.e. both $\Delta\Delta E_{A'-B}$ and $\Delta\Delta E_{B-A} \geq 2$ kcal mol^{-1}) by modifying only intrinsically weak, non-covalent binding modes thus presents a significant challenge. In the next sections we outline some of the different stimuli that have been used to bring about a positional change in the macrocycle in amide-based molecular shuttles.

3.4.2 Adding and Removing Protons to Induce Net Positional Change

The first pH-switched amide-based shuttle to exploit [N – H···anion] hydrogen bonding interactions was recently reported [68]. In [2]rotaxane **18**·H (Scheme 4), formation of the benzylic amide macrocycle is templated by a succinamide station in the thread. However, the thread also contains a cinnamate group. In the neutral form, the cinnamate phenol is a relatively poor hydrogen bonding group and the macrocycle resides on the succinamide station > 95%

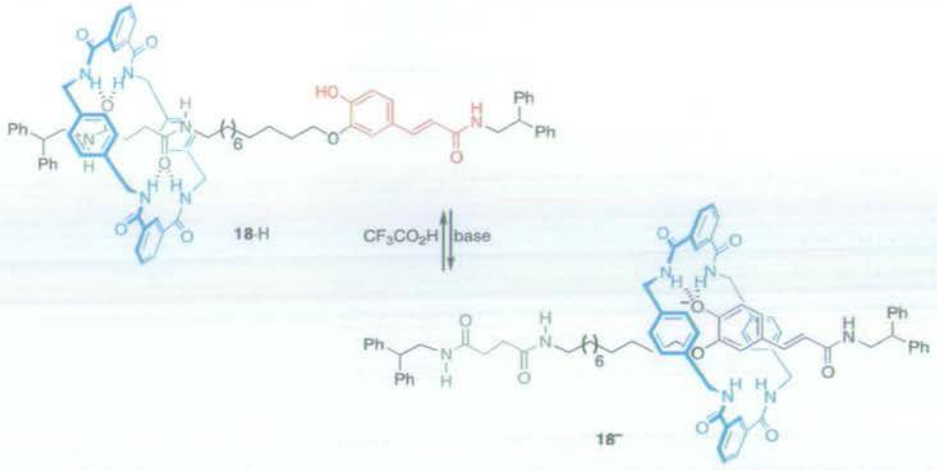

Scheme 4 pH-Switched anion shuttling in a hydrogen bonded [2]rotaxane, **18**·H, in [D_7]DMF at rt. Bases that can be used include LiOH, NaOH, KOH, CsOH, Bu_4NOH, *t*BuOK, DBU, Schwesinger's phosphazine P_1 base, illustrating the lack of influence on shuttling of the accompanying cation

of the time in most solvents at rt. Deprotonation to give 18^- in [D_7]DMF results in the macrocycle binding to the phenolate anion. Reprotonation of the phenol returns the system to its original state. While a wide range of bases (with a variety of counterions) proved efficacious, shuttling was found to be extremely solvent dependent. Hydrogen bond mediated systems usually perform best in "non-competing" solvents—those with low hydrogen bond basicity. Yet, when the deprotonation of **18**·H is carried out in $CDCl_3$ or CD_2Cl_2, a change of position of the macrocycle does not occur. Rather, an intramolecular folding event occurs to allow the phenolate to hydrogen bond with the macrocycle while it remains on the succinamide station. This solvent dependence presumably arises because the phenolate can only satisfy the hydrogen bonding requirements of one isophthalamide unit in the macrocycle. The presence of a hydrogen bond accepting solvent such as DMF can therefore compensate for this loss of stabilization. The strength of binding to the anion is illustrated by the fact that the shuttling process continues to occur even in CD_3CN—only a moderate hydrogen bond acceptor and weaker than the amide groups of the thread. Shuttling is unaffected by the nature of the accompanying cation or the addition of up to 10 equivalents of other anions.

3.4.3
Adding and Removing Electrons to Induce Net Positional Change

[2]Rotaxane **19** contains two potential hydrogen bonding stations for the benzylic amide macrocycle—a succinamide (*succ*) station and a redox-active

3,6-di-*tert*-butyl-1,8-naphthalimide (*ni*) station—separated by a C_{12} aliphatic spacer (Scheme 5) [69, 70].

While the ability of the *succ* station to template formation of the macrocycle is well established, the neutral naphthalimide moiety is a poor hydrogen bond acceptor. To minimize its free energy, the macrocycle in **19** must therefore sit over the succinamide station in non-hydrogen bonding solvents, so co-conformation *succ*-**19** predominates (Scheme 5). In fact, the difference in macrocycle binding affinities is so great that *succ*-**19** is the only translational isomer detectable by ^{1}H NMR in $CDCl_3$, CD_3CN, and [D_8]THF, while even in the strongly hydrogen bond-disrupting [D_6]DMSO, the macrocycle resides over the *succ* station about half of the time. One-electron reduction of the naphthalimide to the corresponding radical anion, however, results in a substantial increase in electron charge density on the imide carbonyls and a concomitant increase in hydrogen bond accepting ability. In **19**, this reverses the relative hydrogen bonding abilities of the two thread stations so that co-conformation *ni*-**19**$^{-\bullet}$ is preferred in the reduced state. Subsequent

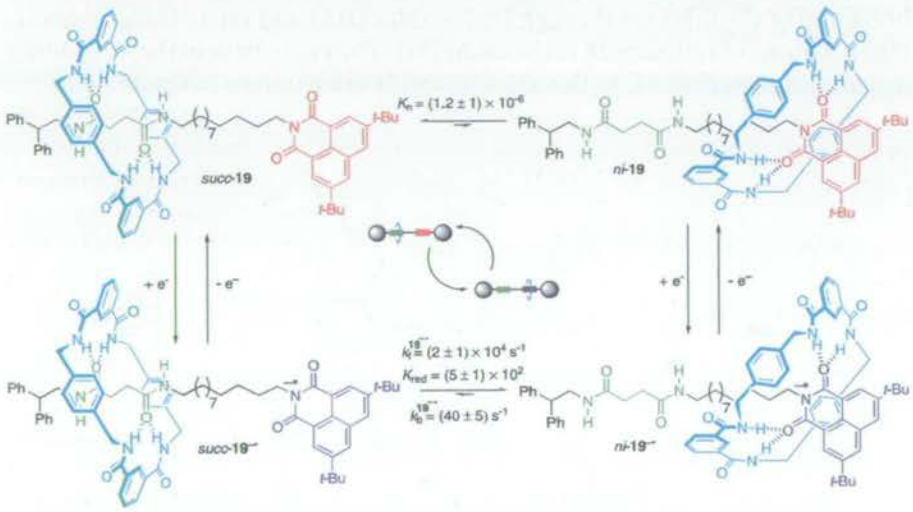

Scheme 5 A photochemically and electrochemically switchable, hydrogen bonded molecular shuttle **19**. In the neutral state, the translational co-conformation *succ*-**19** is predominant as the *ni* station is a poor hydrogen bond acceptor ($K_n = (1.2 \pm 1) \times 10^{-6}$). Upon reduction, the equilibrium between *succ*-**19**$^{-\bullet}$ and *ni*-**19**$^{-\bullet}$ is altered ($K_{red} = (5 \pm 1) \times 10^2$) because *ni*$^{-\bullet}$ is a powerful hydrogen bond acceptor and the macrocycle changes position through biased Brownian motion. Upon re-oxidation, the macrocycle shuttles back to the succinamide station. Repeated reduction and oxidation causes the macrocycle to be displaced forwards and backwards between the two stations. All the values shown refer to cyclic voltammetry experiments in anhydrous THF at 298 K with tetrabutylammonium hexafluorophosphate as the supporting electrolyte. Similar values were determined on photoexcitation and reduction of the ensuing triplet excited state by an external electron donor

re-oxidation to the neutral compound restores the original order of binding site affinities and the shuttle returns to its initial state as co-conformation *succ*-**19**. This process can be stimulated and observed in cyclic voltammetry experiments [70], or alternatively photochemistry can be employed to initiate (through excitation of the naphthalimide group by a nanosecond laser pulse at 355 nm followed by electron transfer from a regenerable external electron donor) and observe (using transient absorption spectroscopy) the change of position of the macrocycle [69]. A number of control experiments proved unequivocally that the dynamic process observed is reversible shuttling of the macrocycle between the stations rather than any other conformational or co-conformational changes [70].

3.4.4
Adding and Removing Covalent Bonds to Induce Net Positional Change

Perhaps surprisingly, the use of covalent bond-forming reactions to bring about positional change in molecular shuttles has been limited to the formation (and breaking) of C – C bonds through Diels–Alder (DA) and retro-Diels–Alder (r-DA) reactions of rotaxane **20** (Scheme 6) [71]. The steric bulk of the DA-adduct displaces the macrocycle to the succinic amide ester station in *Cp*-**20**.

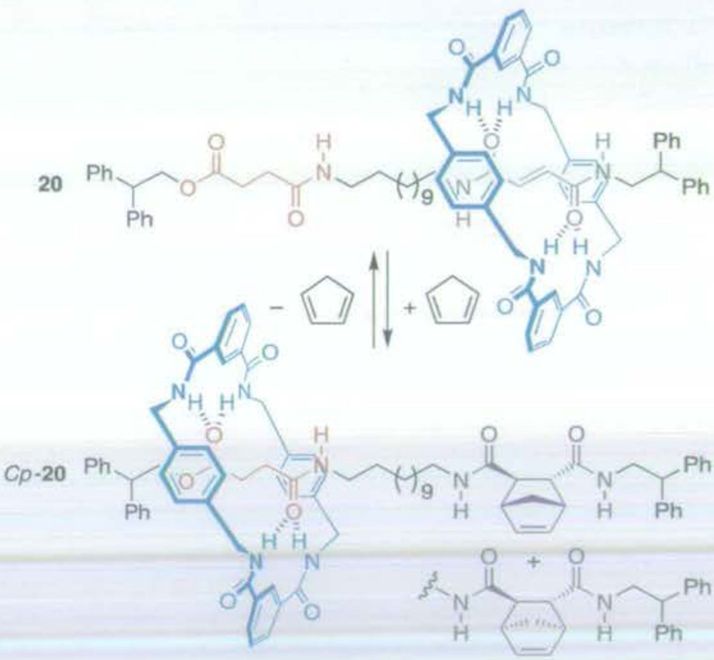

Scheme 6 Shuttling through reversible covalent bond formation. Absolute stereochemistry for *Cp*-**20** is depicted arbitrarily

3.4.5
Changing Configuration to Induce Net Positional Change

As with the control of submolecular motion in covalently bound systems, isomerization processes are an attractive means for controlling shuttling in rotaxanes. Shuttle *E*/*Z*-**21** (Scheme 7) employs the interconversion between fumaramide (*trans*) and maleamide (*cis*) isomers of the olefinic unit [72]. Fumaramide moieties are excellent binding sites for benzylic amide macrocycles: the *trans*-olefin fixes the two strongly hydrogen bond accepting amide carbonyls in a close-to-ideal spatial arrangement for interaction with the amide protons from the macrocycle. Two sets of bifurcated hydrogen bonds between macrocycle and thread result. Although a similar hydrogen bonding surface is presented to the macrocycle, binding to the succinamide station results in both a loss in entropy (due to loss of bond rotation) and also one less intracomponent hydrogen bond which cannot be compensated for by the rigid fumaramide station. The result is that only one major positional isomer of *E*-**21** is observed at room temperature. Photoisomerization of the fumaramide station by irradiation at 254 nm reduces the number of possible intercomponent hydrogen bonds at this station from four to two so that a new co-conformational energy minimum now exists: the macrocycle now sits overwhelmingly on the succinamide station. Unlike the succinamide/naphthalimide system (Scheme 5), this new state is indefinitely stable until a further stimulus is applied—namely thermal or chemical reisomerization of the maleamide unit back to fumaramide, thus restoring the shuttle to its initial state.

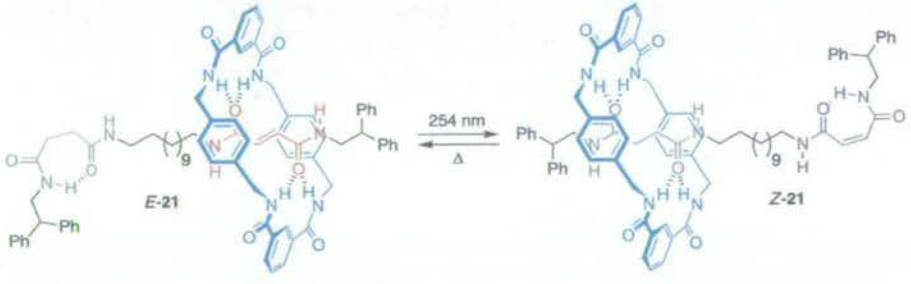

Scheme 7 Bistable molecular shuttle *E*/*Z*-**21** in which self-binding of the "low affinity" station in each state is a major factor in producing excellent positional discrimination

3.4.6
Entropy-Driven Net Positional Change

Most of the shuttles which exhibit excellent positional discrimination are switched using stimuli such as pH, light, polarity of the environment, or electrochemistry to modify the enthalpy of macrocycle binding to one or both

stations. Generally, the effect of temperature is simply to alter the degree of discrimination the macrocycle expresses for the various stations, not to alter the station preference. In [2]rotaxane **22**, however, the macrocycle is actually switched between stations by changing the temperature [73]. In fact, **22** is a *tristable* molecular shuttle: a rotaxane in which the ring can be switched between three different positions on the thread (Scheme 8).

Structurally, **22** is closely related to **21**, the key difference being substitution of the isophthaloyl unit in the macrocycle for a pyridine-2,6-dicarbonyl moiety. In the *E*-**22** form, the macrocycle resides over the strong fumaramide station at all temperatures investigated, as expected. Photoisomerization of *E*-**22** gave the maleamide *Z*-**22** isomer. The ^{1}H NMR spectra of this product showed clearly that shuttling away from the maleamide station had occurred, but the nature of the product was highly temperature dependent. At elevated temperatures (308 K) the expected *succ-Z*-**22** co-conformation was observed; the macrocycle spends nearly all its time over the succinamide station. At lower temperatures, however, the macrocycle occupies neither the succinamide nor the maleamide units, but it is the alkyl chain which exhibits the spectroscopic shifts indicative of encapsulation by the ring. This suggests that the thread adopts an S-shaped conformation with the macrocycle binding to one amide of each station (*dodec-Z*-**22**, Scheme 8). Unlike [2]rotaxane **21**, photochemical *cis*→*trans* isomerization was effective (irradiation of *Z*-**22** at 312 nm gave a photostationary state of > 95 : 5 *E* : *Z* compared to ~ 45 : 55

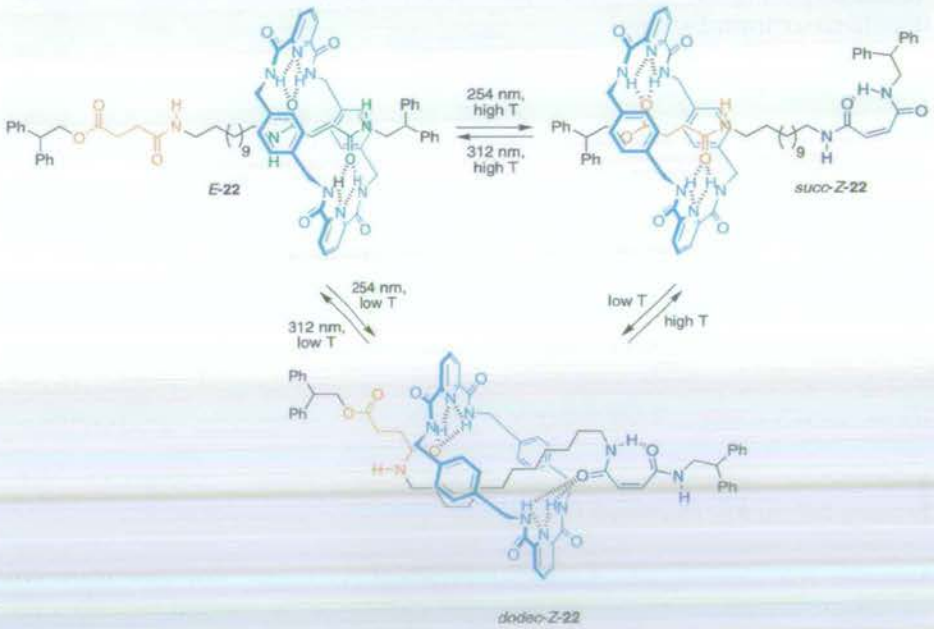

Scheme 8 A tristable molecular shuttle **22**

under the same conditions for **21**) so that no heating is necessary for this step and all the interconversions shown in Scheme 8 are possible.

The origin of this temperature-switchable effect is presumably the large difference in entropy of binding ($\Delta S_{binding}$) to the succinamide and alkyl chain stations which allows the $T\Delta S_{binding}$ term to have a significant overall impact on $\Delta G_{binding}$ as temperature is varied. In the *succ-Z*-**22** co-conformation, the macrocycle forms two strong hydrogen bonds with an amide carbonyl and two, significantly weaker, bonds to the ester carbonyl. The *dodec-Z*-**22** co-conformation, however, allows formation of four strong hydrogen bonds to amide carbonyls making it enthalpically favored by $\sim 2\,kcal\,mol^{-1}$. At low temperatures, where the effects of the entropy term are less significant, the molecule therefore adopts the *dodec-Z*-**22** co-conformation. At higher temperatures, the increased contribution from the $T\Delta S_{binding}$ term requires that the molecule adopt the more entropically favorable *succ-Z*-**22** co-conformation in order to minimize its energy.

This effect seems to be quite structure specific—no other shuttles in this series have shown temperature dependent co-conformational preference. If suitable systems can be successfully designed however, entropy-driven temperature control of positional isomerism could prove a useful addition to the expanding strategies for controlling submolecular motions [74].

Many of the shuttling examples described show remarkable degrees of control over submolecular fragment positioning and dynamics. They utilize a number of different stimuli-induced processes to effect macrocycle shuttling over large amplitudes (up to ~ 15 Å in the case of **14–16** and **18–22**) and operate over a range of timescales (a complete shuttling cycle in **19** is over in $\sim 100\,\mu s$ while, in **21**, both states are indefinitely stable and the time for a full cycle is infinitely variable). Yet it must be remembered that all such shuttles exist as an equilibrium of co-conformations and it is simply the position of the equilibrium that is varied.

3.5
Controlling Rotational Motion: Ring Pirouetting in Rotaxanes

Control of macrocycle pirouetting in rotaxanes presents two challenges—frequency of random pirouetting and directionality. The former has been achieved through temperature, structure, electric fields, light, and solvent effects; the latter has yet to be demonstrated.

Alternating current (a.c.) electric fields are an ideal stimulus with which to control submolecular dynamics for many applications. For two benzylic amide-based hydrogen bonded [2]rotaxanes (**23** and **24**, Fig. 11) it was observed that application of a.c. fields of around 50 Hz resulted in unusual Kerr effect responses which are unique to the interlocked architecture (i.e. are not observed for either of the components alone) [75]. Decreasing the field strength had the same effect as increasing temperature: enhancement of the response; indicating

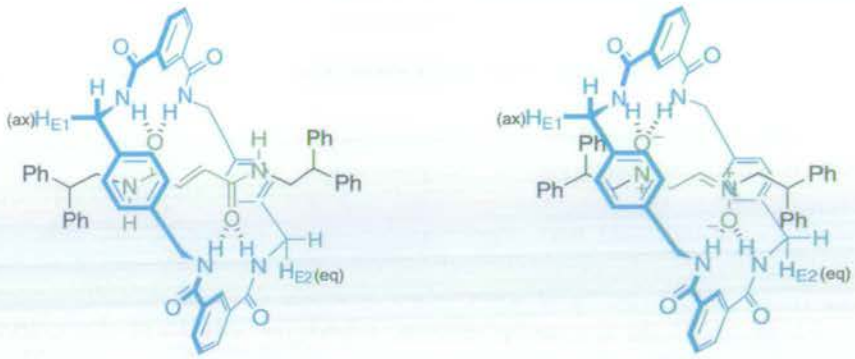

23 **24**

Fig. 11 [2]Rotaxanes **23** and **24** in which the rate of pirouetting is controlled by an alternating current electric field

that the underlying phenomenon is addressable by these two stimuli. Both VT NMR experiments and molecular modeling suggested that macrocycle pirouetting is the only possible dynamic process on this timescale for these structures. The experimental and theoretical studies also predict the slightly more complex Kerr effect response observed experimentally for **23** compared to **24**. It is believed that application of an a.c. electric field therefore attenuates macrocycle pirouetting in **18** and **19**—the extent of the dampening can be varied with the strength of the applied field; even modest fields of ~ 1 V cm^{-1} produce rate reductions of 2–3 orders of magnitude.

An alternative strategy for affecting pirouetting rates would be to apply some stimulus which directly alters the structure or electronics of the thread or macrocycle so as to adjust the strength of intercomponent interactions. This has been achieved for the fumaramide-based [2]rotaxanes *E*/*Z*-**25**–**27** (Scheme 9), which are closely related to **23** [76]. The decrease in intercomponent binding affinity on photoisomerization of the fumaramide units in *E*-**25**–**27** to the *cis*-maleamide isomers gives a huge increase in the rate of pirouetting of more than 6 orders of magnitude. The switching process is also reversible; subjecting the maleamide rotaxanes to heat or various chemical stimuli results in re-isomerization to the more thermally stable *trans*-olefin isomers, with accompanying reinstatement of the strong hydrogen bonding network.

In all of the above systems, the rate of Brownian pirouetting is influenced by applying external stimuli, the direction of these random motions are not affected. It has incorrectly been suggested [77] that unidirectional pirouetting could result from simply derivatizing rotaxanes with chiral or knotted stoppers. Directional rotation can only result from an external energy source being used (more than once in order to achieve circumrotation) to drive a system temporarily away from equilibrium. Under those circumstances, simple 2D asymmetry would be sufficient to induce directional motion.

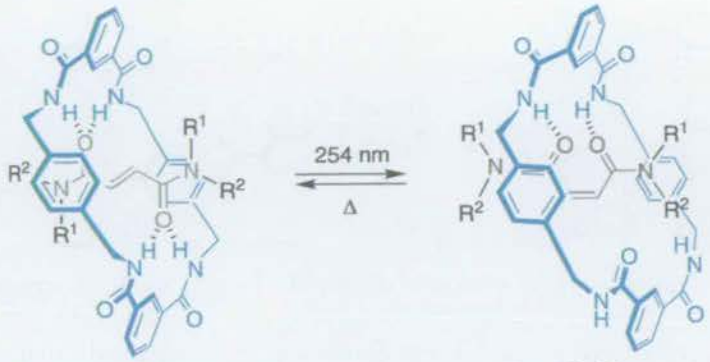

E-25 $R^1 = R^2 = CH_2CO_2CH_2Ph$ *Z*-25
E-26 R^1 Me, $R_2 = CH_2CHPh_2$ *Z*-26
E-27 $R^1 = H$, $R^2 = CH_2CHPh_2$ *Z*-27

Scheme 9 Photoisomerization of [2]rotaxanes *E*-25-27 which results in pirouetting rate enhancements of up to 6 orders of magnitude. The reverse process $Z \rightarrow E$ isomerization can be effected by heating a 0.02 M solution of the *Z*-rotaxanes at 400 K or generating bromine radicals (cat. Br_2, hv 400 nm) or via reversible Michael addition of piperidine (rt, 1 h)

3.6 Controlling Rotational Motion in Catenanes

3.6.1 Two-Way and Three-Way Catenane Positional Switches

The fundamental principles of controlling shuttling in rotaxanes and rotation in catenanes are the same. For example, homocircuit [2]catenane **28**, acts somewhat like the two station degenerate shuttle **14** [78]. In halogenated solvents such as $CDCl_3$, the two macrocycles interact through hydrogen bonding between their aromatic-1,3-diamide groups, resulting in a "host-guest" relationship in which each (constitutionally identical) ring adopts a different conformation and exists in a different chemical environment (*amide-endo*-**28**, Scheme 10). Pirouetting of the two rings interconverts this host-guest relationship and is fast on the NMR timescale in $CDCl_3$ at rt. In a hydrogen bond-disrupting solvent such as $[D_6]$DMSO, however, the preferred coconformation has the amides exposed on the surface where they can interact with the surrounding medium, while the hydrophobic alkyl chains are buried in the middle of the molecule (*amide-exo*-**28**, Scheme 10). Of course, with the disruption of the main non-covalent interactions between the two rings, the frequency of movements is also greatly increased in polar media.

As with rotaxanes, stimuli-induced structural changes can be used to alter the rates of the random intercomponent motions in catenanes. For example, electrochemical reduction of benzylic amide [2]catenane **3** completely halts

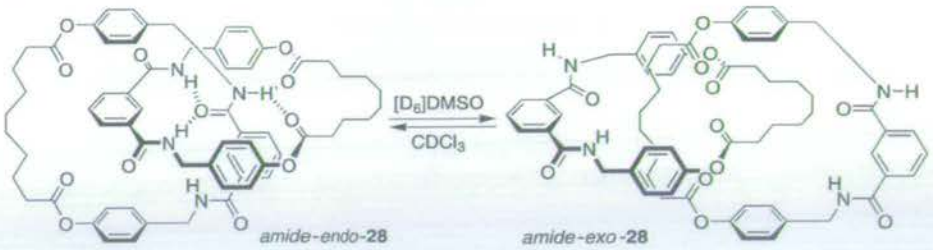

Scheme 10 Translational isomerism in an amphiphilic benzylic amide [2]catenane **28**

the circumrotational process due to formation of an intramolecular covalent bond between the two rings [79].

Sequential movement of one macrocycle between *three* stations on a second ring requires independent switching of the affinities for two of the units so as to change the relative order of binding affinities, as shown schematically in Scheme 11 [80].

In [2]catenane **29** (Fig. 12), this is achieved by employing two fumaramide stations with differing macrocycle binding affinities, one of which (station **A**, green) is located next to a benzophenone unit. This allows selective, photosensitized isomerization of station **A** by irradiation at 350 nm, before direct photoisomerization of the other fumaramide station (station **B**, red) at 254 nm. Station **B**, being a methylated fumaramide residue, has a lower affinity for the macrocycle than station **A**. The third station (station **C**, orange)—a succinic amide ester—is not photoactive and is intermediate in macrocycle

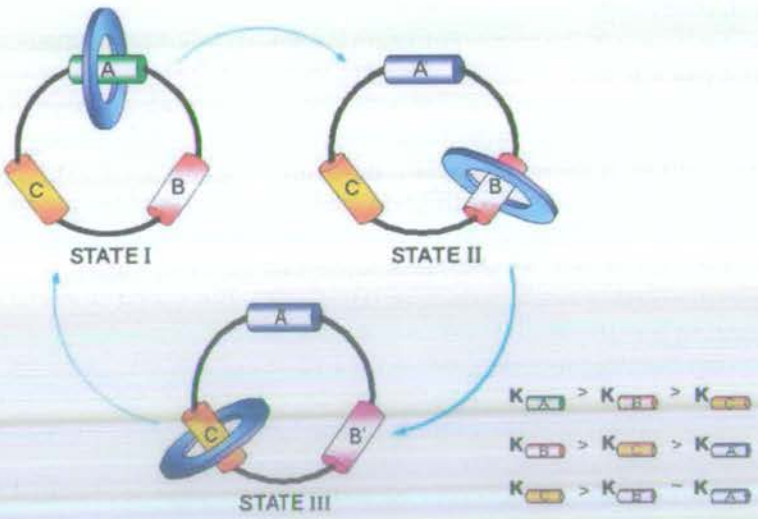

Scheme 11 Stimuli-induced sequential movement of a macrocycle between three different binding sites in a [2]catenane

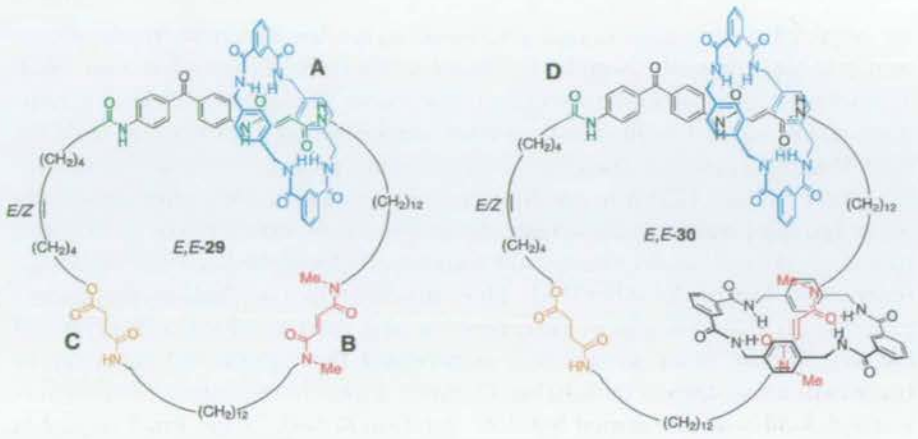

Fig. 12 [2]Catenane **29** and [3]catenane **30** shown as their *E,E*-isomers

binding affinity between the two fumaramide stations and their maleamide counterparts. A fourth station, an isolated amide group (shown as **D** in *E,E*-**30**) which can make fewer intercomponent hydrogen bonding contacts than **A**, **B**, or **C**, is also present but only plays a significant role in the behavior of the [3]catenane.

Consequently, in the initial state (state I, Scheme 11), the small macrocycle resides on the green, non-methylated fumaramide station of [2]catenane **29**. Isomerization of this station (irradiation at 350 nm, green → blue) destabilizes the system and the macrocycle finds its new energy minimum on the red station (state II). Subsequent photoisomerization of this station (irradiation at 254 nm, red → pink) means the macrocycle must now move onto the succinic amide ester unit (orange, state III). Finally, heating the catenane (or treating it with photo-generated bromine radicals or piperidine) results in isomerization of both the *Z*-olefins back to their *E*-forms (pink → red and blue → green) so that the original order of binding affinities is restored and the macrocycle returns to its original position on the green station.

The ^{1}H NMR spectra for each diastereomer show excellent positional integrity of the small macrocycle in this three-way switch at all stages of the process, but the rotation is not directional—over the complete sequence of reactions, an equal number of macrocycles go from **A**, through **B** and **C**, back to **A** again in each direction.

3.6.2 Directional Circumrotation: A [3] Catenane Rotary Motor

Remarkable directional rotary motion has been produced in covalently linked structures in recent years [81–91]. In order to bias the direction the macrocycle takes from station to station in a catenane such as **29**, temporary barriers

are required at each stage to restrict Brownian motion in one particular direction and bias the path taken by the macrocycle from station to station. Such a situation is intrinsically present in [3]catenane **30** (Scheme 12) [80]. Irradiation at 350 nm of *E,E*-**30** causes counter-clockwise (as drawn) rotation of the light blue macrocycle to the succinic amide ester (orange) station to give *Z,E*-**30**. Isomerization (254 nm) of the remaining fumaramide group causes the other (purple) macrocycle to relocate to the single amide (dark green) station (*Z,Z*-**25**) and, again, this occurs counter-clockwise because the clockwise route is blocked by the other (light blue) macrocycle. This "follow-the-leader" process, each macrocycle in turn moving and then blocking a direction of passage for the other macrocycle, is repeated throughout the sequence of transformations shown in Scheme 12. After three diastereomer interconversions, *E,E*-**30** is again formed but 360° rotation of each of the small rings has not yet occurred, they have only swapped places. Complete unidirectional ro-

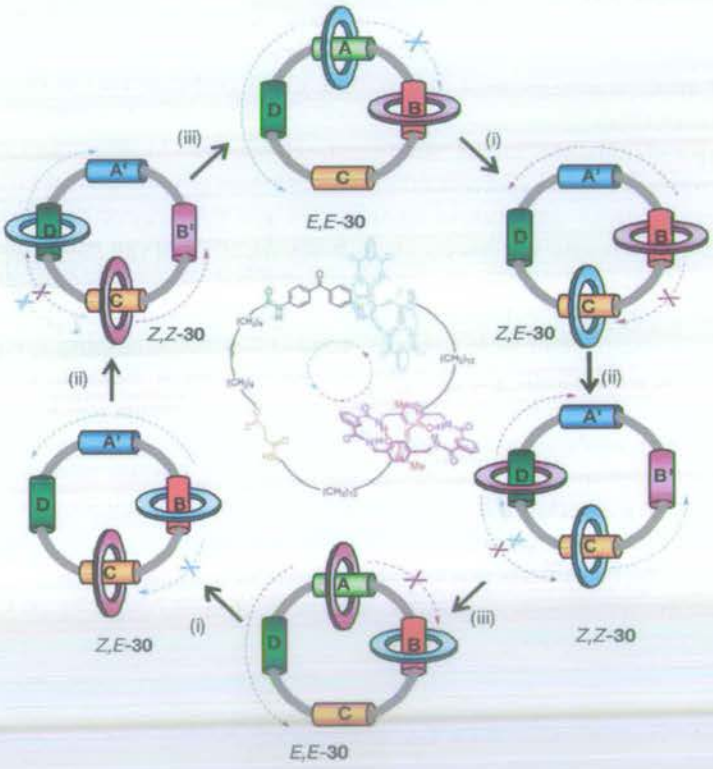

Scheme 12 Stimuli-induced unidirectional rotation in a four station [3]catenane **30**. (i) 350 nm, CH_2Cl_2, 5 min, 67%; (ii) 254 nm, CH_2Cl_2, 20 min, 50%; (iii) 100 °C, $C_2H_2Cl_4$, 24 h, ~ 100%; or catalytic ethylenediamine, 50 °C, 48 h, 65%; or catalytic Br_2, 400–670 nm, CH_2Cl_2, – 78 °C, 10 min, ~ 100%

tation of both small rings occurs only after the synthetic sequence (i)–(iii) has been completed twice.

3.6.3 Selective Rotation in Either Direction: A [2] Catenane Reversible Rotary Motor

Catenane **30** rotates directionally solely through the biasing of random Brownian motion. Over the past decade, a number of theoretical formalisms have been developed using non-equilibrium statistical physics which explain how various types of random fluctuation-driven transport can occur [7, 9–18]. Underlying each of these Brownian ratchet or motor mechanisms are three components: (i) a randomizing element; (ii) an energy input to avoid falling foul of the Second Law of Thermodynamics; and (iii) asymmetry in the energy or information potential in the dimension in which the motion occurs. Such ratchet mechanisms not only account for the general principles behind biological motors but have also been successfully applied to the development of transport and separation devices for mesoscopic particles and macromolecules, microfluidic pumping, the photo-alignment of liquid crystals, and quantum and electronic applications. Accordingly it appeared to us that a consideration of such physical mechanisms could aid the understanding of how to direct intramolecular rotations within chemical structures and we applied these ideas to a catenane architecture [92].

A flashing ratchet is a particular type of energy ratchet mechanism [11], a classic example of which consists in physical terms (Fig. 13) of an asymmetric potential energy surface (a periodic series of two different minima and two different maxima) along which a Brownian particle is directionally transported by sequentially raising and lowering each set of minima and maxima by changing the potential (for example, with an oscillating electric field and a charged particle). *The key to visualizing how the principles of such an energy ratchet can be applied to a catenane architecture is not to consider the whole catenane as a molecular machine, but rather to think of one macrocycle as a motor that transports a substrate—the other ring—directionally around itself*! In its simplest form this results in a [2]catenane such as **31** (Fig. 14) which is able to directionally rotate the smaller ring about the larger one in response to a series of chemical reactions.

Fig. 13 A flashing energy ratchet mechanism for Brownian particle transport along an oscillating potential energy surface

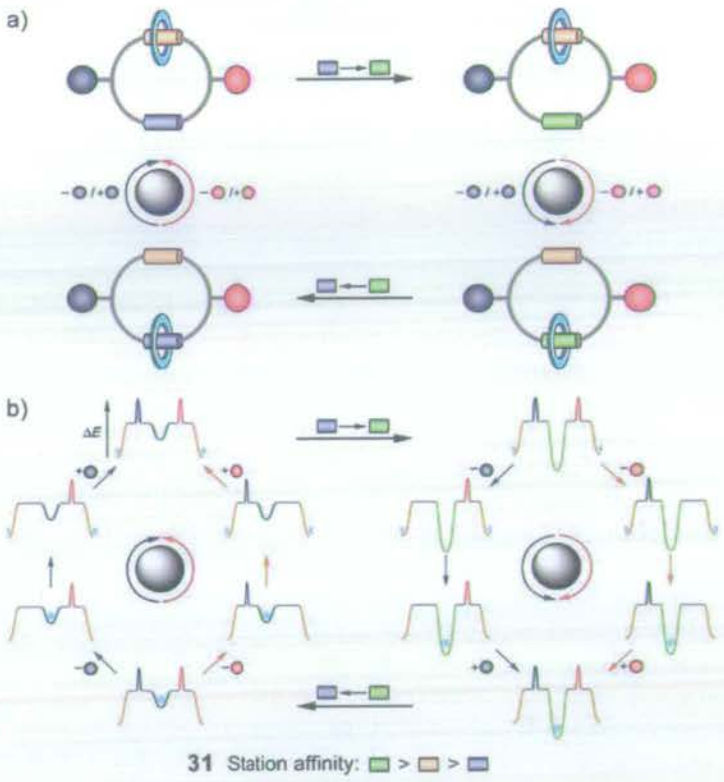

Fig. 14 **a** Schematic illustration and **b** potential energy surface for the blue ring in a minimalist [2]catenane rotary molecular motor, **31**

This concept was realized in chemical terms through the synthesis and operation of catenane **32** (Scheme 13) [92]. Net changes in the position or potential energy of the smaller ring were sequentially achieved by: (i) photoisomerization to the maleamide (→*mal-Z*-**32**); (ii) de-silylation/re-silylation (→*succ-Z*-**32**); (iii) re-isomerization to the fumaramide (→*succ-E*-**32**); and finally, (iv) de-tritylation/re-tritylation to regenerate *fum-E*-**32**, the whole reaction sequence producing a net clockwise (as drawn in Scheme 13) circumrotation of the small ring about the larger one. Exchanging the order of steps (ii) and (iv)—i.e. employing steps (v) and (vi) instead—produced an equivalent counter-clockwise rotation of the small ring.

Biological motors are obviously too complex for the thermodynamic function of individual amino acid movements to be unraveled in detail. In contrast, the simplicity of **32** and the minimalist nature of its design allows insight into the fundamental role each part of the structure plays in the operation of the rotary machine. The various chemical transformations perform two different functions: one pair (the linking/unlinking reactions—steps (ii) and (iv) or (v) and (vi)) modulates whether the small macrocycles can be

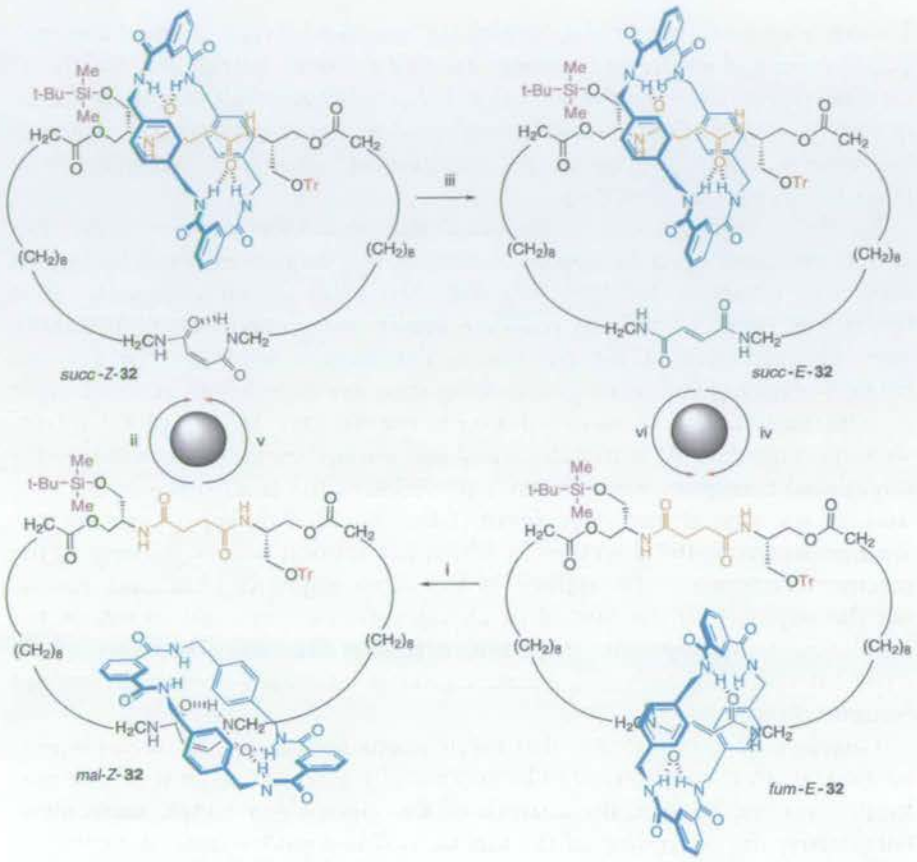

Scheme 13 A reversible [2]catenane rotary motor **32**. i) hν 254 nm, 5 min., 50%; ii) TBAF, 20 min then cool to − 78 °C and add 2,4,6-collidine, TBDMSOTf, 1 h, overall 61%; iii) piperidine, 1 h, ~ 100%; iv) $Me_2S{\cdot}BCl_3$, − 10 °C, 15 min then cool to − 78 °C and add 2,4,6-collidine, TrOTf, 5 h, overall 63%; v) $Me_2S{\cdot}BCl_3$, − 10 °C 10 min and then TrCl, Bu_4NClO_4, 2,4,6-collidine, 16 h, overall 74%; vi) TBAF, 20 min then cool to − 10 °C and add 2,4,6-collidine, TBDMSOTf, 40 min, overall 76%

exchanged between the two binding sites on the big ring or not (i.e. allow the small macrocycle to reach positional equilibrium and become statistically balanced between the two binding sites according to a Boltzmann distribution); the second pair (balance-breaking reactions—steps (i) and (iii)) isomerize the olefin station (either $E \rightarrow Z$ or $Z \rightarrow E$), switching its binding affinity for the small macrocycle either on or off. By changing the relative binding affinities of the two stations in the large ring, each balance-breaking stimulus provides a driving force for re-distribution of the small ring if it is able to move between the binding sites. In other words, the balance-breaking reactions control the *thermodynamics* and *impetus for net transport* by biased

Brownian motion; the linking/unlinking reactions largely control the relative *kinetics* and *ability to exchange*. Raising a kinetic barrier also "ratchets" transportation, allowing the statistical balance of the small ring to be subsequently broken without reversing the preceding net transportation sequence. Lowering a kinetic barrier allows "escapement" of a ratcheted quantity of rings in a particular direction.

To obtain 360° rotation of the small ring about the large ring, the four sets of reactions must be applied in one of two sequences, each taking the form: first a balance-breaking reaction; then a linking/unlinking step; then the second balance-breaking reaction; finally, the second linking/unlinking step. The direction of net rotation is determined solely by the way the balance-breaking and linking/unlinking steps are paired—an external input of information. The sense of rotation is not affected by any of the intrinsic requirements—2D symmetry breaking, energy input, thermal bath—for directional transport. The efficiency or yields of the reactions—or the position of the ring at any stage (even if the machine makes a "mistake")—are immaterial to the direction in which net motion occurs, as long as the reactions continue to be applied in the same sequence. Although reversing the sequence of the four steps changes the pairings and so rotates the small ring in the opposite direction, reversing the entire sequence of six chemical reactions does not, because linking-unlinking operations are not commutative.

Catenane **32** demonstrates that mechanisms formulated from non-equilibrium statistical mechanics can be successfully used to design synthetic molecular motors. In turn, the analysis of this deceptively simple molecule—particularly the separation of the kinetic and thermodynamic requirements for detailed balance—provides experimental insight into how an energy input is essential for directional rotation of a submolecular fragment by Brownian motion. Even though no net energy is used to power the motion, there has to be some processing of chemical energy for net rotation to be directional over a statistically significant number of molecules; a requirement that is absent if the equivalent motion is non-directional. The amount of energy conversion required to induce directionality has an intrinsic lower limit, corresponding to the binding energy difference of the fumaramide and maleamide binding sites, the same value that determines the directional efficiency of rotation and the maximum amount of work the motor can theoretically perform in a single cycle. The link between information and thermodynamics has haunted physics for nearly 150 years [93]. The factors that determine the sense of rotation in **32** (relying on the sequence, not energetics, of balance-breaking and linking/unlinking steps), together with the requirement for finite energy conversion to heat for directional rotation in circumstances when no work is done against an external force, illustrates how fundamental interplay between informational and thermodynamic laws governs directional Brownian rotation in molecular structures.

4
Property Effects Using Amide-Based Synthetic Molecular Machines

Whatever the future application of synthetic molecular machines may be, it is clear practical devices will require that the machine and its components are able to interact with the macroscopic world, either directly or through further interactions with other molecular-scale devices. Stimuli responsive molecular shuttles offer a generic approach which could be taken to create mechanical molecular switches for a variety of distance dependent properties. Suitable functionalization of the macrocycle and one end of the thread can lead to molecular switches that can change a variety of properties in response to a particular switching stimulus (Fig. 15) [94].

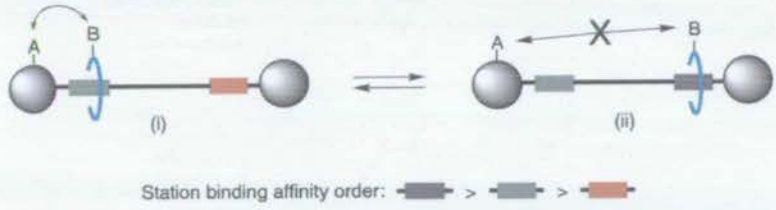

Fig. 15 Exploiting a well-defined, large amplitude positional change to trigger property changes. (i) A and B interact to produce a physical response (fluorescence quenching, specific dipole or magnetic moment, NLO properties, color, creation/concealment of a binding site or reactive/catalytic group, hydrophobic/hydrophilic region, etc.); (ii) moving A and B far apart mechanically switches off the interaction and the corresponding property effect

4.1
Switching On and Off Induced Circular Dichroism with a Molecular Shuttle

In a study of chiral dipeptide [2]rotaxanes, it had been shown that the presence of an intrinsically achiral benzylic amide macrocycle near to the chiral center can induce an asymmetric response in the aromatic ring absorption bands [95]. The induced circular dichroism (ICD) effect is strongest in apolar solvents when intercomponent interactions are maximized and the chirality is transmitted from the amino acid asymmetric center on the thread, via the achiral macrocycle to the aromatic rings of the achiral C-terminal stopper on the thread. These observations led to the design of the chiroptical molecular shuttle *E*/*Z*-**33** (Scheme 14) [96]. Unlike chiroptical switches in which the presence or handedness of chirality is intrinsically altered, *E*/*Z*-**33** remains chiral with the same handedness throughout; it is the *expression* of that chirality that is altered. In the *E*-**33** form, the macrocycle is held over the fumaramide binding site, far from the chiral center of the peptidic station. Correspondingly, the circular dichroism response is zero. In the *Z*-**33**

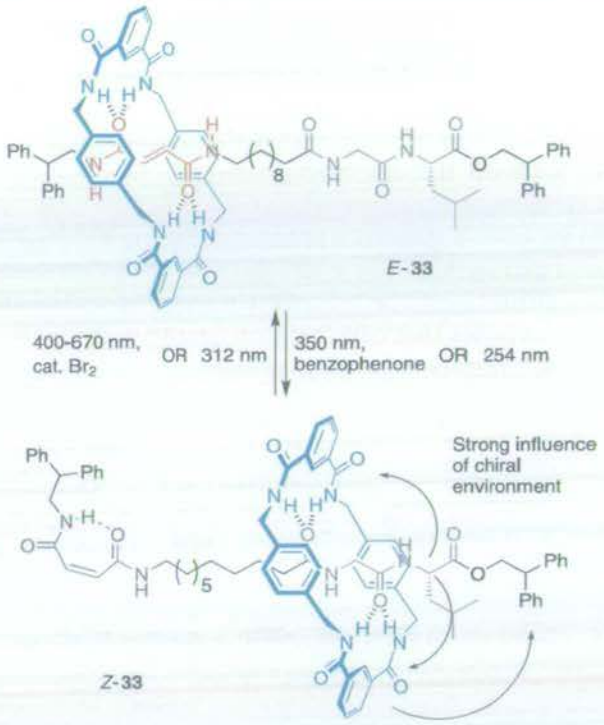

Scheme 14 Chiroptical switching in [2]rotaxane-based molecular shuttle *E*/*Z*-**33**

isomer, however, the macrocycle resides on the peptide station close to the L-Leu residue and a strong (– 13 k deg cm^2 dmol^{-1}), negative ICD response is observed [96]. Preparatively, the $E \rightarrow Z$ isomerization is most efficiently carried out by irradiation at 350 nm in the presence of a benzophenone sensitizer (photostationary state 70 : 30 *Z* : *E*), while the $Z \rightarrow E$ transformation can be achieved almost quantitatively by irradiation at 400–670 nm in the presence of catalytic Br_2.

4.2 Switching On and Off Fluorescence with a Molecular Shuttle

A similar approach has been used to make a molecular shuttle switch for fluorescence, *E*/*Z*-**34** (Scheme 15) [94]. This system also relies on the photoswitchable fumaramide/maleamide station but attached to the intermediate-affinity dipeptide station is an anthracene fluorophore, while the macrocycle now contains pyridinium units—known to quench anthracene fluorescence by electron transfer. In both the free thread and *E*-**34**, strong fluorescence (λ_{exc} = 365 nm) is observed, while shuttling of the macrocycle onto the glycylglycine station in *Z*-**34** quenches this emission almost completely. At the maximum of *E*-**34** emission

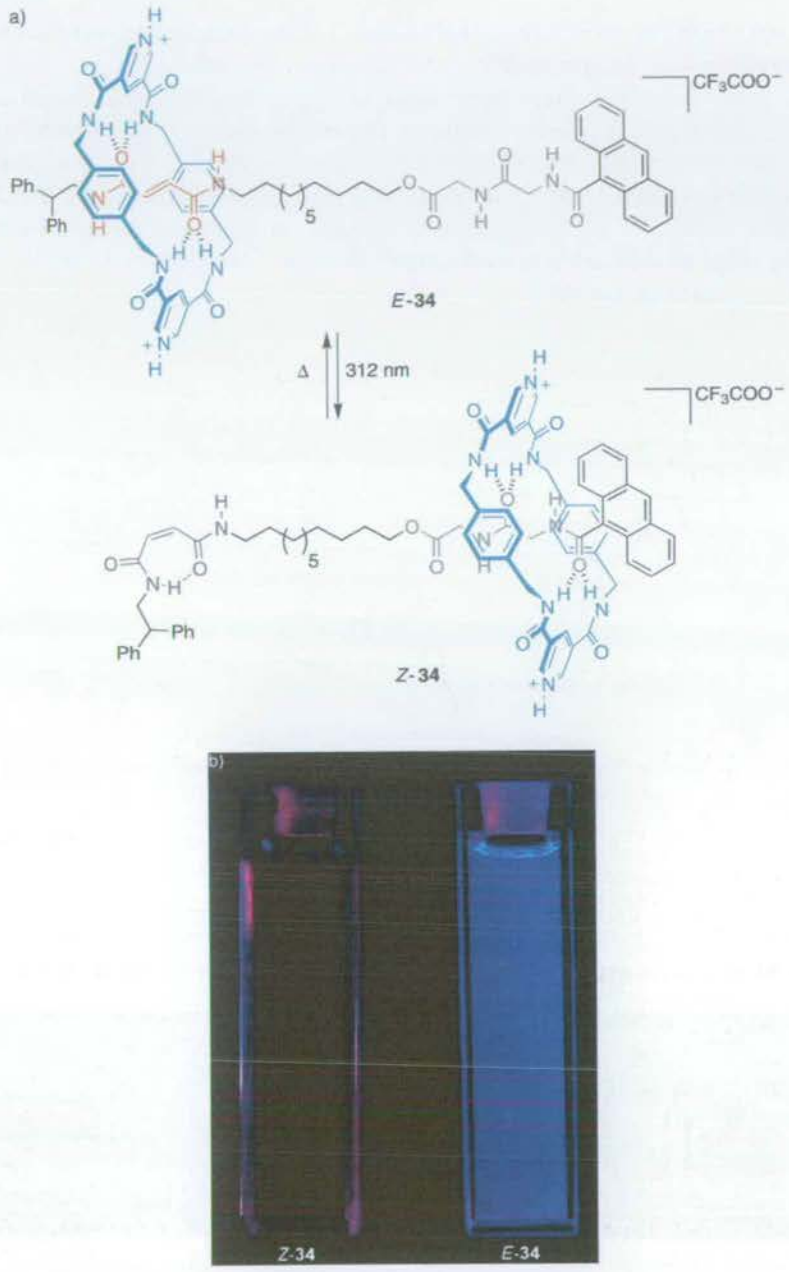

Scheme 15 A fluorescent molecular switch based on [2]rotaxane molecular shuttle *E*/*Z*-34. **a** Interconversion between fluorescent *E*-**34** and non-fluorescent *Z*-**34**; **b** images of cuvettes containing solutions of *Z*-**34** and *E*-**34** respectively (0.8 μM, CH_2Cl_2) demonstrating the clearly visible difference in fluorescence intensity. The photographs were taken while illuminating with UV light (365 nm)

(λ_{max} = 417 nm) there is a remarkable 200 : 1 difference in intensity between the two states—strikingly visible to the naked eye (Scheme 15b).

The same principles have been used to create switches that function in polymer films [97]. Patterns visible to the naked eye were generated using an environment-switchable shuttle covalently derivatized with poly(methyl methacrylate) (PMMA), **35** (Scheme 16 and Fig. 16). A polymer film INHIBIT logic gate based on a combination of control of submolecular positioning and chemical modification (protonation) was also demonstrated (**36**/**36**·2H$^+$, Scheme 16 and Fig. 17) [97].

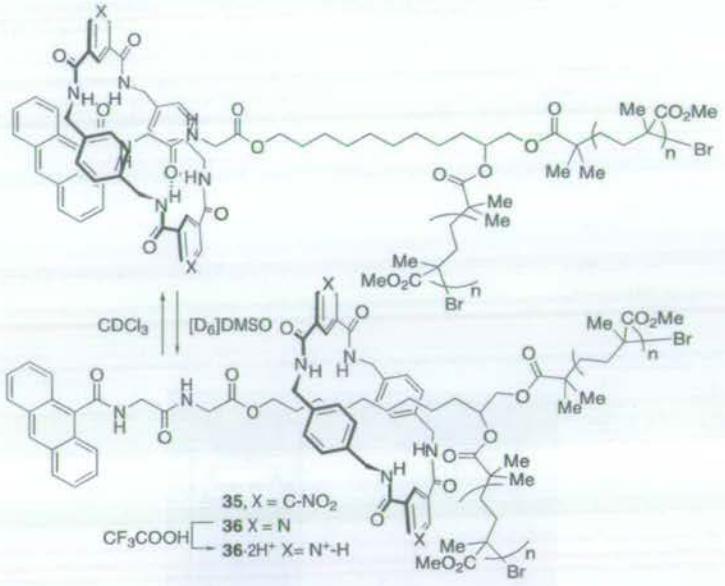

Scheme 16 Polymeric environment-switchable molecular shuttles **35** and **36**/**36**·2H$^+$

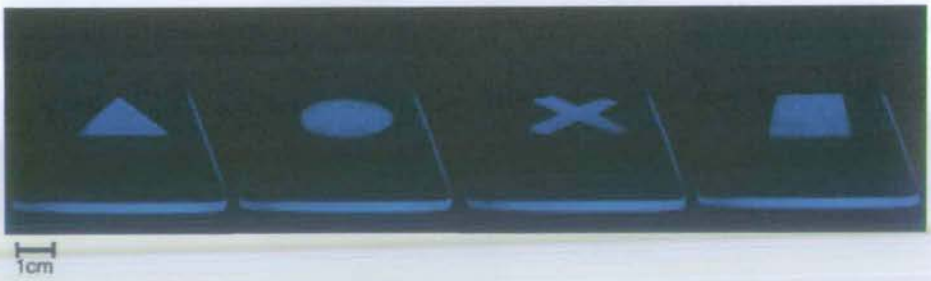

Fig. 16 Images obtained by casting films of polymer **35** on quartz slides, covering them with an aluminum mask and exposing the unmasked area to dimethylsulfoxide vapors for 5 minutes. The photographs were taken while illuminating the slides with UV light (254–350 nm). The symbols of Sony Playstation™ are illustrative of the types of patterns that can be created

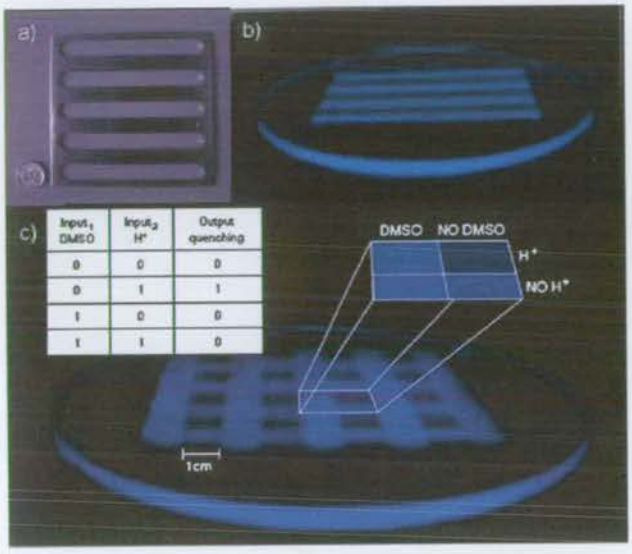

Fig. 17 A molecular shuttle Boolean logic gate that functions in a polymer film. **a** Aluminium grid used in the experiment. The coin shown for scale is a UK 5p piece. **b** Pattern generated when films of **36** were exposed to trifluoroacetic acid vapor for 5 minutes through the aluminium grid mask. **c** Criss-cross pattern obtained by rotating the aluminium grid 90° and exposing the film shown in (**b**) to DMSO vapor for a further 5 minutes. Only regions exposed to trifluoroacetic acid but not to DMSO are quenched. The truth table for an INHIBIT logic gate is shown in the *inset*. The photographs of the slides were taken in the dark while illuminating with UV light (254–350 nm)

4.3 Rotaxane-Based Photoresponsive Surfaces and Macroscopic Transport by Molecular Machines

Perhaps the most dramatic illustration of the potential of controlled molecular level motion in this type of system is a recent demonstration of the creation and utility of photoresponsive surfaces based on rotaxanes (Schemes 17 and 18, Fig. 18) [98]. The millimeter scale directional transport of diiodomethane across a surface (Fig. 18) was achieved using the biased Brownian motion of the components of a stimuli-responsive rotaxane **37** (Scheme 17) to expose or conceal fluoroalkane residues and thereby modify surface tension. The collective operation of a monolayer of the molecular shuttles attached to a self-assembled monolayer of 11-mercaptoundecanoic acid (11-MUA) on Au(111) (Scheme 18) was sufficient to power the movement of a microliter droplet of diiodomethane up a twelve degree incline (Fig. 18e–h).

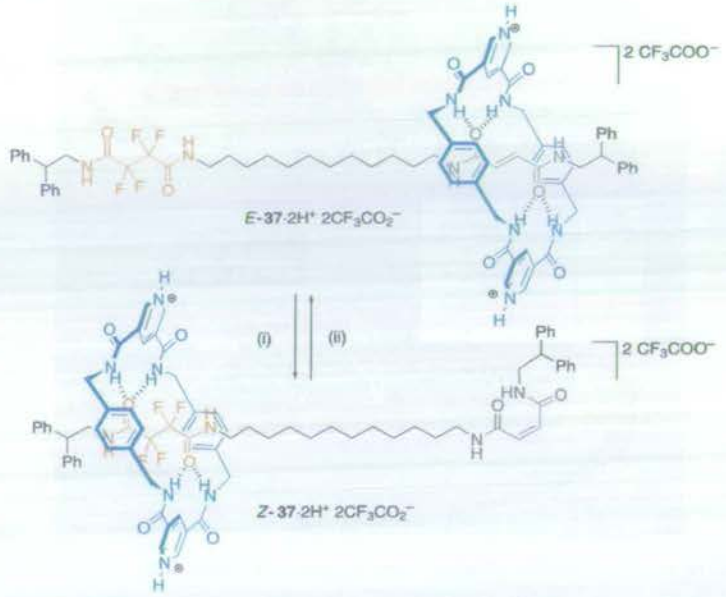

Scheme 17 Stimuli-induced positional change of the macrocycle in a fluorinated molecular shuttle, **37**·$2H^+$. (i) 254 nm, CH_2Cl_2, 5 min, 50%; (ii) piperidine, CH_2Cl_2, rt, 2 h then CF_3CO_2H, 100% or 115°, $C_2H_2Cl_4$, 24 h, 90%

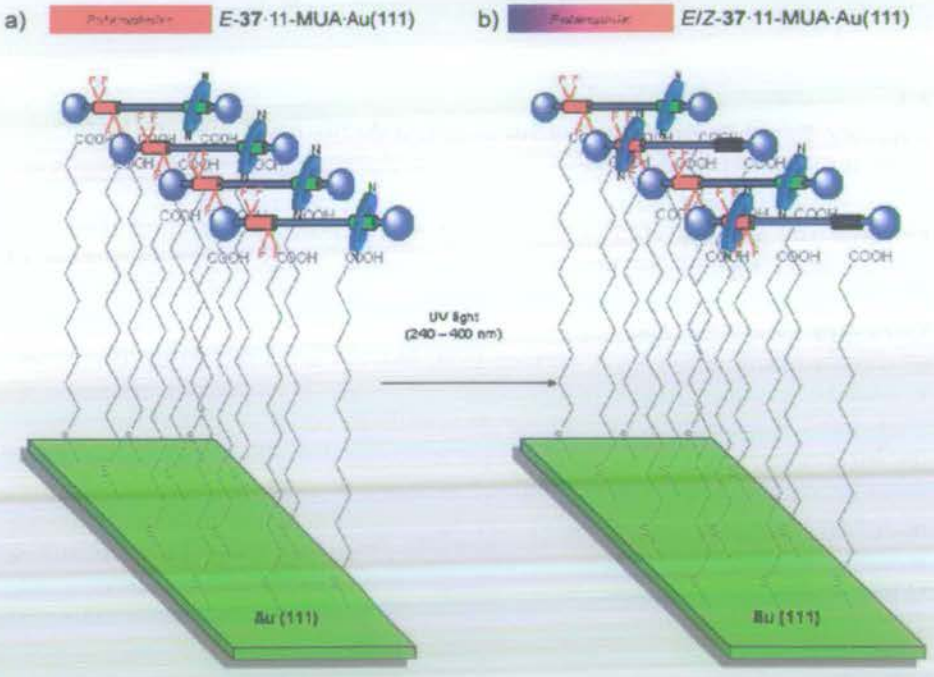

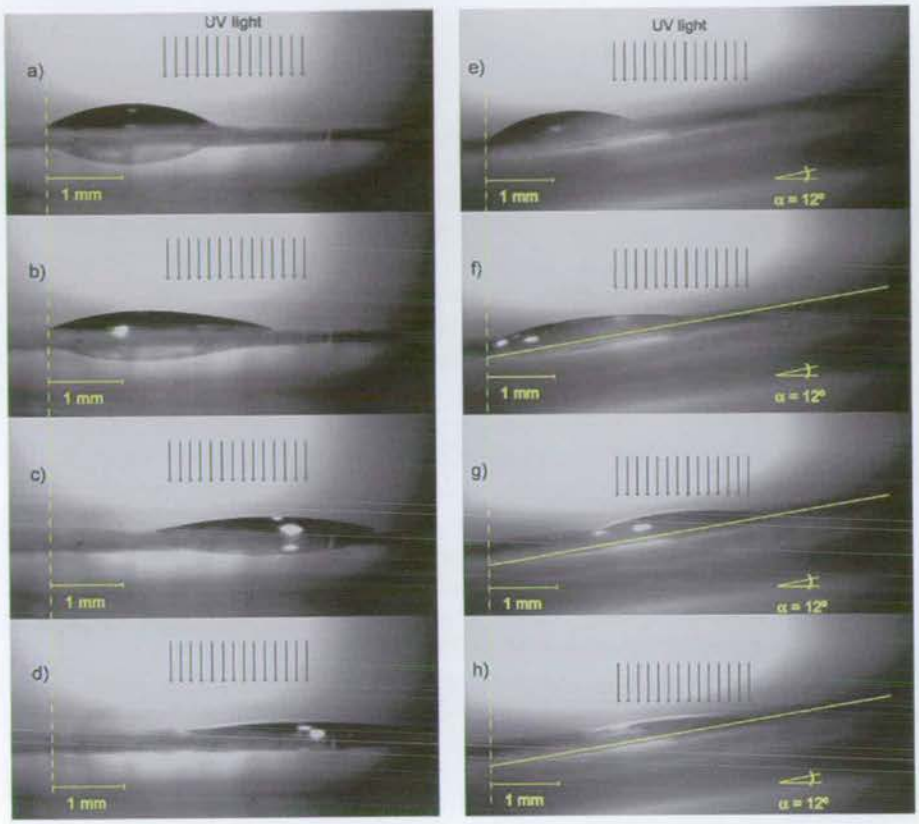

Fig. 18 Lateral photographs of light-driven directional transport of a 1.25 µl diiodomethane drop across the surface of a *E*-**37**·11-MUA·Au(111) substrate on mica arranged flat (**a–d**) and up a twelve degree incline (**e–h**). **a** Before irradiation (pristine *E*-**37**). **b** After 215 s of irradiation (20 s prior to transport) with UV light in the position shown (the right edge of the droplet and the adjacent surface). **c** After 370 s of irradiation (just after transport). **d** After 580 s of irradiation (at the photostationary state). **e** Before irradiation (pristine *E*-**37**). **f** After 160 s of irradiation (just prior to transport) with UV light in the position shown (the right edge of the droplet and the adjacent surface). **g** After 245 s of irradiation (just after transport). **h** After 640 s irradiation (at the photostationary state). For clarity, on photographs **f–h** a *yellow line* is used to indicate the surface of the substrate

◀ **Scheme 18** A photo-responsive surface based on switchable fluorinated molecular shuttles. Light-switchable rotaxanes with the fluoroalkane region (*orange*) exposed (*E*-**37**) were physisorbed onto a SAM of 11-MUA on Au(111) deposited onto either glass or mica to create a polarophobic surface, *E*-**37**·11-MUA·Au(111). Illumination with 240–400 nm light isomerizes some of the *E* olefins to *Z* causing a nanometer displacement of the rotaxane threads in the *Z*-shuttles which encapsulates the fluoroalkane units leaving a more polarophilic surface, *E*/*Z*-**37**·11-MUA·Au(111). The contact angles of droplets of a wide range of liquids change in response to the isomerization process

5 Conclusions

The relative positioning of the components of hydrogen bonded benzylic amide catenanes and rotaxanes can be switched, rotated, speeded up, slowed down and directionally driven in response to a remarkable range of stimuli. In doing so they can affect the nanoscopic and macroscopic properties of the system to which they belong. Whether one chooses to call these and similar systems "motors" and "machines", or rather consider them more classically in terms of specific triggered large amplitude conformational, configurational and structural changes, to appreciate the overriding importance and potential of controlled molecular motion one only has to realize that it is at the heart of virtually every biological process. In contrast, at the start of the 21st century none of mankind's technology (with the notable exception of liquid crystals) exploits controlled molecular-level motion in any way at all. When we learn how to produce molecules that can bias random dynamic processes in response to stimuli in a controlled manner—and discover how to interface their effects with other molecules and the outside world —it will add a completely new dimension to functional molecule and materials design. An improved understanding of physics and biology will also surely follow. There is no question that much of this revolution lies far in the future but it is inevitable nonetheless. The first small steps along this path have been taken.

References

1. Balzani V, Credi A, Raymo FM, Stoddart JF (2000) Angew Chem Int Ed 39:3349
2. Balzani V, Venturi M, Credi A (2003) Molecular devices and machines. A journey into the nanoworld. Wiley-VCH, Weinheim
3. Easton CJ, Lincoln SF, Barr L, Onagi H (2004) Chem Eur J 10:3120
4. Kottas GS, Clarke LI, Horinek D, Michl J (2005) Chem Rev 105:1281
5. Kinbara K, Aida T (2005) Chem Rev 105:1377
6. Kay ER, Leigh DA (2005) Synthetic molecular machines. In: Schrader T, Hamilton AD (eds) Functional artificial receptors. Wiley-VCH, Weinheim, p 333
7. Astumian RD, Hänggi P (2002) Phys Today 55(11):33
8. Jones RAL (2004) Soft machines: nanotechnology and life. OUP, Oxford
9. Hänggi P, Bartussek R (1996) Lect Notes Phys 476:294
10. Jülicher F, Ajdari A, Prost J (1997) Rev Mod Phys 69:1269
11. Reimann P (2002) Phys Rep 361:57
12. Reiman P, Hänggi (2002) Appl Phys A 75:169
13. Parrondo JMR, de Cisneros BJ (2002) Appl Phys A 75:179
14. Gabryœ BJ, Pesz K, Bartkiewicz SJ (2004) Physica A 336:112
15. Astumian RD (1997) Science 276:917
16. Astumian RD (2002) Appl Phys A 75:193
17. Oster G, Wang H (2003) 13:114
18. Kurzyński M, Chełminiak P (2004) Physica A 336:123

19. Schliwa M (ed) (2003) Molecular motors. Wiley-VCH, Weinheim
20. Hess H, Vogel V (2001) Rev Mol Biotechnol 82:67
21. Hess H, Bachand GD, Vogel V (2004) Chem Eur J 10:2110
22. Purcell EM (1977) Am J Phys 45:3
23. Schill G (1971) Catenanes, rotaxanes and knots. Academic Press, New York
24. Walba DM (1985) Tetrahedron 41:3161
25. Amabilino DB, Stoddart JF (1995) Chem Rev 95:2725
26. Leigh DA, Murphy A (1999) Chem Ind 178
27. Breault GA, Hunter CA, Mayers PC (1999) Tetrahedron 55:5265
28. Sauvage J-P, Dietrich-Buchecker CO (eds) (1999) Molecular catenanes, rotaxanes and knots. Wiley-VCH, Weinheim
29. Hannam JS, Kidd TJ, Leigh DA, Wilson AJ (2003) Org Lett 5:1907
30. Block SM (1996) Cell 87:151
31. Block SM (1998) Cell 93:5
32. Skou JC (1998) Angew Chem Int Ed 37:2321
33. Fyfe MCT, Glink PT, Menzer S, Stoddart JF, White AJP, Williams DJ (1997) Angew Chem Int Ed Engl 36:2068
34. Wasserman E (1960) J Am Chem Soc 82:4433
35. Schill G, Lüttringhaus A (1964) Angew Chem Int Ed Engl 3:546
36. Harrison IT, Harrison S (1967) J Am Chem Soc 89:5723
37. Harrison IT (1974) J Chem Soc Perkin Trans 1:301
38. Dietrich-Buchecker CO, Sauvage J-P, Kintzinger JP (1983) Tetrahedron Lett 24:5095
39. Dietrich-Buchecker CO, Sauvage J-P (1987) Chem Rev 87:795
40. Sauvage J-P (1990) Acc Chem Res 32:53
41. Busch DH, Stephenson NA (1990) Coord Chem Rev 100:119
42. Hoss R, Vögtle F (1994) Angew Chem Int Ed Engl 33:375
43. Philp D, Stoddart JF (1996) Angew Chem Int Ed Engl 35:1155
44. Fujita M, Ogura K (1996) Coord Chem Rev 148:249
45. Fyfe MCT, Stoddart JF (1997) Acc Chem Res 30:393
46. Jager R, Vögtle F (1997) Angew Chem Int Ed Engl 36:930
47. Diederich F, Strang PJ (eds) (1999) Templated organic synthesis. Wiley-VCH, Weinheim
48. Fujita M (1999) Acc Chem Res 32:53
49. Hubin TJ, Busch DH (2000) Coord Chem Rev 200:5
50. Furlan RLE, Otto S, Sanders JKM (2002) Proc Natl Acad Sci USA 99:4801
51. Chambron J-C, Collin J-P, Heitz V, Jouvenot D, Kern J-M, Mobian P, Pomeranc D, Sauvage J-P (2004) Eur J Org Chem 1627
52. Hunter CA (1992) J Am Chem Soc 114:5303
53. Vögtle F, Meier S, Hoss R (1992) Angew Chem Int Ed Engl 31:1619
54. Johnston AG, Leigh DA, Pritchard RJ, Deegan MD (1995) Angew Chem Int Ed Engl 34:1209
55. Johnston AG, Leigh DA, Murphy A, Smart JP, Deegan MD (1996) J Am Chem Soc 118:10662
56. Johnston AG, Leigh DA, Nezhat L, Smart JP, Deegan MD (1995) Angew Chem Int Ed Engl 34:1212
57. Leigh DA, Venturini A, Wilson AJ, Wong JKY, Zerbetto F (2004) Chem Eur J 10:4960
58. Leigh DA, Murphy A, Smart JP, Slawin AMZ (1997) Angew Chem Int Ed Engl 36:728
59. Lane AS, Leigh DA, Murphy A (1997) J Am Chem Soc 119:11092
60. Gatti FG, Leigh DA, Nepogodiev SA, Slawin AMZ, Teat SJ, Wong JKY (2001) J Am Chem Soc 123:5983

61. Leigh DA, Murphy A, Smart JP, Deleuze MS, Zerbetto F (1998) J Am Chem Soc 120:6458
62. Deleuze MS, Leigh DA, Zerbetto F (1999) J Am Chem Soc 121:2364
63. Leigh DA, Troisi A, Zerbetto F (2001) Chem Eur J 7:1450
64. Sandström J (1982) Dynamic NMR spectroscopy. Academic Press, London
65. Dahlquist FW, Longmur KJ, Du Vernet RB (1975) J Magn Reson 17:406
66. Leigh DA, Troisi A, Zerbetto F (2000) Angew Chem Int Ed 39:350
67. Anelli PL, Spencer N, Stoddart JF (1991) J Am Chem Soc 113:5131
68. Keaveney CM, Leigh DA (2004) Angew Chem Int Ed 43:1222
69. Brouwer AM, Frochot C, Gatti FG, Leigh DA, Mottier L, Paolucci F, Roffia S, Wurpel GWH (2001) Science 291:2124
70. Altieri A, Gatti FG, Kay ER, Leigh DA, Martel D, Paolucci F, Slawin AMZ, Wong JKY (2003) J Am Chem Soc 125:8644
71. Leigh DA, Pérez EM (2004) Chem Commun 2262
72. Altieri A, Bottari G, Dehez F, Leigh DA, Wong JKY, Zerbetto F (2003) Angew Chem Int Ed 42:2296
73. Bottari G, Dehez F, Leigh DA, Nash PJ, Pérez EM, Wong JKY, Zerbetto F (2003) Angew Chem Int Ed 42:5886
74. Hanke A, Metzler R (2002) Chem Phys Lett 359:22
75. Bermudez V, Capron N, Gase T, Gatti FG, Kajzar F, Leigh DA, Zerbetto F, Zhang SW (2000) Nature 406:608
76. Gatti FG, León S, Wong JKY, Bottari G, Altieri A, Morales MAF, Teat SJ, Frochot C, Leigh DA, Brouwer AM, Zerbetto F (2003) Proc Natl Acad Sci USA 100:10
77. Lukin O, Kubota T, Okamoto Y, Schelhase F, Yoneva A, Müller WM, Müller U, Vögtle F (2003) Angew Chem Int Ed 42:4542
78. Leigh DA, Moody K, Smart JP, Watson KJ, Slawin AMZ (1996) Angew Chem Int Ed Engl 35:306
79. Ceroni P, Leigh DA, Mottier L, Paolucci F, Roffia S, Tetard D, Zerbetto F (1999) J Phys Chem B 103:10171
80. Leigh DA, Wong JKY, Dehez F, Zerbetto F (2003) Nature 424:174
81. Kelly TR, De Silva H, Silva RA (1999) Nature 401:150
82. Kelly TR (2001) Acc Chem Res 34:514
83. Sestelo JP, Kelly TR (2002) Appl Phys A 75:337
84. Koumura N, Zijlstra RWJ, van Delden RA, Harada N, Feringa BL (1999) Nature 401:152
85. Kelly TR, Silva RA, De Silva H, Jasmin S, Zhao YJ (2000) J Am Chem Soc 122:6935
86. Feringa BL (2001) Acc Chem Res 34:504
87. Feringa BL, Koumura N, van Delden RA, ter Wiel MKJ (2002) Appl Phys A 75:301
88. Koumura N, Geertsema EM, van Gelder MB, Meetsma A, Feringa BL (2002) J Am Chem Soc 124:5037
89. Geertsema EM, Koumura N, ter Wiel MKJ, Meetsma A, Feringa BL (2002) Chem Commun 2962
90. ter Wiel MKJ, van Delden RA, Meetsma A, Feringa BL (2003) J Am Chem Soc 125:15076
91. Feringa BL, van Delden RA, ter Wiel MKJ (2003) Pure Appl Chem 75:563
92. Hernández JV, Kay ER, Leigh DA (2004) Science 306:1532
93. Maxwell JC (1867) Letter to PG Tait, 11 December 1867. Quoted in: Knot CG (1911) Life and scientific work of Peter Guthrie Tait. Cambridge University Press, Cambridge, p 213

94. Pérez EM, Dryden DTF, Leigh DA, Teobaldi G, Zerbetto F (2004) J Am Chem Soc 126:12210
95. Asakawa M, Brancato G, Fanti M, Leigh DA, Shimizu T, Slawin AMZ, Wong JKY, Zerbetto F, Zhang SW (2002) J Am Chem Soc 124:2939
96. Bottari G, Leigh DA, Pérez EM (2003) J Am Chem Soc 125:13360
97. Leigh DA, Morales MAF, Pérez EM, Wong JKY, Saiz CG, Slawin AMZ, Carmichael AJ, Haddleton DM, Brouwer AM, Buma WJ, Wurpel GWH, León S, Zerbetto F (2005) Angew Chem Int Ed 44:3062
98. Berná J, Leigh DA, Lubomska M, Mendoza SM, Pérez EM, Rudolf P, Teobaldi G, Zerbetto F (2005) Nature Mater 4:704

J|A|C|S
ARTICLES
Published on Web 03/02/2006

Beyond Switches: Ratcheting a Particle Energetically Uphill with a Compartmentalized Molecular Machine

Manashi N. Chatterjee, Euan R. Kay, and David A. Leigh*
Contribution from the School of Chemistry, University of Edinburgh, The King's Buildings, West Mains Road, Edinburgh EH9 3JJ, United Kingdom
Received November 10, 2005; E-mail: David.Leigh@ed.ac.uk

Abstract: Here we correlate chemical (covalent), physical (thermodynamic), and statistical (population distribution) descriptions of behavior with the way that two new types of simple molecular machines (the threads of rotaxanes) perform the task of transporting a Brownian substrate (the rotaxane macrocycle) between two distinguishable binding sites. The first machine−substrate ensemble is a [2]rotaxane that operates through a mechanism that intrinsically causes it to change the average position of the macrocycle irreversibly. This contrasts with the behavior of classic stimuli-responsive molecular shuttles that act as reversible molecular switches. The second system is a compartmentalized molecular machine that is able to pump its substrate energetically uphill using the energy provided by a photon by means of an olefin photoisomerization. Resetting this compartmentalized molecular machine does not undo the work it has carried out or the task performed, a significant difference to a simple molecular switch and a characteristic we recognize as "ratcheting" (see Scheme 8). The ratcheting mechanism allows the [2]rotaxane to carry out the transport function envisaged for the historical thought-machines, Smoluchowski's Trapdoor and Maxwell's Pressure Demon, albeit via an unrelated mechanism and using an input of energy. We define and exemplify the terms "ratcheting" and "escapement" in mechanical terms for the molecular level and outline the fundamental phenomenological differences that exist between what constitutes a two-state Brownian switch, a two-state Brownian memory or "flip-flop", and a (two-stroke) Brownian motor. We also suggest that considering the relationship between the parts of a molecular machine and a substrate in terms of "statistical balance" and "linkage" could be useful in the design of more complex systems and in helping to understand the role of individual amino acids and peptide fragments during the directional transport of substrates by biological pumps and motors.

Introduction

In recent years it has proved possible to design synthetic molecular systems in which positional displacements of submolecular components result from moving energetically downhill,[1] but what are the structural features necessary for molecules to convert chemical energy into mechanical work? How can we make a synthetic molecular machine that pumps ions against a gradient, say, or moves itself or a substrate energetically uphill along a track? We know that nature has developed such machines and refined them to a high degree of efficiency[2] and yet the chemistry literature is surprisingly poor when it comes to the fundamental guidelines necessary to invent them. Here we examine the way that some simple molecular machines carry out the task of transporting a particle along a one-dimensional, two minimum, potential energy surface and attempt to correlate the chemical (covalent structure), physical potential (thermodynamic and kinetic properties governed by attractive and repulsive noncovalent interactions), and statistical (population distribution) behavior of the system with aspects of the task performance. The results begin to provide the phenomenological framework necessary for chemists to design more complex compartmentalized molecular-level machines (assemblies of simpler machines that each act as components by performing a set task). It may also prove useful in understanding the roles played by individual submolecular fragments during the operation of biological machines.

The Two-Compartment Brownian Particle "Thought-Machines"

The design of tiny machines capable of transporting Brownian particles selectively between two compartments—i.e., effectively along a one-dimensional, two minimum, potential energy surface—was the subject of several celebrated historical "thought-machines" (Figure 1).[3−7] Both Maxwell's Demon[4] (Figure 1a and b) and Smoluchowski's Trapdoor[5] (Figure 1d) were concerned with trying to set up temperature or pressure gradients in systems containing multiple Brownian particles through their

(1) (a) Balzani, V.; Credi, A.; Raymo, F. M.; Stoddart, J. F. *Angew. Chem., Int. Ed.* **2000**, *39*, 3349−3391. (b) Stoddart, J. F., Ed. Special issue on *Molecular Machines. Acc. Chem. Res.* **2001**, *34*, 409−522. (c) Balzani, V.; Venturi, M.; Credi, A. *Molecular Devices and Machines. A Journey into the Nanoworld*; Wiley-VCH: Weinheim, Germany, 2003. (d) Easton, C. J.; Lincoln, S. F.; Barr, L.; Onagi, H. *Chem. Eur. J.* **2004**, *10*, 3120−3128. (e) Flood, A. H.; Ramirez, R. J. A.; Deng, W. Q.; Muller, R. P.; Goddard, W. A.; Stoddart, J. F. *Aust. J. Chem.* **2004**, *57*, 301−322. (f) Crowley, J. D.; Goshe, A. J.; Steele, I. M.; Bosnich, B. *Chem. Eur. J.* **2004**, *10*, 1944−1955. (g) Kottas, G. S.; Clarke, L. I.; Horinek, D.; Michl, J. *Chem. Rev.* **2005**, *105*, 1281−1376. (h) Kinbara, K.; Aida, T. *Chem. Rev.* **2005**, *105*, 1377−1400. (i) Kay, E. R.; Leigh, D. A. In *Functional Artificial Receptors*; Schrader, T., Hamilton, A. D., Eds.; Wiley-VCH: Weinheim, Germany, 2005; pp 333−406. (j) Kelly, T. R., Ed. Volume on *Molecular Machines. Top. Curr. Chem.* **2005**, *262*, 1−236.

(2) *Molecular Motors*; Schliwa, M., Ed.; Wiley-VCH: Weinheim, Germany, 2003.

10.1021/ja057664z CCC: $33.50

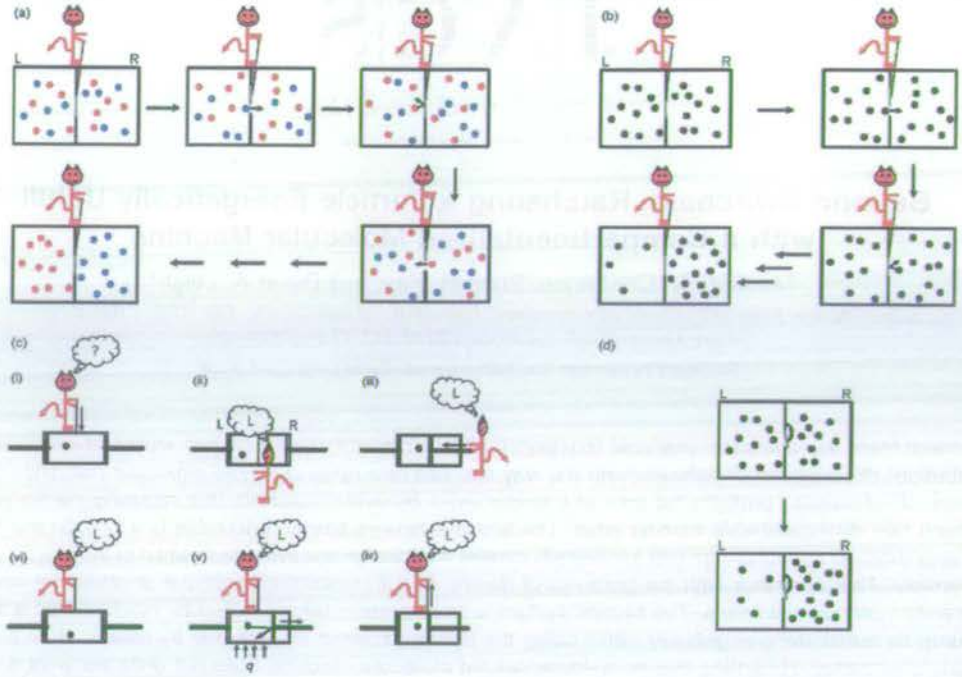

Figure 1. Examples of two-compartment Brownian "thought-machines": (a) Maxwell's "temperature demon" in which a gas at uniform temperature is sorted into "hot" and "cold" molecules.[4] Particles with energy higher than the average are represented by red dots while blue dots represent particles with energies lower than the average. (b) A Maxwellian "pressure demon" in which a pressure gradient would be created if the door was only opened when a particle in the left compartment approached it.[4c] (c) Szilard's Engine, which attempts to do work with a piston using heat drawn from an external reservoir by a pressure demon.[6] (i) Initially, a single Brownian particle occupies a cylinder with a piston at either end. A frictionless partition is put in place to divide the container into two compartments ((i) → (ii), unlinking stimulus). (ii) The demon then detects the particle and determines in which compartment it resides (the left (L) compartment in the depicted example). (iii) Using this information, the demon is able to move the opposite piston into position without meeting any resistance from the particle. (iv) The partition is removed (linking stimulus), allowing (v) the "gas" to expand against the piston, doing work against any attached load. To replenish the energy used by the piston and maintain a constant temperature, heat must flow into the system. To complete the thermodynamic cycle and reset the machine, the demon's memory of where the particle was must be erased ((vi) → (i)). (d) Smoluchowski's Trapdoor: an "automatic" pressure demon. The directionally discriminating behavior is carried out by a wholly mechanical device, a trapdoor that is intended to open when hit from one direction but not the other (note, this still involves the communication of information between the particle and the machine; the demon is incorporated into the door mechanism).[5]

controlled exchange between two compartments; Szilard's Engine[6] (Figure 1c) endeavored to utilize the pressure exerted by one Brownian particle located in one of two compartments to do work. The behaviors of all four "Gedankenmaschinen" were considered without an external energy source (other than a heat reservoir at the same temperature as the Gedankenmaschine system)—their purpose was to test the nature of the

(3) *Maxwell's Demon 2. Entropy, classical and quantum information, computing*; Leff, H. S., Rex, A. F., Eds.; Institute of Physics Publishing: Bristol, U.K., 2003.

(4) The first (a) private and (b) public written discussions of the "temperature demon" were as follows: (a) Maxwell, J. C. *Letter to P. G. Tait, 11 December 1867.* Quoted in Knott, C. G. *Life and Scientific Work of Peter Guthrie Tait*; Cambridge University Press: London, 1911; pp 213–214. (b) Maxwell, J. C. *Theory of Heat*; Longmans, Green and Co.: London, 1871; Chapter 12. (c) Maxwell introduced the idea of a "pressure demon" in a later (undated) letter to Tait, also quoted in Knott, C. G. *Life and Scientific Work of Peter Guthrie Tait*; Cambridge University Press: London, 1911; pp 214–215 and ref (3). A pressure demon is able to operate in a system linked to a constant-temperature reservoir with the sole effect of using energy transferred as heat from that reservoir to do work (see Szilard's engine, Figure 1c, ref 6). This is in conflict with the Kelvin-Planck form of the Second Law, whereas the temperature demon challenges the Clausius definition.

(5) Smoluchowski's Trapdoor [(a) von Smoluchowski, M. *Phys. Z.* **1912**, *13*, 1069–1080. (b) von Smoluchowski, M. *Vortgage über die Kinetische Theorie der Materie und der Elektrizitat*; Planck, M., Ed.; Teubner und Leipzig: Berlin, 1914; pp 89–121] aims to transport particles selectively from the left compartment to the right in Figure 1d. However, in the absence of a mechanism whereby the trapdoor can dissipate energy, it will be at thermal equilibrium with its surroundings. This means it must spend much of its time open, unable to influence particle transport. Rarely, it will be closed when a particle approaches from the right and will open on collision with a particle coming from the left—doing its job as intended. Such events are balanced, however, by the door snapping shut on a particle from the right, pushing it into the left chamber. Overall, the probability of a particle moving from left to right is equal to that for moving right to left and so the trapdoor cannot accomplish its intended function adiabatically.

(6) Szilard, L. *Z. Phys.* **1929**, *53*, 840–856.

(7) Feynman, R. P.; Leighton, R. B.; Sands, M. *The Feynman Lectures on Physics*; Addison-Wesley: Reading, MA, 1963; Vol. 1, Chapter 46.

(8) For the realization of Feynman's ratchet-and-pawl in molecular form see: (a) Kelly, T. R.; Tellitu, I.; Sestelo, J. P. *Angew. Chem., Int. Ed. Engl.* **1997**, *36*, 1866–1868. For nonadiabatic molecular versions which unidirectionally rotate see: (b) Kelly, T. R.; De Silva, H.; Silva, R. A. *Nature* **1999**, *401*, 150–152. (c) Leigh, D. A.; Wong, J. K. Y.; Dehez, F.; Zerbetto, F. *Nature* **2003**, *424*, 174–179. (d) Hernández, J. V.; Kay, E. R.; Leigh, D. A. *Science* **2004**, *306*, 1532–1537. For other types of rotary molecular motors see: (e) Koumura, N.; Zijlstra, R. W. J.; van Delden, R. A.; Harada, N.; Feringa, B. L. *Nature* **1999**, *401*, 152–155. (f) Koumura, N.; Geertsema, E. M.; Meetsma, A.; Feringa, B. L. *J. Am. Chem. Soc.* **2000**, *122*, 12005–12006. (g) Koumura, N.; Geertsema, E. M.; van Gelder, M. B.; Meetsma, A.; Feringa, B. L. *J. Am. Chem. Soc.* **2002**, *124*, 5037–5051. (h) Geertsema, E. M.; Koumura, N.; ter Wiel, M. K. J.; Meetsma, A.; Feringa, B. L. *Chem. Commun.* **2002**, 2962–2963. (i) van Delden, R. A.; Koumura, N.; Harada, N.; Feringa, B. L. *Proc. Natl. Acad. Sci. U.S.A.* **2002**, *99*, 4945–4949. (j) ter Wiel, M. K. J.; van Delden, R. A.; Meetsma, A.; Feringa, B. L. *J. Am. Chem. Soc.* **2003**, *125*, 15076–15086. (k) van Delden, R. A.; Koumura, N.; Schoevaars, A.; Meetsma, A.; Feringa, B. L. *Org. Biomol. Chem.* **2003**, *1*, 33–35. (l) ter Wiel, M. K. J.; van Delden, R. A.; Meetsma, A.; Feringa, B. L. *J. Am. Chem. Soc.* **2005**, *127*, 14208–14222. (m) Pijper, D.; van Delden, R. A.; Meetsma, A.; Feringa, B. L. *J. Am. Chem. Soc.* **2005**, *127*, 17612–17613. (n) ter Wiel, M. K. J.; van Delden, R. A.; Meetsma, A.; Feringa, B. L. *Org. Biomol. Chem.* **2005**, *3*, 4071–4076. (o) van Delden, R. A.; ter Wiel, M. K. J.; Pollard, M. M.; Vicario, J.; Koumura, N.; Feringa, B. L. *Nature* **2005**, *437*, 1337–1340. (p) Fujita, T.; Kuwahara, S.; Harada, N. *Eur. J. Org. Chem.* **2005**, 4533–4543. (q) Kuwahara, S.; Fujita, T.; Harada, N. *Eur. J. Org. Chem.* **2005**, 4544–4556. (r) Fletcher, S. P.; Dumur, F.; Pollard, M. M.; Feringa, B. L. *Science* **2005**, *310*, 80–82. (s) Lin, Y.; Dahl, B. J.; Branchaud, B. P. *Tetrahedron Lett.* **2005**, *46*, 8359–8362.

Scheme 1. Previously Reported[13j] [2]Rotaxane, **1**, that Functions as a Stimuli-Responsive Molecular Shuttle[a]

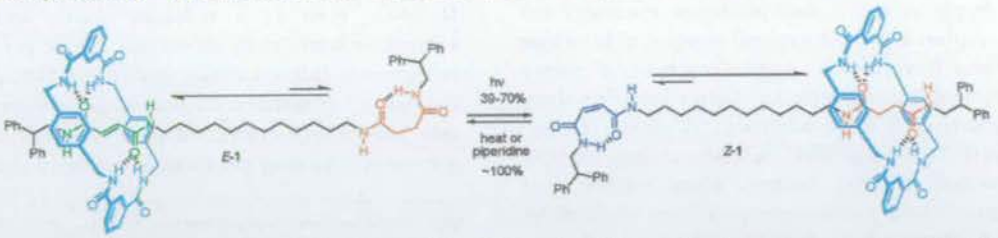

[a] At 254 nm the photostationary state is 61:39 *E*:*Z*,[13j] at 312 nm it is ~50:50, and at 350 nm with a benzophenone sensitizer it is 40:60 *E*:*Z*[13j] and can be increased up to 30:70 *E*:*Z*[20] for some derivatives.

Second Law of Thermodynamics, not to see how a working Brownian machine could be achieved (that was probably first discussed[7,8] by Feynman). However, modern synthetic routes allow us to make molecules in which the Brownian motion of substrates *does* occur between two well-defined locations, e.g., rotaxane-based molecular shuttles. This enables us to re-visit the question of how to transport a Brownian particle between two distinguishable sites, not from the point of view of doing so adiabatically, but rather to see how such a task can be performed by a molecular-level machine.

Rotaxanes and Molecular Shuttles

Rotaxanes are chemical structures in which one or more macrocycles are mechanically prevented from de-threading from linear chains by bulky "stoppers".[9] Even though the rings are not covalently attached to the threads, rotaxanes are molecules—not supramolecular complexes—as covalent bonds must be broken in order to separate the components from each other.[9,10] The interactions generally used to direct the synthesis of rotaxanes often "live-on" in the product, providing a well-defined binding site or "station" for the ring on the thread. If two or more stations are present on a thread with a traversable path between them, the rotaxane can be considered a "molecular shuttle"[11] in which the ring is incessantly and randomly exchanged between the binding sites.[12] Stimuli-responsive molecular shuttles are rotaxanes in which the net position of the macrocycle on the thread (i.e., the statistical distribution of the ring between the stations) changes in response to external triggers (light,[13] heat,[14] electrons,[15] chemical,[16] pH,[17] binding events,[18] etc.). Generally, the external stimulus alters the structure of one of the binding sites so as to change the relative binding affinities of the stations for the macrocycle, placing the system out of co-conformational[19] equilibrium. Relaxation toward the new global minimum subsequently occurs by the macrocycle moving along the thread. A typical example[13j] of a light-switchable amide-based molecular shuttle is shown in Scheme 1.

However, we can also think of stimuli-responsive molecular shuttles in another way; we can consider just the thread portion of such a molecule as a machine that directionally transports a particle—the interlocked macrocycle—between two sites (compartments) on a one-dimensional potential energy surface.[20] The significance of considering a rotaxane in this way is that over

(9) (a) Schill, G. *Catenanes, Rotaxanes and Knots*; Academic Press: New York, 1971. (b) Amabilino, D. B.; Stoddart, J. F. *Chem. Rev.* **1995**, *95*, 2725–2828. (c) *Molecular Catenanes Rotaxanes and Knots*; Sauvage, J.-P., Dietrich-Buchecker, C. O., Eds.; Wiley-VCH: Weinheim, Germany, 1999.

(10) Hannam, J. S.; Lacy, S. M.; Leigh, D. A.; Saiz, C. G.; Slawin, A. M. Z.; Stitchell, S. G. *Angew. Chem., Int. Ed.* **2004**, *43*, 3260–3264.

(11) (a) Anelli, P. L.; Spencer, N.; Stoddart, J. F. *J. Am. Chem. Soc.* **1991**, *113*, 5131–5133. For the first example of an amide-based molecular shuttle see: (b) Lane, A. S.; Leigh, D. A.; Murphy, A. *J. Am. Chem. Soc.* **1997**, *119*, 11092–11093.

(12) The key feature of a rotaxane architecture from the point of view of molecular-level machines is that movement of the macrocycle in any direction other than along the thread is resisted by enormous steric forces up until the breaking point of covalent bonds in the macrocycle or the thread. This is a fundamentally different situation to a host–guest complex when, following de-complexation from the binding site, the motion of the ring is not restricted in any dimension and it is free to exchange with others in the medium. Simple host–guest/supramolecular systems cannot function as nanoscale mechanical machines unless restrictions on the exchange of the unbound species with the bulk apply (as happens with kinetically stable pseudo-rotaxanes) or the binding event brings about a mechanical (i.e., conformational) change in one of the molecular components. Similarly, molecules that are not kinetically stable—this includes some rotaxanes that are thermodynamically stable but kinetically labile—cannot behave as molecular machines if they exchange components with the bulk quicker than the time scale of their stimuli-induced change of position. Molecular machines designed to exploit motion have to be kinetically associated with their substrates throughout the operation of the machine.

(13) For examples of photochemically responsive molecular shuttles see: (a) Benniston, A. C.; Harriman, A. *Angew. Chem., Int. Ed. Engl.* **1993**, *32*, 1459–1461. (b) Benniston, A. C.; Harriman, A.; Lynch, V. M. *Tetrahedron Lett.* **1994**, *35*, 1473–1476. (c) Benniston, A. C.; Harriman, A.; Lynch, V. M. *J. Am. Chem. Soc.* **1995**, *117*, 5275–5291. (d) Murakami, H.; Kawabuchi, A.; Kotoo, K.; Kunitake, M.; Nakashima, N. *J. Am. Chem. Soc.* **1997**, *119*, 7605–7606. (e) Armaroli, N.; Balzani, V.; Collin, J.-P.; Gaviña, P.; Sauvage, J.-P.; Ventura, B. *J. Am. Chem. Soc.* **1999**, *121*, 4397–4408. (f) Ashton, P. R.; Ballardini, R.; Balzani, V.; Credi, A.; Dress, K. R.; Ishow, E.; Kleverlaan, C. J.; Kocian, O.; Preece, J. A.; Spencer, N.; Stoddart, J. F.; Venturi, M.; Wenger, S. *Chem. Eur. J.* **2000**, *6*, 3558–3574. (g) Wurpel, G. W. H.; Brouwer, A. M.; van Stokkum, I. H. M.; Farran, A.; Leigh, D. A. *J. Am. Chem. Soc.* **2001**, *123*, 11327–11328. (h) Brouwer, A. M.; Frochot, C.; Gatti, F. G.; Leigh, D. A.; Mottier, L.; Paolucci, F.; Roffia, S.; Wurpel, G. W. H. *Science* **2001**, *291*, 2124–2128. (i) Stanier, C. A.; Alderman, S. J.; Claridge, T. D. W.; Anderson, H. L. *Angew. Chem., Int. Ed.* **2002**, *41*, 1769–1772. (j) Altieri, A.; Bottari, G.; Dehez, F.; Leigh, D. A.; Wong, J. K. Y.; Zerbetto, F. *Angew. Chem., Int. Ed.* **2003**, *42*, 2296–2300. (k) Abraham, W.; Grubert, L.; Grummt, U. W.; Buck, K. *Chem. Eur. J.* **2004**, *10*, 3562–3568. (l) Murakami, H.; Kawabuchi, A.; Matsumoto, R.; Ido, T.; Nakashima, N. *J. Am. Chem. Soc.* **2005**, *127*, 15891–15899. (m) Schmidt-Schäffer, S.; Grubert, L.; Grummt, U. W.; Buck, K.; Abraham, W. *Eur. J. Org. Chem.* **2006**, 378–398. (n) Wang, Q.-C.; Ma, X.; Qu, D.-H.; Tian, H. *Chem. Eur. J.* **2006**, *12*, 1088–1096. (o) Balzani, V.; Clemente-León, M.; Credi, A.; Ferrer, B.; Venturi, M.; Flood, A. H.; Stoddart, J. F. *Proc. Natl. Acad. Sci. U.S.A.* **2006**, *103*, 1178–1183.

(14) For an example of entropy-driven shuttling see: Bottari, G.; Dehez, F.; Leigh, D. A.; Nash, P. J.; Pérez, E. M.; Wong, J. K. Y.; Zerbetto, F. *Angew. Chem., Int. Ed.* **2003**, *42*, 5886–5889.

(15) For examples of electrochemically responsive molecular shuttles see ref 13e, 13o and (a) Bissell, R. A.; Córdova, E.; Kaifer, A. E.; Stoddart, J. F. *Nature* **1994**, *369*, 133–136. (b) Collin, J.-P.; Gaviña, P.; Sauvage, J.-P. *New J. Chem.* **1997**, 525–528. (c) Ballardini, R.; Balzani, V.; Dehaen, W.; Dell'Erba, A. E.; Raymo, F. M.; Stoddart, J. F.; Venturi, M. *Eur. J. Org. Chem.* **2000**, 591–602. (d) Ashton, P. R.; Ballardini, R.; Balzani, V.; Credi, A.; Dress, K. R.; Ishow, E.; Kleverlaan, C. J.; Kocian, O.; Preece, J. A.; Spencer, N.; Stoddart, J. F.; Venturi, M.; Wenger, S. *Chem. Eur. J.* **2000**, *6*, 3558–3574. (e) Altieri, A.; Gatti, F. G.; Kay, E. R.; Leigh, D. A.; Martel, D.; Paolucci, F.; Slawin, A. M. Z.; Wong, J. K. Y. *J. Am. Chem. Soc.* **2003**, *125*, 8644–8654. (f) Long, B.; Nikitin, K.; Fitzmaurice, D. *J. Am. Chem. Soc.* **2003**, *125*, 15490–15498. (g) Kihara, N.; Hashimoto, M.; Takata, T. *Org. Lett.* **2004**, *6*, 1693–1696. (h) Tseng, H.-R.; Vignon, S. A.; Celestre, P. C.; Perkins, J.; Jeppesen, J. O.; Di Fabio, A.; Ballardini, R.; Gandolfi, M. T.; Venturi, M.; Balzani, V.; Stoddart, J. F. *Chem. Eur. J.* **2004**, *10*, 155–172. (i) Flood, A. H.; Peters, A. J.; Vignon, S. A.; Steuerman, D. W.; Tseng, H.-R.; Kang, S.; Heath, J. R.; Stoddart, J. F. *Chem. Eur. J.* **2004**, *10*, 6558–6564. (j) Tseng, H.-R.; Wu, D. M.; Fang, N. X. L.; Zhang, X.; Stoddart, J. F. *ChemPhysChem* **2004**, *5*, 111–116. (k) Steuerman, D. W.; Tseng, H.-R.; Peters, A. J.; Flood, A. H.; Jeppesen, J. O.; Nielsen, K. A.; Stoddart, J. F.; Heath, J. R. *Angew. Chem., Int. Ed.* **2004**, *43*, 6486–6491. (l) Jeppesen, J. O.; Nygaard, S.; Vignon, S. A.; Stoddart, J. F. *Eur. J. Org. Chem.* **2005**, 196–220.

the past decade physicists have developed formal theoretical mechanisms, deeply rooted in nonequilibrium statistical mechanics, which explain how the directional transport of Brownian particles can occur from periodic changes in a potential energy surface (e.g., by applying an oscillating electric field).[21,22] Many different possible types of these theoretical "Brownian ratchet" mechanisms have been suggested, including energy ratchets, information ratchets, flashing ratchets, tilting ratchets, and rocking ratchets.[22] These mechanisms have been successfully applied to the development of transport and separation devices for mesoscopic particles and macromolecules, microfluidic pumping, and quantum and electronic applications[23,24] and have also been shown to successfully account for the general principles that govern the operation of complex biological motors.[24,25] However, to date it is not known how such theoretical mechanisms correlate with the changes that occur in molecular structure during the operation of biological machines. What do individual peptide fragments do in order to bring about transport of an ion or molecule by a Brownian ratchet mechanism and why? We wondered whether examining how these principles can be applied to some much less sophisticated (in terms of function as well as structure) synthetic molecular machines could tell us something about how they might apply to more complex systems, both artificial and natural.

Statistical Balance of a Dynamically Exchangeable Substrate or Quantity (The Principle of Detailed Balance)

If we ignore the normally small population of rings on the spacer, at equilibrium the macrocycle in a molecular shuttle can be considered to continuously fluctuate between the two stations. However, even for a molecular shuttle with two different stations, at equilibrium no net task can be performed by these movements. This is a consequence of the "Principle of Detailed Balance";[26] at equilibrium transitions between any two states take place in either direction at the same rate so that no flux is generated. This rules out the maintenance of equilibria by cyclic

(16) For examples of chemically responsive molecular shuttles see ref 11b, 15h, 15l, and (a) Gong, C.; Gibson, H. W. *Angew. Chem., Int. Ed. Engl.* **1997**, *36*, 2331−2333. (b) Gong, C. G.; Glass, T. E.; Gibson, H. W. *Macromolecules* **1998**, *31*, 308−313. (c) Jiménez, M. C.; Dietrich-Buchecker, C.; Sauvage, J.-P *Angew. Chem., Int. Ed.* **2000**, *39*, 3284−3287. (d) Lee, J. W.; Kim, K.; Kim, K. *Chem. Commun.* **2001**, 1042−1043. (e) Jimenez-Molero, M. C.; Dietrich-Buchecker, C.; Sauvage, J.-P. *Chem. Eur. J.* **2002**, *8*, 1456−1466. (f) Da Ross, T.; Guldi, D. M.; Farran Morales, A.; Leigh, D. A.; Prato, M.; Turco, R. *Org. Lett.* **2003**, *5*, 689−691. (g) Tseng, H.-R.; Vignon, S. A.; Stoddart, J. F. *Angew. Chem., Int. Ed.* **2003**, *42*, 1491−1495. (h) Laursen, B. W.; Nygaard, S.; Jeppesen, J. O.; Stoddart, J. F. *Org. Lett.* **2004**, *6*, 4167−4170. (i) Huang, T. J.; Tseng, H.-R.; Sha, L.; Lu, W. X.; Brough, B.; Flood, A. H.; Yu, B.-D.; Celestre, P. C.; Chang, J. P.; Stoddart, J. F.; Ho, C.-M. *Nano Lett.* **2004**, *4*, 2065−2071. (j) Leigh, D. A.; Pérez, E. M. *Chem. Commun.* **2004**, 2262−2263. (k) Nørgaard, K.; Laursen, B. W.; Nygaard, S.; Kjaer, K.; Tseng, H.-R.; Flood, A. H.; Stoddart, J. F.; Bjørnholm, T. *Angew. Chem., Int. Ed.* **2005**, *44*, 7035−7039.

(17) For examples of pH-responsive molecular shuttles see ref 15a and (a) Martínez-Díaz, M.-V.; Spencer, N.; Stoddart, J. F. *Angew. Chem., Int. Ed. Engl.* **1997**, *36*, 1904−1907. (b) Ashton, P. R.; Ballardini, R.; Balzani, V.; Baxter, I.; Credi, A.; Fyfe, M. C. T.; Gandolfi, M. T.; Gómez-López, M.; Martínez-Díaz, M.-V.; Piersanti, A.; Spencer, N.; Stoddart, J. F.; Venturi, M.; White, A. J. P.; Williams, D. J. *J. Am. Chem. Soc.* **1998**, *120*, 11932−11942. (c) Elizarov, A. M.; Chiu, S.-H.; Stoddart, J. F. *J. Org. Chem.* **2002**, *67*, 9175−9181. (d) Badjić, J. D.; Balzani, V.; Credi, A.; Silvi, S.; Stoddart, J. F. *Science* **2004**, *303*, 1845−1849. (e) Keaveney, C. M.; Leigh, D. A. *Angew. Chem., Int. Ed.* **2004**, *43*, 1222−1224. (f) Garaudée, S.; Silvi, S.; Venturi, M.; Credi, A.; Flood, A. H.; Stoddart, J. F. *ChemPhysChem.* **2005**, *6*, 2145−2152. (g) Badjić, J. D.; Ronconi, C. M.; Stoddart, J. F.; Balzani, V.; Silvi, S.; Credi, A. *J. Am. Chem. Soc.* **2006**, *128*, 1489−1499.

(18) For examples of molecular shuttles switched by alkali metal ion complexation, competitive binding, or allosteric regulation, see: (a) Vignon, S. A.; Jarrosson, T.; Iijima, T.; Tseng, H.-R.; Sanders, J. K. M.; Stoddart, J. F. *J. Am. Chem. Soc.* **2004**, *126*, 9884−9885. (b) Iijima, T.; Vignon, S. A.; Tseng, H.-R.; Jarrosson, T.; Sanders, J. K. M.; Marchioni, F.; Venturi, M.; Apostoli, E.; Balzani, V.; Stoddart, J. F. *Chem. Eur. J.* **2004**, *10*, 6375−6392. (c) Marlin, D. S.; González Carbrera, D.; Leigh, D. A.; Slawin, A. M. Z. *Angew. Chem., Int. Ed.* **2006**, *45*, 77−83. (d) Marlin, D. S.; González Carbrera, D.; Leigh, D. A.; Slawin, A. M. Z. *Angew. Chem., Int. Ed.* **2006**, *45*, 1385−1390.

(19) "Co-conformation" refers to the relative positions of the mechanically interlocked components with respect to each other, see: Fyfe, M. C. T.; Glink, P. T.; Menzer, S.; Stoddart, J. F.; White, A. J. P.; Williams, D. J. *Angew. Chem., Int. Ed. Engl.* **1997**, *36*, 2068−2070.

(20) Stimuli-induced shuttling has been used to control a number of different properties. See: Fluorescence switching: (a) Pérez, E. M.; Dryden, D. T. F.; Leigh, D. A.; Teobaldi, G.; Zerbetto, F. *J. Am. Chem. Soc.* **2004**, *126*, 12210−12211. (b) Wang, Q.-C.; Qu, D.-H.; Ren, J.; Chen, K.; Tian, H. *Angew. Chem., Int. Ed.* **2004**, *43*, 2661−2665. (c) Qu, D.-H.; Wang, Q.-C.; Ren, J.; Tian, H. *Org. Lett.* **2004**, *6*, 2085−2088. (d) Qu, D.-H.; Wang, Q.-C.; Tian, H. *Mol. Cryst. Liq. Cryst.* **2005**, *430*, 59−65. (e) Leigh, D. A.; Morales, M. A. F.; Pérez, E. M.; Wong, J. K. Y.; Saiz, C. G.; Slawin, A. M. Z.; Carmichael, A. J.; Haddleton, D. M.; Brouwer, A. M.; Buma, W. J.; Wurpel, G. W. H.; León, S.; Zerbetto, F. *Angew. Chem., Int. Ed.* **2005**, *44*, 3062−3067. (f) Qu, D.-H.; Wang, Q.-C.; Tian, H. *Angew. Chem., Int. Ed.* **2005**, *44*, 5296−5299. (g) Qu, D.-H.; Wang, Q.-C.; Ma, X.; Tian, H. *Chem. Eur. J.* **2005**, *11*, 5929−5937. (h) Li, Y.; Li, H.; Li, Y.; Liu, H.; Wang, S.; He, X.; Wang, N.; Zhu, D. *Org. Lett.* **2005**, *7*, 4835−4838. (i) Onagi, H.; Rebek, J. *Chem. Commun.* **2005**, 4604−4606. Expression of chirality: (j) Bottari, G.; Leigh, D. A.; Pérez, E. M. *J. Am. Chem. Soc.* **2003**, *125*, 13360−13361. Conductivity of solid-state electronic junctions: (k) Collier, C. P.; Mattersteig, G.; Wong, E. W.; Luo, Y.; Beverly, K.; Sampaio, J.; Raymo, F. M.; Stoddart, J. F.; Heath, J. R. *Science* **2000**, *289*, 1172−1175. (l) Collier, C. P.; Jeppesen, J. O.; Luo, Y.; Perkins, J.; Wong, E. W.; Heath, J. R.; Stoddart, J. F. *J. Am. Chem. Soc.* **2001**, *123*, 12632−12641. (m) Luo, Y.; Collier, C. P.; Jeppesen, J. O.; Nielsen, K. A.; Delonno, E.; Ho, G.; Perkins, J.; Tseng, H.-R.; Yamamoto, T.; Stoddart, J. F.; Heath, J. R. *ChemPhysChem* **2002**, *3*, 519−525. (n) Diehl, M. R.; Steuerman, D. W.; Tseng, H.-R.; Vignon, S. A.; Star, A.; Celestre, P. C.; Stoddart, J. F.; Heath, J. R. *ChemPhysChem* **2003**, *4*, 1335−1339. Conductivity at electrode interfaces: (o) Willner, I.; Pardo-Yissar, V.; Katz, E.; Ranjit, K. T. *J. Electroanal. Chem.* **2001**, *497*, 172−177. (p) Sheeney-Haj-Ichia, L.; Willner, I. *J. Phys. Chem. B* **2002**, *106*, 13094−13097. (q) Katz, E.; Sheeney-Haj-Ichia, L.; Willner, I. *Angew. Chem., Int. Ed.* **2004**, *43*, 3292−3300. (r) Katz, E.; Lioubashevsky, O.; Willner, I. *J. Am. Chem. Soc.* **2004**, *126*, 15520−15532. Exertion of a mechanical force on a macroscopic object: (s) Huang, T. J.; Brough, B.; Ho, C.-M.; Liu, Y.; Flood, A. H.; Bonvallet, P. A.; Tseng, H.-R.; Stoddart, J. F.; Baller, M.; Magonov, S. *Appl. Phys. Lett.* **2004**, *85*, 5391−5393. (t) Liu, Y.; Flood, A. H.; Bonvallet, P. A.; Vignon, S. A.; Northrop, B. H.; Tseng, H.-R.; Jeppesen, J. O.; Huang, T. J.; Brough, B.; Baller, M.; Magonov, S.; Solares, S. D.; Goddard, W. A.; Ho, C.-M.; Stoddart, J. F. *J. Am. Chem. Soc.* **2005**, *127*, 9745−9759. Access to a nanopore: (u) Nguyen, T. D.; Tseng, H.-R.; Celestre, P. C.; Flood, A. H.; Liu, Y.; Stoddart, J. F.; Zink, J. I. *Proc. Natl. Acad. Sci. U.S.A.* **2005**, *102*, 10029−10034. Surface wettability: ref 20r and (v) Berná, J.; Leigh, D. A.; Lubomska, M.; Mendoza, S. M.; Pérez, E. M.; Rudolf, P.; Teobaldi, G.; Zerbetto, F. *Nat. Mater.* **2005**, *4*, 704−710. The latter also demonstrates the macroscopic transport of a droplet of liquid across a surface using stimuli-responsive molecular shuttles.

(21) For an introduction to Brownian motors see: (a) Astumian, R. D. *Sci. Am.* **2001**, *285* (1), 56−64. (b) Astumian, R. D.; Hänggi, P. *Phys. Today* **2002**, *55* (11), 33−39.

(22) For reviews of Brownian ratchet mechanisms see: (a) Hänggi, P.; Bartussek, R. In *Nonlinear Physics of Complex Systems − Current Status and Future Trends*; Parisi, J., Müller, S. C., Zimmermann, W., Eds.; Lecture Notes in Physics, Vol. 476; Springer: Berlin, 1996; pp 294−308. (b) Astumian, R. D. *Science* **1997**, *276*, 917−922. (c) Jülicher, F.; Ajdari, A.; Prost, J. *Rev. Mod. Phys.* **1997**, *69*, 1269−1281. (d) Special issue on *The constructive role of noise in fluctuation driven transport and stochastic resonance. Chaos* **1998**, *8*, 533−664. (e) Reimann, P. *Phys. Rep.* **2002**, *361*, 57−265. (f) Reimann, P.; Hänggi, P. *Appl. Phys. A* **2002**, *75*, 169−178. (g) Parrondo, J. M. R.; De Cisneros, B. J. *Appl. Phys. A* **2002**, *75*, 179−191. (h) Gabrys, B. J.; Pesz, K.; Bartkiewicz, S. J. *Physica A* **2004**, *336*, 112−122. (i) Linke, H.; Downton, M. T.; Zuckermann, M. J. *Chaos* **2005**, *15*, 026111.

(23) (a) Rousselet, J.; Salome, L.; Ajdari, A.; Prost, J. *Nature* **1994**, *370*, 446−448. (b) Faucheux, L. P.; Bourdieu, L. S.; Kaplan, P. D.; Libchaber, A. J. *Phys. Rev. Lett.* **1995**, *74*, 1504−1507. (c) Bader, J. S.; Hammond, R. W.; Henck, S. A.; Deem, M. W.; McDermott, G. A.; Bustillo, J. M.; Simpson, J. W.; Mulhern, G. T.; Rothberg, J. M. *Proc. Natl. Acad. Sci. U.S.A.* **1999**, *96*, 13165−13169. (d) Linke, H.; Humphrey, T. E.; Lofgren, A.; Sushkov, A. O.; Newbury, R.; Taylor, R. P.; Omling, P. *Science* **1999**, *286*, 2314−2317. (e) Matthias, S.; Müller, F. *Nature* **2003**, *424*, 53−57.

(24) Linke, H., Ed. Special issue on *Ratchets and Brownian motors: Basics, experiments and applications. Appl. Phys. A* **2002**, *75*, 167−352.

(25) (a) Astumian, R. D.; Bier, M. *Biophys. J.* **1996**, *70*, 637−653. (b) Astumian, R. D.; Derényi, I. *Eur. Biophys. J.* **1998**, *27*, 474−489. (c) Lipowsky, R. In *Stochastic Processes in Physics, Chemistry and Biology*; Freund, J. A., Pöschel, T., Eds.; Lecture Notes in Physics, Vol. 557; Springer: Berlin, 2000; pp 21−31. (d) Bustamante, C.; Keller, D.; Oster, G. *Acc. Chem. Res.* **2001**, *34*, 412−420. (e) Astumian, R. D. *Appl. Phys. A* **2002**, *75*, 193−206. (f) Mogilner, A.; Oster, G. *Curr. Biol.* **2003**, *13*, R721−R733. (g) Oster, G.; Wang, H. Y. *Trends Cell Biol.* **2003**, *13*, 114−121. (h) Kurzynski, M.; Chelminiak, P. *Physica A* **2004**, *336*, 123−132.

(26) Onsager, L. *Phys. Rev.* **1931**, *37*, 405−426.

Scheme 2 [a,b]

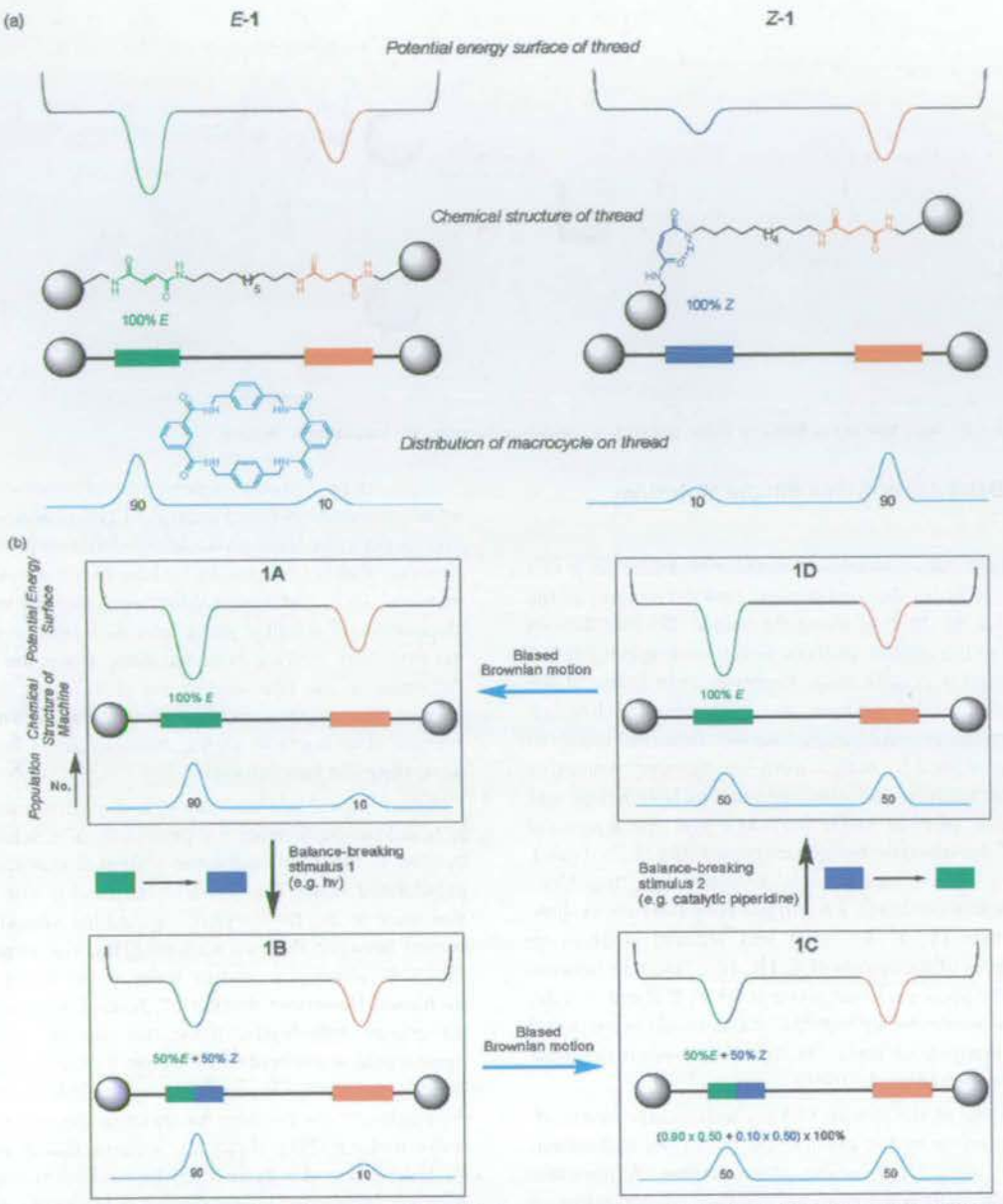

[a] Description of *E*-**1** and *Z*-**1** in covalent, thermodynamic, and statistical terms, assuming a 90:10 distribution of translational isomers in each olefin diastereomer. [b] "Machine-performance representation" of the forward (**1A** → **1C**) and backward (**1C** → **1A**) operations of machine−substrate system **1**, assuming a 50:50 olefin mixture at the photostationary state. The chemical structure of the machine (thread) is shown at each stage in cartoon form with the fraction of olefin diastereomers indicated in terms of color of a station. The potential energy surface shown is the average potential energy surface of the thread for the macrocycle at that stage of the machine operation, i.e., the appropriately weighted combination of the potential energy surfaces for each of the olefin diastereomers (see (a)) contributing to the mixture. The population trace shows the overall distribution of the substrate over the machine.

processes such as A → B → C → A rather than A⇌B + B⇌C + C⇌A (ref 21b) and is a formal indication that a machine such as Smoluchowski's Trapdoor (Figure 1d) cannot operate (at least not in the way originally envisaged). However, in an out-of-equilibrium system, detailed balance is broken and as the system moves spontaneously toward equilibrium net work *can* be done by the fluxional exchange process. It is well-established that breaking detailed balance is a requirement for doing work with stochastic transport systems.[22] However, we recently pointed out that detailed balance could be considered to result from two separate properties of a system;[8d] the statistical distribution of a quantity (an imbalance in which provides the thermodynamic impetus for net transport) and the ability of that quantity to be dynamically exchanged (which provides the communication necessary for transport to occur). It is no coincidence that all four of the Gedankenmaschinen shown in Figure 1 disconnect the compartments at various stages during their operation in order to try and achieve net particle transportation. The molecular examples in this paper (vide infra) show that the deconvolution of the statistical "balance" and the "linkage" of compartments is useful for establishing the phenomenological nature of ratcheting and escapement (the counterpart to ratcheting) in Brownian transport processes.

Scheme 3. A Type of [2]Rotaxane that can Act as an Irreversible Mechanical Switch[a]

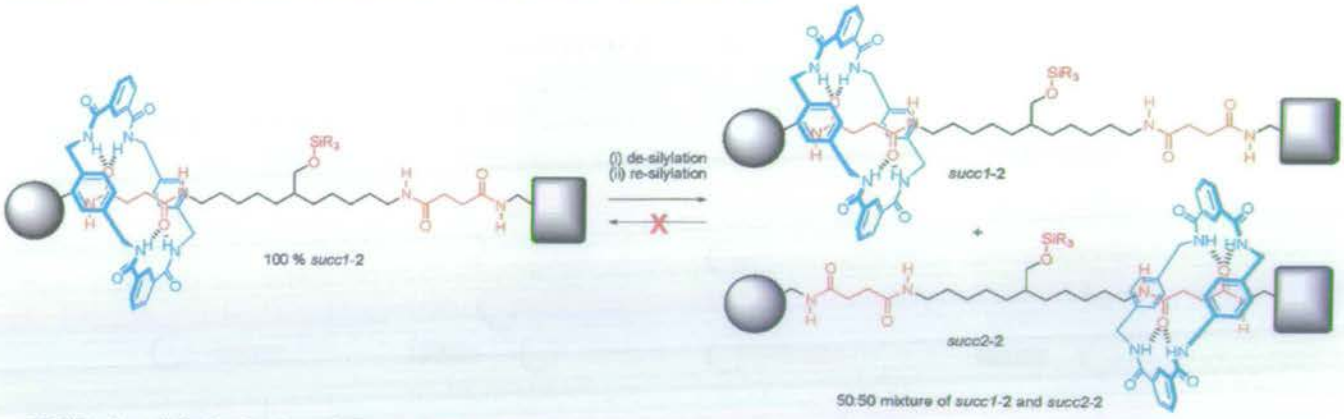

[a] R_3SiO- is a silyl ether that is too bulky to allow macrocycle exchange between the succinamide stations.

Systematic Behavior of Some Simple Molecular Machines

Let us consider how a stimuli-responsive rotaxane such as **1** (Scheme 1) performs the mechanical task of changing the average position of the ring along the thread. So that we can clearly see how the system evolves as this task is performed, we will represent it at each stage (Scheme 2) in terms of the covalent structure of the machine, that is, the thread (chemical status), the average potential energy surface (physical status of the machine, governed by noncovalent interactions—attractive forces between machine and substrate such as H-bonding, and repulsive forces such as steric barriers), and the statistical distribution of the substrate being transported (the macrocycle). In these types of schemes, which we shall call "machine-performance representations", we will use bold numbers to show different systems (**1**, **2**, **3**... etc.) and lettered suffixes to differentiate states of the system (**1A**, **1B**, **1C**.... etc.). In Scheme 2 we assume the photostationary state is 50:50 *E*:*Z* and that the preferred ratio of occupancy between fumaramide (green) and succinamide (orange) stations is 90:10 and between maleamide (dark blue) and succinamide 10:90.

The initial state of the system (**1A**) is statistically balanced. The average position of the macrocycle (from the Boltzmann distribution) is very close to the green station. A photonic stimulus ("balance-breaking stimulus") causes isomerization of some of the olefins from *E* to *Z*, putting the position of the macrocycle in the molecules that are isomerized momentarily out of equilibrium (**1B**, similarly **1D**). The system acts to restore balance through biased Brownian motion of the macrocycles and we arrive at the final state, **1C**. The change in state between **1B** and **1C** (and also between **1D** and **1A**) is not triggered externally; rather it is a thermally activated relaxation step in which the average position of the macrocycle (given by the Boltzmann distributions within the olefin isomers multiplied by their contribution to the photostationary state) moves along the thread toward the orange station. Note, however, that the machine—the thread—cannot use the energy from the photon to perform the transportation task in such a way that the position of the substrate becomes independent of the state of the machine; applying a second stimulus to reset the machine (e.g., adding piperidine to reform the *E*-olefin of the thread) undoes the net displacement of the macrocycle (**1C** → **1A**).

Now let us consider a new type of rotaxane system, **2**, in which a stimuli-induced change of position of the macrocycle also occurs but through a clearly different mechanism to the previous shuttle (Scheme 3). In **2** the two stations are structurally identical (but distinguishable—note the differently depicted stoppers) and a bulky group acts as a barrier which prevents the ring from moving between them. If we start with 100% of the rings on the first station, *succ1*-**2**,[27] and then remove the barrier, the system moves toward equilibrium, causing an average displacement of the macrocycle of half the distance separating the two stations.

Again, we can see how this system evolves more clearly using a "machine-performance representation" (Scheme 4). Unlike system **1**, machine−substrate system **2** starts out statistically unbalanced (**2A**). The stimulus required is also different from that used in the first system: a "linking stimulus" lowers the barrier between the two stations (**2B**), allowing the system to fulfill the impetus to restore balance and move to equilibrium by biased Brownian motion of the macrocycle (**2C**, note that the energy well-depths of the two stations are the same; the macrocycle is not held more tightly by the station it moves to). Raising the barrier by applying an "unlinking stimulus" resets the machine—the thread—but this time the task it has performed is *not* undone (**2D**). However, we note that if we try applying the linking stimulus again after the machine is reset, the machine does not change the average position of the macrocycle because the system is already statistically balanced (Scheme 4).

This stimuli-induced irreversible net change of position of the macrocycle represents a new type of molecular shuttle in phenomenological terms and so we prepared an experimental example, **3**, in single translational isomer form (*succ1*-**3**) according to Scheme 5. The unoccupied thread, **4**, was also synthesized as a comparison for ^{1}H NMR purposes. To be able to distinguish between the two succinamide stations through ^{1}H NMR spectroscopy but still keep them similar in terms of macrocycle binding affinity, the terminal right-hand side (as depicted in Scheme 5) amide group was derivatized with a

(27) The nomenclature used to denote individual rotaxane configurational and translational isomers follows conventions introduced in previous papers (e.g., ref 8d). Namely, a bolded compound number refers to a given structural formula irrespective of functional group configuration or position of the macrocycle; a prefix *E* or *Z* describes the configuration of the olefin; a prefix *succ1*, *succ2*, *fum*, or *mal* denotes the position of the macrocycle in a particular translational isomer.

Scheme 4 [a,b]

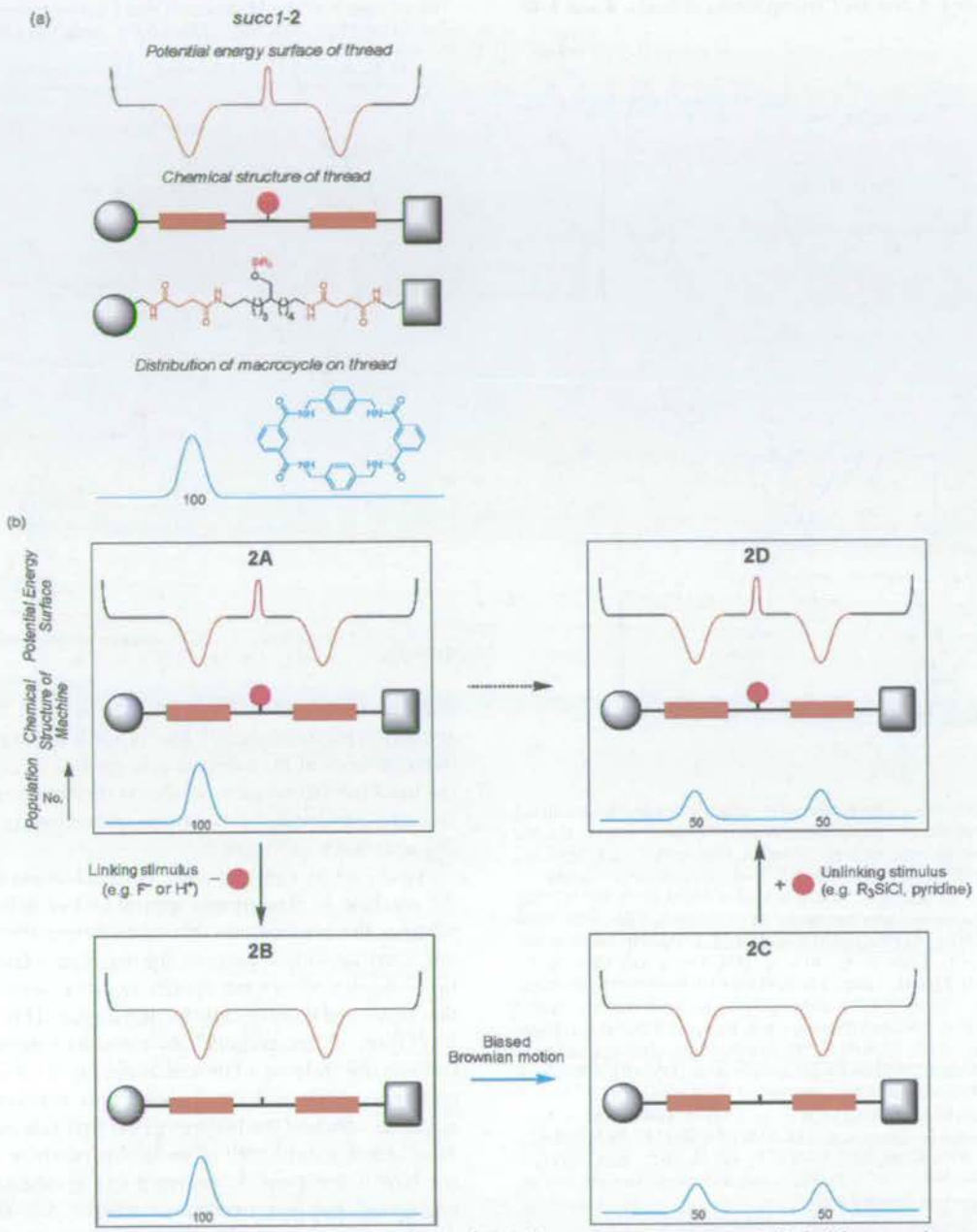

[a] Description of *succ1*-**2** in covalent, thermodynamic, and statistical terms. [b] "Machine-performance representation" of a [2]rotaxane that acts as an irreversible mechanical switch. **2A**: The macrocycle is locked on one of the two energetically identical but distinguishable stations by a large kinetic energy barrier. **2B**: A linking stimulus lowers the barrier. **2C**: The thermal bath restores equilibrium via biased Brownian motion. **2D**: An unlinking stimulus resets the machine. Note that repeating the cycle of chemical reactions would not change the distribution of the macrocycle for a second time.

phenyl group. Aryl-substituted tertiary amides preferentially adopt an *anti*-arrangement of the alkyl groups so there is no complication with slowly interconverting rotamers in the ^{1}H NMR spectra.[28,29] (Tertiary aryl-substituted fumaramide groups are excellent templates for benzylic amide macrocycle rotaxane formation.[30]) A 4-picolyl fragment provides the necessary bulk for the rest of the stopper.

The synthetic route to *succ1*-**3** is worthy of some comment. The "gated" spacer that separates the two stations was prepared by double alkylation (orthogonal amine protecting groups) and subsequent Krapcho decarboxylation[31] of dimethyl malonate (Scheme 5, i−v). A fumaramide group was then attached, both to maximize the yield of rotaxane formation (step viii, 68%) and to provide a common route for the synthesis of *fum-E*-**5** (vide infra). Unmasking of the Fmoc-protected amine, followed by coupling with a succinic acid derivative (step ix), was

(28) Itai, A.; Toriumi, Y.; Saito, S.; Kagechika, H.; Shudo, K. *J. Am. Chem. Soc.* **1992**, *114*, 10649−10650.
(29) Note that there is no indication of multiple tertiary amide rotamers in the ^{1}H NMR spectrum of **4** (Figure 2a). For example, only one signal is observed for H_φ.
(30) Leigh, D. A.; Nash, P. J. Manuscript in preparation.
(31) (a) Krapcho, A. P. *Synthesis* **1982**, 805−822. (b) Krapcho, A. P. *Synthesis* **1982**, 893−914.

Scheme 5. Synthesis of Single Translational Isomer [2]Rotaxanes *succ1*-**3** and *fum*-*E*-**5** and the Corresponding Threads, **4** and *E*-**6**[a]

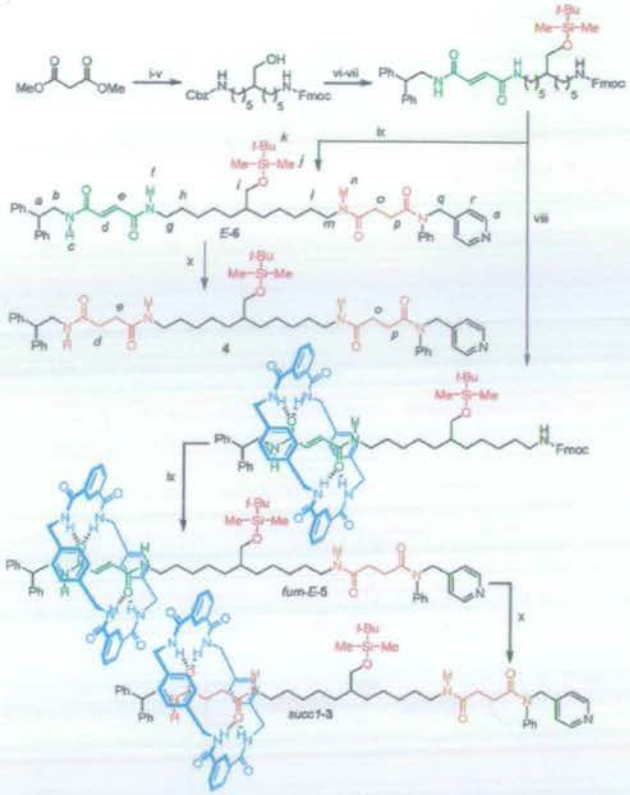

[a] Reaction conditions (unless otherwise stated, reactions were carried out at room temperature): (i) a. NaH, THF, 0 °C to rt, 1 h; b. Bu_4NI, *N*-benzyloxycarbonyl-5-bromo-1-pentylamine, THF, reflux, 12 h, 88%. (ii) a. NaH, THF, 0 °C to rt, 1 h; b. Bu_4NI, *N*-allyloxycarbonyl-5-bromo-1-pentylamine, THF, reflux, 12 h, 58%. (iii) LiCl, DMSO, H_2O, 160 °C, 4 h, 66%. (iv) Diisobutylaluminum hydride (1 M in toluene), THF, −78 °C, 4 h, 68%. (v) a. $PhSiH_3$, $Pd(PPh_3)_4$, CH_2Cl_2, 45 min; b. fluorenylmethylchloroformate (Fmoc-Cl), Et_3N, 0 °C, 30 min, 56%. (vi) a. H_2, 10% Pd/ C, HCl (1 M in Et_2O), MeOH, 1 atm, 1 h; b. (*E*)-3-(2,2-diphenylethylcarbamoyl)-acrylic acid, 1-[3-dimethylaminopropyl]-3-ethylcarbodiimide hydrochloride (EDCI·HCl), 1-hydroxybenzotriazole hydrate (HOBt·H_2O), Et_3N, CH_2Cl_2, 0 °C to rt, 2 h, 60%. (vii) *tert*-Butyldimethylsilyl chloride (TBDMSCl), imidazole, 4-(dimethylamino)pyridine (DMAP), CH_2Cl_2, 1 h, 63%. (viii) *p*-Xylylenediamine, isophthaloyl dichloride, Et_3N, $CHCl_3$, 3 h, 68%. (ix) a. Piperidine, THF:CH_3CN (1:3), 2.5 h; b. 4-oxo-4-(phenyl(pyridin-4-ylmethyl)amino)butanoic acid, EDCI·HCl, HOBt·H_2O, Et_3N, CH_2Cl_2, 0 °C to rt, 14 h, 47% (*E*-**6**), 48% (*fum*-*E*-**5**). (x) H_2, 10% Pd/C, THF, 1 atm, 6 h, 90% (**4**), 90% (*succ1*-**3**). Full experimental procedures can be found in the Supporting Information.

followed by hydrogenation (step x) of the fumaramide moiety. Perhaps surprisingly, the macrocycle appears to offer no significant protection to the thread functionality in this step,[32] which readily affords the two station rotaxane, **3**, as a single translational isomer, *succ1*-**3** (however, careful solvent selection is necessary to avoid cleavage of the silyl ether[33]).

The system functions (Scheme 6) as predicted in Scheme 4. De-silylation of *succ1*-**3** (Scheme 6, step i) followed by re-silylation (step ii) afforded a ~1:1 mixture of the two translational isomers of **3**. Note, because *succ1*-**3** and *succ2*-**3** are not in equilibrium with each other, unlike *fum*-*E*-**1** and *succ*-

Scheme 6. Chemical Representation of the Irreversible Net Translocation of the Macrocycle that Occurs through the Transformation *succ1*-**3** → [*succ2*-**3** + *succ1*-**3**] (50:50 ± 2)[a]

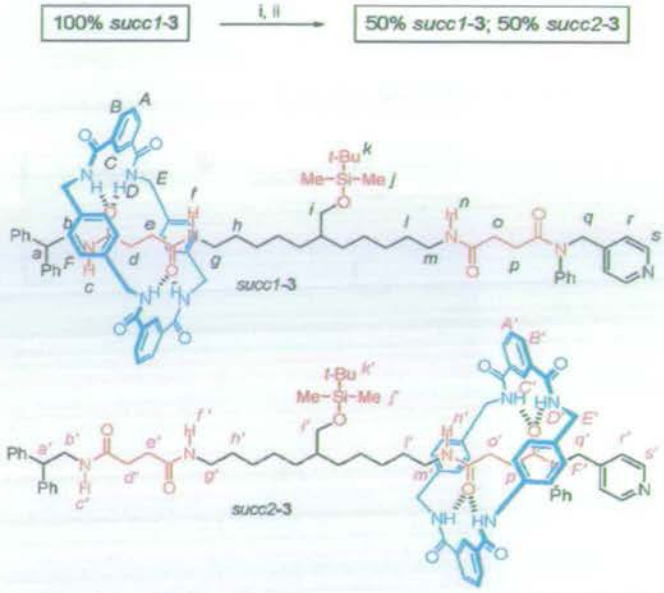

[a] Reaction conditions: (i) 80% aqueous acetic acid, 60 °C, 1 h. (ii) TBDMSCl, imidazole, DMAP, CH_2Cl_2, rt, 1 h.

E-**1** for example (Scheme 1), the translational isomers of **3** are actually diastereoisomers.[10] The ^{1}H NMR spectra of the machine in the absence of the substrate (i.e., the free thread, Figure 2a),[29] the machine−substrate ensemble in its initial state (Figure 2b), and after application of the linking and unlinking stimuli (Figure 2c) are shown in Figure 2.

Again, let us consider what the mechanism of operation of the machine is: The stimuli applied to **3** switch "on" and "off" whether the stations are able to exchange the macrocycle or not. Linking of two parts of the machine which interact with the substrate allows the system to move toward equilibrium, that is, toward a statistically balanced state. This is a molecular-level form of "escapement", the element of the mechanism that controls the release of potential energy to drive mechanical motion in clocks and other macroscopic mechanical devices.[34]

Let us combine the features of the first two rotaxanes, **1** and **3**, to invent a third type of molecular machine system, **5**, and see how it functions. Rotaxane **5** was synthesized as a single configurational and translational isomer, *fum*-*E*-**5**, along with the corresponding thread *E*-**6**, according to Scheme 5. The reaction profile of this rotaxane is outlined in Scheme 7 in standard chemical terms and its performance as a machine−substrate ensemble is shown in Scheme 8.

The xylylene rings of the macrocycle shield the regions of the thread that they encapsulate and the resulting shifts in the ^{1}H NMR spectra are diagnostic of the position of the macrocycle on the thread.[13j] Thus, the operation of the machine and its effect on the substrate can be followed by ^{1}H NMR spectroscopy (Figure 3). In particular, it is instructive to observe the change in intensity of the unoccupied fumaramide station protons $H_{d'}$ and $H_{e'}$ (H_d and H_e in *E*-**6**) during the operation of the machine. In the free thread they appear as a pair of doublets at 6.86 and

(32) Parham, A. H.; Windisch, B.; Vögtle, F. *Eur. J. Org. Chem.* **1999**, 1233−1238.

(33) Sajiki, H.; Ikawa, T.; Hattori, K.; Hirota, K. *Chem. Commun.* **2003**, 654−655.

(34) (a) Britten, F. J. *Escapements: Their Actions Constructions and Proportion*; Arlington Book Co: U.S.A., 1985. (b) Gazeley, W. J. *Clock and Watch Escapements*; Robert Hale & Co.: 1999.

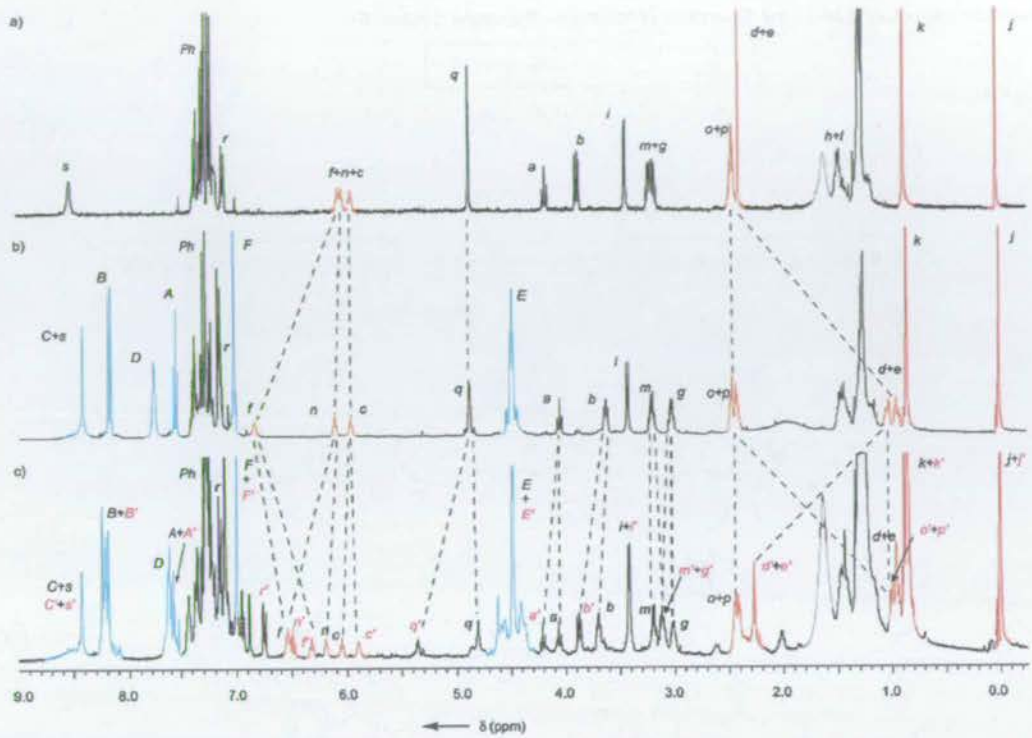

Figure 2. ^{1}H NMR spectra (400 MHz, $CDCl_3$, 298 K) of (a) free thread **4**, (b) *succ1*-**3**, and (c) mixture of translational isomers *succ1*-**3** and *succ2*-**3** after the two-step operation (Scheme 6, (i) and (ii)). Integration shows the *succ1*-**3**:*succ2*-**3** ratio in (c) is 50:50 (±2%). The ^{1}H NMR assignments and coloring correspond to the labeling in Schemes 5 and 6. Residual water peaks are shown in gray.

7.02 ppm (Figure 3a); they are absent in the spectrum of pure *fum*-*E*-**5** (Figure 3b); in the statistically balanced (unlinked) system (Figure 3c) they account for ~15% of the overall population; in the final ratcheted system (Figure 3d) they are ~56% of the reaction mixture.

So, in Scheme 8, the two parts of the machine start out (**5A**) statistically balanced (85% of the macrocycles on the fumaramide station; 15% on the succinamide station) and unlinked (and therefore not in equilibrium). A balance-breaking stimulus (*hν* at 312 nm,[35] which generates a 49:51 ±2% *E*:*Z* photostationary state by ^{1}H NMR, not shown) is applied, giving **5B**. Removal of the barrier ("linking stimulus"; 80% aqueous acetic acid) gives **5C** and allows balance to be restored through moving to equilibrium by biased Brownian motion of the ring (**5D**). Restoring the barrier ("unlinking stimulus"; TBDMSCl, base) makes the system (**5E**) unlinked and not in equilibrium, although statistically balanced. The resetting step (a different balance-breaking stimulus; catalytic piperidine, to promote the $Z \rightarrow E$ olefin isomerization) makes the system statistically unbalanced, unlinked, and not in equilibrium (**5F**).

After the operational cycle of the machine (i.e., **5F**) the unoccupied fumaramide station protons $H_{d'}$ and $H_{e'}$ account for ~56% of the reaction mixture (Figure 3d).[36] Given that the photostationary state from irradiation of *E*-**5** at 312 nm is 49:51 ±2% *E*:*Z*, and that the statistically balanced distribution of the macrocycle is 85:15 between the *fum* and *succ* stations of *E*-**5** (Figure 3c), the final 44:56 *fum*-*E*-**5**:*succ*-*E*-**5** ratio indicates that the equilibrium distribution of translational isomers between the *mal* and *succ* stations in the de-silylated (linked) derivative of *Z*-**5** is ~5:95 in CH_2Cl_2 at room temperature.[37] The transportation of the macrocycle in **5** is repeatedly reversible between the statistically balanced 85:15 and statistically unbalanced 44:56 ratios of *fum*-*E*-**5** to *succ*-*E*-**5**.[38]

The thread has therefore successfully performed the task of directionally changing the net position of the macrocycle—and since the succinamide station binds the macrocycle more weakly than the fumaramide station, the thread has moved the macrocycle energetically uphill!—and the machine, the thread, has returned to its initial state. We recognize this behavior as "ratcheting", a characteristic of the operating mechanism of many biological molecular machines. For the first time, we have a molecular shuttle which is more sophisticated in terms of task performance than a simple mechanical switch. The compartmentalized machine achieves this result by applying four different stimuli which govern in turn the thermodynamics and the kinetics for transport between the two stations: balance-breaking 1; linking; unlinking; balance-breaking 2 (resetting—of the machine, not the substrate).[39]

(35) Some degradation of rotaxane **5** occurs upon irradiation at 254 nm; however, at 312 nm no degradation or side reactions are apparent and the photostationary state is 49:51 ± 2 *E*:*Z* by ^{1}H NMR spectroscopy.

(36) Note how the chemical shifts of some of the protons (e.g., H_d and H_e) in *fum*-*E*-**5** change among Figures 3b, 3c, and 3d, illustrating the sensitivity of the H-bonding between the macrocycle and thread to factors such as moisture, concentration, and possibly, impurities.

(37) This calculation assumes that both translational isomers of de-silylated *Z*-**5** are re-silylated at the same rate. If this is not true, if the position of the macrocycle on a station affects the rate of the unlinking reaction, then it is possible to produce a nonbalanced distribution of the macrocycle through just controlling kinetic energy barriers with the position of the ring—an "information ratchet" (ref 25b).

(38) The pure single translational isomer *fum*-*E*-**5** cannot be regenerated by the operation of the machine but it can be separated from the reaction mixture at any stage using standard purification protocols.

Scheme 7. Chemical Representation of the Operation of Machine–Substrate System **5**[a]

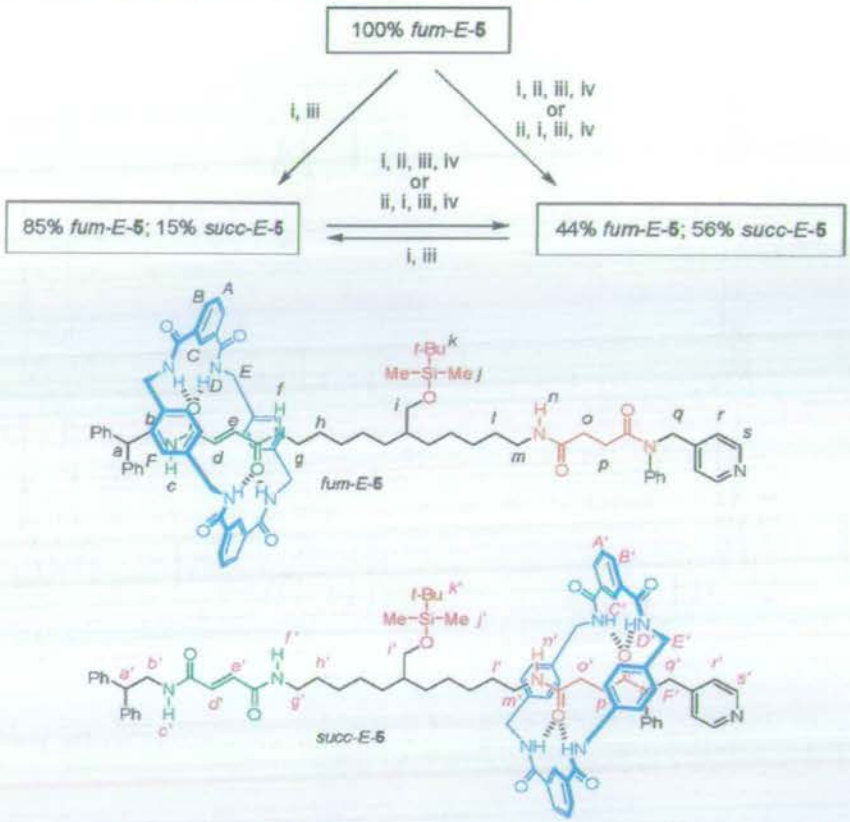

[a] Reaction conditions: (i) 80% aqueous acetic acid, 60 °C, 1 h. (ii) *hν* at 312 nm (5 × 5 min irradiation),[35] CH_2Cl_2, rt. (iii) TBDMSCl, imidazole, DMAP, CH_2Cl_2, rt, 1 h. (iv) Piperidine, CH_2Cl_2, rt, 12 h, quantitative.

Through its operation in Scheme 7/8, rotaxane **5** establishes a thermodynamically unfavorable concentration gradient of the macrocycle between the compartments. This is the function envisaged for the thought-machine pressure demons shown in Figures 1b and 1d, albeit featuring many machines each acting on one Brownian particle in the case of the rotaxane rather than a single machine acting on many Brownian particles. However, the way in which **5** achieves this result is very different from either Gedankenmaschine design. During the operation of **5** the Brownian particle's position does not determine when or whether the linking stimulus is applied. This would require the communication of information regarding the particle's position to the machine, which *is* possible but would correspond to an "information ratchet"[25b] mechanism. Rather the rotaxane machine carries out its operations independent of the position of the particle by varying the potential energy surface minima as well as maxima in a partial so-called "energy ratchet"[25b,8d] mechanism (Figure 4).

As mechanical work is done by its operation, is it correct to categorize **5** as a molecular motor? No. Although the machine component of **5** acts to transport a substrate energetically uphill and can be reset without undoing the work done on the substrate, it cannot do so repetitively—a key requirement of a motor—because the succinamide compartment cannot be emptied of the ratcheted substrate. The escapement of the ratcheted quantity is the missing element required for **5** to operate for a second time without undoing the previously performed task by the action of resetting the machine.[40] This feature is present in a previously reported[8d] [2]catenane, **7**, in which the larger macrocycle acts as a motor that repetitively transports the small macrocycle directionally around itself according to a cyclic reaction scheme (Scheme 9). As with **5**, the olefin isomerization reactions in Scheme 9 are balance-breaking steps (depending on where one starts in the scheme, either can be considered to reset the machine); the manipulation of the trityl and silyl protecting groups are pairs of linking–unlinking steps which determine the pathway through which escapement of the ratcheted substrate occurs. Thus, the molecular machine in Scheme 9 operates by the following sequence: [balance-breaking 1; escapement (pathway A); ratcheting; balance-breaking 2 (reset machine); escapement (pathway B); ratcheting]$_n$.

(39) Starting from state **5A**, the linking and initial balance-breaking stimuli can be applied in either order (or simultaneously) in Scheme 8 for the task to be performed by the machine on the substrate, i.e., net transport of the macrocycle along the thread. In fact, any orthogonal transformations that transpire between two unlinking operations are commutative. Indeed, in a classic energy ratchet mechanism (ref 25b)—say using an oscillating electric field to directionally transport a charged particle—the linking/unlinking and balance-breaking steps happen simultaneously which, of course, would have exactly the same effect as doing them sequentially as envisaged in Scheme 8. Balance-breaking and linking/unlinking steps also occur simultaneously during the operation of molecular shuttles containing cyclodextrins incorporated onto azobenzene or stilbene threads (refs 13d, 13i, 13l, 13n, 20b, 20c, 20d, 20f, and 20g).

(40) Although escapement occurs during the operation of **5**, it is not escapement of a quantity that had been previously ratcheted by the operation of the motor. Prior to escapement, the macrocycles located on the olefin station in **5** have only been statistically unbalanced by the action of the motor, not ratcheted.

Scheme 8 [a,b]

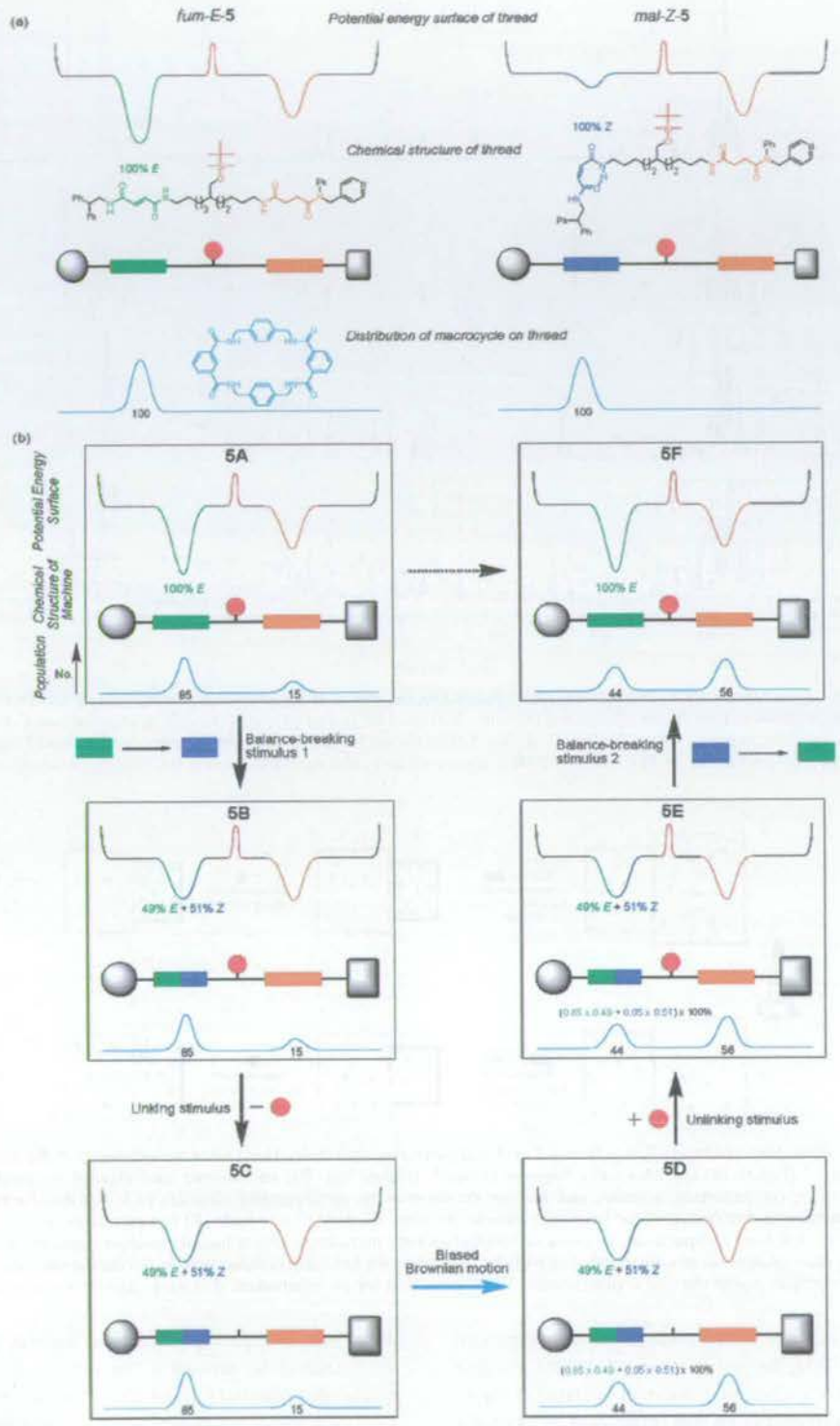

[a] Description of *fum-E*-**5** and *mal-Z*-**5** in covalent, thermodynamic, and statistical terms. [b] "Machine-performance representation" of a compartmentalized molecular machine that can transport a substrate energetically uphill and be reset without undoing the task. **5A**: Initially balanced and unlinked. **5B**: Unbalanced and unlinked. **5C**: Unbalanced and linked (detailed balance is broken). **5D**: Balanced and linked. **5E**: Balanced and unlinked. **5F**: Unbalanced and unlinked. Note the chemical structure of the thread in **5F** is identical to that in **5A**— the machine has been reset—but the population distribution of the macrocycle has changed. The machine has successfully utilized the energy of the photon, via the olefin isomerization reactions, to do the work required to transport the substrate energetically uphill. The stimuli correspond to the reaction conditions given in Scheme 7.

Although rotaxane **5** does not fulfill the requirements for a motor, neither is it a simple switch since the machine part can be reset without influencing the distribution of the substrate. Significantly, examining the state of the machine (the rotaxane thread) in **5** does not provide information regarding the state (distribution) of the substrate. It is only from the history of the

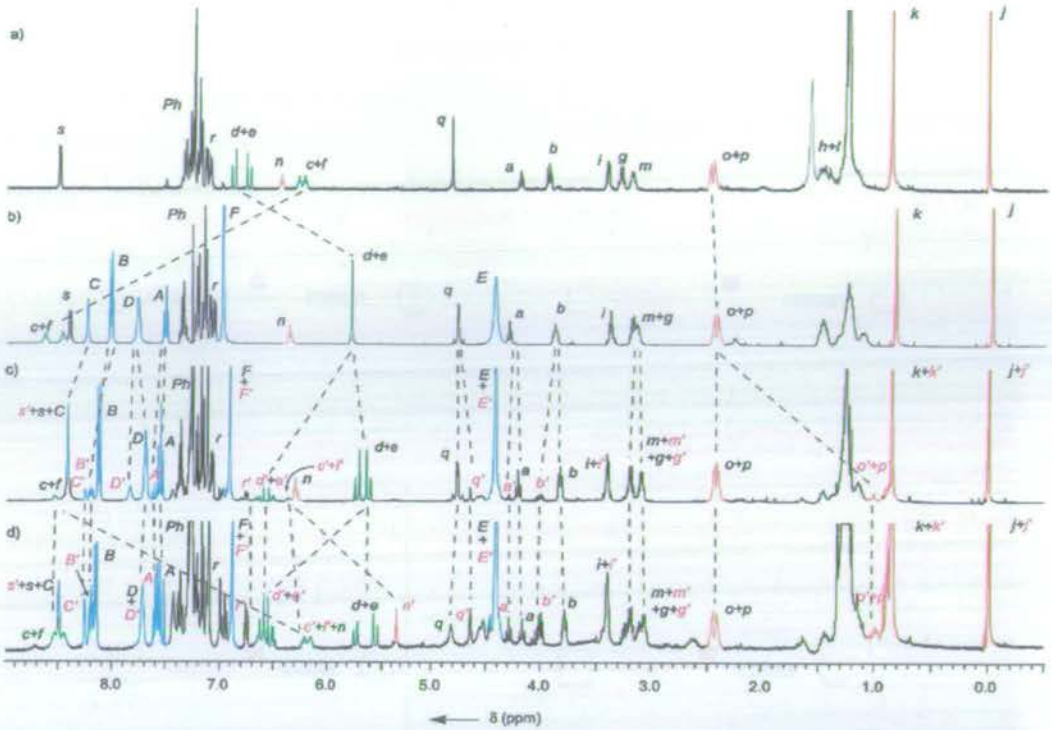

Figure 3. ^{1}H NMR spectra (400 MHz, $CDCl_3$, 298 K) of (a) free thread *E*-**6**, (b) *fum*-*E*-**5**, (c) statistically balanced *E*-**5**, the 85:15 mixture of *fum*-*E*-**5** and *succ*-*E*-**5** that results from desilylation/resilylation of *fum*-*E*-**5** (Scheme 7, (i) and (iii)), and (d) 44:56 (±2%) mixture of *fum*-*E*-**5** and *succ*-*E*-**5** that results from the four-step operation of the machine, either starting from *fum*-*E*-**5** or the 85:15 *fum*-*E*-**5**:*succ*-*E*-**5** statistically balanced mixture (Scheme 7, (i), (ii), (iii), (iv) or (ii), (i), (iii), (iv); Scheme 8, **5A** → **5F**). The ^{1}H NMR assignments and coloring correspond to the labeling in Schemes 5 and 7. Residual water peaks are shown in gray.

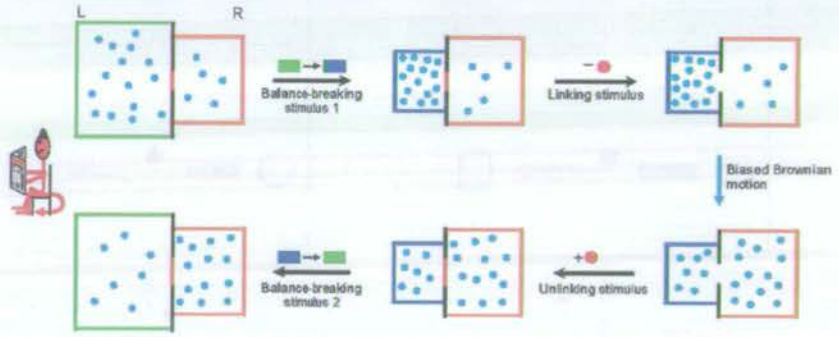

Figure 4. The operation of machine–substrate **5** in Schemes 7 or 8 is the experimental realization (albeit nonadiabatic) of the transportation task required of Smoluchowski's Trapdoor[5] (Figure 1d) and Maxwell's Pressure Demon[4c] (Figure 1b). The mechanistic equivalent of the illustrations from Figure 1 is shown above. The colors of the compartments, particles, and door are the same as the corresponding elements of **5**. The initially balanced (in proportion to the sizes of the two compartments) distribution of the Brownian particles between the left (L) and right (R) compartments becomes statistically unbalanced by a change in volume of the left-hand compartment. Opening the door allows the particles to redistribute themselves according to the new size ratio of the compartments. Closing the door ratchets the new distribution of particles. Restoring the left-hand compartment to its original size then results in a concentration gradient of the Brownian particles across the two compartments. There is no role for an information-gathering demon in this mechanism.

machine's operations that the distribution of the substrate can be known; in other words, the net position of the macrocycle in rotaxane **5** is a consequence of a form of sequential logic. This type of logic is different from that utilized in most of the Boolean logic chemical systems investigated to date, which feature combinational logic (the outputs are solely a function of the inputs at that moment in time).[41] In fact, the behavior of **5** is characteristic of a two-state (one bit) memory or "flip-flop" component in electronics.[42] A flip-flop maintains its effect on a system indefinitely until an input pulse operates on it, causing its output to change to a new indefinitely stable state according to defined rules.[43] Different variants include T-, S-R-, J-K-, and D-type flip-flops. We suggest that a molecule such as **5** should be termed a "two-state" Brownian flip-flop because the substrate must exist in one of two compartments

(41) Combinational logic circuits (NAND, NOR, OR, XOR, EOR, two- and three-input INH, etc.) are assembled by connecting combinations of AND, NOT, and OR gates in various ways. These, in turn, are assembled by connecting simple "on"–"off" switches in various ways. See: (a) Ben-Ari, M. *Mathematical Logic for Computer Science*; Prentice-Hall: Hemel Hempstead, 1993. For reviews on molecular-scale combinational logic systems see: (b) Raymo, F. M. *Adv. Mater.* **2002**, *14*, 401–414 and (c) de Silva, A. P.; McClenaghan, N. D. *Chem. Eur. J.* **2004**, *10*, 574–586. For the sequential operation of combinational logic gates see: (d) de Silva, A. P.; Dixon, I. M.; Gunaratne, H. Q. N.; Gunnlaugsson, T.; Maxwell, P. R. S.; Rice, T. E. *J. Am. Chem. Soc.* **1999**, *121*, 1393–1394 and (e) Raymo, F. M.; Giordani, S. *Org. Lett.* **2001**, *3*, 3475–3478.

Scheme 9. Previously Reported[8d] Synthetic Molecular Rotary Motor **7** that Operates through a Full Brownian Ratchet Mechanism

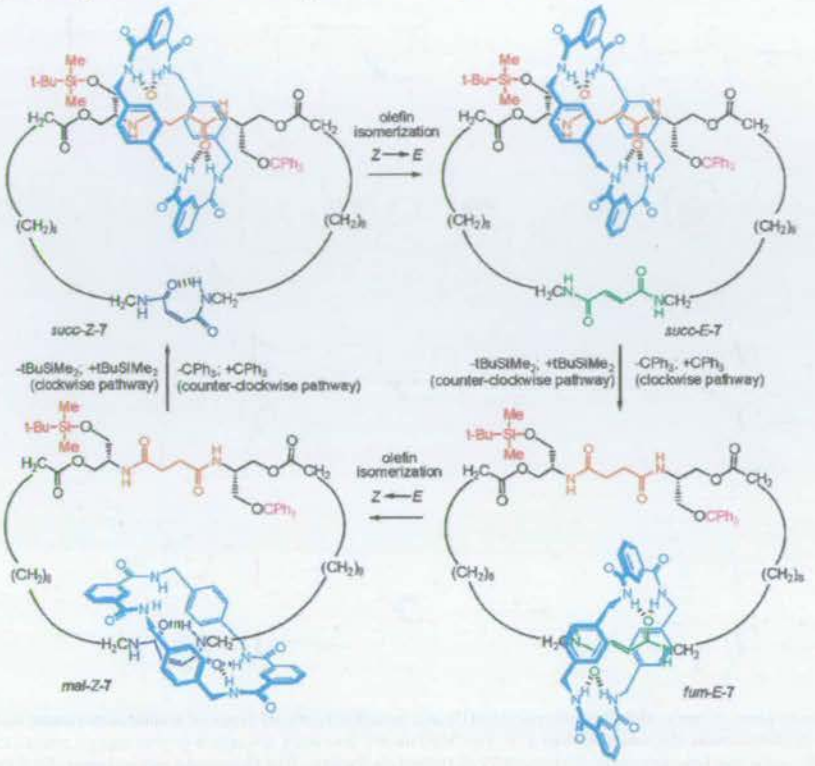

in each molecule. However, there is an important difference that arises because of the statistical nature of a two-state Brownian flip-flop compared to the digital nature of its electronic counterpart. If we wish to utilize the effect of *many* molecules of **5** on a system, the operation of the flip-flop can vary the bulk population distribution of the substrate between the two compartments over a continuum from 85:15 to 44:56 *fum*:*succ* by modifying the balance-breaking reaction parameters (e.g., by changing the time for which the photoisomerization stimulus is applied). If, on the other hand, we use a *single* molecule of **5** to influence a system, its effect is strictly binary—the molecule is in one state or the other—with the *fum*:*succ* ratios corresponding to the *probability* that the substrate will be in a particular compartment given the history of the inputs. In contrast, an electronic flip-flop is always utilized as a single entity in a circuit and its effect is therefore always binary.

Language Necessary To Describe the Operation and Mechanisms of Molecular-Level Mechanical Machines

Up to now the categorization of molecules as machines by chemists has largely been iconic—the structures "look" like pieces of machinery—or they are so-called because they carried out a function that in the macroscopic world would require a machine to perform it.[1] However, as function and mechanism replace imagery as the driving force behind advances in this field, the use of language needs to become more phenomenologically based. For this reason, on the basis of the systems described in this paper and those developed previously by ourselves, Kelly, Feringa, Stoddart and others,[8,10,13–18] we suggest below definitions for four significant phenomenological terms (ratcheting, escapement, balance, and linkage) that are crucial for machines that operate by controlled Brownian motion. Ratcheting is an often used, but previously ill-defined, process in chemical terms. Unfortunately, this vagueness has led to the term sometimes being applied to describe phenomena that are unrelated to Brownian ratchet mechanisms. Escapement is the counterpart to ratcheting and, as far as we are aware, has only rarely been used to describe molecular-level events. The statistical balance of a dynamic substrate and whether the parts of the machine acting on the substrate allow exchange of the substrate or not appear to be key factors that determine whether the machine can perform a task or not. In fact, it appears that the behavior of a molecular machine toward a substrate can be defined by the changing relationship (linked/unlinked; balanced/unbalanced) between the parts of machine interacting with the substrate.

(i) "Ratcheting" is the capturing of a positional displacement of a substrate through the imposition of a kinetic energy barrier which prevents the displacement being reversed when the thermodynamic driving force is removed. The key feature of ratcheting is that the ratcheted part of the system is not linked with (i.e., not allowed to exchange the substrate with) any part of the system that it is ratcheted from. Ratcheting is a crucial requirement for allowing a Brownian machine to be reset without undoing the task it has performed. An example of

(42) (a) Malvino, A. P.; Brown, J. A. *Digital Computer Electronics*, 3rd ed.; Glencoe: Lake Forest, 1993. (b) Mitchell, R. J. *Microprocessor Systems: An introduction*; Macmillan: London, 1995.

(43) A series of stimuli-responsive molecular shuttles have been shown to exhibit relatively long-lived nonequilibrium ("metastable") states when operating in self-assembled monolayers or a polymer electrolyte or at low temperatures (see refs 15i, 15j, and 15k). This may account for the junction hysteresis observed in solid-state electronic devices that utilize such rotaxanes (refs 20k–n). Kinetically stable nonequilibrium co-conformations have also been observed in cyclodextrin-based shuttles; see refs 13l and 16d.

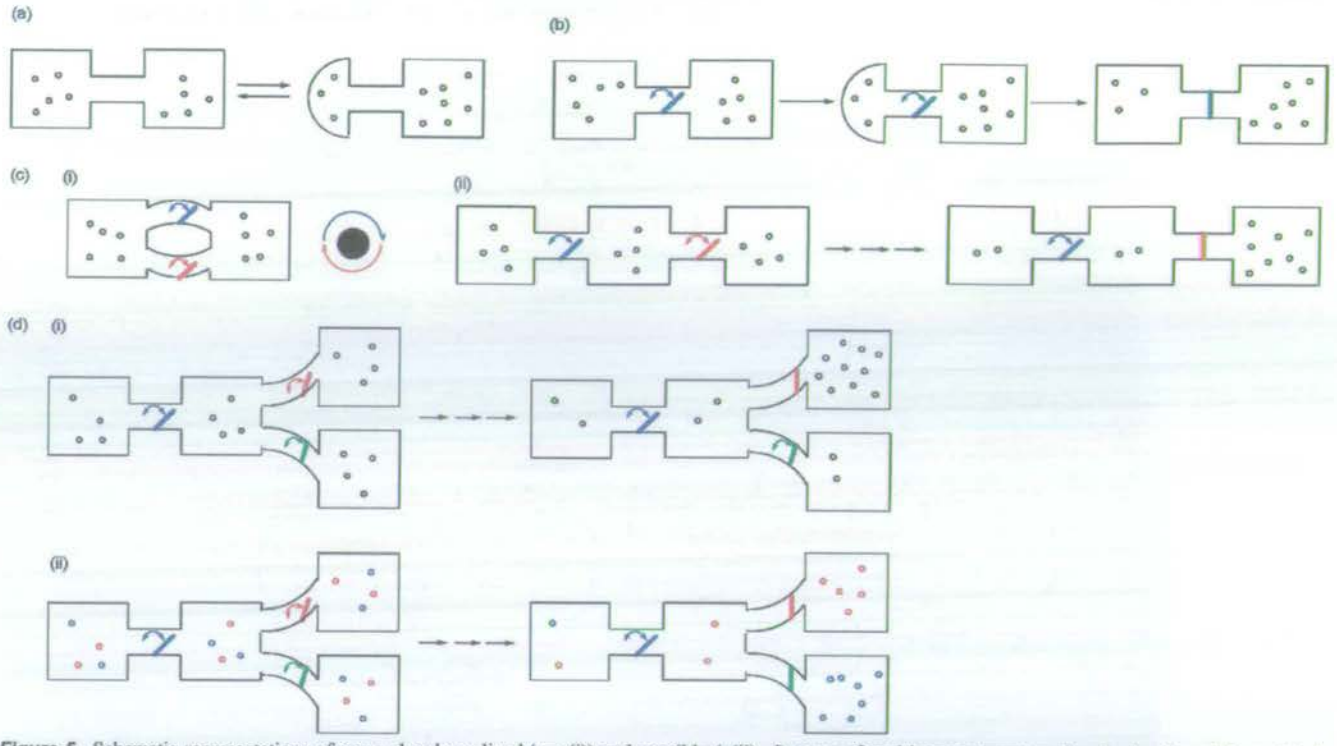

Figure 5. Schematic representations of some already realized (a−c(i)) and possible (c(ii), d) types of multicompartment molecular-level machines. (a) A two-state Brownian switch. (b) A two-state Brownian memory or flip-flop (shown operating through a partial energy ratchet mechanism; other mechanisms are also possible to achieve the same machine function). (c) Examples of Brownian motors: (i) a two-stroke rotary motor; (ii) a three-compartment translational motor. (d) Compartmentalized molecular-level machines that combine ratcheting and escapement with Boolean logic operations: (i) a four-compartment Brownian machine that pumps a substrate in a given (variable) direction. Deciding which one of the red or green gates is used for ratcheting determines whether the substrate is transported to the top compartment or the bottom. (ii) A four-compartment Brownian machine that sorts and separates different ions (e.g., red = Na^+; blue = K^+). A logic operation providing selective access through each of the red and green gates ensures one type of ion is pumped into each compartment.

ratcheting is the unlinking step **5D** → **5E** in Scheme 8. Because it is used to kinetically stabilize an ultimately thermodynamically unfavorable state, ratcheting is intrinsically associated with a sequential logic sequence applied to a Brownian substrate.

(ii) "Escapement" is the (directional) release of a ratcheted substrate in a statistically unbalanced system by lowering a kinetic energy barrier (i.e., by linking). The key feature of escapement is that it requires the linking of two unbalanced parts of a system that were previously unlinked. An escapement step must be subsequently ratcheted in order for a machine to be able to do work repetitively on a substrate. An example of escapement is the de-silylation step during the operation of the irreversible molecular shuttle *succ1*-**3** (Scheme 6, step (i)) or the analogous step for system **5** (**5B** → **5C**, Scheme 8).

(iii) "Balance" is the thermodynamically preferred distribution of an exchangeable quantity or substrate over a machine or parts of a machine. The impetus for net transportation of a substrate comes from balance being broken. (Note that "balance" being broken is not the same as "detailed balance" being broken; "balance" is the thermodynamic driving force for "detailed balance" to be broken.)

(iv) "Linkage" is the communication necessary for transportation of a substrate to occur between parts of a machine. However, the ability to exchange the substrate between the linked parts is not in itself enough for a task to be performed; there must also be a driving force for it to occur (vide supra). Linking and unlinking operations are purely kinetic parameters and so can be accomplished by simply changing the rate of reactions rather than introducing or removing physical steric or electronic barriers.

Types of Compartmentalized Molecular Machines

During development of the terminology necessary to describe molecular-level behavior scientifically, the standard dictionary definitions meant for everyday use are not always appropriate for regimes that the definitions were never intended to cover. As we have seen through the examples given in this paper, the difference between a molecular motor and a molecular switch is fundamental and profound because "motor" and "switch" become different phenomenological descriptors at Brownian length scales, not just iconic classifications of macroscopic objects. As another example, simple switches that operate through biasing Brownian motion do not stay in the same state if the thermodynamic driving force is turned off and it is important to distinguish them from other Brownian machines that do. Indeed, we can identify three different fundamental types of simple Brownian machines that act through various combinations of balance-breaking, linking/unlinking, ratcheting, and escapement steps—a Brownian switch (Figure 5a), a Brownian flip-flop (Figure 5b), and a Brownian motor (Figure 5c). Each of these machine types can also function as components in more complex molecular-level machines (Figure 5d).

(a) A "Two-state (or multistate) Brownian switch" is a machine which can reversibly change the distribution of a Brownian substrate (a moiety which undergoes Brownian motion) between two (or more) distinguishable sites as a

function of state of the machine. It does this by biasing the Brownian motion of the substrate (Figure 5a). Classic stimuli-responsive molecular shuttles, such as *E*/*Z*-**1** and those listed in refs 13−18 and 20, are examples of two-state (or three-state[14]) Brownian switches.

(b) A "Two-state (or multi-state) Brownian flip-flop" is a machine which can reversibly change the distribution of a Brownian substrate between two (or more) distinguishable sites and can be reset without restoring the original distribution of the substrate (Figure 5b). The statistical distribution of the substrate cannot be determined from the state of the flip-flop (unlike a switch, which influences a substrate as a function of state) but rather is determined by the history of operation of the machine, i.e., through a form of sequential logic. Rotaxane **5** is an example of a two-state Brownian flip-flop. It operates through a partial Brownian ratchet mechanism[44] consisting of the following steps applied to a pair of compartments: balance-breaking, escapement, ratcheting, and resetting of the machine (a second balance-breaking step). The original substrate distribution is restored by an escapement−unlinking sequence.

(c) A "Brownian motor" is a machine which can repetitively and progressively change the distribution of a Brownian substrate, during which the machine is reset without restoring the original distribution of the substrate (Figure 5c). Like a flip-flop, a Brownian motor affects a system as a function of the pathway that the machine takes, not as a function of state. Catenane **7** (Scheme 9) is an example of a two-stroke rotary Brownian motor (Figure 5c (i)).[8d] The substrate is repetitively transported between two sites via two alternating pathways. We shall shortly report on the synthesis and operation of a linear three compartment Brownian motor (Figure 5c (ii)).[45]

(d) By combining the three fundamental Brownian machine types which work through combinations of balance-breaking, linking/unlinking, ratcheting, and escapement with other combinational and/or sequential operations based on Boolean logic, machines that can carry out more complex functions, such as variable, directional, travel (Figure 5d (i)), and "sorting and separating" (Figure 5d (ii)), can be envisaged.

Apart from allowing a large amplitude one-dimensional motion to be considered independently of other movements, there is nothing special about rotaxanes in terms of mechanical mechanisms.[12,46] The relationships described in this paper are applicable to any type of molecular-level construct, with controlled motion possible in a kinetically associated structure in two or three dimensions as well as just one. They may also be useful in understanding the changes involved in biological machines as they bring about movement, function, and the transport of Brownian substrates (molecules and ions) in 1-D channels, across membranes, and between parts of a protein.

To appreciate the technological potential of controlled molecular-level motion, one only has to consider that it lies at the heart of virtually every biological process. When we learn how to build synthetic structures that can rectify random dynamic processes and interface their effects directly with other molecular-level substructures and the outside world, it will add a new dimension to functional molecule and materials design. An improved understanding of biological pumps, motors, and other cellular machines will surely also follow.

(44) Since the method of operation of **5** involves varying the relative heights of energy minima and maxima irrespective of the position of the macrocycle, this is a partial "energy ratchet" mechanism (ref 25b). Other types of mechanisms are known (see ref 22), for example, an "information ratchet" which achieves directional transport of a Brownian substrate by varying the relative heights of energy maxima using information provided by the position of the substrate (ref 25b).

(45) Chatterjee, M. N.; Goldup, S.; Kay, E. R.; Leigh, D. A. Manuscript in preparation.

(46) Indeed, their branched topologies rule out rotaxanes as architectures for the particular examples of compartmentalized machines shown in Figure 5d (i) and (ii).

Experimental Procedures for the Operation of Machine−Substrate Systems 3 and 5

Machine−Substrate System 3. Step (i). A solution of [2]rotaxane *succ1*-**3** (80 mg, 0.057 mmol) in aqueous acetic acid (80%, 10 mL) was heated at 60 °C for 1 h. The reaction mixture was concentrated under reduced pressure and traces of acetic acid were removed with a toluene azeotrope (3 × 50 mL). To remove non-rotaxane impurities, the crude reaction mixture was filtered through a plug of silica gel (neat dichloromethane followed by dichloromethane:methanol 95:5) and the solvent removed under reduced pressure to furnish fully de-silylated material.

Step (ii). The de-silylated product from step (i) was dissolved in dichloromethane (20 mL) and treated with imidazole (70 mg, 1.0 mmol), *tert*-butyl-dimethylsilyl chloride (90 mg, 0.60 mmol), and a catalytic amount (5.0 mg) of 4-(dimethylamino)pyridine and the mixture stirred at room temperature for 1 h. To remove non-rotaxane impurities, the crude reaction mixture was filtered through a plug of silica gel (neat dichloromethane followed by dichloromethane:methanol 98:2) and the solvent removed under reduced pressure. The ^{1}H NMR spectrum in $CDCl_3$ of the isomeric mixture of *succ1*-**3** and *succ2*-**3** resulting from this two-step operation is shown in Figure 2c.

Machine−Substrate System 5. Step (i). A solution of [2]rotaxane *fum-E*-**5** (30 mg, 0.021 mmol) in aqueous acetic acid (80%, 2.0 mL) was heated at 60 °C for 1 h. The reaction mixture was concentrated under reduced pressure and traces of acetic acid were removed with a toluene azeotrope (3 × 5 mL). To remove non-rotaxane impurities, the crude reaction mixture was filtered through a plug of silica gel (neat dicholormethane followed by dichloromethane:methanol 95:5) and the solvent removed under reduced pressure to furnish fully de-silylated material.

Step (ii). A solution of the de-silylated product from step (i) (20 mg) in dichloromethane (50 mL) was placed in a quartz vessel, degassed with argon (3 × 5 min), and irradiated at 312 nm using a multilamp photoreactor for five successive 5 min sessions. The progress of the reaction was monitored by ^{1}H NMR spectroscopy. The photostationary state was reached after 20 min (4 × 5 min irradiations). The reaction mixture was concentrated under reduced pressure and used directly in the next step.

Step (iii). The de-silylated photoisomerized material (20 mg) was dissolved in dichloromethane (2.0 mL) and treated with imidazole (20 mg, 0.29 mmol), *tert*-butyldimethylsilyl chloride (26 mg, 0.17 mmol), and a catalytic amount (5.0 mg) of 4-(dimethylamino)pyridine. The reaction mixture was stirred for 2 h, during which time a colorless precipitate appeared. Water (2 mL) was added and the reaction mixture extracted with dichloromethane (5 mL). The organic layer was separated, washed with brine (saturated, 5 mL), dried over Na_2SO_4, and concentrated under reduced pressure to furnish the crude re-silylated isomeric mixture of rotaxanes. To remove non-rotaxane impurities, the mixture was filtered through a plug of silica gel (petroleum ether:ethyl acetate 8:2 followed by dichloromethane:methanol 8:2). This mixture was concentrated under reduced pressure and used directly in the next step.

Step (iv). To a solution of the re-silylated isomeric mixture of four rotaxanes from step (iii) (20 mg) in dichloromethane (1.0 mL) was added piperidine (100 μL, 1.0 mmol). The reaction was stirred for 12 h. To remove non-rotaxane impurities, the crude reaction mixture was filtered through a plug of silica gel (neat dichloromethane followed by

dichloromethane:methanol 8:2) and the solvent removed under reduced pressure. The ^{1}H NMR spectrum in $CDCl_3$ of the isomeric mixture of *fum-E*-**5** and *succ-E*-**5** obtained after the four-step operation is shown in Figure 3d. An essentially identical ^{1}H NMR spectrum was obtained upon reversing the sequence of steps (i) and (ii).

Acknowledgment. This work was supported by the European Union Future and Emerging Technology program *Hy3M*, the EPSRC, and the Carnegie Trust. D.A.L. is an EPSRC Senior Research Fellow and holds a Royal Society-Wolfson Research Merit Award.

Supporting Information Available: Experimental procedures and spectroscopic data for *succ1*-**3** and *fum-E*-**5** and their precursors. This material is available free of charge via the Internet at http://pubs.acs.org. See any current masthead page for ordering information and Web access instructions.

JA057664Z

NATURE|Vol 440|16 March 2006

50 YEARS AGO

"The Arrow of Time"

— It is widely believed that all irreversible mechanical processes involve an increase of entropy, and that 'classical' (that is, non-statistical) mechanics, of continuous media as well as of particles, can describe physical processes only in so far as they are reversible in time. This means that a film taken of a classical process should be reversible, in the sense that, if put into a projector with the last picture first, it should again yield a possible classical process. This is a myth, however, as a trivial counter-example will show. Suppose a film is taken of a large surface of water initially at rest into which a stone is dropped. The reversed film will show contracting circular waves of increasing amplitude. Moreover, immediately behind the highest wave crest, a circular region of undisturbed water will close in towards the centre. This cannot be regarded as a possible classical process. (It would demand a vast number of distant coherent generators of waves the co-ordination of which, to be explicable, would have to be shown, in the film, as originating from one centre. This, however, raises precisely the same difficulty again, if we try to reverse the amended film.) **K. R. Popper**

From *Nature* 17 March 1956.

100 YEARS AGO

Journals dealing with the chemical aspects of physiological and pathological research have long been current in Germany; but up to the present time English-speaking workers have had to rely on periodicals dealing with all branches of physiology and pathology for the publication of their results... the need has for long been felt of a special journal, and we have to chronicle the advent of one — the *Bio-chemical Journal*... In America also a similar want has been met by the issue of the first numbers of what is there called the *Journal of Biological Chemistry*.

From *Nature* 15 March 1906.

50 & 100 YEARS AGO

PHOTOCHEMISTRY

Lighting up nanomachines

Euan R. Kay and David A. Leigh

A cleverly engineered molecule uses light to generate a charge-separated state and so cause one of its components to move. It's the latest study of a molecular machine that exploits nature's most plentiful energy source.

Nature runs the nanomachinery that makes life possible using the last word in clean, free and readily available power sources — sunlight. In photosynthetic bacteria and green plants, photon absorption by chlorophyll generates a charge-separated state, from which the electron is quickly passed down a cascade of electron carriers, ultimately generating energy in a convenient chemical form. Can similar capabilities be engineered? An exemplary effort to do just this is given by Balzani *et al.* who, writing in *Proceedings of the National Academy of Sciences*[1], describe photochemical experiments on an artificial machine that uses light to displace a fragment of its unimolecular structure.

Those who seek to harness the Sun's energy for synthetic molecular machines find that chemistry is always throwing up obstacles. In particular, charge recombination typically occurs thousands or millions of times faster than the nuclear movements on which such machines rely, making charge-separated states difficult to exploit. This problem can be overcome using bimolecular systems: here, the charged partners quickly diffuse apart so their energy can be used, for example, to achieve switching in a rotaxane[2]. This class of molecule, consisting of a ring that shuttles randomly and incessantly along a string, stopped only by bulky groups at the string's termini, is also that used by Balzani and colleagues[1].

Their rotaxane[3] (Fig. 1) incorporates two structurally different bipyridinium sites — 'stations' 1 and 2 — that slow the shuttling ring's motion through strong short-range electrostatic interactions. The ring thus divides its time between station 1, station 2 and the rest of the string in the ratio of around 95:5:<1. At room temperature, the ring shuttles between the stations tens of thousands of times per second, but the net flux is zero. So no work can be done, or useful task performed, by the shuttling action (the 'principle of detailed balance'[4]).

One of the bulky end-groups of the rotaxane's string is a ruthenium trisbipyridine complex. This can absorb a photon of visible light and so form a reactive, excited state that donates an electron to the more easily reduced of the two bipyridinium sites — station 1, the ring's preferred binding site. One would normally expect the resulting charge imbalance to be corrected by back-transfer of an electron on

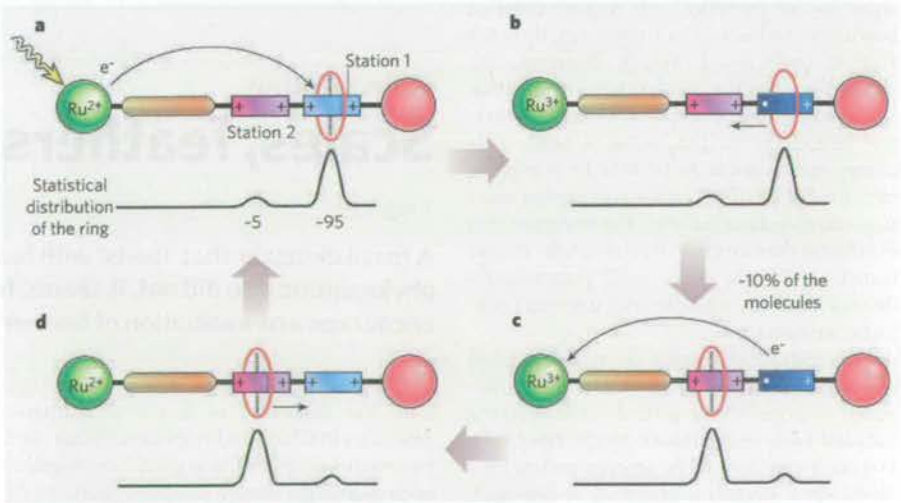

Figure 1 | Light-driven molecular shuttle. Balzani and colleagues' rotaxane[1-3] consists of a molecular ring free to move along a molecular string. **a**, At equilibrium in the ground state, the ring spends most of the time over station 1, as a result of attractive, non-covalent interactions. But irradiation of the ruthenium complex (green) at one end of the string generates a highly reducing excited state, resulting in electron transfer to station 1, and the weakening of this station's electrostatic interactions with the ring. **b**, Normally, charge recombination is fast in comparison with nuclear motions, but here a delay allows approximately 10% of the molecules to undergo significant brownian motion, shifting the distribution of these rings to favour station 2. **c**, When charge recombination eventually does take place, the higher binding affinity of station 1 is restored, and **d**, the system relaxes to restore the original statistical distribution of rings.

the sub-microsecond timescale, even given the considerable distance between the ruthenium complex and the stations (which also slows down the rate of the forward electron-transfer reaction). In fact, the charge-separated state has an average lifetime of around 10 microseconds.

Reduced bipyridinium is a very much poorer binding site for the ring, and the charge-separated state survives long enough for about 10% of the rings to undergo significant brownian motion. Detailed balance is broken and a net flux of rings occurs as they shift their allegiance to the unreduced station 2. After 10 microseconds, however, as back electron transfer finally takes place, station 1 regains its stickiness. A net flux of rings occurs back from station 2, the system returns to its original equilibrium, and a machine cycle has taken place. The process can be repeated for at least a thousand cycles.

This is a fascinating system, working (as do most other light-driven shuttles[2,5–8]) without the consumption of chemical fuels or the formation of waste products. It can be properly called a machine because component displacements occur in response to an external stimulus. But is it really best described as a 'nanomotor'? Chemists are still pondering the most useful way to understand the behaviour of the contemporary, early generations of synthetic molecular machines, but physics and biology offer many useful phenomenon-based ideas in this regard. Brownian motors, for example, use mechanisms[9] that harness random molecular-level motion like that of the ring motion in rotaxanes.

Such brownian ratchet mechanisms, which are believed to account for the behaviour of some motor proteins[10], all require detailed balance to be broken to allow a net, directed flux of particles. Crucially, however, the 'ratchet' part of the mechanism ensures that the resulting change in particle distribution is not undone when the motor is reset. This allows the machine to be able to pump the particle distribution further and further away from equilibrium (as with the enzymes that synthesize the currency of intracellular energy transfer, ATP) or move itself progressively down a track (as with the cell's internal packhorse, kinesin).

This feature is missing from Balzani and colleagues' rotaxane[1], and other simple molecular shuttles[2,5–8]: the work done in breaking detailed balance is undone by the reset step. For such a system to be understood to be a motor by a statistical physicist or biologist, therefore, the rings would have to be diverted along a different track during the reset phase (making a rotary motor), or remain where they are while the machine is reset (making a linear motor or pump). The former is the basis of several wholly synthetic molecular motors[11–15]; the latter has thus far been achieved only with artificial structures made from DNA[16].

Balzani and colleagues' shuttle operates through a fully autonomous photochemical cycle; but can these molecules repetitively do work as long as sunlight is available? The authors did not use sunlight in the experiments they report, but instead treated the rotaxanes with a single 10-nanosecond laser pulse at a visible-light wavelength. If continuously irradiated with sunlight, the distribution of the rings between the two stations would reach a steady state (the exact distribution depending on the intensity of the light) within a few milliseconds. To generate net flows of rings between the stations after that, it appears one would have to switch the light source rapidly on and off.

This is in contrast to the performance of another family of machine molecules that have components that rotate directionally, rather than shuttle linearly[12,17]. When these rotary molecules reach a steady state under continuous irradiation, as with the rotaxanes the bulk distribution of the machine components no longer changes. But even at the steady state, at a sufficiently high temperature, net fluxes of the rotor components still occur through different pathways between four different rotary isomers that are present. Under constant irradiation, the molecules thus operate continuously as directionally rotating motors[17].

Synthetic molecular motors and machines are very much in their infancy, and chemists are still learning the most basic rules for their design and operation. It is a field that can usefully draw on input from physicists, biologists, engineers and materials scientists. For a deeper understanding of molecular machine systems to evolve, therefore, it would be highly beneficial if the terminology used to describe them were to become consistent across all the contributing disciplines. Balzani and colleagues' latest photochemical experiments[1] represent a fascinating advance in our understanding of how a charge-separated state can be used to bring about a nuclear displacement in a unimolecular machine. It will doubtless prove an important stage on the route towards autonomous artificial nanomotors powered by sunlight. ■

Euan R. Kay and David A. Leigh are in the School of Chemistry, University of Edinburgh, King's Buildings, West Mains Road, Edinburgh EH9 3JJ, UK.
e-mail: david.leigh@ed.ac.uk

1. Balzani, V. *et al. Proc. Natl Acad. Sci. USA* **103,** 1178–1183 (2006).
2. Brouwer, A. M. *et al. Science* **291,** 2124–2128 (2001).
3. Ashton, P. R. *et al. Chem. Eur. J.* **6,** 3558–3574 (2000).
4. Onsager, L. *Phys. Rev.* **37,** 405–426 (1931).
5. Murakami, H., Kawabuchi, A., Kotoo, K., Kunitake, M. & Nakashima, N. *J. Am. Chem. Soc.* **119,** 7605–7606 (1997).
6. Wurpel, G. W. H., Brouwer, A. M., van Stokkum, I. H. M., Farran, A. & Leigh, D. A. *J. Am. Chem. Soc.* **123,** 11327–11328 (2001).
7. Altieri, A. *et al. Angew. Chem. Int. Edn* **42,** 2296–2300 (2003).
8. Wang, Q.-C., Qu, D.-H., Ren, J., Chen, K. & Tian, H. *Angew. Chem. Int. Edn* **43,** 2661–2665 (2004).
9. Reimann, P. *Phys. Rep.* **361,** 57–265 (2002).
10. Astumian, R. D. *Science* **276,** 917–922 (1997).
11. Kelly, T. R., De Silva, H. & Silva, R. A. *Nature* **401,** 150–152 (1999).
12. Koumura, N., Zijlstra, R. W. J., van Delden, R. A., Harada, N. & Feringa, B. L. *Nature* **401,** 152–155 (1999).
13. Leigh, D. A., Wong, J. K. Y., Dehez, F. & Zerbetto, F. *Nature* **424,** 174–179 (2003).
14. Hernández, J. V., Kay, E. R. & Leigh, D. A. *Science* **306,** 1532–1537 (2004).
15. Fletcher, S. P., Dumur, F., Pollard, M. M. & Feringa, B. L. *Science* **310,** 80–82 (2005).
16. Kelly, T. R. *Angew. Chem. Int. Edn* **44,** 4124–4127 (2005).
17. Feringa, B. L., Koumura, N., van Delden, R. A. & ter Wiel, M. K. J. *Appl. Phys. A* **75,** 301–308 (2002).

PALAEONTOLOGY

Scales, feathers and dinosaurs

Xing Xu

A fossil dinosaur that 'nests' with feathered relations in the dinosaur phylogenetic tree did not, it seems, have feathers. The discovery will encourage a re-evaluation of feather evolution.

Only birds have feathers — or so we thought until the discovery of fossils of feathered dinosaurs in China and elsewhere[1]. Since then, palaeontologists and biologists have together been painting a simple picture of feather evolution based on evidence from fossils and from developmental biology. A new example of a predatory dinosaur, described by Göhlich and Chiappe on page 329 of this issue[2], makes that picture a little bit more complicated.

The context is provided by Figure 1 (overleaf), which shows the generally understood relationships among the main groups of dinosaur (Aves — the birds — is the only one of these groups to have extant members). Feathers are thought to be characteristic of the Coelurosauria, a group of theropod dinosaurs that includes Aves and several other groups. Because feathers are unique and therefore innovative in developmental and evolutionary terms[3], we can infer their presence in extinct forms using a method called phylogenetic bracketing. Based on the presence of feathers in some extinct coelurosaurs and all living birds, this approach suggests that all coelurosaurs, with the possible exception of gigantic species such as *Tyrannosaurus rex*, are feathered[4].

The small coelurosaur described by Göhlich and Chiappe now enters the picture. This new